

https://dspace.org/

Signal transduction pathways controlling the induction of bone formation by macroporous biomimetic matrices

Klar, Roland Manfred

2015-03-27
http://hdl.handle.net/10539/17353

Downloaded from a DSpace repository. https://dspace.org/

SIGNAL TRANSDUCTION PATHWAYS CONTROLLING THE INDUCTION OF BONE FORMATION BY MACROPOROUS BIOMIMETIC MATRICES

Roland Manfred Klar

A thesis submitted to the Faculty of Health Sciences, University of the Witwatersrand, South Africa, in fulfillment of the requirements for the degree of Doctor of Philosophy

Johannesburg, 2014

DECLARATION

I declare that this thesis is my own work. It is being submitted for the degree of Doctor of Philosophy at the University of the Witwatersrand, Johannesburg, South Africa. It has not been submitted before for any degree or examination at this or any other University.

Roland Klar

Roland Manfred Klar

10 day of October, 2014

ABSTRACT

In spite of vigorous research efforts to date the induction of bone formation by macroporous coral-derived constructs when implanted heterotopically in the *rectus abdominis* muscle of the non-human primate Chacma baboon *Papio ursinus* has not yet been resolved and needs to be assigned. More importantly, the apparent redundancy of molecular signals singly initiating the induction of bone formation in primate species and the heterotopic induction of endochondral bone formation by the mammalian recombinant human transforming growth factor $-\beta_3$ (rhTGF-β_3) isoform have not yet been assigned and need to be mechanistically resolved. Using the r*ectus abdominis* muscle of *Papio ursinus* the study sought to molecularly determine how coral-derived macroporous constructs and doses of the hTGF-β_3 isoform initiate the induction of bone formation. To elucidate the function of osteoclastogenesis and Ca^{2+}, biomimetic coral-derived 7% hydroxyapatite/calcium carbonate (7% HA/CC) devices were supplemented either with 240 μg zoledronate bisphosphonate, an osteoclast binding antagonist, or 500 μg of the calcium channel blocker verapamil hydrochloride. Additionally but in separate coral-derived bioreactors, 125 μg rhTGF-β_3 and/or 125 μg hNoggin were added to answer the question of how TGF-β_3 induces bone formation. All devices were then subsequently implanted within heterotopic sites of the *rectus abdominis* muscle of 6 *Papio ursinus* and left *in vivo* for 15, 60 and 90 days. Harvested specimens were subjected to histomorphometrical and quantitative reverse transcription polymerase chain reaction (qRT-PCR) analysis. *Collagen Type IV* expression supported by extensive vascularisation was detected and observed respectively in all implants after 15 days *in vivo*. Importantly the zoledronate treated specimens possessed delayed tissue patterning and morphogenesis,

an observation not as pronounced as within the verapamil hydrochloride treated specimens. However, both treatment modalities showed a lack or minimal bone formation. The gene expression experiments revealed that *Noggin* was elevated whereas *bone morphogenetic protein-2 (BMP-2)* was greatly downregulated in the verapamil or zoledronate treated devices, indicating that bone formation by macroporous coral-derived devices is through the BMP-pathway. Therefore Ca^{2+} release may be the driving force behind the bone induction mechanism by both regulating stem cell differentiation and the BMP-pathway.

In 7% HA/CC constructs preloaded with 125ug hNoggin there was downregulation of *BMP-2* and lack of *TGF-β_3* activity. Minimal bone formation characterised the hNoggin treated bioreactor. The hTGF-β_3/hNoggin treated devices exhibited *BMP-2* upregulation on day 90 and significant *Noggin* downregulation on day 60 and 90. Downregulation of *Noggin* corresponded to limited bone formation at the periphery of the device at day 90. In the TGF-β_3 loaded 7% HA/CC constructs there was significant downregulation of *BMP-2* expression on day 15, followed by upregulation on day 60 and 90. *BMP-2* upregulation was accompanied by the concomitant upregulation of *RUNX-2* and *Osteocalcin*, along with prominent induction of bone formation. These results unequivocally show that in the *rectus abdominis* muscle of *Papio ursinus* TGF-β_3 induces bone formation by upregulating BMP expression *via* Noggin transcription, together with controlling the differentiation of a progenitor stem cell niche to enhance osteoblastic cell differentiation and proliferation.

PUBLICATIONS FROM THIS THESIS

Ripamonti U, **Klar RM**, Renton LH, Ferretti C.

Synergistic induction of bone formation by hOP-1, hTGF-β3 and inhibition by zoledronate in macroporous coral-derived hydroxyapatites.

Biomaterials. 2010 Sep; 31 (125): 6400-6410.

PMID: 20493522

(Chapter Three)

Klar RM, Duarte R, Dix-Peek T, Dickens C, Ferretti C, Ripamonti U**.**

Calcium ions and osteoclastogenesis initiate the induction of bone formation by coral-derived macroporous constructs.

J Cell Mol Med. 2013 Aug; 17 (11): 1444-1457

PMID: 24106923

(Chapter Four)

Klar RM, Duarte R, Dix-Peek T, Ripamonti U.

The induction of bone formation by the recombinant human transforming growth factor-β_3.

Biomaterials. 2013/14 Dec; 23 (X): 1-16

Manuscript No.: http://dx.doi.org/10.1016/j.biomaterials.2013.12.062

(Chapter Five)

OTHER PUBLICATIONS

Ripamonti U, **Klar RM**

Regenerative frontiers in craniofacial reconstruction: grand challenges and opportunities for the mammalian growth factor-β proteins.

Front Physiol. 2010 Nov; 1 (143): 1-7.

PMID: 21423383

Ripamonti U. **Klar RM**.

Redundancy of osteogenic soluble molecular signals initiating the induction of bone formation.

Science in Africa. 2010 Nov.

(http://www.scienceinafrica.co.za/2010/november/bone_regeneration_ full.htm)

Klar RM.

Bone induction: regeneration through chaos.

Front Physiol. 2011 May; 2 (21): 1-2.

PMCID: PMC3106174

Ripamonti U, Roden LC, Ferretti C, **Klar RM**.

Biomimetic matrices self-initiating the induction of bone formation.

J Craniofac Surg. 2011 Sep; 22 (5): 1859-1870.

Ripamonti U, Roden L, Renton L, **Klar RM**, Petiti J.-C.

The influence of geometry on bone: formation by autoinduction

Science in Africa. 2012

(http://www.scienceinafrica.co.za/2012/The%20influence%20of%20geometry%20on%20bone%20%20SIA.%205.5.12.pdf)

Ripamonti U, Magan A, **Klar RM**, Teare J.

Chapter 2: Calvarial and periodontal tissue induction by autogenous striated muscle cells.

In: Muscle Cells (ed. Pezzo B)

Nova Science Publishing Inc. 2013

ISBM: 978-1-62147-233-5

PRESENTATIONS AT MEETINGS/CONFERENCES

Klar RM, Ripamonti U.

Cementogenesis and mRNA: Breaking the protein paradigm.

Research Day & Postgraduate Expo 2010, University Witwatersrand, Faculty of Health Sciences, Johannesburg, South Africa (Poster)

Klar RM, Ripamonti U.

Calvarial tissue segregation restores the induction of bone formation by the mammalian TGF-β_3 isoform.

Research Day & Postgraduate Expo 2012, University Witwatersrand, Faculty of Health Sciences, Johannesburg, South Africa (Oral)

Klar RM, Ripamonti U.

Bone formation by biomimetic macroporous devices: Novel hTGF-β_3 functions and mechanistic insights.

Research Day & Postgraduate Expo 2012, University Witwatersrand, Faculty of Health Sciences, Johannesburg, South Africa (Poster)

I dedicate this work to my

Austrian grandfather Franz Eigner, who taught me that the "wisest men follow their own direction." (Proverb by Aristotle)

ACKNOWLEDGEMENTS

I would like to articulate my deepest and sincerest gratitude to the following individuals for their invaluable support and contribution to this work.

To my supervisor, Professor Ugo Ripamonti, for his patience, his guidance and his scientific stimulation every step of the way. Thank you for having allowed me to do this PhD in your Bone Research Laboratory and that I was able to meaningfully contribute to the expansion of principles of bone regeneration by induction,

To my Co-supervisor, Doctor Raquel Duarte, for all her assistance, moral support and especially her friendship which helped me to believe in myself and to express my theories, concepts and who remembered me to follow my own direction,

To all co-authors for their valuable input and thought provoking theories, ideas and help in the write-up and construction of the articles, especially that of Professor Ripamonti's expertise and guidance.

To colleagues, especially

Mrs. Ruqaya Parak, for her assistance in histology and histomorphometry, but especially her friendship and moral support in always being honest and truthful. Thank you for having been a shoulder to lean and cry on in the hardest of times. God bless you for always,

Miss. Caroline Dickens and Miss Therese Dix-Peel for having been helpful in teaching and expanding my knowledge and protocol basis on quantitative gene procedures.

Professor Carlo Ferretti for his suggestion to test zoledronate and verapamil and their effect on bone formation by induction.

To Professor Rosemary Crouch, for her assistance through her inspiration to help me overcome my prejudice of my scientific writing. Thank you for all your

inspirational/loving words and guidance, which allowed me to confidently write this thesis.

On a personal note,

To my family; Lucia Klar (mother) and Wolfgang Klar (father), for all their love and support throughout this project.

To God, who helped me get through every challenge and face every problem with an open heart.

To Dr. M. Conradie, my ophthalmologist, who kept my eyes functioning so that I can fullfill my dreams and purpose.

This work was partially funded by the AD-HOC grant of the Bone research Laboratory, the National Research Foundation's (NRF) Incentive funding for rated researchers grant (Grant no. 76605) and the University of Witwatersrand, Faculty of Health Sciences Research grant (FHS), from South Africa.

TABLE OF CONTENTS **Page**

DECLARATION……ii

ABSTRACT……iii

PUBLICATIONS FROM THIS THESIS…….…...v

OTHER PUBLICATIONS…….……..vi

PRESENTATIONS AT MEETINGS/CONFERENCES…….……..viii

ACKNOWLEDGEMENTS…….……....x

TABLE OF CONTENTS…….……...xii

LIST OF TABLES…….……xv

LIST OF FIGURES……..……..xvi

ABBREVIATIONS.....….....xx

PREFACE.....……1

CHAPTER ONE

INTRODUCTION WITH LITERATURE REVIEW.....4

1. Introduction…….....5

1.1 Osteogenesis.....5

1.2 Bone remodelling.....8

1.3 Bone formation by autoinduction-a basic historical perspective.....12

1.4 Induction of bone formation by coral-derived macroporous biomimetic matrices...17

1.5 Bone formation by TGF-β superfamily members.....22

1.6 Molecular redundancy of the initiation of bone formation by induction.....30

CHAPTER TWO

RESEARCH AIMS AND OBJECTIVES.....32

2.1 Significance of Research.....33

2.2 Aims and objectives.....33

CHAPTER THREE

SYNERGISTIC INDUCTION OF BONE FORMATION BY hOP-1, hTGF-β_3 AND INHIBITION BY ZOLEDRONATE IN MACROPOROUS CORAL-DERIVED HYDROXYAPATITES.....34

CHAPTER FOUR

CALCIUM IONS AND OSTEOCLASTOGENESIS INITIATE THE INDUCTION OF BONE FORMATION BY CORAL-DERIVED MACROPOROUS CONSTRUCTS.....46

CHAPTER FIVE

THE INDUCTIONOF BONE FORMATION BY THE RECOMBINANT HUMAN TRANSFORMING GROWTH FACTOR-β_3 61

CHAPTER SIX

SUMMARISING DISCUSSION.....78

6.1 A compositional standard for future bone inductive biomaterials.....79

6.2 TGF-β_3: modulation and indirect initiation of bone formation by induction.....85

CHAPTER SEVEN

CONCLUSION.....89

APPENDIX A.....93

APPENDIX B.....96

APPENDIX C.....127

GENERAL REFERENCES.....226

LIST OF TABLES

Page

Chapter 3

Table 1. Primer sequences and cycling conditions used for each qRT-PCR run....37

Table 2. Volume fraction (%) of tissue components in 7%HA/CC macroporous constructs *solo*, pre-loaded with bisphosphonate (Zometa®), osteogenic protein-1 (hOP-1), transforming growth factor-β_3 (TGF-β_3), and binary application of both recombinant morphogens on the induction of bone formation within the macroporous spaces 90 days after implantation in the *rectus abdominis* muscle.....37

Chapter 5

Table 1. Primer sequence.....49

Chapter 6

Table 1. Primer sequence.....64

LIST OF FIGURES

Page

Chapter 1

Figure 1. Diagram of intramembraneous ossification.....6

Figure 2. The bone remodelling cycle.....12

Figure 3. The BMP pathway.....26

Figure 4. The TGF-β pathway.....29

Chapter 3

Figure 1. Heterotopic *rectus abdominis* surgical model and implantation design in 3 adult male baboons *Papio ursinus*.....37

Figure 2. Spontaneous induction of bone formation within macroporous spaces of coral-derived 7%HA/CC constructs.....38

Figure 3. Tissue induction and morphogenesis by coral-derived 7%HA/CC pre-loaded with 0.24mg zoledronate.....39

Figure 4. Induction of bone formation by 7%HA/CC constructs pre-loaded with 125μg human recombinant osteogenic protein-1 (hOP-1) and 125μg human recombinant transforming growth factor-β_3 (hTGF-β_3).....40

Figure 5. Digital radiographic images of 7%HA/CC specimens.....41

Figure 6. Synergistic induction of bone formation by binary application of 125μg hOP-1 and 125μg hTGF-β_3.....42

Figure 7. Changes in *OP-1* and *TGF-β_3* mRNA synthesis in macroporous constructs.....43

Chapter 4

Figure 1. Heterotopic intramuscular *rectus abdominis* surgical model and implantation design in adult non-human primates Chacma baboon *Papio ursinus*.....49

Figure 2. Untreated control 7% HA/CC coral-derived macroporous constructs on days 15 and 60 after heterotopic intramuscular implantation.....50

Figure 3. Relative change in gene expression.....51

Figure 4. Morphometric analysis of induced bone by 7%HA/CC untreated control *versus* verapamil hydrochloride and zoledronate treated specimens.....52

Figure 5. Untreated control 7%HA/CC macroporous constructs on day 90.....53

Figure 6. Zoledronate-treated 7%HA/CC macroporous constructs on day 15, 60 and 90.....54

Figure 7. Ca^{++} channel blocker verapamil hydrochloride-treated 7%HA/CC macroporous constructs on day 15, 60 and 90.....57

Chapter 5

Figure 1. Heterotopic intramuscular rectus abdominis surgical model and implantation design in six adult non-human primates Chacma baboon Papio ursinus.....63

Figure 2. Morphometric analyses of the induction of bone formation by treated and untreated coral-derived macroporous bioreactors implanted in the rectus abdominis muscle of 6 non-human primates *Papio ursinus* and harvested at day 15, 60 and 90 after heterotopic implantation and tissue formation.....64

Figure 3. Tissue induction, morphogenesis and pattern formation by coral-derived macroporous constructs pre-treated with 125 μg hTGF-β_3 and harvested 15 days upon intramuscular implantation in the rectus abdominis muscle of *Papio ursinus*.....65

Figure 4. Significant and substantial induction of bone formation by coral-derived macroporous constructs pre-treated with 125 μg hTGF- β_3 on day 30 after heterotopic implantation in *Papio ursinus*.....66

Figure 5. Tissue induction and morphogenesis by coral-derived macroporous constructs pre-treated with 125 μg hTGF- β_3 harvested 60 days upon intramuscular implantation in the rectus abdominis muscle of *Papio ursinus*. 67

Figure 6. Induction of bone formation by coral-derived macroporous constructs pre-treated with 125 μg hTGF- β_3 on day 90 after heterotopic implantation in *Papio ursinus***.** 68

Figure 7. Tissue morphogenesis by coral-derived macroporous constructs pre-treated by binary applications of 125 μg g hTGF- β_3 and 125 μg hNoggin harvested on day 15, 60 and 90 after intramuscular implantation in the rectus abdominis muscle of *Papio ursinus*. 69

Figure 8. Tissue morphogenesis by coral-derived macroporous constructs pre-treated by 125 μg hNoggin harvested on day 15, 60 and 90 after intramuscular implantation in the rectus abdominis muscle of *Papio ursinus*. 70

Figure 9. Induction of bone formation by untreated control macroporous constructs on day 15, 60 and 90 after intramuscular implantation of coral-derived macroporous bioreactors. 71

Figure 10. Relative change in gene expression of *BMP-2*, *TGF-β_3* and *Noggin* at day 15 (15d), 60 (60d) and 90 (90d) within untreated 7% HA/CC control (solo), hNoggin, hTGF-β_3 and hTGF-β_3/hNoggin pre-treated 7% HA/CC. 72

Figure 11. Relative change in gene expression of *type IV collagen*, *RUNX-2* and *Osteocalcin* at day 15 (15d), 60 (60d) and 90 (90d) within untreated 7% HA/CC control (solo), hNoggin and/or hTGF-β_3 pre-treated 7% HA/CC.....73

Chapter 6

Figure 1. The RANK/RANKL pathway 83

Figure 2. The BMP-2 – cAMP – CREB pathway.....84

ABBREVIATIONS

kDa	kilo Daltons
kg	kilograms
mg	milligrams
mM	milliMolar
µg	micrograms
µl	microlitres
µm	micrometers
ALP	alkaline phosphotase
BC	before Christ
BMP	bone morphogenetic protein
BMPRIA	BMP receptor type I alpha
BMPRIB	BMP receptor type I β
BMPRII	BMP receptor type II
BMU	basic multicellular unit
BRL	Bone Research Laboratory
Ca^{2+} or Ca^{++}	calcium ion
cAMP	cyclic Adenosine monophosphate
CDMP	cartilage-derived morphogenetic protein
CREB	cAMP response element binding protein
C_t or C_q	threshold cycle
DBM	demineralised bone matrix
Dpp	decapentaplegic
FGF	fibroblast growth factor

FVA	fibrovascular tissue
GDF	growth differentiation factor
HA/CC	hydroxyapatite/calcium carbonate
HA/β-TCP	hydroxyapatite/β-tricalcium phosphate
hOP-1	human osteogenic protein-1
ICBM	insoluble collagenous bone matrix
LTBP	latent transforming growth factor-β binding protein
mRNA	messenger ribose nucleic acid
$NFAT_{c1}$	nuclear factor of activated T-cells cytoplasmic 1
NF-κB	nuclear factor-kappa B
OC	osteocalcin
OPs	osteogenic proteins
$PPAR_{\gamma}R$	peroxisome proliferator-activated gamma receptor
PCR	polymerase chain reaction
pH	power of hydrogen
qPCR	quantitative PCR
qRT-PCR	quantitative reverse transcription/real time PCR
RANK	receptor activator of nuclear factor-kappa B
RANK-L	RANK-ligand
rh	recombinant human
RNA	ribose nucleic acid
Runx-2	runt-related transcription factor 2
RT-PCR	reverse transcription PCR
Shh	sonic hedge hog

Smad	Smad family member
TβRI	transforming growth factor-β receptor I
TβRII	transforming growth factor-β receptor II
TGF-β	transforming growth factor β
Wnt3a	wingless-type MMTV integration site family member A

PREFACE

The biological activities of the soluble molecular signals of the transforming growth factor-β (TGF-β) supergene family are inexorably linked to biomaterial sciences (Reddi, 1994). The *connubium* of a soluble and an insoluble signal is epitomized by the biological evidence that when implanted in heterotopic extraskeletal sites of animal models singly they lack the capacity of initiating the induction of bone formation (Sampath and Reddi 1981). The soluble signal needs to be reconstituted or recombined with an insoluble signal or substratum to trigger the ripple-like cascade of bone formation by induction (Sampath and Reddi 1981; Sampath and Reddi 1983). Thus the greatest challenges of bone tissue engineering have been, on the one hand, to understand how topographical surface modifications of the insoluble signals or substratum set into motion the molecular and cellular cascade leading to tissue induction and morphogenesis (Fu *et al*. 2010; Chou *et al.* 1995; Curran *et al.* 2006; Vlacic-Zischke *et al.* 2011; Gittens *et al.* 2011; Wilkinson *et al.* 2011; McNamara *et al.;* 2011; Ripamonti *et al.* 2012), and on the other hand, to define the initiating soluble signals that start bone formation (Ripamonti *et al.* 1997; Ripamonti *et al.*2004; Ripamonti *et al.*2008; Ripamonti and Roden 2010).

The insights of Urist (1965), Reddi and Huggins (1972), Sampath and Reddi (1981; Sampath and Reddi 1983), Wozney *et al.* (1988), Celeste *et al*. (1990), Özkaynak *et al.* (1990) permitted the isolation, characterisation and molecular cloning of an entirely new family of protein initiators collectively called bone morphogenetic/osteogenic proteins (BMPs/OPs), members of the TGF-β supergene family (Wozney *et al.* 1988; Ripamonti *et al.* 2004; Ripamonti 2006). BMPs/OPs when implanted in heterotopic extraskeletal sites of animal models including non-human primates induce the formation of new bone (Reddi

1994; Reddi 2000; Ripamonti 2004; Ripamonti 2006). The substantial induction of bone formation in pre-clinical animal studies prematurely convinced basic scientists and skeletal reconstructioneers that an application of a single dose of a recombinant human bone morphogenetic protein would induce tissue morphogenesis, in a clinical environment (Friedlaender *et al*. 2001; Govender *et al.* 2002). However, this theoretical potential has so far not been successfully translated to clinical context. Clinical trials of craniofacial orthopaedic applications such as mandibular reconstruction have indicated that supra physiological doses of a single recombinant human BMPs/OPs (hBMPs/OPs) are needed to often induce clinically unacceptable induction of bone, which still falls short of autogenous bone grafts (Ripamonti *et al.* 2006; Ripamonti *et al*. 2007; Ripamonti 2009; Garrison *et al*. 2007; Mussano *et al*. 2007). Because of the often substandard regeneration of osseous defects in humans implanted with hBMPs/OPs, this thesis now finally asks the prevocative question: are the BMPs/OPs the only initiators of the induction of bone formation?

Implantation of coral-derived calcium carbonate-based macroporous constructs alone or combined with recombinant human TGF-β_3 (rhTGF-β_3) induces bone formation in heterotopic intramuscular sites of the non-human primate *Papio ursinus* (*Papio ursinus*) (Ripamonti 1990; Ripamonti 1991; Ripamonti *et al*. 2008; Ripamonti *et al*. 2012). Taken in context of how gene expression, the algorithm formula for all biological life (Mendel, 1886), affects and directs cellular form and function, the present thesis sought to define some of the mechanisms by which coral-derived macroporous constructs and hTGF-β_3 induce bone formation in heterotopic sites of *Papio ursinus*.

CHAPTER 1

INTRODUCTION WITH LITERATURE REVIEW

1. Introduction

A great unsolved challenge in regenerative medicine and tissue engineering is to restore craniofacial and appendicular bony defects brought about by genetic mutations, pathologies or trauma (Ripamonti *et al*. 1997). Substantial research has been committed towards understanding what it is that confers to the skeleton its remarkable repair potential, which as been observed since Hippocratic times (quoted by Reddi 1994; Reddi 2000). What are the molecular and cellular signals that are set into motion to induce the cascade of bone differentiation? This Introduction with associated Literature Review provides an overview of the signals and mechanisms that initiate and maintain the fascinating scenario of "*Bone: formation by autoinduction*" (Urist 1965; Reddi and Huggins 1972).

1.1 Osteogenesis

Osteogenesis is the process by which new bone is formed. There are two ways by which bone is formed. The aggregation and conversion of mesenchymal cells into osteoblasts laying down newly formed bone is defined as intramembraneous ossification (Gilbert 2000). The craniofacial bones are formed by intramembraneous ossification. Endochondral ossification is the process whereby the appendicular skeleton is formed and it involves the formation of a cartilage anlage that forms the cellular strut for vascular invasion, chondrolysis, bone marrow formation and osteoblastic-like cell differentiation with synthesis of bone matrix (Gilbert 2000).

- **Intramembraneous ossification**

Neural crest-derived mesenchymal cells proliferate and form dense condensations of aggregated mesenchymal cells (Gilbert 2000) where new bone is to be formed later by differentiating osteoblasts. Whilst a constituent of these condensed cells are utilised for capillary formation, the greater majority transform into osteoblasts, the precursor cells required for the successful deposition of new bone matrix (**Fig. 1**).

The osteoblasts secrete a collagen-proteoglycan matrix (osteoid) that has a high binding affinity for calcium salts (Gilbert 2000). When calcium salts associate with the osteoid it becomes mineralized. The osteoblasts then are separated from the region of mineralization by a layer of osteoid matrix, i.e. newly deposited as yet to be mineralized bone matrix (Gilbert 2000). Osteoblasts are then later entrapped within the newly formed and mineralized matrix as osteocytes.

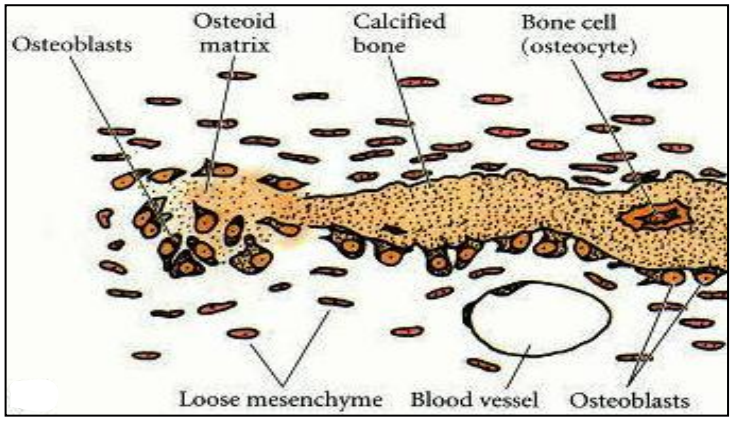


Figure 1. Diagram of intramembraneous ossification. Mesenchymal cells condense and transform into osteoblasts, which deposit osteoid. Osteoid matrix becomes calcified resulting in bone. (Adapted from Gilbert 2000)

- **Endochondral ossification**

Endochondral ossification is characterised by a cartilage anlage that provides the strut for tissue induction, angiogenesis and vascular invasion followed by chondrolysis and osteoblastic cell differentiation (Horton 1990; Gilbert 2000).

Mesenchymal cells differentiate into cartilage cells, i.e. chondroblasts which express cartilage associated genes (Cserjesi *et al.* 1995; Sosic *et al.* 1997). Later chondroblasts condense into compact nodules and complete their transition into chondrocytes (Gilbert 2000). As chondrocytes differentiate they undergo mitosis rapidly. The third stage of endochondral bone formation is characterised by rapidly proliferating chondrocytes that assemble themselves in a cartilage anlage of a model where bone will form. Once properly arranged within this pre-structure bone model, chondrocytes enter a quiescent phase. Chondrocytes increase in size and volume effectively becoming hyper chondrocytes (Gilbert 2000). Hyperthrophic chondrocytes deposite further cartilaginous matrix notably with abundant fibronectin and type X collagen and additionally secrete small membrane-bound vesicles into the extracellular matrix. These vesicles contain enzymes that set into motion the mineralization process within the cartilaginous matrix (Wu *et al.* 1997). The induction of bone formation is brought about by angiogenesis and vascular invasion of the cartilage. Vascular invasion is followed by apoptosis of the hyperthrophic chondrocytes or chondrolysis, that is the lysis of newly formed mineralized cartilage later to become the newly formed marrow spaces sourronded by newly formed bone (Hatori *et al. 1*995; Rajpurokit *et al.* 1999). Cells surrounding the dying hypertrophic chondrocytes differentiate into osteoblasts and form new bone on the degrading cartilaginous

matrix (Bruder and Caplan 1989; Hatori *et al.* 1995).

These two processes of osteogenesis occur primarily during embryogenesis within vertebrates (Gilbert 2000). However bone formation is not a singular event as over the course of a vertebrate's life, bone is constantly being re-formed by resorption and remodelling (Reddi 1994; Reddi 1997; Gilbert 2000). These events have been shown to be crucial for maintaining the bones structural integrity, as well as repairing the bone should it be damaged (Reddi 1997; Gilbert 2000).

1.2 Bone remodelling

The remodelling of bone, as reported by Eriksen (1986), is a continuous process which occurs during specific stages of foetal life and continues once the skeleton has fully formed in vertebrates. The bone remodelling cycle is categorised by a series of crticial and step by step molecular and cellular events (Eriksen 1986; Parfitt 1994). During remodelling, two cell lineages are critical - the mesenchymal osteoblastic and the hematopoietic osteoclastic lineages (Raisz 1999). Resorption and formation exist within a balanced homeostatic equilibrium (Frost 1990). Old bone is continuously replaced by newly formed bone as the bone adapts to mechanical loads and strains (Frost 1990). Several studies have indicated that bone remodelling is controlled by several molecular, ionic and cellular mechanisms ultimatly controlling bone resorption coupled with bone deposition (Boyce *et al.* 2012; Boyle *et al.* 2003; Caudarella *et al.* 2011; Hwang and Putney 2011; Hadjidakis and Androulakis 2006).

Osteoclasts and osteoblasts are known to cooperate closely with each other in the remodelling process in what is called a basic multicellular unit (BMU) (Hadjidakis and Androulakis 2006). The BMUs are organized differently throughout cortical and trabecular bone, the latter housing the bone marrow. Within the cortical bone the BMU has been shown to cut, at an estimated rate of 20 μm per day, a cylindrical canal, approximately 2,000 μm in length and 150–200 μm in width, within the mineralized bone (Petryl, 1996). It has thus been suggested that during 24 hours, ~10 osteoclasts excavate a circular tunnel in the dominant loading direction (Petryl 1996), which is filled in with new bone *via* several thousands of osteoblasts (Parfitt 1994). Thus per annum about 2- 5% of cortical bone is being remodelled in this way. In contrast to this, trabecular bone is more actively remodelled than cortical bone. Trabecular bone surface to volume ratio has been shown to be much greater (Hadjidakis and Androulakis 2006). Time loop experimentation indicated that osteoclasts move across the trabecular bone surface at speeds of up to 25 μm per day, excavating trenches at an approximate depth of 55 μm (Hadjidakis and Androulakis 2006) allowing bone remodelling to occur efficiently and effectively within a relative small amount of time.

The remodelling cycle (**Fig. 2**) has been shown to consist of three consecutive phases: resorption, reversal and formation (Gilbert 2000; Parfitt 1994; Hadjidakis and Androulakis 2006). The induction of bone formation relies on these three phases to be initiated and though several molecular signals have been linked to the remodelling cycle, it is yet still unclear which are the specific signals and/or signal that initiate the remodelling cycle. The present doctoral thesis attempted to study *in vivo* the control of the remodelling cycle by inhibiting osteoclastic activity, essential for bone formation to occur.

The first stage of the remodelling cycle or quiescent phase is morphologically characterized by trabeculae of bone lined by flattened mesenchymal cells not as yet activated but rather in a quiescent state (Parfitt 1994). Mononuclear pre-osteoclasts migrate to the surface of the bone as directed there either by calcium ion release (Boyce *et al.* 2012; Boyle *et al.* 2003; Caudarella *et al.* 2011; Hwang and Putney 2011) or soluble signals secreted by either osteocytes, osteoblasts and/or endothelial cells (Hadjidakis and Androulakis 2006) or possibly even by just the activated quiescent lining cells. Pre-osteoclasts undergo their transition into multinucleated giant cells and attach to the mineralized bone surface. Testing of pH revealed that an acidic pH is created in the zone of resorption created by osteoclasts (Vaananen *et al.* 2000). Osteoclasts secrete hydrogen ions together with lysosomal enzymes, primarily Cathepsin K, and eventually dissolve the mineralized component of the bone matrix (Vaananen *et al.* 2000). The resorption process by osteoclasts produces irregular scalloped concavities of various dimensions , radii and/or curvatures on the bone surface, which are referred to as Howship lacunae, or cylindrical Haversian canals in the cortical bone (Gilbert 2000; Hadjidakis and Androulakis 2006). After the completion of osteoclastic resorption, the reversal phase is entered (Parfitt, 1994).

Mononuclear cells appear on the bone surface (Parfitt 1994). These cells prime the surface by promoting further degradation of the bone collagenous matrix, depositing proteoglycans to form a so-called cement line and release specific growth factors, which then initiate the formation/deposition phase of new bone at the site of the osteoclastic cut concavities (Parfitt 1994).

In the final formation phase, the differentiated osteoblasts, which have differentiated from

mesenchymal precursors, then deposit new bone matrix until the resorbed area within the bone is completely replaced by new osteogenic material (Parfitt 1994; Gilbert 2000; Hadjidakis and Androulakis 2006). Once this stage has been completed the surface of the site of new bone within pre-existing bone is covered once again by flattened lining cells and a prolonged quiescent phase begins until the remodelling cycle is re-initiated (Parfitt 1994; Gilbert 2000).

The remodelling cycle of the osteonic cortical bone with the three continuous phases of resorption, reversal and formation may possibly relate to the often extraordinary repair capacity of the bone matrix and of the skeleton in several animal models including humans. This remarkable potential to heal without scarring has fascinated scientists for centuries and has led to the development of a continuous effort to mechanistically understand the capacity of bone repair and the induction of bone formation which would become known as the “bone induction principle” (Urist *et al*. 1967; Urist *et al*.1968).

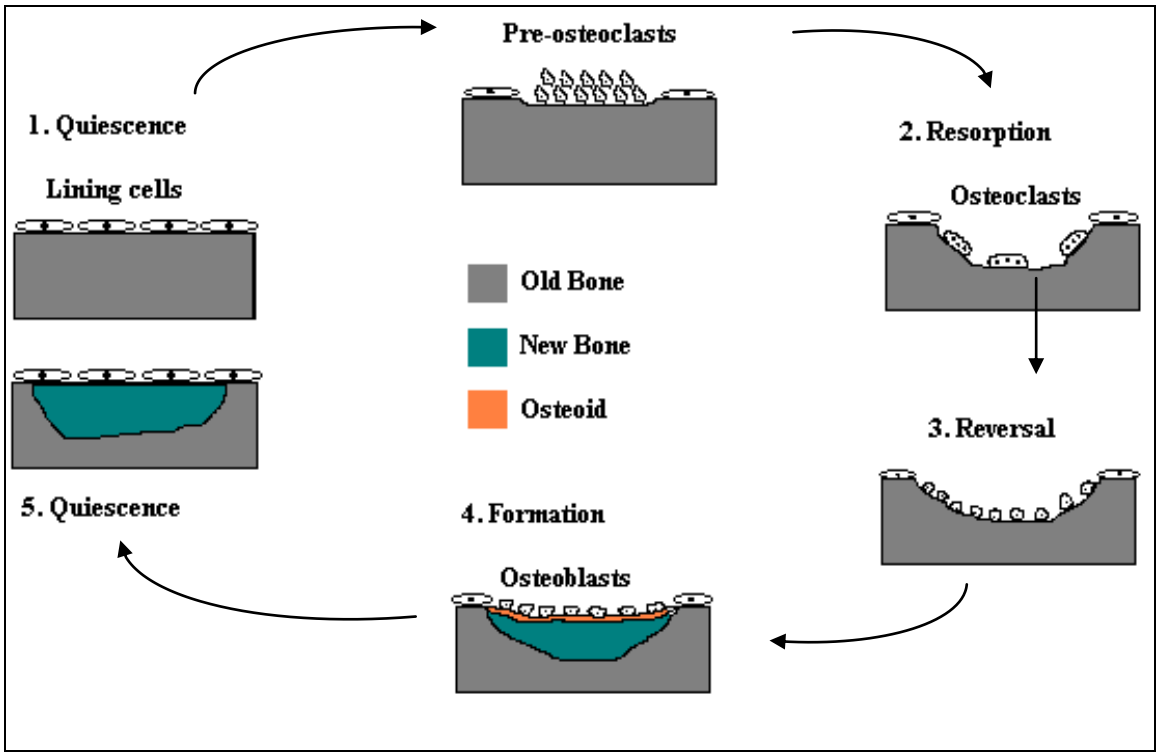


Figure 2. The bone remodeling cycle. Flattened mesenchymal cells line the surface of the bone (1). Pre-osteoclasts migrate to the surface of the bone and differentiate into osteoclasts that resorb an area of bone, producing concavities (2). Monocytes then prime the surface of the newly cut concavities (3), which permits mesenchymal derived osteoblasts to deposit new osteoid within the cut area, which is then converted to new bone (4). A prolonged quiescence phase is then entered (5) before the next remodeling cycle begins (Adapted from Parfitt 1994).

1.3 Bone: formation by autoinduction – a basic historical perspective

The history of regenerative medicine and bone tissue engineering has been shaped from the pioneering scientific work of several scientists across the world, which firstly developed and later set the basic principles of bone tissue engineering.

Senn (1889) was one of the first pioneers to investigate bone regeneration by implanting decalcified bone segments in skull defects of canines. Perceptively, Senn (1889) after having observed that the decalcified bone matrix was incorporated by a mass of embryonic

tissue, stated that this was a necessary condition required for the proper formation of new bone at the site of the implantation (Senn 1889). The concept that postnatal bone formation after implantation of devitalized bone matrices develops by recapitulating embryonic developmental processes was possibly first alluded to by Senn (1889).

Important contributions where brought about by Trueta (1963) who, through in depth morphological analyses, established that angiogenesis is a prerequisite for osteogenesis. However, the pioneering work of Levander (1938) provided important discoveries as well as terminology from which the bone induction principle would further develop. Levander (1938) used the term "tissue induction" upon implantation of bone matrices. Levander (1938) showed that bone formation could be "induced" within heterotopic intramuscular sites when implanting ethanol-treated partially extracted bone matrices. Levander (1938) suggested that heterotopic intramuscular formation of bone was induced by "*some substance extracted by alcohol from the skeletal tissue, a substance having the power to activate the non-specific mesenchymal tissue into the formation of bone tissue, either directly or via the embryonic prenatal stage of bone, viz. cartilage*" (Levander 1938; Levander and Willestaedt 1946). Levander (Levander 1938; Levander and Willestaedt 1946) thus additionally identified that the induction of bone formation in postnatal life is a repeat of embryonic development.

Later Lacroix (1945) would aptly name this hypothetical substance or substances as "osteogenins." It was however the fundamental work of Urist (1965), who established, from the previously published experimental works of Senn, Levander and Lacroix, the so called "bone induction principle" ((Urist *et al.* 1967; Urist *et* al.1968; Reddi 2000;

Ripamonti 2006). Marshall Urist routinely established the use of demineralized bone matrices to induce the differentiation of bone (Urist 1965). The constant reproducible induction of bone formation by demineralized bone matrices resulted in his classic Science paper titled "*Bone: formation by autoinduction*" (Urist, 1965). Importantly however the classic papers of Urist on the "bone induction principle" (Urist 1965; Urist *et al.* 1967; Urist *et al*. 1968) were also the result of previous published experiments in particular by Senn (1889) and Levander (1938), the former implanting demineralized bone matrix blocks, the latter speculating on the induction phenomena brought about by some "unknown substance" within the bone matrix (for review see Ripamonti *et al*. 2006). A further seminal contribution was the introduction of the morphogenetic concept of a hypothetical bone morphogenetic protein complex that initiates the induction of bone morphogenesis within the bone matrix. Urist's studies on the induction of bone formation in a variety of animal models including humans but particularly in the selection of the term "bone morphogenetic protein" (Urist and Strates 1971) have been the cornerstone for the emergence of all the studies on the "*bone induction principle*" (Urist *et al.* 1967; Urist *et* al.1968; Reddi 2000; Ripamonti *et* al. 2006; Ripamonti 2006).

Seminal work on the biochemical and morphological cascades of bone differentiation by induction followed shortly (Reddi and Huggins 1972; Reddi 1984) with partial purification (Sampath and Reddi 1981; Sampath and Reddi 1983) to apparent homogeneity of the still "elusive" morphogenetic factors (Sampath *et al.* 1987; Luyten *et al*. 1989; Ripamonti *et al*. 1992).

Previous studies have shown that osteogenesis can be induced by ligation of the renal

arteries (Sacerdotti and Frattin 1901) or surgically lacerating the urinary bladder wall (Huggins 1931; Friedenstein 1968). Friedenstein (1968) asked how the induction "stimulus" is transferred from the transitional epithelium and other matrices, including demineralized bone matrices, to the surrounding responding cells. Friedenstein implied that there must be the presence of a "soluble inductor," a signal that was responsible for the induction of bone formation (Friedenstein 1962). This query would become the foundation that would shape and later define the "bone induction principle" and the "osteogenic activity" of transplanted matrices, including dentine, uroepithelium and bone (for review Ripamonti *et al*. 2006).

As per Urist hypothesis (Urist and Strates 1971), a bone morphogenetic protein complex within demineralized bone and dentine matrices would provide reproducible evidence of bone formation by induction upon implantation in heterotopic sites. The identification of this elusive bone morphogenetic protein complex was problematic however, since the extracellular matrix of bone "*exists in a solid state*" (Reddi 1997), with the resident morphogenetic proteins tightly bound to the inorganic and organic components of the bone matrix (Sampath and Reddi 1984).

Sampath and Reddi (1981) bypassed "*the bone matrix in the solid state*" (Reddi 1997) by successfully dissociatively extracting the bone matrix using chaotropic agents such as guanidinum and/or urea hydrochloride. This resulted in the preparation of an insoluble inactive collagenous residue and soluble signals, the "putative" extracted osteogenic proteins (Sampath and Reddi 1981; Sampath and Reddi 1983). Separately neither of the two phases, i.e. the extracted solubilised proteins nor the insoluble collagenous bone

matrix (ICBM), induced bone formation when implanted subcutaneously in rodents (Sampath and Reddi 1981). The osteogenic activity of the intact demineralized bone matrix disappeared when it was separated by chaotropic extraction (Sampath and Reddi 1981). Only when the two components separated by chaotropic extraction, i.e. the molecular signals in a soluble state were recombined or reconstituted with the insoluble signal of the ICBM was the inductive potential restored (Sampath and Reddi 1981). The discovery that bone matrix could be dissociatively extracted yielding soluble morphogenetic signals that when reconstituted with the inactive residue restored the osteogenic activity of the intact demineralized bone matrix, showed that the extracellular matrix of bone is a reservoir for soluble morphogenetic signals that initiate the cascade of bone formation by induction (Sampath and Reddi 1981; Sampath and Reddi 1983; Ripamonti and Reddi 1995; Reddi, 2000).

Additionally, the chaotropic dissociative extraction provided a bioassay by which proteins could be identified and classified *in vivo* for its osteoinductive potential (Sampath and Reddi 1983). Bone formation is only induced when a soluble signal is recombined with an insoluble signal or substratum implanted in heterotopic extraskeletal sites *in vivo* (Sampath and Reddi 1981; Sampath and Reddi 1983; Reddi 2000).

The operational reconstitution of a soluble morphogenetic signal with an insoluble signal or substratum is now known as the "*bone tissue engineering paradigm*" (Sampath and Reddi 1981; 1983; Khouri *et al.* 1991; Ripamonti and Reddi 1995; Reddi 2000). Of note however, homologous xenogeneic proteins recombined with recipient allogeneic insoluble collagenous matrix could also induce bone formation (Sampath and Reddi 1983;

Ripamonti and Reddi 1995) but not *vice versa*. This implied that bone inductive signals share important homologies across mammalian species whereas the insoluble collagenous bone matrix retains the antigenic load across species (Sampath and Reddi 1983; Ripamonti and Reddi 1995).

After the realization that the hypothised morphogenetic proteins were tightly bound to the bone matrix and could be dissociatively extracted from bone matrix (Sampath and Reddi 1981; Sampath and Reddi1983), the soluble signals were eventually identified, purified and isolated, yielding an entirely new family of protein initiators collectively called the bone morphogenetic/osteogenic proteins (BMPs/OPs) (Wang *et al*. 1988; Wozney *et al*. 1988). BMPs/OPs were determined to belong to the transforming growth factor-β (TGF-β) supergene family (Wozney *et al.* 1988; Özkaynak *et al.* 1990; Reddi 2000; Ripamonti *et al.* 2004; Ripamonti 2006). The molecular cloning of the now available recombinant human BMPs/OPs has resulted in extensive testing *in vitro* and *in vivo* including pre-clinical experimentation in non-human primates (Ripamonti *et al*. 2001; Ripamonti 2006). This has culminated in the use of recombinant human OP-1 (hOP-1) and hBMP-2 in clinical context (Reddi 2000; Ripamonti *et al*. 2000; Ripamonti *et al*. 2001; Ripamonti *et al*. 2007; Friedlaender *et al.* 2001; Govender *et al*. 2002; Ripamonti, 2006; Ripamonti 2010)

1.4 Induction of bone formation by coral-derived macroporous biomimetic matrices

The understanding of the fascinating phenomenon of "*Bone: formation by autoinduction*" (Urist 1965; Reddi and Huggins 1972) has been vital for the construction of the biological

algorithms in inductive tissue engineering. To successfully induce tissue formation a soluble recombinant molecular signal must be combined with an insoluble substratum, which then activates the morphogenetic and tissue inductive processes (Reddi 1994; Ripamonti *et al.* 2004; Ripamonti 2006; Ripamonti *et al.* 2006; Reddi 2000; Ripamonti 2004a). Additional requirements to obtain successful morphogenesis, as established by Reddi (2000), were the extracellular matrix, responding stem cells and inductive soluble signals. The extracellular matrix is the macro-environment, and can be functionally duplicated by the supra-molecular assembly of new biomimetic matrices (Reddi 2000; Ripamonti *et al.* 2007a; Ripamonti 2009). In order to induce the morphogenesis of specialised organs and tissues, without the need to rely on a multitude of highly diverse proteomic regulators, Nature has come up with simple solution. By adjusting the protein structure, through minor variations in the amino-acid structure within highly conserved carboxy-terminal regions, a single protein family can perform multiple functions. The transforming growth factor-β (TGF-β) supergene family is a classical example of pleotropic activity (Ripamonti 2006; Ripamonti *et al.* 2006; Ripamonti *et al*. 2007a).

The theory for the best possible induction of bone formation relies on the joint action of a complementary substratum together with a soluble osteogenic molecular signal is of pivotal importance for the development of future therapeutic strategies (Ripamonti and Reddi 1995; Ripamonti and Duneas 1996; Ripamonti and Duneas 1998; Reddi 2000). Indeed, biomimetic matrices that imitate or replicate biological structures in mammals have been shown to initiate the induction of bone formation even in the absence of exogenously applies BMPs/OPs (Ripamonti 1990; Ripamonti 2009).

Replication of the remodelling process and subsequent bone formation can be achieved by biomimetic matrices which are constructed with cyclical concavities, e.g. biphasic or highly crystalline hydroxyapatite/β-tricalcium phosphate, as they possess the geometric configuration that set into motion the induction of bone formation (Ripamonti *et al*. 2007a; Ripamonti *et al*. 2008; Ripamonti *et al*. 2009; Ripamonti 2004a; Ripamonti 2009). Research in *Papio ursinus* has shown that the biomimetism of extracellular matrix directs the function of the designed molecular biomimetic matrices (Ripamonti *et al*. 2007; Ripamonti *et al*. 2009; Ripamonti 2004; Ripamonti 2009). The geometric blueprint of the biomaterial influences the inductive potential of the molecular osteogenic signals to initiate the induction of bone formation (Ripamonti 2004). "*The language of shape is the language of geometry, and the language of geometry is a sequence of repetitive concavities cut within biomimetic matrices that biomimetize the remodeling cycle of osteonic bone in primates*" (Ripamonti 2004; Ripamonti 2009)

A very interesting occurrence is the "*spontaneous*" induction of bone formation when utilizing a variety of porous biomimetic matrices (Ripamonti 2004; Ripamonti 2006: Habibovic *et al.* 2006). Selye *et al*. (1960) was the first to report on the induction of bone, cartilage and hematopoietic tissue formation in rodents. Later Winter and Simpson (1996) showed that porous poly-hydroxethyl-methacrylate implanted within heterotopic sites of Large White pigs could also induce bone formation. However it would be the systematic studies of Ripamonti (1990; Ripamonti 1991; Ripamonti *et al* 1993; Ripamonti *et al*. 1996; Ripamonti *et al*. 2009) that showed that calcium phosphate based bioreactors, implanted

within the heterotopic sites of the non-human primate *Papio ursinus* could spontaneously and reproducibly induce new bone formation. The morphogenesis of bone following heterotopic implantation of coral-derived macroporous constructs has been instrumental for the development of highly sintered crystalline hydroxyapatite with a series of self-inducing repetitive concavities (Ripamonti *et al.* 1999), culminating in the construction of '*smart'* biphasic/ tri-calcium phosphate macroporous constructs inducing significant amount of bone formation in both heterotopic and orthotopic sites of *Papio ursinus* (Ripamonti *et al*. 2008).

Coral-derived macroporous constructs have yielded important information on the induction of bone formation and on the induction of the osteogenic phenotype when implanted heterotopically in the *rectus abdominis* muscle of the non-human primate *Papio ursinus* (Ripamonti 1990; Ripamonti 1991; Ripamonti *et al.* 1993; Ripamonti 1996: Ripamonti 2009; Ripamonti *et al*. 2009). Time studies *in vivo* have suggested that myoblastic and/or pericytic stem cells attach to the surface of the macroporous construct, differentiating and proliferating into osteoblastic-like cells (Ripamonti *et al.* 1993; Ripamonti *et al*. 2009). Morphological analyses have shown a continuous stream of stem cells migrating from the vascular compartment towards the osteoblastic compartment attached to the implanted substratum (Ripamonti *et al.* 1993).

Immunohistochemical staining of the implanted macroporous constructs have further shown the presence of alkaline phosphatase and laminin expression within the invading capillaries that sprout within the macroporous spaces (Ripamonti *et al.* 1993). Collagenous condensations that form within the macroporous spaces and undergoing mineralization

together, with the differentiation of osteoblastic-like cells and deposition of osteoid matrix have also been observed (Ripamonti *et al.* 1993). The differentiation of mesenchymal collagenous condensations at the interface of the hydroxyapatite has been suggested to be a prominent differentiating event predating the induction of bone formation within coral-derived macroporous constructs (Ripamonti 1990; Ripamonti 1991; Ripamonti 2009; Ripamonti *et al.* 1993).

Since then, coral-derived macroporous constructs, highly sintered crystalline hydroxyapatites and biphasic hydroxyapatite/β-tricalcium phosphate have been shown to "spontaneously" induce bone formation when implanted in the *rectus abdominis* muscle of *Papio ursinus,* and without any exogenous applications of osteogenic molecular signals (Ripamonti 1990; Ripamonti 1991; Ripamonti *et al.* 1993; Ripamonti *et al* 1999; Ripamonti *et al* 2001; Ripamonti *et al* 2004; Ripamonti *et al* 2011; van Eeden and Ripamonti 1994; Ripamonti 1996; Ripamonti 2000; Ripamonti 2004a; Ripamonti 2006; Ripamonti 2009; Magan and Ripamonti 1996; Ripamonti and Roden 2010).

To summarise, the basic principle of bone formation by induction is to combine an insoluble substrata with a soluble osteogenic molecular signal that through their union form a support that resembles the original shape and function of *in* vivo bone (Sampath and Reddi 1981; Khouri *et al*. 1991; Reddi 1994; Reddi 2000; Ripamonti *et al.* 1993; Ripamonti 2006). However, the above paradigm has since then been modified in which it is proposed that the initiation of bone formation within heterotopic extraskeletal sites can be induced by biometic biomaterial matrices without the exogenously applied soluble osteogenic molecular signal (Ripamonti 2004; Ripamonti 2006).

Hence, how then do coral-derived calcium phosphate-based macroporous constructs initiate the induction of bone formation? This was the first important question the present doctoral study sought to answer.

1.5 Bone formation by TGF-β superfamily members

The incisive work of Wozney *et al*. (1988) finally permitted the molecular cloning of several BMPs/OPs, which were found to be members of the TGF-β supergene family. Proteins were firstly isolated after increasingly chromatographic purification methods (Urist *et al*. 1984; Sampath *et al*. 1987; Luyten *et al.* 1989; Wang *et al.* 1988; Ripamonti *et al.* 1992). Amino acid sequence motifs of batches of purified proteins were then used for molecular cloning of an entirely new family of proteins initiators, collectively called the BMPs/OPs (Wozney *et al*. 1988; Celeste *et al*. 1990; Özkaynak *et al.* 1990; Hammonds *et al*. 1991; Sampath *et al*. 1992). We have since then learned that BMPs/OPs are a family of highly conserved secreted pleitropic proteins that intiate cartilage and bone formation *in vivo* (Wosney *et al.* 1988; Sampath et al. 1992; Reddi 200; Ripamonti 2006; Ripamonti *et al*. 2004).

BMPs/OPs have also been shown to be involved in pattern formation during embryonic organogenesis (Reddi 2005). A remarkable characteristic of BMPs/OPs gene products is that when implanted heterotopically extraskeletally in animal models they induce *de novo* endochondral bone formation (Reddi 2000; Ripamonti *et al.* 2004; Ripamonti 2006).

- **The BMPs/OPs and their signal transduction pathway**

Development, embryogenesis, pattern formation and organo-and skeletogenesis require the action of BMPs (Alliston *et al*. 2008). BMP signalling is regulated *via* their localised expression, the action of specific antagonists and a series of negative and positive feedback loops (Alliston *et al.* 2008) (**Fig. 3**). During skeletal development BMPs-2 - 7 have an overlapping pattern of expression to ensure development occurs in an ordered manner (Solloway *et al.* 1998). Whilst BMP receptors type II and type I alpha (BMPRII and BMPRIA), like most members of the TGF-β family, are ubiquitously expressed (Kawabata *et al.* 1995), BMPR type I beta (BMPRIB), as shown by Ishidou *et al*. (1995), they are principally transcribed only within developing bone and cartilage. Only when bone, in adult life, is damaged are all BMP receptors expressed (Onishi *et al*. 1998), as they facilitate the activation of the bone regeneration cycle. Subsequently, further research studies by Rickard *et al.* (1998), Mundy *et al.* (1999) and Rawadi *et al.* (2003) have shown that additional proteins, specifically statins, estrogen and wingless-type MMTV integration site family member 3A (Wnt3a), are also capable of activating the BMPs.

The activities of the BMPs are highly regulated by a series of antagonists and agonists. Chordin, Follistatin, Gremlin, Noggin and Sclerostin are specific antagonists known to inhibit the BMP pathway activation and thus bone formation (Alliston *et al*. 2008). Research studies have revealed BMPs are also capable of activating the expression of their inhibitors including Noggin and the intracellular BMP pathway inhibitory Smad family members 6 and 7 (Smad6 and Smad7) (**Fig.3**) (Gazerro *et al.* 1998; Takase *et al.* 1998; Ishiskai *et al.* 1999; Pereira *et al.* 2000; van Bezoojien *et al.* 2005). Additionally, members

of the entire BMP signalling pathway, including their initiators and antagonist are subjected to further regulation by a series of positive and negative feedback signalling loops that interact with other signalling pathways (Alliston *et al*. 2008).

BMP signalling commences when a BMP ligand binds first to either the BMPR1A or BMPRIB, after which it forms a receptor complex with BMPRII, i.e. BMPRIA/B + BMPRII (Berk *et al.* 1997; Hayashi *et al.* 1997; Imamura *et al.* 1997; Yoshida *et al.* 2000; Sowa *et al.* 2004). This active complex then activates the Smad transcription receptor complex to regulate nuclear transcription factor activity (Berk *et al.* 1997; Hayashi *et al.* 1997; Imamura *et al.* 1997; Nakao *et al.* 1997; Yoshida *et al.* 2000; Sowa *et al.* 2004). It is this spatial and temporal regulation of the various components of the BMP pathway that ensure proper skeleto-and organogenesis during embryo development as well as the maintenance of bone later in postnatal life (Alliston *et al.* 2008).

Storm *et al.* (1994) revealed that Growth differentiation factor (GDF)-5, -6 and -7, also referred to as cartilage-derived morphogenetic proteins (CDMP-1, -2, and -3) (Chang *et al.* 1994; Storm *et al.* 1994) are involved in bone formation and development *in vivo* (Mikic *et al.* 2002). GDF-5 to -7 have been found, *via* gene knocked studies, to control the length of long bone formation in limbs and regulate patterning of segments in the digits, chondrogenesis and longitudinal bone growth (Storm *et al.* 1994; Storm and Kingsley 1996; Storm and Kingsley 1999). GDFs have also been shown to induce osteogenic differentiation within *in vitro* stem cell differentiation studies (Erlacher *et al.* 1998; Yeh *et al.* 2005).

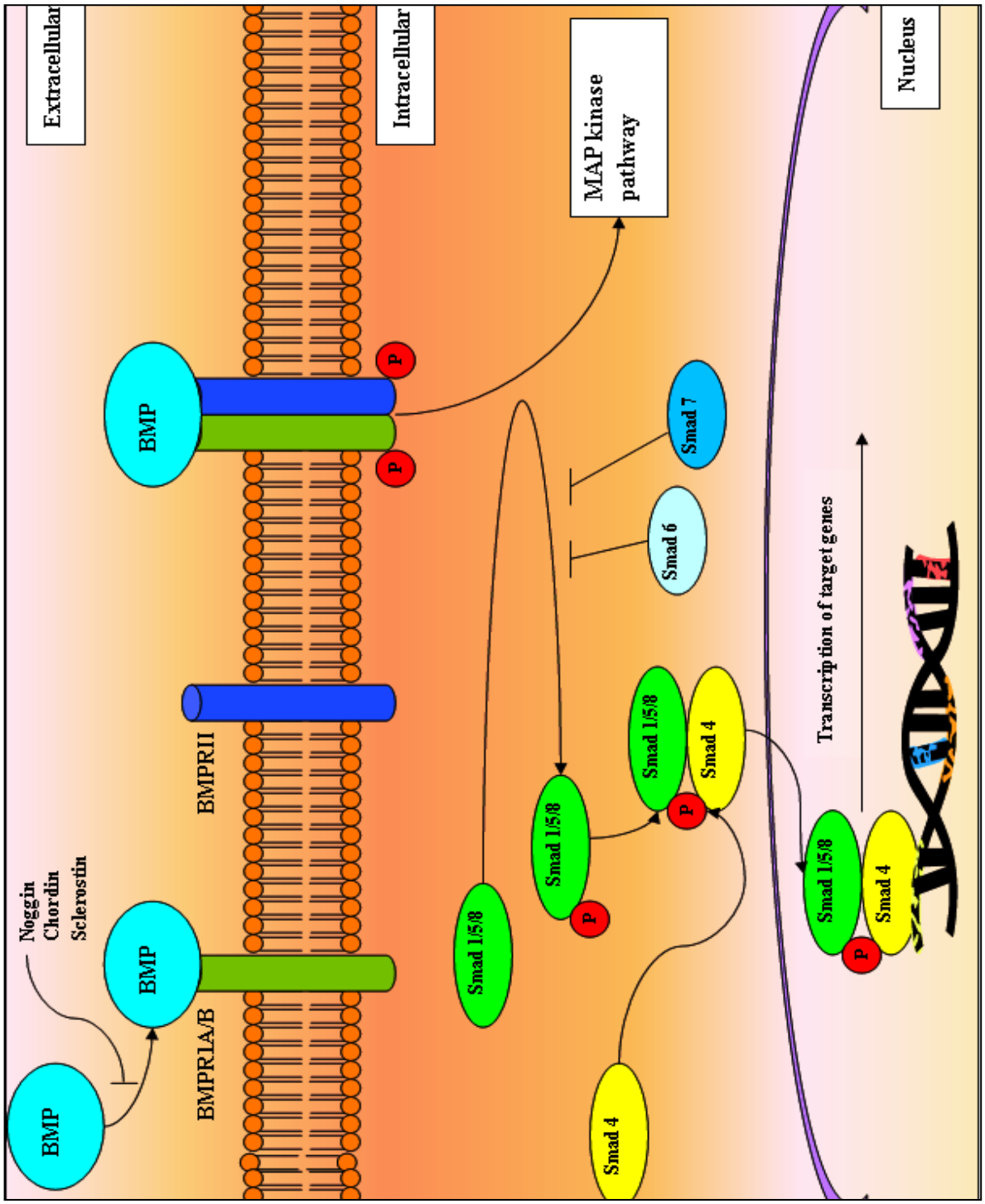


Figure 3. The Bone morphogenetic protein (BMP) pathway. BMPs form a heteromeric complex with type I and type II BMP receptors (BMPRI and BMPRII). Subsequent to this complex formation the BMPRII receptor phosphorylates (P) the BMPRI receptor, upon which the Smad family member 1(Smad 1), Smad5 or Smad8 are phosphorylated. Phosphorylated Smad1/5/6 then forms a complex with Smad4 transforming into a transcription factor, which migrates to the nucleus and transcribes various genes.

→ **activation**

⊣ **inhibition**

- **The TGF-β isoforms and signal transduction pathway**

The three mammalian TGF-β isoforms, TGF-β_1, TGF-β_2 and TGF-β_3 have been shown to signal through receptor complexes of the TGF-β type II receptor (TßRII) and TßRI (Alliston *et al.* 2008) (**Fig. 4)**. *In vitro* research has shown that all three of TGF-β isoforms function similarly at the cellular level (Alliston *et al.* 2008) but differently throughout embryonic osteogenesis (Alliston *et al.* 2008). In knockout studies during murine development each corresponding gene produced unique phenotypic deviations, which reflect their different spatio-temporal distributions and roles. Knock-out studies of TGF-β_1 resulted in abnormal bone quality (Shull *et al.* 1992; Kulkarni *et al.* 1993), whereas deletions of TGF-β_2 or TGF-β_3 impaired epithelial-mesenchymal transdifferentiation, cyto-proliferation and palate formation of the skull (Kaartinen *et al.* 1995; Proetzel *et al.* 1995; Sanford *et al.* 1997).

During bone formation in skeletogenesis the expression patterns of the various TGF-β isoforms are further modulated by a series of positive and negative feedback loops (Alliston *et al*. 2008). However, there are apparent differences between the mRNA and protein expression patterns, which regulate TGF-β isoform storage in cartilage and bone (Alliston and Derynck 2000). Pelton *et al.* (1991) found that extracellular matrix proteins from bone interact with certain of TGF-β isoforms, particularly TGF-β_1, to allow for them to be stored within bone. In the mesenchyme, all TGF-β isoforms are expressed and during condensation of the mesenchyme their expression increases (Alliston *et al*. 2008). Experimental research has revealed that TGF-β_3 is expressed at high levels during the early development of cartilage formation, whereas TGF-β_1 and TGF-β_2 expression is very low

(Pelton *et al.* 1990; Pelton 1991). As bone development progresses, TGF-β_3 levels diminish and TGF-β_1 and TGF-β_2 levels increase (Pelton *et al.* 1990). Primarily it seems that TGF-β_3 levels are highest in tissues associated with skeletogenesis and bone formation, whereas TGF-β_2 is highly transcribed in areas of new bone mineralization (Alliston *et al.* 2008).

In previous research studies of mouse cartilage, TGF-β_3 expression is higher than in relation to the other TGF-β isoforms (Pelton *et al.* 1990; Pelton 1991). Subsequently other research studies on the mouse growth plate have found that whilst TGF-β_2 is transcribed throughout all the regions of the developing plate, whereas TGF-β_1 and TGF-β_3 are restricted to only the hypertrophic and proliferative areas (Sandberg *et al.* 1988; Millian *et al.* 1991; Thorp *et al.* 1992; Horner *et al.* 1998). The periosteums of endochondral and intramembraneous bones show high levels of expression of TGF-β_1 and TGF-β_2 respectively, whilst osteoclasts and osteoblast show varied expression patterns in TGF-β isoforms (Pelton *et al.*(1991)..

In developing bones the TβRI and TβRII are transcribed throughout the developing embryonic skeleton (Horner *et al.* 1998), but in hypertrophic chondrocytes and mineralized osteophyte tissue their expression is reduced and lost, respectively (Horner *et al.* 1998). The Smads, known regulators of the TGF-β pathway, are also subject to regulation in skeletal tissue (Sakou *et al.* 1999). *In* vitro cell culture experiments have shown that Smad2, Smad3 and Smad4 including the inhibitory Smads, Smad6 and 7 are all differentially expressed within proliferating chondrocytes and bone cells (Sakou *et al.* 1999; Alliston *et al*. 2008).

Inactivation and storage of TGF-β isoforms has been shown to be facilitated by latent TGF-β-binding proteins (LTBPs) (Shipley *et al.* 2000). Among the four isoforms of LTBPs-(1-4), all but LTBP-2 have been shown to bind to the TGF-β isoforms (Shipley *et al.* 2000). Although all four LTBPs are broadly expressed and regulated, LPBT-3 expression as shown by Shipley *et al.* (2000) is the highest in bone with LTBP-2 primarily expressed in chondrogenic condensations (Shipley *et al.* 2000). Although other studies have shown that there are ways in which the formation and storage of TGF-β complexes can be regulated (Kwok *et al.* 2005; Oreffo *et al.* 1989; Oursler 1994; Dallas *et al.* 2002), LTBPs are considered the primary mode during skeletal bone formation.

The importance of BMPs and TGF-β isoform involvement in embryonic bone formation has been shown by various studies. However how BMPs and TGF-βs operate during the induction of bone formation is raising awareness especially with regards to which of these two pathways initiate and/or modulate the formation of bone by induction.

Figure 4. The Transforming growth factor- beta (TGF-β) pathway. TGF-β isoforms are produced as a latent protein that is activated by various factors. In their active form TGF-β isoforms bind to the TGF-β type I receptor (TβRI). The TβRI then forms a heteromeric receptor complex with TGF-β type II receptor (TβRII). Smad family member 2 (Smad2) or Smad3 are then phosphorylated (P) and form a transcription complex with Smad4. This transcription factor then migrates to the nucleus where it transcribes various genes.

→ **activation**

⊣ **inhibition**

1.6 Molecular redundancy of the initiation of bone formation by induction

We define the induction of bone formation as the *de novo* induction of endochondral bone when putative osteogenic proteins and/or biomimetic matrices are implanted heterotopically in different animal models. Recombinant hOP-1 induces bone differentiation in the non-human primate model *Papio ursinus* (Ripamonti *et al.* 2000a; Ripamonti 2005). Before 1993, the heterotopic bone formation could only be induced by BMP/OPs morphogens (Reddi 2000; Ripamonti *et al.* 2004; Ripamonti 2006). Homologues of the BMPs/OPs genes where subsequently identified and isolated from *Drosophila melanogaster***,** i.e *decapentaplegic* (*Dpp*) and *60A* genes (Sampath *et al.* 1993; Reddi 2000; Ripamonti 2006) revealing that BMPs/OPS are an ancient gene group that was important for the evolution of all vertebrate life (Ripamonti 2006). Indeed a research study conducted by Sampath *et al*. (1993) showed just how conserved these two gene/protein families were, when he successfully induced the formation of bone within heterotopic extraskeletal sites of rodents upon implantation of recombinant Dpp and 60A. This proved that embryonic patterning either in the fruit fly or vertebrates was linked, helping explain many aspects of embryonic development including hominid evolution (Ripamonti 2009).

Some genes that are upregulated upon implantation of BMPs/OPs within heterotopic sites are *OP-1, BMP-3, TGF-β_1,* and *Type IV collagen,* which as Ripamonti (2005) postulated are expressed during different developmental stages for different time intervals thus helping guide the formation of new bone formation by induction.

Though the induction of bone formation was previously only allocated to the BMPs/OPs, this categorization has since then become redundant since the three mammalian TGF-β isoforms, i.e. TGF-β_1 TGF-β_2 and TGF-β_3, were shown to somehow induce new bone formation within heterotopic extraskeletal sites (Ripamonti *et al*. 1997; Ripamonti *et al*. 2000; Ripamonti *et al*. 2008; Ripamonti *et al*. 2009 Ripamonti and Roden 2010). Whilst this function has still been restricted only to *Papio* ursinus, as previous experiments in the rodent and lagomorph models have failed to demonstrate the induction of bone formation by the three mammalian TGF-β isoforms (Roberts *et al.* 1986; Saadeh *et al.* 1999; Sampath *et al.* 1987; Hammonds *et al.* 1991; Shinozaki *et al.* 1997; Shah *et al.* 1995; Ripamonti *et al.* 2004), an important question has since been raised: how do TGF-β isoforms induce bone formation?

Though there are suggestions that the TGF-β isoforms may induce heterotopic bone differentiation by modulating the BMPs/OPs through their antagonist Noggin (Ripamonti and Roden 2010), this doctoral research sought to further define, more clearly, the bone inductive potential of TGF-β_3, molecularly, so as to help pioneer the way for future therapeutical clinical applications.

CHAPTER 2

RESEARCH AIMS AND OBJECTIVES

2.1 Significance of Research

This research sought to clarify which molecular signals, cellular mechanisms and /or genes initiate and regulate the bone induction cascade by coral-derived calcium carbonate/ hydroxyapatite-based macroporous constructs to expand the current paradigm of bone formation by autoinduction in the primate *Papio ursinus*.

2.2 Aim and Objectives

The aim of this study was to determine how coral-derived macroporous biomimetic matrices and hTGF-β_3 induce bone formation when implanted in heterotopic intramuscular sites of the non-human primate *Papio ursinus* and was addressed by the following two objectives.

Study Objective 1:

To determine the role of osteoclastogenesis and calcium ions in the induction of bone formation by coral-derived macroporous constructs.

Study Objective2:

To determine how mammalian recombinant hTGF-β_3 induces bone formation when combined to coral-derived macroporous constructs implanted within intramuscular sites of *Papio ursinus*.

CHAPTER 3

SYNERGISTIC INDUCTION OF BONE FORMATION BY hOP-1, hTGF-β_3 AND INHIBITION BY ZOLEDRONATE IN MACROPOROUS CORAL-DERIVED HYDROXYAPATITES

Published: Biomaterials 2010; 31: 6400-6410

Biomaterials 31 (2010) 6400–6410

Contents lists available at ScienceDirect

Biomaterials

journal homepage: www.elsevier.com/locate/biomaterials

Synergistic induction of bone formation by hOP-1, hTGF-β_3 and inhibition by zoledronate in macroporous coral-derived hydroxyapatites

Ugo Ripamonti [a,*], Roland M. Klar [a], Louise F. Renton [a], Carlo Ferretti [a,b]

[a] Bone Research Unit, Medical Research Council/University of the Witwatersrand, Johannesburg, South Africa
[b] Division of Oral and Maxillofacial Surgery, University of the Witwatersrand, Johannesburg, South Africa

ARTICLE INFO

Article history:
Received 22 February 2010
Accepted 21 April 2010
Available online 21 May 2010

Keywords:
Osteoclastic topographical modifications
Bisphosphonate zoledronate Zometa
Osteogenic proteins
Synergistic induction of bone formation
Biomimetism

ABSTRACT

Thirty coral-derived calcium carbonate-based macroporous constructs with limited hydrothermal conversion to hydroxyapatite (7% HA/CC) were implanted in the *rectus abdominis* of three adult non-human primate *Papio ursinus* to investigate the intrinsic induction of bone formation. Macroporous constructs with 125 μg human recombinant osteogenic protein-1 (hOP-1) or 125 μg human recombinant transforming growth factor-β_3 (hTGF-β_3) were also implanted. The potential synergistic interaction between morphogens was tested by implanting binary applications of hOP-1 and hTGF-β_3 5:1 by weight, respectively. To evaluate the role of osteoclastic activity on the implanted macroporous surfaces, coral-derived constructs were pre-loaded with 0.24 mg of bisphosphonate zoledronate (Zometa®). To correlate the morphology of tissue induction with osteogenic gene expression and activation, harvested specimens on day 90 were analyzed for changes in *OP-1* and *TGF-β_3* mRNA synthesis by quantitative real-time polymerase chain reaction (qRT-PCR). The induction of bone formation in 7% HA/CC *solo* correlated with *OP-1* expression. Massive bone induction formed by binary applications of the recombinant morphogens. Single applications of hOP-1 and hTGF-β_3 also resulted in substantial bone formation, not comparable however to synergistic binary applications. Zoledronate-treated macroporous constructs showed limited bone formation and in two specimens bone formation was altogether absent; qRT-PCR showed a prominent reduction of *OP-1* gene expression whilst *TGF-β_3* expression was far greater than *OP-1*. The lack of bone formation by zoledronate-treated specimens indicates that osteoclastic activity on the implanted coral-derived constructs is critical for the spontaneous induction of bone formation. Indirectly, zoledronate-treated samples showing lack of *OP-1* gene expression and absent or very limited bone formation by induction confirm that the spontaneous induction of bone formation by coral-derived macroporous constructs is initiated by secreted BMPs/OPs, in context the OP-1 isoform.

© 2010 Elsevier Ltd. All rights reserved.

1. Introduction

The fundamental tenet of the induction of bone formation is to combine osteogenic soluble molecular signals with insoluble signals or substrata that erect scaffolds of biomimetic biomaterial matrices mimicking the supramolecular assembly of the extracellular matrix of bone [1–7]. Our laboratories have modified the above paradigm by constructing biomimetic biomaterial matrices that *per se* initiate the ripple-like cascade of bone differentiation by induction [7,8]. The induction of bone initiates even if the macroporous constructs are implanted in heterotopic extraskeletal sites and without the exogenous application of the osteogenic soluble molecular signals of the transforming growth factor-β (TGF-β) supergene family [7,8]. The morphogenesis of bone was first reported using coral-derived hydroxyapatite/calcium carbonate macroporous constructs when implanted in the *rectus abdominis* muscle of the adult non-human primate *Papio ursinus* [9,10].

Using biphasic hydroxyapatite/β-tricalcium phosphate (HA/β-TCP) biomimetic matrices, we have shown that micro- and macro-topographical modifications in the form of resorption lacunae, pits and concavities cut by osteoclasts are regulators of the spontaneous induction of bone formation [11]. Heterotopic implantation in the *rectus abdominis* muscle of adult *Papio ursinus* has also suggested that myoblastic/myoendothelial and/or pericytic/endothelial stem cells may respond to the topography of the surface micro- and macro-environments differentiating into osteoblastic cell lines expressing, secreting and embedding osteogenic soluble molecular signals of the TGF-β supergene family into the biomimetic matrices initiating the induction of bone formation as a secondary response [8,11].

* Corresponding author. Tel.: +27 11 717 2144; fax: +27 11 717 2300.
E-mail address: ugo.ripamonti@wits.ac.za (U. Ripamonti).

0142-9612/$ – see front matter © 2010 Elsevier Ltd. All rights reserved.
doi:10.1016/j.biomaterials.2010.04.037

The intrinsic and/or spontaneous induction of bone formation by coral-derived hydroxyapatite constructs and by sintered highly crystalline macroporous scaffolds [12,13] is profoundly enhanced by recombining the calcium phosphate-based carriers with naturally-derived or recombinant human bone morphogenetic/osteogenic proteins (BMPs/OPs) [7,14]. Uniquely so far in the non-human primate *Papio ursinus*, heterotopic implantation of the mammalian TGF-β_1, -β_2, and -β_3 combined with either allogeneic insoluble collagenous or macroporous calcium phosphate matrices induce endochondral bone formation [15–18]. Importantly, the induction of bone can be significantly enhanced by the synergistic induction of bone formation [15] in which relatively low doses of the mammalian TGF-β_1 isoform synergize with recombinant human osteogenic protein-1 (hOP-1) to initiate the rapid induction of bone formation in heterotopic *rectus abdominis* and orthotopic calvarial sites [15,19].

To further our knowledge on the synergistic induction of bone formation, three adult non-human primates of the species *Papio ursinus* were used to study the induction of bone by coral-derived macroporous constructs implanted heterotopically in the *rectus abdominis* muscle *solo* or recombined with doses of hOP-1 and hTGF-β_3. The synergistic interaction between morphogens was extended to the hTGF-β_3 isoform by implanting doses of both recombinant proteins. To correlate the morphology of tissue induction with osteogenic gene expression and activation, harvested generated tissues were analyzed for changes in *OP-1* and *TGF-β_3* mRNA synthesis by quantitative real-time polymerase chain reaction (qRT-PCR).

To evaluate the role of osteoclastic activity on the implanted coral-derived macroporous constructs, the bisphosphonate zoledronate (Zometa®) was loaded onto the macroporous surfaces to inhibit osteoclastic activity after intramuscular implantation. Osteoclasts surfacing and modifying the macroporous surfaces of the implanted biomimetic constructs might be the critical step for the initiation of bone formation by carving topographical modifications releasing calcium ions (Ca^{2+}). Ca^{2+} could initiate the ripple-like cascade of myoblastic/myoendothelial and/or pericytic/endothelial stem cell differentiation culminating in the induction of the osteoblastic phenotype without the exogenous application of the osteogenic soluble molecular signals of the TGF-β supergene family [8,11,13].

The prominent induction of bone formation by the synergistic hOP-1/hTGF-β_3 binary applications and the inhibition of bone formation by zoledronate-treated coral-derived macroporous constructs form the basis of this communication.

2. Materials and methods

2.1. Macroporous coral-derived calcium carbonate/hydroxyapatite constructs

Corals (class: Anthozoa) precipitate calcium carbonate in the form of aragonite on a skeletal organic matrix template [20]. The precipitation pattern is highly controlled between colonies; the resulting exoskeletal morphological structures between colonies, i.e. fenestrated partitions or sceroseptae, are highly repetitive geometries used as primary phenotypic markers of genera and species [20]. Macroporous hydroxyapatite replicas of the calcium carbonate exoskeletal microstructure of the coral genus *Goniopora* were prepared by hydrothermal chemical exchange with phosphate [9,10,12,21,22]. Macroporous replicas were constructed to the protocol specifications by Interpore International (Irvine CA, USA) [21]; limited conversion to hydroxyapatite resulted in calcium carbonate (CC) constructs with 7% hydroxyapatite (HA) designated as 7% hydroxyapatite/calcium carbonate (7% HA/CC) constructs [12,21]. Implants for heterotopic implantation were rods 7 mm in diameter and 20 mm in length. The solid components of the framework average 130 μm in diameter and their interconnection 220 μm; the average porosity is 600 μm and their interconnections average 260 μm in diameter [9,10,12,21,22]. Macroporous HA/CC constructs are optimal biomimetic substrata for cell attachment, proliferation and differentiation, acting as non-immunogenic carriers for the biological activity of the osteogenic proteins of the TGF-β supergene family [9,10,12–14]. Macroporous 7% HA/CC constructs were coated with 125 μg hOP-1, 125 μg hTGF-β_3, binary application of both recombinant morphogens and 0.24 mg bisphosphonate zoledronate Zometa® in 200 μl liquid vehicle per macroporous construct.

2.2. Recombinant hOP-1, hTGF-β_3 and preparation of the osteogenic devices

Recombinant human osteogenic protein-1 (hOP-1) was from Creative BioMolecules/Stryker Biotech (Hopkinton, MA, USA) [23]. Mature recombinant human transforming growth factor-β_3 (hTGF-β_3), a glycosylated 25-kDa homodimer with a C-terminal domain of 112 amino acids [24–26] was from Novartis AG, Basel, Switzerland [17]. Stock solutions of the recombinant morphogens were prepared with hOP-1 in 5 mM hydrochloric acid and hTGF-β_3 in 20% ethanol 100 mM acetic acid pH 5.5. Six 7% HA/CC constructs were loaded with 125 μg hOP-1, and six with 125 μg hTGF-β_3 in 200 μl liquid vehicle. Six 7% HA/CC constructs were loaded with binary applications of 125 μg hOP-1 and 25 μg hTGF-β_3 in the ratio of 5:1 by weight of hOP-1 and hTGF-β_3, respectively, to evaluate the synergistic induction of bone formation as initiated by the as yet untested hTGF-β_3 isoform with recombinant hOP-1. Pre-loading of recombinant morphogens was done by pipetting the required amount of liquid vehicle with a 200 μl sterile tip over the central part of the specimens vertically positioned in a laminar flow cabinet [14].

2.3. Pre-loading with the bisphosphonate zoledronate Zometa®

Osteoclastic topographical alterations of the macroporous calcium carbonate/calcium phosphate constructs have been suggested to be a critical event initiating the spontaneous induction of bone formation [11–13]. To test this hypothesis, an additional 6 macroporous constructs were pre-loaded with 0.24 mg of the osteoclastic inhibitor zoledronate before implantation in the *rectus abdominis* muscle.

2.4. Primate model for tissue induction and morphogenesis

Three clinically healthy adult Chacma baboons *Papio ursinus* with a mean weight of 18.6 ± 2.3 kg were selected from the primate colony of the University of the Witwatersrand, Johannesburg. Criteria for selection, housing conditions and diets were as described [6–12]. *Papio ursinus* species share similar bone physiology and osteonic bone remodeling with man [27]. Research protocols were approved by the Animal Ethics Screening Committee and conducted according to the *Guidelines for the care and use of Experimental Animals* prepared by the University and in compliance with the National Code for Animal Use in Research, Education and Diagnosis in South Africa [28]. The heterotopic *rectus abdominis* model of tissue induction and morphogenesis by osteoinductive biomimetic matrices and soluble osteogenic molecular signals has been described in detail [7–18]. A total of 10 7% HA/CC specimens *solo* or pre-treated with soluble signals were implanted bilaterally in 10 intramuscular pouches created by sharp and blunt dissection in the *rectus abdominis* muscle of each animal (Fig. 1). Implants in the pouches flanked the *linea alba* of the *rectus abdominis* are were aligned longitudinally (Fig. 1) approximately 2 cm apart.

2.5. Tissue harvest, histology and histomorphometry

After harvesting of heterotopic tissue for quantitative real-time polymerase chain reaction (qRT-PCR), anaesthetized animals were subjected to bilateral carotid perfusion with buffered saline and harvest of specimens with surrounding *rectus abdominis* muscle as described [8–12]. Harvested tissue was further fixed in phosphate buffered formalin for 48 h, rinsed in tap water and stored in 70% ethanol [10–12]. Fixed specimens were demineralized in a Sakura TDE™ 30 decalcifying unit (Sakura, Fintek, USA) and processed for paraffin wax embedding. Thirty sections were cut sequentially at 4 μm to obtain a full cross sectional area of each specimen. The 1st and every 10th section was stained with a modified Goldner's trichrome and used for histomorphometrical analyses. Sections were examined with a Provis AX70 research microscope (Olympus Optical Co., Japan) equipped with a calibrated Zeiss Integration Platte II (Oberkochem, Germany) with 100 lattice points for determination by the point-counting technique [29] of the fractional volume (in %) of each of the following morphological components: newly formed bone, fibrovascular tissue (including marrow) and the residual hydroxyapatite substratum [9–12]. Morphometry was performed in two sections per implant on two sources per section several μm apart analyzing 15.68 mm^2 per section for a total of 450.24 mm^2 of 30 sections in three animals.

Remaining fixed undecalcified tissue of the binary hOP-1/TGF-β_3 large regenerates was treated according to the method of Donath and Breuner [30] with minor modifications. Briefly, the tissues were processed in ascending grades of ethanol in an automatic tissue processor (Tissue – Tek, V.I.P.; Miles Inc, Elkhart, USA), under pressure vacuum cycles. Samples were infiltrated with ascending concentration of Technovit 7200 VLC (Heraeus Kulzer GmbH, Wehrheim, Germany) and embedded in a fresh solution of the same resin. Undecalcified sections were then ground and polished to 10 μm and stained with a modified Goldner's trichrome. All sample preparation was performed using the EXAKT precision cutting and grinding system (EXAKT Apparatebau, Nordestedt, Hamburg, Germany) [30].

2.6. Relative quantitative real-time polymerase chain reaction (qRT-PCR) analyses

Total RNA was extracted from heterotopic specimens harvested on day 90 using a Total Qiagen RNA extraction kit (Qiagen, South Africa). Samples from only two animals were available for the qRT-PCR analysis. RNA concentration and quality was

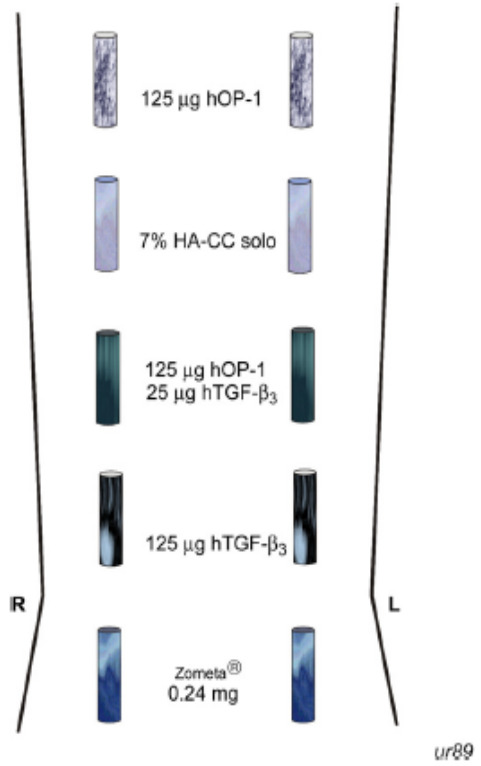


Fig. 1. Heterotopic *rectus abdominis* surgical model and implantation design in 3 adult male baboons *Papio ursinus*. In each animal, ten cylinders of coral-derived calcium carbonate macroporous constructs with limited hydrothermal conversion to hydroxyapatite (7% HA/CC) were implanted heterotopically in duplicate, five 7% HA/CC specimens on each side of the *rectus abdominis* muscle. 7% HA/CC constructs were implanted *solo*, pre-loaded with 125 µg recombinant human osteogenic protein-1 (hOP-1), binary applications of 125 µg hOP-1 and 25 µg recombinant human transforming growth factor-β_3 (hTGF-β_3) ratio 5:1, 125 µg hTGF-β_3, and with 0.24 mg of the bisphosphonate zoledronate Zometa®.

determined spectrophotometrically at A_{260}/A_{280}. Equivalent amounts of RNA (1 µg) were reverse transcribed using a cDNA synthesis kit (Applied Biosystems, South Africa), for first strand cDNA synthesis using random primers. PCR was performed using gene-specific primers to determine optimal cycling conditions (Table 1). PCR coupled with BLASTn (www.pubmed.com) also served to eliminate possible artifactual amplification. Utilizing the Applied Biosystems Software 7500 v12.3 and a PCR machine from Applied Biosystems, South Africa, the relative quantity of the genes were determined through the use of the C_t (threshold cycle). A quantitative value between the endogenous control (muscle tissue) and the treated samples was the calculated using the C_t values.

2.7. Statistical analyses

The data were analyzed with an Analysis of Variance Procedure; pair-wise comparisons of mean values between treatments were obtained by Bonferroni's multiple comparison test and are presented in Table 2. The critical level of statistical significance chosen was $p < 0.01$.

Table 1
Primer sequences and cycling conditions used for each qRT-PCR run.

Gene	Sequence (5′–3′)	Cycling conditions	Amplicon (bp)
TGF-β_3	F: GGTTTTCCGCTTCAATGTGT R: GCTCGATCCTCTGCTCATTC	40 cycles: 94 °C 30 s, 58 °C 30 s, 72 °C 45 s	119
OP-1	F: TGCAGGCAAAACCTAGCA R: ACAGGAACTTCCGGGTCA	40 cycles: 94 °C 1 min, 56 °C 2 min, 72 °C 3 min	215

3. Results

3.1. Induction of bone formation by macroporous hydroxyapatite/calcium carbonate constructs

At harvest, specimens were firmly attached to the ventral fascia of the *rectus abdominis* muscle and to the surrounding muscular tissue without fibrous encapsulation. On day 90 the macroporous spaces showed fibrovascular tissue invasion across the porous spaces (Fig. 2A and B). Collagenic condensations as previously described [9,10,22] were differentiating within the macroporous spaces attached to the inductive hydroxyapatite substratum (Fig. 2A and C). Implantation of macroporous 7% HA/CC *solo* resulted in the morphogenesis of bone (Fig. 2A and B). The spontaneous induction of bone formation also showed bone marrow development surrounded by the newly formed bone (Fig. 2).

3.2. Zoledronate pre-treated macroporous constructs

Zoledronate pre-treated macroporous constructs showed fibrovascular invasion and collagenous condensations across the macroporous spaces tightly attached to the implanted substratum (Fig. 3A and B). In two specimens, the spontaneous induction of bone formation was altogether absent (Fig. 3A and B). Morphological analyses of the remaining specimens showed that minor amounts of bone had formed by induction at the periphery of the implanted pre-treated macroporous scaffolds. The induction of bone, albeit limited at the periphery (Fig. 3C–F), may be the result of incomplete diffusion of the zoledronate throughout the entirety of the macroporous spaces.

3.3. Induction of bone formation by macroporous constructs pre-treated with 125 µg hOP-1 and 125 µg hTGF-β_3 applied singly

hOP-1-treated samples induced substantial osteogenesis across the macroporous spaces (Fig. 4A and B, Table 2). The induction of bone formation surrounded newly formed hematopoietic bone marrow (Fig. 4B). The newly formed bone had remodeled to thin layers of newly induced bone attached to the macroporous constructs (Fig. 4A).

Substantial bone formation had formed in coral-derived 7% HA/CC specimens pre-treated with 125 µg hTGF-β_3 (Fig. 4C–F, Table 2); the prominent induction of bone formation across the macroporous spaces was coupled to the induction of hematopoietic bone marrow supported by prominent angiogenesis and capillary sprouting (Fig. 4D and F). Morphologically, remodeling of the newly formed bone was different as compared to the hOP-1-treated specimens

Table 2
Volume fraction (%) of tissue components in 7% HA/CC macroporous constructs *solo* pre-loaded with bisphosphonate (Zometa®), osteogenic protein-1 (hOP-1), transforming growth factor-β_3 (TGF-β_3), and binary applications of both recombinant morphogens on the induction of bone formation within the macroporous spaces 90 days after implantation in the *rectus abdominis* muscle.

Treatment	Bone (%)	FVA (%)	Substratum (%)
7% HA/CC *solo*	4.7 ± 2.0	56.1 ± 4.7	40.0 ± 5.6
0.24 mg Zometa®	2.8 ± 2.6*	53.4 ± 10.6	45.7 ± 10.2
125 µg hOP-1	19.6 ± 5.2	41.8 ± 5.7	38.6 ± 6.1
125 µg TGF-β_3	14.9 ± 4.7	42.6 ± 3.6	42.6 ± 2.3
125 µg hOP-1 + 25 µg TGFβ_3	24.8 ± 5.7**	38.2 ± 7.3	37.0 ± 8.8

Volume fraction compositions were calculated using a Zeiss Integration Platte II with 100 lattice points superimposed over two sources per two sections per implant. Values (in %) are given as means ± standard error of the mean. FVA: Fibrovascular tissue.
*$p < 0.01$ *vs.* 7% HA/CC *solo*; **$p < 0.01$ *vs.* 125 µg hTGF-β_3; and $p < 0.01$ *vs.* 125 µg hOP-1.

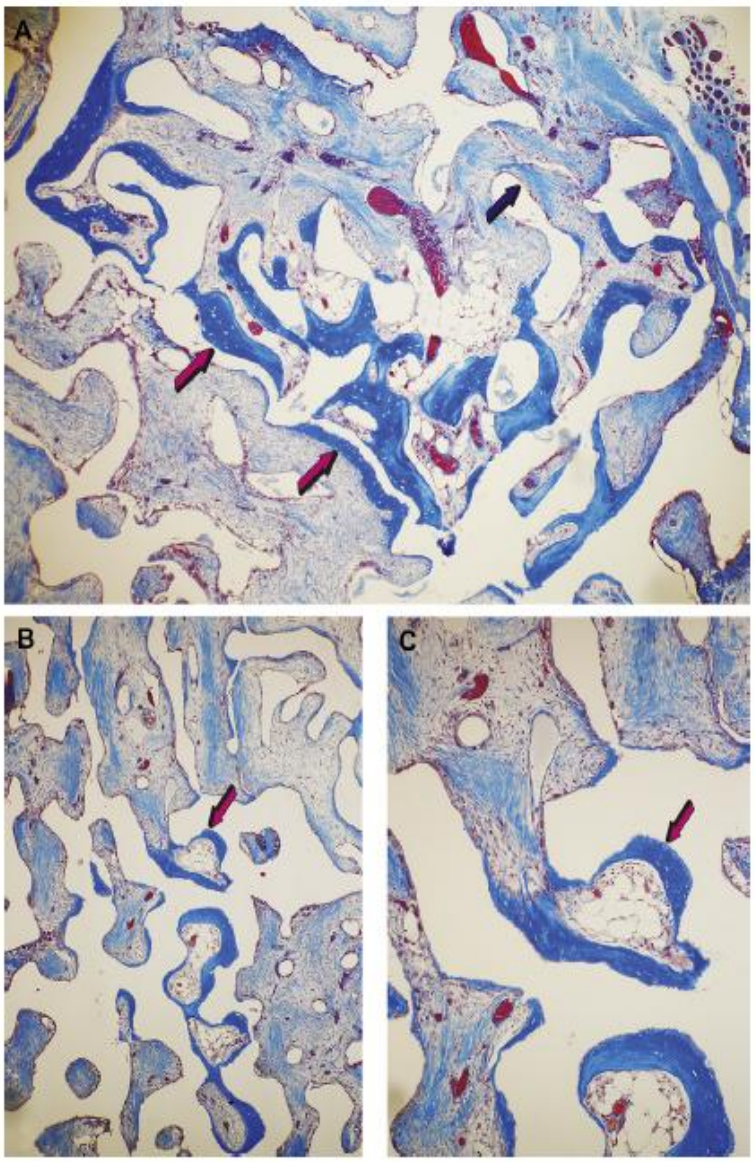


Fig. 2. 'Spontaneous' induction of bone formation within the macroporous spaces of coral-derived 7% HA-CC constructs harvested from the *rectus abdominis* muscle 90 days after heterotopic implantation. (A) Induction of bone (magenta arrows) with bone marrow within the macroporous spaces. Collagenous condensations (blue arrow) form against the coral-derived construct. (B,C) Induction of bone formation (magenta arrows) surrounding bone marrow within the macroporous spaces without the exogenous application of the osteogenic soluble molecular signals of the transforming growth factor-β supergene family. Decalcified sections cut at 4 μm stained with Goldner's trichrome (A) original magnification x21; (B) x27; (C) x75.

with solid blocks of newly induced bone within the macroporous spaces (Fig. 4D and F). In two specimens, there was prominent induction of bone formation mainly at the periphery with a central area characterized by fibrovascular tissue invasion (not shown).

3.4. *hTGF-β_3 and hOP-1 synergize to induce corticalized large ossicles in the rectus abdominis muscle of* Papio ursinus

Binary application of hOP-1 and hTGF-β_3 in the ratio of 5:1 by weight induced substantial bone formation as evaluated at tissue harvest and by radiographic (Fig. 5) and morphological analyses (Fig. 6). Binary applications resulted in the generation of single massive ossicles (Fig. 5B–D) displacing both the dorsal and ventral fasciae of the *rectus abdominis* muscle (Fig. 6A–D). Cut surfaces showed mineralization of the external cortices and were macroscopically brownish-red in colour indicating hematopoietic bone marrow with endosteal vascularization. Decalcified and undecalcified sections showed substantial induction of bone formation not only across the macroporous spaces of the implanted substratum, but prominently exceeding the profile of the implanted biomimetic matrices as evaluated by radiographic and morphological analyses (Figs. 5 and 6). Trabeculae of newly formed bone

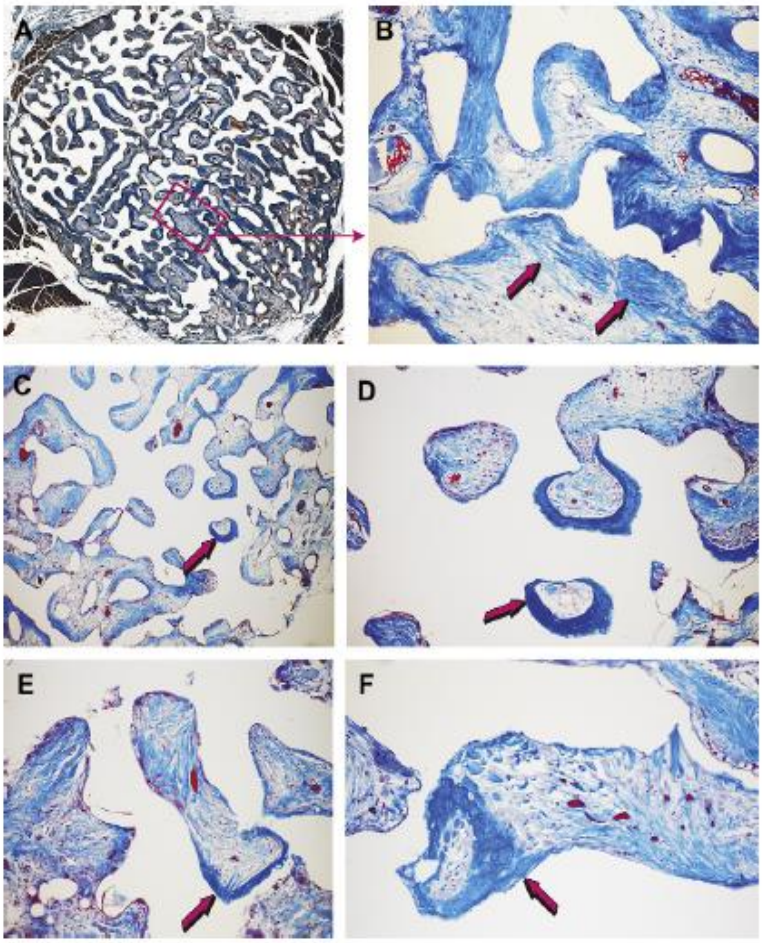


Fig. 3. Tissue induction and morphogenesis by coral-derived 7% HA-CC pre-treated with 0.24 mg zoledronate 90 days after implantation in the *rectus abdominis* muscles of adult baboons *Papio ursinus*. (A) Low power view showing fibrovascular tissue invasion within the macroporous spaces with the induction of collagenous condensations at the interfaces magnified in (B arrow). (B) Detail highlighted in (A) showing the collagenous condensations throughout the macroporous spaces but lack of bone differentiation. (C,D) Limited induction of bone formation in a zoledronate pre-treated specimen (C) magnified in (D) indicated by magenta arrows. (E,F) High power views of another zoledronate pre-treated specimen showing minor induction of bone formation (magenta arrows). The induction of bone (arrows) has formed at the periphery of the implanted coral-derived construct only. Decalcified sections cut at 4 μm stained with Goldner's trichrome (A) original magnification x3.7; (B) x27; (C) x17; (D,E) x47; (F) x125.

were covered by osteoid seams populated by contiguous osteoblasts surrounding newly formed hematopoietic bone marrow facing both the *rectus abdominis* and the peritoneal fascia of the recipient muscle (Fig. 6B, D and I)

3.5. *Morphometric analyses: effect of macroporous constructs solo, zoledronate-treated macroporous constructs, hOP-1 and hTGF-β_3 applied singly or in binary application*

Volume fractions of tissue components in coral-derived macroporous constructs are presented in Table 2. Implantation of macroporous constructs *solo* resulted in the induction of bone differentiation (Fig. 2, Table 2). Zoledronate-treated specimens showed minimal bone differentiation by induction ($p < 0.001$ *vs.* untreated 7% CC/HA constructs, Table 2) with two specimens showing complete lack of bone differentiation (Fig. 3A and B). 7% CC/HA constructs pre-treated with 125 μg hOP-1, 125 μg hTGF-β_3 and binary applications of both recombinant morphogens induced substantial bone differentiation within the macroporous spaces with the induction of hematopoietic bone marrow (Figs. 4 and 6, Table 2). Although higher, the amount of bone in 7% CC/HA preloaded with 125 μg hOP-1 did not differ significantly when compared to 7% CC/HA pre-loaded with 125 μg hTGF-β_3 (Table 2); binary application of both morphogens differ significantly when compared to hOP-1 and hTGF-β_3–treated specimens when the substantial newly formed bone that had formed outside the profile of the implanted 7% CC/HA constructs (Fig. 6, Table 2 $p < 0.01$ *vs.* all other treatments) was also included in the analysis.

3.6. *Relative quantitative real-time polymerase chain reaction (qRT-PCR) analyses*

The intensity of the expression of *OP-1* and *TGF-β_3* are presented in Fig. 7. Harvested and homogenized specimens from the *rectus abdominis* muscle of animal 1 and 2 showed a variable degree of expression of *OP-1* and *TGF-β_3*. In general, *TGF-β_3* expression was far greater than the observed *OP-1* expression (Fig. 7). Binary applications of hOP-1/hTGF-β_3 resulted in *OP-1* mRNA synthesis

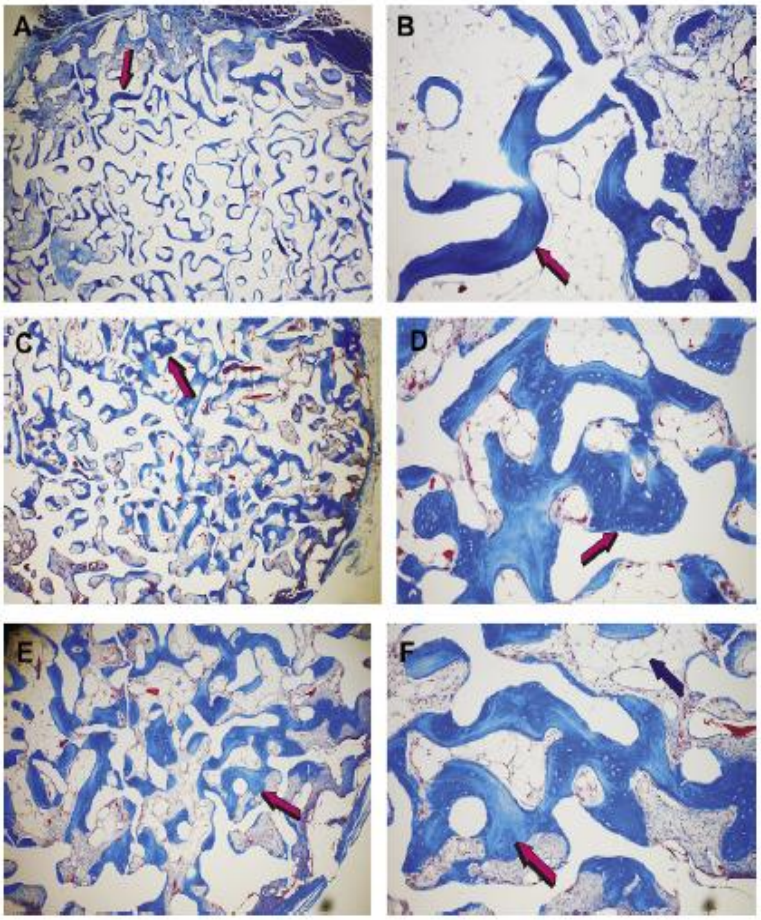


Fig. 4. Induction of bone formation by 7% HA-CC constructs pre-loaded with 125 μg human recombinant osteogenic protein-1 (hOP-1) (A,B) and 125 μg human recombinant transforming growth factor-β_3 (hTGFF-β_3) (C,D,E,F) harvested 90 days after implantation in the *rectus abdominis* muscle of adult baboons *Papio ursinus*. (A) Low power view of the induction of bone formation by hOP-1 throughout the macroporous spaces. (B) Remodeled bone (magenta arrow) facing hematopoietic bone marrow. (C,E) Low power views of 7% HA-CC constructs pre-loaded with 125 μg hTGFF-β_3. Bone induction throughout the macroporous spaces with thick trabeculae of newly formed bone (magenta arrows) (D,F) permeating the macro porosities and facing newly formed hematopoietic bone marrow (blue arrow in F). Decalcified sections cut at 4 μm stained with Goldner's trichrome (A,C) original magnification x5.7; (B,D,F) x27; (E) x17.

several fold lower than *OP-1* expression in both 7% HA/CC constructs *solo* or hTGF-β_3 pre-treated samples (Fig. 7). *TGF-β_3* gene expression did not vary between treatments save for macroporous construct specimens pre-treated with 125 μg hOP-1 in which TGF-β_3 mRNA synthesis showed a 25% increase (Fig. 7). In animal 2 (Fig. 7B), *OP-1* expression was minimal and *TGF-β3* expression was significantly upregulated in specimens pre-treated with 125 μg hOP-1. *OP-1* gene expression was found to be reduced in specimens pre-treated with hTGF-β_3 or binary applications of hOP-1/TGF-β_3. A considerable reduction of *OP-1* gene expression was found in specimens pre-treated with 0.24 mg zoledronate; there was limited *OP-1* expression as compared to *TGF-β_3* mRNA synthesis which showed a 30-fold increase *vs. OP-1* expression (Fig. 7).

4. Discussion

We have shown that partially converted coral-derived hydroxyapatite/calcium carbonate macroporous constructs *solo*, pre-treated with 125 μg hOP-1 or hTGF-β_3 induce the morphogenesis of bone when implanted in heterotopic *rectus abdominis* sites of the non-human primate *Papio ursinus*. Binary applications of the recombinant morphogens showed that the third mammalian hTGF-β isoform also synergizes with hOP-1 to induce large heterotopic ossicles well beyond the profile of the implanted HA/CC constructs. The synergistic induction was very clear even though the ratio of hOP-1 to hTGF-β_3 was set at 5:1 as compared to previous studies in which the tested and optimal ratio was set at 20:1 hOP-1 to hTGF-β_1, respectively [15]. We hypothesized that the ratio of 5:1 would rapidly induce large heterotopic ossicles due to the most powerful osteogenic activity of the TGF-β_3 protein [17].

Significantly, macroporous constructs pre-treated with 0.24 mg zoledronate showed very limited bone formation and two specimens lacked the initiation of bone formation altogether. Osteoclastic post-implantation modifications of the implanted macroporous substrata are thus critical for the induction of macro- and micro-patterned topographies highly suitable for the differentiation of resident stem cells into osteoblastic-like cells expressing the soluble osteogenic molecular signals of the TGF-β supergene family.

Sustained release of calcium ions (Ca^{2+}) provided by the implanted scaffold and the release of intracellular fluid with Ca^{2+}

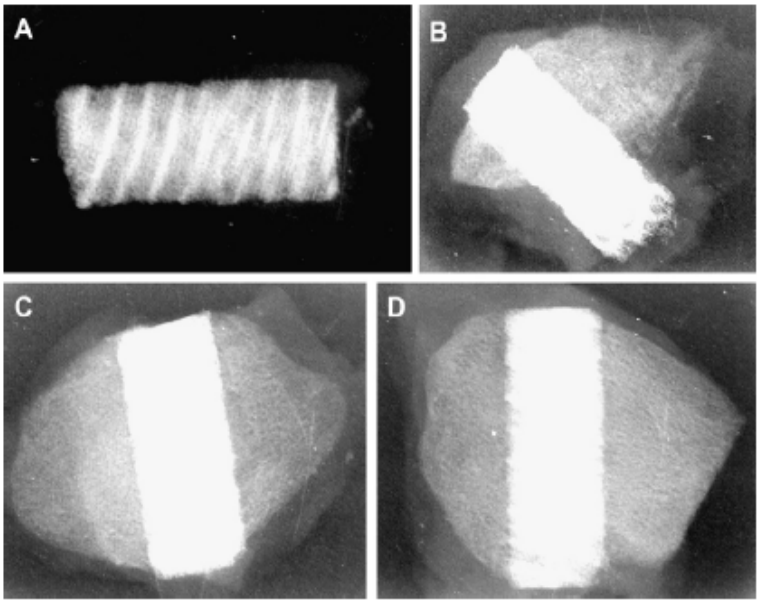


Fig. 5. Digital radiographic images of 7% HA-CC specimens harvested 90 days after implantation in the *rectus abdominis* muscle of three adult baboons *Papio ursinus*. (A) 7% macroporous construct 'solo' with no addition of osteogenic proteins. (B,C, D) Macroporous constructs pre-loaded with binary applications of 125 μg hOP-1 and 25 μg hTGF-β_3 showing massive induction of mineralized bone prominently away from the profile of the coral-derived implanted constructs. (A,B,C,D) original magnification x3.7.

from cells during surgical implantation set into motion the mechanisms of host defence [31]. Extracellular Ca^{2+} elicits a chemokinetic response from monocytes/macrophages [32]. Ca^{2+} also influences the conversion of monocytes to multinucleated macrophages starting osteoclastogenesis [32–34]. Osteoclasts differentiation is mediated by colony stimulating factor, RANKL and NFATc1 [35] further releasing Ca^{2+} within the micro- and macroporous microenvironments. Ca^{2+} release also promotes angiogenesis [36–38] and cell differentiation [39–41]. Of note, recent data have indicated that osteoclasts express and synthesize bone morphogenetic proteins [42,43]; this suggests a possible path to anabolic calcium phosphate remodeling [42,43]. Secreted BMPs/OPs may differentiate resident stem cells into the osteoblastic phenotype. The recruitment and differentiation of mature functional osteoblasts amplified by elevated Ca^{2+} concentrations emphasizes the balanced coupling of bone resorption to formation as initiated by several molecular signals [41–45].

Lack of resorption pits and lacunae cut by osteoclasts within the implanted biomimetic constructs coupled with limited release of Ca^{2+} might have resulted in limited angiogenesis, cell differentiation [36–41] and lack of bone formation. The above data indicate that osteoclastic activity on the macroporous implanted constructs is pivotal for the subsequent differentiation of local stem cells into osteoblastic-like cells. The observed changes in *OP-1* gene expression in zoledronate-treated samples directly correlate with the morphological analyses showing lack of bone differentiation. Indirectly, zoledronate-treated samples showing lack of *OP-1* gene expression and absent or limited bone formation by induction confirm that the spontaneous induction of bone formation by coral-derived macroporous constructs is initiated by secreted proteins of the BMPs/OPs supergene family, in context the OP-1 isoform. The lack of osteoclastic activity negates nanoscale topographical modifications [46] and resorptive surface patterning [11,13]. In previous experiments using hydroxyapatite/β-tricalcium phosphate (HA/β-TCP) constructs implanted long term in *Papio ursinus* [11,13], we have shown that the insoluble signal or substratum resorbs *via* downstream molecular and cellular cascades that sculpt resorption pits and lacunae in the geometric form of concavities [11,13]. The present experiments clearly confirm that topographical modifications of the implanted HA/CC macroporous constructs are the biological *continuum* for the induction of bone formation and essential for the differentiation of the osteoblastic phenotype. Zoledronates, used therapeutically to treat systemic bone loss resulting from ageing or metastatic tumour activity [47], are readily internalized by osteoclasts [48], and once within the cell, negate osteoclastic activity by disruption of the cytoskeleton by interference with the formation of actin rings [48]. These are essential for sealing the osteoclasts to the bone/implant surface to initiate resorption of the underlying matrix by acid hydrolysis [58].

In previous experiments, we have postulated [8,11–13] that myoblastic/myoendothelial [49] and/or pericytic/endothelial stem cells [50–54] might differentiate into osteoblastic-like cells [51–54]. Differentiated osteoblasts then express, secrete and embed soluble molecular signals into the biomimetic matrices [7,8,11,13] initiating bone formation as a secondary response. Classic studies have indicated that perivascular pericytic cells are the responding differentiating cells initiating the induction of bone formation upon implantation of demineralized bone matrix and/or partially purified naturally-derived bone morphogenetic protein [55,56]. Native pericytes express several markers of mesenchymal stem cells reinforcing the *status* of pericytes as ancestors to mesenchymal stem cells [57]. As reported by Chen *et al.* [54], current research has outlined strong similarities between vascular pericytes and mesenchymal stem cells, the latter in essence an '*artifactual cell*' [54]. Though the question '*are all the mesenchymal stem cells in descent of pericytes?*' [54] has not been definitely answered as yet, unpublished data indicate the existence of an even more primitive and distinct stem cell lineage than perivascular pericytes [54].

The level of tissue morphogenesis induced by hOP-1 and hTGF-β_3 applied singly was raised several fold by the binary application of

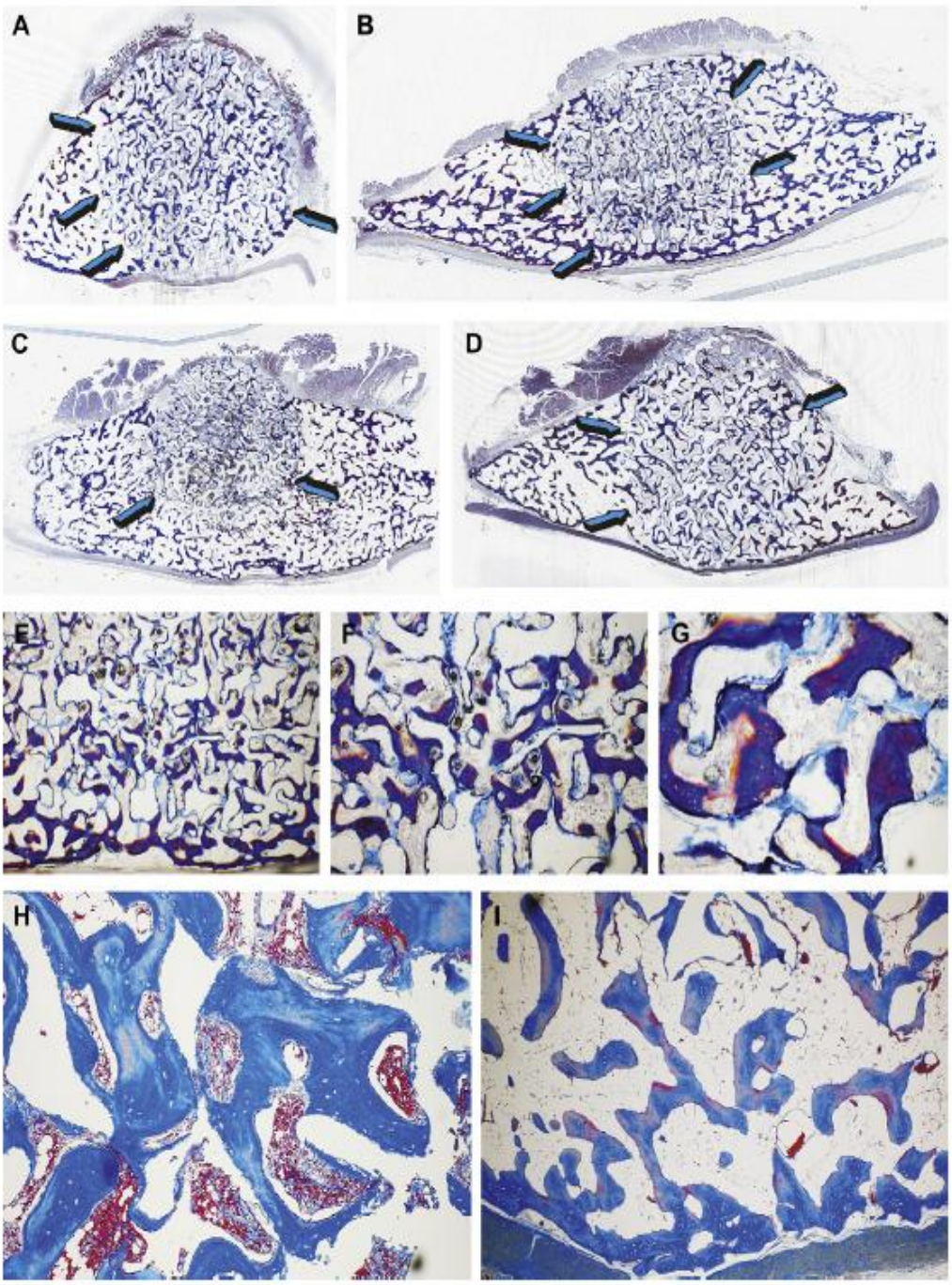


Fig. 6. Synergistic induction of bone formation by binary application of 125 μg hOP-1 and 25 μg hTGF-β_3 pre-loaded onto the macroporous constructs of coral-derived 7% HA-CC specimens harvested from the *rectus abdominis* muscle 90 days after heterotopic implantation. (A,B,C,D) Massive induction of bone formation well beyond the profile of the implanted macroporous constructs (blue arrows) extending through the *rectus abdominis* displacing both the muscle and the peritoneal fascia. (E,F,G) Details of previous undecalcified low power sections highlighting mineralized bone in *blue* surfaced by *red/orange* osteoid seams invading the macroporous spaces of the coral-derived specimens. (H,I) Details of decalcified sections showing newly formed bone in light blue within the macroporous spaces (H) and away from the scaffold profile (I) within the *rectus abdominis* muscle with generated foci of hematopoietic bone marrow (I) just above the peritoneal fascia. (A,B,C,D) Undecalcified sections prepared by the EXAKT cutting – grinding system [37] ground and polished to 10 μm stained with Goldner's trichrome for undecalcified microscopy. (A,B,C,D) original magnification x2.7; (E,F,G) original magnification x17 (E); x 21 (F); x75 (G). (H,I) Decalcified sections cut at 4 μm stained with Goldner's trichrome. (H) original magnification x77; (I) x27.

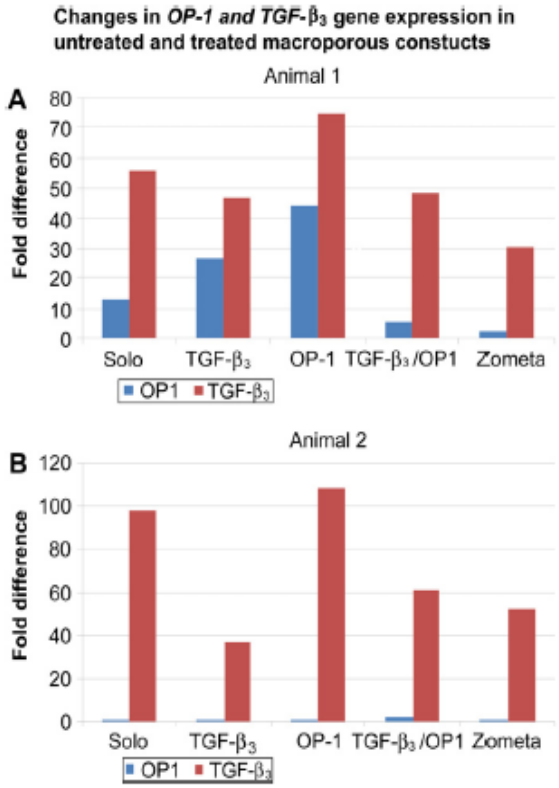


Fig. 7. Changes in *OP-1* and *TGF-β_3* mRNA synthesis in macroporous constructs implanted 'solo', pre-loaded with 125 μg hOP-1, 125 μg hTGF-β_3, binary applications of 125 μg hOP-1/25 μg hTGF-β_3 and 0.24 mg of the bisphosphonate zoledronate implanted in the *rectus abdominis* muscle of two *Papio ursinus* and harvested on day 90.

comparatively low doses of the recombinant hTGF-β_3 isoform, which by itself induces bone formation in the *rectus abdominis* at doses of 5 μg per 100 mg of collagenous matrix as carrier [17]. Binary applications of both recombinant morphogens in the ratio of 5:1 resulted in the induction of large corticalized ossicles as evaluated by radiographic and morphological analyses. The induction of bone formed well outside the profile of the implanted macroporous constructs with the generation of large heterotopic ossicles displacing the ventral and dorsal fasciae of the *rectus abdominis* muscle.

We have shown that the mammalian TGF-β isoforms are determinant of the induction of endochondral bone formation in non-human primates *Papio* sp. [15–19]. Studies in rodents and lagomorphs have confirmed that heterotopic implantation of the three mammalian TGF-β isoforms results in the induction of granulation tissue and of a fibrogenic response only, without cartilage or bone formation [58–60]. The apparent redundancy of molecular signals initiating the induction of bone formation remains largely uncharacterized; also the exact mechanisms by which TGF-β signaling results in the induction of endochondral bone formation in the non-human primate *Papio ursinus* [15–19]. In a number of systematic studies in the different microenvironments of heterotopic intramuscular and orthotopic craniofacial sites including the *rectus abdominis* muscle, the calvarium, the mandible and mandibular periodontal furcation defects, respectively, we have shown that primate tissues and microenvironments respond remarkably differently when compared to rodents, lagomorphs and canine tissues at identical doses of the various osteogenic proteins of the TGF-β superfamily [7,15–19,61–63]. Although structurally similar, BMPs/OPs and TGF-β receptors bind in dramatically different modes, mediating graded and switch-like assembly mechanisms that may have co-evolved with branch-specific groups of cytoplasmic effectors [64].

Members of the TGF-β supergene family of proteins are conserved in structure but diverse in recognition [65]. The crystal structure of BMP-7 in complex with the type II activin receptor shows a different receptor binding site on the ligand compared to that observed in the TGF-β_3 and receptor complex [65]. The limited number of serine threonine kinase receptors and Smads may elucidate the vast pleiotropic activity of the TGF-β superfamily of proteins [6,66]. BMPs/OPs-like molecules exist in the fruit fly *Drosophila melanogaster* as Decapentaplegic (DPP) and 60A but there is lack of bone differentiation in invertebrates [66]. Recombinant human DPP and 60A induce heterotopic endochondral bone formation in mammals [67]. Remarkably thus, a phylogenetically ancient signaling carboxy-terminal domain deployed for dorsal-ventral patterning in the fruit fly *D. melanogaster* is also operational to engineer the induction of bone formation and skeletogenesis, unique traits of the vertebrate mammals responsible for ambulation, body erection, freeing the upper limbs generating the *Homo* clade [13]

Understanding the mechanism which bestows significant differences in biological activities of the mammalian TGF-β isoforms amongst different mammalian species will improve our ability to predict interspecies variations with significant implications in clinical contexts. As Myazono *et al.* have recently asked [66] "*what could be the mechanisms for such diverse biological activities induced by the TGF-β superfamily proteins?*" This vast pleiotropic activity could be the result of the multiple interactions of the phosphorylated Smad gene products with various proteins and transcription factors [45,66]. Activity of Smad proteins is also modified by signaling cross-talk with other signaling pathways which may also lead to the establishment of diverse pleiotropic responses [44,45,64].

The bioactive biomimetic matrix may orchestrate guidance information to responding stem cells instructing collective cell migration within the concavities of either myoblastic/myoendothelial or pericytic/endothelial stem cells from the adjacent highly vascular striated muscular tissue. The concavities *per se* [8,13] may generate physical forces upon invading progenitor stem cells by the *vacuum* of the topographical structure setting into motion the ripple-like cascade of migration, contact guidance and differentiation [68,69]. Cell/matrix interactions during progenitor stem cells migration perforce induce remodeling of the extracellular matrix thereby sculpting local microenvironments [68]; mechanical forces that originate during the orchestration of mesenchymal collagenous condensations with contraction of resident mesenchymal cells induce gradient of mechanical stresses; such forces deployed within the multicellular and vascularized collagenous condensations result in tissue patterning and morphogenesis with tissue geometry and mechanical stress as inductive cues [68,69]. Gradients of mechanical stresses generated within multicellular aggregates invading and colonizing the carved topographies and organized by the substratum concavities can act in a morphogenetic capacity [68–70] to induce spatial patterning, cellular proliferation and the induction of the osteoblastic phenotype. Published mechanical models of tissue morphogenesis have predicted that the geometry of a multicellular structure defines patterns of mechanical stresses [68,69] eventually conducive to cellular differentiation and to the induction of bone formation.

Together with Ca^{2+} release, angiogenesis [36–38] and cellular differentiation [39–41], the establishment of a dynamic reciprocal communication between invading stem cells and the organized collagenous condensations of the extracellular matrix may result in tissue patterning and osteogenesis within the macroporous

calcium phosphate-based biomimetic matrices. The observed lack of bone differentiation by zoledronate-treated macroporous constructs with minimal *OP-1* expression perforce indicates that the spontaneous and intrinsic osteoinductivity of coral-derived macroporous constructs is certainly initiated *via* the OP-1/BMP-7 pathway in the non-human primate *Papio ursinus*.

5. Conclusions

This non-human primate study establishes that that micro- and macro-topographical modifications cut by osteoclasts after heterotopic implantation of macroporous coral-derived constructs are regulators of the spontaneous induction of bone formation as shown by the lack of bone differentiation in zoledronate-treated specimens; hTGF-β_3 synergizes with hOP-1 to induce large mineralized and corticalized ossides providing a realistic therapeutic strategy for human osteoinduction.

Acknowledgements

This research on the '*intrinsic*' induction of bone formation by macroporous calcium phosphate-based biomimetic matrices and on the transforming growth factor-β isoforms has been continuously supported by the South African Medical Research Council, the University of the Witwatersrand, Johannesburg, the South African National Research Foundation and *ad hoc* grants to the Bone Research Unit. We thank Mike Ponticiello of Interpore International USA for the preparation of the coral-derived hydroxyapatite/calcium carbonate constructs, Ruqayya Parak for preparing undecalcified sections on the synergistic induction of bone formation specimens and Piet Becker, Biostatistics Unit, Medical Research Council, for the data analysis. Special thanks to Creative BioMolecules/Stryker Biotech USA and to Novartis AG Basel Switzerland for supplying the recombinant hOP-1 and hTGF-β_3 proteins, respectively, and to the Central Animal Services of the University for the help with primate experimentation.

Appendix

Figures with essential colour discrimination. Certain figures in this article, particularly Figs 1–4 and 6,7 are difficult to interpret in black and white. The full colour images can be found in the online version, at doi:10.1016/j.biomaterials.2010.04.037.

References

[1] Sampath TK, Reddi AH. Dissociative extraction and reconstitution of extracellular matrix components involved in local bone differentiation. Proc Natl Acad Sci USA 1981;78:7599–603.
[2] Khouri RK, Koudsi B, Reddi AH. Tissue transformation into bone in vivo. A potential practical application. J Am Med Assoc 1991;226:1953–5.
[3] Reddi AH. Symbiosis of biotechnology and biomaterials: applications in tissue engineering of bone and cartilage. J Cell Biochem 1994;56:192–5.
[4] Reddi AH. Morphogenesis and tissue engineering of bone and cartilage: inductive signals, stem cells, and biomimetic biomaterials. Tissue Eng 2000; 6:351–9.
[5] Ripamonti U, Duneas N. Tissue engineering of bone by osteoinductive biomaterials. MRS Bull 1996;21:36–9.
[6] Ripamonti U, van den Heever B, Crooks J, Rueger DC, Reddi AH. Long-term evaluation of bone formation by osteogenic protein 1 in the baboon and relative efficacy of bone-derived bone morphogenetic proteins delivered by irradiated xenogeneic collagenous matrices. J Bone Miner Res 2000;15: 1798–809.
[7] Ripamonti U. Soluble osteogenic molecular signals and the induction of bone formation. Biomaterials 2006;27:807–22.
[8] Ripamonti U, Richter PW, Thomas ME. Self-inducing shape memory geometric cues embedded within *smart* hydroxyapatite-based biomimetic matrices. Plast Reconstr Surg 2007;120:1796–807.
[9] Ripamonti U. Inductive bone matrix and porous hydroxylapatite composites in rodents and nonhuman primates. Handbook of bioactive ceramics, vol. II. CRC Press; 1990. 245–53.
[10] Ripamonti U. The morphogenesis of bone in replicas of porous hydroxyapatite obtained from conversion of calcium carbonate exoskeletons of coral. J Bone Joint Surg Am 1991;73:692–703.
[11] Ripamonti U, Richter PW, Nilen RWN, Renton L. The induction of bone formation by smart biphasic hydroxyapatite tricalcium phosphate biomimetic matrices in the non-human primate *Papio ursinus*. J Cell Mol Med 2008;12:1029–48.
[12] Ripamonti U, Crooks J, Khoali L, Roden L. The induction of bone formation by coral-derived calcium carbonate/hydroxyapatite constructs. Biomaterials 2009;30:1428–39.
[13] Ripamonti U. Biomimetism, biomimetic matrices and the induction of bone formation. J Cell Mol Med 2009;12(6B):2609–21.
[14] Ripamonti U, Crooks J, Rueger DC. Induction of bone formation by recombinant human osteogenic protein-1 and sintered porous hydroxyapatite in adult primates. Plast Reconstr Surg 2001;107:977–88.
[15] Ripamonti U, Duneas N, van den Heever B, Bosch C, Crooks J. Recombinant transforming growth factor-β_1 induces endochondral bone in the baboon and synergizes with recombinant osteogenic protein-1 (bone morphogenetic protein-7) to initiate rapid bone formation. J Bone Miner Res 1997;2:1584–95.
[16] Ripamonti U, Crooks J, Matsaba T, Tasker J. Induction of endochondral bone formation by recombinant human transforming growth factor-β_2 in the baboon (*Papio ursinus*). Growth Factors 2000;17:269–85.
[17] Ripamonti U, Ramoshebi LN, Teare J, Renton L, Ferretti C. The induction of endochondral bone formation by transforming growth factor-β_3: experimental studies in the non-human primate *Papio ursinus*. J Cell Mol Med 2008;12:1029–48.
[18] Ripamonti U, Roden L. The induction of bone formation by transforming growth factor-β_2 in the non-human primate *Papio ursinus* and its modulation by skelretal muscle responding stem cells. Cell Prolif 2010;43:207–18.
[19] Duneas N, Crooks J, Ripamonti U. Transforming growth factor-β_1: induction of bone morphogenetic protein genes expression during endochondral bone formation in the baboon, and synergistic interaction with osteogenic protein-1 (BMP-7). Growth Factors 1998;15:259–77.
[20] Helman Y, Natale F, Sherrell RM, LaVigne M, Starovoytov V, Gorbunov MY, et al. Extracellular matrix production and calcium carbonate precipitation by coral cells in vitro. Proc Natl Acad Sci USA 2008;105:54–5.
[21] Shors EC. Coralline bone graft substitutes. Orthop Clin North Am 1999; 30:599–613.
[22] Ripamonti U, van den Heever B, van Wyk J. Expression of the osteogenic phenotype in porous hydroxyapatite implanted extra skeletally in baboons. Matrix 1993;13:491–502.
[23] Sampath TK, Maliakal JC, Hauschka PV, Jones WK, Sasak H, Tucker RF, et al. Recombinant human osteogenic protein-1 (hOP-1) induces new bone formation in vivo with a specific activity comparable with natural bovine osteogenic protein and stimulates osteoblast proliferation and differentiation in vitro. J Biol Chem 1992;267:20352–62.
[24] ten Dijke P, Hansen P, Iwata KK, Pieler C, Foulkes JG. Identification of another member of the transforming growth facor type β gene family. Proc Natl Acad Sci U S A 1988;85:4715–9.
[25] ten Dijke P, Iwata KK, Goddard C, Pieler C, Canalis E, McCarthy TL, et al. Recombinant transforming growth factor type β_3: biological activities and receptor binding properties in isolated bone cells. Mol Cell Biol 1990;10:4473–9.
[26] ten Dijke P, Iwata KK, Thorikay M, Schwedes J, Stewart A, Pieler C. Molecular characterization of transforming growth factor type β_3. Ann N Y Acad Sci 1990;593:26–42.
[27] Schnitzler CM, Ripamonti U, Mesquita JM. Histomorphometry of iliac crest trabecular bone in adult male baboons in captivity. Calcif Tissue Int 1983;52:447–54.
[28] Public Service Department. National code for animal use in research, education, diagnosis and testing of drugs and related substances in South Africa. Pretoria, South Africa: Public Service Department; 1990.
[29] Parfitt AM. Stereologic basis of bone histomorphometry; theory of quantitative microscopy and reconstruction of the third dimension. In: Recker RR, editor. Bone histomorphometry: techniques and interpretation. Boca Raton FL USA: CRC Press; 1983. p. 53–87.
[30] Donath K, Breuner G. A method for the study of undecalcified bones and teeth with attached soft tissue – the "Säge Schliff" (sawing and grinding) technique. J Oral Pathol 1982;11:318–26.
[31] Bar-Shavit Z. The osteoclasts: a multinucleated, hematopoietic-origin, bone resorbing osteoimmune cell. J Cell Biochem 2007;102:1130–9.
[32] Olszak IT, Poznansky MC, Evans RH, Olson D, Kos C, Pollak MR, et al. Extracellular calcium elicits a chemokinetic response from monocytes in vitro and in vivo. J Clin Invest 2000;105:1299–305.
[33] Sabokbar A, Pandey R, Diaz J, Quinn JMW, Murray DW. Hydroxyapatite particles are capable of inducing osteoclasts formation. J Mater Sci Mater Med 2001;12:659–64.
[34] Detsch R, Mayr H, Ziegler G. Formation of osteoclast-like cells on HA and TCP ceramics. Acta Biomater 2008;4:139–48.
[35] Neigishi-Koga T, Takayanagi H. Ca^{2+}–NFATc1 signaling is an essential axis of osteoclasts differentiation. Immunol Rev 2009;231:241–56.
[36] Kohn E, Alessandro R, Spoonster J, Wersto RP, Liotta LA. Angiogenesis: role of calcium-mediated signal transduction. Proc Natl Acad Sci USA 1995; 92:1307–11.

[37] Munaron L. Intracellular calcium, endothelial cells and angiogenesis. Recent Pat Anticancer Drug Discov 2006;1:105–19.
[38] Wu Q, Shao H, Eton D, Li J, Li J, Yang B, et al. Extracellular calcium increases CXCR4 expression on bone marrow-derived cells and enhances pro-angiogenesis therapy. J Cell Mol Med 2009;13:1–10.
[39] Zayzafoon M. Calcium/calmodulin signaling controls osteoblast growth and differentiation. J Cell Biochem 2006;97:56–70.
[40] Ohgushi H, Dohi Y, Tamai S, Tabata S. Osteogenic differentiation of marrow stromal stem cells in porous hydroxyapatite ceramics. J Biomed Mater Res 1993;27:1401–7.
[41] Kanatani M, Sugimoto T, Fukase M, Fujita T. Effect of elevated extracellular calcium on the proliferation of osteoblastic MC3T3-E1 cells: it direct and indirect effects via monocytes. Biochem Biophys Res Commun 1991;181:1425–30.
[42] Karsdal MA, Neutzsky-Wulff, Dziegiel MH, Christiansen C, Henriksen K. Osteoclasts secrete non-bone derived signals that induce bone formation. Biochem Biophys Res Commun 2008;366:483–8.
[43] Carimella R, Tague SE, Zhang J, Belibi F, Nahar N, Sun BH, et al. Expression and synthesis of bone morphognetic proteins by osteoclasts: a possible path to anabolic bone remodeling. J Histochem Cytochem 2008;56:569–77.
[44] Piek E, Helsin C-H, ten Dijke P. Specificity, diversity, and regulation in TGF-β superfamily signaling. FASEB J 1999;13:2105–24.
[45] Feng X-H, Derynck R. Specificity and versatility in TGF-β signaling through Smads. Annu Rev Cell Dev Biol 2005;21:659–93.
[46] Dalby MJ, Gadegaard N, Tare R, Andar A, Riehle MO, Herzyk P, et al. The control of human mesenchymal cell differentiation using nanoscale symmetry and disorder. Nat Mater 2007;6:997–1003.
[47] Weinstein RS, Roberson PK, Manolagas SC. Giant osteoclast formation and long-term oral bisphosphonate therapy. N Engl J Med 2009;360:53–62.
[48] Saltel F, Destaing O, Bard F, Eichert D, Jurdic P. Apatite-mediated actin dynamics in resorbing osteoclasts. Mol Biol Cell 2004;12:5231–41.
[49] Zheng B, Cao B, Crisan M, Sun B, Li G, Logar A, et al. Prospective identification of myogenic endothelial cells in human skeletal muscle. Nat Biotechnol 2007;25:102534.
[50] Trueta J. The role of the vessels in osteogenesis. J Bone Joint Surg 1963;45B:402–18.
[51] Doherty MJ, Ashton BA, Walsh S, Beresford JN, Grant ME, Canfield AE. Vascular pericytes express osteogenic potential in vitro and in vivo. J Bone Miner Res 1998;13:828–38.
[52] Benjamin LE, Hemo I, Keshet E. A plasticity window for blood vessel remodeling is defined by pericyte coverage of the preformed endothelial network and is regulated by PDGF-B and VEGF. Development 1998;125:1591–8.
[53] Kovacic JC, Boehm M. Resident vascular progenitor cells: an emerging role for non-terminally differentiated vessel-resident cells in vascular biology. Stem Cell Res 2009;2:2–15.
[54] Chen C-W, Montelatici E, Crisan M, Coselli M, Huard J, Lazzari L, et al. Perivascular multi-lineage progenitor cells in human organs: regenerative units, cytokine sources or both? Cytokine Growth Factor Rev 2009;20:429–34.
[55] Urist MR. Bone: formation by autoinduction. Science 1965;50:255–66.
[56] Urist MR, Huo YK, Brownell AG, Hohl WM, Buyske J, Lietze A, et al. Purification of bone morphogenetic protein by hydroxyapatite chromatography. Proc Natl Acad Sci USA 1984;81:371–5.
[57] Crisan M, Chen CW, Corselli M, Andriolo G, Lazzari L, Péault B. Perivascular multipotent progenitor cells in human organs. Proc Natl Acad Sci USA 2009;1176:118–23.
[58] Roberts AB, Sporn MB, Assoian RK, Smith JM, Roche NS, Wakefield LM, et al. Transforming growth factor type β: rapid induction of fibrosis and angiogenesis in vivo and stimulation of collagen formation in vitro. Proc Natl Acad Sci U S A 1986;83:4167–71.
[59] Sampath TK, Muthukumaran N, Reddi AH. Isolation of osteogenin, an extracellular matrix-associated bone-inductive protein, by heparin affinity chromatography. Proc Natl Acad Sci USA 1987;90:6004–8.
[60] Shinozaki M, Kawara S, Hayashi N, Kakinuma T, Igarashi A, Takehara K. Induction of subcutaneous tissue fibrosis in newborn mice by transforming growth factor β – simultaneous application with basic fibroblast growth factor causes persistent fibrosis. Biochem Biophys Res Commun 1997;237:292–6.
[61] Ripamonti U. The Marshall Urist lecture. Bone: formation by autoinduction. In: Vukicevic S, Reddi AH, editors. Proceedings of the 6th international conference on bone morphogenetic proteins. Dubrovnik: Depol Org; 2006. p. 1.
[62] Ripamonti U, Parak R, Petit J- C. Induction of cementogenesis and periodontal ligament regeneration by recombinant human transforming growth factor-β_3 in Matrigel with *rectus abdominis* responding cells. J Periodont Res 2009;44:1–87.
[63] Ripamonti U, Ferretti C, Teare J, Blann L. Transforming growth factor-β isoforms and the induction of bone formation: implications for reconstructive craniofacial surgery. J Craniofac Surg 2009;20:1544–55.
[64] Groppe J, Hinck CS, Samavarchi-Tehrani, Zubieta C, Schuermann P, Taylor AB, et al. Cooperative assembly of TGF-β superfamily signaling complexes is mediated by two disparate mechanisms and distinct modes of receptor binding. Cell 2008;29:157–68.
[65] Sun PD. Conserved in structure but diverse in recognition. Structure 2003;11:362–3.
[66] Miyazono K, Kusanagi K, Inoue H. Divergence and convergence of TGF-β/BMP signaling. J Cell Physiol 2001;187:265–76.
[67] Sampath TK, Rashka KE, Doctor JS, Tucker RF, Hoffmann FM. Drosophila TGF-β superfamily proteins induce endochondral bone formation in mammals. Proc Natl Acad Sci U S A 1993;90:6004–8.
[68] Gjorevski N, Nelson CM. Bidirectional extracellular matrix signaling during tissue morphogenesis. Cytokine Growth Factor Rev 2009;20:459–65.
[69] Nelson CM, Jean RP, Tan JL, Liu WF, Sniadecki NJ, Spector AA. Emergent patterns of growth controlled by multicellular form and mechanics. Proc Natl Acad Sci U S A 2005;102:11594–9.
[70] Ingber DE. Mechanical control of tissue morphogenesis during embryological development. Int J Dev Biol 2006;50:255–66.

CHAPTER 4

CALCIUM IONS AND OSTEOCLASTOGENESIS INITIATE THE INDUCTION OF BONE FORMATION BY CORAL_DERIVED MACROPOROPUS CONSTRUCTS

Published: J Cell Mol Med 2013; 17: 1444-1457

J. Cell. Mol. Med. Vol 17, No 11, 2013 pp. 1444-1457

Calcium ions and osteoclastogenesis initiate the induction of bone formation by coral-derived macroporous constructs

Roland M Klar [a], Raquel Duarte [b], Therese Dix-Peek [b], Caroline Dickens [b], Carlo Ferretti [a], Ugo Ripamonti [a, *]

[a] Bone Research Laboratory, School of Physiology, Faculty of Health Sciences, University of the Witwatersrand, Johannesburg, South Africa
[b] Department of Internal Medicine, University of the Witwatersrand, Johannesburg, South Africa

Received: March 16, 2013; Accepted: August 12, 2013

Abstract

Coral-derived calcium carbonate/hydroxyapatite macroporous constructs of the genus Goniopora with limited hydrothermal conversion to hydroxyapatite (7% HA/CC) initiate the induction of bone formation. Which are the molecular signals that initiate pattern formation and the induction of bone formation? To evaluate the role of released calcium ions and osteoclastogenesis, 7% HA/CC was pre-loaded with either 500 μg of the calcium channel blocker, verapamil hydrochloride, or 240 μg of the osteoclast inhibitor, biphosphonate zoledronate, and implanted in the *rectus abdominis* muscle of six adult Chacma baboons *Papio ursinus*. Generated tissues on days 15, 60 and 90 were analysed by histomorphometry and qRT-PCR. On day 15, up-regulation of *type IV collagen* characterized all the implanted constructs correlating with vascular invasion. Zoledronate-treated specimens showed an important delay in tissue patterning and morphogenesis with limited bone formation. Osteoclastic inhibition yielded minimal, if any, bone formation by induction. 7% HA/CC pre-loaded with the Ca^{++} channel blocker verapamil hydrochloride strongly inhibited the induction of bone formation. Down-regulation of *bone morphogenetic protein-2 (BMP-2)* together with up-regulation of *Noggin* genes correlated with limited bone formation in 7% HA/CC pre-loaded with either verapamil or zoledronate, indicating that the induction of bone formation by coral-derived macroporous constructs is *via* the BMPs pathway. The spontaneous induction of bone formation is initiated by a local peak of Ca^{++} activating stem cell differentiation and the induction of bone formation.

Keywords: calcium channel blocker verapamil hydrochloride • osteoclast inhibitor biphosphonate zoledronate • Ca^{++} • functionalized nano-patterned topographies • qRT-PCR

Introduction

The future of the continuing evolution of biomaterials [1] is to functionalize the implanted biomaterials surfaces by activating the surface biology to directly induce specific molecular and tissue biology phenomena initiating regenerative responses as inductive biomaterials [2–12]. Self-inductive biomaterials *per se*, without the exogenous application of soluble molecular signals, trigger the ripple-like cascade of pattern formation and tissue induction initiating the generation of form and function, or morphogenesis [3, 5, 6, 10, 12–14].

The basic bone tissue engineering paradigm is tissue induction and morphogenesis by combinatorial molecular protocols whereby soluble molecular signals are re-combined with insoluble signals or substrata acting as tridimensional constructs for the initiation of *de novo* tissue induction and morphogenesis [15–21]. The paradigm has been modified by the language of geometry [4–6, 12, 22]; a number of systematic studies in heterotopic sites of the Chacma baboon *Papio ursinus* have shown that the driving force of the intrinsic osteoinductivity by bioactive biomaterial matrices is the shape and surface characteristics of the implanted scaffold [4, 5]. The language of shape is the language of geometry; the language of geometry is the

*Correspondence to: Ugo RIPAMONTI, M.D., Ph.D.,
Bone Research Laboratory, School of Physiology,
Faculty of Health Sciences,
University of the Witwatersrand,
7 York Road, Parktown,
Johannesburg 2193, South Africa.
Tel.: +27 11 717 2144
Fax: + 27 11 717 2300
E-mail: ugo.ripamonti@wits.ac.za

doi: 10.1111/jcmm.12125

© 2013 The Authors.
Journal of Cellular and Molecular Medicine Published by John Wiley & Sons Ltd and Foundation for Cellular and Molecular Medicine.
This is an open access article under the terms of the Creative Commons Attribution License, which permits use, distribution and reproduction in any medium, provided the original work is properly cited.

J. Cell. Mol. Med. Vol 17, No 11, 2013

language of a sequence of repetitive concavities that biomimetize the remodelling cycle of the primate osteonic bone [5, 6, 22–24]. This has resulted in a hydroxyapatite-coated titanium implant endowed with the intrinsic capacity of inducing bone formation as a result of functionalized tissue-inducing geometric bioreactors constructed along the titanium surfaces [25].

The morphogenesis of bone by calcium phosphate-based macroporous bioceramics when implanted in heterotopic sites was first reported when implanting coral-derived fully converted hydroxyapatite constructs in the *rectus abdominis* muscle of adult non-human primates *P. ursinus* [13, 14]. Systematic studies in *P. ursinus* were then initiated to further understand the induction of bone formation by coral-derived macroporous constructs harvested at different time periods [3, 26–29]. Because of the availability of comprehensive acquired data all obtained in *P. ursinus*, further mechanistic studies were performed in the same animal model.

Which are the molecular signals that set into motion cell differentiation, pattern formation and the induction of bone formation by coral-derived macroporous constructs? To mechanistically further our knowledge on the spontaneous and intrinsic induction of bone formation by coral-derived macroporous constructs, a series of treated and untreated coral-derived biomimetic matrices were implanted in the *rectus abdominis* muscle of the Chacma baboon *P. ursinus*. Generated tissues at different time-points were harvested and evaluated morphologically, histomorphometrically and by qRT-PCR.

Osteoclastic-driven functionalized nano-patterned topographies with calcium ions (Ca^{++}) release re-programmed somatic stem cells to initiate *de novo* bone formation. The induction of *bone morphogenetic protein-2 (BMP-2)* gene expression, the prominent expression of *type IV collagen* pre-dating the induction of bone formation together with down-regulation of *BMP-2* and up-regulation of *Noggin* with corresponding limited bone formation by treated macroporous constructs with the Ca^{++} channels blocker, verapamil hydrochloride and the osteoclast inhibitor, biphosphonate zoledronate, form the basis of this communication.

Materials and methods

Macroporous coral-derived calcium carbonate/hydroxyapatite constructs

Macroporous replicas of coral-derived calcium carbonate exoskeletons of the genus Gonipora were prepared by hydrothermal chemical exchange with phosphate [14, 30]. Limited conversion to hydroxyapatite resulted in calcium carbonate constructs with 7% hydroxyapatite defined as 7% HA/CC (Biomet, Interpore Cross, Irvine, CA, USA). 7% HA/CC constructs were rods 8 mm in diameter and 20 mm in length [29]. The solid components of the hydroxyapatite/calcium carbonate replica average 130 μm in diameter and their interconnections 220 μm; the average porosity is 600 μm and their interconnections average 260 μm in diameter [14, 30].

Pre-loading of coral-derived constructs with the calcium ion channel blocker, verapamil hydrochloride and the osteoclast inhibitor, biphosphonate zoledronate

Topographical osteoclastic modifications of the 7% HA/CC macroporous surfaces have been suggested to be a critical event initiating the spontaneous induction of bone formation [29]. Release of calcium ions by osteoclasts during bone resorption regulates cellular differentiation and induces angiogenesis [31–36]. Macroporous 7% HA/CC constructs were loaded with either 240 μg of the biphosphonate zoledronate (Zometa®, Novartis, Kempton Park, Johannesburg, South Africa), an osteoclast inhibitor analogue, or 500 μg of verapamil hydrochloride (Isoptin®, Knoll Pharmaceutical, Port Elizabeth, South Africa), an L-type voltage gated calcium channel blocker. Untreated 7% HA/CC constructs were used as control. Under laminar flow, pre-loading of the re-suspended inhibitors was by pipetting the required amount of liquid vehicle onto both proximal and distal regions of the 7% HA/CC constructs to ensure an even distribution of the various added components throughout the macroporous spaces.

Primate model for tissue induction and morphogenesis

Six clinically healthy adult *P. ursinus* with a mean weight of 21.2 (±1.48) kg were selected from the primate colony of the University of the Witwatersrand, Johannesburg. Criteria for selection, housing conditions and diets were as described [14]. *Papio ursinus* species share similar bone physiology and osteonic bone remodelling with humans [37]. Research protocols were approved by the Animal Ethics Screening Committee of the University, and conducted according to the *Guidelines for the Care and Use of Experimental Animals* prepared by the University and in compliance with the National Code for Animal Use in Research, Education and Diagnosis in South Africa [38]. Premedication, before induction of general anaesthesia, was by midazolam hydrochloride (Dormicum® 3 mg/kg IM, Roche, Illovo, South Africa). Animals were anaesthetized with ketamine hydrochloride (5–15 mg/kg; Eutaphent Kyron Laboratories, Johannesburg, South Africa) and general anaesthesia maintained by Isofor (1.5–2%; Safe Line Pharmaceutical, Johannesburg, South Africa), after oro-tracheal intubation [28, 29]. A total of nine 7% HA/CC untreated and treated macroporous constructs were implanted bilaterally in intramuscular pouches surgically created by sharp and blunt dissection within the *rectus abdominis* muscle of each animal (Fig. 1), three on day 0, three on day 30 and three on day 75. Implants were aligned longitudinally ~2 cm apart [29]. Post-operative pain and inflammation were controlled by buprenorphine hydrochloride (Temgesic 0.3 mg/kg IM), and carpofan (Rimadyl 3 mg/kg *subcutis*).

Tissue harvest, histology and histomorphometry

On day 90, animals were anaesthetized with an injection of ketamine (5–15 mg/kg) and maintained under general anaesthesia with Isofor (1.5–2%). Specimens were harvested together with muscle tissue (baseline control). Following harvest, animals were killed with an intravenous

© 2013 The Authors.

Journal of Cellular and Molecular Medicine Published by John Wiley & Sons Ltd and Foundation for Cellular and Molecular Medicine.

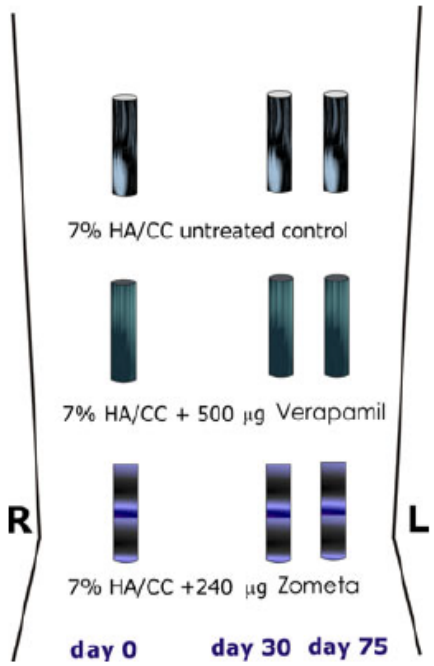


Fig. 1 Heterotopic intramuscular *rectus abdominis* surgical model and implantation design in six adult non-human primates Chacma baboon *Papio ursinus*. In each animal, a total of nine coral-derived calcium carbonate macroporous constructs with limited hydrothermal conversion to hydroxyapatite (7% HA/CC) were implanted heterotopically in triplicate. Three 7% HA/CC constructs representing one treatment modality each were implanted at days 0, 30 and 75, thus providing tissue constructs with invading differentiating tissues to be harvested at days 90, 60 and 15 after heterotopic implantation. Implants were aligned longitudinally ~8 and 2 cm apart.

overdose of sodium pentobarbitone (Anaket, Isando, South Africa). Harvested specimens provided regenerating tissues at 15, 60 and 90 days after intramuscular implantation. A 4 mm fragment of each harvested 7% HA/CC construct with invading differentiating tissues within the macroporous spaces was cut with sterile blades, and flash frozen in liquid Nitrogen. Remaining tissues were fixed in 10% phosphate buffered formalin for 48 hrs, rinsed in tap water and stored in 70% ethanol [29, 30]. Specimens were demineralized in a Sakura TDE™ 30 decalcifying unit (Sakura, Fintek, Torrance, CA, USA) and processed for paraffin wax embedding. Thirty sections were cut sequentially at 4 μm to obtain a full cross-sectional area of each specimen. The 1st and every 10th section was stained with a modified Goldner's Trichrome stain for histological and histomorphometric analyses [28, 29].

Images of the histological sections were captured and digitalized with a Provis AX70 research microscope (Olympus Optical Co., Shinjuku, Tokyo, Japan) attached to a video camera (Olympus). Histomorphometric analysis was then performed with the Stream Essentials software v.1.6 (Olympus). The *ratios* of the total area of the devices and the area of newly formed bone generated within the evaluated macroporous spaces were established, and values were expressed, as a mean percentage of bone generated within the evaluated macroporous spaces. Results were analysed with a Student's *t*-test using STATISTICA version 10 (Statsoft Inc., Tulsa, OK, USA).

qRT-PCR

Under sterile conditions, redundant soft tissue was removed from heterotopic specimens, and the 4 mm fragments of each harvested specimens were then ground to powder in liquid Nitrogen with a mortar and pestle. Total RNA was extracted from 30 mg of pulverized specimen with the Total RNA Mini Kit (Bio-Rad, Hercules, CA, USA). RNA concentration was determined spectrophotometrically at $A_{260/280}$ with a Nanodrop 2000 (Thermo Scientific, Waltham, MA, USA) and RNA quality was assessed with a Pico6000 RNA kit (Agilent Technologies, Santa Clara, CA, USA) on a Bioanalyzer 2100 (Agilent Technologies). RNA integrity numbers were between 8.0 and 9.0. RNA was reverse transcribed with the High Capacity cDNA Reverse Transcription kit (Applied Biosystems, Foster City, CA, USA). qRT-PCR was performed, in duplicate with EvaGreen Master Mix (Bio-Rad) on a CFX-96 thermocycler (Bio-Rad). Each reaction contained 10 ng cDNA; 1× EvaGreen Mix and 10 μM of each primer (Table 1). Primers were designed with Gene fisher v. 2.0 (http://bibiserv.techfak.uni-bielefeld.de/genefisher2). Thermocycling parameters included a denaturation step of 94°C for 2 min.; 40 cycles of 95°C for 10 sec., 60°C for 10 sec. and 72°C for 30 sec.; and a final extension at 72°C for 5 min. Genes assayed included *BMP-2; Type IV Collagen* and *Noggin*. Gene expression was normalized against four reference genes: *β-Actin; Succinate dehydrogenase complex subunit A (SDHA); Ribosomal Protein L13A (RPL13a) and Ribosomal Protein Large P0 (RPLP0)*. Use of GeNorm (http://medgen.ugent.be/~jvdesomp/genorm/) established that these were the most appropriate internal reference genes to use. Amplified PCR products underwent sequencing (Inqaba Biotech, Pretoria, South Africa) to confirm that the correct sequence had been amplified.

Gene expression from the harvested macroporous devices was normalized to muscle tissue in each animal. Calibrated normalized relative quantities (CNRQs), which reflect the $\log_{10}^{-\Delta\Delta Ct}$, were determined with qBase analysis software (http://www.biogazelle.com). A Student's *t*-test (STATISTICA version 10, Statsoft Inc.) was used to determine statistical significance at $p < 0.05$.

Table 1 Primer sequence

Gene	Primer Sequence (5′–3′)
BMP-2	F: AGTTGCGGCTGCTCAGCATGTT R: ACATGTCTCTTGGAGACACCT
Collagen type IV	F: GTTGGTCTACCGGGACTCAA R: GTTCACCTCTGATCCCCTGA
Noggin	F: GAGGAAGTTACAGATGTGGCT R: CACTCGGAAATGATGGGGTAC
SDHA (reference)	F: TGGGAACAAGAGGGCATCTG R: CCACCACTGCATCAAATTCATG
RPL13a (reference)	F: CCTGGAGGAGAAGAGGAAAGAGA R: TGAGGACCTCTGTGTATTTGTCAA
β-actin (reference)	F: CTCTTCCAGCCTTCCTTCCT R: AGCACTGTGTTGGCGTACAG
RPLP0 (reference)	F: AGCTGATCAAGACTGGAGACA R: TCCAGGAAGCGAGAATGCAGAGTT

© 2013 The Authors.
Journal of Cellular and Molecular Medicine Published by John Wiley & Sons Ltd and Foundation for Cellular and Molecular Medicine.

J. Cell. Mol. Med. Vol 17, No 11, 2013

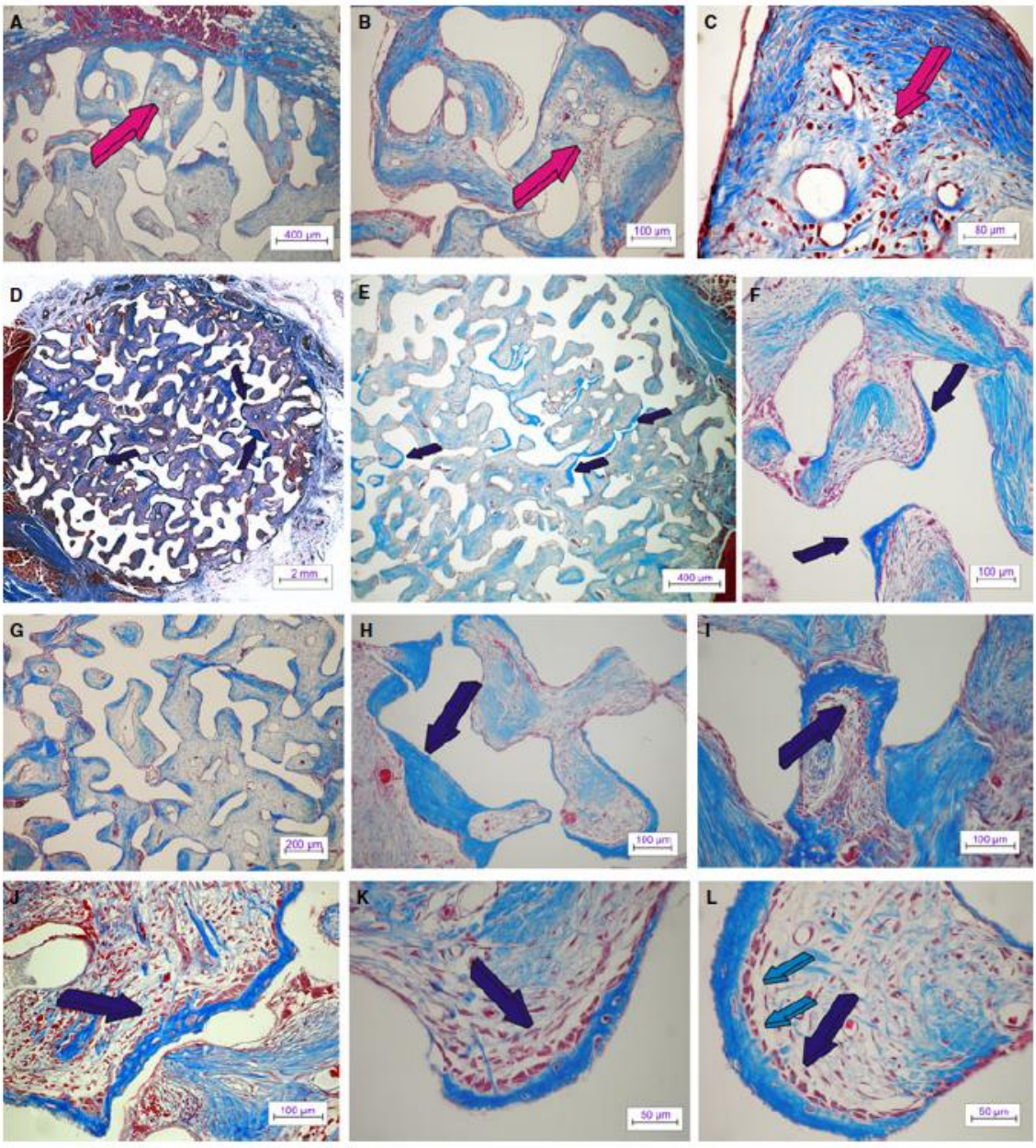


Fig. 2 Untreated control 7% HA/CC coral-derived macroporous constructs on days 15 and 60 after heterotopic intramuscular implantation. Macroporous self-inducing geometric cues of untreated coral-derived biomimetic constructs induce angiogenesis with capillary sprouting and invasion, cellular trafficking, pattern formation and the morphogenesis of collagenous condensations attached to the macroporous surfaces facing a highly vascular penetrating mesenchymal tissue (magenta arrows in **A**–**C**) as early as 15 days after intramuscular implantation. By day 60 (**D**–**H**), there are further remodelling and tissue patterning with the induction of bone formation (dark blue arrows). Bone preferentially forms by induction within concavities of the 7% HA/CC macroporous constructs (dark blue arrows in **F**, **H**, **K** and **L**). Newly formed bone by induction with embedded osteocytes is tightly connected to the implanted biomatrix (**I**–**L**); the newly induced bone matrix is surfaced by plump contiguous secreting osteoblasts facing a highly angiogenic mesenchymal supporting matrix (dark blue arrows in **K** and **L**). Note how capillary basement membranes touch osteoblastic cells lining newly formed bone within concavities of the substratum (large arrow in **L**). (Decalcified sections cut at 4 µm stained with Goldner's trichrome).

© 2013 The Authors.

Journal of Cellular and Molecular Medicine Published by John Wiley & Sons Ltd and Foundation for Cellular and Molecular Medicine.

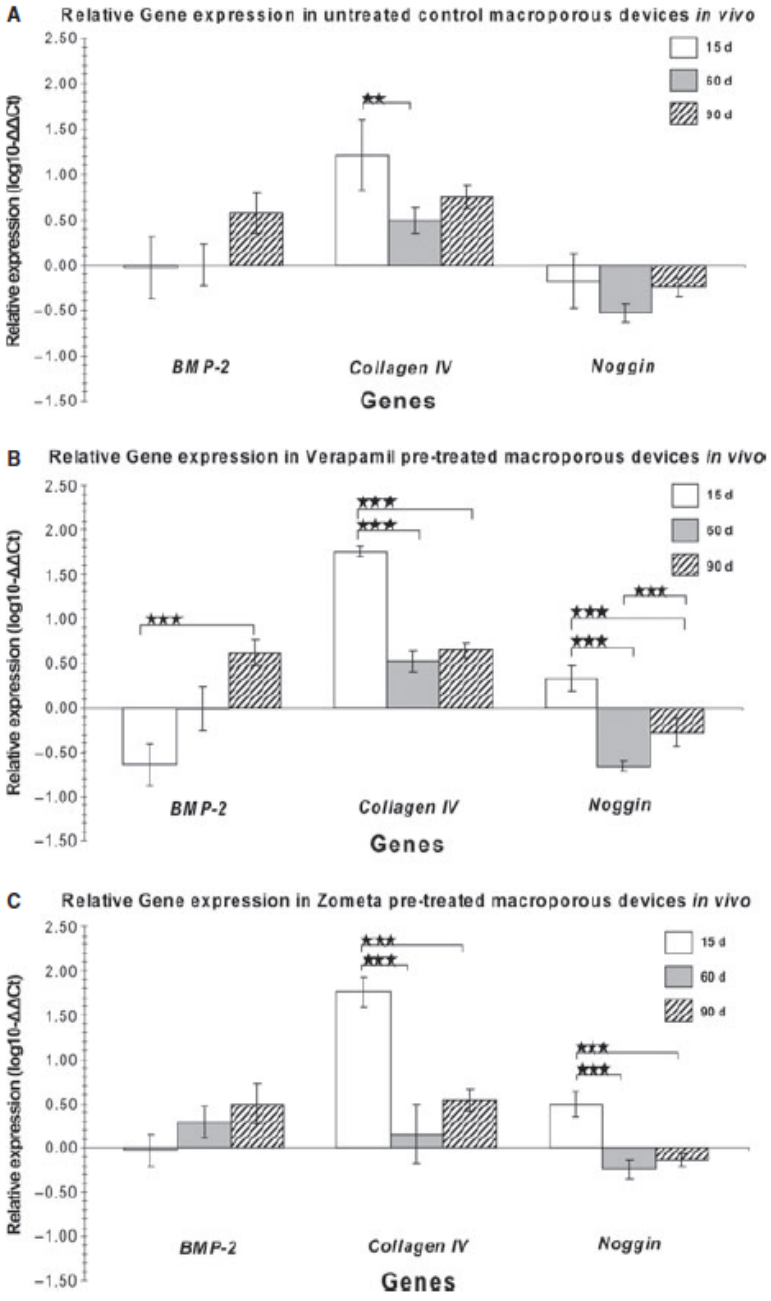


Fig. 3 Relative change in gene expression of BMP-2, collagen type IV and Noggin at days 15 (15d), 60 (60d) and 90 (90d) within untreated 7% HA/CC control (**A**), verapamil (**B**) and zoledronate-pre-treated 7% HA/CC (**C**) implanted within the *rectus abdominis* muscle of six adult Chacma baboons *Papio ursinus* (**$p < 0.05$, ***$p < 0.01$).

Results

Bone formation by autoinduction in 7% HA/CC untreated macroporous constructs

Digital iconographic images of 7% HA/CC untreated control are presented in Figure 2, at 15 and 60 days, and Figure 5, at 90 days. At harvest, all implants were firmly attached to the ventral fascia and the surrounding *rectus abdominis* muscle. On day 15, the most peripheral macroporous spaces were invaded by a highly vascular connective tissue matrix (Fig. 2A–C). Vascular invasion and capillary sprouting was pronounced in all treatment modalities. Previous experiments in the non-human primate *P. ursinus* have shown that the specific geometry and surface characteristics of the coral-derived substratum are conducive to rapid vessels ingrowths' and capillary sprouting within the early mesenchyme penetrating the macroporous spaces [3].

© 2013 The Authors.
Journal of Cellular and Molecular Medicine Published by John Wiley & Sons Ltd and Foundation for Cellular and Molecular Medicine.

J. Cell. Mol. Med. Vol 17, No 11, 2013

Angiogenesis correlated with *type IV collagen* up-regulation irrespective of the treatment modalities (Fig. 3). 7% HA/CC untreated controls showed pronounced capillary sprouting and vascular invasion within the peripheral macroporous spaces (Fig. 2A–C). Morphogenesis and tissue patterning of collagenous condensations were well advanced on day 15 (Fig. 2B and C) with remodelling and further development on day 60 (Fig. 2D–F). Areas with prominent angiogenesis showed a pronounced capillary sprouting and invasion with hypercellularity (Fig. 2B and C). Paravascular pericytic cells showed enlarged hyper-chromatic nuclei with several cells migrating between the vascular compartment and the paravascular extracellular matrix (Fig. 2C).

On day 60, untreated macroporous constructs showed bone formation by autoinduction throughout several macroporous spaces (Fig. 2D–F) correlating with the morphometric analyses (Fig. 4). Histological analyses at high magnification showed that bone was tightly opposed to the macroporous spaces surfaced by contiguous plumped and secreting osteoblasts facing a highly vascularized matrix (Fig. 2H–L). Of note, several areas of newly auto induced bone had formed preferentially in concavities of the substratum (Fig. 2K and L) following a repetitive sequence of events as highlighted by the '*geometric induction of bone formation*' [9, 10, 23]. Importantly, osteoblastic cells were directly opposed to the basement membranes of the capillaries that had formed within the macroporous spaces as shown in Figure 2L (light blue arrows).

By day 90, auto induced bone by untreated macroporous constructs increased significantly (Fig. 4), and remodelled in blocks of osteonic lamellar bone throughout the macroporous spaces (Fig. 5A–F) with osteocytes embedded within the newly formed matrix (Fig. 5G and H). Capillary sprouting was associated with osteoclastic activity remodelling the newly formed bone (Fig. 5H).

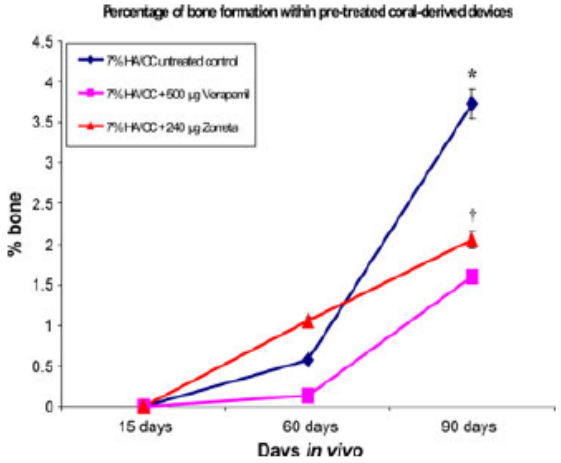


Fig. 4 Morphometric analyses of induced bone by 7% HA/CC untreated control *versus* verapamil hydrochloride and zoledronate-treated specimens. Note the pronounced and significant inhibitory effects on the induction of bone formation by both verapamil hydrochloride- and zoledronate-treated specimens *versus* untreated control on day 90 (*$p < 0.05$). Zoledronate-treated specimens showed the least bone formation by induction on day 90 also when compared with verapamil hydrochloride-treated specimens (†$p < 0.05$).

Biphosphonate zoledronate-treated macroporous constructs

Digital iconographic images of 7% HA/CC biphosphonate zoledronate-treated macroporous constructs are presented in Figure 6, at 15, 60 and 90 days. On day 15, the most peripheral macroporous spaces were invaded by a rather loose and less organized fibro-vascular tissue when compared with untreated control specimens (Fig. 6A) without tissue patterning as in control specimens, which already showed the morphogenesis of mesenchymal collagenous condensations on day 15 (Fig. 2A–C). Collagenous fibres were as yet to be patterned and assembled interacting with a poorly organized fibrovascular tissue with capillary sprouting (Fig. 6B and C).

Collagenous condensations against the macroporous surfaces were seen to be still organizing on day 60 facing a rather loose yet vascular connective tissue matrix (Fig. 6D–F). In general, tissue patterning and morphogenesis were greatly delayed when compared with untreated control specimens. On day 90, collagenous condensations were more organized, but not patterned as in 7% HA-CC untreated control, still facing a rather loose connective tissue matrix (Fig. 6J–M). On day 90 at the periphery of the specimens, there was occasionally the induction of bone formation (Fig. 6N and O).

Calcium ion channel blocker verapamil pre-treated macroporous constructs

Digital iconographic images of 7% HA/CC Ca^{++} channel blocker verapamil pre-treated constructs are presented in Figure 7, at 15, 60 and 90 days. On day 15, there was fibrovascular tissue invasion within the most peripheral macroporous spaces with morphogenesis of cellular condensations along the macroporous surfaces of the implanted 7% HA/CC constructs (Fig. 7A–C). Vascular invasion and capillary sprouting were well pronounced (Fig. 7B and C) correlating with the up- regulation of the *type IV collagen* gene (Fig. 3B).

On day 60, there were morphogenesis and remodelling of collagenous condensations against the macroporous spaces (Fig. 7D–F). Minimal bone formation, when found, was only present at the very periphery of the implanted matrix, bordering with the fibro-muscular tissue surrounding the harvested specimens (Fig. 7E and G). Tissue patterning and morphogenesis of mesenchymal collagenous condensations were delayed when compared with untreated control. A thorough morphological analysis of treated and untreated macroporous samples indicated that the greater delays in tissue patterning and morphogenesis of collagenous condensations were seen in macroporous constructs pre-treated with 240 µg of the biphosphonate zoledronate (Fig. 6).

On day 90, the macroporous spaces of Ca^{++} channel blocker verapamil pre-treated constructs were invaded by fibrovascular tissue

© 2013 The Authors.

Journal of Cellular and Molecular Medicine Published by John Wiley & Sons Ltd and Foundation for Cellular and Molecular Medicine.

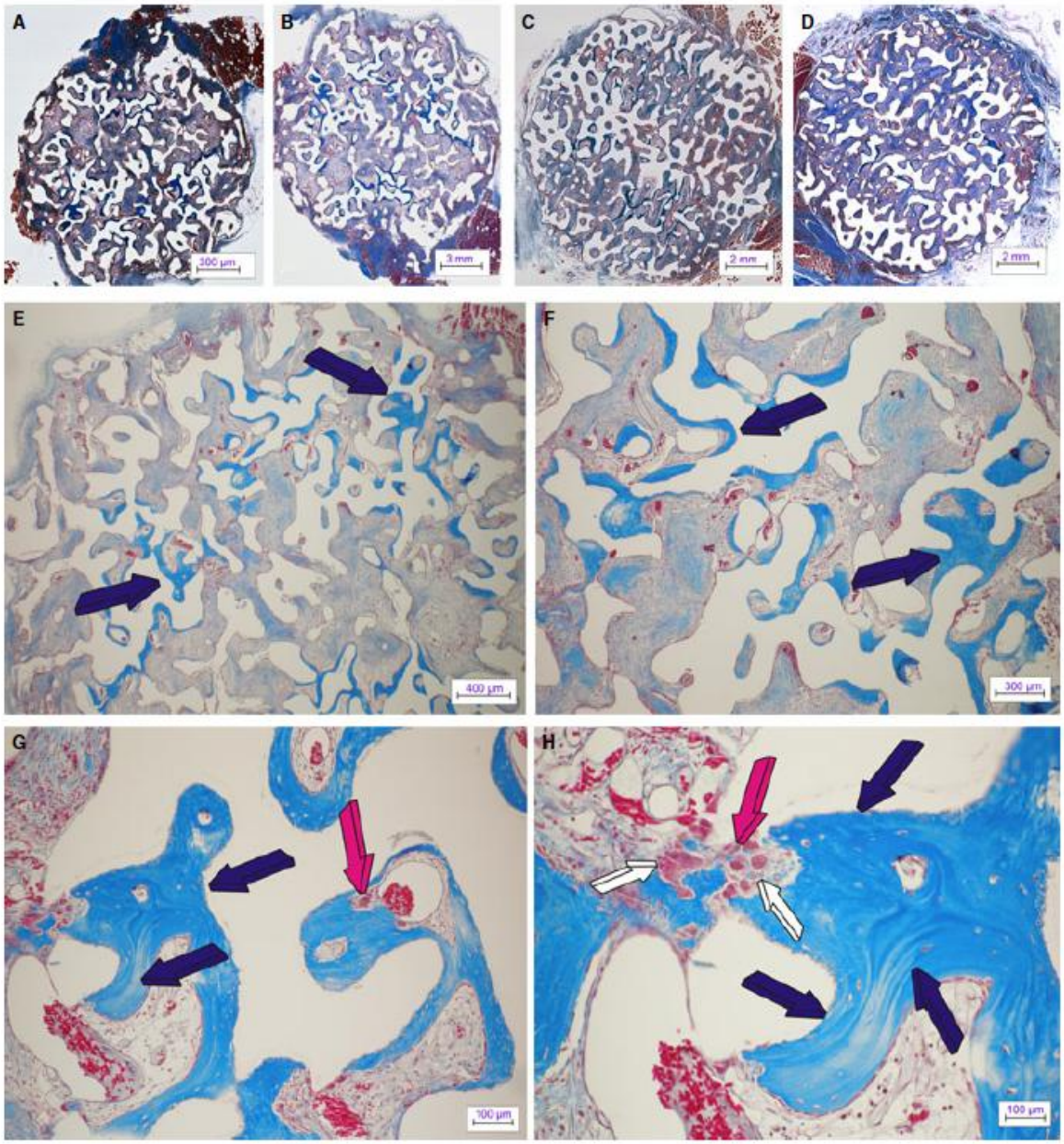


Fig. 5 Untreated control 7% HA/CC macroporous constructs on day 90. 'Spontaneous' and 'intrinsic' bone differentiation and remodelling in untreated control 7% HA/CC biomimetic constructs harvested on day 90 after intramuscular heterotopic implantation. (**A**–**D**) Low power views showing tissue patterning, remodelling of collagenous condensations and bone formation by induction within selected macroporous spaces. (**E** and **F**) High power views of previous sections (**A** and **B**) showing the induction of bone formation (dark blue arrows) supported by a pronounced vascular invasion across the macroporous spaces. (**G** and **H**) There is prominent remodelling with osteoclastogenesis (magenta arrows) of the newly formed corticalized lamellar bone (dark blue arrows). Note the intimacy of vascular invasion with newly differentiated large multinucleated osteoclastic cells within the remodelled bone matrix (white arrows). Decalcified sections cut at 4 µm stained with Goldner's trichrome.

with scattered condensations throughout the implanted matrix (Fig. 7H and I). Tissue patterning and morphogenesis of collagenous condensations were greatly delayed when compared with untreated control specimens (Figs 2 and 5).

qRT-PCR

The intensity of the expression together with the relative changes in gene expression of *BMP-2*, *type IV collagen*, and *Noggin* are pre-

© 2013 The Authors.
Journal of Cellular and Molecular Medicine Published by John Wiley & Sons Ltd and Foundation for Cellular and Molecular Medicine.

J. Cell. Mol. Med. Vol 17, No 11, 2013

sented in Figure 3. *Type IV collagen* was up-regulated on day 15 ($p < 0.05$) in all the homogenized treated and untreated constructs; of interest, this up-regulation was independent of the treatment modalities. *Type IV collagen* up-regulation was directly correlated with the morphological pattern of vascular tissue invasion and capillary sprouting within the macroporous spaces that characterized morphologically all treatment modalities when evaluated on day 15. Of interest, *type IV collagen* expression, although reduced, was also present on day 90, correlating with the continuous induction of bone formation sustained by capillary sprouting as seen morphologically within the treated and untreated macroporous constructs (Fig. 3). Of note, limited angiogenesis and capillary sprouting in biphosphonate zoledronate-treated samples showed a significant reduction in *type IV collagen* expression on day 60 (Fig. 3C). *Bone morphogenetic protein-2* was up-regulated on day 90 in untreated control specimens (Fig. 3A). Verapamil hydrochloride-treated samples showed down-regulation of the *BMP-2* gene on day 15, with significant up-regulation on day 90 (Fig. 3B). *Noggin* expression was significantly up-regulated on day 15 in tissue specimens of both verapamil- and zoledronate-treated samples (Fig. 3B and C). To the contrary, untreated control specimens showed down-regulation of *Noggin* at all time periods (Fig. 3A). Importantly, up-regulation of *Noggin* was more pronounced in biphosphonate zoledronate-treated specimens than in verapamil hydrochloride-treated constructs (Fig. 3C).

Discussion

The future of the continuing evolution of biomaterials [1] is to functionalize the implanted biomaterials' surfaces to evoke a pattern of gene expression that invocates selected tissue biology and morphological cascades [3, 6, 10, 25]. Such novel biomaterials when interacting with multipotent pleiotropic stem cells 'niches' induce specific molecular and tissue biology phenomena initiating regenerative responses as inductive biomaterials [2, 3, 6, 25]. Importantly, the induction of tissue formation occurs without the exogenous application of the soluble molecular signals of the transforming growth factor-β (TGF-β) supergene family [3–5].

The micro crystallinity of the implanted biomatrices, lacunae, pits and concavities cut by osteoclastogenesis together with Ca^{++} release are the driving morphogenetic and ionic cues that set into motion the induction of bone formation [28, 29]. Responding stem cells' differentiation and the induction of the osteogenic phenotype are controlled by Ca^{++} release within the protected microenvironment of the secluded macroporous spaces after nano-topographical modifications of the implanted macroporous surfaces primarily by osteoclastic cells [39–42].

By harvesting samples at an earlier time period, *i.e.* 15 days, the present study has shown prominent vascular invasion and capillary sprouting within the most peripheral macroporous spaces of all the implanted macroporous constructs. This prominent and remarkable angiogenesis is molecularly initiated by the up-regulation of *type IV collagen* in treated and untreated samples. Type IV collagen is essential for the morphogenesis of the basement membrane of the sprouting and invading capillaries [17, 43].

Previous results have shown that there is a temporally and spatially related sequence of tissue alkaline phosphatase expression during the developmental processes culminating in bone differentiation [3]; of interest, the induction of bone differentiation has been also related to the developmental sequence of the induction of collagenous condensations, which pre-date the induction of bone formation [3, 13, 14] together with invading capillaries. These, interpreted as the '*osteogenetic vessels*' of Trueta's definition [44], promote the cascade of bone differentiation.

The present iconographic digital data show how the vascular bundle supported by collagenic fibres enters and proceeds within the macroporous spaces from the most peripheral areas of the implanted construct. Classic studies have shown that the extracellular matrix components of type IV collagen and laminin bind morphogenetic proteins involved both in angiogenesis, *i.e.* basic fibroblast growth factor [45, 46], TGF-β_1 [47] and osteogenesis, *i.e.* osteogenin and OP-1 [48, 49]. Bound angiogenic and bone morphogenetic proteins are then presented locally in an immobilized form to responding stem cells and osteoprogenitors-alike to initiate osteogenesis in angiogenesis [43, 50].

The sprouting invading capillaries almost touch the calcium phosphate-based substratum as well as the osteoblasts, and release a continuous flow of paravascular/pericytic stem cells from the vascular compartment to the differentiating osteogenic compartment attached to the coral-derived biomimetic matrix [3, 4, 43, 50]. Based on the fundamental insights of Trueta [44], classic *in vitro* experiments have indicated that bone-forming cells are in contact with the basement membrane of the invading capillaries playing a key role in formation of a network of cytoplasmic processes resembling the osteocytes' canalicular network [51]. Our morphological images show the exquisite relationship between osteoblastic cells polarized on the secreted bone matrix with the invading sprouting capillary whose basement membrane components touch the polarized osteoblastic cells.

Recent papers, expanding on *in vivo* manufacturing of vascularized autogenous skeletal replacement parts [21], investigated axial vascularization to promote and enhance angiogenesis in osteoconductive matrices [52–54]. A direct comparison with the reported vascular invasion within the macroporous spaces of the intramuscularly implanted coral-derived constructs is, however, difficult. Further studies in *P. ursinus* should be planned using coral-derived constructs supported by the arteriovenous loop approach [52–54] to additionally investigate the critical role of axial vascularization in the induction of bone formation by coral-derived macroporous constructs.

On day 15, biphosphonate-treated specimens showed minimal, if any, *BMP-2* expression, but up-regulation of the *Noggin* gene. More importantly, however, besides the limited bone formation as evaluated histomorphometrically, zoledronate-treated specimens showed a profoundly delayed tissue patterning with poorly constructed collagenous condensations, so critically important for the induction of bone formation [3, 13, 14]. Delayed tissue patterning and poorly constructed mesenchymal tissue condensations, and later cell differentiation and osteogenesis, are as a result of the lack of osteoclastic-driven nano-patterned geometric configurations, which result in Ca^{++} release with the expression of the osteogenic phenotype [7–11, 29, 55–57]. Importantly, lack of osteoclastic activity does result in limited, if any,

© 2013 The Authors.

Journal of Cellular and Molecular Medicine Published by John Wiley & Sons Ltd and Foundation for Cellular and Molecular Medicine.

Ca^{++} release; a reduction in Ca^{++} release results in lack of angiogenesis and stem-cell differentiation [31–36, 58], thus effectively controlling *ab initio* the induction of bone formation.

The importance of tissue patterning and the induction of mesenchymal tissue condensations are critically shown by the lack of osteoclastic activity in zoledronate-treated specimens. In previous experiments using coral-derived macroporous constructs, morphological and immunocytochemistry analyses have suggested the critical morphogenetic role of the morphogenesis of mesenchymal tissue condensations against the implanted substratum, further indicating that condensations pre-date the induction of bone formation [3, 13, 14].

Cellular and extracellular matrix condensations are pivotal in the development of skeletal tissues [59]. Zoledronate-treated specimens showed a profound delay in tissue patterning and morphogenesis; molecularly, this tissue patterning disarray is pre-dated by *Noggin* up-regulation together with minimal, if any, *BMP-2* expression on day 15. The data indicate the critical role of BMPs in setting tissue patterning and morphogenesis before the induction of bone formation.

Zoledronate-treated specimens showed *Noggin* up-regulation on day 15 as compared with untreated control samples. Noggin prevents BMP binding to the BMP receptor [60] and as such inhibits bone formation. The loss of osteoclast binding resulted in a temporary up-regulation of *Noggin* on day 15; this up-regulation generated minimal bone formation by induction on days 60 and 90. Our results further suggest that the biphosphonate zoledronate' effect is temporary, possibly degraded by days 60 and 90, with down-regulation of *Noggin,* resulting in delayed and minimal bone induction yet again at the periphery of the implanted macroporous constructs only.

When the L-type voltage-gated ion channel for Ca^{++} was blocked by pre-loading the macroporous constructs with verapamil hydrochloride, morphological and histomorphometric analyses showed limited bone formation. Tissue patterning was not as disorganized and delayed as in zoledronate-treated specimens. Verapamil-treated samples showed down-regulation of *BMP-2* together with up-regulation of *Noggin* on day 15, suggesting that Ca^{++} regulates gene expression [61] and thus controlling the induction of bone formation. Limited induction of bone formation on days 60 and 90, although preferentially at the periphery of the implanted macroporous constructs, may indicate degradation of the implanted verapamil-hydrochloride. Lack of active verapamil with delayed bone induction on day 90 is accompanied by recovery of *BMP-2* expression and notably by *Noggin* down-regulation on days 60 and 90.

The acidic microenvironment of the implanted intramuscular pouch may also result in dissolution of hydroxyl apatite and carbonate bound calcium resulting in higher extracellular calcium concentrations within the protected macroporous spaces of the coral-derived constructs. Of note, implanted macroporous calcium carbonate constructs were partially converted to 7% hydroxyapatite, which could possibly release Ca^{++} at minor intramuscular pH changes during healing [28–30]. The biological effects of several ions have been well documented, including the induction of angiogenesis by triggering the secretion of angiogenic morphogens [62]. Underlying cellular migration and differentiation are exceedingly complex intracellular events focused on cytosolic flooding by calcium ions either from the endoplasmic reticulum or the extracellular domain *via* calcium channels in the cell membrane [63].

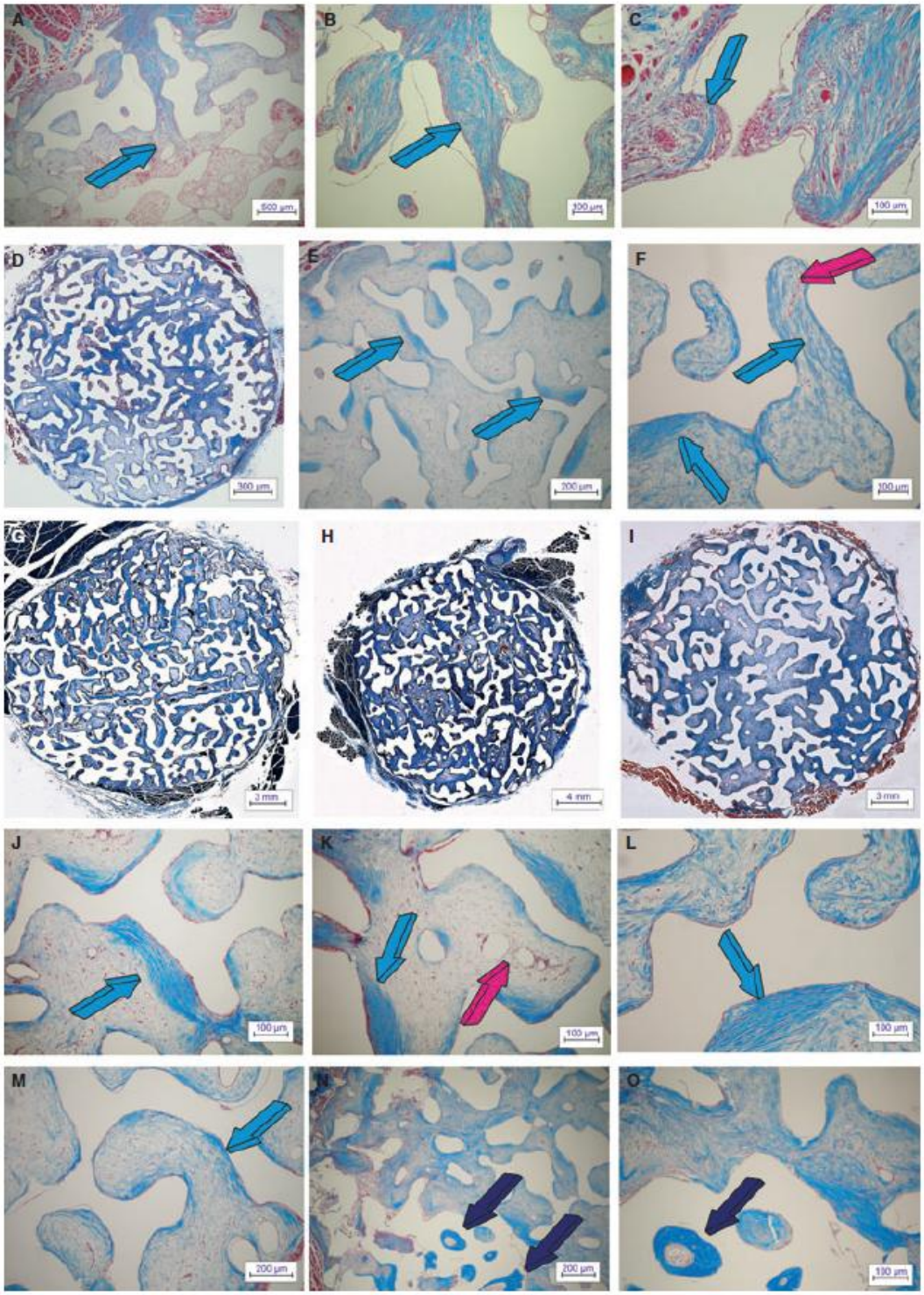
The most likely triggering events for the spontaneous induction of bone formation are, on the one hand, ionic with Ca^{++} release in the protected microenvironment of the macroporous spaces and, on the other, cellular and morphological whereby osteoclastic-based nanopatterned surface modifications with Ca^{++} release differentiate locally responding stem cells into secreting osteoblasts. The coral-derived macroporous constructs are thus richly vascularized because of the calcium gradient; vascularization with capillary sprouting populate the macroporous spaces with mesenchymal stem cells of vascular/paravascular derivation capable of responding both to the newly carved functionalized nano-patterned topographies [7–12, 39–41, 52, 53, 64–67] and to the calcium ions concentration peak [32, 34–36]. *In vitro*, the proliferation of human vascular smooth muscle cells is inhibited by the addition of the L-type voltage-gated calcium channel blocker verapamil [42]. Verapamil blocks extracellular calcium ingress to cytosol of several cells involved in the angiogenic response and irreparably halts the nascent angiogenic phase [42].

The formation of bone by osteoblasts and its remodelling by osteoclasts are a closely integrated homeostatic system [68]. The bone remodelling cycle is the cumulative result of the intimate and complex interaction of the cellular components of the basic multicellular unit (BMU) [23, 24, 69]. Mineralized surfaces including hydroxyapatite and tricalcium phosphate substrata recruit and induce osteoclast formation [70, 71]. The mesenchymal cellular condensations cued by the nanotopography of the implanted macroporous surfaces, together with the Ca^{++} concentration peak facilitated by the protected microenvironment of the secluded macroporous spaces, will attract circulating osteoclast precursor cells (OCP) to populate the coral-derived

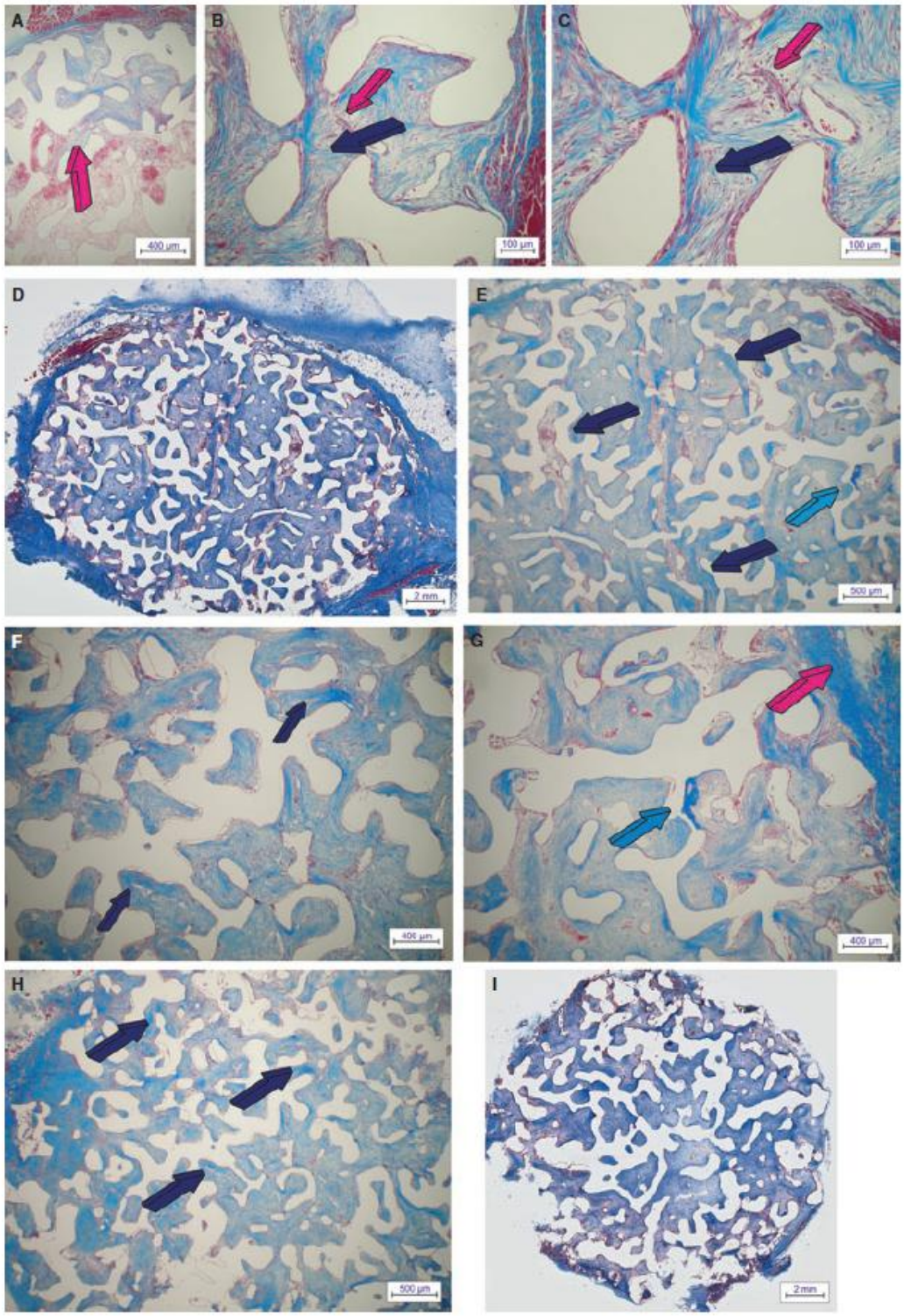
Fig. 6 Zoledronate-treated 7% HA/CC macroporous constructs on days 15, 60 and 90. Tissue patterning and morphogenesis of fibrovascular mesenchymal tissue penetrating the macroporous spaces of biphosphonate zoledronate-treated macroporous 7% HA/CC constructs. The angiogenic fibroblastic front advances within the interconnected macroporous spaces invading the loose vascular matrix suspended by the remaining fibrin/fibronectin scaffold that has formed within the macroporous spaces (light blue arrow in **A**). Tissue patterning and morphogenesis of collagenous condensations not yet tightly attached to the biomimetic matrix (light blue arrows in **B** and **C**). (**D**–**F**) Remodelling, tissue patterning and morphogenesis of collagenous condensations against the implanted biomatrix on day 60 is still profoundly delayed when compared with tissue invasion and morphogenesis as evaluated in untreated control specimens even when harvested on day 15 (Fig. 2A–C). (**G**–**I**) Low power views of tissue incorporation and mesenchymal tissue invasion in zoledronate-treated macroporous 7% HA/CC constructs harvested on day 90 showing delayed mesenchymal tissue patterning facing a very loose fibrovascular tissue. (**J**–**M**) Delayed tissue patterning and morphogenesis of collagenous condensations against the macroporous constructs (light blue arrows) with still prominent vascular invasion (magenta arrow). (**N** and **O**) On day 90, and at the periphery of the macroporous constructs, possibly related to the lack of diffusion of the pipetted biphosphonate zoledronate, there is occasionally the induction of bone formation (dark blue arrows). Decalcified sections cut at 6 μm stained with Goldner's trichrome.

© 2013 The Authors.
Journal of Cellular and Molecular Medicine Published by John Wiley & Sons Ltd and Foundation for Cellular and Molecular Medicine.

J. Cell. Mol. Med. Vol 17, No 11, 2013



© 2013 The Authors.
Journal of Cellular and Molecular Medicine Published by John Wiley & Sons Ltd and Foundation for Cellular and Molecular Medicine.



© 2013 The Authors.
Journal of Cellular and Molecular Medicine Published by John Wiley & Sons Ltd and Foundation for Cellular and Molecular Medicine.

Fig. 7 Ca^{++} channel blocker verapamil hydrochloride-treated 7% HA/CC macroporous constructs on days 15, 60 and 90. Tissue induction, morphogenesis and tissue patterning of mesenchymal fibrovascular tissue invasion in 7% HA/CC macroporous spaces pre-loaded with the Ca^{++} channel blocker verapamil hydrochloride implanted in the *rectus abdominis* muscle of *Papio ursinus* and harvested on days 15 (**A**–**C**), 60 (**D**–**G**) and 90 (**H** and **I**). (**A**) Tissue patterning of fibrovascular tissue invasion on day 15 with fibrovascular bundles invading the loose fibrin-fibronectin vascular matrix (magenta arrow) within the more internal macroporous spaces. (**B** and **C**) Early tissue morphogenesis of collagenous condensations (dark blue arrows) supported by a rich vascular invasion (magenta arrows). (**D** and **E**) Low power views of a verapamil hydrochloride-treated constructs implanted in the *rectus abdominis* of *P. ursinus* and harvested on day 60. Morphogenesis and tissue patterning of collagenous condensations (dark blue arrows) with the induction of an island of bone at the very periphery of the implanted macroporous construct (light blue arrow in **E**). (**F**) Remodelling of the fibrovascular tissue invasion and mesenchymal collagenous condensations (dark blue arrows) and (**G**) detail of newly formed bone (light blue arrow) at the periphery of the implanted macroporous construct surrounded by the *rectus abdominis* fascia (magenta arrow). (**H** and **I**) Delayed tissue patterning and collagenous condensations in Verapamil hydrochloride-treated specimens harvested on day 90. Limited organization and tissue patterning of collagenous condensations with, however, prominent vascularization across the macroporous spaces. Decalcified sections cut at 4 μm stained with Goldner's trichrome.

macroporous surfaces and initiate the osteogenic activity of the BMU by setting the activation phase of resorption and by recruiting osteoblastic precursor cells. The nanotopographical geometric configurations set by osteoclastogenesis together with Ca^{++} ions release differentiate myoblastic/paravascular and/or pericytic stem cells into osteoblastic cell lines.

The inductive surface microstructure of various hydroxyapatite-based macroporous constructs is the common denominator of materials endowed with the striking prerogative of initiating *de novo* bone formation by induction [72]. Surface microstructure resulting from micro surface porosity may be drastically affected by sintering, thereby affecting the induction of bone formation when implanted in heterotopic sites [72].

Differentiated osteoblasts will express and secrete osteogenic proteins of the TGF-β supergene family to be embedded into the matrix initiating the induction of bone formation as a secondary response. There are temporally and spatially related phenotypic transitions ultimately culminating in the differentiation of osteoblastic-like cells and the induction of bone formation [3]. The angiogenic response penetrating the macroporous spaces of the coral-derived constructs is a prominent morphological feature. This was shown by the pattern of alkaline phosphatase activity of the invading capillaries [3] as well as by the expression of *type IV collagen* on day 15 in the present study. It is likely that the temporal induction of *type IV collagen* and angiogenesis is initiated long before the inhibitory activities of both the calcium ion blocker, verapamil hydrochloride and the osteoclast inhibitor, biphosphonate zoledronate.

Finally, the presented study is the only experiment *in vivo* correlating tissue morphology with the gene expression of the generated tissues by macroporous constructs at different time-points and in a non-human primate model [73]. The nascent tissue induction and tissue patterning as seen morphologically have been studied by qRT-PCR; because of the lack of *in vivo* studies, we still do not know the level and the extent of tissue induction changes, which impact gene expression. The opposite is perhaps more true and important: we have not grasped as yet the extent of gene expression changes necessary to set into motion the quantity and quality of regenerated tissue morphology particularly in primate species. The knowledge of this fine molecular/morphological tuning would be exceedingly complicated to gather from *in vivo* studies, particularly in primates, but may well be the next boundary in regenerative medicine and tissue engineering.

Lastly, the harvested tissue for the molecular biology studies may not fully represent or capture the quantity and quality of tissue morphology changes that occur at the microenvironment level, calling for a more sophisticated approach in studying the events at the cell/matrix interface.

In conclusion, this non-human primate study establishes the critical role of osteoclastogenesis to regulate the induction of bone formation by coral-derived biomimetic matrices. It further shows the regulatory role of Ca^{++} and L-type voltage-gated ion channels in controlling the induction of bone formation. Osteoclastogenesis is required to set nano-patterned geometric topographies, which, together with Ca^{++} release, induce angiogenesis and capillary sprouting, cellular differentiation, osteoblastic cell attachment and synthesis to the implanted biomimetic matrix. Expression of *BMPs* is followed by the embedding of the secreted gene products into the implanted macroporous surfaces inducing bone formation as a secondary response. The induction of *BMPs*, together with *Noggin* controlling the extent of bone differentiation by induction, indicates that the induction of bone formation by coral-derived biomimetic matrices is initiated and maintained *via* the *BMPs* pathway.

The induction of bone formation as initiated by macroporous coral-derived constructs might require fewer amounts in hBMPs/hOPs when applied in clinical contexts.

Acknowledgements

The studies on the "*intrinsic induction of bone formation by macroporous coral-derived constructs*" have been constantly supported by the University of the Witwatersrand, Johannesburg, the Faculty of Health Sciences and the National Research Foundation of South Africa since the first histological of bone sections cut by Barbara van den Heever in 1988 showing the morphogenesis by coral-derived macroporous constructs. The South African Medical Research Council partly supported the presented research. The molecular insights of Marco Weinberg are greatly acknowledged. A special word of thanks to Ruquayya Parak for the histological processing and part of the evaluation, and Mike Ponticiello, Biomet USA, for the kind supply of the coral-derived macroporous constructs.

Conflicts of interest

The authors confirm that there are no conflicts of interest.

© 2013 The Authors.

Journal of Cellular and Molecular Medicine Published by John Wiley & Sons Ltd and Foundation for Cellular and Molecular Medicine.

References

1. **Williams D.** The continuing evolution of biomaterials. *Biomaterials*. 2011; 32: 1–2.
2. **Ripamonti U, Duneas N.** Tissue engineering of bone by osteoinductive biomaterials. *MRS Bull*. 1996; 21: 36–9.
3. **Ripamonti U, van den Heever B, van Wyk J.** Expression of the osteogenic phenotype in porous hydroxyapatite implanted extraskeletally in baboons. *Matrix*. 1993; 13: 491–502.
4. **Ripamonti U, Crooks J, Kirkbride AN.** Sintered porous hydroxyapatites with intrinsic osteoinductive activity: geometric induction of bone formation. *S Afr J Sci*. 1999; 95: 335–43.
5. **Ripamonti U.** Soluble, insoluble and geometric signals sculpt the architecture of mineralized tissues. *J Cell Mol Med*. 2004; 8: 169–80.
6. **Ripamonti U, Richter PW, Thomas ME.** Self-inducing shape memory geometric cues embedded within *smart* hydroxyapatite-based biomimetic matrices. *Plast Reconstr Surg*. 2007; 120: 1796–807.
7. **Buxboim A, Ivanovska IL, Discher DE.** Matrix elasticity, cytoskeletal forces and physics of the nucleus: how deeply do cells 'feel' outside and in? *J Cell Sci*. 2010; 123: 297–308.
8. **Fu J, Wang YK, Yang MT, *et al.*** Mechanical regulation of cell function with geometrically modulated elastomeric substrates. *Nat Methods*. 2010; 7: 733–6.
9. **Vlacic-Zischke J, Hamlet SM, Friis T, *et al.*** The influence of surface microroughness and hydrophilicity of titanium on the up-regulation of TGFβ/BMP signalling in osteoblasts. *Biomaterials*. 2011; 32: 665–71.
10. **McNamara LE, Sjöström T, Burgess KE, *et al.*** Skeletal stem cell physiology on functionally distinct titania nanotopographies. *Biomaterials*. 2011; 32: 7403–10.
11. **Watari S, Hayashi K, Wood JA, *et al.*** Modulation of osteogenic differentiation in hMSCs cells by submicron topographically-patterned ridges and grooves. *Biomaterials*. 2012; 33: 128–36.
12. **Ripamonti U.** The concavity: the 'shape of life and the control of bone differentiation. Available at http://www.scienceinafrica.co.za/2012/ripamonti_bone.htm (accessed 7 May 2012).
13. **Ripamonti U.** Inductive bone matrix and porous hydroxyapatite composites in rodents and non-human primates. In: Yamamuro T, Wilson-Hench J, Hench LL, editors. *The handbook of bioactive ceramics, volume II: calcium phosphate and hydroxyapatite ceramics*. Florida: CRC Press; 1990. pp. 245–53.
14. **Ripamonti U.** The morphogenesis of bone in replicas of porous hydroxyapatite obtained from conversion of calcium carbonate exoskeletons of coral. *J Bone Joint Surg Am*. 1991; 73: 692–703.
15. **Reddi AH.** Symbiosis of biotechnology and biomaterials: applications in tissue engineering of bone and cartilage. *J Cell Biochem*. 1994; 56: 192–5.
16. **Ripamonti U, Reddi AH.** Bone morphogenetic proteins: applications in plastic and reconstructive surgery. *Adv Plast Reconstr Surg*. 1995; 11: 47–65.
17. **Reddi AH.** Morphogenesis and tissue engineering of bone and cartilage: inductive signals, stem cells, and biomimetic biomaterials. *Tissue Eng*. 2000; 6: 351–9.
18. **Ripamonti U, Ramoshebi LN, Patton J, *et al.*** Soluble signals and insoluble substrata: novel molecular cues instructing the induction of bone. In: Massaro EJ, Rogers JM, editors. *The skeleton*. New York: Humana Press; 2004. pp. 217–27.
19. **Sampath TK, Reddi AH.** Dissociative extraction and reconstitution of extracellular matrix components involved in local bone differentiation. *Proc Natl Acad Sci USA*. 1981; 78: 7599–603.
20. **Sampath TK, Reddi AH.** Homology of bone-inductive proteins from human, monkey, bovine, and rat extracellular matrix. *Proc Natl Acad Sci USA*. 1983; 80: 6591–5.
21. **Khouri RK, Koudsi B, Reddi H.** Tissue transformation into bone *in vivo*. A potential practical application. *JAMA*. 1991; 266: 1953–5.
22. **Ripamonti U.** Biomimetism, biomimetic matrices and the induction of bone formation. *J Cell Mol Med*. 2009; 13: 2953–72.
23. **Parfitt AM.** Osteonal and hemi-osteonal remodeling: the spatial and temporal framework for signal traffic in adult human bone. *J Cell Biochem*. 1994; 55: 273–86.
24. **Manolagas SC, Jilka RL.** Bone marrow, cytokines, and bone remodeling. Emerging insights into the pathophysiology of osteoporosis. *N Engl J Med*. 1995; 332: 305–11.
25. **Ripamonti U, Roden LC, Renton LF.** Osteoinductive hydroxyapatite-coated titanium implants. *Biomaterials*. 2012; 33: 3813–23.
26. **van Eeden SP, Ripamonti U.** Bone differentiation in porous hydroxyapatite in baboons is regulated by the geometry of the substratum: implications for reconstructive craniofacial surgery. *Plast Reconstr Surg*. 1994; 93: 959–66.
27. **Ripamonti U.** Osteoinduction in porous hydroxyapatite implanted in heterotopic sites of different animal models. *Biomaterials*. 1996; 17: 31–5.
28. **Ripamonti U, Crooks J, Khoali L, *et al.*** The induction of bone formation by coral-derived calcium carbonate/hydroxyapatite constructs. *Biomaterials*. 2009; 30: 1428–39.
29. **Ripamonti U, Klar RM, Renton LF, *et al.*** Synergistic induction of bone formation by hOP-1, hTGF-β, and inhibition by zoledronate in macroporous coral-derived hydroxyapatites. *Biomaterials*. 2010; 31: 6400–10.
30. **Shors EC.** Coralline bone graft substitutes. *Orthop Clin North Am*. 1999; 30: 599–613.
31. **Kanatani M, Sugimoto T, Fukase M, *et al.*** Effect of elevated extracellular calcium on the proliferation of osteoblastic MC3T3-E1 cells: its direct and indirect effects *via* human monocytes. *Biochem Biophys Res Commun*. 1991; 181: 1425–30.
32. **Kohn EC, Alessandro R, Spoonster J, *et al.*** Angiogenesis: role of calcium-mediated signal transduction. *Proc Natl Acad Sci USA*. 1995; 92: 1307–11.
33. **Matsuoka H, Akiyama H, Okada Y, *et al.*** *In vitro* analysis of the stimulation of bone formation by highly bioactive apatite- and wollastonite-containing glass-ceramic: released calcium ions promote osteogenic differentiation in osteoblastic ROS17/2.8 cells. *J Biomed Mater Res*. 1999; 47: 176–88.
34. **Munaron L.** Intracellular calcium, endothelial cells and angiogenesis. *Recent Pat Anticancer Drug Discov*. 2006; 1: 105–19.
35. **Wu Q, Shao H, Eton D, *et al.*** Extracellular calcium increases CXCR4 expression on bone marrow-derived cells and enhances pro-angiogenesis therapy. *J Cell Mol Med*. 2009; 13: 1–10.
36. **Zayzafoon M.** Calcium/calmodulin signaling controls osteoblast growth and differentiation. *J Cell Biochem*. 2006; 97: 56–70.
37. **Schnitzler CM, Ripamonti U, Mesquita JM.** Histomorphometry of iliac crest trabecular bone in adult male baboons in captivity. *Calcif Tissue Int*. 1993; 52: 447–54.
38. **Public Service Department.** *National code for animal use in research education, diagnosis and testing of drugs and related substances in South Africa*. Pretoria, South Africa: Public Service Department; 1990.
39. **McNamara LE, McMurray RJ, Biggs MJ, *et al.*** Nanotopographical control of stem cell differentiation. *J Tissue Eng*. 2010; 1: 1–13.
40. **Gittens RA, McLachlan T, Oliveres-Navarrete R, *et al.*** The effect of combined

© 2013 The Authors.
Journal of Cellular and Molecular Medicine Published by John Wiley & Sons Ltd and Foundation for Cellular and Molecular Medicine.

micron-/submicron-scale surface roughness and nanoscale features on cell proliferation and differentiation. *Biomaterials*. 2011; 32: 3395–403.

41. **Wilkinson A, Hewitt RN, McNamara LE, *et al.*** Biomimetic microtopography to enhance osteogenesis *in vitro*. *Acta Biomater*. 2011; 7: 2919–25.
42. **Yoo HJ, Kozaki K, Akishita M, *et al.*** Augmented Ca^{2+} influx is involved in the mechanism of enhanced proliferation of cultured vascular smooth muscle cells from spontaneous diabetic Goto-Kahizaki rats. *Atherosclerosis*. 1997; 2: 167–75.
43. **Ripamonti U, Ferretti C, Heliotis M.** Soluble and insoluble signals and the induction of bone formation: molecular therapeutics recapitulating development. *J Anat*. 2006; 209: 447–68.
44. **Trueta J.** The role of the vessels in osteogenesis. *J Bone Joint Surg*. 1963; 45: 402–18.
45. **Vlodavsky I, Folkman J, Sullivan R, *et al.*** Endothelial cell-derived basic fibroblast growth factor: synthesis and deposition into subendothelial extracellular matrix. *Proc Natl Acad Sci USA*. 1987; 84: 2292–6.
46. **Folkman J, Klagsbrun M, Sasse J, *et al.*** A heparin binding angiogenic protein basic fibroblast growth factor-is stored within basement membranes. *Am J Pathol*. 1988; 130: 393–400.
47. **Paralkar VM, Vukicevic S, Reddi AH.** Transforming growth factor β type 1 binds to collagen type IV of basement membrane matrix: implications for development. *Dev Biol*. 1991; 143: 303–9.
48. **Paralkar VM, Nandedkar AKN, Pointer RH, *et al.*** Interaction of osteogenin, a heparin binding bone morphogenetic protein, with type IV collagen. *J Biol Chem*. 1990; 265: 17281–4.
49. **Vukicevic S, Latin V, Chen P, *et al.*** Localization of osteogenic protein-1 (bone morphogenetic protein-7) during human embryonic development: high affinity binding to basement membranes. *Biochem Biophys Res Commun*. 1994; 198: 693–700.
50. **Ripamonti U.** Soluble osteogenic molecular signals and the induction of bone formation. *Biomaterials*. 2006; 27: 807–22.
51. **Vukicevic S, Luyten FP, Kleinman HK, *et al.*** Differentiation of canalicular cell processes in bone cells by basement membrane matrix components: regulation by discrete domains of laminin. *Cell*. 1990; 63: 437–45.
52. **Kneser U, Polykandriotis E, Ohnolz J, *et al.*** Engineering of vascularized transplantable bone tissue: induction of axial vascularization in an osteoconductive matrix using an arteriovenous loop. *Tissue Eng*. 2006; 12: 1721–31.
53. **Polykandriotis E, Arkudas A, Beier JP, *et al.*** Intrinsic axial vascularization of an osteoconductive bone matrix by means of an arteriovenous vascular bundle. *Plast Reconstr Surg*. 2007; 120: 855–68.
54. **Beier JP, Horch RE, Hess A, *et al.*** Axial vascularization of a large volume calcium phosphate ceramic bone substitute in the sheep AV loop model. *J Tissue Eng Regen Med*. 2010; 4: 216–23.
55. **Discher DE, Janmey P, Wang YL.** Tissue cells feel and respond to the stiffness of their substrata. *Science*. 2005; 310: 1139–43.
56. **Dalby MJ, Gadegaard N, Tare R, *et al.*** The control of human mesenchymal cell differentiation using nanoscale symmetry and disorder. *Nat Mater*. 2007; 6: 997–1003.
57. **Discher DE, Mooney DJ, Zandstra PW.** Growth factors, matrices, and forces combine and control stem cells. *Science*. 2009; 324: 1673–7.
58. **Ohgushi H, Dohi Y, Tamai S, *et al.*** Osteogenic differentiation of marrow stromal stem cells in porous hydroxyapatite ceramics. *J Biomed Mater Res*. 1993; 27: 1401–7.
59. **Hall BK, Miyake T.** All for one and one for all: condensations and the initiation of skeletal development. *BioEssays*. 2000; 22: 138–47.
60. **Zimmerman LB, De Jesus-Escobar JM, Harland RM.** The Spemann organizer signal noggin binds and inactivates bone morphogenetic protein 4. *Cell*. 1996; 96: 599–606.
61. **Barbado H, Fablet K, Ronjat M, *et al.*** Gene regulation by voltage-dependant calcium channels. *Biochem Biophys Acta*. 2009; 1793: 1096–104.
62. **Li H, Chang J.** Stimulation of proangiogenesis by calcium silicate bioactive ceramic. *Acta Biomater*. 2012; 12: 1742–61.
63. **Wei C, Wang X, Zheng M, *et al.*** Calcium gradients underlying cell migration. *Curr Opin Cell Biol*. 2012; 2: 254–61.
64. **Gray C, Boyde A, Jones SJ.** Topographically induced bone formation *in vitro*: implication for bone implants and bone grafts. *Bone*. 1996; 2: 115–23.
65. **Wieland M, Textor M, Spenor ND, *et al.*** Wavelength-dependant roughness: a quantitative approach to characterising the topography of rough titanium surfaces. *Int J Oral Maxillofac Implants*. 2001; 2: 163–81.
66. **Chou L, Firth JD, Uitto VJ, *et al.*** Substratum surface topography allows cell shape and regulates fibronectin mRNA levels, mRNA stability, secretion and assembly in human fibroblasts. *J Cell Sci*. 1995; 4: 1563–73.
67. **Curran JM, Chen R, Hunt JA.** The guidance of human mesenchymal stem cell differentiation *in vitro* by controlled modifications to cell substrate. *Biomaterials*. 2006; 27: 4783–93.
68. **Reddi AH.** Bone morphogenesis and modelling: soluble signals sculpt osteosomes in the solid state. *Cell*. 1997; 89: 159–61.
69. **Parfitt AM, Mundy GR, Roodman GD, *et al.*** A new model for the regulation of bone with the particular reference to the effect of bisphosphonates. *J Bone Miner Res*. 1996; 11: 150–9.
70. **Sabokbar A, Panddey R, Díaz J, *et al.*** Hydroxyapatite particles are capable of inducing osteoclast formation. *J Mater Sci Mater Med*. 2001; 12: 659–64.
71. **Detsch R, Mayr H, Ziegler G.** Formation of osteoclast-like cells on HA and TCP ceramics. *Acta Biomater*. 2008; 4: 139–48.
72. **Le Nihouannen D, Daculsi G, Saffarzadeh A, *et al.*** Ectopic bone formation by microporous calcium phosphate ceramic particles in sheep muscles. *Bone*. 2005; 36: 1086–93.
73. **Ripamonti U.** Bone induction by recombinant human osteogenic protein-1 (hOP-1, BMP-7) in the primate *Papio ursinus* with expression of mRNA of gene products of the TGF-β superfamily. *J Cell Mol Med*. 2005; 4: 911–28.

© 2013 The Authors.
Journal of Cellular and Molecular Medicine Published by John Wiley & Sons Ltd and Foundation for Cellular and Molecular Medicine.

CHAPTER 5

THE INDUCTION OF BONE FORMATION BY THE RECOMBINANT HUMAN TRANSFORMING GROWTH FACTOR – β_3

Published: Biomaterials 2014; XX: 1-16.

ARTICLE IN PRESS

Biomaterials xxx (2014) 1–16

Contents lists available at ScienceDirect

Biomaterials

journal homepage: www.elsevier.com/locate/biomaterials

The induction of bone formation by the recombinant human transforming growth factor-β_3

Roland M. Klar [a], Raquel Duarte [b], Therese Dix-Peek [b], Ugo Ripamonti [a,*]

[a] Bone Research Laboratory, School of Physiology, Faculty of Health Sciences, Medical School, University of the Witwatersrand, Parktown, Johannesburg 2193 South Africa

[b] Department of Internal Medicine, School of Clinical Medicine, University of the Witwatersrand, Johannesburg, South Africa

ARTICLE INFO

Article history:
Received 22 November 2013
Accepted 19 December 2013
Available online xxx

Keywords:
Transforming growth factor-β_3
Bone morphogenetic proteins
Tissue induction
Noggin
Primates
qRT-PCR

ABSTRACT

Implantation of recombinant human transforming growth factor-β_3 (hTGF-β_3) with coral-derived calcium carbonate-based macroporous bioreactors with limited conversion to hydroxyapatite (7% HA/CC) in the *rectus abdominis* muscle of the non-human primate Chacma baboon *Papio ursinus* induces endochondral bone formation. The exact mechanisms by which hTGF-β_3 signalling induces bone in heterotopic sites of *P. ursinus* are not known. Coral-derived 7% HA/CC bioreactors with and without 125 μg hTGF-β_3 were implanted in triplicate in the *rectus abdominis* muscle of 6 adult baboons. 7% HA/CC bioreactors either with or without hTGF-β_3 were loaded with 125 μg of recombinant human Noggin (hNoggin), a bone morphogenetic proteins (BMPs) antagonist. Tissues on day 15, 60 and 90 were analysed by histomorphometry and quantitative reverse-transcriptase polymerase chain reaction (qRT-PCR). Down-regulation of *BMP-2* characterized 7% HA/CC constructs preloaded with 125 μg hNoggin with *Noggin* down-regulated on day 60 and 90 together with lack of *TGF-β_3* expression. Down-regulation of *BMP-2* correlated with minimal bone formation by induction. hTGF-β_3/hNoggin pre-treated bioreactors up-regulated *BMP-2* but only on day 90 together with a significant down-regulation of *Noggin* on day 60 and 90, correlating with the induction of bone formation, albeit limited, on day 90 at the periphery of the macroporous bioreactors only. hTGF-β_3 treated bioreactors significantly down-regulated *BMP-2* on day 15 whilst up-regulating *BMP-2* on day 60 and 90, together with down-regulation of *Noggin* on day 60 and 90 correlating with the prominent induction of bone formation. hTGF-β_3 significantly up-regulated *RUNX-2* and *Osteocalcin* expression on day 15 controlling the differentiation of progenitor stem cells into the osteoblastic lineage. The induction of bone as initiated by hTGF-β_3 in the *rectus abdominis* muscle of *P. ursinus* is *via* the BMPs pathway with hTGF-β_3 controlling the induction of bone formation by regulating the expression of *BMPs via Noggin* expression. These results unequivocally demonstrate that hTGF-β_3 elicits bone induction by up-regulation of endogenous *BMP-2* and is blocked by hNoggin.

© 2013 Elsevier Ltd. All rights reserved.

1. Introduction

The induction of bone formation during embryonic development and postnatal tissue induction and morphogenesis is set by complex seemingly redundant cascades of molecular and morphogenetic events that sculpt the multicellular mineralized and non-mineralized structures of bone that have ultimately engineered the emergence of the skeleton and thus of the vertebrates [1–3].

The transforming growth factor-β (TGF-β) supergene family comprises several multifactorial gene products endowed with a vast pleiotropic activity regulating embryonic development, tissue patterning, postnatal tissue induction and morphogenesis, immunoregulation and fibrosis, initiating the morphogenesis of several tissues and organs including the skeleton and the bone matrix [1,2,4–7]. In recent years, different studies have cast additional light on the specific role of the three mammalian transforming growth factor-β (TGF-β) isoforms within the bone matrix [8,9]. Balooch et al. [8] identified TGF-β as the key regulator of the mechanical properties and composition of the bone matrix, additionally as the ultimate morphogen to maintain functional parameters of bone quality, bone mass, elastic modulus and hardness, mineral concentration and resistance to fracture, controlling the structure and function of the skeleton [8]. Additionally, mRNA expression of TGF-β gene products regulates joint morphogenesis [9].

* Corresponding author.
E-mail addresses: ugo.ripamonti@wits.ac.za, ugo.ripamonti@gmail.com (U. Ripamonti).

0142-9612/$ – see front matter © 2013 Elsevier Ltd. All rights reserved.
http://dx.doi.org/10.1016/j.biomaterials.2013.12.062

ARTICLE IN PRESS

Strikingly, and in marked contrast to rodents [7,10–16], systematic studies in the non-human primate *Papio ursinus* have discovered a previously unreported biological function of the three mammalian TGF-β isoforms. The isoforms are determinant of a prominent and rapid induction of endochondral bone formation when implanted in heterotopic intramuscular sites of *P. ursinus* [17–20].

The presence of several related but molecularly different isoforms endowed with osteogenic activity poses important questions about the biological significance of this apparent redundancy [7,17,19,21], indicating multiple interactions of several molecularly different yet homologous isoforms deployed synchronously and synergistically during the cascade of bone formation by induction [7,19]. The induction of bone formation thus proceeds *via* the combinatorial action of several osteogenic proteins of the TGF-β superfamily [22,23], including the bone morphogenetic proteins (BMPs) and the three mammalian TGF-β isoforms [17–19]. The temporal window during which *TGF-β_1* mRNA expression is essential for optimal osteogenesis has been unambiguously illustrated by the endochondral osteoinductivity of the three mammalian TGF-β isoforms in *P. ursinus* [17–19] and by the biphasic temporal expression of *TGF-β_1* mRNA in heterotopic constructs harvested at different time periods from the *rectus abdominis* muscle [24].

The apparent redundancy of molecular signals initiating the induction of bone formation and the mechanisms by which TGF-β signalling results in the induction of bone formation in the *rectus abdominis* of the non-human primate *P. ursinus* are still not known and need to be assigned. How does the hTGF-β_3 isoform initiate the cascade of heterotopic bone induction in *P. ursinus*? Can we extrapolate unique results from *P. ursinus* to *Homo sapiens* in clinical contexts?

Using quantitative reverse-transcriptase polymerase chain reaction (qRT-PCR), the expression patterns of the *BMP-2*, *TGF-β_3*, *Noggin*, *Type IV collagen*, *Osteocalcin* (*OC*) and *RUNX-2* at 15, 60 and 90 days after implantation were analysed and correlated to the extent of bone formation by induction. The molecular biological working hypothesis of the present communication is that recombinant human transforming growth factor-β_3 (hTGF-β_3) signalling induces endochondral bone differentiation by regulating Noggin expression and therefore BMPs activities [19,20]. If these molecular and cellular scenarios are correct, the binary application of Noggin with hTGF-β_3 would inhibit osteogenic activity of the expressed and secreted proteins resulting in limited and/or no bone formation by induction. Alternatively, though unlikely, the mammalian hTGF-β isoforms initiate the induction of endochondral bone formation *via* a non-BMPs pathway and in primates only [20].

2. Materials and methods

2.1. Macroporous coral-derived calcium carbonate/hydroxyapatite constructs

Macroporous replicas of coral-derived calcium carbonate exoskeletons of the genus Gonipora were prepared by hydrothermal chemical exchange with phosphate [25–27]. Limited conversion to hydroxyapatite resulted in calcium carbonate constructs with 7% hydroxyapatite defined as 7% HA/CC (Biomet, Indiana, USA) [28,29]. 7% HA/CC constructs were rods 8 mm in diameter and 20 mm in length [28,29]. The solid components of the hydroxyapatite/calcium carbonate replica average 130 μm in diameter and their interconnections 220 μm; the average porosity is 600 μm and their interconnections average 260 μm in diameter [25–29].

2.2. Pre-loading of coral-derived constructs with the recombinant hTGF-β_3 and recombinant human Noggin proteins

Recombinant human transforming growth factor-β_3 (hTGF-β_3) and recombinant human Noggin (hNoggin) were obtained from Novartis AG (Basel, Switzerland) and Regeneron Pharmaceuticals (USA), respectively. Stock solutions of hTGF-β_3 were prepared in 20% ethanol/100 mM acetic acid, pH 4.5, to a final volume of 200 μl with 125 μg hTGF-β_3 dispensed by micro-pipetting onto the macroporous bioreactors. Stock solutions of hNoggin were prepared in 200 μl of 20% ethanol/100 mM acetic acid pH 5.5. 125 μg hNoggin were loaded in liquid vehicle into eighteen 7% HA/CC bioreactors. Additional macroporous bioreactors were loaded with a combination of 125 μg hTGF-β_3 and 125 μg hNoggin prepared in 5 mM hydrochloric acid to a final concentration of 0.625 μg/μl 7% HA/CC macroporous constructs were also implanted in the *rectus abdominis* as untreated control.

Pre-loading of recombinant morphogens was performed under laminar flow by pipetting the required amount of liquid vehicle with a 0.2 ml sterile tip onto both proximal and distal regions of the rods to ensure an even distribution of loaded proteins throughout the macroporous spaces.

2.3. Primate model for tissue induction and morphogenesis

Six clinically healthy adult *P. ursinus* with a mean weight of 21.2 (±1.48) kg were selected from the primate colony of the University of the Witwatersrand, Johannesburg. Criteria for selection, housing conditions and diets were as described [25,26]. *P. ursinus* species share similar bone physiology and osteonic bone remodelling with humans [30]. Research protocols were approved by the Animal Ethics Screening Committee of the University, and conducted according to the *Guidelines for the Care and Use of Experimental Animals* prepared by the University and in compliance with the National Code for Animal Use in Research, Education and Diagnosis in South Africa [31]. Premedication before induction of general

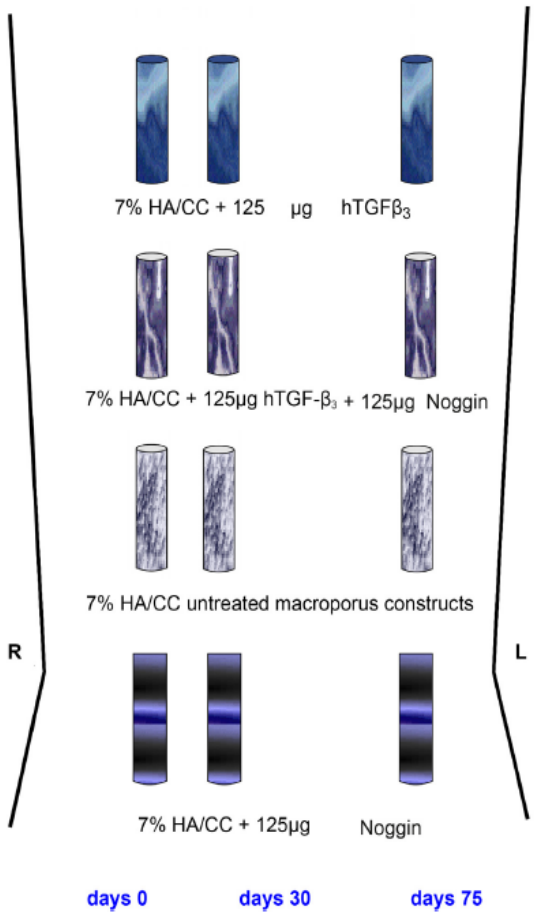


Fig. 1. Heterotopic intramuscular *rectus abdominis* surgical model and implantation design in six adult non-human primates Chacma baboon *Papio ursinus*. In each animal, a total of twelve coral-derived calcium carbonate macroporous constructs with limited hydrothermal conversion to hydroxyapatite (7% HA/CC constructs) were implanted in the *rectus abdominis* muscle of each animal in triplicate. Three 7% HA/CC constructs each representing one treatment modality were implanted at day 0, 30 75 thus providing macroporous bioreactors with differentiating tissues according to each treatment modality to be harvested at days 90, 60 and 15 after heterotopic implantation. Implants were aligned longitudinally ~8 and 2 cm apart.

ARTICLE IN PRESS

anaesthesia was by midazolam hydrochloride (Dormicum® 3 mg/kg IM; Roche, Illovo, South Africa). Animals were anaesthetized with ketamine hydrochloride (5–15 mg/kg) (Eutaphent Kyron Laboratories, Johannesburg, South Africa) and general anaesthesia maintained by Isofor (1.5%–2%) (Safe Line Pharmaceutical, Johannesburg, South Africa) after oro-tracheal intubation [26,28,29]. A total of twelve 7% HA/CC untreated and treated macroporous bioreactors were implanted bilaterally in intramuscular pouches surgically created by sharp and blunt dissection within the *rectus abdominis* muscle of each animal (Fig. 1), four on day 0, four on day 30 and four on day 75, representing a total of eighteen macroporous bioreactors per treatment modality. Implants were aligned longitudinally approximately 2 cm apart [28,29].

2.4. Tissue harvest, histology and histomorphometry

On day 90, animals were anaesthetized with an injection of ketamine (5–15 mg/kg) and maintained under general anaesthesia with Isofor (1.5%–2%). Specimens were harvested together with muscle tissue (baseline control). Following harvest, animals were killed with an intravenous overdose of sodium pentobarbitone (Anaket, Isando, South Africa). Harvested specimens provided regenerating tissues at 15, 60 and 90 days after intramuscular implantation. A 4 mm apical fragment of each harvested 7% HA/CC construct with invading differentiating tissues within the macroporous spaces was cut with sterile blades, and flash frozen in liquid Nitrogen for qRT-PCR. Remaining tissues were fixed in 10% phosphate buffered formalin for 48 h, rinsed in dH_2O and stored in 70% ethanol [28,29]. Specimens were demineralized in a Sakura TDE™ 30 decalcifying unit (Sakura Fintek, Torrance, USA) and processed for paraffin wax embedding. Thirty sections were cut sequentially at 4 μm to obtain a full cross sectional area of each specimen. The 1st and every 10th section was stained using a modified Goldner's Trichrome stain for histological and histomorphometric analyses [28,29].

Images of the histological sections were captured and digitalized using a Provis AX70 research microscope (Olympus Optical Co., Shinjuku, Tokyo Japan) attached to a video camera (Olympus, Shinjuku, Tokyo, Japan). Histomorphometric analysis was then performed using the Stream Essentials software v.1.6 (Olympus, Shinjuku, Tokyo, Japan). The ratios of the total area of the devices and the area of newly formed bone generated within the evaluated macroporous spaces were established, and values were expressed, as a mean percentage of bone generated within the evaluated macroporous spaces (Fig. 2) [32]. Results were analysed with a Student's *t*-test using STATISTICA version 10 (Statsoft, Inc., Tulsa, OK, USA).

2.5. Quantitative reverse transcriptase polymerase chain reaction (qRT-PCR)

Under sterile conditions, redundant soft tissue was removed from heterotopic specimens which were then ground to powder in liquid Nitrogen using a mortar and pestle. Total RNA was extracted from 30 mg of pulverized specimen using the Total RNA Mini Kit (Bio-Rad, Hercules, CA, USA). RNA concentration was determined spectrophotometrically at $A_{260/280}$ with a Nanodrop 2000 (Thermo Scientific, Waltham, MA, USA) and RNA quality was assessed using a Pico6000 RNA kit (Agilent Technologies, Santa Clara, CA, USA) on a Bioanalyzer 2100 (Agilent Technologies, Santa Clara, CA, USA). RNA integrity numbers were between 8.0 and 9.0 for all samples. RNA was reverse transcribed using the High Capacity cDNA Reverse Transcription kit (Applied Biosystems, Foster City, CA, USA). qRT-PCR was performed, in duplicate using EvaGreen Master Mix (Bio-Rad, Hercules, CA, USA) on a CFX-96 thermocycler (Bio-Rad, Hercules, CA, USA). Each reaction contained 10 ng cDNA; 1 x EvaGreen Mix and 10 μM of each primer (Table 1). Primers were designed using Gene fisher v. 2.0 (http://bibiserv.techfak.uni-bielefeld.de/genefisher2). Thermocycling parameters included a denaturation step of 94 °C for 2 min; 40 cycles of 95 °C for 10 s, 60 °C for 10 s and 72 °C for 30 s; and a final extension at 72 °C for 5 min. Genes assayed included *Bone morphogenetic protein-2* (*BMP-2*); *Transforming growth factor-β_3*; *Type IV Collagen*, *Noggin*, *RUNX-2 and Osteocalcin* (*OC*). Gene expression was normalized against 4 reference genes: β-Actin; Succinate dehydrogenase complex subunit A (SDHA); Ribosomal Protein L13A (RPL13a) and Ribosomal Protein Large *PO* (*RPLPO*). Use of GeNorm (*http://medgen.ugent.be/~jvdesomp/genorm/*) established that these were the most appropriate internal reference genes to use. Amplified PCR products underwent sequencing (Inqaba Biotech, Pretoria, South Africa) to confirm that the correct sequence had been amplified [32].

Gene expression from the harvested macroporous devices was normalized to muscle tissue in each animal. Calibrated normalized relative quantities, which reflect the $\log_{10}\ 2^{-\Delta\Delta Ct}$, were determined using qBase analysis software (http://www.biogazelle.com). A Student's *t*-test (STATISTICA version 10, Statsoft, Inc., Tulsa, OK, USA) was used to determine statistical significance at $p < 0.05$.

Table 1
Primer sequence.

Gene	Sequence (5′–3′)
BMP-2	F: GAGTTGCGGCTGCTCAGCATGTT R: ACATGTCTCTTGGAGACACCT
TGF-β_3	F: GGTTTTCCGCTTCAATGTCT R: GCTCGATCCTCTGCTCATTC
Collagen type IV	F: GTTGGTCTACCGGGACTCAA R: GTTCACCTCTGATCCCCTGA
Noggin	F: GAGGAAGTTACAGATGTGGCT R: CACTCGGAAATGATGGGGTAC
RUNX-2	F: CCCCACGACAACCGCACCAT R: CACTCCGGCCCACAAATC
Osteocalcin	F: AGGTGCAGCCTTTTGTGTCCAAG R: GCAAGGGGAAGAGGAAAGAAGG
SDHA (reference)	
RPL13a (reference)	F: TGGGAACAAGAGGGCATCTG R: CCACCACTGCATCAAATTCATG
β-actin (reference)	F: CCTGGAGGAGAAGAGGAAAGAGA R: TGAGGACCTCTGTGTATTTGTCAA
RPLP0 (reference)	F: CTCTTCCAGCCTTCCTTCCT R:AGCACTGTGTTGGCGTACAG F:AGCTGATCAAGACTGGAGACA R:TCCAGGAAGCGAGAATGCAGAGTT

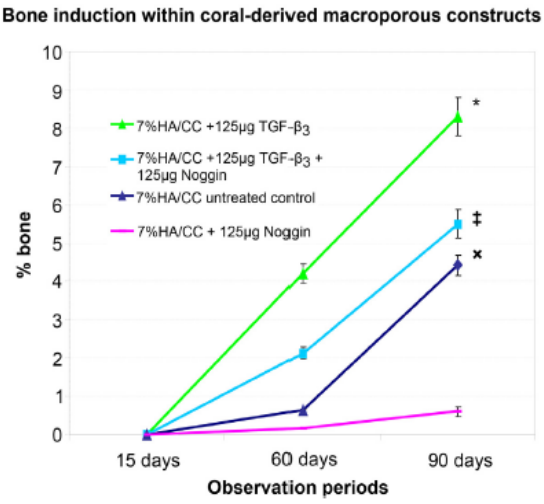


Fig. 2. Morphometric analyses of the induction of bone formation by treated and untreated coral-derived macroporous bioreactors implanted in the *rectus abdominis* muscle of 6 non-human primates *Papio ursinus* and harvested at day 15, 60 and 90 after heterotopic implantation and tissue formation. Significant induction of bone formation by macroporous bioreactors pre-treated with 125 μg hTGF-β_3 (*) *vs.* 125 μg hTGF-β_3 with 125 μg hNoggin (‡), *vs.*7% HA/CC untreated control specimens (×) and *vs.* hNoggin-treated-bioreactors. Note the significant (‡) inhibitory effects on the induction of bone formation by binary application of 125 μg hTGF-β_3 with 125 μg hNoggin. hNoggin-treated specimens showed the least bone formation by induction at all-time points ($p < 0.01$).

3. Results

3.1. Induction of bone formation by hTGF-β_3 treated 7% HA/CC macroporous bioreactors

At harvest, treated and untreated control 7% HA/CC macroporous bioreactors were firmly attached to the ventral fascia of the *rectus abdominis* muscle. On day 15, hTGF-β_3 treated specimens showed fibrovascular tissue invasion across the macroporous spaces (Fig. 3A,B). Such fibrovascular invasion blended into haematopoietic corpuscolated material predominantly red blood cells embedded within a fibrin/fibronectin network across the internal and central macroporous spaces (Fig. 3C,D). The fibrin network was organized in concentric rings progressively invading the macroporous spaces (Fig. 3D,E). In selected specimens on day 15, the morphogenesis of fibrin rings was noteworthy tri-dimensionally organizing tissue induction and morphogenesis by the exogenously applied hTGF-β_3 (Fig. 3D,E).

ARTICLE IN PRESS

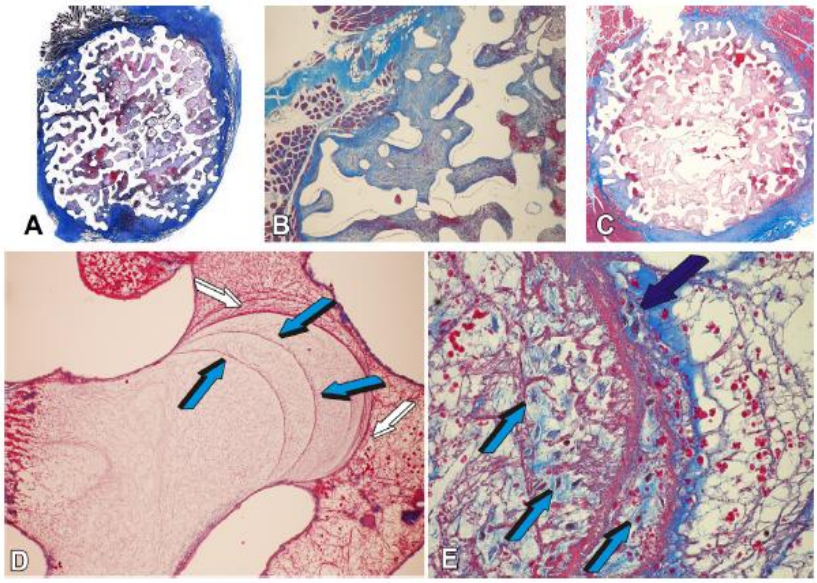


Fig. 3. Tissue induction, morphogenesis and pattern formation by coral-derived macroporous constructs pre-treated with 125 μg hTGF-β_3 and harvested 15 days upon intramuscular implantation in the *rectus abdominis* muscle of *P. ursinus*. (A) Low power view indicating complete fibro vascular tissue invasion within the macroporous spaces highlighted in (B). (C) Low power view showing haematopoietic corpuscolated material with the construction and assembly of extracellular matrix material interpreted to be a fibrin/fibronectin network (D,E) assembling within the macroporous spaces (blue arrows in D) progressing by compressing the surrounding extracellular matrix (white arrows in D) (D,E). (E) Complex tissue patterning and cell differentiation into osteoblastic-like cells (dark blue arrow) secreting the very first extracellular matrix of bone (blue arrows E) patterned by condensing extracellular matrix rings progressing within the invaded macroporous spaces. Decalcified sections cut at 6 μm stained with Goldner's trichrome. Original magnification: (A, C) ×2.7; (B) ×75; (D) ×87; (E) ×250. (For interpretation of the references to colour in this figure legend, the reader is referred to the web version of this article.)

Of note, fibrin/fibronectin rings were expanding within the macroporous spaces mechanically organizing the invading extracellular matrix that had invaded the macroporous bioreactors (Fig. 3D,E). High power views show distinctly organized rings of extracellular matrix progressing within the invaded macroporous spaces (Fig. 3D) transporting differentiating cellular elements interspersed within the generated tridimensional matrix scaffold (Fig. 3E).

Morphological analyses on serial sections stained with the modified Goldner's trichrome showed that the concentric fibrin/fibronectin rings were advancing within the macroporous spaces (Fig. 3D). The advancing movement as determined by tractional forces generated between fibrin and fibronectin is transporting the concentric rings compressing the extracellular matrix ahead of the patterning advancing rings (Fig. 3D).

In hTGF-β_3 treated macroporous bioreactors, the advancing rings provide structural anchorage for plump nucleated hyperchromatic cells interpreted as differentiating osteoblasts (Fig. 3E) reprogrammed by the hTGF-β_3 protein from invading myoblastic/pericytic differentiated cells. The observed cells secrete the very first extracellular matrix of bone deposited onto the patterned extracellular matrix, the induced rings thus structurally organizing the induction of bone formation by the hTGF-β_3 isoform (Fig. 3E). Of note, *RUNX-2* and *Osteocalcin* expression are significantly up-regulated in hTGF-β_3 treated bioreactors particularly on day 15 (Fig. 11) supporting the morphological observations of cell differentiation into the osteoblastic phenotype with hyper cellular osteoblastic activity and extracellular matrix secretion as early as day 15 post-implantation in adult non-human primates (Fig. 3E).

The morphology of the induction of bone formation by coral-derived macroporous bioreactors super activated by 125 μg hTGF-β_3 would be incomplete without digitalized iconographic material on day 30 after implantation in the *rectus abdominis* muscle. 7% HA/CC macroporous constructs pre-loaded with 125 μg hTGF-β_3 were harvested from additional animals on day 30 (Fig. 4). Morphological analyses showed the substantial induction of bone formation throughout the macroporous spaces (Fig. 4A) characterized by multicellular osteoblastic activity and cellular trafficking supported by pronounced capillary sprouting and invasion (Fig. 4B–D).

Newly formed bone was populated by contiguous osteoblasts actively secreting bone matrix (Fig. 4B–D). Osteoblasts were often seen in a close relationship with invading sprouting capillaries (Fig. 4C,D) as well as with large multinucleated osteoclastic-like cells (Fig. 4B–E).

On day 60, in selected hTGF-β_3 treated macroporous specimens, substantial bone had formed (Fig. 5A–C). Induced bone had remodelled in trabeculae of lamellar osteonic-like bone supported by prominent vascular invasion and capillary sprouting within the invaded macroporous spaces (Fig. 5D–F).

Of note, hTGF-β_3 treated 7% HA/CC macroporous constructs showed the generation of rapid and prominent induction of bone formation at the periphery of the implanted macroporous bioreactors invading the *rectus abdominis* muscle (Fig. 5D–F). hTGF-β_3 treated 7% HA/CC macroporous specimens showed extensive induction of bone formation both attached to the substratum as well as invading the macroporous spaces with trabeculae of newly formed bone populated by contiguous plumped secreting osteoblasts touching the invading sprouting capillaries (Fig. 5B,C). Of note, in spite of the extensive induction of bone formation at the periphery of the macroporous bioreactors, limited if any bone formation occurred within the more internal and central regions of the treated macroporous bioreactors (Fig. 5D–F).

By day 90, newly formed bone had remodelled into solid blocks of lamellar/osteonic bone (Fig. 6A–C) with osteoclastic activity supported by a still prominent vascular invasion with capillary sprouting promoting active osteoclastogenesis and remodelling (Fig. 6E,G).

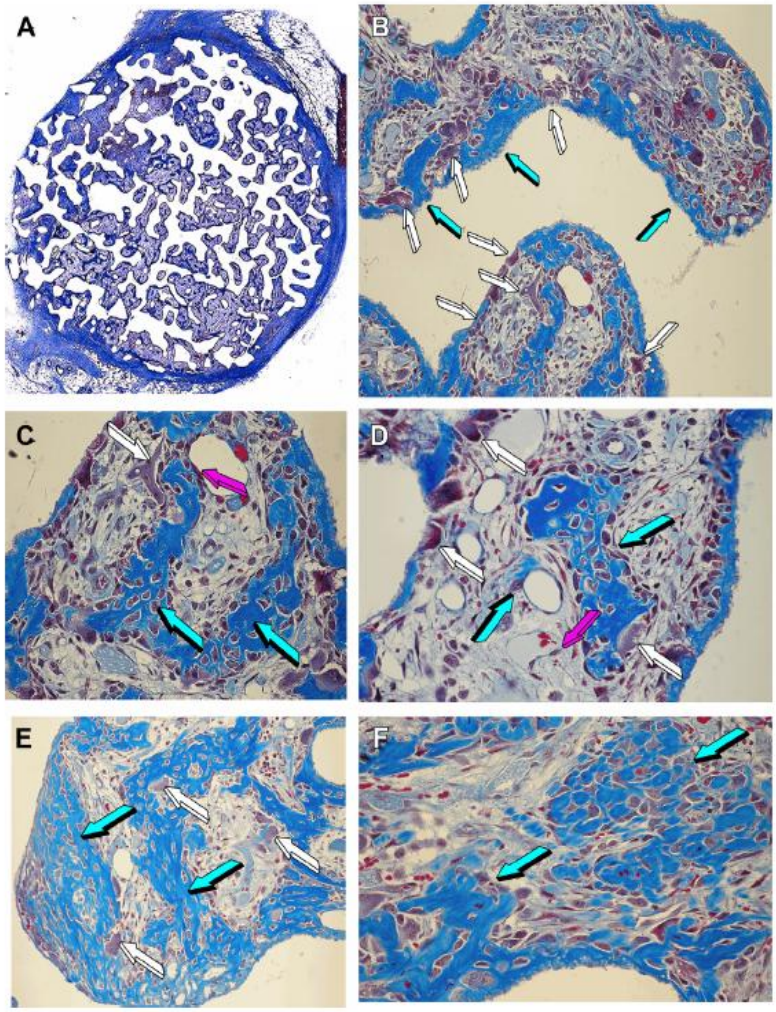


Fig. 4. Significant and substantial induction of bone formation by coral-derived macroporous constructs pre-treated with 125 μg hTGF-β_3 on day 30 after heterotopic implantation in *P. ursinus*. (A) Low power view indicating macroporous spaces with substantial trabeculae of newly formed bone attached to the mineralized substratum (B) with significant cellularity, bone matrix deposition and osteoclastic multinucleated giant cells (white arrows in B–D) in close relationship with both osteoblastic cells (B–D) and sprouting capillaries (D). (C,D) Prominent cellularity and osteoblastic-like cells activity with matrix deposition and endothelial cells in close relationship with the cellular osteoblastic compartment of the newly formed bone by induction (magenta arrows C,D). (E,F) Multicellularity, osteoblastic synthesis and bone matrix deposition (light blue arrows in E,F), multinucleated giant cells (white arrows B,C,D,E) and capillary sprouting with bone matrix tightly attached the calcium carbonate/hydroxyapatite substratum. Decalcified sections cut at 6 μm stained with Goldner's trichrome. Original magnification: (A) ×2.7; (B) ×75; (C, E) ×125; (D, F) ×175. (For interpretation of the references to colour in this figure legend, the reader is referred to the web version of this article.)

3.2. Tissue morphogenesis by hTGF-β_3/hNoggin-treated 7% HA/CC macroporous bioreactors

On day 15, there was limited fibrovascular tissue invasion even within the most peripheral macroporous spaces (Fig. 7A–C); fibrovascular bundles merged within corpuscolated haematopoietic material supported by a fibrin network which showed the absence of fibrin-like rings as characteristically observed in hTGF-β_3 treated 7% HA/CC macroporous constructs. On day 60 (Fig. 7D–G) there was still limited fibrovascular tissue invasion across the macroporous spaces; there was a delayed tissue patterning as compared to hTGF-β_3 treated 7% macroporous bioreactors with limited tissue patterning and organization of the invading collagenous condensations (Fig. 7E–G). Delayed tissue patterning and limited organization of invading collagenous condensations were particularly evident within the centre of the treated-macroporous constructs (Fig. 7D,E). On day 90, hTGF-β_3/hNoggin-treated 7% HA/CC macroporous specimens persistently showed haphazardly constructed and limited patterned collagenous condensations with poorly invaded vascularised central macroporous areas (Fig. 7H–J). Specimens often showed that collagenous condensations were in the form of single collagenous bundles intersecting within the macroporous spaces surrounding a central core characterized by limited tissue invasion and vascularisation (Fig. 7H *inset*). Single collagenous bundles were separated by invading capillaries with attached mesenchymal stem cells (Fig. 7H *inset*).

On day 90, hTGF-β_3/hNoggin-treated specimens showed limited induction of bone formation within the most peripheral

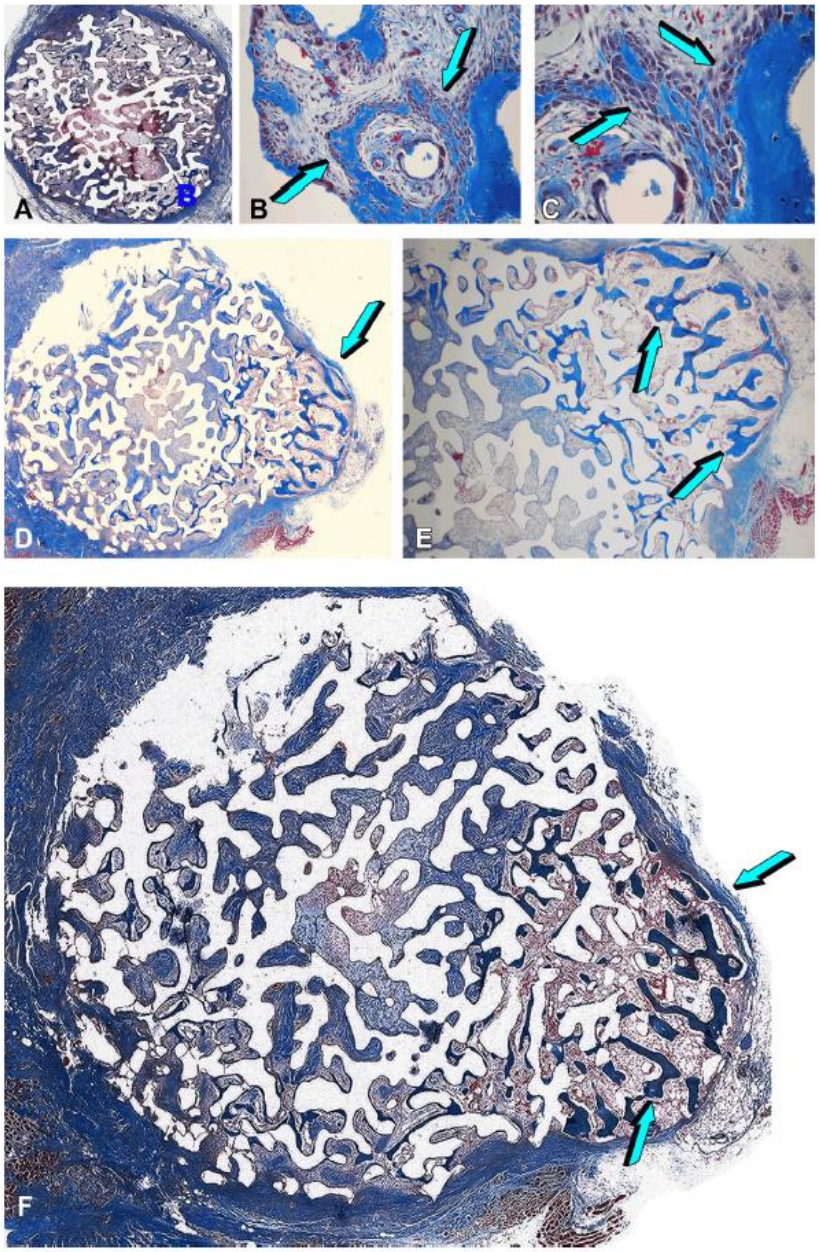


Fig. 5. Tissue induction and morphogenesis by coral-derived macroporous constructs pre-treated with 125 μg hTGF-β_3 harvested 60 days upon intramuscular implantation in the *rectus abdominis* muscle of *P. ursinus*. (A) Low power view showing the induction of bone formation across multiple macroporous spaces with hyper cellularity, capillary sprouting and osteoblastic cells lining newly formed bone matrix (*light blue* arrows in B,C). (D–F) Substantial induction of bone formation protruding through the peripheral outline of the hTGF-β_3/pre-treated bioreactors when harvested 60 days upon implantation in heterotopic sites (*light blue* arrows in D–F). Of interest, central macroporous spaces show the lack of bone formation (F). Decalcified sections cut at 6 μm stained with Goldner's trichrome. Original magnification: (A, D, F) ×2.7; (B) ×125; (C) ×175; (E) ×75. (For interpretation of the references to colour in this figure legend, the reader is referred to the web version of this article.)

macroporous spaces only (Fig. 7H–J). Induced bone faced a central/internal core with limited tissue invasion with delayed tissue patterning and organogenesis of collagenous condensations often poorly organized as single bundles of collagenic material (Fig. 7 *inset*).

hTGF-β_3/hNoggin-treated 7% HA/CC macroporous constructs were thus characterized by contrasting tissue morphogenesis spatially related to selected areas of the implanted macroporous constructs.

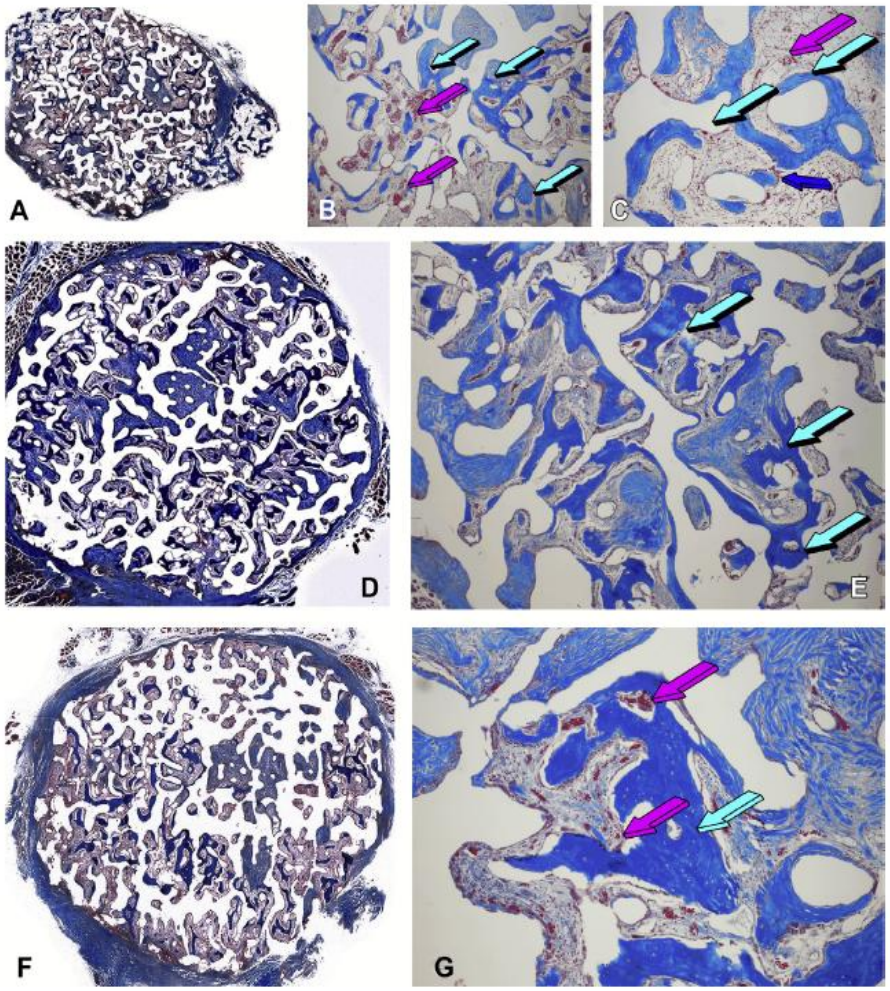


Fig. 6. Induction of bone formation by coral-derived macroporous constructs pre-treated with 125 μg hTGF-β_3 on day 90 after heterotopic implantation in *P. ursinus*. (A) Low power view newly formed bone across the macroporous spaces. (B,C) Induction of substantial bone formation with prominent vascular invasion induction (*magenta* arrows B,C,G) within the macroporous spaces supporting bone remodelling by osteoclastic activity (E,G) across the newly formed bone (*light blue* arrows. (D,F) Prominent vascular invasion and capillary sprouting with remodelling of solid blocks of newly formed bone across the macroporous spaces of the treated calcium carbonate/hydroxyapatite constructs. Decalcified sections cut at 6 μm stained with Goldner's trichrome. Original magnification: (A) ×2.7; (B, E) ×25; (C) ×47; (D, F) ×3; (G) ×75. (For interpretation of the references to colour in this figure legend, the reader is referred to the web version of this article.)

3.3. *Tissue morphogenesis by hNoggin-treated 7% HA/CC macroporous bioreactors*

hNoggin-treated 7% HA/CC macroporous specimens on day 15 were characterized by very limited fibrovascular tissue invasion which, when present, was only seen at the very periphery of the macroporous constructs (Fig. 8A–C). On day 60 isolated rare fibrovascular bundles were seen occasionally at the very periphery of the macroporous hNoggin-treated specimens with supporting angiogenesis (Fig. 8D–F). On day 60, there was still limited tissue patterning with delayed organization of haphazardly patterned mesenchymal tissue condensations against the macroporous surfaces of the coral-derived constructs (Fig. 8G,H). High power views (Fig. 8I) showed mesenchymal tissue invasion but lack of patterning within the macroporous spaces with lack of bone differentiation (Fig. 8J,K).

On day 90, in spite of some organization of collagenous condensations within the macroporous spaces, there was lack of bone differentiation by induction even in the most peripheral macroporous paces (Fig. 8L–O). hNoggin-treated 7% HA/CC macroporous specimens at all time periods were characterized by a profoundly delayed and limited tissue patterning of collagenous condensations ultimately resulting in limited if any induction of bone formation on day 90 (Fig. 2). This haphazardly altered tissue patterning has also been found in coral-derived macroporous constructs when treated with both the Ca^{++} blocker verapamil hydrochloride and the biphosphonate osteoclast inhibitor zoledronate [29,32]. Both treatment modalities yielded limited or absent induction of bone formation which molecularly is now ascribed to the significant up-regulation of *Noggin* expression. Up-regulation of the *Noggin* gene or the exogenously applied doses of the recombinant hNoggin gene product result in severe delayed tissue patterning with poorly

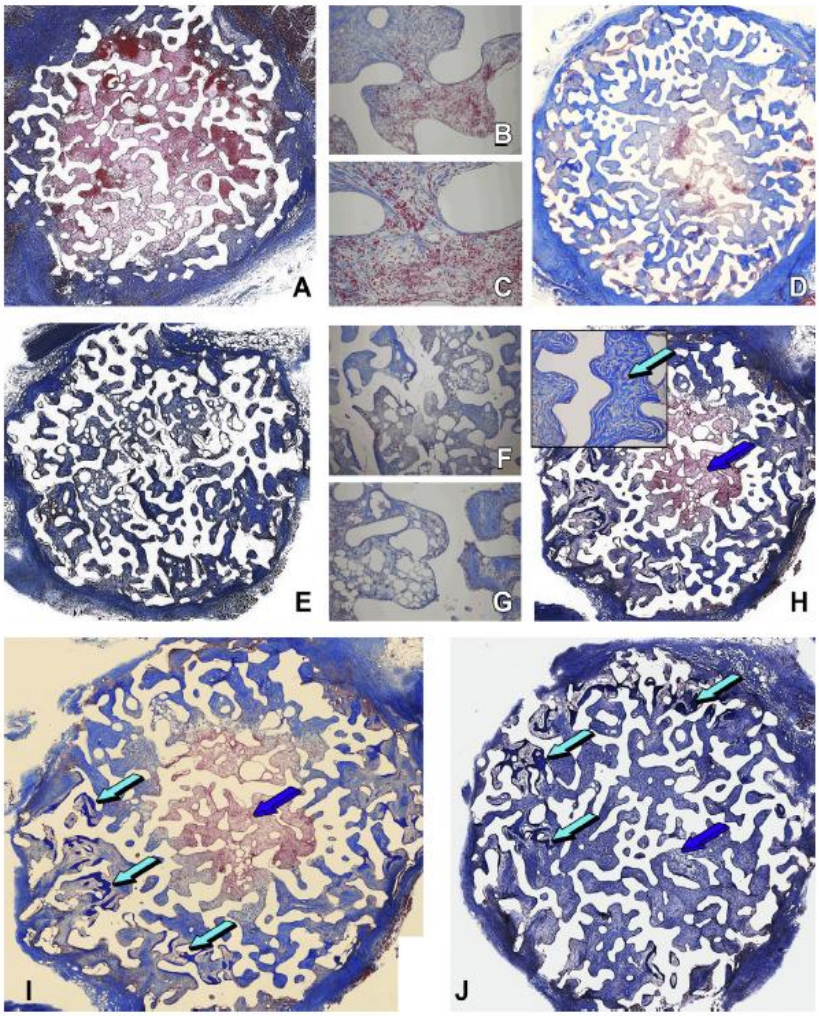


Fig. 7. Tissue morphogenesis by coral-derived macroporous constructs pre-treated by binary applications of 125 μg hTGF-β_3 and 125 μg hNoggin harvested on day 15 (A–C), 60 (D–G) and 90 (H–J) after intramuscular implantation in the *rectus abdominis* muscle of *P. ursinus*. (A) Low power view showing minimal tissue invasion within the most peripheral macroporous spaces (B,C) merging within corpuscolated haematopoietic material. (D–G) As yet limited fibro vascular invasion and mesenchymal tissue patterning of mesenchymal condensations within the macroporous spaces (F,G) in specimens harvested 60 days after heterotopic implantation. (H–J) Incomplete patterning and alignment of collagenous condensations in macroporous constructs harvested on day 90. Minimal if any tissue patterning in the most central areas of hNoggin co-treated specimens showing limited fibro vascular tissue invasion and complete lack of patterned mesenchymal collagenous condensations (*dark blue* arrows in H–J). Incomplete patterned collagenous condensations are shown in H *inset* haphazardly generated within the macroporous spaces with lack of bone differentiation by induction. (I,J) On day 90, limited formation by induction is shown at the periphery of the implanted macroporous constructs only (*light blue* arrows I,J). Decalcified sections cut at 6 μm stained with Goldner's trichrome. Original magnification: (A, D, E, H, I, J) ×2.7; (B, G) ×75; (C) ×125; (F) ×25. (For interpretation of the references to colour in this figure legend, the reader is referred to the web version of this article.)

constructed collagenous condensations so critically important for *de novo* generation of bone within the invaded and patterned macroporous spaces [3,26,33].

3.4. Spontaneous induction of bone formation by untreated control 7% HA/CC macroporous bioreactors

On day 15, untreated control 7% HA/CC macroporous bioreactors (Fig. 9A) showed fibrovascular tissue invasion with cellular and collagenic alignment along the peripheral macroporous surfaces (Fig. 9A,B). As early as day 15, untreated control specimens showed differentiation and tissue patterning of mesenchymal collagenous condensations along the macroporous spaces (Fig. 9B). Fibrovascular tissue invasion blended into haematopoietic corpuscolated material within the more internal macroporous spaces (Fig. 9B). By day 60, there was further remodelling and morphogenesis of collagenous condensation with the induction of bone formation preferentially within concavities of the macroporous constructs (Fig. 9C). By day 90, untreated control 7% HA/CC macroporous bioreactors showed significant induction of bone formation across the macroporous spaces (Fig. 2; Fig. 9D–I) tightly attached to the macroporous substratum supported by still pronounced angiogenesis with remodelling and capillary sprouting (Fig. 9H,I).

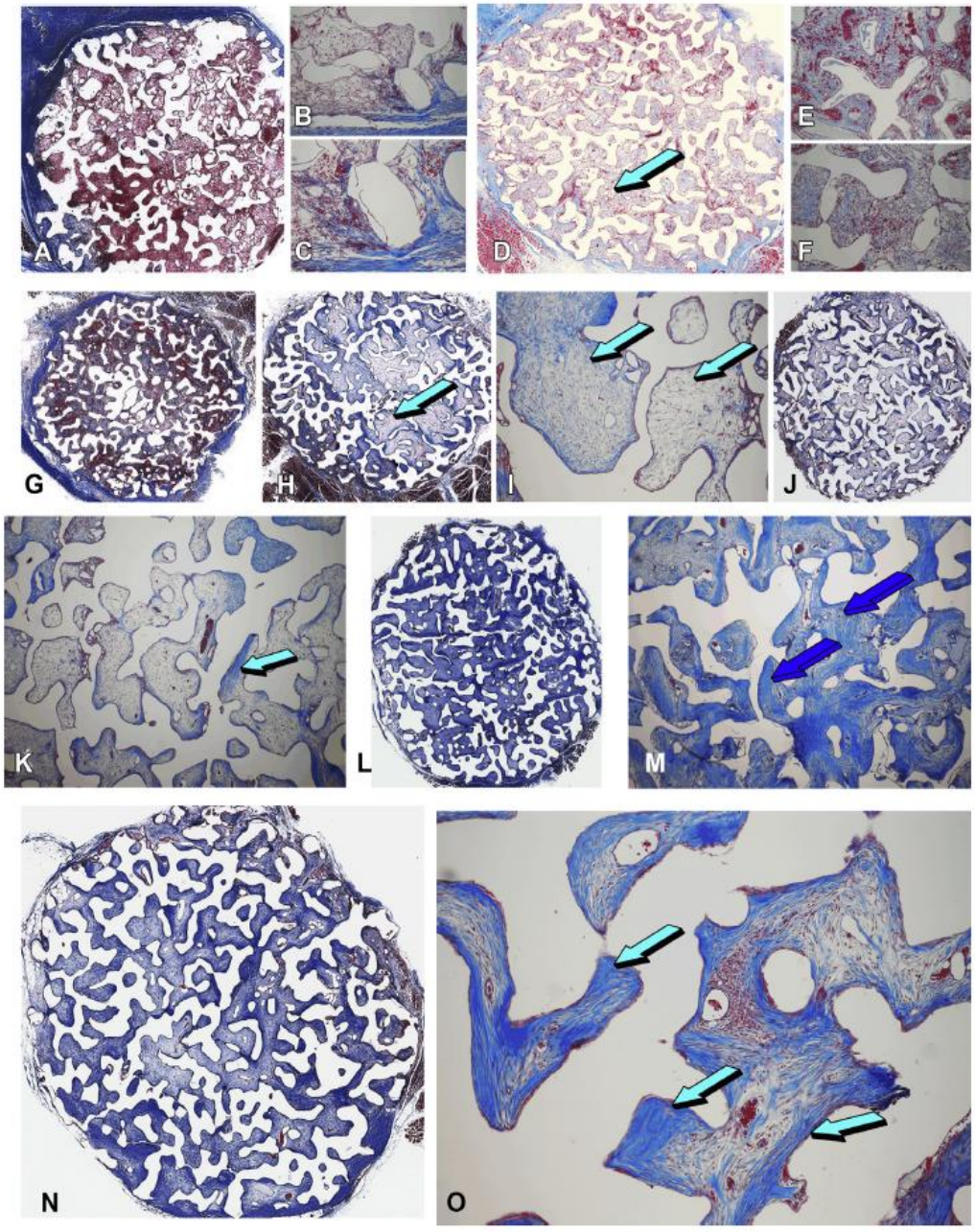


Fig. 8. Tissue morphogenesis by coral-derived macroporous constructs pre-treated by 125 μg hNoggin harvested on day 15 (A–C), 60 (D–K) and 90 (L,M,N,O,J) after intramuscular implantation in the *rectus abdominis* muscle of *P. ursinus*. (A) Low power view showing limited tissue invasion across the macroporous spaces of the treated constructs with minimal fibro vascular invasion even at the most peripheral macroporous spaces (B,C). (D–F) Prominent inhibition of tissue patterning (light blue arrows in D) and fibro vascular tissue invasion within the macroporous spaces of hNohggin-pre-treated constructs (D–F). (G,H,J,K) low power views of hNoggin-treated constructs consistently showing lack fibro vascular invasion as well as tissue patterning against the implanted constructs with sparse tissue invasion and haphazardly generated tissue invasion (I) with lack of connective tissue alignment (light blue arrows H,I) and bone differentiation. On day 60, one specimen only showed some tissue patterning compatible with some organizational degree of collagenous condensations (J,K, light blue arrows K). (L–O) Consistently lack of collagenous condensations patterning and alignment in hNoggin-pre-treated constructs (dark blue and light blue arrows in M,O) correlating to the lack of bone differentiation by induction. Decalcified sections cut at 6 μm stained with Goldner's trichrome. Original magnification: (A, D, G, H, J, L, N) ×2.7; (B, E, I) ×75; (C, F) ×125; (K, M) ×25; (O) ×27. (For interpretation of the references to colour in this figure legend, the reader is referred to the web version of this article.)

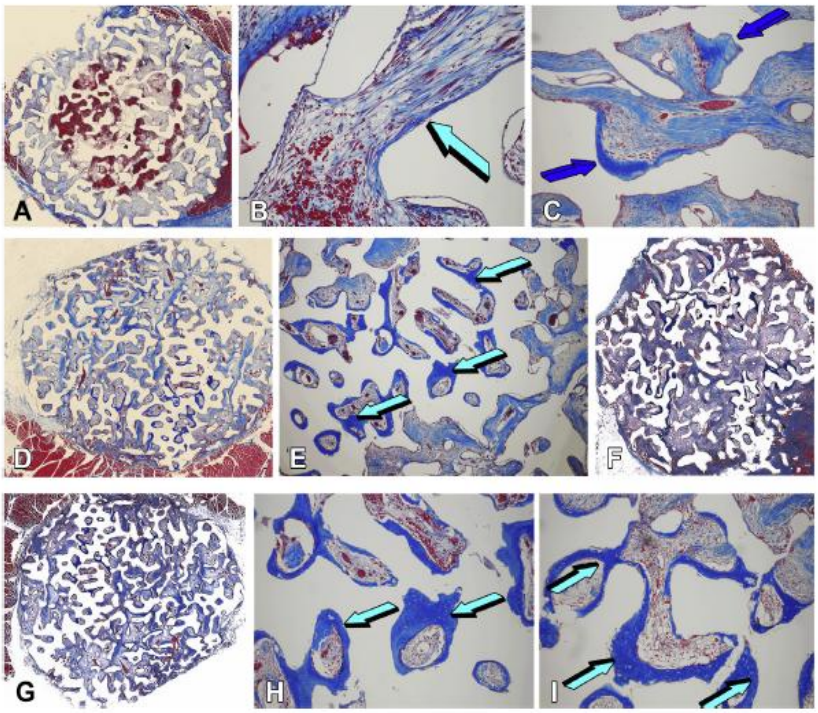


Fig. 9. Induction of bone formation by untreated control macroporous constructs on day 15 (A,B), 60 (C) and 90 (D–I) after intramuscular implantation of coral-derived macroporous bioreactors. (A) Fibro vascular tissue invasion and tissue patterning across the macroporous spaces predominantly at the periphery and internal areas of the implanted macroporous constructs with tissue patterning and alignment of collagenous condensations (light blue arrows B). (C) Induction of bone formation within concavities of the substratum (dark blue arrows C) on day 60 after implantation of the coral-derived macroporous constructs. (D,E,F,G,H,I) Substantial induction of bone formation by coral-derived macroporous constructs implanted in the *rectus abdominis* muscle of *P. ursinus* and harvested on day 90 after intramuscular implantation. Remodelled newly formed bone (light blue arrows E,H,I) supported by still prominent angiogenesis across the macroporous spaces. Decalcified sections cut at 6 μm stained with Goldner's trichrome. Original magnification: (A, D, F, G) ×2.7; (B, C) ×125; (E) ×25; (H, I) ×47. (For interpretation of the references to colour in this figure legend, the reader is referred to the web version of this article.)

3.5. Gene expression analysis by qRT-PCR

Quantitative RT-PCR was performed to monitor the relative change in *BMP-2*, *TGF-β_3*, *Type collagen IV*, *Noggin*, *OC* and *RUNX-2* expression. The results represent a snapshot for the above genes on days 15, 60 and 90 after tissue induction and differentiation within the macroporous spaces of the implanted 7% HA/CC bioreactors. Results are expressed relative to RNA extracted from control muscle tissue harvested adjacent to the site of implantation of the various macroporous constructs. The results have been normalised to 4 control genes (*RPL13a*, *RPLPO*, *SDHA* and *β-actin*) and expressed as $\log_{10} 2^{-\Delta\Delta Ct}$.

Fifteen days after implantation of untreated control 7% HA/CC constructs, *BMP-2* expression was found to be up-regulated relative to the expression observed in normal control muscle tissue (Fig. 10A,C). *BMP-2* expression increases from day 60–90, corresponding to the morphogenesis of bone within the macroporous spaces as evaluated morphometrically (Fig. 2). Gene expression analyses of RNA extracted from 7% HA/CC macroporous constructs treated with 125 μg hNoggin, showed that *BMP-2* expression was down-regulated on day 15 (Fig. 10A, C, D2). Thereafter *BMP-2* expression in hNoggin-treated constructs on day 60 and 90 was found to recover to similar levels to that observed in control bioreactors (Fig. 10A,C,D2).

Quantitative RT-PCR of 7% HA/CC macroporous constructs pre-treated with 125 μg hTGF-β_3, showed a significant reduction of *BMP-2* expression on day 15 (Fig. 10A,B3,C). Over 60 and 90 days there was a significant increase in the expression of *BMP-2* relative to the expression on day 15, such that by day 90, the level of *BMP-2* expression in hTGF-β_3 treated 7% HA/CC bioreactors was similar to that observed in untreated control constructs (Fig. 10A,B3,C). In hTGF-β_3/hNoggin-pretreated constructs, the expression of *BMP-2* on day 15 was significantly down-regulated (Fig. 10C). On day 60, there is a significant increase of *BMP-2* expression relative to day 15 (Fig. 10A,C). By day 90, the levels of *BMP-2* expression recovered to similar levels as recorded in 7% HA/CC treated and untreated macroporous constructs (Fig. 10A,C).

The levels of *TGF-β_3* expression, whilst up-regulated from the normal muscle control tissue, remained at a relatively constant level from day 15 to day 90 in untreated control 7% HA/CC specimens (Fig. 10B1). On day 15, hNoggin-treated bioreactors displayed a marked downregulation of *TGF-β_3* (Fig. 10B2). Of note, this down-regulation is negated by the simultaneous administration of hTGF-β_3 as observed in hTGF-β_3/Noggin pre-treated 7% HA/CC macroporous bioreactors (Fig. 10B4).

From day 15–90, the expression of *Noggin* was down-regulated in untreated control 7% HA/CC macroporous constructs (Fig. 10D1). Of note, an increase in *BMP-2* expression correlated to a decrease in *Noggin* expression, i.e. there was an inverse relationship between the expression of *BMP-2* and *Noggin* (Fig 10D1), further reflecting tissue induction and morphogenesis of bone evaluated morphologically and histomorphometrically (Fig. 2). *Noggin* expression was significantly down-regulated in hTGF-β_3 and hTGF-β_3/hNoggin treated bioreactors on day 60 (Fig. 10D3,D4) relative to untreated

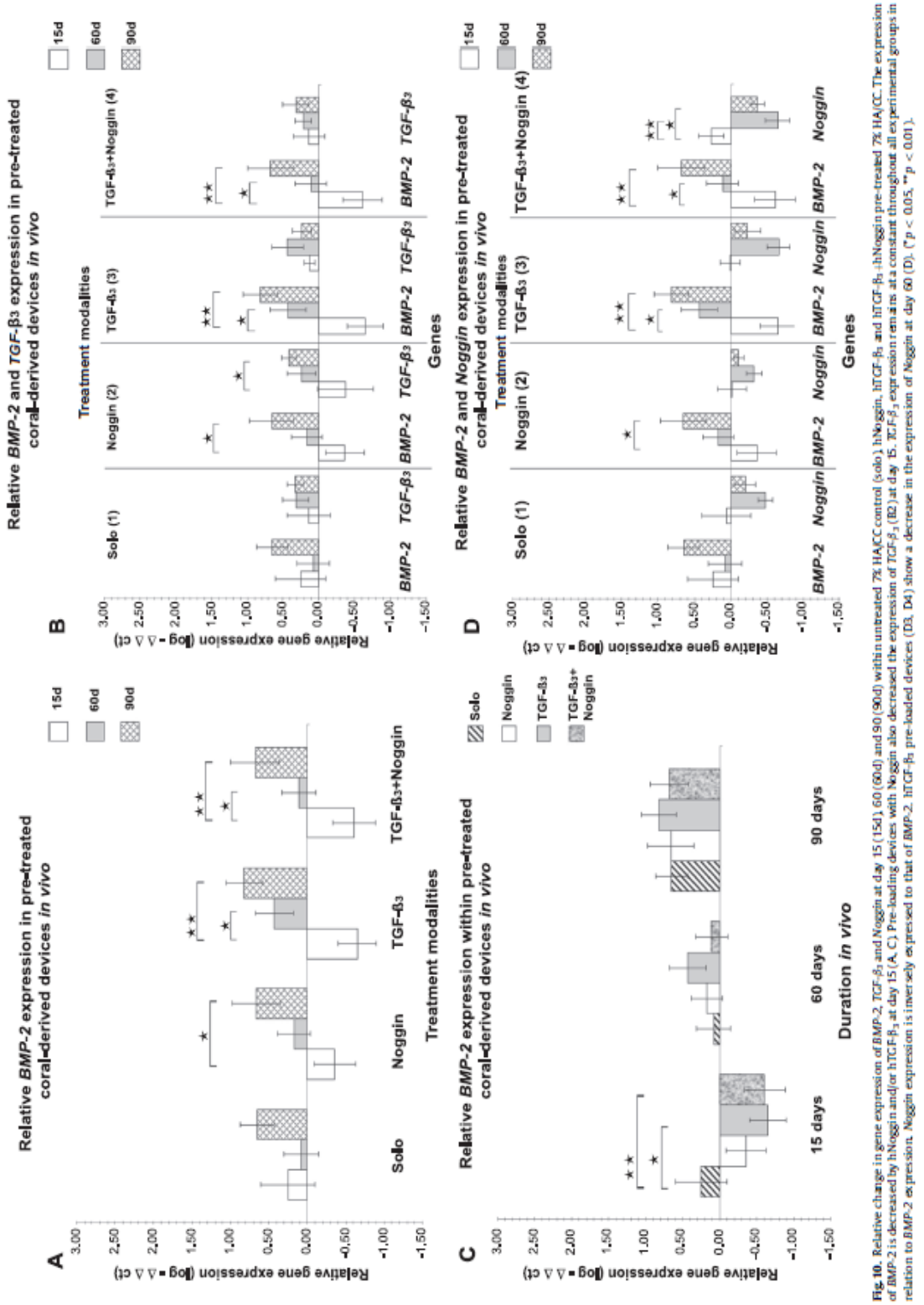


Fig. 10. Relative change in gene expression of *BMP-2*, *TGF-β3* and Noggin at day 15 (15d), 60 (60d) and 90 (90d) within untreated 7% HAC/C control (solo), hNoggin, hTGF-β3 and hTGF-β3 +hNoggin pre-treated 7% HA/CC. The expression of *BMP-2* is decreased by hNoggin and/or hTGF-β3 at day 15 (A, C). Pre-loading devices with Noggin also decreased the expression of TGF-β3 (B2) at day 15. *TGF-β3* expression remains at a constant throughout all experimental groups in relation to *BMP-2* expression. Noggin expression is inversely expressed to that of *BMP-2*. hTGF-β3 pre-loaded devices (D3, D4) show a decrease in the expression of Noggin at day 60 (D). (*$p < 0.05$, **$p < 0.01$).

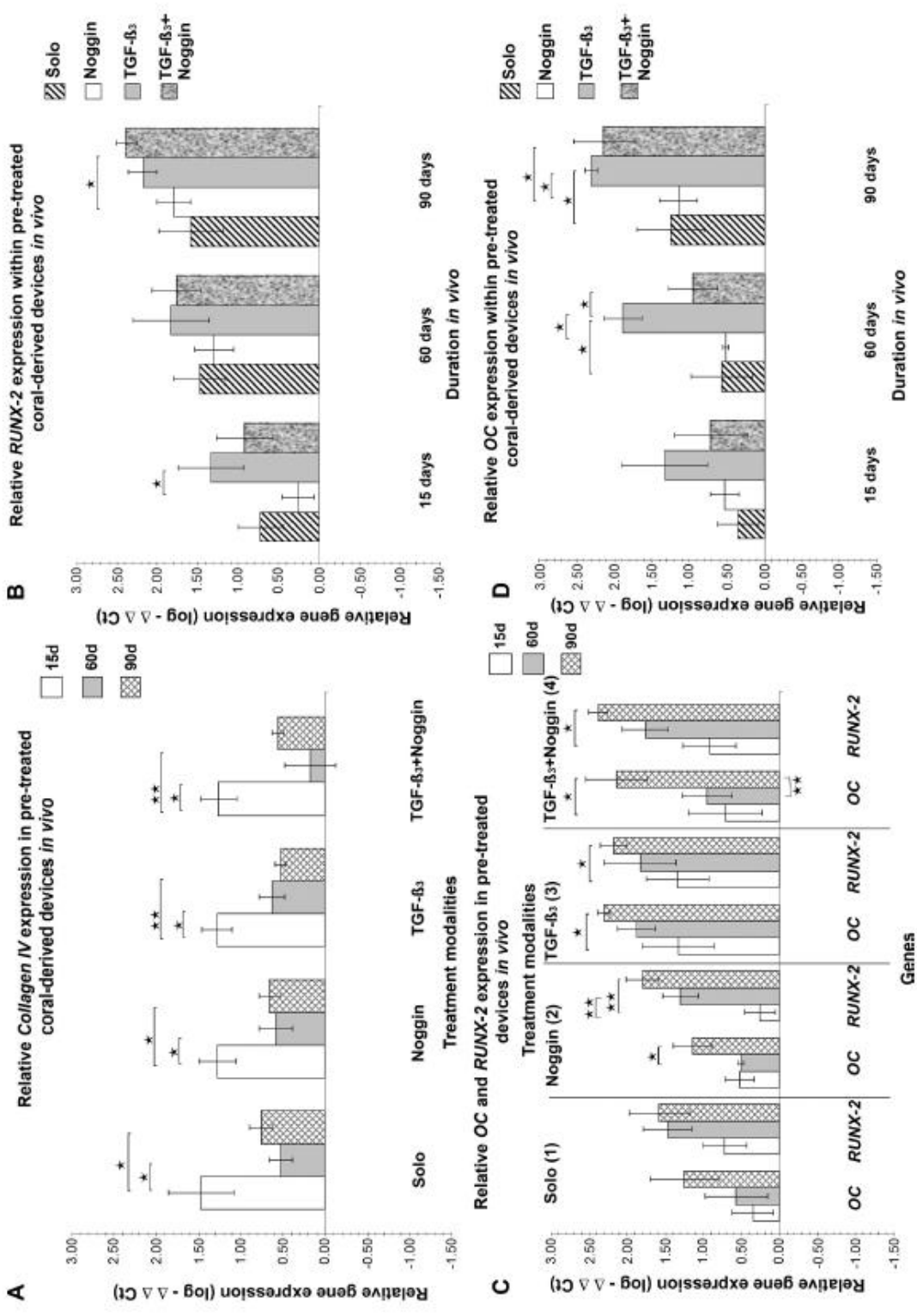


Fig. 11. Relative change in gene expression of type IV collagen, RUNX-2 and Osteocalcin at day 15 (15d), 60 (60d) and 90 (90d) within untreated 7% HA/CC control (solo), hNoggin and/or hTGF-β_3 pre-treated 7% HA/CC. Type IV collagen expression was increased by day 15 in all experimental treatment and control devices after which it decreases by day 60 and 90 (A). Runx-2 and OC increase slowly in expression from day 15–90 in untreated control devices (B, C1, D) showing the progression of bone formation over time. Runx-2 and OC expression was decreased within hNoggin pre-loaded devices and greatly increased within hTGF-β_3 pre-treated devices (B, C2, C3, D). (*$p < 0.05$, **$p < 0.01$).

7% HA/CC control specimens. However, *Noggin* was up-regulated in hTGF-β_3/Noggin constructs on day 15 (Fig. 10D4).

By day 15, *Type IV collagen* expression was up-regulated in untreated control 7% HA/CC macroporous constructs relative to muscle control tissue. (Fig. 11 A). Of interest, *Type IV collagen* expression as observed on day 15 was similar throughout all treatment modalities (Fig. 11A) suggesting that the coral-derived macroporous constructs are *per se* intrinsically angiogenic when implanted in the *rectus abdominis* muscle of *P. ursinus*. There was however a significant decrease in level of *Type IV collagen* expression on day 60 and 90 after heterotopic implantation.

From day 15 through 90 a steady increase of *RUNX-2* and *OC* expression was recorded in untreated control bioreactors (Fig. 11 B). The expression of *RUNX-2* was found to be significantly lower on day 15 in hNoggin treated 7% HA/CC constructs than in the untreated control bioreactors (Fig. 11B1). From day 60–90 there was a recovery in the expression of *RUNX-2* within Noggin treated 7% HA/CC devices (Fig. 11). *RUNX-2* was significantly up-regulated in hTGF-β_3/treated bioreactors on day 15 (Fig. 11B); this up-regulation is maintained throughout days 60 and 90 (Fig. 11B). On day 15, *RUNX-2* expression remained unchanged between hTGF-β_3/hNoggin treated and untreated control bioreactors (Fig. 11B). By day 60 and 90, *RUNX-2* expression reached similar levels in the hTGF-β_3/Noggin, and hTGF-β_3 treated 7% HA/CC constructs (Fig. 11 B, C).

The expression pattern of the *OC* gene, in untreated control 7% HA/CC devices and hNoggin/treated macroporous constructs, were similar, in that both showed an increased expression at subsequent time points (Fig. 11C). hTGF-β_3 treated 7% HA/CC bioreactors showed a highly significant increase in *Osteocalcin* expression, recorded from day 15 to day 90 (Fig. 11C). In hTGF-β_3/hNoggin treated constructs, *OC* showed limited expression on day 15 and 60, with however high expression on day 90 when compared to hTGF-β_3 treated 7% HA/CC macroporous constructs (Fig. 10D4), corresponding to the induction of bone formation on day 90 albeit limited at the periphery of the hTGF-β_3/hNoggin treated macroporous constructs only.

4. Discussion

Understanding gene expression changes during regenerative medicine is vital to unlock the mechanisms that control, recapitulate and induce the regenerative potential of morphogenetic matrices. This study was directed to unravel some of the complexities surrounding the signalling events that occur during the induction of bone formation when hTGF-β_3 treated macroporous bioreactors are implanted in heterotopic intramuscular sites of *P. ursinus*.

In a number of systematic studies in different microenvironments of heterotopic intramuscular and orthotopic craniofacial sites including the *rectus abdominis* muscle, the calvarium, the mandible and periodontal furcation defects, we have shown that primate tissues and microenvironments respond remarkably differently when compared to rodent and lagomorph tissues when implanted in heterotopic sites with identical osteogenic proteins of the TGF-β supergene family [7,19,21]. Our data have shown that the mammalian TGF-β isoforms are determinant of substantial endochondral bone formation by induction in the non-human primate *P. ursinus* [17–20].

Our previous combined data using the three mammalian hTGF-β isoforms have indicated that the TGF-β proteins may act upstream to the bone morphogenetic proteins and may induce the induction of heterotopic bone by expressing BMPs-related gene products ultimately directing the induction of bone formation [17–20]. Northern blot analyses of generated tissue by naturally-derived TGF-β_1 and recombinant hTGF-β_2 show the expression of BMP-3 and OP-1 mRNAs [18,20,34]. This underlies the importance of the BMPs pathway even when molecularly different but related osteogenic proteins induce *de novo* heterotopic bone formation in primate species.

The results of the present study highlight the modulation of *BMP-2* expression together with the down-regulation of *Noggin* correlating with the induction of bone morphogenesis within the heterotopically implanted macroporous bioreactors. The reported data indicate that hTGF-β_3 signalling induces endochondral bone differentiation by regulating *Noggin* expression and BMPs activities, and thus, the induction of bone formation. Indeed, the binary application of hNoggin with equal doses of the hTGF-β_3 protein significantly inhibited the extent of bone formation by induction when compared to coral-derived macroporous bioreactors pre-treated with hTGF-β_3.

Importantly, the addition of the hNoggin protein to the coral-derived macroporous constructs profoundly inhibited the sequential morphogenetic cascade of tissue patterning and alignment of collagenous condensations so critical for the induction of bone formation as initiated by coral-derived macroporous constructs [3,25,26,33]. Indirectly thus, pre-treatment of hNoggin shows that the spontaneous and intrinsic osteoinductivity of coral-derived macroporous constructs is initiated *via* the BMPs pathway during collagenous condensations, alignment and tissue patterning before osteoblastic cell differentiation with expression of BMPs gene products and the deposition of bone as a secondary response [3,33].

The mammalian TGF-β_3 is one of the major regulators of mesenchymal fate choice that control the early stages of osteoblastic cell differentiation [5,35,36]. Members of the TGF-β supergene family, BMPs and TGF-βs isoforms, are critical for the induction, maintenance and expansion of cartilage and bone [2,4,7]. The three mammalian TGF-β isoforms are responsible for the proliferation, early differentiation and commitment of bone progenitors by signalling through Smad2/3 and TAK1-MMK-p38 [36]. Members of the BMP family *via* BMP-2, -4, -5, -6 and -7 are osteogenic inducers [7,37]. At the same time, however, it has been shown that *BMP-2* expression is sufficient for full commitment to osteogenesis [38] and even short term expression of *BMP-2* is sufficient to induce bone formation irreversibly [39].

Our previous and current results have shown that coral-derived macroporous bioreactors initiate the induction of bone formation without exogenously applied BMPs and/or TGF-β isoforms even when implanted in heterotopic intramuscular sites of *P. ursinus* [3,28,33]. Of note, a loss of *BMP-2* signalling would thus result in limited osteogenesis; this is clearly supported by the limited induction of bone formation by 7% HA/CC macroporous constructs pre-treated with hNoggin. Noggin is a known antagonist of BMPs signalling and inhibits the binding of BMP to its receptor [40]. An important as yet unreported observation is the loss of *TGF-β_3* expression on day 15 in macroporous bioreactors pre-treated with hNoggin which further shows the complexities of the relationships of *BMPs* with *TGF-β_3* expression *in vivo*.

BMP-2 signals independently through type I and II BMP and ALK2 receptors to activate the Smad1/5/8 pathway [41]. However, both BMP and TGF-β signals converge to regulate the expression of *RUNX-2*, the master transcriptional regulator of osteogenesis through Dlx5 [42,43]. There is considerable cross talk in the pathways that control bone formation. TGF-β signalling interacts with elements of the Wnt, FGF and the pituitary hormone (PTH) pathways, whilst BMPs interacts with components of the Notch, FGF and Wnt signalling pathways [44,45]. Modulation of the vast pleiotropic activities of BMPs and of the mammalian TGF-β isoforms is highly complex, and several extracellular antagonists regulate the pleiotropic activities of the gene products of the TGF-β supergene family including *Noggin*, *Chordin*, *Cerberus*, and *Gremlin* [46–52].

ARTICLE IN PRESS

It is clear that complex signalling dynamics exist during the induction of bone formation by macroporous bioreactors pre-treated with hTGF-β_3 in *P. ursinus*. The results show that on day 15 in TGF-β_3 pre-treated bioreactors there is down-regulation of *BMP-2*, which is recovered on days 60 and 90. Recent studies [53,54] have made similar observations on the effect of TGF-β on BMP-2 and BMP-7 signalling. It was shown that in cultures of isolated primary human osteoblasts the addition of hTGF-β could completely block BMP-2 and -7 signalling by inhibiting Smad1/5/8 expression [53,54].

The present results indicate that endogenous TGF-β_3 acts upstream to the bone morphogenetic proteins modulating the temporal and spatial patterns of *BMPs* expression and the rate of bone formation by controlling *RUNX-2* and *Osteocalcin* thus affecting cellular differentiation and proliferation pathways of mesenchymal stem cells into the osteoblastic lineage. This is achieved by regulating both inhibitory bone inductive signals, such as Noggin, and promoting osteoblastic cellular differentiation markers *RUNX-2* and *Osteocalcin*, respectively. Firstly BMPs, in context *BMP-2*, induce the formation of bone within the macroporous bioreactors. *TGF-β_3* is then expressed at the same time but at a more constant rate modulating *BMP-2* effect by preventing *Noggin* expression protecting the bone induction cascade from inhibition. Our results clearly show that hTGF-β_3 treated coral-derived bioreactors display a constant decrease in the transcription of *Noggin*, which is further negatively enhanced on day 60 in both hTGF-β_3 and hTGF-β_3/hNoggin pre-treated macroporous constructs.

The results show that hTGF-β_3 controls *RUNX-2* and *Osteocalcin* and thus, as observed by the addition of exogenously applied recombinant protein, there is significant up-regulation of the above osteoblastic cellular differentiation markers on day 15. These data in the non-human primate *P. ursinus* indicate that the dose of the exogenously applied hTGF-β_3 controls the induction of bone formation. In *P. ursinus*, the hTGF-β_3 isoform is a vital component of this process; this is shown by hNoggin pre-treated constructs in which there is a profound down-regulation of osteogenic differentiation markers *RUNX-2* and *Osteocalcin*, together with the loss of *BMP-2* on day 15 corresponding to a profound delay in tissue patterning and morphogenesis with lack of bone differentiation by induction.

The recruitment of responding stem cells is clearly a phenomenon that results in the profound and rapid cascade of bone differentiation by induction when the mammalian hTGF-β_3 isoform, combined with coral-derived macroporous bioreactors, is implanted in the *rectus abdominis* muscle of the non-human primate *P. ursinus*. The available morphological data show that the induction of bone rapidly forms between 15 and 30 days, with osteoblasts multicellularity and vascular invasion with capillary sprouting by day 30 predated by up-regulation of *Collagen type IV*, *RUNX-2* and *Osteocalcin* on day 15. Osteoblasts differentiation, secretion and multicellularity as seen and predicted morphologically between 15 and 30 days are molecularly driven by high expression of *Osteocalcin* but particularly *RUNX-2* on day 15 in hTGF-β_3 treaded macroporous bioreactors.

The images presented in Fig. 3 indicate the extent of structural organization of the extracellular matrix directly modulated by the of hTGF-β_3 isoform. The presented digital images are highly suggestive of hTGF-β_3 reprogramming resident invading recruited myoblastic and/or pericytic/perivascular cells into secreting functionalized osteoblasts by day 15 depositing bone matrix onto patterned extracellular matrix rings induced within the coral-derived macroporous constructs. The induction of advancing extracellular matrix rings within the macroporous bioreactors super activated by the hTGF-β_3 isoform provides structural anchorage for hyper chromatic osteoblastic-like cells reprogrammed by the hTGF-β_3 from invading myoblastic/pericytic cells.

Taken together, these unique morphological results together with up-regulation of *RUNX-2*, a master control gene of osteogenic differentiation [42,43,55], suggest that the 125 μg dose of the hTGF-β_3 protein is successfully reprogramming differentiated myoblastic/pericytic cells into the induction of pluripotent stem cells [56,57] for rapid transformation into active secreting osteoblasts. The essential role of *RUNX-2* in osteoblast differentiation [42,43,55] has been shown in null-mutation mice that had a cartilaginous skeleton with complete absence of osteoblasts [42,55,58]. Transgenic expression of *RUNX-2* in chondrocytes results in heterotopic chondrocytes hypertrophy and endochondral ossification [59]. The induction of chondrocytes hypertrophy and endochondral ossification indicate that *RUNX-2* controls chondrocytes and osteoblast differentiation ultimately regulating the induction of endochondral ossification [42,55,59].

The rapidity of tissue induction and transformation into bone by the hTGF-β_3 protein is further morphologically shown by the induction of bone formation well beyond the perimeter of the implanted macroporous bioreactors with however lack of bone differentiation within the central regions of the coral derived macroporous constructs as shown on day 60. As previously hypothesized using the hTGF-β_1 isoform [17], the extensive osteoinduction surrounding the implanted hTGF-β_3 treated bioreactors could be the result of desorption of the applied morphogen from the coral-derived constructs, as suggested in previous experiments in the non-human primate *P. ursinus* when using insoluble collagenous bone matrix as carrier [17] also for the recombinant human osteogenic protein-1 [22,60], with subsequent diffusion and biological activity into the extracellular space away from the implanted matrices [17,22,60]. Whether such an extended range of action is due to a diffusion gradient or to the initiation of a sequential chain of cellular induction [61,62] cannot be deduced from the available data. The data do however indicate the rapidity of stem cells/responding cells induction into bone long before migrating cells are within the pre-treated bioreactors' macroporous spaces thus transformed into bone when still at the periphery of the implanted bioreactors super activated by the adsorbed hTGF-β_3 signal.

Further molecular and morphological studies are now necessary to precisely resolve the remarkable endochondral osteoinductivity of the hTGF-β_3 isoform in primates only. Our current and previous experiments using the hTGF-β_3 protein in *P. ursinus* have shown rapid and substantial bone induction when hTGF-β_3 reconstituted osteogenic device are implanted in heterotopic intramuscular *rectus abdominis* sites with *BMP-2*, *TGF-β_1*, *TGF-β_3*, *RUNX-2*, *Osteocalcin* and *Type IV collagen* expression, hypercellular osteoblastic activity and capillary sprouting which are now the molecular and morphological basis to rapidly construct bone in clinical contexts [19,63].

The substantial induction of bone formation by 125 μg hTGF-β_3 but particularly the prominent induction of bone by 250 μg hTGF-β_3 by day 20 when combined with coral-derived macroporous bioreactors [64], has been translated in clinical contexts resulting in significant induction of bone formation in a large mandibular defect after hemi-mandibulectomy in a human patient [63,64] now further evaluated by CT-scans 6 months after implantation of the 250 μg hTGF-β_3 osteogenic device.

Finally, mandatory research will have now to be devoted to address the following question: why the mammalian TGF-β_3 induces prominent bone formation when implanted in heterotopic intramuscular sites of the *rectus abdominis* muscle of *P. ursinus* and not when implanted in heterotopic sites of rodents and lagomorphs? Mechanistically, the question raises rather complicated avenues of apparent redundancy of genes and related secreted molecular signals in primate tissues *vs.* rodents and lagomorphs.

Molecular redundancy with associated different biological functions in primate tissues may simply represent the fine tuning of speciation-related molecular evolution in anthropoid apes at the early Pliocene boundary which resulted in a more capable tuning of the bone induction cascade in primate species.

Importantly, a large proportion of molecular evolution across many phylogenies of different clades is associated with speciation events which have prompted the hypothesis that speciation *per se* causes a burst of genetic evolution [65,66] which indeed drives molecular evolution. Alternatively, the heterotopic induction of bone formation in *P. ursinus* as a result of bursts of cladistic evolution is now redundant but yet still activated by high doses of the recombinant morphogen to induce prominent and rapid induction of bone formation.

5. Conclusions

The mammalian TGF-β_3 isoform is a vital constituent of the bone induction cascade in heterotopic sites of the non-human primate *P. ursinus*. The results unequivocally demonstrate that hTGF-β_3 elicits the induction of bone formation by up-regulating endogenous BMP-2 and is blocked by Noggin, a BMP antagonist. The data provocatively suggest a role for hTGF-β_3 in recruiting and reprogramming resident progenitor cells including pericytic/perivascular stem cells into active secreting osteoblasts. The rapid and prominent induction of bone formation has been translated in clinical contexts. The potential manipulation of a pluripotent stem cell *niche* by the heterotopically applied hTGF-β_3 osteogenic device is an exciting avenue of fervent future investigation in the unique model system of bone induction that has been provided by *P. ursinus*.

Acknowledgements

The controversial research on the hTGF-β_3 in *Papio ursinus* and its translation in clinical contexts have been continuously supported by *ad hoc* grants of the Bone Research Laboratory and by a grant from Novartis AG in the late nineties. Aris Economides and Peter ten Dijke are gratefully acknowledged for the kind donation of the recombinant human Noggin and for suggesting the use of the Noggin protein to highlight some the mechanisms of this unique apparent redundancy of soluble molecular signals initiating the induction of bone formation in primate species. The significant help of Barbara van den Heever, Manolis Heliotis, Laura Roden née Yeates and Carlo Ferretti is gratefully acknowledged. A special word of thank to Ruquayya Parak for the histological processing and some of the evaluation, to Caroline Dickens for critical help with the qRT-PCR, and to Mike Ponticiello Biomet USA for the kind supply of the implanted coral-derived macroporous constructs. Hari Reddi significantly contributed by initiating the senior author to the induction of bone formation and by sharply discussing the 2nd last manuscript draft. This paper and the significant efforts of this never ending journey on the hTGF-β_3 isoform are dedicated to the Bone Research Laboratory of the University of the Witwatersrand, Johannesburg.

References

[1] Reddi AH. Bone morphogenesis and modelling: soluble signals sculpt osteosomes in the solid state. Cell 1997;89:159–61.
[2] Reddi AH. Morphogenesis and tissue engineering of bone and cartilage: inductive signals, stem cells, and biomimetic biomaterials. Tissue Eng 2000;6:351–9.
[3] Ripamonti U. Biomimetism, biomimetic matrices and the induction of bone formation. J Cell Mol Med 2009;13:2953–72.
[4] Wozney JM, Rosen V, Celeste AJ, Mitsock LM, Whitters MJ, Kriz RW, et al. Novel regulators of bone formation: molecular clones and activities. Science 1988;242:1528–34.
[5] ten Dijke P, Iwata KK, Goddard C, Pieter C, Canalis E, McCarthy TL, et al. Recombinant transforming growth factor type beta 3: biological activities and receptor-binding properties in isolated bone cells. Mol Cell Biol 1990;10:4473–9.
[6] Massagué J. How cells read TGF-β signals. Nat Rev Mol Cell Biol 2000;3:169–78.
[7] Ripamonti U. Soluble osteogenic molecular signals and the induction of bone formation. Biomaterials 2006;27:807–22.
[8] Balooch G, Balooch M, Nalla RK, Schilling S, Filvaroff EH, Marshal GW, et al. TGFβ regulates the mechanical properties and composition of bone matrix. Proc Natl Acad Sci U S A 2005;102:18813–8.
[9] Spagnoli A, O'Rear L, Chandler RL, Granero-Molto F, Mortlock DP, Gorska AE, et al. TGF-β signalling is essential for joint morphogenesis. J Cell Biol 2007;177:1105–17.
[10] Roberts AB, Sporn MB, Assoian RK, Smith JM, Roche NS, Wakefield LM, et al. Transforming growth factor type β: rapid induction of fibrosis and angiogenesis *in vivo* and stimulation of collagen formation *in vitro*. Proc Natl Acad Sci U S A 1986;83:4167–71.
[11] Saadeh PB, Mehrara BJ, Steinbrech DS, Dudziak ME, Greenwald JA, Luchs JS, et al. Transforming growth factor-β_1 modulates the expression of vascular endothelial growth factor by osteoblasts. Am J Phys 1999;277:C628–37.
[12] Sampath TK, Muthukumaran N, Reddi AH. Isolation of osteogenin, an extracellular matrix-associated, bone-inductive protein, by heparin affinity chromatography. Proc Natl Acad Sci U S A 1987;84:7109–13.
[13] Hammonds RG, Schwall R, Dudley A, Berkemeier L, Lai C, Lee J, et al. Bone inducing activity of mature BMP-2b produced from a hybrid BMP-2a/2b precursor. Mol Endocrinol 1991;5:149–55.
[14] Shinozaki M, Kawara S, Hayashi N, Kakinuma T, Igarashi A, Takehara K. Induction of subcutaneous tissue fibrosis in newborn mice by transforming growth factor β-simultaneous application with basic fibroblast growth factor causes persistent fibrosis. Biochem Biophys Res Commun 1997;240:292–7.
[15] Shah M, Foreman DM, Ferguson MW. Neutralisation of TGF-β1 and TGF-β2 or exogenous addition of TGF-β3 to cutaneous rat wounds reduces scarring. J Cell Sci 1995;108:985–1002.
[16] Ripamonti U, Ramoshebi LN, Patton J, Matsaba T, Teare J, Renton L. Soluble signals and insoluble substrata: novel molecular cues instructing the induction of bone. In: Massaro EJ, Rogers JM, editors. The skeleton. New York: Humana Press; 2004. pp. 217–27.
[17] Ripamonti U, Duneas N, van den Heever B, Bosch C, Crooks J. Recombinant transforming growth factor-β_1 induces endochondral bone in the baboon and synergizes with recombinant osteogenic protein-1 (bone morphogenetic protein-7) to initiate rapid bone formation. J Bone Miner Res 1997;2:1584–95.
[18] Ripamonti U, Crooks J, Matsaba T, Taskar J. Induction of endochondral bone formation by recombinant human transforming growth factor-β_2 in the baboon (*Papio ursinus*). Growth Factors 2000;17:269–85.
[19] Ripamonti U, Ramoshebi LN, Teare J, Renton L, Ferretti C. The induction of endochondral bone formation by transforming growth factor-β_3: experimental studies in the non-human primate *Papio ursinus*. J Cell Mol Med 2008;12:1029–48.
[20] Ripamonti U, Roden LC. The induction of bone formation by transforming growth factor-β_2 in the non-human primate *Papio ursinus* and its modulation by skeletal muscle responding stem cells. Cell Prolif 2010;43:207–18.
[21] Ripamonti U, Ferretti C, Teare J, Blann L. Transforming growth factor-β isoforms and the induction of bone formation: Implications for reconstructive craniofacial surgery. J Craniofac Surg 2009;20:1544–55.
[22] Ripamonti U, Van Den Heever B, Crooks J, Tucker MM, Sampath TK, Rueger DC, et al. Long-term evaluation of bone formation by osteogenic protein 1 in the baboon and relative efficacy of bone-derived bone morphogenetic proteins delivered by irradiated xenogeneic collagenous matrices. J Bone Miner Res 2000;9:1798–809.
[23] Ripamonti U. Osteogenic proteins of the transforming growth factor-β superfamily. In: Henry HL, Norman AW, editors. Encyclopaedia of hormones. Texas: Austin Academic Press; 2003. pp. 80–6.
[24] Ripamonti U. Bone induction by recombinant human osteogenic protein-1 (hOP-1, BMP-7) in the primate *Papio ursinus* with expression of mRNA of gene products of the TGF-β superfamily. J Cell Mol Med 2005;9:911–28.
[25] Ripamonti U. Inductive bone matrix and porous hydroxyapatite composites in rodents and non-human primates. In: Yamamuro T, Wilson-Hench J, Hench LL, editors. Handbook of bioactive ceramics, calcium phosphate and hydroxylapatite ceramics, vol. II. Florida: CRC Press; 1990. pp. 245–53.
[26] Ripamonti U. The morphogenesis of bone in replicas of porous hydroxyapatite obtained from conversion of calcium carbonate exoskeletons of coral. J Bone Joint Surg Am 1991;73:692–703.
[27] Shors EC. Coralline bone graft substitutes. Orthop Clin North Am 1999;30:599–613.
[28] Ripamonti U, Crooks J, Khoali L, Roden L. The induction of bone formation by coral-derived calcium carbonate/hydroxyapatite constructs. Biomaterials 2009;30:1428–39.
[29] Ripamonti U, Klar RM, Renton LF, Ferretti C. Synergistic induction of bone formation by hOP-1, hTGF-β3 and inhibition by zoledronate in macroporous coral-derived hydroxyapatites. Biomaterials 2010;31:6400–10.
[30] Schnitzler CM, Ripamonti U, Mesquita JM. Histomorphometry of iliac crest trabecular bone in adult male baboons in captivity. Calcif Tissue Int 1993;52:447–54.

ARTICLE IN PRESS

[31] Public Service Department. National code for animal use in research education, diagnosis and testing of drugs and related substances in South Africa. Pretoria, South Africa: Public Service Department; 1990.

[32] Klar RM, Duarte R, Dix-Peek T, Dickens C, Ferretti C, Ripamonti U. Calcium ions and osteoclastogenesis initiate the induction of bone formation by coral-derived macroporous constructs. J Cell Mol Med 2013. http://dx.doi.org/10.1111/jcmm.12125.

[33] Ripamonti U, van Den Heever B, van Wyk J. Expression of the osteogenic phenotype in porous hydroxyapatite implanted extraskeletally in baboons. Matrix 1993;13:491–502.

[34] Duneas N, Crooks J, Ripamonti U. Transforming growth factor-β_1: induction of bone morphogenetic protein genes expression during endochondral bone formation in the baboon, and synergistic interaction with osteogenic protein-1 (BMP-7). Growth Factors 1998;15:259–77.

[35] Shi Y, Massagué J. Mechanisms of TGF-β signaling from cell membrane to the nucleus. Cell 2003;113:685–700.

[36] Matsunobu T, Torigoe K, Ishikawa M, de Vega S, Kulkarni AB, Iwamoto Y, et al. Critical roles of the TGF-β type I receptor ALK5 in perichondrial formation and function, cartilage integrity, and osteoblast differentiation during growth plate development. Dev Biol 2009;2:325–38.

[37] Bandyopadhyay A, Tsuji K, Cox K, Harfe BD, Rosen V, Tabin CJ. Genetic analysis of the roles of BMP2, BMP4, and BMP7 in limb patterning and skeletogenesis. PLoS Genet 2006;12:e216.

[38] Huang Z, Ren PG, Ma T, Smith RL, Goodman SB. Modulating osteogenesis of mesenchymal stem cells by modifying growth factor availability. Cytokine 2010;51:305–10.

[39] Noel D, Gazit D, Bouquet C, Apparailly F, Bony C, Plence P, et al. Short-term BMP-2 expression is sufficient for *in vivo* osteochondral differentiation of mesenchymal stem cells. Stem Cells 2004;22:74–85.

[40] Zimmerman LB, De Jesus-Escobar JM, Harland RM. The Spemann organizer signal noggin binds and inactivates bone morphogenetic protein 4. Cell 1996;96:599–606.

[41] Zhou Z, Xie J, Lee D, Liu Y, Jung J, Zhou L, et al. Neogenin regulation of BMP-induced canonical Smad signaling and endochondral bone formation. Dev Cell 2010;19:90–102.

[42] Ducy P, Zhang R, Geoffroy V, Ridall AL, Karsenty G. Osf2/Cbfa1: a transcriptional activator of osteoblast differentiation. Cell 1997;89:747–54.

[43] Pretheeban T, Lemos DR, Paylor B, Zhang RH, Rossi FM. Role of stem/progenitor cells in reparative disorders. Fibrogenesis Tissue Repair 2012;5:1–20.

[44] De Robertis EM. Evo-Devo: the merging of evolutionary and developmental biology. In: The scientific legacy of the 20th centuryPontif Acad Sci Acta, vol. 21; 2011. pp. 221–35.

[45] Chen G, Deng C, Li YP. TGF-β and BMP signaling in osteoblast differentiation and bone formation. Int J Biol Sci 2012;8:272–88.

[46] Miyazono K, Kusanagi K, Inoue H. Divergence and convergence of TGF-β/BMP signaling. J Cell Physiol 2001;187:265–76.

[47] Heldin CH, Miyazono K, ten Dijke P. TGF-β signalling from cell membrane to nucleus through SMAD proteins. Nature 1997;390:465–71.

[48] Miyazono K, ten Dijke P, Heldin CH. TGF-β signaling by Smad proteins. Adv Immunol 2000;75:115–57.

[49] Miyazono K. Positive and negative regulation of TGF-β signaling. J Cell Sci 2000;113:1101–9.

[50] Cooper GM, Usas A, Olshanski A, Mooney MP, Losee JE, Huard J. Ex vivo Noggin gene therapy inhibits bone formation in a mouse model of postoperative resynostosis. Plast Reconstr Surg 2009;123:94S–103S.

[51] Onichtchouk D, Chen YG, Dosch R, Gawantka V, Delius H, Massagué J, et al. Silencing of TGF-beta signalling by the pseudoreceptor BAMBI. Nature 1999;401:480–5.

[52] Gazzerro E, Smerdel-Ramoya A, Zanotti S, Stadmeyer L, Durant D, Economides AN, et al. Conditional deletion of gremlin causes a transient increase in bone formation and bone mass. J Biol Chem 2007;282:31549–57.

[53] Ehnert S, Baur J, Schmitt A, Neumaier M, Lucke M, Dooley S, et al. TGF-β_1 as possible link between loss of bone mineral density and chronic inflammation. PLoS One 2010;5:e14073.

[54] Ehnert S, Zhao J, Pscherer S, Freude T, Dooley S, Kolk A, et al. Transforming growth factor β_1 inhibits bone morphogenic protein (BMP)-2 and BMP-7 signaling *via* upregulation of Ski-related novel protein N (SnoN): possible mechanism for the failure of BMP therapy? BMC Med 2012;10:101.

[55] Komori T, Yagi H, Nomura S, Yamaguchi A, Sasaki K, Deguchi K, et al. Targeted disruption of Cbfa1 results in a complete lack of bone formation owing to maturational arrest of osteoblasts. Cell 1997;89:755–64.

[56] Takahashi K, Yamanaka S. Induction of pluripotent stem cells from mouse embryonic and adult fibroblast cultures by defined factors. Cell 2006;126:663–76.

[57] Takahashi K, Tanabe K, Ohnuki M, Narita M, Ichisaka T, Tomoda K, et al. Induction of pluripotent stem cells from adult human fibroblasts by defined factors. Cell 2007;131:1–12.

[58] Harada S, Rodan GA. Control of osteoblast function and regulation of bone mass. Nature 2003;423:349–55.

[59] Takeda S, Bonnamy JP, Owen MJ, Ducy P, Karsenty G. Continuous expression of Cbfa1 in non-hypertrophic chondrocytes uncovers its ability to induce hypertrophic chondrocyte differentiation and partially rescues Cbfa1-deficient mice. Genes Dev 2001;15:467–81.

[60] Ripamonti U, van den Heever B, Sampath TK, Tucker MM, Rueger DC, Reddi AH. Complete regeneration of bone in the baboon by recombinant human osteogenic protein-1 (hOP-1, bone morphogenetic protein-7). Growth Factors 1996;13:273–89.

[61] Slack JMW. Morphogenetic gradients – past and present. Trends Biochem 1987;12:200–4.

[62] Lander AD. Morpheus unbound: reimagining the morphogen gradient. Cell 2007;128:245–56.

[63] Ripamonti U, Ferretti C. Grand challenges for craniomandibularfacialreconstruction by human recombinant transforming growth fac tor-β_3. In: Tuan RS, Guilak F, Atala A, editors. Keystone symposia on regenerative tissue engineering. Breckenridge CO. http://www.keystonesymposia.org; 2012.

[64] Ripamonti U, Teare J, Ferretti C. A macroporous bioreactor super activated by the recombinant human transforming growth factor-β3. Front Physiol 2012;3:1–18.

[65] Webster AJ, Payne RJH, Pagel M. Molecular phylogenies link rates of evolution and speciation. Science 2003;301:478.

[66] Ezard THG, Thomas GH, Purvis A. Inclusion of a near-complete fossil record reveals speciation-related molecular evolution. Methods Ecol Evol 2013;4:745–53.

CHAPTER 6

SUMMARISING DISCUSSION

6.1 A compositional standard for bone inductive biomaterials

Coral-derived macroporous biomimetic matrices have emerged to be an effective biomaterial capable of autoinducing bone formation. Results of this study (Ripamonti *et al.* 2010 (**Chapter 3**); Klar *et al.* 2013 (**Chapter 4**); Klar *et al.* 2014 (**Chapter 5**) have unraveled some of the cellular and molecular mechanisms underlying the induction of bone formation when macroporous bioreactors are implanted in heterotopic intramuscular sites of *Papio ursinus*.

The intrinsic nature of the implanted biomatrices with its lacunae and concavities, which are further enhanced by osteoclastogenesis, in combination with Ca^{2+} release, are compelling morphogenic and ionic signals that promote the induction of bone formation (Klar *et al*. 2013). Residing stem cells are induced to differentiate along the osteoblastic lineage by Ca^{2+} release within the macroporous spaces after modification of the surface of the implanted device by osteoclasts (McNamara *et al.* 2010; Ripamonti *et al*. 2010; Wilkinson *et al.* 2011).

As previous observations by Ripamonti *et al.* (Ripamonti 1990; Ripamonti 1991; Ripamonti *et al*. 1993; Ripamonti 2006) have shown, blood vessel and connective tissue formation and invasion occurs prior to the onset of bone formation. Prominent angiogenesis was supported in the present study by the observation that *Collagen type IV* was highly expressed at day 15 (Klar *et al.* 2013; Klar *et al*. 2014) in all samples. Type IV collagen is critical for the development of basement membrane in sprouting and invading capillaries (Reddi 2000). Once the foundation of collagenous condensation has been established, what follows is a systematic sequence of developmental processes triggered by

changes in the expression of key genes that promote the bone differentiation cascade, particularly the *BMPs* (Huang *et al.* 2010).

As shown by Klar *et al.* (2013), important chemical and cellular cues are required to set into motion the induction of bone formation within the implanted coral-derived macroporous constructs. Klar *et al.* (2013) have demonstrated that osteoclastogenesis and Ca^{2+} plays an important role in establishing and maintaining the various signalling and expression pathways required to induce bone formation.

Monocytes/macrophages differentiate into osteoclasts as they come in to contact with the Ca^{2+} which is released from the hydroxyapatite and calcium carbonate based biomimetic constructs when it is implanted in the acidic microenvironment of the surgical healing wound of the heterotopic intramuscular pouch (Kanatani *et al.* 1991, Müller *et al.* 2008). It is known that without topographical geometric alterations by the osteoclasts, in the shape of macro and micro-concavities, bone formation may be inhibited (Ripamonti *et al.* 1999; Ripamonti 2004; Ripamonti *et al*. 2009; Ripamonti *et al.* 2010). In addition osteoclasts also release Ca^{2+} (Teitelbaum, 2000), which then triggers a cascade of cellular events including osteoblastogenesis which deposits new bone matrix in the excavated concavities. However the present research also demonstrates that osteoclastogenesis exerts gene expression changes and indicates how subtle changes in this process can affect bone formation within the converted calcium carbonate derived devices (Klar *et al.* 2013).

The loss in osteoclast binding due to zoledronate treatment of samples results in a temporary upregulation of *Noggin* at day 15 when compared to the untreated control samples and this corresponded morphologically to a delay in the formation of bone (Klar *et*

al. 2013). In addition to the upregulation of *Noggin* there is minimal expression of *BMP-2.* Noggin is known to prevent BMP binding to the BMP receptor (BMPR) (Zimmerman *et al.* 1996) and thereby inhibits bone formation by altering downstream signalling pathways.

A possible mechanism for the observed upregulation of *Noggin* has been proposed based on the findings of Wei and Wan (2013) that have shown that osteoclasts display the peroxisome proliferator- activated gamma receptor ($PPA_{\gamma}R$). $PPA_{\gamma}R$ is activated when osteoclasts bind to their respective surface material (Wei and Wan 2013) and prevents the activation of the downstream acting transcription factor β-catenin (Wei and Wan 2013). B-catenin is a known activator of *Noggin* expression (Domingos *et al*. 2001). Thus $PPA_{\gamma}R$ activation through osteoclast binding would lead to the downregulation of Noggin. Inversely if $PPA_{\gamma}R$ is not activated, because osteoclasts are prevented from binding, it would lead to β-catenin activation and hence increased *Noggin* expression. Indeed this deduction helps explains why in Klar *et al.* (2013) *Noggin* expression was increased. Lack of osteoclast binding produces an activation of β-catenin resulting in increased gene expression levels of *Noggin* and thus the inhibition of bone formation.

When the L-type voltage gated ion channel for calcium was blocked by the preloading of the macroporous constructs with verapamil, bone formation within coral-derived devices was scant as observed by morphological and histomorphometric analysis (Klar *et al.* 2013). Whilst tissue patterning was not as disorganized or delayed as in the zometa-treated samples, at the molecular level there was the reduced expression in *BMP-2* and the significant upregulation of *Noggin* at day 15. The qRT-PCR results show that in the absence of Ca^{2+}, gene expression is greatly affected. *In vitro* studies performed by Bais *et*

al. (2009) supported these current findings. The alteration in gene expression profiles as a result of the Ca^{2+} modulation is a possible explanation why bone formation was so affected within coral-derived macroporous constructs pre-treated with Verapamil.

There are a number of signal transduction pathways that affect bone formation by mediating cell differentiation into either osteoclast or osteoblasts (**Fig. 1**). Monocytes/macrophages are known to differentiate into osteoclasts when the receptor activator of nuclear factor-κB ligand (RANK-L) binds to the RANK receptor (Dougall *et al.* 1999; Ducy *et al.* 1997) ultimately resulting in the expression of *BMPs* (Csiszar *et al.* 2005). As BMPs are released from osteoclasts they attach to the BMPRI and II receptors on pericytes causing these to differentiate into osteoblasts (Zhao *et al.* 2009) and begin depositing new bone. In osteoblasts, the cAMP response element-binding protein (CREB)-transcription factor is activated by cyclic adenosine monophosphate (cAMP) (Zhang *et al.* 2011), as initiated by BMPs, which then transcribes various genes including *BMP-2* (Zhang *et al.* 2011). However when investigating these pathways it was found that both the RANK-L pathway and BMP-cAMP-CREB pathway require Ca^{2+}. RANK-L, through various signalling intermediaries activates the downstream effector nuclear factor kappa B (NF-κB). For this transcription factor to successfully activate the transcription of relevant genes, including *BMP-2*, and hence affect the differentiation of osteoclasts, it is required to form a complex with the Nuclear factor of activated T-cells cytoplasmic 1 ($NFAT_{C1}$). $NFAT_{C1}$ is the downstream phosphorylated protein activated from the successful activation of calmodulin by Ca^{2+}. Calmodulin is only activated provided there is sufficient Ca^{2+} present in the cytoplasm of the cell as was shown by Zyzafoon (2009).

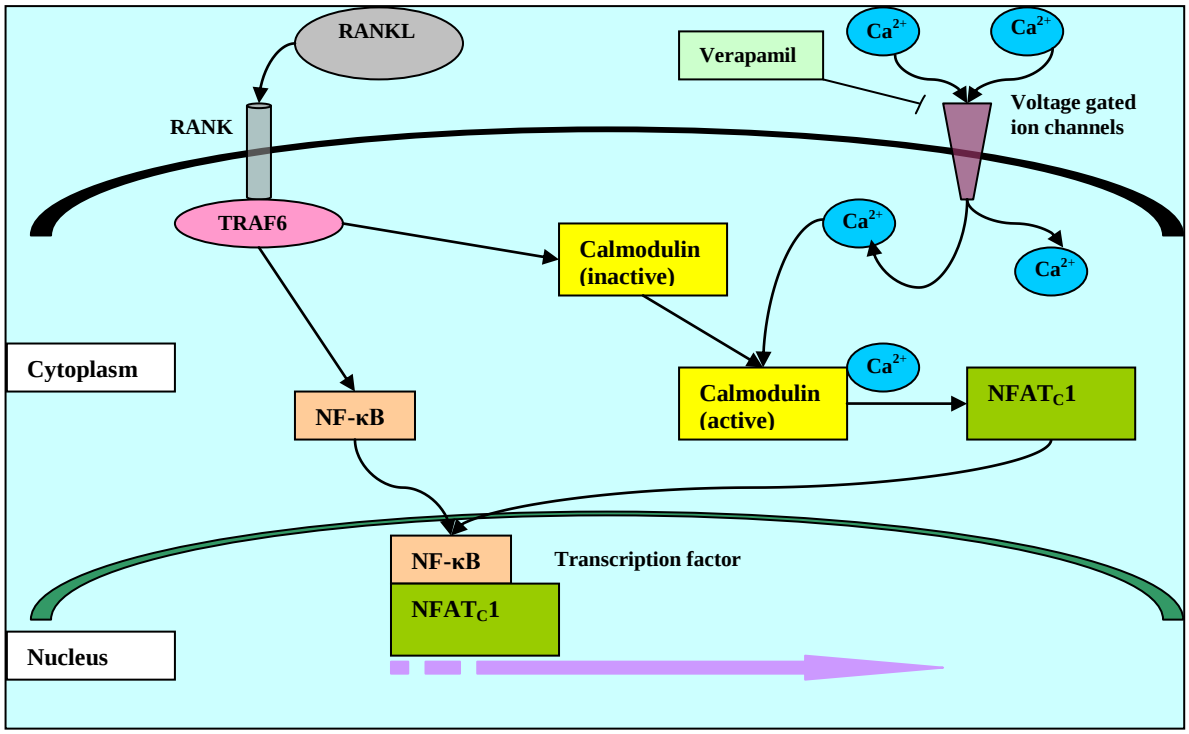


Figure 1. The RANK/RANKL pathway. RANKL binds and activates RANK receptor, which activates the formation of the NF-κB and inactive calmodulin. Calmodulin becomes fully active only when calcium binds to it. Calmodulin activates $NFAT_C1$ which in turn forms the transcriptional complex with NF-κB. This transcription factor then activates various gene targets. (Constructed from material provided in Dougall *et al*. 1999; Cisiszar *et al*. 2009, Zyzafoon 2009; Zhang *et al*. 2011).

Osteoblast differentiation (**Fig. 2**) and its accompanying gene expression program rely on the successful activation of cAMP. cAMP requires phosphorylation via a downstream activated kinase, through the successful activation of a membrane bound receptor, the BMPR. Furthermore, cAMP requires that the concentration of calcium ions within the cytosol of these cells be sufficient (Barbado *et al.* 2009). If the Ca^{2+} is too low within the cytosol it prevents the activation of cAMP even when cAMP has been phosphorylated (Barbado *et al.* 2009). If cAMP is successfully activated the CREB transcription factor is phosphorylated permitting the expression of genes and especially that of *BMP-2*. A loss in *BMP-2* expression prevent bone formation (Bais *et al.* 2009) as BMPs have long been

shown to be involved in the induction of bone formation (Wang *et al.* 1988; Wang *et al.* 1990; Reddi 2000; Ripamonti 2006).

Results of the present study clearly reiterate this, as a decrease in calcium ion migration in verapamil treated bioreactors reduced the level of *BMP-2* expression which culminated in reduced bone formation by induction. The expression of *BMP-2* seems to be able to maintain the differentiation of both osteoblasts and osteoclasts (Klar *et al.* 2013), only if there is sufficient Ca^{2+} within the cytosol of target cells. Hence the findings points to the importance of Ca^{2+} not just for the formation of new bone, but for cellular differentiation and for the successful signaling of *BMP* responsive pathways required for bone formation.

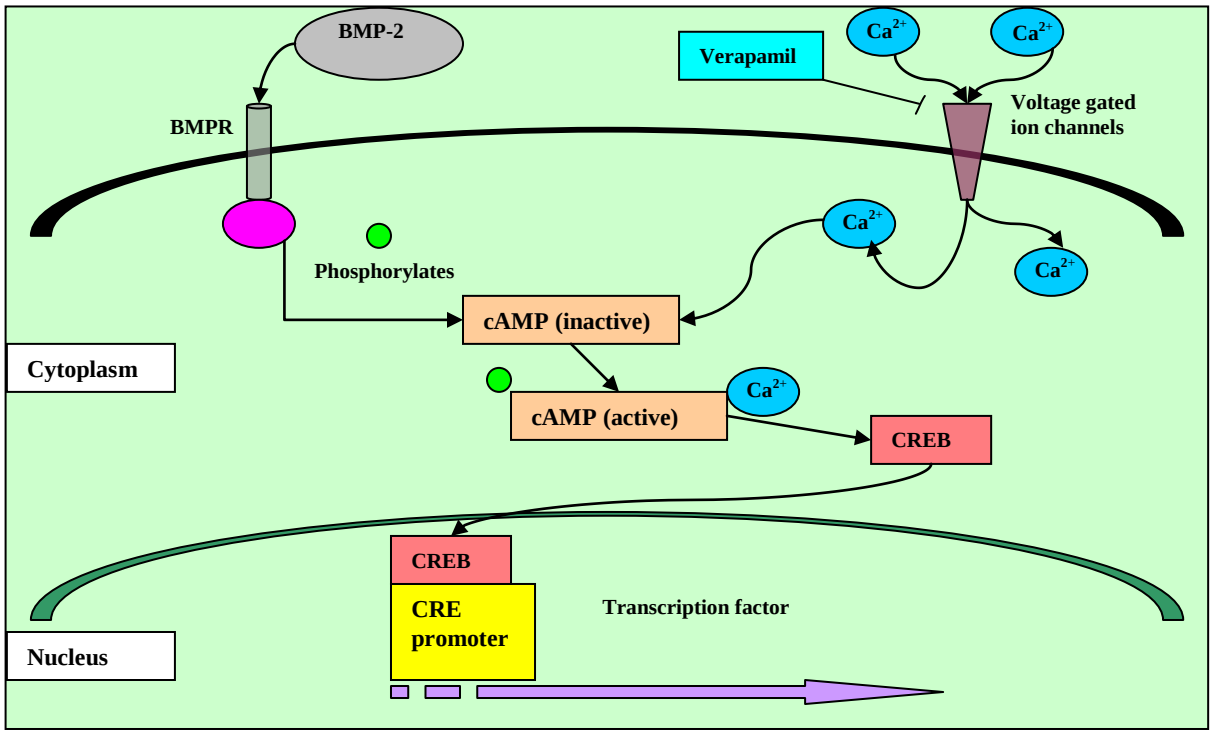


Figure 2. The BMP-2 – cAMP – CREB pathway. cAMP pathway is activated upon BMP-2 binding to the BMP receptor (BMPR). This association phosphorylates and activates cAMP. Only in the presence of calcium ions does cAMP become fully active. cAMP then actives CREB which in turn forms binds CRE promoter elements of CRE responsive genes. (Constructed from material provided in Barbado *et al*. 2009; Bais *et al*. 2009)

Ripamonti *et al.* 2010 and Klar *et al.* (2013) have shown the importance of calcium ions and osteoclasts within the bone induction cascade as initiated by implantation of coral-derived macroporous constructs.

A subsequent interesting phenomenon observed in all the studies using coral-derived macroporous constructs was that the induction of bone formation within coral-derived macroporous constructs occurs *via* the intramembraneous ossification process (Ripamonti *et al.* 2010; *Klar et al*. 2013) instead of progressing through a cartilage anlage as is the case for endochondral bone formation (Gilbert 2000). This trend seems to be conserved throughout all experiments that involve biomimetic osteoinductive devices and furthermore is not restricted to the site of implantation (Habibovic *et al* 2006). Why bone formation takes the direct route of bone formation instead of the cartilaginous pathway is still unclear. Perhaps, as Ripamonti (1991; Ripamonti 1993) suggested, it may be because of mesenchymal condensation at the hydroxyapatite interface that prevent cartilage formation, instead favoring direct ossification; or as the present study also showed, especially through the extensive *Collagen Type IV* expression at day 15 (Klar *et al*. 2013), that the highly vascularized network that forms within the spaces of the coral-derived devices, creates an inhibitory microenvironment that antagonizes chondrogenesis. Whatever the reason may be, future research might be necessary to clarify this aspect as it may enhance the inductive activity of biomimetic devices.

6.2 TGF-β_3: modulation and initiation of bone formation by induction

Mammalian TGF-β isoforms have been shown to induce bone formation when combined

with coral-derived and collagen matrices implanted in heterotopic extraskeletal sites of non-human primates by influencing BMP related gene expression (Ripamonti *et al.* 1997; Ripamonti *et* al. 2000; Ripamonti *et al.* 2008). However, a key question regarding the induction of bone formation by the TGF-β isoforms, especially the mammalian TGF-β_3, as suggested by Ripamonti *et al.* (2008; 2010), was whether TGF- β_3 is directly inducing bone formation or acting as a modulator by expressing BMPs/OPs ultimately responsible for the induction of bone formation.

The results of the present study demonstrate that the induction of *BMP-2* expression in association with the downregulation of *Noggin* corresponds to the induction of bone in heterotopically implanted bioreactors pre-loaded with doses of the hTGF-β_3 isoform. Therefore hTGF- β_3 signaling induces bone formation by regulating Noggin and BMP activity and hence the induction of bone formation. A simultaneous application of the hNoggin with hTGF-β_3 significantly inhibited bone formation compared to the hTGF-β_3 pre-treated devices. The administration of hNoggin severely inhibits morphogenesis by perturbing tissue patterning and the collagenous condensations so vital for the bone induction process.

TGF- β_3 is an essential regulator of mesenchymal fate controlling early osteoblastic cell differentiation (ten Dijke *et al.* 1990; Shi *et al.* 2003). All three mammalian TGF-β's are important for the proliferation, differentiation and commitment of bone progenitor cells. Signalling takes place through Smad 2/3 and TAK1-MMK-p38 with BMP-2, -4, -5, -6 and -7 acting as inducers in this pathway (Matsunobu *et al.* 2009; Bandyopadhyay *et al.* 2006). An important and unexplored observation is the apparent loss of TGF-β_3 expression on day

15 in the hNoggin treated devices which is indicative of the complex relationships of *BMP* and *TGF-β* expression in the context of bone induction.

In contrast, BMP-2 has been shown to independently signal through type I and II BMP and ALK2 receptors resulting in activation of the Smad1/5/8 pathway (Zhou *et al.* 2010). Both the BMP and TGF-β signalling pathways converge to activate expression of the master osteogenesis regulator *RUNX-2* (Pretheeban *et al.* 2012). It is recognized that during bone formation there is considerable cross talk between the regulatory pathways where TGF-β interacts with the Wnt, FGF and pituitary hormone (PTH) pathway, whilst BMP interacts with Notch, FGF and Wnt signaling pathways (Chen *et al.* 2012). Clearly the modulations of the activities of the members of the TGF-β supergene family is very complex and are controlled by a range of gene products which include Noggin (Cooper *et al.* 2009).

The complexities in the dynamics of bone formation are clearly illustrated in the TGF- β_3 treated macroporous constructs (Klar *et al*. 2014). On day 15, hTGF- β_3 downregulates *BMP-2* expression. Recent studies in isolated primary human osteoblasts has also shown the impact of TGF- β treatment on BMP-2 and -7 with both genes showing a significant inhibition of expression through modulation of the Smad 1/5/8 pathway (Ehnert *et al.* 2010; Ehnert *et al.* 2012).

Endogenous TGF- β_3 acting upstream to BMPs appears to be an important controller of the rate of bone formation as it is seen to greatly affect *RUNX-2* and thus *Osteocalcin* (*OC)* gene expression (Klar *et al.,* 2014). TGF- β_3 also regulates the differentiation of progenitor mesenchymal stem cells into the osteoblastic lineage by regulating inductive and inhibitory signals (such as Noggin) through the osteoblastic differentiation markers, *RUNX2* and OC.

Results from this study clearly show an increased percentage of bone that had formed in both the TGF-β_3 and TGF-β_3 /Noggin treatment groups (Klar *et al.* 2014) together with the concomitant decrease in the expression of the inhibitor *Noggin*.

This rapid induction of the bone differentiation when the exogenously applied hTGF-$\beta_{3,}$ in combination with the coral-derived macroporous construct, is inserted in the intramuscular sites of *Papio ursinus* was shown morphologically on day 30 with extensive vascular invasion and increased osteoblast muticellularity and accompanied by a marked increased expression of the *Collagen type IV*, *OC* and *RUNX-2* genes already by day 15.

The rapid induction of bone induction by the hTGF- β_3 is further illustrated morphologically by the induction of bone well outside the border of the implanted bioreactors and a distinctive lack of bone formation in the central regions. It has been hypothesized that the induction of bone in areas surrounding the device may be due to the desorption of the morphogen from the construct with the subsequent diffusion and activity into the extracellular microenvironment (Ripamonti *et al.* 1997). What follows is the rapid recruitment of responding cells with the peripheral microenvironment, structural organization of the matrix and possibly reprogramming of resident myoblastic and pericytic cells into functional osteoblasts. The hTGF-β_3, together with the other mammalian TGF-β isoforms, could be a novel viable molecular signal to induce bone formation in man. The rapid and prominent induction of bone formation has been translated in clinical context (Ripamonti *et al*. 2012a; Ripamonti and Ferretti 2012).

CHAPTER 7

CONCLUSION

This research sought to clarify which molecular signals, cellular mechanisms, morphogens and/or genes initiate and modulate the bone induction cascade to expand the current paradigm of bone formation by auto induction in the primate *Papio ursinus*.

Firstly, this study was directed at establishing the key signals, initiators and modulators of the spontaneous induction of bone formation when coral-derived macroporous constructs are implanted heterotopically in the *rectus abdominis* muscle of *Papio ursinus*. The first critical signal is calcium ions which are released from the implanted construct and migrate across their relevant voltage-gated ion channels of responding cells. Without calcium ions present in the cytoplasm of responsive cells, vital downstream signals of both the BMP and TGF-β pathways including important regulatory transcription factors associated with bone formation, are not properly activated. Therefore, perturbation of Ca^{2+} ion channelling and signalling has an impact on bone formation. Osteoclastogenesis is the cellular mechanism and a response that requires the presence of calcium to be initiated. Osteoclastogenesis is responsible for the progression of new bone formation by geometrically configuring the biomimetic construct to permit osteoblasts to deposit new bone matrix. The geometric patterning in combination with the Ca^{2+} release induces a series of cellular events critical to the induction of bone formation, which are angiogenesis, capillary formation and differentiation of osteoblasts. The subsequent expression of members of the BMP family, and the resultant gene products of BMP signalling, are secreted and embedded in the implanted devices inducing the induction of bone formation as a secondary response.

Secondly, this study has also revealed how hTGF-β_3 induces the bone induction cascade in the non-human primate *Papio ursinus*. Findings from this study reiterate that it is the

BMPs/OPs, in context the *BMP-2* gene activation, that in part initiate bone formation in coral-derived macroporous constructs. However, it is hTGF-β_3 that initiates bone formation by modulating the expression of *BMP-2 via* Noggin and by regulating the differentiation of progenitor mesenchymal stem cells into the osteoblastic lineage, respectively. hTGF-β_3 is also responsible for the rapid and potent induction of bone suggesting that at the highest non-inhibitory dose, hTGF-β_3 could reduce the time at which bone induction is initiated and increase the rate of the newly formed bone. These finding demonstrate why the mammalian hTGF-β_3 isoform should be considered for future clinical applications to regenerate bone in humans.

The combined morphological and molecular data analyses and evaluation have indicated that hTGF-β_3 significantly upregulated *RUNX-2* and *Osteocalcin* expression on day 15 controlling the differentiation of progenitor stem cells into the osteoblastic lineage. The induction of bone as initiated by the hTGF-β_3 in the *rectus abdominis* muscle of *Papio ursinus* is *via* the BMPs pathway with hTGF-β_3 controlling the induction of bone formation by regulating the expression of *BMPs via Noggin* expression. The presented data unequivocally demonstrated that hTGF-β_3 elicits bone induction by up-regulation of endogenous *BMP-2* and is blocked by hNoggin.

On day 15, harvested hTGF-β_3 bioreactors show advancing extracellular matrix rings that provide structural anchorage for hyper chromatic cells interpreted as differentiating osteoblasts reprogrammed by the hTGF-β_3 from invading myoblastic/pericytic differentiated cells (Klar *et al*. 2014; Ripamonti *et al*. 2014).

RUNX-2 and *Osteocalcin* are significantly upregulated in hTGF-β_3 treated bioreactors on day 15 supporting the morphological observations of invading cell differentiating into the osteoblastic phenotype with hyper cellular osteoblastic activity and extracellular matrix secretion (Klar *et al*. 2014; Ripamonti *et al*. 2014).

The rapid induction of bone formation by the hTGF-β_3 in *Papio ursinus* has been translated in clinical contexts to regenerate severe mandibulo-facial defects in human patients (Ripamonti and Ferretti 2012; Ripamonti *et al*. 2012; Klar *et al*. 2014).

The manipulation and rapid induction of a pluripotent stem cell niche harboured in primate striated muscle engineering microenvironments super activated by hTGF-β_3 reprogramming recruited differentiated pericytes into highly active secreting osteoblasts in primate striated muscle (Ripamonti et al. 2014) with *RUNX-2*, *Osteocalcin*, *TGF-β_3*, *BMP-2* and *OP-1* expression together with angiogenesis, hyper cellular osteoblastic activity, and osteoid synthesis are the novel molecular and morphological basis for the induction of bone formation in clinical contexts (Ripamonti *et al.* 2008; Klar *et al.* 2014; Ripamonti *et al*. 2014).

APPENDIX A Animal Ethics Clearance/Modifications and Extensions

AESC 3

UNIVERSITY OF THE WITWATERSRAND, JOHANNESBURG

STRICTLY CONFIDENTIAL

ANIMAL ETHICS SCREENING COMMITTEE (AESC)

CLEARANCE CERTIFICATE NO. 2009/18/04

APPLICANT: Mr. RM Klar

SCHOOL:
DEPARTMENT: Bone Research Unit
LOCATION:

PROJECT TITLE: **Bone induction by porous hydroxyapatite based biometric matrices in Papio ursinus and Macaca mulatta**

Number and Species

2 M/F *Papio ursinus* and 2 M/F *Macaca mulatta* with the following conditions

Approval was given for the use of animals for the project described above at an AESC meeting held on 28.04.2009. This approval remains valid until 28.04.2011

The use of these animals is subject to AESC guidelines for the use and care of animals, is limited to the procedures described in the application form and to the following additional conditions:

- **Clarity on the animal implant procedure to be provided.**
- **Clarify the size of the implant, and whether it is feasible to place 4 implants at 4 sites in the *latissimus dorsi* muscle.**
- **Clarify the duration of the surgery and any post-operative care (analgesia, antibiotics, and dressings in particular) that will be required (if any).**

Signed: _____ Date: 18/05/2009
(Chairperson, AESC)

I am satisfied that the persons listed in this application are competent to perform the procedures therein, in terms of Section 23 (1) (c) of the Veterinary and Para-Veterinary Professions Act (19 of 1982)

Signed: _____ Date: 18/05/2009
(Registered Veterinarian)

cc: Supervisor:
Director: CAS

Works 2000/lain0015/AESCCert.wps

AESC 2009

ANIMAL ETHICS SCREENING COMMITTEE

MODIFICATIONS AND EXTENSIONS TO EXPERIMENTS

a. Name: Roland M. Klar

b. Department: BONE RESEARCH UNIT

c. Experiment to be modified / extended **AESC NO:**

Original AESC number	2009	18	04
Other M&E's :			

d. Project Title: Bone induction by porous hydroxyapatite based-biometric matrices in *Papio ursinus* and *Chlorobecus pygerythrus*

e.	Number and species of animals **originally approved:**	4	
f.	Number of additional animals **previously allocated on M&Es:**	0	
g.	Total number of animals **allocated** to the experiment to date:	4	
h.	Number of animals **used** to date:	0	

i. Specific modification / extension requested:

a.) Two edentulized baboons AEC no. 2006/71/05 awaiting mandibular scaffold implantation will be used to maximize animal usage and prevent wasting of specimens.

b.) Modify implantation period. Since the mandibular implants need to be *in vivo* for 180 days heterotopic and orthotopic implants will be implanted at day 150, 165, 173 and 177, so that specimens will remain *in vivo* for 180 (mandibular only), 30 (orthotopic and heterotopic), 15, 7 and 3 days (heterotopic only) respectively. Euthanasia will occur at 180 days and all implants will be processed.

c.) Change form *Macaca mulatta* to *Chlorobecus pygerythrus* n=2.

j. Motivation for modification / extension:

a.) So as not to waste tissue specimens.

b.) The HA/TCP TGFβ_3 will be implanted at day 150 and so forth as mandibular implanted HA scaffolds need to be *in vivo* for 180 days.

c.) The *Macaca mulatta* are being used for a separate study and so *Chlorobecus pygerythrus* will replace this loss. The procedures including implantation scheme and the time periods at which implantation will occur are unaltered as previously described in the approved AESC application form 2009/18/04. The 180 day concept for the baboons and edentulized procedure will not apply to the Vervet monkeys. Implantation will occur at day 0, 15, 23 and 27 with euthanasia at day 30 where implants will be harvested and processed.

AESC 2009

ANIMAL ETHICS SCREENING COMMITTEE

MODIFICATIONS AND EXTENSIONS TO EXPERIMENTS

a. Name: Roland M. Klar/Ugo Ripamonti

b. Department: BONE RESEARCH UNIT

c. Experiment to be modified / extended

AESC NO:

Original AESC number	2009	18	05
Other M&E's:			

d. Project Title: Signal transduction pathways controlling the induction of bone formation in the non-human primates

e.	Number and species of animals **originally approved**:	4	
f.	Number of additional animals **previously allocated on M&Es**:	2	
g.	Total number of animals **allocated** to the experiment to date:	6	
h.	Number of animals **used** to date:	6	

i. Specific modification / extension requested:
Addition of two adult baboons *Papio ursinus* presently available at the University of the Orange Free State

j. Motivation for modification / extension:
Using coral-derived macroporous substrata we obtained important results on the spontaneous induction of bone formation as implanted in baboons: we are currently evaluating the important inhibitory effect of Zometa upon bone induction and still wishing to study the effect of calcium ions inhibitors on the induction of bone formation; our latest results on bone formation by macroporous devices were somehow altered and highly variable between the two *Papio ursinus* because of chronic mandibular inflammation in one of the animals; we wish to add and repeat important results data on the ideal *Papio ursinus* model we have tested since the late eighties

Date: 18 November 2010 Signature:

RECOMMENDATIONS:

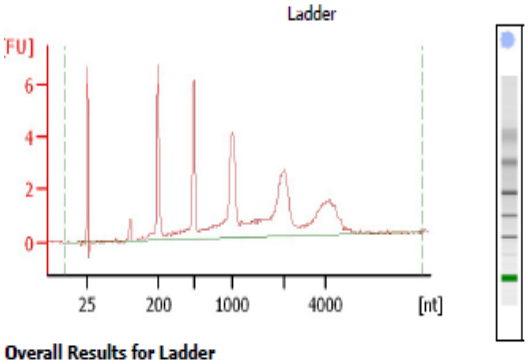
Approved

Date: 18/11/2010 Signature: Chairman, AESC

APPENDIX B RNA Integrity Numbers (RIN) for all samples

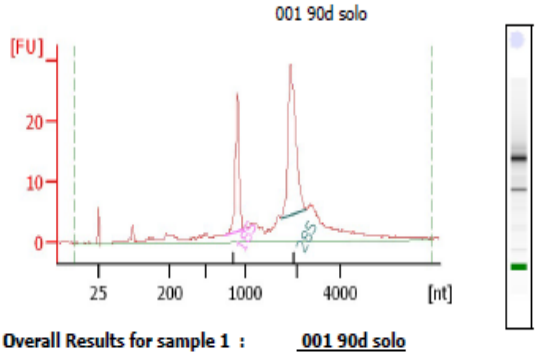
(Please note that samples are labelled according to animal number, days *in vivo* and treatment type e.g. 001 90d Solo or 001 90d Noggin = Animal number 001, specimen left 90 days *in vivo*, untreated or treated with Noggin...)

Electropherogram Summary



Overall Results for Ladder

RNA Area:	58.1
RNA Concentration:	1,000 pg/µl
Result Flagging Color:	
Result Flagging Label:	All Other Samples

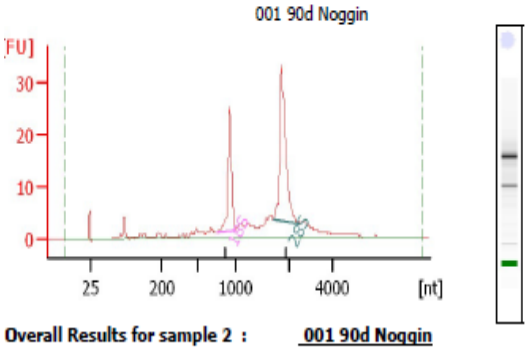


Overall Results for sample 1 : 001 90d solo

RNA Area:	226.6
RNA Concentration:	3,902 pg/µl
rRNA Ratio [28s / 18s]:	1.9
RNA Integrity Number (RIN):	9 (B.02.07)
Result Flagging Color:	
Result Flagging Label:	RIN:9

Fragment table for sample 1 : 001 90d solo

Name	Start Size [nt]	End Size [nt]	Area	% of total Area
18S	732	979	30.9	13.6
28S	1,680	2,426	59.0	26.1

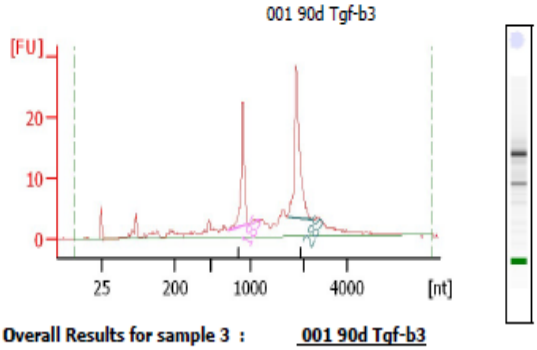


Overall Results for sample 2 : 001 90d Noggin

RNA Area:	195.6
RNA Concentration:	3,369 pg/µl
rRNA Ratio [28s / 18s]:	1.6
RNA Integrity Number (RIN):	9 (B.02.07)
Result Flagging Color:	
Result Flagging Label:	RIN:9

Fragment table for sample 2 : 001 90d Noggin

Name	Start Size [nt]	End Size [nt]	Area	% of total Area
18S	743	994	32.1	16.4
28S	1,696	2,502	52.9	27.0

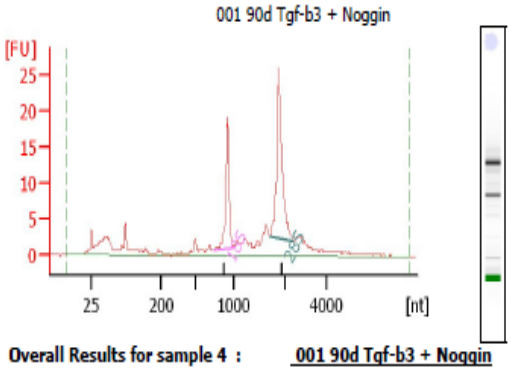


Overall Results for sample 3 : 001 90d Tgf-b3

RNA Area:	186.3
RNA Concentration:	3,209 pg/µl
rRNA Ratio [28s / 18s]:	1.6
RNA Integrity Number (RIN):	8.7 (B.02.07)
Result Flagging Color:	
Result Flagging Label:	RIN: 8.70

Fragment table for sample 3 : 001 90d Tgf-b3

Name	Start Size [nt]	End Size [nt]	Area	% of total Area
18S	718	979	27.9	15.0
28S	1,689	2,409	44.2	23.7

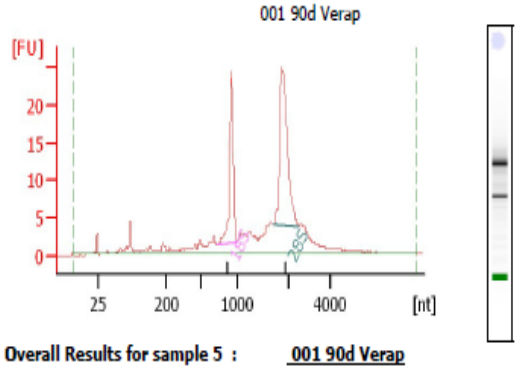


Overall Results for sample 4 : **001 90d Tgf-b3 + Noggin**

RNA Area:	174.4
RNA Concentration:	3,002 pg/µl
rRNA Ratio [28s / 18s]:	1.7
RNA Integrity Number (RIN):	8.9 (B.02.07)
Result Flagging Color:	
Result Flagging Label:	RIN: 8.90

Fragment table for sample 4 : **001 90d Tgf-b3 + Noggin**

Name	Start Size [nt]	End Size [nt]	Area	% of total Area
18S	743	996	24.3	14.0
28S	1,714	2,434	41.9	24.1

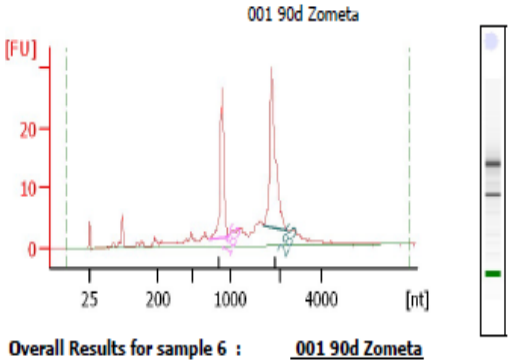


Overall Results for sample 5 : **001 90d Verap**

RNA Area:	213.1
RNA Concentration:	3,670 pg/µl
rRNA Ratio [28s / 18s]:	1.5
RNA Integrity Number (RIN):	8.6 (B.02.07)
Result Flagging Color:	
Result Flagging Label:	RIN: 8.60

Fragment table for sample 5 : **001 90d Verap**

Name	Start Size [nt]	End Size [nt]	Area	% of total Area
18S	725	985	33.4	15.7
28S	1,696	2,502	51.0	23.9

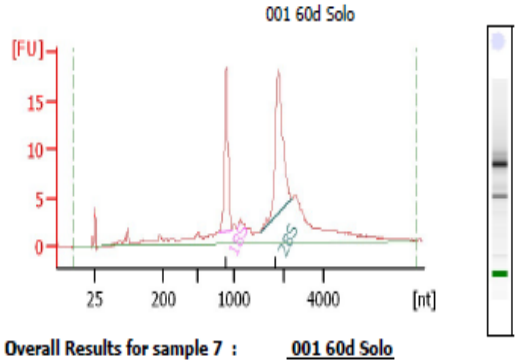


Overall Results for sample 6 : **001 90d Zometa**

RNA Area:	192.8
RNA Concentration:	3,320 pg/µl
rRNA Ratio [28s / 18s]:	1.5
RNA Integrity Number (RIN):	8.8 (B.02.07)
Result Flagging Color:	
Result Flagging Label:	RIN: 8.80

Fragment table for sample 6 : **001 90d Zometa**

Name	Start Size [nt]	End Size [nt]	Area	% of total Area
18S	708	974	33.6	17.4
28S	1,670	2,341	49.8	25.8

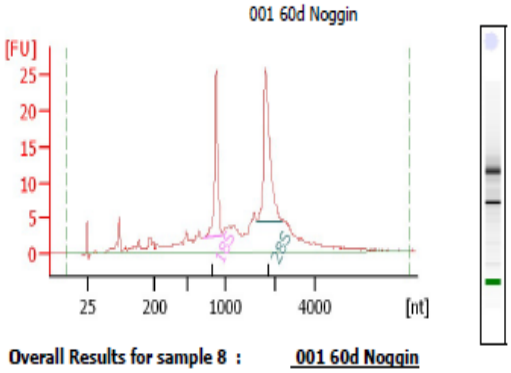


Overall Results for sample 7 : **001 60d Solo**

RNA Area:	169.6
RNA Concentration:	2,921 pg/µl
rRNA Ratio [28s / 18s]:	1.7
RNA Integrity Number (RIN):	8.7 (B.02.07)
Result Flagging Color:	
Result Flagging Label:	RIN: 8.70

Fragment table for sample 7 : **001 60d Solo**

Name	Start Size [nt]	End Size [nt]	Area	% of total Area
18S	792	976	21.8	12.9
28S	1,534	2,448	37.4	22.0

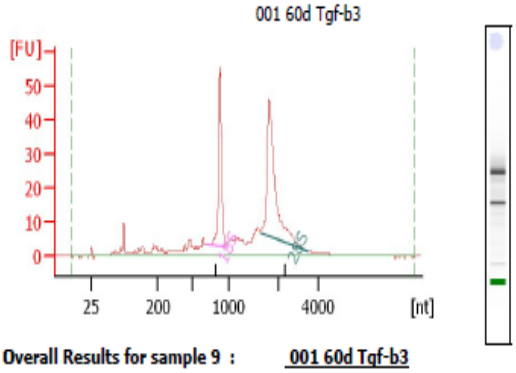


Overall Results for sample 8 : **001 60d Noggin**

RNA Area:	249.7
RNA Concentration:	4,300 pg/µl
rRNA Ratio [28s / 18s]:	1.6
RNA Integrity Number (RIN):	8.1 (B.02.07)
Result Flagging Color:	
Result Flagging Label:	RIN: 8.10

Fragment table for sample 8 : **001 60d Noggin**

Name	Start Size [nt]	End Size [nt]	Area	% of total Area
18S	718	965	31.6	12.6
28S	1,640	2,357	49.1	19.6

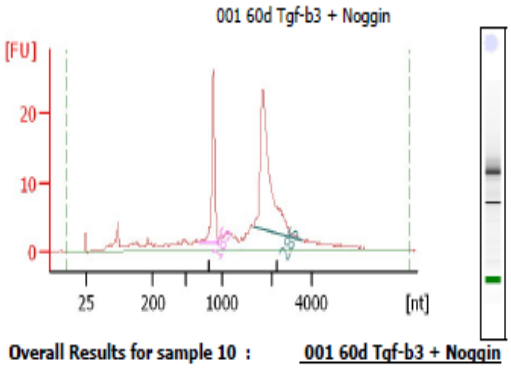


Overall Results for sample 9 : **001 60d Tgf-b3**

RNA Area:	423.4
RNA Concentration:	7,291 pg/µl
rRNA Ratio [28s / 18s]:	1.6
RNA Integrity Number (RIN):	8.6 (B.02.07)
Result Flagging Color:	
Result Flagging Label:	RIN: 8.60

Fragment table for sample 9 : **001 60d Tgf-b3**

Name	Start Size [nt]	End Size [nt]	Area	% of total Area
18S	706	968	69.8	16.5
28S	1,662	3,516	113.9	26.9

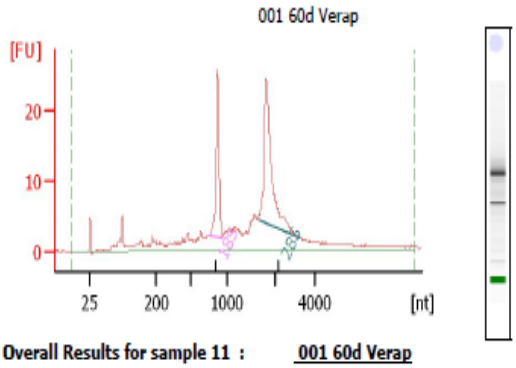


Overall Results for sample 10 : **001 60d Tgf-b3 + Noggin**

RNA Area:	228.8
RNA Concentration:	3,939 pg/µl
rRNA Ratio [28s / 18s]:	2.1
RNA Integrity Number (RIN):	8.9 (B.02.07)
Result Flagging Color:	
Result Flagging Label:	RIN: 8.90

Fragment table for sample 10 : **001 60d Tgf-b3 + Noggin**

Name	Start Size [nt]	End Size [nt]	Area	% of total Area
18S	689	952	33.8	14.8
28S	1,635	3,496	70.8	30.9

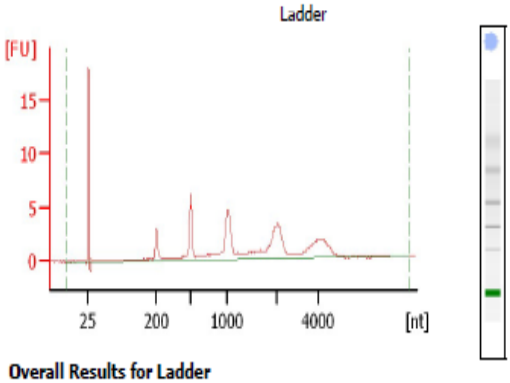


Overall Results for sample 11 : **001 60d Verap**

RNA Area:	226.1
RNA Concentration:	3,894 pg/µl
rRNA Ratio [28s / 18s]:	1.8
RNA Integrity Number (RIN):	8.5 (B.02.07)
Result Flagging Color:	
Result Flagging Label:	RIN: 8.50

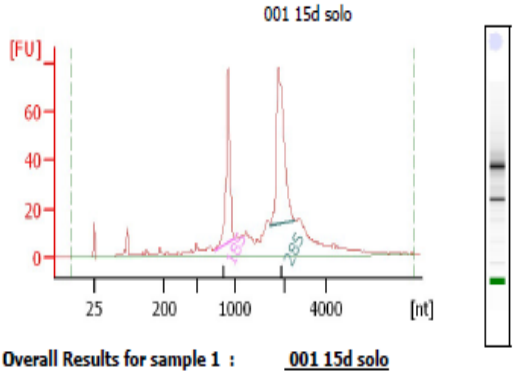
Fragment table for sample 11 : **001 60d Verap**

Name	Start Size [nt]	End Size [nt]	Area	% of total Area
18S	760	952	30.7	13.6
28S	1,643	3,221	56.5	25.0



Overall Results for Ladder

RNA Area:	59.6
RNA Concentration:	1,000 pg/µl
Result Flagging Color:	
Result Flagging Label:	All Other Samples

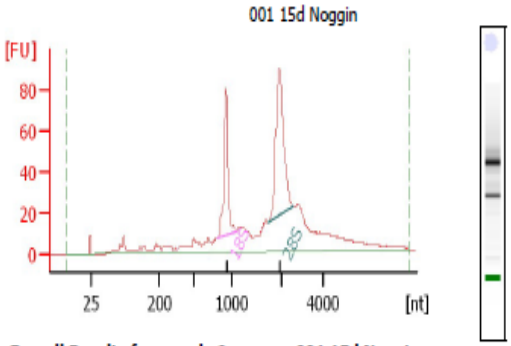


Overall Results for sample 1 : 001 15d solo

RNA Area:	666.8
RNA Concentration:	11,191 pg/µl
rRNA Ratio [28s / 18s]:	1.5
RNA Integrity Number (RIN):	9 (B.02.07)
Result Flagging Color:	
Result Flagging Label:	RIN:9

Fragment table for sample 1 : 001 15d solo

Name	Start Size [nt]	End Size [nt]	Area	% of total Area
18S	731	992	104.0	15.6
28S	1,717	2,520	159.3	23.9

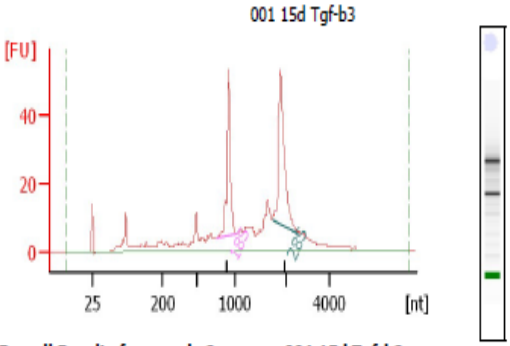


Overall Results for sample 2 : 001 15d Noggin

RNA Area:	879.4
RNA Concentration:	14,760 pg/µl
rRNA Ratio [28s / 18s]:	1.7
RNA Integrity Number (RIN):	8.6 (B.02.07)
Result Flagging Color:	
Result Flagging Label:	RIN: 8.60

Fragment table for sample 2 : 001 15d Noggin

Name	Start Size [nt]	End Size [nt]	Area	% of total Area
18S	812	1,122	112.3	12.8
28S	1,757	2,577	187.7	21.3

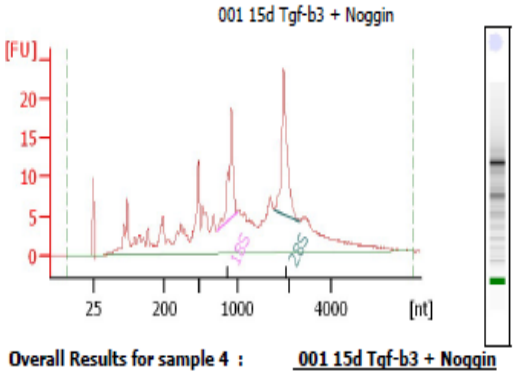


Overall Results for sample 3 : 001 15d Tgf-b3

RNA Area:	460.2
RNA Concentration:	7,724 pg/µl
rRNA Ratio [28s / 18s]:	1.3
RNA Integrity Number (RIN):	8.1 (B.02.07)
Result Flagging Color:	
Result Flagging Label:	RIN: 8.10

Fragment table for sample 3 : 001 15d Tgf-b3

Name	Start Size [nt]	End Size [nt]	Area	% of total Area
18S	754	1,010	66.6	14.5
28S	1,724	2,530	89.6	19.5

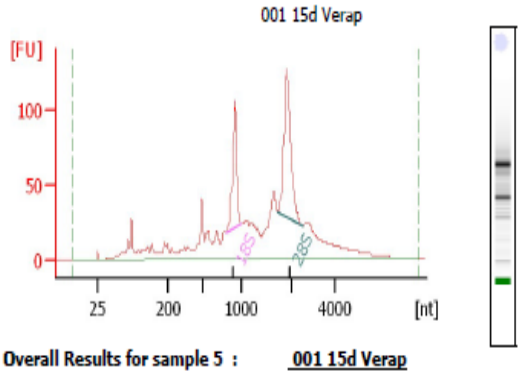


Overall Results for sample 4 : **001 15d Tgf-b3 + Noggin**

RNA Area:	328.9
RNA Concentration:	5,520 pg/µl
rRNA Ratio [28s / 18s]:	1.4
RNA Integrity Number (RIN):	6.5 (B.02.07)
Result Flagging Color:	
Result Flagging Label:	RIN: 6.50

Fragment table for sample 4 : **001 15d Tgf-b3 + Noggin**

Name	Start Size [nt]	End Size [nt]	Area	% of total Area
18S	740	997	24.3	7.4
28S	1,731	2,501	34.0	10.3

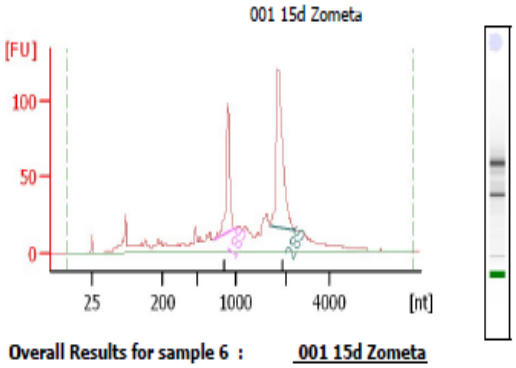


Overall Results for sample 5 : **001 15d Verap**

RNA Area:	1,525.3
RNA Concentration:	25,600 pg/µl
rRNA Ratio [28s / 18s]:	1.6
RNA Integrity Number (RIN):	7.3 (B.02.07)
Result Flagging Color:	
Result Flagging Label:	RIN: 7.30

Fragment table for sample 5 : **001 15d Verap**

Name	Start Size [nt]	End Size [nt]	Area	% of total Area
18S	806	1,000	133.5	8.8
28S	1,727	2,498	218.1	14.3

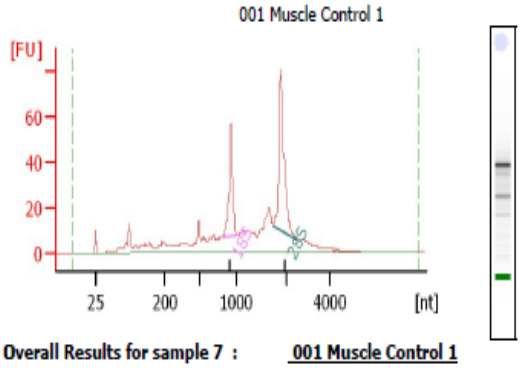


Overall Results for sample 6 : **001 15d Zometa**

RNA Area:	1,050.6
RNA Concentration:	17,633 pg/µl
rRNA Ratio [28s / 18s]:	1.7
RNA Integrity Number (RIN):	8 (B.02.07)
Result Flagging Color:	
Result Flagging Label:	RIN:8

Fragment table for sample 6 : **001 15d Zometa**

Name	Start Size [nt]	End Size [nt]	Area	% of total Area
18S	727	1,000	121.0	11.5
28S	1,686	2,465	208.7	19.9

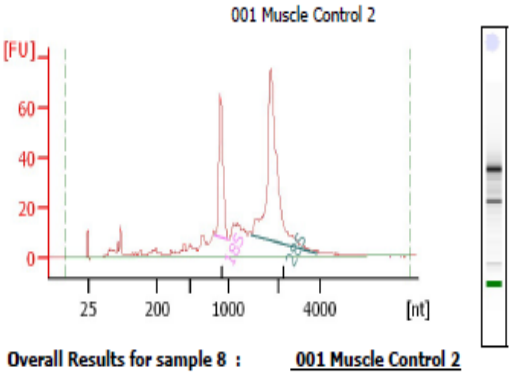


Overall Results for sample 7 : **001 Muscle Control 1**

RNA Area:	616.0
RNA Concentration:	10,339 pg/µl
rRNA Ratio [28s / 18s]:	1.7
RNA Integrity Number (RIN):	7.8 (B.02.07)
Result Flagging Color:	
Result Flagging Label:	RIN: 7.80

Fragment table for sample 7 : **001 Muscle Control 1**

Name	Start Size [nt]	End Size [nt]	Area	% of total Area
18S	804	1,016	68.0	11.0
28S	1,724	2,424	116.0	18.8

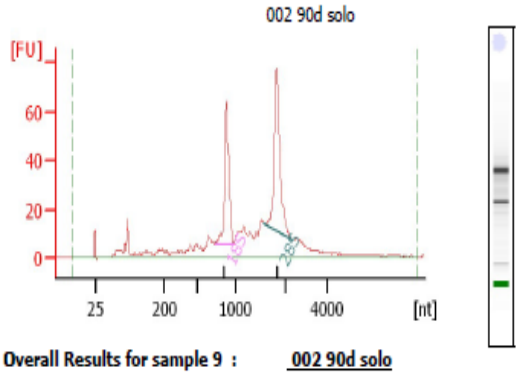


Overall Results for sample 8 : **001 Muscle Control 2**

RNA Area:	679.8
RNA Concentration:	11,410 pg/µl
rRNA Ratio [28s / 18s]:	2.7
RNA Integrity Number (RIN):	8.8 (B.02.07)
Result Flagging Color:	
Result Flagging Label:	RIN: 8.80

Fragment table for sample 8 : **001 Muscle Control 2**

Name	Start Size [nt]	End Size [nt]	Area	% of total Area
18S	835	1,000	82.5	12.1
28S	1,489	3,874	219.9	32.3

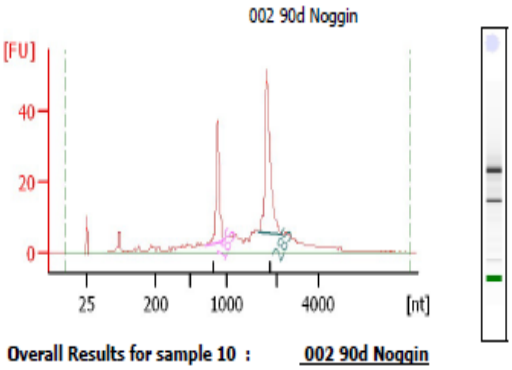


Overall Results for sample 9 : **002 90d solo**

RNA Area:	624.9
RNA Concentration:	10,489 pg/µl
rRNA Ratio [28s / 18s]:	1.5
RNA Integrity Number (RIN):	8.3 (B.02.07)
Result Flagging Color:	
Result Flagging Label:	RIN: 8.30

Fragment table for sample 9 : **002 90d solo**

Name	Start Size [nt]	End Size [nt]	Area	% of total Area
18S	736	981	86.6	13.9
28S	1,593	2,365	133.6	21.4

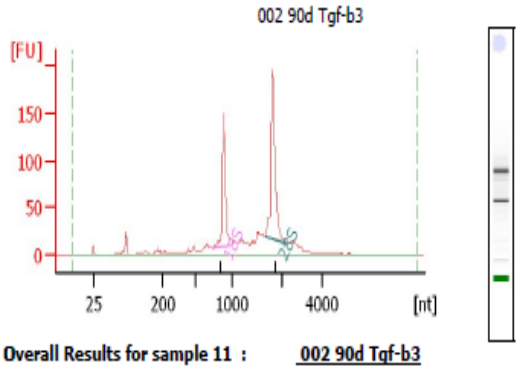


Overall Results for sample 10 : **002 90d Noggin**

RNA Area:	326.2
RNA Concentration:	5,475 pg/µl
rRNA Ratio [28s / 18s]:	1.9
RNA Integrity Number (RIN):	8.9 (B.02.07)
Result Flagging Color:	
Result Flagging Label:	RIN: 8.90

Fragment table for sample 10 : **002 90d Noggin**

Name	Start Size [nt]	End Size [nt]	Area	% of total Area
18S	711	961	44.5	13.6
28S	1,650	2,289	85.6	26.3

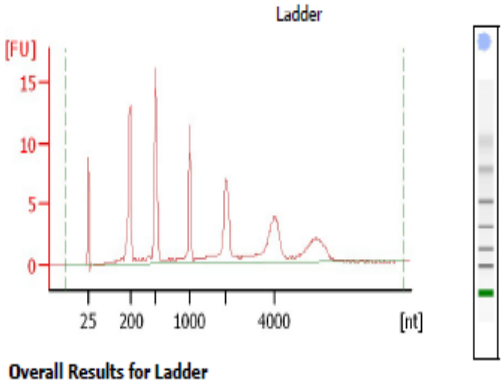


Overall Results for sample 11 : **002 90d Tgf-b3**

RNA Area:	1,017.4
RNA Concentration:	17,076 pg/µl
rRNA Ratio [28s / 18s]:	1.5
RNA Integrity Number (RIN):	9 (B.02.07)
Result Flagging Color:	
Result Flagging Label:	RIN:9

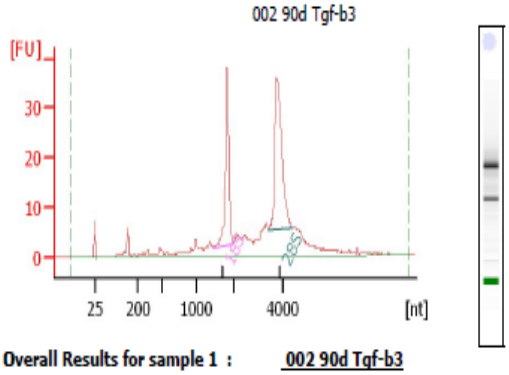
Fragment table for sample 11 : **002 90d Tgf-b3**

Name	Start Size [nt]	End Size [nt]	Area	% of total Area
18S	732	974	181.1	17.8
28S	1,659	2,280	279.3	27.5



Overall Results for Ladder

RNA Area:	116.7
RNA Concentration:	1,000 pg/µl
Result Flagging Color:	
Result Flagging Label:	All Other Samples

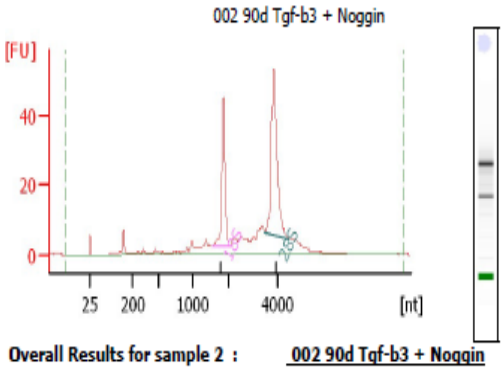


Overall Results for sample 1 : 002 90d Tgf-b3

RNA Area:	294.3
RNA Concentration:	2,522 pg/µl
rRNA Ratio [28s / 18s]:	1.4
RNA Integrity Number (RIN):	8.9 (B.02.07)
Result Flagging Color:	
Result Flagging Label:	RIN: 8.90

Fragment table for sample 1 : 002 90d Tgf-b3

Name	Start Size [nt]	End Size [nt]	Area	% of total Area
18S	1,443	1,995	49.0	16.6
28S	3,455	4,453	68.6	23.3

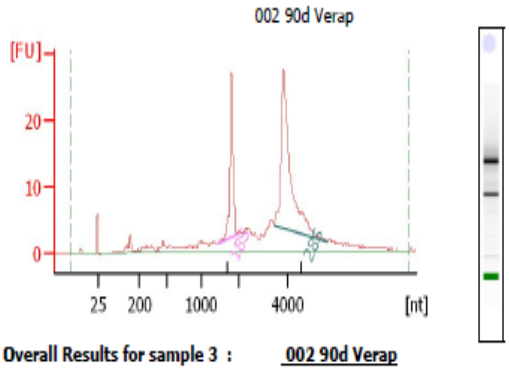


Overall Results for sample 2 : 002 90d Tgf-b3 + Noggin

RNA Area:	328.1
RNA Concentration:	2,811 pg/µl
rRNA Ratio [28s / 18s]:	1.5
RNA Integrity Number (RIN):	8.8 (B.02.07)
Result Flagging Color:	
Result Flagging Label:	RIN: 8.80

Fragment table for sample 2 : 002 90d Tgf-b3 + Noggin

Name	Start Size [nt]	End Size [nt]	Area	% of total Area
18S	1,548	2,050	56.0	17.1
28S	3,482	4,492	84.9	25.9

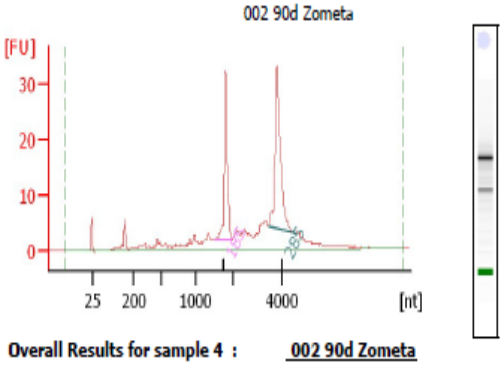


Overall Results for sample 3 : 002 90d Verap

RNA Area:	245.5
RNA Concentration:	2,103 pg/µl
rRNA Ratio [28s / 18s]:	2.1
RNA Integrity Number (RIN):	9.1 (B.02.07)
Result Flagging Color:	
Result Flagging Label:	RIN: 9.10

Fragment table for sample 3 : 002 90d Verap

Name	Start Size [nt]	End Size [nt]	Area	% of total Area
18S	1,441	1,975	34.6	14.1
28S	3,473	5,606	73.2	29.8

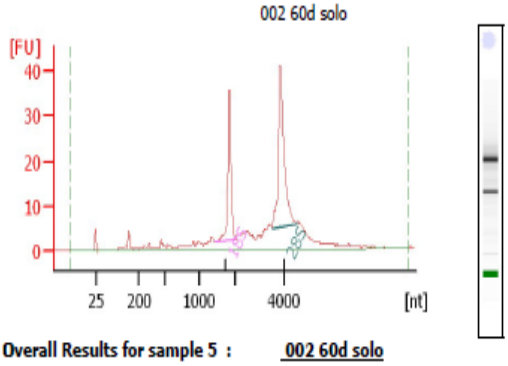


Overall Results for sample 4 : 002 90d Zometa

RNA Area:	222.4
RNA Concentration:	1,906 pg/µl
rRNA Ratio [28s / 18s]:	1.5
RNA Integrity Number (RIN):	8.6 (B.02.07)
Result Flagging Color:	
Result Flagging Label:	RIN: 8.60

Fragment table for sample 4 : 002 90d Zometa

Name	Start Size [nt]	End Size [nt]	Area	% of total Area
18S	1,524	1,994	38.5	17.3
28S	3,473	4,512	55.9	25.1

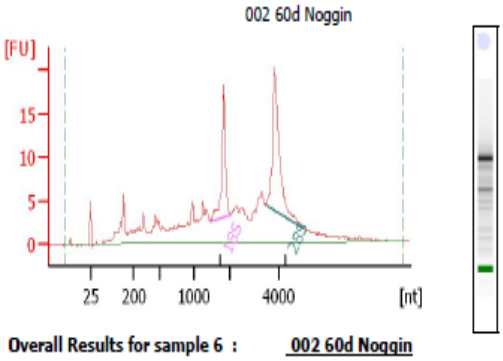


Overall Results for sample 5 : 002 60d solo

RNA Area:	280.7
RNA Concentration:	2,405 pg/µl
rRNA Ratio [28s / 18s]:	1.6
RNA Integrity Number (RIN):	8.9 (B.02.07)
Result Flagging Color:	
Result Flagging Label:	RIN: 8.90

Fragment table for sample 5 : 002 60d solo

Name	Start Size [nt]	End Size [nt]	Area	% of total Area
18S	1,482	1,990	45.6	16.2
28S	3,491	4,481	72.1	25.7

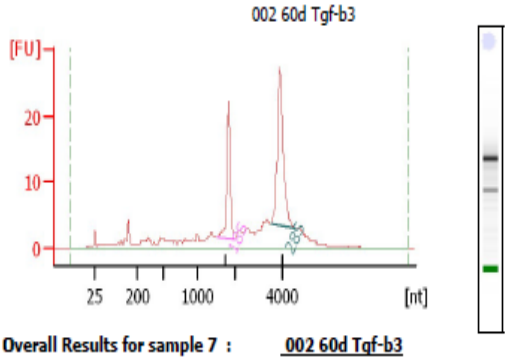


Overall Results for sample 6 : 002 60d Noggin

RNA Area:	264.4
RNA Concentration:	2,265 pg/µl
rRNA Ratio [28s / 18s]:	1.7
RNA Integrity Number (RIN):	7.1 (B.02.07)
Result Flagging Color:	
Result Flagging Label:	RIN: 7.10

Fragment table for sample 6 : 002 60d Noggin

Name	Start Size [nt]	End Size [nt]	Area	% of total Area
18S	1,452	2,013	22.2	8.4
28S	3,477	4,955	38.7	14.6

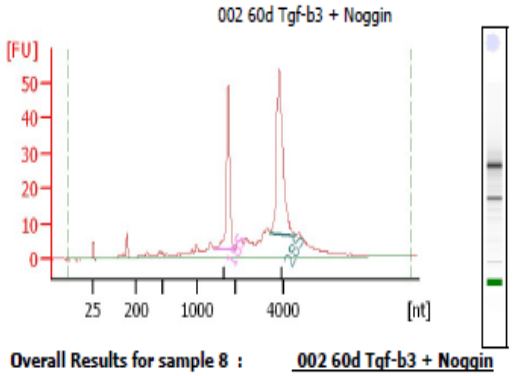


Overall Results for sample 7 : 002 60d Tgf-b3

RNA Area:	223.4
RNA Concentration:	1,914 pg/µl
rRNA Ratio [28s / 18s]:	1.6
RNA Integrity Number (RIN):	8.2 (B.02.07)
Result Flagging Color:	
Result Flagging Label:	RIN: 8.20

Fragment table for sample 7 : 002 60d Tgf-b3

Name	Start Size [nt]	End Size [nt]	Area	% of total Area
18S	1,541	2,024	29.2	13.1
28S	3,508	4,488	47.7	21.4

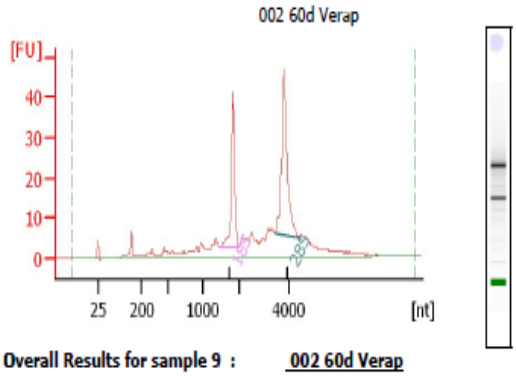


Overall Results for sample 8 : **002 60d Tgf-b3 + Noggin**

RNA Area:	368.3
RNA Concentration:	3,156 pg/µl
rRNA Ratio [28s / 18s]:	1.4
RNA Integrity Number (RIN):	8.8 (B.02.07)
Result Flagging Color:	
Result Flagging Label:	RIN: 8.80

Fragment table for sample 8 : **002 60d Tgf-b3 + Noggin**

Name	Start Size [nt]	End Size [nt]	Area	% of total Area
18S	1,466	1,988	62.3	16.9
28S	3,466	4,432	90.1	24.5

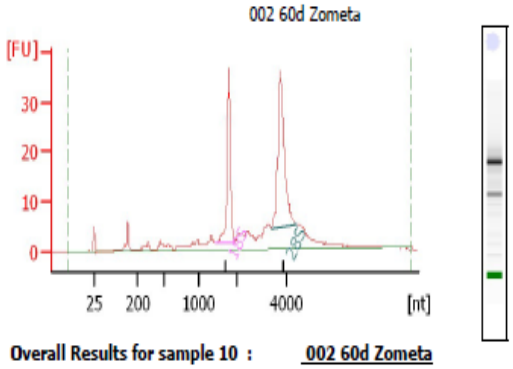


Overall Results for sample 9 : **002 60d Verap**

RNA Area:	325.9
RNA Concentration:	2,792 pg/µl
rRNA Ratio [28s / 18s]:	1.4
RNA Integrity Number (RIN):	8.4 (B.02.07)
Result Flagging Color:	
Result Flagging Label:	RIN: 8.40

Fragment table for sample 9 : **002 60d Verap**

Name	Start Size [nt]	End Size [nt]	Area	% of total Area
18S	1,462	1,981	51.5	15.8
28S	3,421	4,439	73.8	22.6

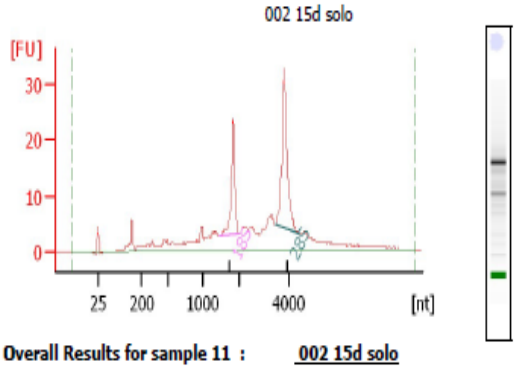


Overall Results for sample 10 : **002 60d Zometa**

RNA Area:	255.5
RNA Concentration:	2,189 pg/µl
rRNA Ratio [28s / 18s]:	1.4
RNA Integrity Number (RIN):	8.9 (B.02.07)
Result Flagging Color:	
Result Flagging Label:	RIN: 8.90

Fragment table for sample 10 : **002 60d Zometa**

Name	Start Size [nt]	End Size [nt]	Area	% of total Area
18S	1,427	1,954	46.3	18.1
28S	3,382	4,436	66.3	25.9

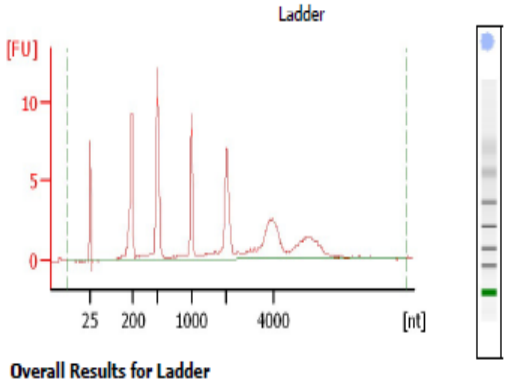


Overall Results for sample 11 : **002 15d solo**

RNA Area:	269.0
RNA Concentration:	2,305 pg/µl
rRNA Ratio [28s / 18s]:	1.6
RNA Integrity Number (RIN):	7.9 (B.02.07)
Result Flagging Color:	
Result Flagging Label:	RIN: 7.90

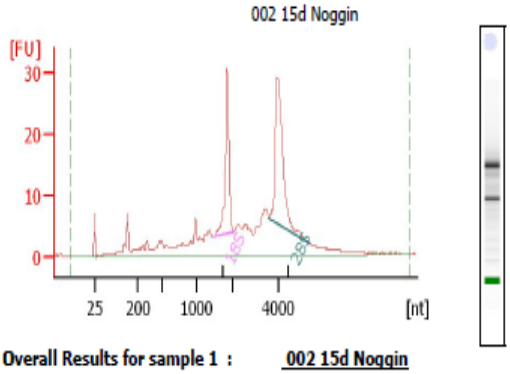
Fragment table for sample 11 : **002 15d solo**

Name	Start Size [nt]	End Size [nt]	Area	% of total Area
18S	1,452	1,981	30.0	11.1
28S	3,435	4,383	48.9	18.2



Overall Results for Ladder

RNA Area:	86.8
RNA Concentration:	1,000 pg/µl
Result Flagging Color:	
Result Flagging Label:	All Other Samples

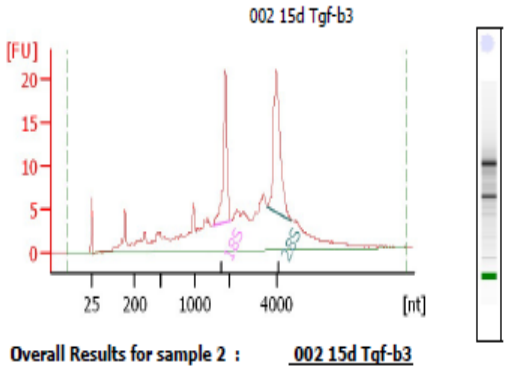


Overall Results for sample 1 : 002 15d Noggin

RNA Area:	314.6
RNA Concentration:	3,625 pg/µl
rRNA Ratio [28s / 18s]:	1.5
RNA Integrity Number (RIN):	7.9 (B.02.07)
Result Flagging Color:	
Result Flagging Label:	RIN: 7.90

Fragment table for sample 1 : 002 15d Noggin

Name	Start Size [nt]	End Size [nt]	Area	% of total Area
18S	1,466	2,066	39.8	12.7
28S	3,579	5,327	58.4	18.6

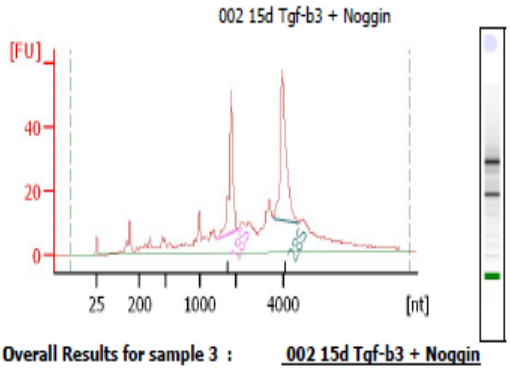


Overall Results for sample 2 : 002 15d Tgf-b3

RNA Area:	260.1
RNA Concentration:	2,998 pg/µl
rRNA Ratio [28s / 18s]:	1.3
RNA Integrity Number (RIN):	7.2 (B.02.07)
Result Flagging Color:	
Result Flagging Label:	RIN: 7.20

Fragment table for sample 2 : 002 15d Tgf-b3

Name	Start Size [nt]	End Size [nt]	Area	% of total Area
18S	1,526	2,068	26.8	10.3
28S	3,621	4,633	35.4	13.6

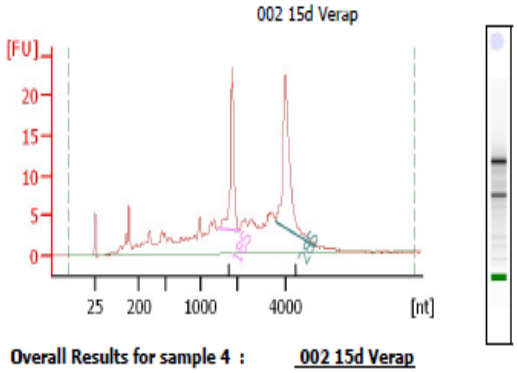


Overall Results for sample 3 : 002 15d Tgf-b3 + Noggin

RNA Area:	582.8
RNA Concentration:	6,717 pg/µl
rRNA Ratio [28s / 18s]:	1.4
RNA Integrity Number (RIN):	7.7 (B.02.07)
Result Flagging Color:	
Result Flagging Label:	RIN: 7.70

Fragment table for sample 3 : 002 15d Tgf-b3 + Noggin

Name	Start Size [nt]	End Size [nt]	Area	% of total Area
18S	1,480	2,048	68.6	11.8
28S	3,586	4,643	95.7	16.4

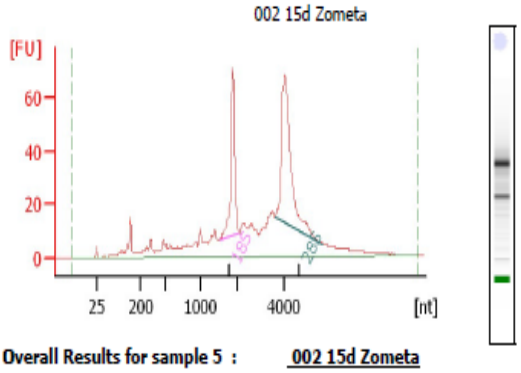


Overall Results for sample 4 : 002 15d Verap

RNA Area:	259.6
RNA Concentration:	2,992 pg/µl
rRNA Ratio [28s / 18s]:	1.4
RNA Integrity Number (RIN):	7.3 (B.02.07)
Result Flagging Color:	
Result Flagging Label:	RIN: 7.30

Fragment table for sample 4 : 002 15d Verap

Name	Start Size [nt]	End Size [nt]	Area	% of total Area
18S	1,509	2,062	30.5	11.8
28S	3,599	5,237	43.5	16.7

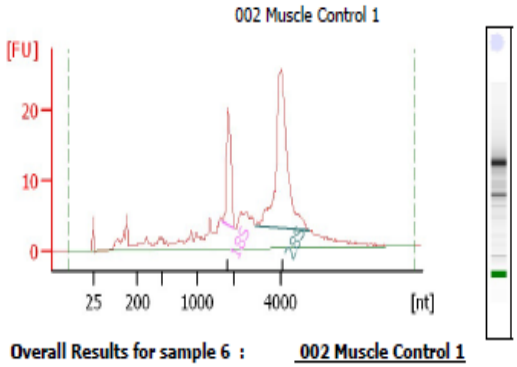


Overall Results for sample 5 : 002 15d Zometa

RNA Area:	773.2
RNA Concentration:	8,910 pg/µl
rRNA Ratio [28s / 18s]:	1.7
RNA Integrity Number (RIN):	8 (B.02.07)
Result Flagging Color:	
Result Flagging Label:	RIN:8

Fragment table for sample 5 : 002 15d Zometa

Name	Start Size [nt]	End Size [nt]	Area	% of total Area
18S	1,523	2,110	96.3	12.5
28S	3,608	5,591	162.6	21.0

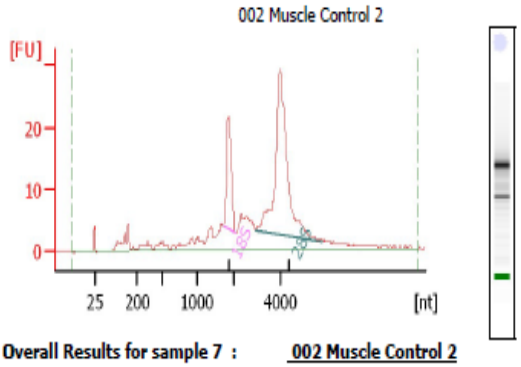


Overall Results for sample 6 : 002 Muscle Control 1

RNA Area:	280.9
RNA Concentration:	3,238 pg/µl
rRNA Ratio [28s / 18s]:	2.9
RNA Integrity Number (RIN):	8.5 (B.02.07)
Result Flagging Color:	
Result Flagging Label:	RIN: 8.50

Fragment table for sample 6 : 002 Muscle Control 1

Name	Start Size [nt]	End Size [nt]	Area	% of total Area
18S	1,687	2,037	28.8	10.3
28S	2,903	5,194	84.3	30.0

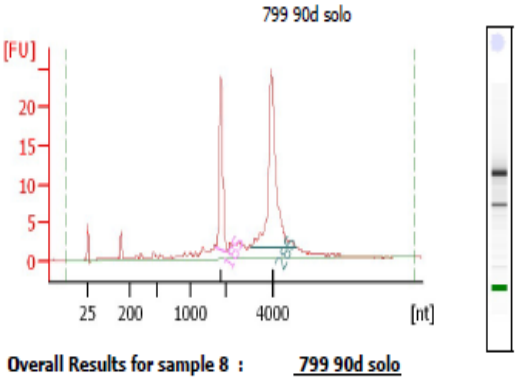


Overall Results for sample 7 : 002 Muscle Control 2

RNA Area:	289.6
RNA Concentration:	3,338 pg/µl
rRNA Ratio [28s / 18s]:	3.4
RNA Integrity Number (RIN):	9 (B.02.07)
Result Flagging Color:	
Result Flagging Label:	RIN:9

Fragment table for sample 7 : 002 Muscle Control 2

Name	Start Size [nt]	End Size [nt]	Area	% of total Area
18S	1,743	2,100	30.3	10.4
28S	2,963	5,805	103.5	35.7

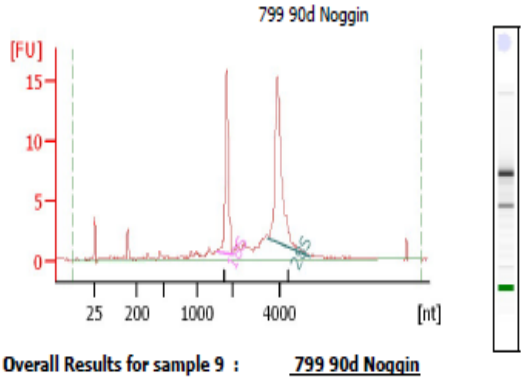


Overall Results for sample 8 : 799 90d solo

RNA Area:	164.6
RNA Concentration:	1,897 pg/µl
rRNA Ratio [28s / 18s]:	2.2
RNA Integrity Number (RIN):	9.4 (B.02.07)
Result Flagging Color:	
Result Flagging Label:	RIN: 9.40

Fragment table for sample 8 : 799 90d solo

Name	Start Size [nt]	End Size [nt]	Area	% of total Area
18S	1,708	2,005	28.1	17.1
28S	3,068	4,870	61.1	37.1

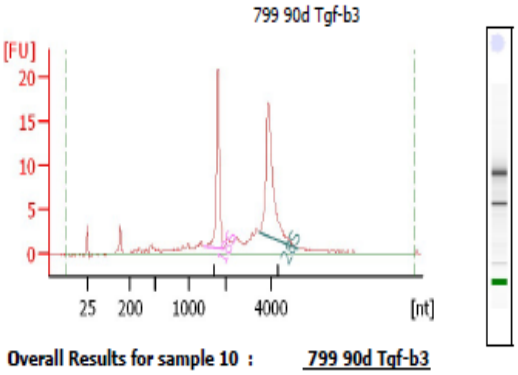


Overall Results for sample 9 : 799 90d Noggin

RNA Area:	104.4
RNA Concentration:	1,203 pg/µl
rRNA Ratio [28s / 18s]:	1.7
RNA Integrity Number (RIN):	9.3 (B.02.07)
Result Flagging Color:	
Result Flagging Label:	RIN: 9.30

Fragment table for sample 9 : 799 90d Noggin

Name	Start Size [nt]	End Size [nt]	Area	% of total Area
18S	1,571	1,983	19.5	18.7
28S	3,502	5,255	32.8	31.4

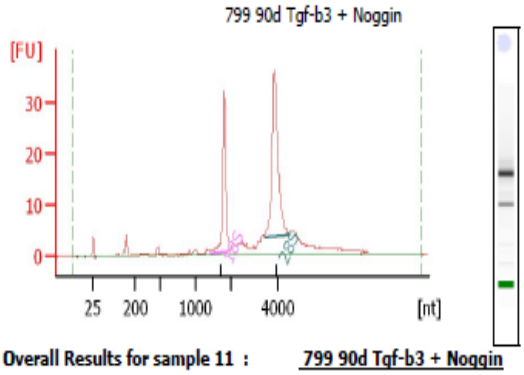


Overall Results for sample 10 : 799 90d Tgf-b3

RNA Area:	132.9
RNA Concentration:	1,532 pg/µl
rRNA Ratio [28s / 18s]:	1.4
RNA Integrity Number (RIN):	9.1 (B.02.07)
Result Flagging Color:	
Result Flagging Label:	RIN: 9.10

Fragment table for sample 10 : 799 90d Tgf-b3

Name	Start Size [nt]	End Size [nt]	Area	% of total Area
18S	1,428	1,961	27.5	20.7
28S	3,475	5,130	39.3	29.5

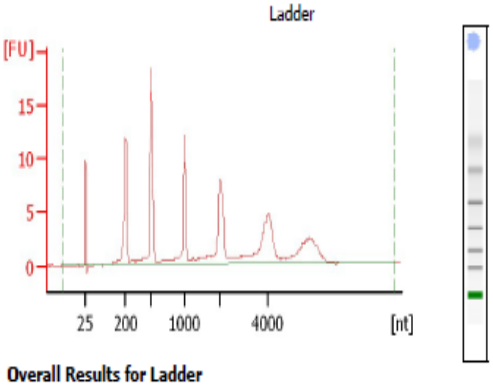


Overall Results for sample 11 : 799 90d Tgf-b3 + Noggin

RNA Area:	220.6
RNA Concentration:	2,543 pg/µl
rRNA Ratio [28s / 18s]:	1.7
RNA Integrity Number (RIN):	9.6 (B.02.07)
Result Flagging Color:	
Result Flagging Label:	RIN: 9.60

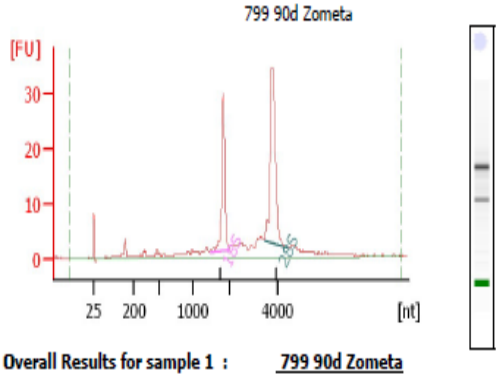
Fragment table for sample 11 : 799 90d Tgf-b3 + Noggin

Name	Start Size [nt]	End Size [nt]	Area	% of total Area
18S	1,443	1,988	41.5	18.8
28S	3,477	4,520	71.1	32.2



Overall Results for Ladder

RNA Area:	124.9
RNA Concentration:	1,000 pg/µl
Result Flagging Color:	
Result Flagging Label:	All Other Samples

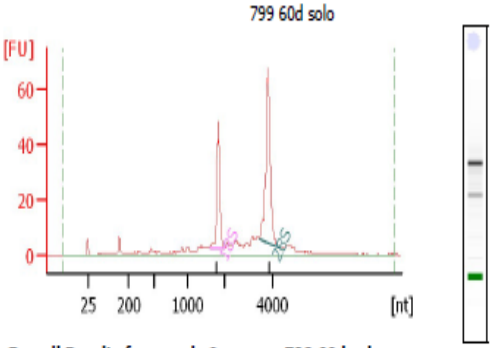


Overall Results for sample 1 : 799 90d Zometa

RNA Area:	178.8
RNA Concentration:	1,431 pg/µl
rRNA Ratio [28s / 18s]:	1.5
RNA Integrity Number (RIN):	9.2 (B.02.07)
Result Flagging Color:	
Result Flagging Label:	RIN: 9.20

Fragment table for sample 1 : 799 90d Zometa

Name	Start Size [nt]	End Size [nt]	Area	% of total Area
18S	1,462	1,995	36.1	20.2
28S	3,459	4,436	52.4	29.3

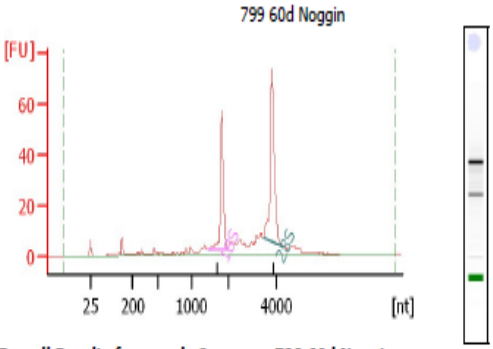


Overall Results for sample 2 : 799 60d solo

RNA Area:	312.3
RNA Concentration:	2,501 pg/µl
rRNA Ratio [28s / 18s]:	1.7
RNA Integrity Number (RIN):	9.1 (B.02.07)
Result Flagging Color:	
Result Flagging Label:	RIN: 9.10

Fragment table for sample 2 : 799 60d solo

Name	Start Size [nt]	End Size [nt]	Area	% of total Area
18S	1,606	2,010	56.4	18.1
28S	3,484	4,374	95.7	30.6

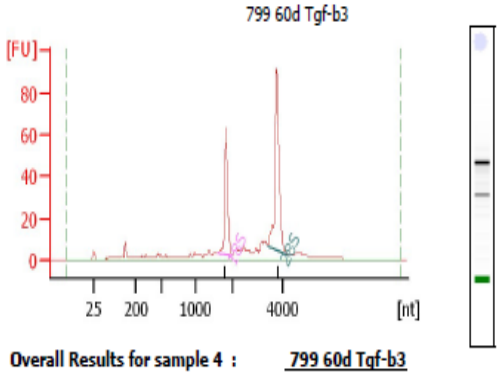


Overall Results for sample 3 : 799 60d Noggin

RNA Area:	352.5
RNA Concentration:	2,823 pg/µl
rRNA Ratio [28s / 18s]:	1.6
RNA Integrity Number (RIN):	9.2 (B.02.07)
Result Flagging Color:	
Result Flagging Label:	RIN: 9.20

Fragment table for sample 3 : 799 60d Noggin

Name	Start Size [nt]	End Size [nt]	Area	% of total Area
18S	1,453	1,986	66.8	18.9
28S	3,448	4,313	104.2	29.6

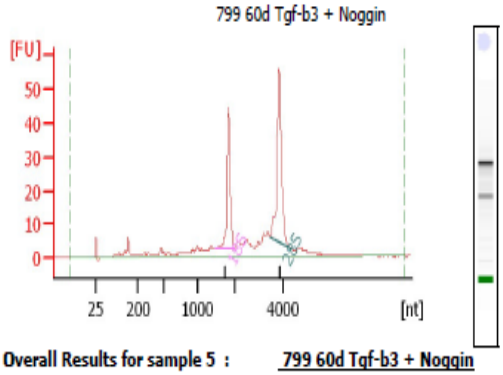


Overall Results for sample 4 : 799 60d Tgf-b3

RNA Area:	390.3
RNA Concentration:	3,125 pg/µl
rRNA Ratio [28s / 18s]:	1.7
RNA Integrity Number (RIN):	9.3 (B.02.07)
Result Flagging Color:	
Result Flagging Label:	RIN: 9.30

Fragment table for sample 4 : 799 60d Tgf-b3

Name	Start Size [nt]	End Size [nt]	Area	% of total Area
18S	1,584	1,978	74.4	19.1
28S	3,433	4,269	126.8	32.5

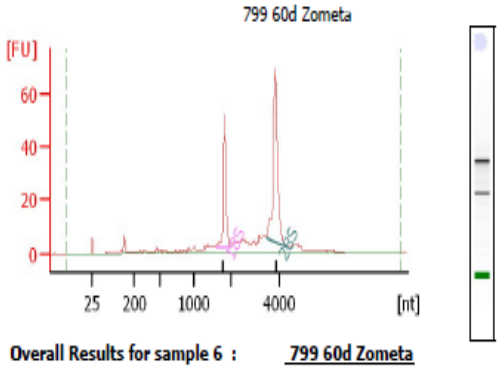


Overall Results for sample 5 : 799 60d Tgf-b3 + Noggin

RNA Area:	319.7
RNA Concentration:	2,560 pg/µl
rRNA Ratio [28s / 18s]:	1.4
RNA Integrity Number (RIN):	8.7 (B.02.07)
Result Flagging Color:	
Result Flagging Label:	RIN: 8.70

Fragment table for sample 5 : 799 60d Tgf-b3 + Noggin

Name	Start Size [nt]	End Size [nt]	Area	% of total Area
18S	1,464	2,015	56.8	17.8
28S	3,480	4,336	81.2	25.4

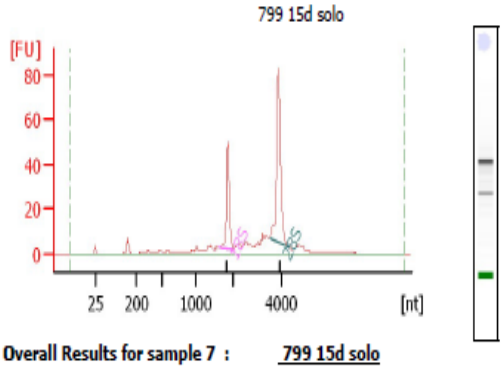


Overall Results for sample 6 : 799 60d Zometa

RNA Area:	312.0
RNA Concentration:	2,498 pg/µl
rRNA Ratio [28s / 18s]:	1.7
RNA Integrity Number (RIN):	9.3 (B.02.07)
Result Flagging Color:	
Result Flagging Label:	RIN: 9.30

Fragment table for sample 6 : 799 60d Zometa

Name	Start Size [nt]	End Size [nt]	Area	% of total Area
18S	1,603	2,002	59.2	19.0
28S	3,480	4,336	100.7	32.3

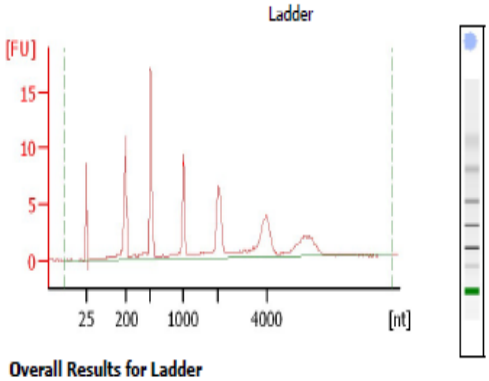


Overall Results for sample 7 : 799 15d solo

RNA Area:	353.5
RNA Concentration:	2,830 pg/µl
rRNA Ratio [28s / 18s]:	2.0
RNA Integrity Number (RIN):	9.2 (B.02.07)
Result Flagging Color:	
Result Flagging Label:	RIN: 9.20

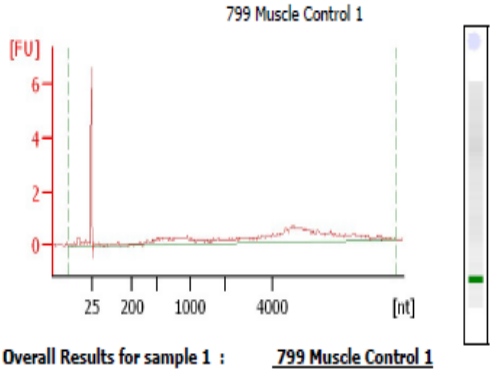
Fragment table for sample 7 : 799 15d solo

Name	Start Size [nt]	End Size [nt]	Area	% of total Area
18S	1,590	2,040	59.3	16.8
28S	3,510	4,315	116.6	33.0



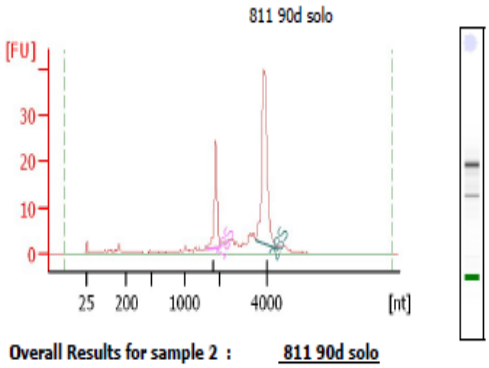
Overall Results for Ladder

RNA Area:	103.2
RNA Concentration:	1,000 pg/µl
Result Flagging Color:	
Result Flagging Label:	All Other Samples



Overall Results for sample 1 : 799 Muscle Control 1

RNA Area:	17.6
RNA Concentration:	170 pg/µl
rRNA Ratio [28s / 18s]:	0.0
RNA Integrity Number (RIN):	1 (B.02.07)
Result Flagging Color:	
Result Flagging Label:	RIN:1

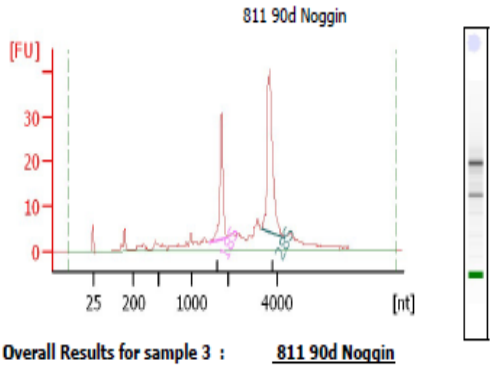


Overall Results for sample 2 : 811 90d solo

RNA Area:	176.6
RNA Concentration:	1,712 pg/µl
rRNA Ratio [28s / 18s]:	2.3
RNA Integrity Number (RIN):	9.5 (B.02.07)
Result Flagging Color:	
Result Flagging Label:	RIN: 9.50

Fragment table for sample 2 : 811 90d solo

Name	Start Size [nt]	End Size [nt]	Area	% of total Area
18S	1,636	2,031	27.4	15.5
28S	3,497	4,451	63.9	36.2

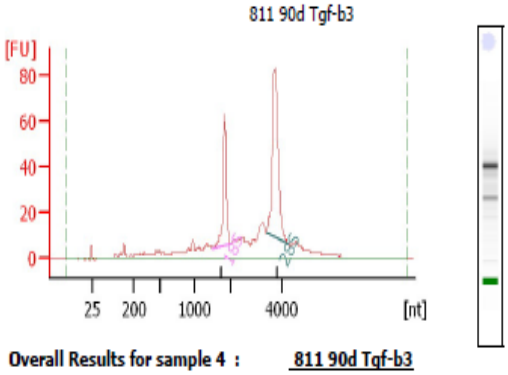


Overall Results for sample 3 : 811 90d Noggin

RNA Area:	266.7
RNA Concentration:	2,586 pg/µl
rRNA Ratio [28s / 18s]:	1.7
RNA Integrity Number (RIN):	8.5 (B.02.07)
Result Flagging Color:	
Result Flagging Label:	RIN: 8.50

Fragment table for sample 3 : 811 90d Noggin

Name	Start Size [nt]	End Size [nt]	Area	% of total Area
18S	1,492	1,973	36.0	13.5
28S	3,377	4,317	61.4	23.0

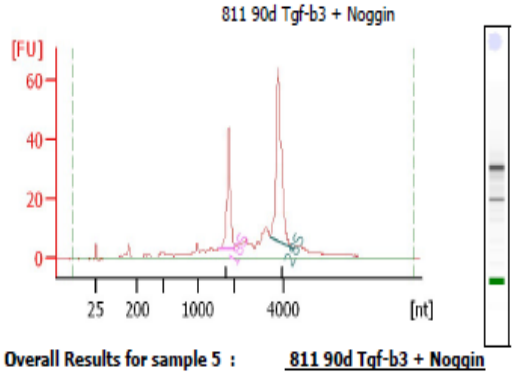


Overall Results for sample 4 : **811 90d Tgf-b3**

RNA Area:	548.3
RNA Concentration:	5,316 pg/µl
rRNA Ratio [28s / 18s]:	1.7
RNA Integrity Number (RIN):	8.4 (B.02.07)
Result Flagging Color:	
Result Flagging Label:	RIN: 8.40

Fragment table for sample 4 : **811 90d Tgf-b3**

Name	Start Size [nt]	End Size [nt]	Area	% of total Area
18S	1,508	1,972	76.0	13.9
28S	3,379	4,266	132.8	24.2

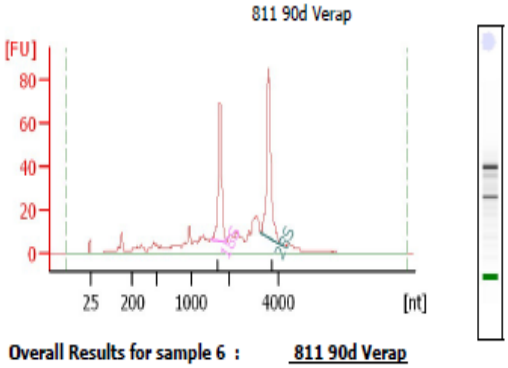


Overall Results for sample 5 : **811 90d Tgf-b3 + Noggin**

RNA Area:	363.3
RNA Concentration:	3,522 pg/µl
rRNA Ratio [28s / 18s]:	1.9
RNA Integrity Number (RIN):	8.9 (B.02.07)
Result Flagging Color:	
Result Flagging Label:	RIN: 8.90

Fragment table for sample 5 : **811 90d Tgf-b3 + Noggin**

Name	Start Size [nt]	End Size [nt]	Area	% of total Area
18S	1,598	2,017	52.9	14.6
28S	3,427	4,368	102.7	28.3

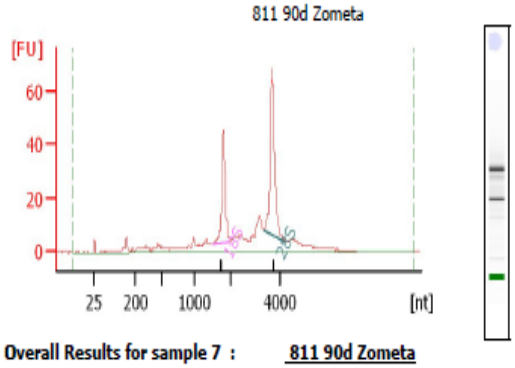


Overall Results for sample 6 : **811 90d Verap**

RNA Area:	509.0
RNA Concentration:	4,934 pg/µl
rRNA Ratio [28s / 18s]:	1.4
RNA Integrity Number (RIN):	8 (B.02.07)
Result Flagging Color:	
Result Flagging Label:	RIN:8

Fragment table for sample 6 : **811 90d Verap**

Name	Start Size [nt]	End Size [nt]	Area	% of total Area
18S	1,535	1,947	79.5	15.6
28S	3,302	4,226	114.6	22.5

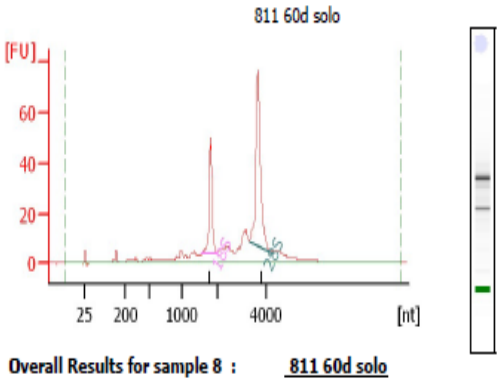


Overall Results for sample 7 : **811 90d Zometa**

RNA Area:	396.0
RNA Concentration:	3,839 pg/µl
rRNA Ratio [28s / 18s]:	1.8
RNA Integrity Number (RIN):	8.7 (B.02.07)
Result Flagging Color:	
Result Flagging Label:	RIN: 8.70

Fragment table for sample 7 : **811 90d Zometa**

Name	Start Size [nt]	End Size [nt]	Area	% of total Area
18S	1,474	1,967	55.6	14.0
28S	3,336	4,217	100.9	25.5

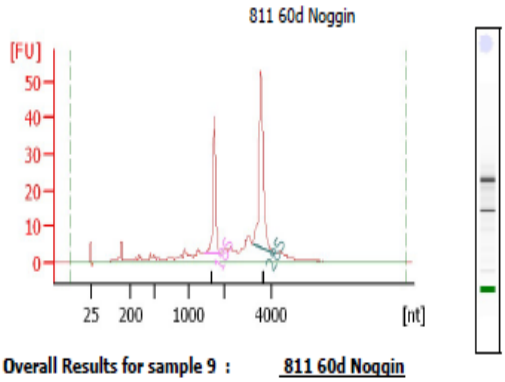


Overall Results for sample 8 : **811 60d solo**

RNA Area:	427.8
RNA Concentration:	4,147 pg/µl
rRNA Ratio [28s / 18s]:	2.0
RNA Integrity Number (RIN):	8.8 (B.02.07)
Result Flagging Color:	
Result Flagging Label:	RIN: 8.80

Fragment table for sample 8 : **811 60d solo**

Name	Start Size [nt]	End Size [nt]	Area	% of total Area
18S	1,548	1,970	59.8	14.0
28S	3,314	4,261	118.9	27.8

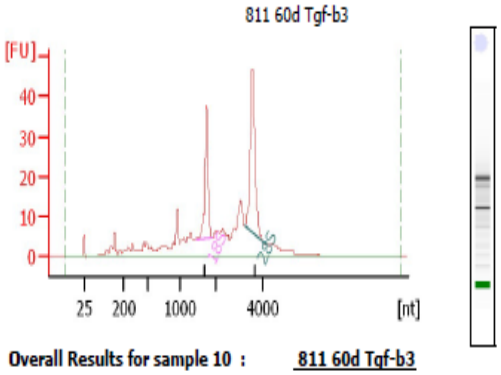


Overall Results for sample 9 : **811 60d Noggin**

RNA Area:	283.3
RNA Concentration:	2,746 pg/µl
rRNA Ratio [28s / 18s]:	1.6
RNA Integrity Number (RIN):	8.7 (B.02.07)
Result Flagging Color:	
Result Flagging Label:	RIN: 8.70

Fragment table for sample 9 : **811 60d Noggin**

Name	Start Size [nt]	End Size [nt]	Area	% of total Area
18S	1,464	1,895	47.0	16.6
28S	3,214	4,117	76.7	27.1

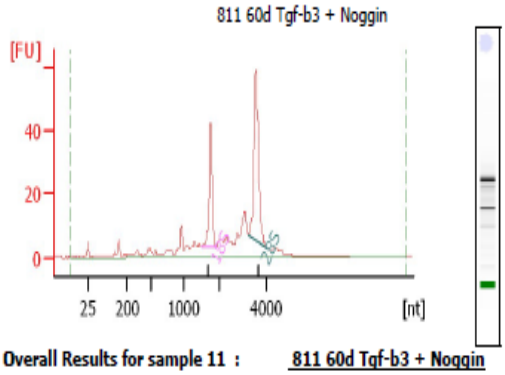


Overall Results for sample 10 : **811 60d Tgf-b3**

RNA Area:	377.1
RNA Concentration:	3,656 pg/µl
rRNA Ratio [28s / 18s]:	1.5
RNA Integrity Number (RIN):	7.6 (B.02.07)
Result Flagging Color:	
Result Flagging Label:	RIN: 7.60

Fragment table for sample 10 : **811 60d Tgf-b3**

Name	Start Size [nt]	End Size [nt]	Area	% of total Area
18S	1,435	1,899	45.5	12.1
28S	3,217	4,086	66.0	17.5

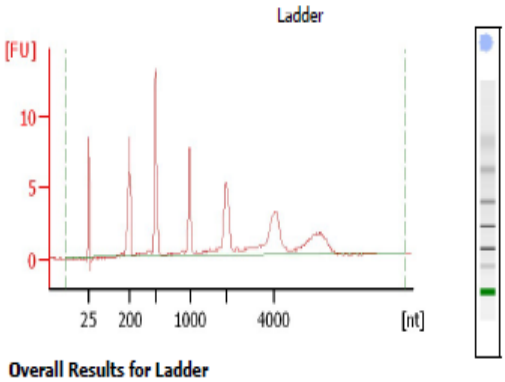


Overall Results for sample 11 : **811 60d Tgf-b3 + Noggin**

RNA Area:	349.1
RNA Concentration:	3,384 pg/µl
rRNA Ratio [28s / 18s]:	1.6
RNA Integrity Number (RIN):	8.3 (B.02.07)
Result Flagging Color:	
Result Flagging Label:	RIN: 8.30

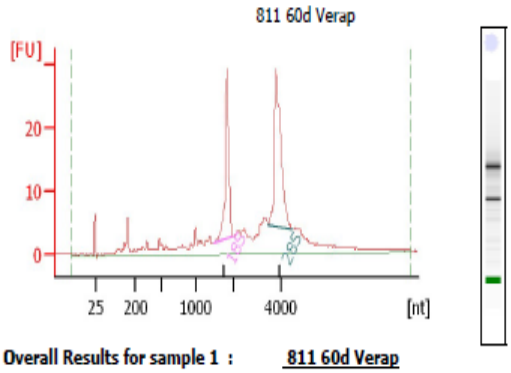
Fragment table for sample 11 : **811 60d Tgf-b3 + Noggin**

Name	Start Size [nt]	End Size [nt]	Area	% of total Area
18S	1,515	1,904	50.5	14.5
28S	3,234	4,094	82.6	23.7



Overall Results for Ladder

RNA Area:	83.5
RNA Concentration:	1,000 pg/µl
Result Flagging Color:	
Result Flagging Label:	All Other Samples

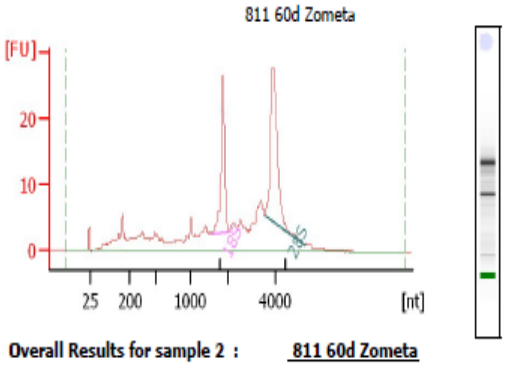


Overall Results for sample 1 : 811 60d Verap

RNA Area:	250.9
RNA Concentration:	3,004 pg/µl
rRNA Ratio [28s / 18s]:	1.4
RNA Integrity Number (RIN):	8.4 (B.02.07)
Result Flagging Color:	
Result Flagging Label:	RIN: 8.40

Fragment table for sample 1 : 811 60d Verap

Name	Start Size [nt]	End Size [nt]	Area	% of total Area
18S	1,467	2,003	37.3	14.9
28S	3,472	4,432	52.7	21.0

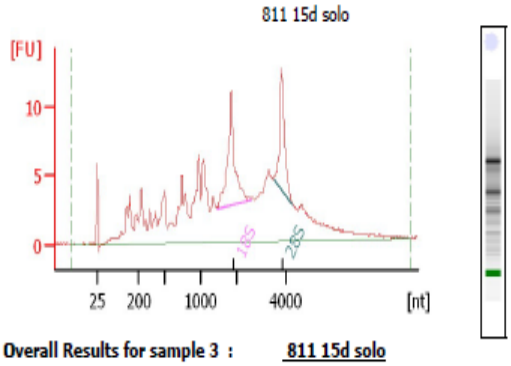


Overall Results for sample 2 : 811 60d Zometa

RNA Area:	297.2
RNA Concentration:	3,558 pg/µl
rRNA Ratio [28s / 18s]:	1.5
RNA Integrity Number (RIN):	7.5 (B.02.07)
Result Flagging Color:	
Result Flagging Label:	RIN: 7.50

Fragment table for sample 2 : 811 60d Zometa

Name	Start Size [nt]	End Size [nt]	Area	% of total Area
18S	1,570	2,074	34.1	11.5
28S	3,557	5,195	50.5	17.0

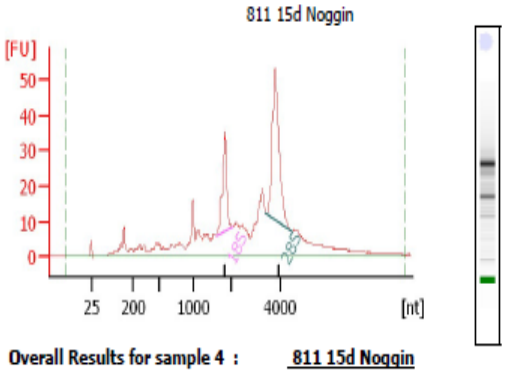


Overall Results for sample 3 : 811 15d solo

RNA Area:	244.1
RNA Concentration:	2,922 pg/µl
rRNA Ratio [28s / 18s]:	0.7
RNA Integrity Number (RIN):	6.2 (B.02.07)
Result Flagging Color:	
Result Flagging Label:	RIN: 6.20

Fragment table for sample 3 : 811 15d solo

Name	Start Size [nt]	End Size [nt]	Area	% of total Area
18S	1,455	2,568	23.1	9.4
28S	3,490	4,241	15.3	6.3

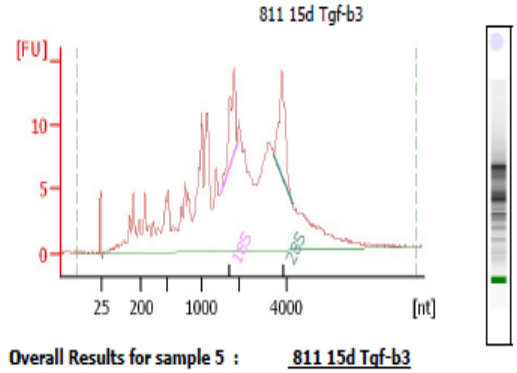


Overall Results for sample 4 : **811 15d Noggin**

RNA Area:	564.5
RNA Concentration:	6,757 pg/µl
rRNA Ratio [28s / 18s]:	2.0
RNA Integrity Number (RIN):	7.6 (B.02.07)
Result Flagging Color:	
Result Flagging Label:	RIN: 7.60

Fragment table for sample 4 : **811 15d Noggin**

Name	Start Size [nt]	End Size [nt]	Area	% of total Area
18S	1,610	2,056	48.2	8.5
28S	3,436	4,481	95.2	16.9

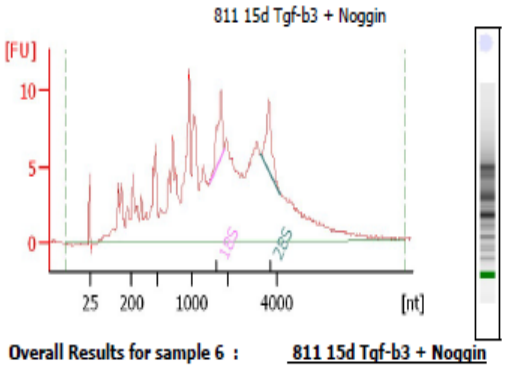


Overall Results for sample 5 : **811 15d Tgf-b3**

RNA Area:	350.4
RNA Concentration:	4,195 pg/µl
rRNA Ratio [28s / 18s]:	1.2
RNA Integrity Number (RIN):	4.2 (B.02.07)
Result Flagging Color:	
Result Flagging Label:	RIN: 4.20

Fragment table for sample 5 : **811 15d Tgf-b3**

Name	Start Size [nt]	End Size [nt]	Area	% of total Area
18S	1,532	1,955	13.8	3.9
28S	3,472	4,235	16.3	4.7

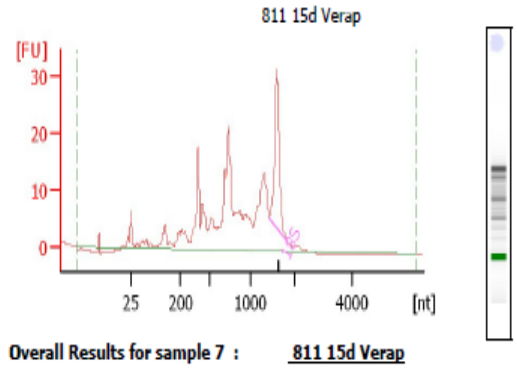


Overall Results for sample 6 : **811 15d Tgf-b3 + Noggin**

RNA Area:	302.1
RNA Concentration:	3,617 pg/µl
rRNA Ratio [28s / 18s]:	1.1
RNA Integrity Number (RIN):	3.5 (B.02.07)
Result Flagging Color:	
Result Flagging Label:	RIN: 3.50

Fragment table for sample 6 : **811 15d Tgf-b3 + Noggin**

Name	Start Size [nt]	End Size [nt]	Area	% of total Area
18S	1,488	1,900	8.4	2.8
28S	3,344	4,147	9.0	3.0

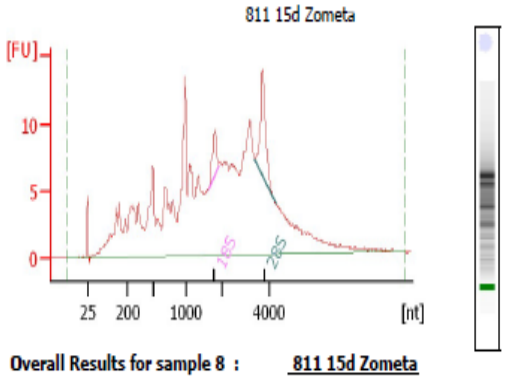


Overall Results for sample 7 : **811 15d Verap**

RNA Area:	312.8
RNA Concentration:	3,745 pg/µl
rRNA Ratio [28s / 18s]:	0.0
RNA Integrity Number (RIN):	5.2 (B.02.07)
Result Flagging Color:	
Result Flagging Label:	RIN: 5.20

Fragment table for sample 7 : **811 15d Verap**

Name	Start Size [nt]	End Size [nt]	Area	% of total Area
18S	1,413	1,839	46.9	15.0

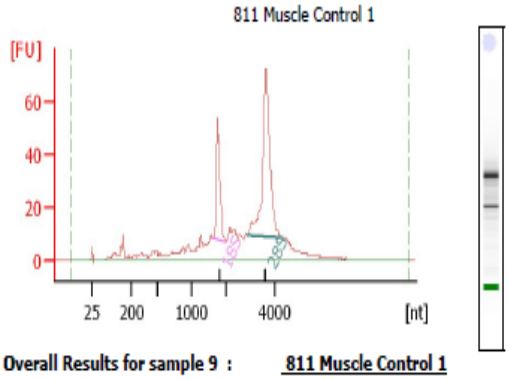


Overall Results for sample 8 : 811 15d Zometa

RNA Area:	360.6
RNA Concentration:	4,317 pg/µl
rRNA Ratio [28s / 18s]:	2.7
RNA Integrity Number (RIN):	3.3 (B.02.07)
Result Flagging Color:	
Result Flagging Label:	RIN: 3.30

Fragment table for sample 8 : 811 15d Zometa

Name	Start Size [nt]	End Size [nt]	Area	% of total Area
18S	1,627	1,905	5.8	1.6
28S	3,398	4,234	15.5	4.3

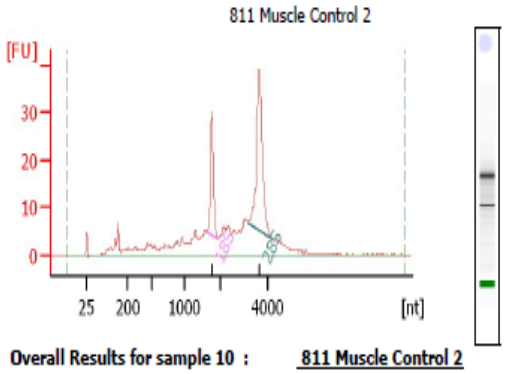


Overall Results for sample 9 : 811 Muscle Control 1

RNA Area:	657.2
RNA Concentration:	7,868 pg/µl
rRNA Ratio [28s / 18s]:	2.5
RNA Integrity Number (RIN):	8.4 (B.02.07)
Result Flagging Color:	
Result Flagging Label:	RIN: 8.40

Fragment table for sample 9 : 811 Muscle Control 1

Name	Start Size [nt]	End Size [nt]	Area	% of total Area
18S	1,619	1,963	69.3	10.5
28S	2,880	4,346	176.6	26.9

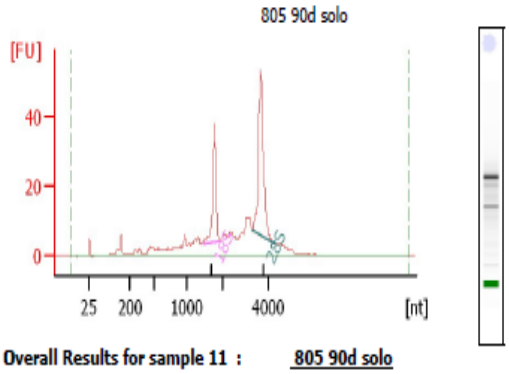


Overall Results for sample 10 : 811 Muscle Control 2

RNA Area:	329.4
RNA Concentration:	3,944 pg/µl
rRNA Ratio [28s / 18s]:	2.0
RNA Integrity Number (RIN):	7.9 (B.02.07)
Result Flagging Color:	
Result Flagging Label:	RIN: 7.90

Fragment table for sample 10 : 811 Muscle Control 2

Name	Start Size [nt]	End Size [nt]	Area	% of total Area
18S	1,603	1,921	35.2	10.7
28S	3,169	4,225	71.0	21.6

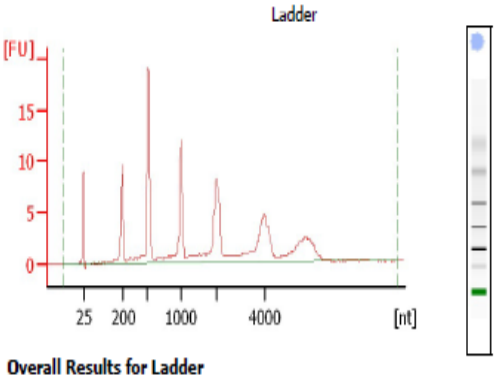


Overall Results for sample 11 : 805 90d solo

RNA Area:	373.3
RNA Concentration:	4,469 pg/µl
rRNA Ratio [28s / 18s]:	1.7
RNA Integrity Number (RIN):	8.1 (B.02.07)
Result Flagging Color:	
Result Flagging Label:	RIN: 8.10

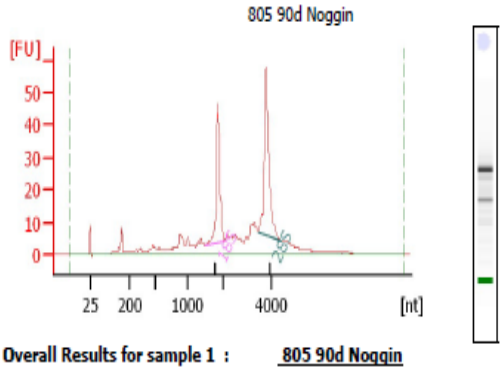
Fragment table for sample 11 : 805 90d solo

Name	Start Size [nt]	End Size [nt]	Area	% of total Area
18S	1,440	1,935	46.6	12.5
28S	3,304	4,252	77.4	20.7



Overall Results for Ladder

RNA Area:	132.7
RNA Concentration:	1,000 pg/µl
Result Flagging Color:	
Result Flagging Label:	All Other Samples

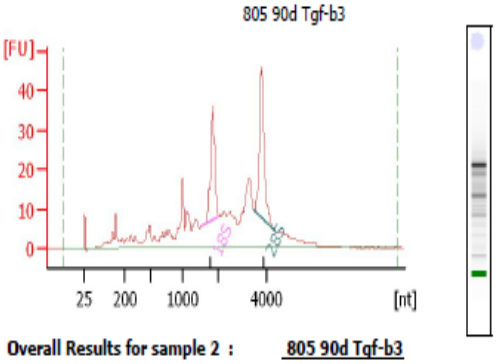


Overall Results for sample 1 : 805 90d Noggin

RNA Area:	404.1
RNA Concentration:	3,044 pg/µl
rRNA Ratio [28s / 18s]:	1.5
RNA Integrity Number (RIN):	8.2 (B.02.07)
Result Flagging Color:	
Result Flagging Label:	RIN: 8.20

Fragment table for sample 1 : 805 90d Noggin

Name	Start Size [nt]	End Size [nt]	Area	% of total Area
18S	1,497	2,029	57.5	14.2
28S	3,449	4,433	88.9	22.0

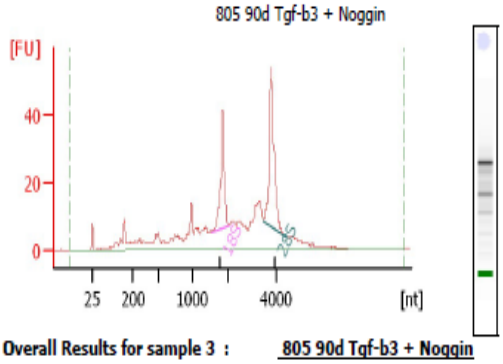


Overall Results for sample 2 : 805 90d Tgf-b3

RNA Area:	497.6
RNA Concentration:	3,748 pg/µl
rRNA Ratio [28s / 18s]:	1.5
RNA Integrity Number (RIN):	7 (B.02.07)
Result Flagging Color:	
Result Flagging Label:	RIN:7

Fragment table for sample 2 : 805 90d Tgf-b3

Name	Start Size [nt]	End Size [nt]	Area	% of total Area
18S	1,532	1,985	44.1	8.9
28S	3,445	4,282	66.6	13.4

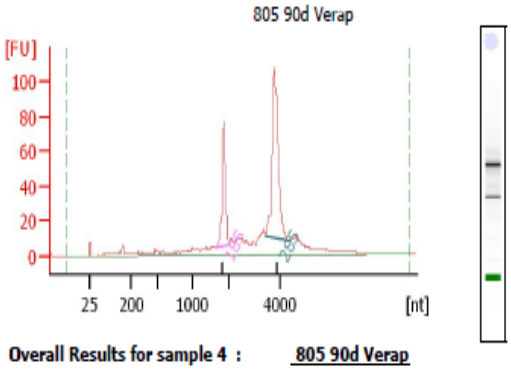


Overall Results for sample 3 : 805 90d Tgf-b3 + Noggin

RNA Area:	468.2
RNA Concentration:	3,527 pg/µl
rRNA Ratio [28s / 18s]:	1.5
RNA Integrity Number (RIN):	7.5 (B.02.07)
Result Flagging Color:	
Result Flagging Label:	RIN: 7.50

Fragment table for sample 3 : 805 90d Tgf-b3 + Noggin

Name	Start Size [nt]	End Size [nt]	Area	% of total Area
18S	1,550	2,041	49.4	10.6
28S	3,467	4,408	75.7	16.2

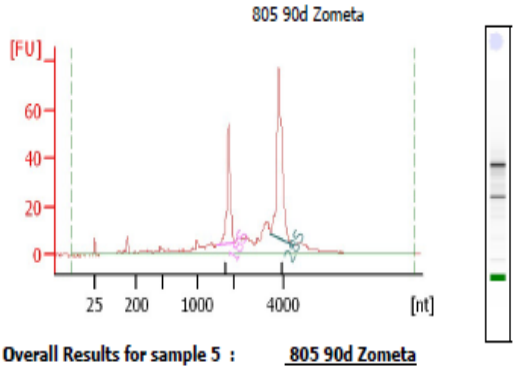


Overall Results for sample 4 : 805 90d Verap

RNA Area:	610.5
RNA Concentration:	4,599 pg/µl
rRNA Ratio [28s / 18s]:	2.0
RNA Integrity Number (RIN):	9.2 (B.02.07)
Result Flagging Color:	
Result Flagging Label:	RIN: 9.20

Fragment table for sample 4 : 805 90d Verap

Name	Start Size [nt]	End Size [nt]	Area	% of total Area
18S	1,618	1,991	91.9	15.1
28S	3,451	4,418	182.8	29.9

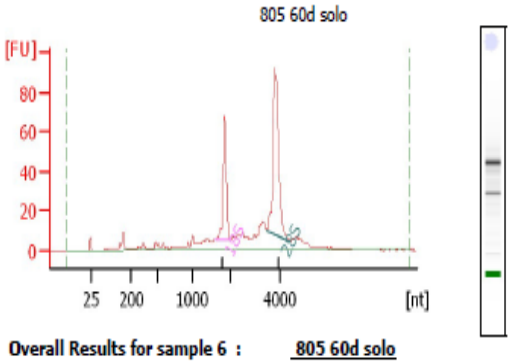


Overall Results for sample 5 : 805 90d Zometa

RNA Area:	442.8
RNA Concentration:	3,336 pg/µl
rRNA Ratio [28s / 18s]:	1.8
RNA Integrity Number (RIN):	8.7 (B.02.07)
Result Flagging Color:	
Result Flagging Label:	RIN: 8.70

Fragment table for sample 5 : 805 90d Zometa

Name	Start Size [nt]	End Size [nt]	Area	% of total Area
18S	1,532	2,027	67.0	15.1
28S	3,480	4,380	118.0	26.6

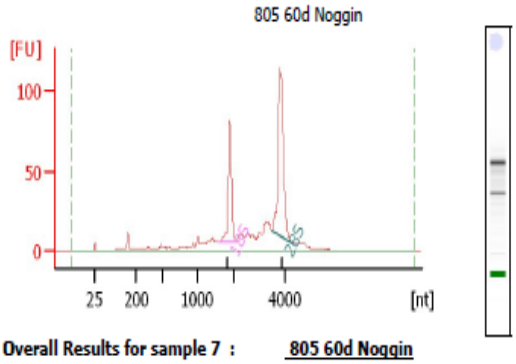


Overall Results for sample 6 : 805 60d solo

RNA Area:	539.2
RNA Concentration:	4,062 pg/µl
rRNA Ratio [28s / 18s]:	1.7
RNA Integrity Number (RIN):	8.6 (B.02.07)
Result Flagging Color:	
Result Flagging Label:	RIN: 8.60

Fragment table for sample 6 : 805 60d solo

Name	Start Size [nt]	End Size [nt]	Area	% of total Area
18S	1,611	2,017	82.1	15.2
28S	3,477	4,414	141.8	26.3

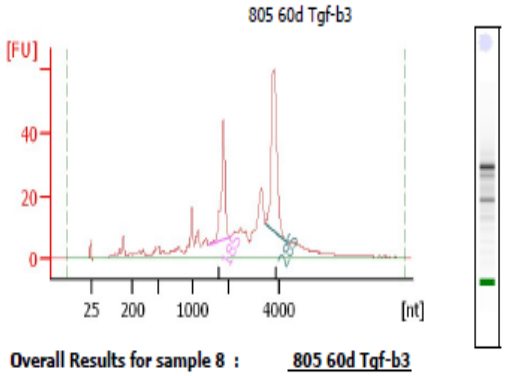


Overall Results for sample 7 : 805 60d Noggin

RNA Area:	632.3
RNA Concentration:	4,763 pg/µl
rRNA Ratio [28s / 18s]:	1.7
RNA Integrity Number (RIN):	8.7 (B.02.07)
Result Flagging Color:	
Result Flagging Label:	RIN: 8.70

Fragment table for sample 7 : 805 60d Noggin

Name	Start Size [nt]	End Size [nt]	Area	% of total Area
18S	1,590	2,057	98.1	15.5
28S	3,507	4,376	167.2	26.4

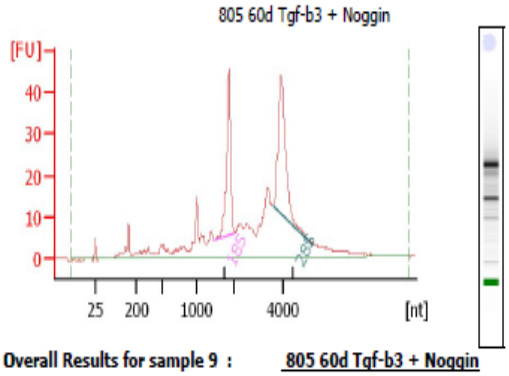


Overall Results for sample 8 : **805 60d Tgf-b3**

RNA Area:	516.8
RNA Concentration:	3,893 pg/µl
rRNA Ratio [28s / 18s]:	1.6
RNA Integrity Number (RIN):	7.7 (B.02.07)
Result Flagging Color:	
Result Flagging Label:	RIN: 7.70

Fragment table for sample 8 : **805 60d Tgf-b3**

Name	Start Size [nt]	End Size [nt]	Area	% of total Area
18S	1,473	2,005	55.8	10.8
28S	3,476	4,328	89.5	17.3

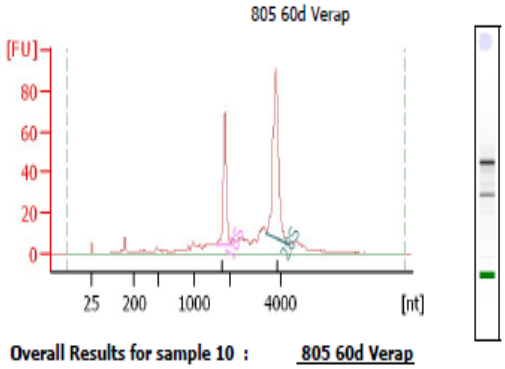


Overall Results for sample 9 : **805 60d Tgf-b3 + Noggin**

RNA Area:	517.4
RNA Concentration:	3,898 pg/µl
rRNA Ratio [28s / 18s]:	1.3
RNA Integrity Number (RIN):	7.7 (B.02.07)
Result Flagging Color:	
Result Flagging Label:	RIN: 7.70

Fragment table for sample 9 : **805 60d Tgf-b3 + Noggin**

Name	Start Size [nt]	End Size [nt]	Area	% of total Area
18S	1,494	2,062	63.5	12.3
28S	3,598	5,203	83.8	16.2

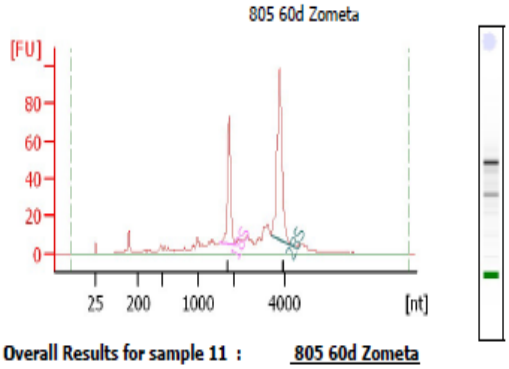


Overall Results for sample 10 : **805 60d Verap**

RNA Area:	515.9
RNA Concentration:	3,886 pg/µl
rRNA Ratio [28s / 18s]:	1.8
RNA Integrity Number (RIN):	8.8 (B.02.07)
Result Flagging Color:	
Result Flagging Label:	RIN: 8.80

Fragment table for sample 10 : **805 60d Verap**

Name	Start Size [nt]	End Size [nt]	Area	% of total Area
18S	1,600	1,997	82.0	15.9
28S	3,444	4,387	147.1	28.5

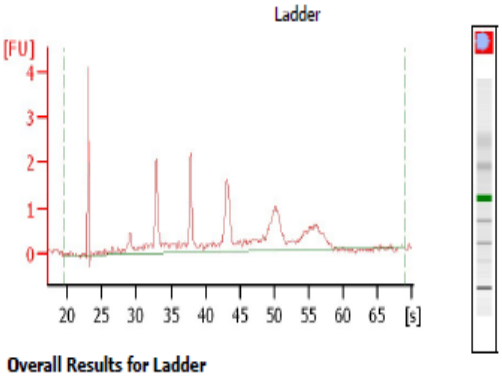


Overall Results for sample 11 : **805 60d Zometa**

RNA Area:	556.8
RNA Concentration:	4,194 pg/µl
rRNA Ratio [28s / 18s]:	1.7
RNA Integrity Number (RIN):	8.5 (B.02.07)
Result Flagging Color:	
Result Flagging Label:	RIN: 8.50

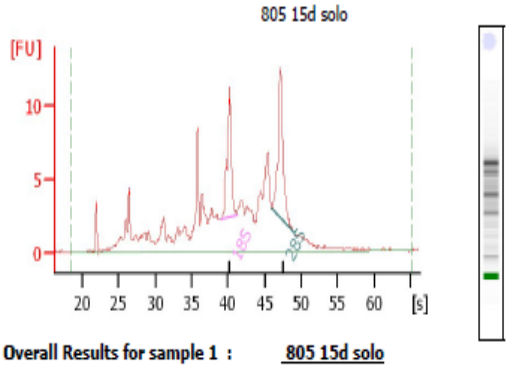
Fragment table for sample 11 : **805 60d Zometa**

Name	Start Size [nt]	End Size [nt]	Area	% of total Area
18S	1,609	2,024	84.9	15.2
28S	3,458	4,387	142.9	25.7



Overall Results for Ladder

RNA Area:	25.0
RNA Concentration:	1,000 pg/µl
Result Flagging Color:	
Result Flagging Label:	All Other Samples

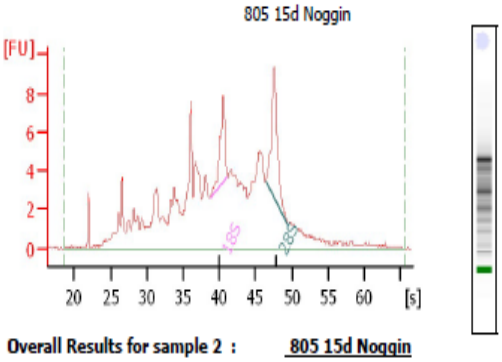


Overall Results for sample 1 : 805 15d solo

RNA Area:	183.2
RNA Concentration:	7,327 pg/µl
rRNA Ratio [28s / 18s]:	1.2
RNA Integrity Number (RIN):	6.3 (B.02.07)
Result Flagging Color:	
Result Flagging Label:	RIN: 6.30

Fragment table for sample 1 : 805 15d solo

Name	Start Size [nt]	End Size [nt]	Area	% of total Area
18S	0	0	14.4	7.9
28S	0	0	16.8	9.2

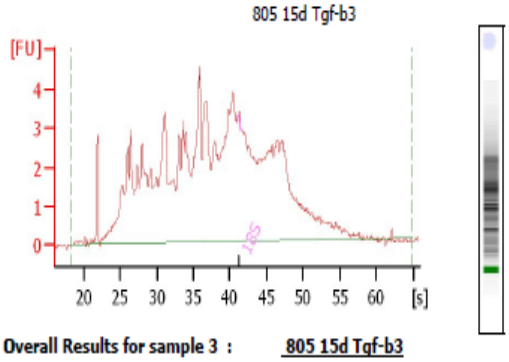


Overall Results for sample 2 : 805 15d Noggin

RNA Area:	204.7
RNA Concentration:	8,189 pg/µl
rRNA Ratio [28s / 18s]:	1.5
RNA Integrity Number (RIN):	5 (B.02.07)
Result Flagging Color:	
Result Flagging Label:	RIN:5

Fragment table for sample 2 : 805 15d Noggin

Name	Start Size [nt]	End Size [nt]	Area	% of total Area
18S	0	0	9.1	4.4
28S	0	0	13.6	6.6

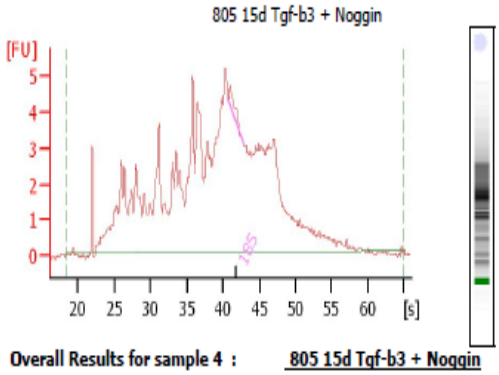


Overall Results for sample 3 : 805 15d Tgf-b3

RNA Area:	159.1
RNA Concentration:	6,363 pg/µl
rRNA Ratio [28s / 18s]:	0.0
RNA Integrity Number (RIN):	2.2 (B.02.07)
Result Flagging Color:	
Result Flagging Label:	RIN: 2.20

Fragment table for sample 3 : 805 15d Tgf-b3

Name	Start Size [nt]	End Size [nt]	Area	% of total Area
18S	0	0	0.1	0.1

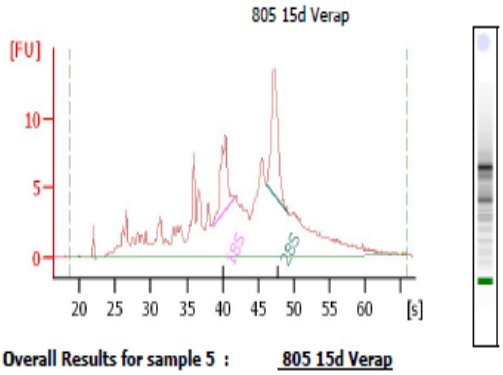


Overall Results for sample 4 : **805 15d Tgf-b3 + Noggin**

RNA Area:	172.0
RNA Concentration:	6,880 pg/µl
rRNA Ratio [28s / 18s]:	0.0
RNA Integrity Number (RIN):	2.4 (B.02.07)
Result Flagging Color:	
Result Flagging Label:	RIN: 2.40

Fragment table for sample 4 : **805 15d Tgf-b3 + Noggin**

Name	Start Size [nt]	End Size [nt]	Area	% of total Area
18S	0	0	1.3	0.7

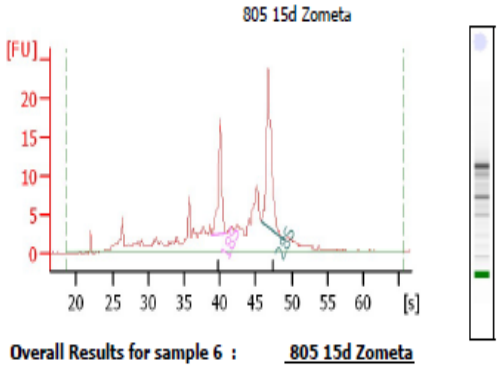


Overall Results for sample 5 : **805 15d Verap**

RNA Area:	238.4
RNA Concentration:	9,536 pg/µl
rRNA Ratio [28s / 18s]:	1.3
RNA Integrity Number (RIN):	5.5 (B.02.07)
Result Flagging Color:	
Result Flagging Label:	RIN: 5.50

Fragment table for sample 5 : **805 15d Verap**

Name	Start Size [nt]	End Size [nt]	Area	% of total Area
18S	0	0	14.6	6.1
28S	0	0	19.4	8.1

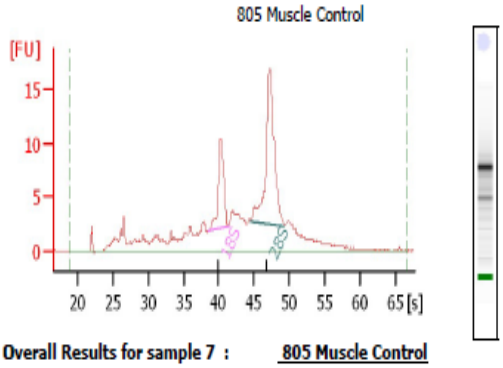


Overall Results for sample 6 : **805 15d Zometa**

RNA Area:	210.3
RNA Concentration:	8,414 pg/µl
rRNA Ratio [28s / 18s]:	1.6
RNA Integrity Number (RIN):	7.4 (B.02.07)
Result Flagging Color:	
Result Flagging Label:	RIN: 7.40

Fragment table for sample 6 : **805 15d Zometa**

Name	Start Size [nt]	End Size [nt]	Area	% of total Area
18S	0	0	21.5	10.2
28S	0	0	34.1	16.2

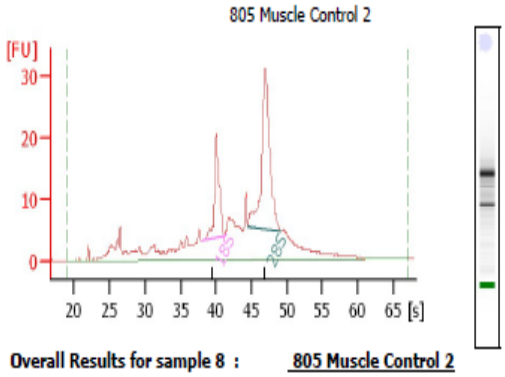


Overall Results for sample 7 : **805 Muscle Control**

RNA Area:	197.4
RNA Concentration:	7,896 pg/µl
rRNA Ratio [28s / 18s]:	2.4
RNA Integrity Number (RIN):	8.1 (B.02.07)
Result Flagging Color:	
Result Flagging Label:	RIN: 8.10

Fragment table for sample 7 : **805 Muscle Control**

Name	Start Size [nt]	End Size [nt]	Area	% of total Area
18S	0	0	17.1	8.7
28S	0	0	41.7	21.1

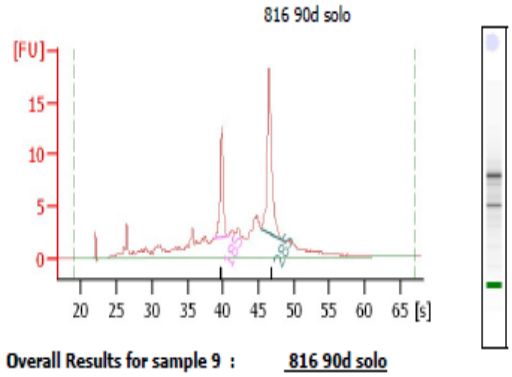


Overall Results for sample 8 : **805 Muscle Control 2**

RNA Area:	350.3
RNA Concentration:	14,013 pg/µl
rRNA Ratio [28s / 18s]:	2.4
RNA Integrity Number (RIN):	8.3 (B.02.07)
Result Flagging Color:	
Result Flagging Label:	RIN: 8.30

Fragment table for sample 8 : **805 Muscle Control 2**

Name	Start Size [nt]	End Size [nt]	Area	% of total Area
18S	0	0	32.6	9.3
28S	0	0	77.0	22.0

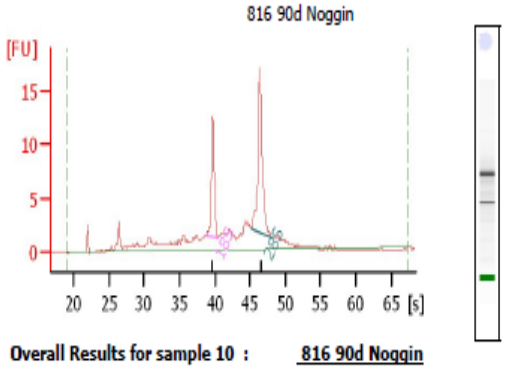


Overall Results for sample 9 : **816 90d solo**

RNA Area:	143.4
RNA Concentration:	5,738 pg/µl
rRNA Ratio [28s / 18s]:	1.8
RNA Integrity Number (RIN):	7.6 (B.02.07)
Result Flagging Color:	
Result Flagging Label:	RIN: 7.60

Fragment table for sample 9 : **816 90d solo**

Name	Start Size [nt]	End Size [nt]	Area	% of total Area
18S	0	0	14.3	10.0
28S	0	0	26.3	18.3

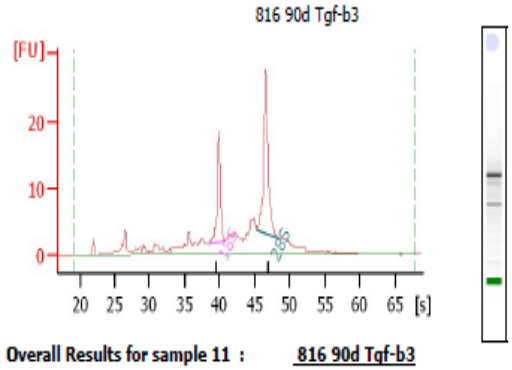


Overall Results for sample 10 : **816 90d Noggin**

RNA Area:	110.3
RNA Concentration:	4,413 pg/µl
rRNA Ratio [28s / 18s]:	1.8
RNA Integrity Number (RIN):	8 (B.02.07)
Result Flagging Color:	
Result Flagging Label:	RIN:8

Fragment table for sample 10 : **816 90d Noggin**

Name	Start Size [nt]	End Size [nt]	Area	% of total Area
18S	0	0	14.2	12.8
28S	0	0	25.1	22.8

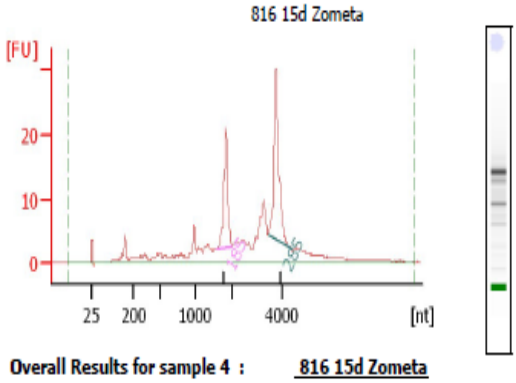


Overall Results for sample 11 : **816 90d Tgf-b3**

RNA Area:	190.0
RNA Concentration:	7,599 pg/µl
rRNA Ratio [28s / 18s]:	1.7
RNA Integrity Number (RIN):	8.2 (B.02.07)
Result Flagging Color:	
Result Flagging Label:	RIN: 8.20

Fragment table for sample 11 : **816 90d Tgf-b3**

Name	Start Size [nt]	End Size [nt]	Area	% of total Area
18S	0	0	23.0	12.1
28S	0	0	40.0	21.0

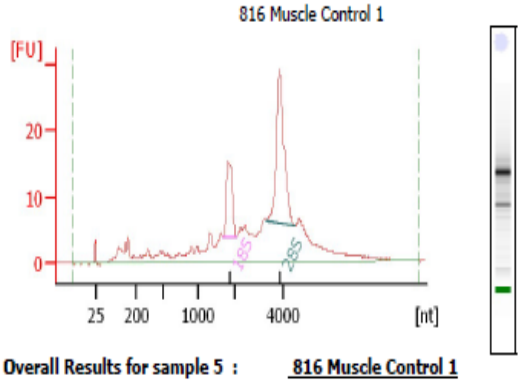


Overall Results for sample 4 : 816 15d Zometa

RNA Area:	228.9
RNA Concentration:	2,701 pg/µl
rRNA Ratio [28s / 18s]:	1.7
RNA Integrity Number (RIN):	7.9 (B.02.07)
Result Flagging Color:	
Result Flagging Label:	RIN: 7.90

Fragment table for sample 4 : 816 15d Zometa

Name	Start Size [nt]	End Size [nt]	Area	% of total Area
18S	1,613	2,031	25.7	11.2
28S	3,451	4,384	43.3	18.9

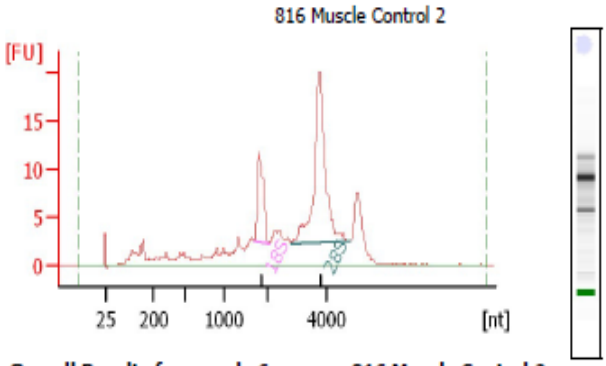


Overall Results for sample 5 : 816 Muscle Control 1

RNA Area:	321.2
RNA Concentration:	3,790 pg/µl
rRNA Ratio [28s / 18s]:	2.4
RNA Integrity Number (RIN):	7.8 (B.02.07)
Result Flagging Color:	
Result Flagging Label:	RIN: 7.80

Fragment table for sample 5 : 816 Muscle Control 1

Name	Start Size [nt]	End Size [nt]	Area	% of total Area
18S	1,702	2,082	24.8	7.7
28S	3,329	4,437	59.8	18.6



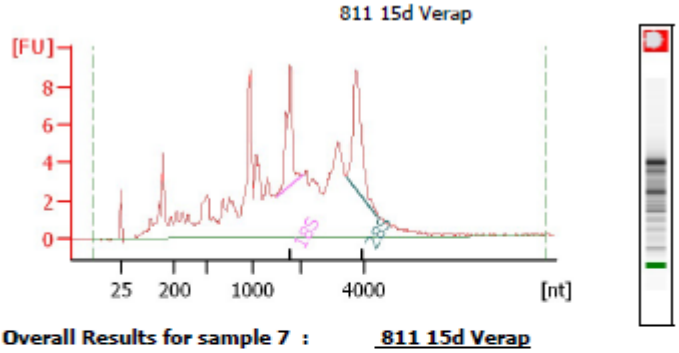
Overall Results for sample 6 : 816 Muscle Control 2

RNA Area:	213.2
RNA Concentration:	2,515 pg/µl
rRNA Ratio [28s / 18s]:	3.4
RNA Integrity Number (RIN):	8.4 (B.02.07)
Result Flagging Color:	
Result Flagging Label:	RIN: 8.40

Fragment table for sample 6 : 816 Muscle Control 2

Name	Start Size [nt]	End Size [nt]	Area	% of total Area
18S	1,681	2,024	17.1	8.0
28S	2,782	4,777	58.1	27.2

Samples repeated from old stock or after new RNA extraction (note: (new) = new RNA extraction)

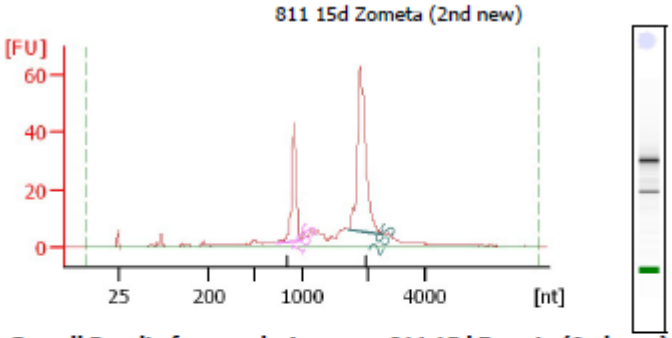


Overall Results for sample 7 : 811 15d Verap

RNA Area:	176.4
RNA Concentration:	2,082 pg/µl
rRNA Ratio [28s / 18s]:	1.2
RNA Integrity Number (RIN):	N/A (B.02.07)
Result Flagging Color:	
Result Flagging Label:	RIN N/A

Fragment table for sample 7 : 811 15d Verap

Name	Start Size [nt]	End Size [nt]	Area	% of total Area
18S	1,500	2,116	12.4	7.0
28S	3,448	4,426	15.0	8.5

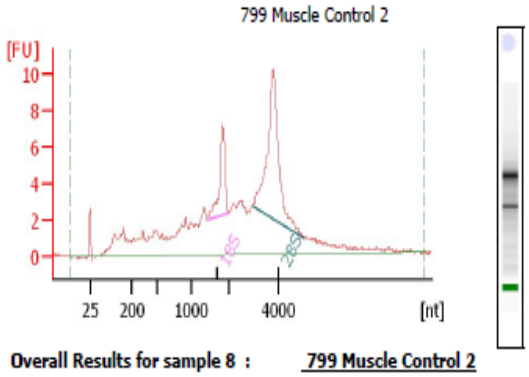


Overall Results for sample 4 : 811 15d Zometa (2nd new)

RNA Area:	342.5
RNA Concentration:	3,612 pg/µl
rRNA Ratio [28s / 18s]:	2.1
RNA Integrity Number (RIN):	9.4 (B.02.07)
Result Flagging Color:	
Result Flagging Label:	RIN: 9.40

Fragment table for sample 4 : 811 15d Zometa (2nd new)

Name	Start Size [nt]	End Size [nt]	Area	% of total Area
18S	728	980	54.4	15.9
28S	1,700	2,511	114.1	33.3

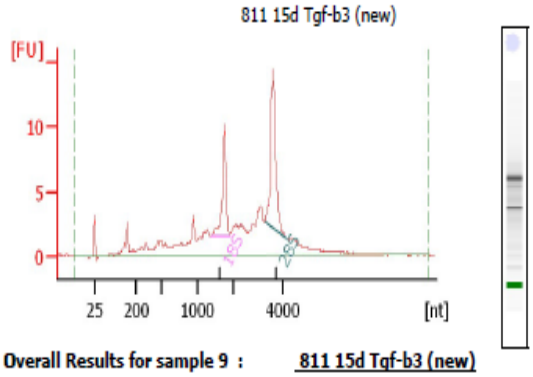


Overall Results for sample 8 : **799 Muscle Control 2**

RNA Area:	167.1
RNA Concentration:	1,972 pg/µl
rRNA Ratio [28s / 18s]:	2.8
RNA Integrity Number (RIN):	7.7 (B.02.07)
Result Flagging Color:	
Result Flagging Label:	RIN: 7.70

Fragment table for sample 8 : **799 Muscle Control 2**

Name	Start Size [nt]	End Size [nt]	Area	% of total Area
18S	1,429	2,021	11.7	7.0
28S	2,953	5,031	32.4	19.4

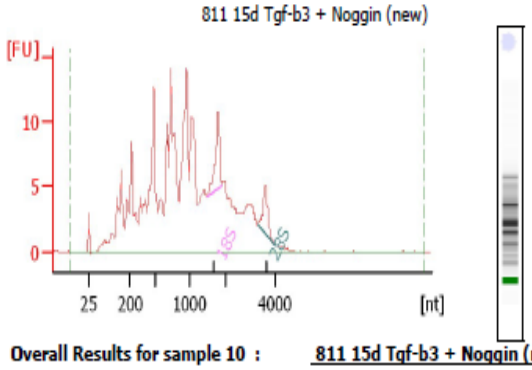


Overall Results for sample 9 : **811 15d Tgf-b3 (new)**

RNA Area:	128.9
RNA Concentration:	1,521 pg/µl
rRNA Ratio [28s / 18s]:	1.5
RNA Integrity Number (RIN):	7.4 (B.02.07)
Result Flagging Color:	
Result Flagging Label:	RIN: 7.40

Fragment table for sample 9 : **811 15d Tgf-b3 (new)**

Name	Start Size [nt]	End Size [nt]	Area	% of total Area
18S	1,402	1,909	13.0	10.1
28S	3,267	4,111	19.7	15.3

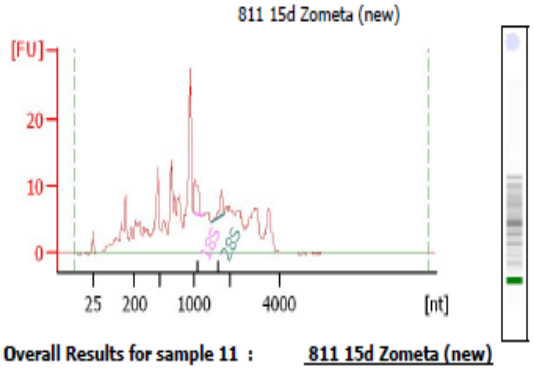


Overall Results for sample 10 : **811 15d Tgf-b3 + Noggin (new)**

RNA Area:	318.5
RNA Concentration:	3,758 pg/µl
rRNA Ratio [28s / 18s]:	0.6
RNA Integrity Number (RIN):	3.4 (B.02.07)
Result Flagging Color:	
Result Flagging Label:	RIN: 3.40

Fragment table for sample 10 : **811 15d Tgf-b3 + Noggin (new)**

Name	Start Size [nt]	End Size [nt]	Area	% of total Area
18S	1,480	1,873	10.0	3.1
28S	3,242	3,949	5.9	1.9

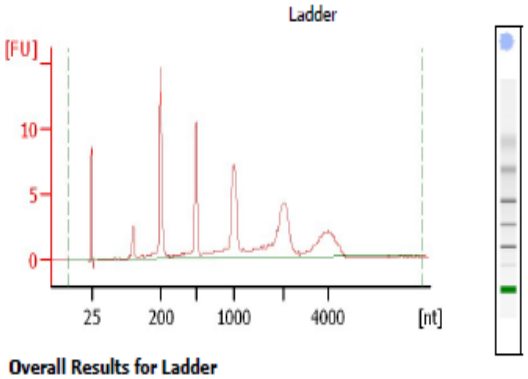


Overall Results for sample 11 : **811 15d Zometa (new)**

RNA Area:	351.0
RNA Concentration:	4,141 pg/µl
rRNA Ratio [28s / 18s]:	0.5
RNA Integrity Number (RIN):	2.8 (B.02.07)
Result Flagging Color:	
Result Flagging Label:	RIN: 2.80

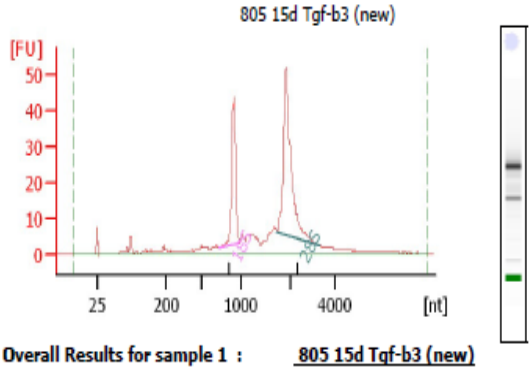
Fragment table for sample 11 : **811 15d Zometa (new)**

Name	Start Size [nt]	End Size [nt]	Area	% of total Area
18S	983	1,234	9.0	2.6
28S	1,480	1,814	4.7	1.4



Overall Results for Ladder

RNA Area:	94.8
RNA Concentration:	1,000 pg/µl
Result Flagging Color:	
Result Flagging Label:	All Other Samples

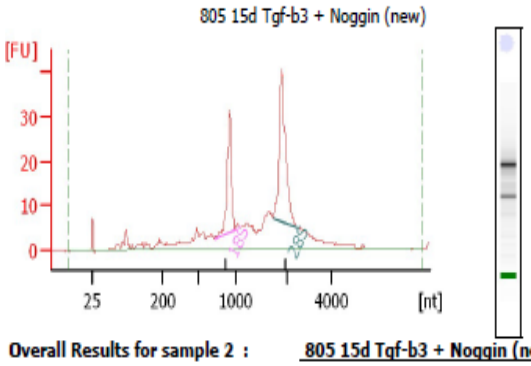


Overall Results for sample 1 : 805 15d Tgf-b3 (new)

RNA Area:	354.2
RNA Concentration:	3,735 pg/µl
rRNA Ratio [28s / 18s]:	2.0
RNA Integrity Number (RIN):	9.3 (B.02.07)
Result Flagging Color:	
Result Flagging Label:	RIN: 9.30

Fragment table for sample 1 : 805 15d Tgf-b3 (new)

Name	Start Size [nt]	End Size [nt]	Area	% of total Area
18S	728	991	56.3	15.9
28S	1,716	3,272	114.9	32.4

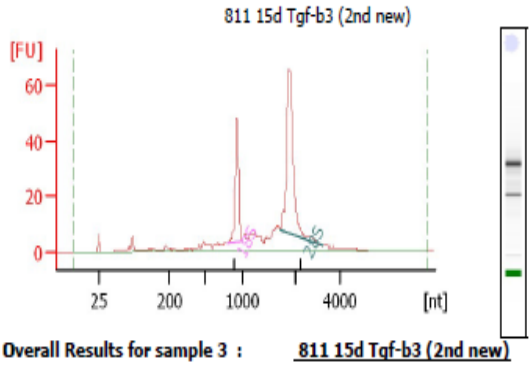


Overall Results for sample 2 : 805 15d Tgf-b3 + Noggin (new)

RNA Area:	348.2
RNA Concentration:	3,672 pg/µl
rRNA Ratio [28s / 18s]:	1.7
RNA Integrity Number (RIN):	8.1 (B.02.07)
Result Flagging Color:	
Result Flagging Label:	RIN: 8.10

Fragment table for sample 2 : 805 15d Tgf-b3 + Noggin (new)

Name	Start Size [nt]	End Size [nt]	Area	% of total Area
18S	721	983	39.9	11.4
28S	1,715	2,455	69.6	20.0



Overall Results for sample 3 : 811 15d Tgf-b3 (2nd new)

RNA Area:	384.9
RNA Concentration:	4,059 pg/µl
rRNA Ratio [28s / 18s]:	2.0
RNA Integrity Number (RIN):	9.2 (B.02.07)
Result Flagging Color:	
Result Flagging Label:	RIN: 9.20

Fragment table for sample 3 : 811 15d Tgf-b3 (2nd new)

Name	Start Size [nt]	End Size [nt]	Area	% of total Area
18S	795	985	59.4	15.4
28S	1,713	3,228	121.6	31.6

APPENDIX C Quantitative RT-PCR reports (Plate setup, amplification curves, $C_{t/q}$ values, target gene)

Plate bactin 15d.pcrd

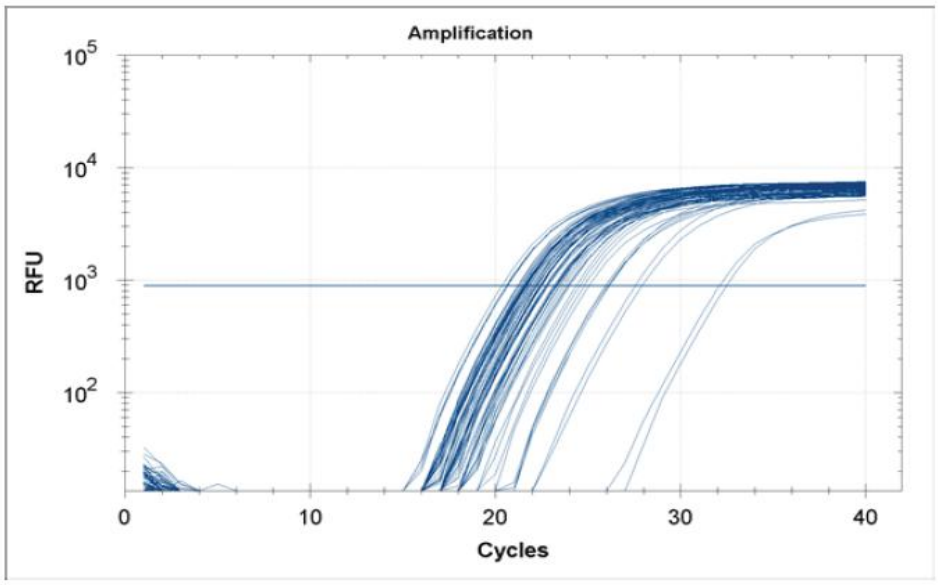
2013/08/21 12:33 PM

Run Setup

Plate Display

	1	2	3	4	5	6	7	8	9	10	11	12
A	Unk-1 Actin 001 S15	Unk-1 Actin 001 S15	Unk-7 Actin 002 S15	Unk-7 Actin 002 S15	Unk-13 Actin 799 S15	Unk-13 Actin 799 S15	Unk-18 Actin 811 S15	Unk-18 Actin 811 S15	Unk-24 Actin 805 S15	Unk-24 Actin 805 S15	Unk-30 Actin 816 S15	Unk-30 Actin 816 S15
B	Unk-2 Actin 001 N15	Unk-2 Actin 001 N15	Unk-8 Actin 002 N15	Unk-8 Actin 002 N15	Unk-14 Actin 799 N15	Unk-14 Actin 799 N15	Unk-19 Actin 811 N15	Unk-19 Actin 811 N15	Unk-25 Actin 805 N15	Unk-25 Actin 805 N15	Unk-31 Actin 816 N15	Unk-31 Actin 816 N15
C	Unk-3 Actin 001 T15	Unk-3 Actin 001 T15	Unk-9 Actin 002 T15	Unk-9 Actin 002 T15	Unk-15 Actin 799 T15	Unk-15 Actin 799 T15	Unk-20 Actin 811 T15	Unk-20 Actin 811 T15	Unk-26 Actin 805 T15	Unk-26 Actin 805 T15	Unk-32 Actin 816 T15	Unk-32 Actin 816 T15
D	Unk-4 Actin 001 T+N15	Unk-4 Actin 001 T+N15	Unk-10 Actin 002 T+N15	Unk-10 Actin 002 T+N15	Unk-16 Actin 799 T+N15	Unk-16 Actin 799 T+N15	Unk-21 Actin 811 T+N15	Unk-21 Actin 811 T+N15	Unk-27 Actin 805 T+N15	Unk-27 Actin 805 T+N15	Unk-33 Actin 816 T+N15	Unk-33 Actin 816 T+N15
E	Unk-5 Actin 001 V15	Unk-5 Actin 001 V15	Unk-11 Actin 002 V15	Unk-11 Actin 002 V15	Unk-17 Actin 799 Z15	Unk-17 Actin 799 Z15	Unk-22 Actin 811 V15	Unk-22 Actin 811 V15	Unk-28 Actin 805 V15	Unk-28 Actin 805 V15	Unk-34 Actin 816 V15	Unk-34 Actin 816 V15
F	Unk-6 Actin 001 Z15	Unk-6 Actin 001 Z15	Unk-12 Actin 002 Z15	Unk-12 Actin 002 Z15			Unk-23 Actin 811 Z15	Unk-23 Actin 811 Z15	Unk-29 Actin 805 Z15	Unk-29 Actin 805 Z15	Unk-35 Actin 816 Z15	Unk-35 Actin 816 Z15
G	Pos-36 Actin 804 PC	Pos-36 Actin 804 PC	NTC-37 Actin H2O	NTC-37 Actin H2O	NTC-38 Actin H2O	NTC-38 Actin H2O	Unk-39 Actin Pooled MC 10ng	Unk-39 Actin Pooled MC 10ng	Unk-40 Actin Pooled MC 15ng	Unk-40 Actin Pooled MC 15ng	Unk-41 Actin Pooled MC 5ng	Unk-41 Actin Pooled MC 5ng
H												

Quantification



Quantification Data

Well	Fluor	Target	Content	Sample	Cq	Cq Mean	Cq Std. Dev
A01	FAM	Actin	Unkn-01	001 S15	23.13	23.17	0.056
A02	FAM	Actin	Unkn-01	001 S15	23.21	23.17	0.056
A03	FAM	Actin	Unkn-07	002 S15	21.64	21.54	0.132
A04	FAM	Actin	Unkn-07	002 S15	21.45	21.54	0.132
A05	FAM	Actin	Unkn-13	799 S15	23.19	23.20	0.026
A06	FAM	Actin	Unkn-13	799 S15	23.22	23.20	0.026
A07	FAM	Actin	Unkn-18	811 S15	23.42	23.07	0.505
A08	FAM	Actin	Unkn-18	811 S15	22.71	23.07	0.505
A09	FAM	Actin	Unkn-24	805 S15	32.41	32.24	0.236
A10	FAM	Actin	Unkn-24	805 S15	32.08	32.24	0.236
A11	FAM	Actin	Unkn-30	816 S15	22.74	23.00	0.372
A12	FAM	Actin	Unkn-30	816 S15	23.27	23.00	0.372
B01	FAM	Actin	Unkn-02	001 N15	22.63	22.52	0.161
B02	FAM	Actin	Unkn-02	001 N15	22.40	22.52	0.161
B03	FAM	Actin	Unkn-08	002 N15	21.53	21.45	0.115
B04	FAM	Actin	Unkn-08	002 N15	21.37	21.45	0.115
B05	FAM	Actin	Unkn-14	799 N15	22.34	22.33	0.021
B06	FAM	Actin	Unkn-14	799 N15	22.32	22.33	0.021
B07	FAM	Actin	Unkn-19	811 N15	21.77	21.99	0.313
B08	FAM	Actin	Unkn-19	811 N15	22.21	21.99	0.313
B09	FAM	Actin	Unkn-25	805 N15	24.73	24.88	0.212
B10	FAM	Actin	Unkn-25	805 N15	25.03	24.88	0.212
B11	FAM	Actin	Unkn-31	816 N15	23.85	23.77	0.112
B12	FAM	Actin	Unkn-31	816 N15	23.70	23.77	0.112
C01	FAM	Actin	Unkn-03	001 T15	21.47	21.64	0.239
C02	FAM	Actin	Unkn-03	001 T15	21.81	21.64	0.239
C03	FAM	Actin	Unkn-09	002 T15	21.38	21.31	0.087
C04	FAM	Actin	Unkn-09	002 T15	21.25	21.31	0.087
C05	FAM	Actin	Unkn-15	799 T15	21.94	22.01	0.095
C06	FAM	Actin	Unkn-15	799 T15	22.08	22.01	0.095
C07	FAM	Actin	Unkn-20	811 T15	20.56	20.57	0.016
C08	FAM	Actin	Unkn-20	811 T15	20.59	20.57	0.016
C09	FAM	Actin	Unkn-26	805 T15	21.74	21.69	0.067
C10	FAM	Actin	Unkn-26	805 T15	21.65	21.69	0.067
C11	FAM	Actin	Unkn-32	816 T15	23.11	23.18	0.100
C12	FAM	Actin	Unkn-32	816 T15	23.25	23.18	0.100
D01	FAM	Actin	Unkn-04	001 T+N15	22.38	22.37	0.015
D02	FAM	Actin	Unkn-04	001 T+N15	22.35	22.37	0.015
D03	FAM	Actin	Unkn-10	002 T+N15	21.51	21.50	0.010
D04	FAM	Actin	Unkn-10	002 T+N15	21.50	21.50	0.010
D05	FAM	Actin	Unkn-16	799 T+N15	22.42	22.42	0.003
D06	FAM	Actin	Unkn-16	799 T+N15	22.43	22.42	0.003
D07	FAM	Actin	Unkn-21	811 T+N15	24.48	24.39	0.122
D08	FAM	Actin	Unkn-21	811 T+N15	24.30	24.39	0.122
D09	FAM	Actin	Unkn-27	805 T+N15	22.03	22.07	0.068
D10	FAM	Actin	Unkn-27	805 T+N15	22.12	22.07	0.068
D11	FAM	Actin	Unkn-33	816 T+N15	21.94	21.94	0.010

Well	Fluor	Target	Content	Sample	Cq	Cq Mean	Cq Std. Dev
D12	FAM	Actin	Unkn-33	816 T+N15	21.95	21.94	0.010
E01	FAM	Actin	Unkn-05	001 V15	22.73	22.73	0.003
E02	FAM	Actin	Unkn-05	001 V15	22.74	22.73	0.003
E03	FAM	Actin	Unkn-11	002 V15	21.20	21.17	0.038
E04	FAM	Actin	Unkn-11	002 V15	21.14	21.17	0.038
E05	FAM	Actin	Unkn-17	799 Z15	21.61	21.59	0.018
E06	FAM	Actin	Unkn-17	799 Z15	21.58	21.59	0.018
E07	FAM	Actin	Unkn-22	811 V15	23.36	23.36	0.004
E08	FAM	Actin	Unkn-22	811 V15	23.36	23.36	0.004
E09	FAM	Actin	Unkn-28	805 V15	23.90	23.95	0.074
E10	FAM	Actin	Unkn-28	805 V15	24.00	23.95	0.074
E11	FAM	Actin	Unkn-34	816 V15	22.38	22.54	0.225
E12	FAM	Actin	Unkn-34	816 V15	22.70	22.54	0.225
F01	FAM	Actin	Unkn-06	001 Z15	21.53	21.55	0.025
F02	FAM	Actin	Unkn-06	001 Z15	21.57	21.55	0.025
F03	FAM	Actin	Unkn-12	002 Z15	21.50	21.42	0.112
F04	FAM	Actin	Unkn-12	002 Z15	21.34	21.42	0.112
F07	FAM	Actin	Unkn-23	811 Z15	20.52	20.40	0.164
F08	FAM	Actin	Unkn-23	811 Z15	20.29	20.40	0.164
F09	FAM	Actin	Unkn-29	805 Z15	23.25	23.40	0.216
F10	FAM	Actin	Unkn-29	805 Z15	23.56	23.40	0.216
F11	FAM	Actin	Unkn-35	816 Z15	22.63	22.72	0.125
F12	FAM	Actin	Unkn-35	816 Z15	22.81	22.72	0.125
G01	FAM	Actin	Pos Ctrl-36	804 PC	22.16	22.18	0.018
G02	FAM	Actin	Pos Ctrl-36	804 PC	22.19	22.18	0.018
G03	FAM	Actin	NTC-37	H2O	N/A	0.00	0.000
G04	FAM	Actin	NTC-37	H2O	N/A	0.00	0.000
G05	FAM	Actin	NTC-38	H2O	N/A	0.00	0.000
G06	FAM	Actin	NTC-38	H2O	N/A	0.00	0.000
G07	FAM	Actin	Unkn-39	Pooled MC 10ng	25.92	25.97	0.067
G08	FAM	Actin	Unkn-39	Pooled MC 10ng	26.01	25.97	0.067
G09	FAM	Actin	Unkn-40	Pooled MC 15ng	26.12	26.10	0.016
G10	FAM	Actin	Unkn-40	Pooled MC 15ng	26.09	26.10	0.016
G11	FAM	Actin	Unkn-41	Pooled MC 5ng	27.48	27.68	0.281
G12	FAM	Actin	Unkn-41	Pooled MC 5ng	27.88	27.68	0.281

Gene Expression

Target Names

Name	Full Name	Reference	Auto Efficiency	Efficiency
Actin	Actin	True	Yes	100.0%

Plate bactin 60d.pcrd

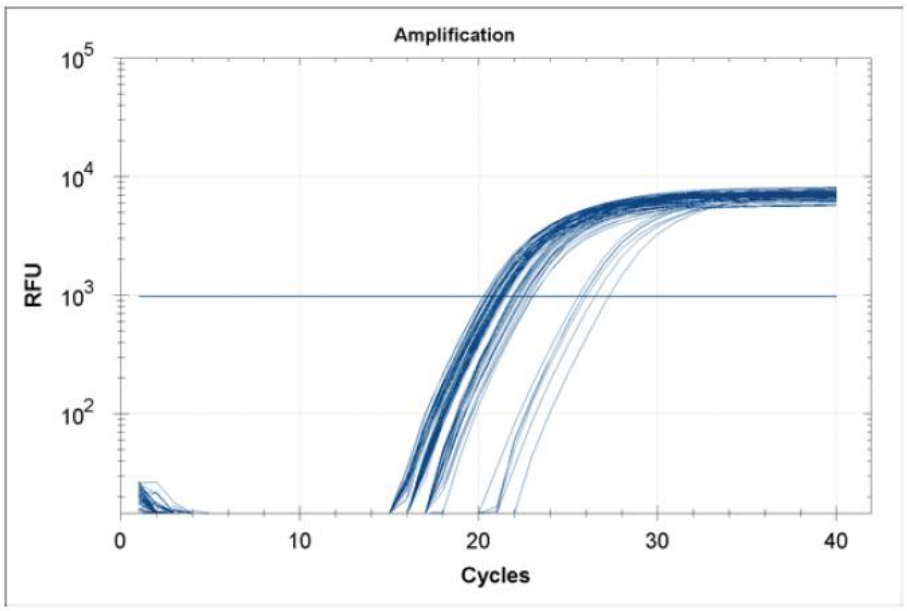
2013/08/21 12:32 PM

Run Setup

Plate Display

	1	2	3	4	5	6	7	8	9	10	11	12
A	Unk-1 Actin 001 S60	Unk-1 Actin 001 S60	Unk-7 Actin 002 S60	Unk-7 Actin 002 S60	Unk-13 Actin 799 S60	Unk-13 Actin 799 S60	Unk-18 Actin 811 S60	Unk-18 Actin 811 S60	Unk-24 Actin 805 S60	Unk-24 Actin 805 S60	Unk-30 Actin 816 S60	Unk-30 Actin 816 S60
B	Unk-2 Actin 001 N60	Unk-2 Actin 001 N60	Unk-8 Actin 002 N60	Unk-8 Actin 002 N60	Unk-14 Actin 799 N60	Unk-14 Actin 799 N60	Unk-19 Actin 811 N60	Unk-19 Actin 811 N60	Unk-25 Actin 805 N60	Unk-25 Actin 805 N60	Unk-31 Actin 816 N60	Unk-31 Actin 816 N60
C	Unk-3 Actin 001 T60	Unk-3 Actin 001 T60	Unk-9 Actin 002 T60	Unk-9 Actin 002 T60	Unk-15 Actin 799 T60	Unk-15 Actin 799 T60	Unk-20 Actin 811 T60	Unk-20 Actin 811 T60	Unk-26 Actin 805 T60	Unk-26 Actin 805 T60	Unk-32 Actin 816 T60	Unk-32 Actin 816 T60
D	Unk-4 Actin 001 T+N60	Unk-4 Actin 001 T+N60	Unk-10 Actin 002 T+N60	Unk-10 Actin 002 T+N60	Unk-16 Actin 799 T+N60	Unk-16 Actin 799 T+N60	Unk-21 Actin 811 T+N60	Unk-21 Actin 811 T+N60	Unk-27 Actin 805 T+N60	Unk-27 Actin 805 T+N60	Unk-33 Actin 816 T+N60	Unk-33 Actin 816 T+N60
E	Unk-5 Actin 001 V60	Unk-5 Actin 001 V60	Unk-11 Actin 002 V60	Unk-11 Actin 002 V60	Unk-17 Actin 799 Z60	Unk-17 Actin 799 Z60	Unk-22 Actin 811 V60	Unk-22 Actin 811 V60	Unk-28 Actin 805 V60	Unk-28 Actin 805 V60	Unk-34 Actin 816 V60	Unk-34 Actin 816 V60
F	Unk-6 Actin 001 Z60	Unk-6 Actin 001 Z60	Unk-12 Actin 002 Z60	Unk-12 Actin 002 Z60			Unk-23 Actin 811 Z60	Unk-23 Actin 811 Z60	Unk-29 Actin 805 Z60	Unk-29 Actin 805 Z60	Unk-35 Actin 816 Z60	Unk-35 Actin 816 Z60
G	Pos-36 Actin 804 PC	Pos-36 Actin 804 PC	NTC-37 Actin H2O	NTC-37 Actin H2O	NTC-38 Actin H2O	NTC-38 Actin H2O	Unk-39 Actin Pooled MC 10ng	Unk-39 Actin Pooled MC 10ng	Unk-40 Actin Pooled MC 15ng	Unk-40 Actin Pooled MC 15ng	Unk-41 Actin Pooled MC 5ng	Unk-41 Actin Pooled MC 5ng
H												

Quantification



Quantification Data

Well	Fluor	Target	Content	Sample	Cq	Cq Mean	Cq Std. Dev
A01	FAM	Actin	Unkn-01	001 S60	21.10	21.14	0.047
A02	FAM	Actin	Unkn-01	001 S60	21.17	21.14	0.047
A03	FAM	Actin	Unkn-07	002 S60	20.66	20.71	0.068
A04	FAM	Actin	Unkn-07	002 S60	20.76	20.71	0.068
A05	FAM	Actin	Unkn-13	799 S60	21.27	21.26	0.007
A06	FAM	Actin	Unkn-13	799 S60	21.26	21.26	0.007
A07	FAM	Actin	Unkn-18	811 S60	22.25	22.20	0.073
A08	FAM	Actin	Unkn-18	811 S60	22.15	22.20	0.073
A09	FAM	Actin	Unkn-24	805 S60	21.00	21.05	0.069
A10	FAM	Actin	Unkn-24	805 S60	21.10	21.05	0.069
A11	FAM	Actin	Unkn-30	816 S60	23.02	23.00	0.020
A12	FAM	Actin	Unkn-30	816 S60	22.99	23.00	0.020
B01	FAM	Actin	Unkn-02	001 N60	21.37	21.38	0.024
B02	FAM	Actin	Unkn-02	001 N60	21.40	21.38	0.024
B03	FAM	Actin	Unkn-08	002 N60	22.46	22.46	0.004
B04	FAM	Actin	Unkn-08	002 N60	22.45	22.46	0.004
B05	FAM	Actin	Unkn-14	799 N60	21.23	21.29	0.087
B06	FAM	Actin	Unkn-14	799 N60	21.35	21.29	0.087
B07	FAM	Actin	Unkn-19	811 N60	21.20	21.15	0.075
B08	FAM	Actin	Unkn-19	811 N60	21.10	21.15	0.075
B09	FAM	Actin	Unkn-25	805 N60	20.63	20.65	0.030
B10	FAM	Actin	Unkn-25	805 N60	20.67	20.65	0.030
B11	FAM	Actin	Unkn-31	816 N60	21.93	22.00	0.100
B12	FAM	Actin	Unkn-31	816 N60	22.07	22.00	0.100
C01	FAM	Actin	Unkn-03	001 T60	20.51	20.60	0.134
C02	FAM	Actin	Unkn-03	001 T60	20.70	20.60	0.134
C03	FAM	Actin	Unkn-09	002 T60	21.22	21.17	0.078
C04	FAM	Actin	Unkn-09	002 T60	21.11	21.17	0.078
C05	FAM	Actin	Unkn-15	799 T60	20.64	20.70	0.086
C06	FAM	Actin	Unkn-15	799 T60	20.76	20.70	0.086
C07	FAM	Actin	Unkn-20	811 T60	21.86	21.90	0.054
C08	FAM	Actin	Unkn-20	811 T60	21.93	21.90	0.054
C09	FAM	Actin	Unkn-26	805 T60	22.46	22.44	0.017
C10	FAM	Actin	Unkn-26	805 T60	22.43	22.44	0.017
C11	FAM	Actin	Unkn-32	816 T60	21.12	21.19	0.097
C12	FAM	Actin	Unkn-32	816 T60	21.26	21.19	0.097
D01	FAM	Actin	Unkn-04	001 T+N60	20.25	20.23	0.033
D02	FAM	Actin	Unkn-04	001 T+N60	20.21	20.23	0.033
D03	FAM	Actin	Unkn-10	002 T+N60	20.81	20.82	0.012
D04	FAM	Actin	Unkn-10	002 T+N60	20.83	20.82	0.012
D05	FAM	Actin	Unkn-16	799 T+N60	20.36	20.38	0.033
D06	FAM	Actin	Unkn-16	799 T+N60	20.41	20.38	0.033
D07	FAM	Actin	Unkn-21	811 T+N60	21.50	21.45	0.072
D08	FAM	Actin	Unkn-21	811 T+N60	21.40	21.45	0.072
D09	FAM	Actin	Unkn-27	805 T+N60	21.81	21.90	0.131
D10	FAM	Actin	Unkn-27	805 T+N60	22.00	21.90	0.131
D11	FAM	Actin	Unkn-33	816 T+N60	21.15	21.17	0.034

Well	Fluor	Target	Content	Sample	Cq	Cq Mean	Cq Std. Dev
D12	FAM	Actin	Unkn-33	816 T+N60	21.19	21.17	0.034
E01	FAM	Actin	Unkn-05	001 V60	21.05	21.03	0.030
E02	FAM	Actin	Unkn-05	001 V60	21.01	21.03	0.030
E03	FAM	Actin	Unkn-11	002 V60	20.39	20.40	0.007
E04	FAM	Actin	Unkn-11	002 V60	20.40	20.40	0.007
E05	FAM	Actin	Unkn-17	799 Z60	20.84	20.82	0.022
E06	FAM	Actin	Unkn-17	799 Z60	20.80	20.82	0.022
E07	FAM	Actin	Unkn-22	811 V60	21.29	21.28	0.007
E08	FAM	Actin	Unkn-22	811 V60	21.28	21.28	0.007
E09	FAM	Actin	Unkn-28	805 V60	20.48	20.47	0.013
E10	FAM	Actin	Unkn-28	805 V60	20.46	20.47	0.013
E11	FAM	Actin	Unkn-34	816 V60	20.83	20.92	0.118
E12	FAM	Actin	Unkn-34	816 V60	21.00	20.92	0.118
F01	FAM	Actin	Unkn-06	001 Z60	20.88	20.83	0.082
F02	FAM	Actin	Unkn-06	001 Z60	20.77	20.83	0.082
F03	FAM	Actin	Unkn-12	002 Z60	21.33	21.31	0.033
F04	FAM	Actin	Unkn-12	002 Z60	21.29	21.31	0.033
F07	FAM	Actin	Unkn-23	811 Z60	22.00	21.96	0.055
F08	FAM	Actin	Unkn-23	811 Z60	21.92	21.96	0.055
F09	FAM	Actin	Unkn-29	805 Z60	22.80	22.74	0.078
F10	FAM	Actin	Unkn-29	805 Z60	22.69	22.74	0.078
F11	FAM	Actin	Unkn-35	816 Z60	22.07	22.12	0.069
F12	FAM	Actin	Unkn-35	816 Z60	22.16	22.12	0.069
G01	FAM	Actin	Pos Ctrl-36	804 PC	22.57	22.47	0.137
G02	FAM	Actin	Pos Ctrl-36	804 PC	22.38	22.47	0.137
G03	FAM	Actin	NTC-37	H2O	N/A	0.00	0.000
G04	FAM	Actin	NTC-37	H2O	N/A	0.00	0.000
G05	FAM	Actin	NTC-38	H2O	N/A	0.00	0.000
G06	FAM	Actin	NTC-38	H2O	N/A	0.00	0.000
G07	FAM	Actin	Unkn-39	Pooled MC 10ng	25.50	25.64	0.204
G08	FAM	Actin	Unkn-39	Pooled MC 10ng	25.79	25.64	0.204
G09	FAM	Actin	Unkn-40	Pooled MC 15ng	25.78	25.89	0.161
G10	FAM	Actin	Unkn-40	Pooled MC 15ng	26.01	25.89	0.161
G11	FAM	Actin	Unkn-41	Pooled MC 5ng	26.43	26.83	0.563
G12	FAM	Actin	Unkn-41	Pooled MC 5ng	27.22	26.83	0.563

Gene Expression

Target Names

Name	Full Name	Reference	Auto Efficiency	Efficiency
Actin	Actin	True	Yes	100.0%

Plate bactin 90d.pcrd

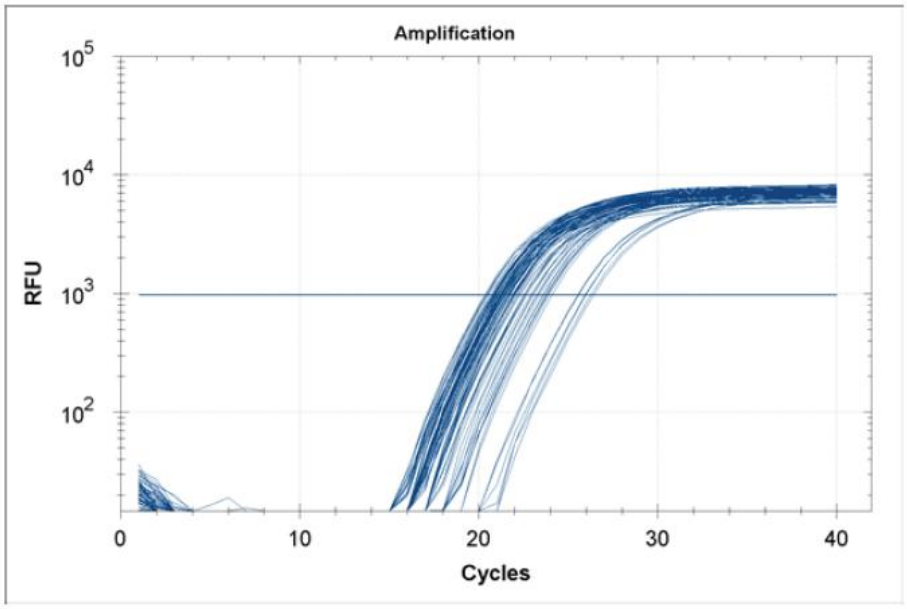
2013/08/21 12:21 PM

Run Setup

Plate Display

	1	2	3	4	5	6	7	8	9	10	11	12
A	Unk-1 Actin 001 S90	Unk-1 Actin 001 S90	Unk-8 Actin 002 S90	Unk-8 Actin 002 S90	Unk-15 Actin 799 S90	Unk-15 Actin 799 S90	Unk-21 Actin 811 S90	Unk-21 Actin 811 S90	Unk-28 Actin 805 S90	Unk-28 Actin 805 S90	Unk-35 Actin 816 S90	Unk-35 Actin 816 S90
B	Unk-2 Actin 001 N90	Unk-2 Actin 001 N90	Unk-9 Actin 002 N90	Unk-9 Actin 002 N90	Unk-16 Actin 799 N90	Unk-16 Actin 799 N90	Unk-22 Actin 811 N90	Unk-22 Actin 811 N90	Unk-29 Actin 805 N90	Unk-29 Actin 805 N90	Unk-36 Actin 816 N90	Unk-36 Actin 816 N90
C	Unk-3 Actin 001 T90	Unk-3 Actin 001 T90	Unk-10 Actin 002 T90	Unk-10 Actin 002 T90	Unk-17 Actin 799 T90	Unk-17 Actin 799 T90	Unk-23 Actin 811 T90	Unk-23 Actin 811 T90	Unk-30 Actin 805 T90	Unk-30 Actin 805 T90	Unk-37 Actin 816 T90	Unk-37 Actin 816 T90
D	Unk-4 Actin 001 T+N90	Unk-4 Actin 001 T+N90	Unk-11 Actin 002 T+N90	Unk-11 Actin 002 T+N90	Unk-18 Actin 799 T+N90	Unk-18 Actin 799 T+N90	Unk-24 Actin 811 T+N90	Unk-24 Actin 811 T+N90	Unk-31 Actin 805 T+N90	Unk-31 Actin 805 T+N90	Unk-38 Actin 816 T+N90	Unk-38 Actin 816 T+N90
E	Unk-5 Actin 001 V90	Unk-5 Actin 001 V90	Unk-12 Actin 002 V90	Unk-12 Actin 002 V90	Unk-19 Actin 799 Z90	Unk-19 Actin 799 Z90	Unk-25 Actin 811 V90	Unk-25 Actin 811 V90	Unk-32 Actin 805 V90	Unk-32 Actin 805 V90	Unk-39 Actin 816 V90	Unk-39 Actin 816 V90
F	Unk-6 Actin 001 Z90	Unk-6 Actin 001 Z90	Unk-13 Actin 002 Z90	Unk-13 Actin 002 Z90			Unk-26 Actin 811 Z90	Unk-26 Actin 811 Z90	Unk-33 Actin 805 Z90	Unk-33 Actin 805 Z90	Unk-40 Actin 816 Z90	Unk-40 Actin 816 Z90
G	Unk-7 Actin 001 MC	Unk-7 Actin 001 MC	Unk-14 Actin 002 MC	Unk-14 Actin 002 MC	Unk-20 Actin 799 MC	Unk-20 Actin 799 MC	Unk-27 Actin 811 MC	Unk-27 Actin 811 MC	Unk-34 Actin 805 MC	Unk-34 Actin 805 MC	Unk-41 Actin 816 MC	Unk-41 Actin 816 MC
H	Pos-42 Actin 804 PC	Pos-42 Actin 804 PC	NTC-43 Actin H2O	NTC-43 Actin H2O	NTC-44 Actin H2O	NTC-44 Actin H2O	Unk-45 Actin Pooled MC 15ng	Unk-45 Actin Pooled MC 15ng	Unk-46 Actin Pooled MC 10ng	Unk-46 Actin Pooled MC 10ng	Unk-47 Actin Pooled MC 5ng	Unk-47 Actin Pooled MC 5ng

Quantification



Quantification Data

Well	Fluor	Target	Content	Sample	Cq	Cq Mean	Cq Std. Dev
A01	FAM	Actin	Unkn-01	001 S90	21.18	21.27	0.119
A02	FAM	Actin	Unkn-01	001 S90	21.35	21.27	0.119
A03	FAM	Actin	Unkn-08	002 S90	21.38	21.26	0.166
A04	FAM	Actin	Unkn-08	002 S90	21.14	21.26	0.166
A05	FAM	Actin	Unkn-15	799 S90	21.34	21.44	0.142
A06	FAM	Actin	Unkn-15	799 S90	21.54	21.44	0.142
A07	FAM	Actin	Unkn-21	811 S90	21.66	21.62	0.065
A08	FAM	Actin	Unkn-21	811 S90	21.57	21.62	0.065
A09	FAM	Actin	Unkn-28	805 S90	22.01	21.92	0.130
A10	FAM	Actin	Unkn-28	805 S90	21.83	21.92	0.130
A11	FAM	Actin	Unkn-35	816 S90	22.20	22.23	0.045
A12	FAM	Actin	Unkn-35	816 S90	22.26	22.23	0.045
B01	FAM	Actin	Unkn-02	001 N90	21.00	21.02	0.023
B02	FAM	Actin	Unkn-02	001 N90	21.04	21.02	0.023
B03	FAM	Actin	Unkn-09	002 N90	20.62	20.56	0.087
B04	FAM	Actin	Unkn-09	002 N90	20.50	20.56	0.087
B05	FAM	Actin	Unkn-16	799 N90	20.26	20.30	0.049
B06	FAM	Actin	Unkn-16	799 N90	20.33	20.30	0.049
B07	FAM	Actin	Unkn-22	811 N90	21.63	21.76	0.181
B08	FAM	Actin	Unkn-22	811 N90	21.89	21.76	0.181
B09	FAM	Actin	Unkn-29	805 N90	20.86	20.91	0.068
B10	FAM	Actin	Unkn-29	805 N90	20.96	20.91	0.068
B11	FAM	Actin	Unkn-36	816 N90	21.39	21.34	0.073
B12	FAM	Actin	Unkn-36	816 N90	21.29	21.34	0.073
C01	FAM	Actin	Unkn-03	001 T90	21.16	21.19	0.033
C02	FAM	Actin	Unkn-03	001 T90	21.21	21.19	0.033
C03	FAM	Actin	Unkn-10	002 T90	21.30	21.26	0.057
C04	FAM	Actin	Unkn-10	002 T90	21.22	21.26	0.057
C05	FAM	Actin	Unkn-17	799 T90	21.16	21.18	0.024
C06	FAM	Actin	Unkn-17	799 T90	21.20	21.18	0.024
C07	FAM	Actin	Unkn-23	811 T90	21.29	21.26	0.042
C08	FAM	Actin	Unkn-23	811 T90	21.23	21.26	0.042
C09	FAM	Actin	Unkn-30	805 T90	22.45	22.52	0.106
C10	FAM	Actin	Unkn-30	805 T90	22.60	22.52	0.106
C11	FAM	Actin	Unkn-37	816 T90	21.65	21.77	0.180
C12	FAM	Actin	Unkn-37	816 T90	21.90	21.77	0.180
D01	FAM	Actin	Unkn-04	001 T+N90	21.08	21.08	0.005
D02	FAM	Actin	Unkn-04	001 T+N90	21.09	21.08	0.005
D03	FAM	Actin	Unkn-11	002 T+N90	20.82	20.80	0.033
D04	FAM	Actin	Unkn-11	002 T+N90	20.78	20.80	0.033
D05	FAM	Actin	Unkn-18	799 T+N90	20.74	20.83	0.118
D06	FAM	Actin	Unkn-18	799 T+N90	20.91	20.83	0.118
D07	FAM	Actin	Unkn-24	811 T+N90	20.81	20.76	0.084
D08	FAM	Actin	Unkn-24	811 T+N90	20.70	20.76	0.084
D09	FAM	Actin	Unkn-31	805 T+N90	21.95	22.02	0.099
D10	FAM	Actin	Unkn-31	805 T+N90	22.09	22.02	0.099
D11	FAM	Actin	Unkn-38	816 T+N90	22.51	22.55	0.062

Well	Fluor	Target	Content	Sample	Cq	Cq Mean	Cq Std. Dev
D12	FAM	Actin	Unkn-38	816 T+N90	22.60	22.55	0.062
E01	FAM	Actin	Unkn-05	001 V90	20.80	20.82	0.029
E02	FAM	Actin	Unkn-05	001 V90	20.84	20.82	0.029
E03	FAM	Actin	Unkn-12	002 V90	21.48	21.46	0.036
E04	FAM	Actin	Unkn-12	002 V90	21.43	21.46	0.036
E05	FAM	Actin	Unkn-19	799 Z90	21.56	21.55	0.027
E06	FAM	Actin	Unkn-19	799 Z90	21.53	21.55	0.027
E07	FAM	Actin	Unkn-25	811 V90	21.67	21.77	0.139
E08	FAM	Actin	Unkn-25	811 V90	21.87	21.77	0.139
E09	FAM	Actin	Unkn-32	805 V90	20.80	20.71	0.124
E10	FAM	Actin	Unkn-32	805 V90	20.62	20.71	0.124
E11	FAM	Actin	Unkn-39	816 V90	21.25	21.30	0.073
E12	FAM	Actin	Unkn-39	816 V90	21.35	21.30	0.073
F01	FAM	Actin	Unkn-06	001 Z90	20.75	20.75	0.002
F02	FAM	Actin	Unkn-06	001 Z90	20.75	20.75	0.002
F03	FAM	Actin	Unkn-13	002 Z90	20.36	20.38	0.026
F04	FAM	Actin	Unkn-13	002 Z90	20.40	20.38	0.026
F07	FAM	Actin	Unkn-26	811 Z90	21.98	21.84	0.199
F08	FAM	Actin	Unkn-26	811 Z90	21.70	21.84	0.199
F09	FAM	Actin	Unkn-33	805 Z90	21.14	21.10	0.057
F10	FAM	Actin	Unkn-33	805 Z90	21.06	21.10	0.057
F11	FAM	Actin	Unkn-40	816 Z90	21.99	22.05	0.088
F12	FAM	Actin	Unkn-40	816 Z90	22.11	22.05	0.088
G01	FAM	Actin	Unkn-07	001 MC	23.72	23.64	0.114
G02	FAM	Actin	Unkn-07	001 MC	23.56	23.64	0.114
G03	FAM	Actin	Unkn-14	002 MC	23.03	23.00	0.042
G04	FAM	Actin	Unkn-14	002 MC	22.97	23.00	0.042
G05	FAM	Actin	Unkn-20	799 MC	23.20	23.21	0.020
G06	FAM	Actin	Unkn-20	799 MC	23.22	23.21	0.020
G07	FAM	Actin	Unkn-27	811 MC	23.50	23.42	0.117
G08	FAM	Actin	Unkn-27	811 MC	23.33	23.42	0.117
G09	FAM	Actin	Unkn-34	805 MC	24.06	23.97	0.126
G10	FAM	Actin	Unkn-34	805 MC	23.88	23.97	0.126
G11	FAM	Actin	Unkn-41	816 MC	23.69	23.74	0.074
G12	FAM	Actin	Unkn-41	816 MC	23.79	23.74	0.074
H01	FAM	Actin	Pos Ctrl-42	804 PC	22.50	22.68	0.252
H02	FAM	Actin	Pos Ctrl-42	804 PC	22.86	22.68	0.252
H03	FAM	Actin	NTC-43	H2O	N/A	0.00	0.000
H04	FAM	Actin	NTC-43	H2O	N/A	0.00	0.000
H05	FAM	Actin	NTC-44	H2O	N/A	0.00	0.000
H06	FAM	Actin	NTC-44	H2O	N/A	0.00	0.000
H07	FAM	Actin	Unkn-45	Pooled MC 15ng	25.47	25.48	0.020
H08	FAM	Actin	Unkn-45	Pooled MC 15ng	25.50	25.48	0.020
H09	FAM	Actin	Unkn-46	Pooled MC 10ng	25.96	25.94	0.029
H10	FAM	Actin	Unkn-46	Pooled MC 10ng	25.91	25.94	0.029
H11	FAM	Actin	Unkn-47	Pooled MC 5ng	26.21	26.28	0.091
H12	FAM	Actin	Unkn-47	Pooled MC 5ng	26.34	26.28	0.091

Gene Expression

Target Names

Name	Full Name	Reference	Auto Efficiency	Efficiency
Actin	Actin	True	Yes	100.0%

RPL13a 15d.pcrd

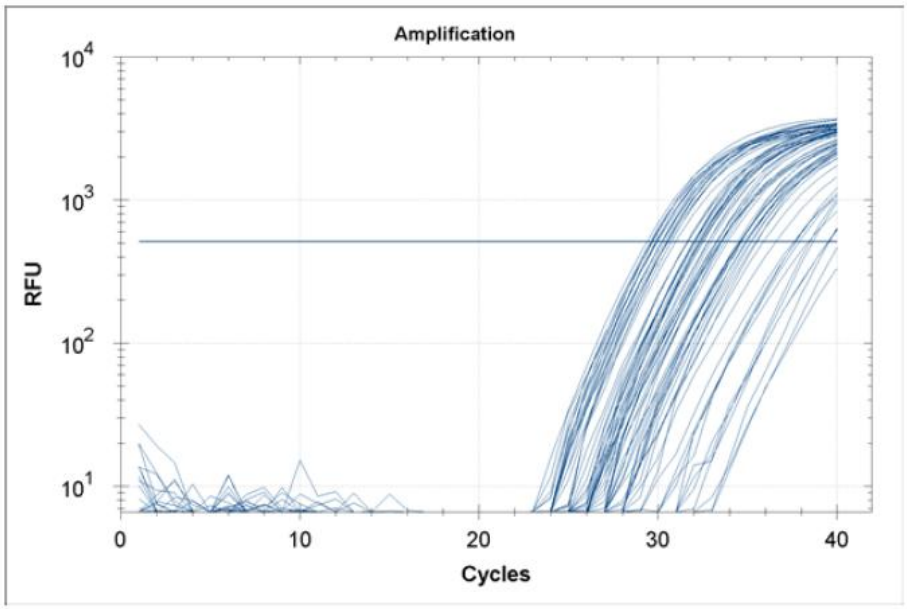
2013/08/21 12:35 PM

Run Setup

Plate Display

	1	2	3	4	5	6	7	8	9	10	11	12
A	Unk-1 RPL13a 001 S15	Unk-1 RPL13a 001 S15	Unk-7 RPL13a 002 S15	Unk-7 RPL13a 002 S15	Unk-13 RPL13a 799 S15	Unk-13 RPL13a 799 S15	Unk-18 RPL13a 811 S15	Unk-18 RPL13a 811 S15	Unk-24 RPL13a 805 S15	Unk-24 RPL13a 805 S15	Unk-30 RPL13a 816 S15	Unk-30 RPL13a 816 S15
B	Unk-2 RPL13a 001 N15	Unk-2 RPL13a 001 N15	Unk-8 RPL13a 002 N15	Unk-8 RPL13a 002 N15	Unk-14 RPL13a 799 N15	Unk-14 RPL13a 799 N15	Unk-19 RPL13a 811 N15	Unk-19 RPL13a 811 N15	Unk-25 RPL13a 805 N15	Unk-25 RPL13a 805 N15	Unk-31 RPL13a 816 N15	Unk-31 RPL13a 816 N15
C	Unk-3 RPL13a 001 T15	Unk-3 RPL13a 001 T15	Unk-9 RPL13a 002 T15	Unk-9 RPL13a 002 T15	Unk-15 RPL13a 799 T15	Unk-15 RPL13a 799 T15	Unk-20 RPL13a 811 T15	Unk-20 RPL13a 811 T15	Unk-26 RPL13a 805 T15	Unk-26 RPL13a 805 T15	Unk-32 RPL13a 816 T15	Unk-32 RPL13a 816 T15
D	Unk-4 RPL13a 001 T+N15	Unk-4 RPL13a 001 T+N15	Unk-10 RPL13a 002 T+N15	Unk-10 RPL13a 002 T+N15	Unk-16 RPL13a 799 T+N15	Unk-16 RPL13a 799 T+N15	Unk-21 RPL13a 811 T+N15	Unk-21 RPL13a 811 T+N15	Unk-27 RPL13a 805 T+N15	Unk-27 RPL13a 805 T+N15	Unk-33 RPL13a 816 T+N15	Unk-33 RPL13a 816 T+N15
E	Unk-5 RPL13a 001 V15	Unk-5 RPL13a 001 V15	Unk-11 RPL13a 002 V15	Unk-11 RPL13a 002 V15	Unk-17 RPL13a 799 Z15	Unk-17 RPL13a 799 Z15	Unk-22 RPL13a 811 V15	*Unk-22 RPL13a 811 V15	*Unk-28 RPL13a 805 V15	Unk-28 RPL13a 805 V15	Unk-34 RPL13a 816 V15	Unk-34 RPL13a 816 V15
F	Unk-6 RPL13a 001 Z15	Unk-6 RPL13a 001 Z15	Unk-12 RPL13a 002 Z15	Unk-12 RPL13a 002 Z15			Unk-23 RPL13a 811 Z15	*Unk-23 RPL13a 811 Z15	Unk-29 RPL13a 805 Z15	Unk-29 RPL13a 805 Z15	Unk-35 RPL13a 816 Z15	Unk-35 RPL13a 816 Z15
G	Pos-36 RPL13a 804 PC	Pos-36 RPL13a 804 PC	NTC-37 RPL13a H2O	NTC-37 RPL13a H2O	NTC-38 RPL13a H2O	NTC-38 RPL13a H2O	Unk-39 RPL13a Pooled MC 10ng	Unk-39 RPL13a Pooled MC 10ng	Unk-40 RPL13a Pooled MC 15ng	Unk-40 RPL13a Pooled MC 15ng	Unk-41 RPL13a Pooled MC 5ng	Unk-41 RPL13a Pooled MC 5ng
H												

Quantification



Quantification Data

Well	Fluor	Target	Content	Sample	Cq	Cq Mean	Cq Std. Dev
A01	FAM	RPL13a	Unkn-01	001 S15	30.48	30.59	0.150
A02	FAM	RPL13a	Unkn-01	001 S15	30.69	30.59	0.150
A03	FAM	RPL13a	Unkn-07	002 S15	30.97	30.31	0.932
A04	FAM	RPL13a	Unkn-07	002 S15	29.65	30.31	0.932
A05	FAM	RPL13a	Unkn-13	799 S15	N/A	0.00	0.000
A06	FAM	RPL13a	Unkn-13	799 S15	39.51	39.51	0.000
A07	FAM	RPL13a	Unkn-18	811 S15	30.34	30.12	0.305
A08	FAM	RPL13a	Unkn-18	811 S15	29.91	30.12	0.305
A09	FAM	RPL13a	Unkn-24	805 S15	38.60	38.52	0.122
A10	FAM	RPL13a	Unkn-24	805 S15	38.43	38.52	0.122
A11	FAM	RPL13a	Unkn-30	816 S15	29.90	29.87	0.039
A12	FAM	RPL13a	Unkn-30	816 S15	29.84	29.87	0.039
B01	FAM	RPL13a	Unkn-02	001 N15	30.19	29.91	0.404
B02	FAM	RPL13a	Unkn-02	001 N15	29.62	29.91	0.404
B03	FAM	RPL13a	Unkn-08	002 N15	29.97	29.65	0.440
B04	FAM	RPL13a	Unkn-08	002 N15	29.34	29.65	0.440
B05	FAM	RPL13a	Unkn-14	799 N15	33.26	33.38	0.164
B06	FAM	RPL13a	Unkn-14	799 N15	33.50	33.38	0.164
B07	FAM	RPL13a	Unkn-19	811 N15	30.44	30.02	0.601
B08	FAM	RPL13a	Unkn-19	811 N15	29.59	30.02	0.601
B09	FAM	RPL13a	Unkn-25	805 N15	32.78	32.86	0.122
B10	FAM	RPL13a	Unkn-25	805 N15	32.95	32.86	0.122
B11	FAM	RPL13a	Unkn-31	816 N15	32.01	32.16	0.210
B12	FAM	RPL13a	Unkn-31	816 N15	32.31	32.16	0.210
C01	FAM	RPL13a	Unkn-03	001 T15	31.57	30.87	0.986
C02	FAM	RPL13a	Unkn-03	001 T15	30.18	30.87	0.986
C03	FAM	RPL13a	Unkn-09	002 T15	30.52	30.36	0.221
C04	FAM	RPL13a	Unkn-09	002 T15	30.21	30.36	0.221
C05	FAM	RPL13a	Unkn-15	799 T15	32.00	32.16	0.229
C06	FAM	RPL13a	Unkn-15	799 T15	32.32	32.16	0.229
C07	FAM	RPL13a	Unkn-20	811 T15	32.77	32.20	0.801
C08	FAM	RPL13a	Unkn-20	811 T15	31.64	32.20	0.801
C09	FAM	RPL13a	Unkn-26	805 T15	32.41	32.41	0.007
C10	FAM	RPL13a	Unkn-26	805 T15	32.40	32.41	0.007
C11	FAM	RPL13a	Unkn-32	816 T15	32.30	32.39	0.133
C12	FAM	RPL13a	Unkn-32	816 T15	32.48	32.39	0.133
D01	FAM	RPL13a	Unkn-04	001 T+N15	33.86	33.54	0.450
D02	FAM	RPL13a	Unkn-04	001 T+N15	33.22	33.54	0.450
D03	FAM	RPL13a	Unkn-10	002 T+N15	32.14	31.89	0.356
D04	FAM	RPL13a	Unkn-10	002 T+N15	31.64	31.89	0.356
D05	FAM	RPL13a	Unkn-16	799 T+N15	35.22	34.82	0.565
D06	FAM	RPL13a	Unkn-16	799 T+N15	34.42	34.82	0.565
D07	FAM	RPL13a	Unkn-21	811 T+N15	37.63	36.11	2.139
D08	FAM	RPL13a	Unkn-21	811 T+N15	34.60	36.11	2.139
D09	FAM	RPL13a	Unkn-27	805 T+N15	32.04	30.78	1.780
D10	FAM	RPL13a	Unkn-27	805 T+N15	29.52	30.78	1.780
D11	FAM	RPL13a	Unkn-33	816 T+N15	30.68	31.36	0.963

Well	Fluor	Target	Content	Sample	Cq	Cq Mean	Cq Std. Dev
D12	FAM	RPL13a	Unkn-33	816 T+N15	32.05	31.36	0.963
E01	FAM	RPL13a	Unkn-05	001 V15	34.95	34.94	0.013
E02	FAM	RPL13a	Unkn-05	001 V15	34.93	34.94	0.013
E03	FAM	RPL13a	Unkn-11	002 V15	33.51	33.51	0.004
E04	FAM	RPL13a	Unkn-11	002 V15	33.51	33.51	0.004
E05	FAM	RPL13a	Unkn-17	799 Z15	35.13	35.02	0.157
E06	FAM	RPL13a	Unkn-17	799 Z15	34.91	35.02	0.157
E07	FAM	RPL13a	Unkn-22	811 V15	37.87	37.87	0.000
E10	FAM	RPL13a	Unkn-28	805 V15	33.68	33.68	0.000
E11	FAM	RPL13a	Unkn-34	816 V15	34.53	34.56	0.040
E12	FAM	RPL13a	Unkn-34	816 V15	34.59	34.56	0.040
F01	FAM	RPL13a	Unkn-06	001 Z15	38.39	35.81	3.649
F02	FAM	RPL13a	Unkn-06	001 Z15	33.23	35.81	3.649
F03	FAM	RPL13a	Unkn-12	002 Z15	34.53	33.97	0.793
F04	FAM	RPL13a	Unkn-12	002 Z15	33.41	33.97	0.793
F07	FAM	RPL13a	Unkn-23	811 Z15	37.65	37.65	0.000
F09	FAM	RPL13a	Unkn-29	805 Z15	32.23	33.39	1.638
F10	FAM	RPL13a	Unkn-29	805 Z15	34.55	33.39	1.638
F11	FAM	RPL13a	Unkn-35	816 Z15	35.43	36.50	1.505
F12	FAM	RPL13a	Unkn-35	816 Z15	37.56	36.50	1.505
G01	FAM	RPL13a	Pos Ctrl-36	804 PC	34.77	34.12	0.913
G02	FAM	RPL13a	Pos Ctrl-36	804 PC	33.48	34.12	0.913
G03	FAM	RPL13a	NTC-37	H2O	N/A	0.00	0.000
G04	FAM	RPL13a	NTC-37	H2O	N/A	0.00	0.000
G05	FAM	RPL13a	NTC-38	H2O	N/A	0.00	0.000
G06	FAM	RPL13a	NTC-38	H2O	N/A	0.00	0.000
G07	FAM	RPL13a	Unkn-39	Pooled MC 10ng	35.87	36.21	0.479
G08	FAM	RPL13a	Unkn-39	Pooled MC 10ng	36.55	36.21	0.479
G09	FAM	RPL13a	Unkn-40	Pooled MC 15ng	35.47	37.48	2.836
G10	FAM	RPL13a	Unkn-40	Pooled MC 15ng	39.48	37.48	2.836
G11	FAM	RPL13a	Unkn-41	Pooled MC 5ng	39.46	39.46	0.000
G12	FAM	RPL13a	Unkn-41	Pooled MC 5ng	N/A	0.00	0.000

Gene Expression

Target Names

Name	Full Name	Reference	Auto Efficiency	Efficiency
RPL13a	RPL13a	False	Yes	100.0%

RPL13a 60d.pcrd

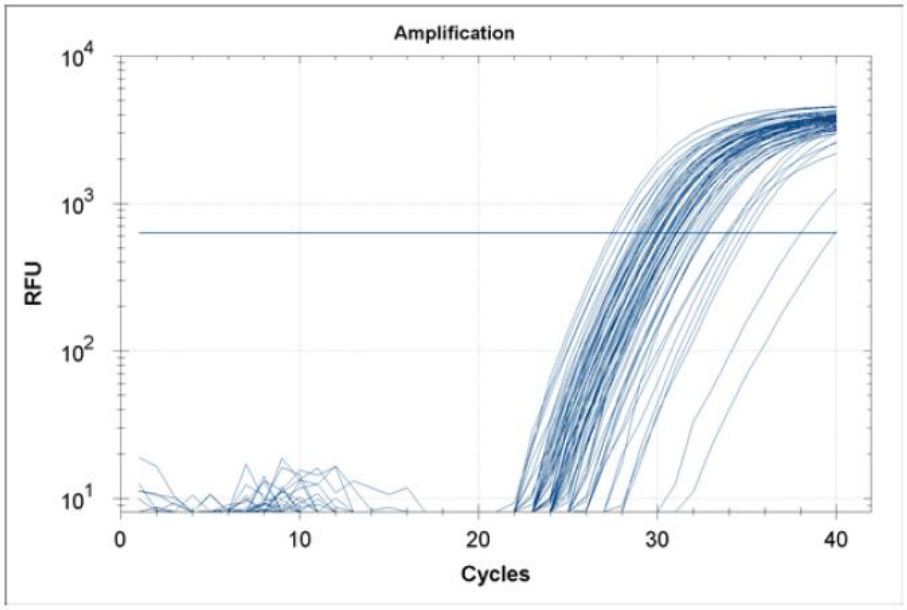
2013/08/21 12:37 PM

Run Setup

Plate Display

	1	2	3	4	5	6	7	8	9	10	11	12
A	Unk-1 RPL13a 001 S60	Unk-1 RPL13a 001 S60	Unk-7 RPL13a 002 S60	Unk-7 RPL13a 002 S60	Unk-13 RPL13a 799 S60	Unk-13 RPL13a 799 S60	Unk-18 RPL13a 811 S60	Unk-18 RPL13a 811 S60	Unk-24 RPL13a 805 S60	Unk-24 RPL13a 805 S60	Unk-30 RPL13a 816 S60	Unk-30 RPL13a 816 S60
B	Unk-2 RPL13a 001 N60	Unk-2 RPL13a 001 N60	Unk-8 RPL13a 002 N60	Unk-8 RPL13a 002 N60	Unk-14 RPL13a 799 N60	Unk-14 RPL13a 799 N60	Unk-19 RPL13a 811 N60	Unk-19 RPL13a 811 N60	Unk-25 RPL13a 805 N60	Unk-25 RPL13a 805 N60	Unk-31 RPL13a 816 N60	Unk-31 RPL13a 816 N60
C	Unk-3 RPL13a 001 T60	Unk-3 RPL13a 001 T60	Unk-9 RPL13a 002 T60	Unk-9 RPL13a 002 T60	Unk-15 RPL13a 799 T60	Unk-15 RPL13a 799 T60	Unk-20 RPL13a 811 T60	Unk-20 RPL13a 811 T60	Unk-26 RPL13a 805 T60	Unk-26 RPL13a 805 T60	Unk-32 RPL13a 816 T60	Unk-32 RPL13a 816 T60
D	Unk-4 RPL13a 001 T+N60	Unk-4 RPL13a 001 T+N60	Unk-10 RPL13a 002 T+N60	Unk-10 RPL13a 002 T+N60	Unk-16 RPL13a 799 T+N60	*Unk-16 RPL13a 799 T+N60	Unk-21 RPL13a 811 T+N60	Unk-21 RPL13a 811 T+N60	Unk-27 RPL13a 805 T+N60	Unk-27 RPL13a 805 T+N60	Unk-33 RPL13a 816 T+N60	Unk-33 RPL13a 816 T+N60
E	Unk-5 RPL13a 001 V60	Unk-5 RPL13a 001 V60	Unk-11 RPL13a 002 V60	Unk-11 RPL13a 002 V60	Unk-17 RPL13a 799 Z60	Unk-17 RPL13a 799 Z60	Unk-22 RPL13a 811 V60	Unk-22 RPL13a 811 V60	Unk-28 RPL13a 805 V60	Unk-28 RPL13a 805 V60	Unk-34 RPL13a 816 V60	Unk-34 RPL13a 816 V60
F	Unk-6 RPL13a 001 Z60	Unk-6 RPL13a 001 Z60	Unk-12 RPL13a 002 Z60	Unk-12 RPL13a 002 Z60			Unk-23 RPL13a 811 Z60	Unk-23 RPL13a 811 Z60	Unk-29 RPL13a 805 Z60	Unk-29 RPL13a 805 Z60	Unk-35 RPL13a 816 Z60	Unk-35 RPL13a 816 Z60
G	Pos-36 RPL13a 804 PC	Pos-36 RPL13a 804 PC	NTC-37 RPL13a H2O	NTC-37 RPL13a H2O	NTC-38 RPL13a H2O	NTC-38 RPL13a H2O	Unk-39 RPL13a Pooled MC 10ng	Unk-39 RPL13a Pooled MC 10ng	Unk-40 RPL13a Pooled MC 15ng	Unk-40 RPL13a Pooled MC 15ng	Unk-41 RPL13a Pooled MC 5ng	Unk-41 RPL13a Pooled MC 5ng
H												

Quantification



Quantification Data

Well	Fluor	Target	Content	Sample	Cq	Cq Mean	Cq Std. Dev
A01	FAM	RPL13a	Unkn-01	001 S60	33.93	31.82	2.991
A02	FAM	RPL13a	Unkn-01	001 S60	29.70	31.82	2.991
A03	FAM	RPL13a	Unkn-07	002 S60	31.47	30.42	1.484
A04	FAM	RPL13a	Unkn-07	002 S60	29.37	30.42	1.484
A05	FAM	RPL13a	Unkn-13	799 S60	29.17	29.57	0.566
A06	FAM	RPL13a	Unkn-13	799 S60	29.97	29.57	0.566
A07	FAM	RPL13a	Unkn-18	811 S60	30.46	29.99	0.671
A08	FAM	RPL13a	Unkn-18	811 S60	29.51	29.99	0.671
A09	FAM	RPL13a	Unkn-24	805 S60	31.05	29.55	2.114
A10	FAM	RPL13a	Unkn-24	805 S60	28.06	29.55	2.114
A11	FAM	RPL13a	Unkn-30	816 S60	28.83	30.16	1.882
A12	FAM	RPL13a	Unkn-30	816 S60	31.49	30.16	1.882
B01	FAM	RPL13a	Unkn-02	001 N60	30.06	30.24	0.250
B02	FAM	RPL13a	Unkn-02	001 N60	30.42	30.24	0.250
B03	FAM	RPL13a	Unkn-08	002 N60	33.82	33.07	1.053
B04	FAM	RPL13a	Unkn-08	002 N60	32.33	33.07	1.053
B05	FAM	RPL13a	Unkn-14	799 N60	28.69	28.85	0.222
B06	FAM	RPL13a	Unkn-14	799 N60	29.00	28.85	0.222
B07	FAM	RPL13a	Unkn-19	811 N60	31.03	29.94	1.554
B08	FAM	RPL13a	Unkn-19	811 N60	28.84	29.94	1.554
B09	FAM	RPL13a	Unkn-25	805 N60	31.08	29.34	2.459
B10	FAM	RPL13a	Unkn-25	805 N60	27.60	29.34	2.459
B11	FAM	RPL13a	Unkn-31	816 N60	30.82	30.43	0.554
B12	FAM	RPL13a	Unkn-31	816 N60	30.03	30.43	0.554
C01	FAM	RPL13a	Unkn-03	001 T60	31.56	31.96	0.567
C02	FAM	RPL13a	Unkn-03	001 T60	32.36	31.96	0.567
C03	FAM	RPL13a	Unkn-09	002 T60	31.03	30.17	1.215
C04	FAM	RPL13a	Unkn-09	002 T60	29.31	30.17	1.215
C05	FAM	RPL13a	Unkn-15	799 T60	32.55	32.10	0.633
C06	FAM	RPL13a	Unkn-15	799 T60	31.65	32.10	0.633
C07	FAM	RPL13a	Unkn-20	811 T60	32.70	31.62	1.528
C08	FAM	RPL13a	Unkn-20	811 T60	30.54	31.62	1.528
C09	FAM	RPL13a	Unkn-26	805 T60	32.03	32.11	0.117
C10	FAM	RPL13a	Unkn-26	805 T60	32.20	32.11	0.117
C11	FAM	RPL13a	Unkn-32	816 T60	28.38	29.44	1.501
C12	FAM	RPL13a	Unkn-32	816 T60	30.50	29.44	1.501
D01	FAM	RPL13a	Unkn-04	001 T+N60	29.07	28.56	0.720
D02	FAM	RPL13a	Unkn-04	001 T+N60	28.05	28.56	0.720
D03	FAM	RPL13a	Unkn-10	002 T+N60	29.59	30.03	0.616
D04	FAM	RPL13a	Unkn-10	002 T+N60	30.46	30.03	0.616
D05	FAM	RPL13a	Unkn-16	799 T+N60	31.07	31.07	0.000
D07	FAM	RPL13a	Unkn-21	811 T+N60	31.01	30.25	1.066
D08	FAM	RPL13a	Unkn-21	811 T+N60	29.50	30.25	1.066
D09	FAM	RPL13a	Unkn-27	805 T+N60	32.72	32.24	0.675
D10	FAM	RPL13a	Unkn-27	805 T+N60	31.77	32.24	0.675
D11	FAM	RPL13a	Unkn-33	816 T+N60	30.55	30.28	0.380
D12	FAM	RPL13a	Unkn-33	816 T+N60	30.01	30.28	0.380

Well	Fluor	Target	Content	Sample	Cq	Cq Mean	Cq Std. Dev
E01	FAM	RPL13a	Unkn-05	001 V60	29.39	29.77	0.529
E02	FAM	RPL13a	Unkn-05	001 V60	30.14	29.77	0.529
E03	FAM	RPL13a	Unkn-11	002 V60	30.12	29.75	0.524
E04	FAM	RPL13a	Unkn-11	002 V60	29.38	29.75	0.524
E05	FAM	RPL13a	Unkn-17	799 Z60	30.93	30.93	0.000
E06	FAM	RPL13a	Unkn-17	799 Z60	N/A	0.00	0.000
E07	FAM	RPL13a	Unkn-22	811 V60	29.24	29.97	1.035
E08	FAM	RPL13a	Unkn-22	811 V60	30.70	29.97	1.035
E09	FAM	RPL13a	Unkn-28	805 V60	29.36	28.37	1.392
E10	FAM	RPL13a	Unkn-28	805 V60	27.39	28.37	1.392
E11	FAM	RPL13a	Unkn-34	816 V60	29.67	29.45	0.310
E12	FAM	RPL13a	Unkn-34	816 V60	29.23	29.45	0.310
F01	FAM	RPL13a	Unkn-06	001 Z60	28.95	28.66	0.410
F02	FAM	RPL13a	Unkn-06	001 Z60	28.37	28.66	0.410
F03	FAM	RPL13a	Unkn-12	002 Z60	31.23	30.64	0.829
F04	FAM	RPL13a	Unkn-12	002 Z60	30.06	30.64	0.829
F07	FAM	RPL13a	Unkn-23	811 Z60	30.69	31.05	0.514
F08	FAM	RPL13a	Unkn-23	811 Z60	31.42	31.05	0.514
F09	FAM	RPL13a	Unkn-29	805 Z60	31.06	30.92	0.190
F10	FAM	RPL13a	Unkn-29	805 Z60	30.79	30.92	0.190
F11	FAM	RPL13a	Unkn-35	816 Z60	30.16	30.42	0.377
F12	FAM	RPL13a	Unkn-35	816 Z60	30.69	30.42	0.377
G01	FAM	RPL13a	Pos Ctrl-36	804 PC	29.92	30.14	0.312
G02	FAM	RPL13a	Pos Ctrl-36	804 PC	30.36	30.14	0.312
G03	FAM	RPL13a	NTC-37	H2O	N/A	0.00	0.000
G04	FAM	RPL13a	NTC-37	H2O	N/A	0.00	0.000
G05	FAM	RPL13a	NTC-38	H2O	N/A	0.00	0.000
G06	FAM	RPL13a	NTC-38	H2O	N/A	0.00	0.000
G07	FAM	RPL13a	Unkn-39	Pooled MC 10ng	39.91	38.96	1.347
G08	FAM	RPL13a	Unkn-39	Pooled MC 10ng	38.01	38.96	1.347
G09	FAM	RPL13a	Unkn-40	Pooled MC 15ng	34.35	34.19	0.222
G10	FAM	RPL13a	Unkn-40	Pooled MC 15ng	34.03	34.19	0.222
G11	FAM	RPL13a	Unkn-41	Pooled MC 5ng	34.73	34.90	0.244
G12	FAM	RPL13a	Unkn-41	Pooled MC 5ng	35.07	34.90	0.244

Gene Expression

Target Names

Name	Full Name	Reference	Auto Efficiency	Efficiency
RPL13a	RPL13a	False	Yes	100.0%

RPL13a 90d.pcrd

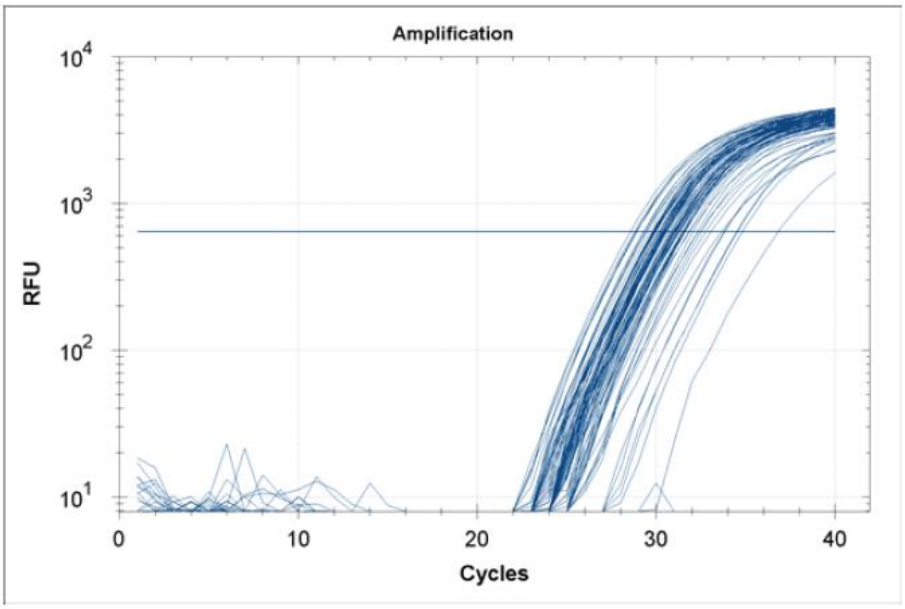
2013/08/21 12:38 PM

Run Setup

Plate Display

	1	2	3	4	5	6	7	8	9	10	11	12
A	Unk-1 RPL13a 001 S90	Unk-1 RPL13a 001 S90	Unk-8 RPL13a 002 S90	Unk-8 RPL13a 002 S90	Unk-15 RPL13a 799 S90	Unk-15 RPL13a 799 S90	Unk-21 RPL13a 811 S90	Unk-21 RPL13a 811 S90	Unk-28 RPL13a 805 S90	Unk-28 RPL13a 805 S90	Unk-35 RPL13a 816 S90	Unk-35 RPL13a 816 S90
B	Unk-2 RPL13a 001 N90	Unk-2 RPL13a 001 N90	Unk-9 RPL13a 002 N90	Unk-9 RPL13a 002 N90	Unk-16 RPL13a 799 N90	Unk-16 RPL13a 799 N90	Unk-22 RPL13a 811 N90	Unk-22 RPL13a 811 N90	Unk-29 RPL13a 805 N90	Unk-29 RPL13a 805 N90	Unk-36 RPL13a 816 N90	Unk-36 RPL13a 816 N90
C	Unk-3 RPL13a 001 T90	Unk-3 RPL13a 001 T90	Unk-10 RPL13a 002 T90	Unk-10 RPL13a 002 T90	Unk-17 RPL13a 799 T90	Unk-17 RPL13a 799 T90	Unk-23 RPL13a 811 T90	Unk-23 RPL13a 811 T90	Unk-30 RPL13a 805 T90	Unk-30 RPL13a 805 T90	Unk-37 RPL13a 816 T90	Unk-37 RPL13a 816 T90
D	Unk-4 RPL13a 001 T+N90	Unk-4 RPL13a 001 T+N90	Unk-11 RPL13a 002 T+N90	Unk-11 RPL13a 002 T+N90	Unk-18 RPL13a 799 T+N90	Unk-18 RPL13a 799 T+N90	Unk-24 RPL13a 811 T+N90	Unk-24 RPL13a 811 T+N90	Unk-31 RPL13a 805 T+N90	Unk-31 RPL13a 805 T+N90	Unk-38 RPL13a 816 T+N90	Unk-38 RPL13a 816 T+N90
E	Unk-5 RPL13a 001 V90	Unk-5 RPL13a 001 V90	Unk-12 RPL13a 002 V90	Unk-12 RPL13a 002 V90	Unk-19 RPL13a 799 Z90	Unk-19 RPL13a 799 Z90	Unk-25 RPL13a 811 V90	Unk-25 RPL13a 811 V90	Unk-32 RPL13a 805 V90	Unk-32 RPL13a 805 V90	Unk-39 RPL13a 816 V90	Unk-39 RPL13a 816 V90
F	Unk-6 RPL13a 001 Z90	Unk-6 RPL13a 001 Z90	Unk-13 RPL13a 002 Z90	Unk-13 RPL13a 002 Z90			Unk-26 RPL13a 811 Z90	Unk-26 RPL13a 811 Z90	Unk-33 RPL13a 805 Z90	Unk-33 RPL13a 805 Z90	Unk-40 RPL13a 816 Z90	Unk-40 RPL13a 816 Z90
G	Unk-7 RPL13a 001 MC	Unk-7 RPL13a 001 MC	Unk-14 RPL13a 002 MC	Unk-14 RPL13a 002 MC	Unk-20 RPL13a 799 MC	Unk-20 RPL13a 799 MC	Unk-27 RPL13a 811 MC	Unk-27 RPL13a 811 MC	Unk-34 RPL13a 805 MC	Unk-34 RPL13a 805 MC	Unk-41 RPL13a 816 MC	Unk-41 RPL13a 816 MC
H	Pos-42 RPL13a 804 PC	Pos-42 RPL13a 804 PC	NTC-43 RPL13a H2O	NTC-43 RPL13a H2O	NTC-44 RPL13a H2O	NTC-44 RPL13a H2O	Unk-45 RPL13a Pooled MC 15ng	Unk-45 RPL13a Pooled MC 15ng	Unk-46 RPL13a Pooled MC 10ng	Unk-46 RPL13a Pooled MC 10ng	Unk-47 RPL13a Pooled MC 5ng	Unk-47 RPL13a Pooled MC 5ng

Quantification



Quantification Data

Well	Fluor	Target	Content	Sample	Cq	Cq Mean	Cq Std. Dev
A01	FAM	RPL13a	Unkn-01	001 S90	33.06	33.34	0.398
A02	FAM	RPL13a	Unkn-01	001 S90	33.62	33.34	0.398
A03	FAM	RPL13a	Unkn-08	002 S90	31.24	31.14	0.143
A04	FAM	RPL13a	Unkn-08	002 S90	31.03	31.14	0.143
A05	FAM	RPL13a	Unkn-15	799 S90	32.75	32.27	0.670
A06	FAM	RPL13a	Unkn-15	799 S90	31.80	32.27	0.670
A07	FAM	RPL13a	Unkn-21	811 S90	29.81	29.53	0.399
A08	FAM	RPL13a	Unkn-21	811 S90	29.25	29.53	0.399
A09	FAM	RPL13a	Unkn-28	805 S90	31.45	31.22	0.331
A10	FAM	RPL13a	Unkn-28	805 S90	30.98	31.22	0.331
A11	FAM	RPL13a	Unkn-35	816 S90	30.93	30.72	0.300
A12	FAM	RPL13a	Unkn-35	816 S90	30.51	30.72	0.300
B01	FAM	RPL13a	Unkn-02	001 N90	31.87	32.13	0.360
B02	FAM	RPL13a	Unkn-02	001 N90	32.38	32.13	0.360
B03	FAM	RPL13a	Unkn-09	002 N90	30.54	30.09	0.643
B04	FAM	RPL13a	Unkn-09	002 N90	29.63	30.09	0.643
B05	FAM	RPL13a	Unkn-16	799 N90	30.54	30.39	0.219
B06	FAM	RPL13a	Unkn-16	799 N90	30.23	30.39	0.219
B07	FAM	RPL13a	Unkn-22	811 N90	31.24	31.03	0.302
B08	FAM	RPL13a	Unkn-22	811 N90	30.82	31.03	0.302
B09	FAM	RPL13a	Unkn-29	805 N90	29.47	29.16	0.438
B10	FAM	RPL13a	Unkn-29	805 N90	28.85	29.16	0.438
B11	FAM	RPL13a	Unkn-36	816 N90	29.89	33.34	4.889
B12	FAM	RPL13a	Unkn-36	816 N90	36.80	33.34	4.889
C01	FAM	RPL13a	Unkn-03	001 T90	31.09	31.09	0.004
C02	FAM	RPL13a	Unkn-03	001 T90	31.09	31.09	0.004
C03	FAM	RPL13a	Unkn-10	002 T90	30.11	30.29	0.249
C04	FAM	RPL13a	Unkn-10	002 T90	30.47	30.29	0.249
C05	FAM	RPL13a	Unkn-17	799 T90	32.49	32.38	0.160
C06	FAM	RPL13a	Unkn-17	799 T90	32.26	32.38	0.160
C07	FAM	RPL13a	Unkn-23	811 T90	30.73	30.63	0.148
C08	FAM	RPL13a	Unkn-23	811 T90	30.52	30.63	0.148
C09	FAM	RPL13a	Unkn-30	805 T90	31.02	31.30	0.395
C10	FAM	RPL13a	Unkn-30	805 T90	31.58	31.30	0.395
C11	FAM	RPL13a	Unkn-37	816 T90	30.95	30.95	0.000
C12	FAM	RPL13a	Unkn-37	816 T90	N/A	0.00	0.000
D01	FAM	RPL13a	Unkn-04	001 T+N90	29.92	30.27	0.503
D02	FAM	RPL13a	Unkn-04	001 T+N90	30.63	30.27	0.503
D03	FAM	RPL13a	Unkn-11	002 T+N90	29.31	29.59	0.397
D04	FAM	RPL13a	Unkn-11	002 T+N90	29.87	29.59	0.397
D05	FAM	RPL13a	Unkn-18	799 T+N90	31.45	31.41	0.054
D06	FAM	RPL13a	Unkn-18	799 T+N90	31.38	31.41	0.054
D07	FAM	RPL13a	Unkn-24	811 T+N90	30.21	30.17	0.066
D08	FAM	RPL13a	Unkn-24	811 T+N90	30.12	30.17	0.066
D09	FAM	RPL13a	Unkn-31	805 T+N90	31.07	30.74	0.465
D10	FAM	RPL13a	Unkn-31	805 T+N90	30.41	30.74	0.465
D11	FAM	RPL13a	Unkn-38	816 T+N90	31.48	31.51	0.036

Well	Fluor	Target	Content	Sample	Cq	Cq Mean	Cq Std. Dev
D12	FAM	RPL13a	Unkn-38	816 T+N90	31.53	31.51	0.036
E01	FAM	RPL13a	Unkn-05	001 V90	29.38	29.76	0.542
E02	FAM	RPL13a	Unkn-05	001 V90	30.14	29.76	0.542
E03	FAM	RPL13a	Unkn-12	002 V90	29.85	29.82	0.033
E04	FAM	RPL13a	Unkn-12	002 V90	29.80	29.82	0.033
E05	FAM	RPL13a	Unkn-19	799 Z90	29.96	30.14	0.261
E06	FAM	RPL13a	Unkn-19	799 Z90	30.33	30.14	0.261
E07	FAM	RPL13a	Unkn-25	811 V90	31.11	31.15	0.064
E08	FAM	RPL13a	Unkn-25	811 V90	31.20	31.15	0.064
E09	FAM	RPL13a	Unkn-32	805 V90	31.21	30.61	0.854
E10	FAM	RPL13a	Unkn-32	805 V90	30.00	30.61	0.854
E11	FAM	RPL13a	Unkn-39	816 V90	30.25	30.76	0.729
E12	FAM	RPL13a	Unkn-39	816 V90	31.28	30.76	0.729
F01	FAM	RPL13a	Unkn-06	001 Z90	28.89	28.82	0.104
F02	FAM	RPL13a	Unkn-06	001 Z90	28.74	28.82	0.104
F03	FAM	RPL13a	Unkn-13	002 Z90	29.37	29.74	0.524
F04	FAM	RPL13a	Unkn-13	002 Z90	30.11	29.74	0.524
F07	FAM	RPL13a	Unkn-26	811 Z90	31.16	31.00	0.217
F08	FAM	RPL13a	Unkn-26	811 Z90	30.85	31.00	0.217
F09	FAM	RPL13a	Unkn-33	805 Z90	30.38	29.44	1.325
F10	FAM	RPL13a	Unkn-33	805 Z90	28.51	29.44	1.325
F11	FAM	RPL13a	Unkn-40	816 Z90	31.54	31.27	0.382
F12	FAM	RPL13a	Unkn-40	816 Z90	31.00	31.27	0.382
G01	FAM	RPL13a	Unkn-07	001 MC	30.45	30.42	0.031
G02	FAM	RPL13a	Unkn-07	001 MC	30.40	30.42	0.031
G03	FAM	RPL13a	Unkn-14	002 MC	30.00	29.45	0.776
G04	FAM	RPL13a	Unkn-14	002 MC	28.91	29.45	0.776
G05	FAM	RPL13a	Unkn-20	799 MC	30.46	30.38	0.116
G06	FAM	RPL13a	Unkn-20	799 MC	30.30	30.38	0.116
G07	FAM	RPL13a	Unkn-27	811 MC	30.96	30.38	0.821
G08	FAM	RPL13a	Unkn-27	811 MC	29.79	30.38	0.821
G09	FAM	RPL13a	Unkn-34	805 MC	31.09	30.72	0.529
G10	FAM	RPL13a	Unkn-34	805 MC	30.34	30.72	0.529
G11	FAM	RPL13a	Unkn-41	816 MC	30.46	30.96	0.716
G12	FAM	RPL13a	Unkn-41	816 MC	31.47	30.96	0.716
H01	FAM	RPL13a	Pos Ctrl-42	804 PC	29.76	30.03	0.378
H02	FAM	RPL13a	Pos Ctrl-42	804 PC	30.30	30.03	0.378
H03	FAM	RPL13a	NTC-43	H2O	N/A	0.00	0.000
H04	FAM	RPL13a	NTC-43	H2O	N/A	0.00	0.000
H05	FAM	RPL13a	NTC-44	H2O	N/A	0.00	0.000
H06	FAM	RPL13a	NTC-44	H2O	N/A	0.00	0.000
H07	FAM	RPL13a	Unkn-45	Pooled MC 15ng	33.81	32.93	1.253
H08	FAM	RPL13a	Unkn-45	Pooled MC 15ng	32.04	32.93	1.253
H09	FAM	RPL13a	Unkn-46	Pooled MC 10ng	34.79	34.28	0.726
H10	FAM	RPL13a	Unkn-46	Pooled MC 10ng	33.77	34.28	0.726
H11	FAM	RPL13a	Unkn-47	Pooled MC 5ng	34.50	34.47	0.038
H12	FAM	RPL13a	Unkn-47	Pooled MC 5ng	34.45	34.47	0.038

Gene Expression

Target Names

Name	Full Name	Reference	Auto Efficiency	Efficiency
RPL13a	RPL13a	False	Yes	100.0%

RPLP0 15d.pcrd

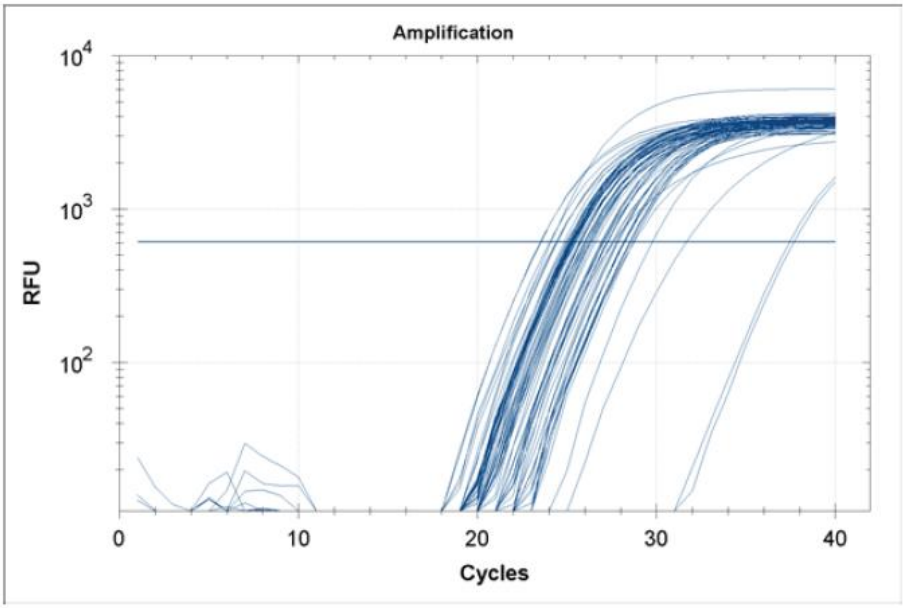
2013/08/21 12:41 PM

Run Setup

Plate Display

	1	2	3	4	5	6	7	8	9	10	11	12
A	Unk-1 RPLP0 001 S15	Unk-1 RPLP0 001 S15	Unk-7 RPLP0 002 S15	Unk-7 RPLP0 002 S15	Unk-13 RPLP0 799 S15	Unk-13 RPLP0 799 S15	Unk-18 RPLP0 811 S15	Unk-18 RPLP0 811 S15	Unk-24 RPLP0 805 S15	Unk-24 RPLP0 805 S15	Unk-30 RPLP0 816 S15	Unk-30 RPLP0 816 S15
B	Unk-2 RPLP0 001 N15	Unk-2 RPLP0 001 N15	Unk-8 RPLP0 002 N15	Unk-8 RPLP0 002 N15	Unk-14 RPLP0 799 N15	Unk-14 RPLP0 799 N15	Unk-19 RPLP0 811 N15	Unk-19 RPLP0 811 N15	Unk-25 RPLP0 805 N15	Unk-25 RPLP0 805 N15	Unk-31 RPLP0 816 N15	Unk-31 RPLP0 816 N15
C	Unk-3 RPLP0 001 T15	Unk-3 RPLP0 001 T15	Unk-9 RPLP0 002 T15	Unk-9 RPLP0 002 T15	Unk-15 RPLP0 799 T15	Unk-15 RPLP0 799 T15	Unk-20 RPLP0 811 T15	Unk-20 RPLP0 811 T15	Unk-26 RPLP0 805 T15	Unk-26 RPLP0 805 T15	Unk-32 RPLP0 816 T15	Unk-32 RPLP0 816 T15
D	Unk-4 RPLP0 001 T+N15	Unk-4 RPLP0 001 T+N15	Unk-10 RPLP0 002 T+N15	Unk-10 RPLP0 002 T+N15	Unk-16 RPLP0 799 T+N15	Unk-16 RPLP0 799 T+N15	Unk-21 RPLP0 811 T+N15	Unk-21 RPLP0 811 T+N15	Unk-27 RPLP0 805 T+N15	Unk-27 RPLP0 805 T+N15	Unk-33 RPLP0 816 T+N15	Unk-33 RPLP0 816 T+N15
E	Unk-5 RPLP0 001 V15	Unk-5 RPLP0 001 V15	Unk-11 RPLP0 002 V15	Unk-11 RPLP0 002 V15	Unk-17 RPLP0 799 Z15	Unk-17 RPLP0 799 Z15	Unk-22 RPLP0 811 V15	Unk-22 RPLP0 811 V15	Unk-28 RPLP0 805 V15	Unk-28 RPLP0 805 V15	Unk-34 RPLP0 816 V15	Unk-34 RPLP0 816 V15
F	Unk-6 RPLP0 001 Z15	Unk-6 RPLP0 001 Z15	Unk-12 RPLP0 002 Z15	Unk-12 RPLP0 002 Z15			Unk-23 RPLP0 811 Z15	Unk-23 RPLP0 811 Z15	Unk-29 RPLP0 805 Z15	Unk-29 RPLP0 805 Z15	Unk-35 RPLP0 816 Z15	Unk-35 RPLP0 816 Z15
G	Pos-36 RPLP0 804 PC	Pos-36 RPLP0 804 PC	NTC-37 RPLP0 H2O	NTC-37 RPLP0 H2O	NTC-38 RPLP0 H2O	NTC-38 RPLP0 H2O	Unk-39 RPLP0 Pooled MC 10ng	Unk-39 RPLP0 Pooled MC 10ng	Unk-40 RPLP0 Pooled MC 15ng	Unk-40 RPLP0 Pooled MC 15ng	Unk-41 RPLP0 Pooled MC 5ng	Unk-41 RPLP0 Pooled MC 5ng
H												

Quantification



Quantification Data

Well	Fluor	Target	Content	Sample	Cq	Cq Mean	Cq Std. Dev
A01	FAM	RPLP0	Unkn-01	001 S15	25.95	26.76	1.138
A02	FAM	RPLP0	Unkn-01	001 S15	27.56	26.76	1.138
A03	FAM	RPLP0	Unkn-07	002 S15	25.48	25.21	0.372
A04	FAM	RPLP0	Unkn-07	002 S15	24.95	25.21	0.372
A05	FAM	RPLP0	Unkn-13	799 S15	25.99	25.62	0.513
A06	FAM	RPLP0	Unkn-13	799 S15	25.26	25.62	0.513
A07	FAM	RPLP0	Unkn-18	811 S15	26.32	26.28	0.048
A08	FAM	RPLP0	Unkn-18	811 S15	26.25	26.28	0.048
A09	FAM	RPLP0	Unkn-24	805 S15	37.40	37.52	0.174
A10	FAM	RPLP0	Unkn-24	805 S15	37.64	37.52	0.174
A11	FAM	RPLP0	Unkn-30	816 S15	26.11	26.59	0.680
A12	FAM	RPLP0	Unkn-30	816 S15	27.07	26.59	0.680
B01	FAM	RPLP0	Unkn-02	001 N15	25.19	25.31	0.160
B02	FAM	RPLP0	Unkn-02	001 N15	25.42	25.31	0.160
B03	FAM	RPLP0	Unkn-08	002 N15	25.21	25.24	0.043
B04	FAM	RPLP0	Unkn-08	002 N15	25.27	25.24	0.043
B05	FAM	RPLP0	Unkn-14	799 N15	24.09	24.66	0.814
B06	FAM	RPLP0	Unkn-14	799 N15	25.24	24.66	0.814
B07	FAM	RPLP0	Unkn-19	811 N15	27.45	27.20	0.358
B08	FAM	RPLP0	Unkn-19	811 N15	26.95	27.20	0.358
B09	FAM	RPLP0	Unkn-25	805 N15	27.06	27.13	0.109
B10	FAM	RPLP0	Unkn-25	805 N15	27.21	27.13	0.109
B11	FAM	RPLP0	Unkn-31	816 N15	28.48	29.10	0.886
B12	FAM	RPLP0	Unkn-31	816 N15	29.73	29.10	0.886
C01	FAM	RPLP0	Unkn-03	001 T15	25.95	26.10	0.210
C02	FAM	RPLP0	Unkn-03	001 T15	26.25	26.10	0.210
C03	FAM	RPLP0	Unkn-09	002 T15	25.34	25.29	0.076
C04	FAM	RPLP0	Unkn-09	002 T15	25.24	25.29	0.076
C05	FAM	RPLP0	Unkn-15	799 T15	25.17	25.15	0.038
C06	FAM	RPLP0	Unkn-15	799 T15	25.12	25.15	0.038
C07	FAM	RPLP0	Unkn-20	811 T15	24.34	24.18	0.217
C08	FAM	RPLP0	Unkn-20	811 T15	24.03	24.18	0.217
C09	FAM	RPLP0	Unkn-26	805 T15	24.99	25.15	0.222
C10	FAM	RPLP0	Unkn-26	805 T15	25.31	25.15	0.222
C11	FAM	RPLP0	Unkn-32	816 T15	27.55	27.88	0.462
C12	FAM	RPLP0	Unkn-32	816 T15	28.20	27.88	0.462
D01	FAM	RPLP0	Unkn-04	001 T+N15	26.05	26.23	0.256
D02	FAM	RPLP0	Unkn-04	001 T+N15	26.42	26.23	0.256
D03	FAM	RPLP0	Unkn-10	002 T+N15	24.39	24.78	0.541
D04	FAM	RPLP0	Unkn-10	002 T+N15	25.16	24.78	0.541
D05	FAM	RPLP0	Unkn-16	799 T+N15	25.11	24.76	0.498
D06	FAM	RPLP0	Unkn-16	799 T+N15	24.41	24.76	0.498
D07	FAM	RPLP0	Unkn-21	811 T+N15	28.56	28.61	0.080
D08	FAM	RPLP0	Unkn-21	811 T+N15	28.67	28.61	0.080
D09	FAM	RPLP0	Unkn-27	805 T+N15	26.11	26.19	0.109
D10	FAM	RPLP0	Unkn-27	805 T+N15	26.27	26.19	0.109
D11	FAM	RPLP0	Unkn-33	816 T+N15	25.74	25.75	0.010

Well	Fluor	Target	Content	Sample	Cq	Cq Mean	Cq Std. Dev
D12	FAM	RPLP0	Unkn-33	816 T+N15	25.75	25.75	0.010
E01	FAM	RPLP0	Unkn-05	001 V15	27.72	28.22	0.710
E02	FAM	RPLP0	Unkn-05	001 V15	28.72	28.22	0.710
E03	FAM	RPLP0	Unkn-11	002 V15	25.23	25.27	0.050
E04	FAM	RPLP0	Unkn-11	002 V15	25.30	25.27	0.050
E05	FAM	RPLP0	Unkn-17	799 Z15	25.34	25.07	0.381
E06	FAM	RPLP0	Unkn-17	799 Z15	24.81	25.07	0.381
E07	FAM	RPLP0	Unkn-22	811 V15	25.68	25.69	0.012
E08	FAM	RPLP0	Unkn-22	811 V15	25.69	25.69	0.012
E09	FAM	RPLP0	Unkn-28	805 V15	28.17	27.97	0.280
E10	FAM	RPLP0	Unkn-28	805 V15	27.77	27.97	0.280
E11	FAM	RPLP0	Unkn-34	816 V15	26.90	26.95	0.081
E12	FAM	RPLP0	Unkn-34	816 V15	27.01	26.95	0.081
F01	FAM	RPLP0	Unkn-06	001 Z15	26.55	26.36	0.261
F02	FAM	RPLP0	Unkn-06	001 Z15	26.18	26.36	0.261
F03	FAM	RPLP0	Unkn-12	002 Z15	25.39	28.52	4.424
F04	FAM	RPLP0	Unkn-12	002 Z15	31.65	28.52	4.424
F07	FAM	RPLP0	Unkn-23	811 Z15	23.47	23.48	0.015
F08	FAM	RPLP0	Unkn-23	811 Z15	23.49	23.48	0.015
F09	FAM	RPLP0	Unkn-29	805 Z15	25.09	25.08	0.024
F10	FAM	RPLP0	Unkn-29	805 Z15	25.06	25.08	0.024
F11	FAM	RPLP0	Unkn-35	816 Z15	27.25	27.22	0.037
F12	FAM	RPLP0	Unkn-35	816 Z15	27.19	27.22	0.037
G01	FAM	RPLP0	Pos Ctrl-36	804 PC	25.12	25.36	0.337
G02	FAM	RPLP0	Pos Ctrl-36	804 PC	25.59	25.36	0.337
G03	FAM	RPLP0	NTC-37	H2O	N/A	0.00	0.000
G04	FAM	RPLP0	NTC-37	H2O	N/A	0.00	0.000
G05	FAM	RPLP0	NTC-38	H2O	N/A	0.00	0.000
G06	FAM	RPLP0	NTC-38	H2O	N/A	0.00	0.000
G07	FAM	RPLP0	Unkn-39	Pooled MC 10ng	27.86	28.01	0.225
G08	FAM	RPLP0	Unkn-39	Pooled MC 10ng	28.17	28.01	0.225
G09	FAM	RPLP0	Unkn-40	Pooled MC 15ng	28.45	28.29	0.226
G10	FAM	RPLP0	Unkn-40	Pooled MC 15ng	28.13	28.29	0.226
G11	FAM	RPLP0	Unkn-41	Pooled MC 5ng	28.47	28.46	0.009
G12	FAM	RPLP0	Unkn-41	Pooled MC 5ng	28.45	28.46	0.009

Gene Expression

Target Names

Name	Full Name	Reference	Auto Efficiency	Efficiency
RPLP0	RPLP0	False	Yes	100.0%

RPLP0 60d.pcrd

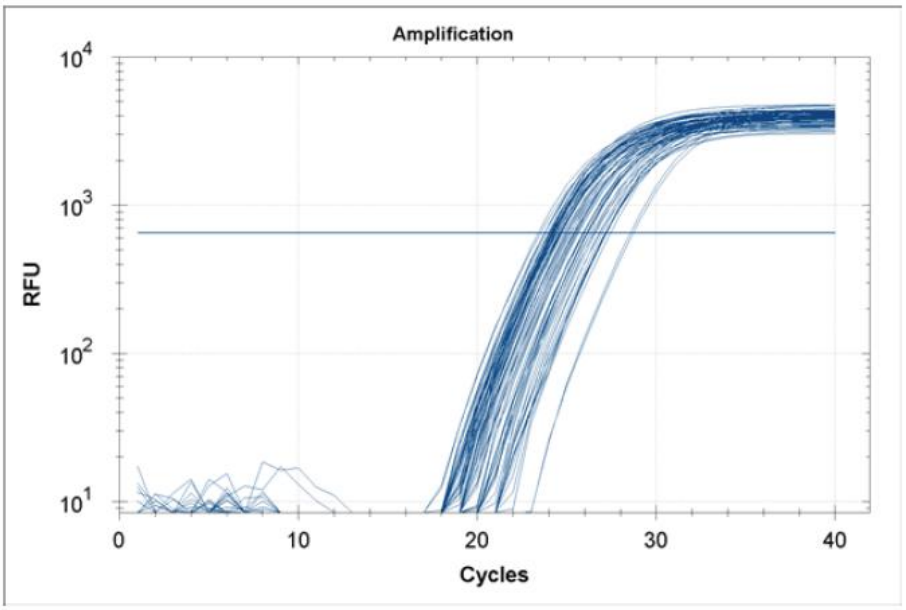
2013/08/21 12:43 PM

Run Setup

Plate Display

	1	2	3	4	5	6	7	8	9	10	11	12
A	Unk-1 RPLP0 001 S60	Unk-1 RPLP0 001 S60	Unk-7 RPLP0 002 S60	Unk-7 RPLP0 002 S60	Unk-13 RPLP0 799 S60	Unk-13 RPLP0 799 S60	Unk-18 RPLP0 811 S60	Unk-18 RPLP0 811 S60	Unk-24 RPLP0 805 S60	Unk-24 RPLP0 805 S60	Unk-30 RPLP0 816 S60	Unk-30 RPLP0 816 S60
B	Unk-2 RPLP0 001 N60	Unk-2 RPLP0 001 N60	Unk-8 RPLP0 002 N60	Unk-8 RPLP0 002 N60	Unk-14 RPLP0 799 N60	Unk-14 RPLP0 799 N60	Unk-19 RPLP0 811 N60	Unk-19 RPLP0 811 N60	Unk-25 RPLP0 805 N60	Unk-25 RPLP0 805 N60	Unk-31 RPLP0 816 N60	Unk-31 RPLP0 816 N60
C	Unk-3 RPLP0 001 T60	Unk-3 RPLP0 001 T60	Unk-9 RPLP0 002 T60	Unk-9 RPLP0 002 T60	Unk-15 RPLP0 799 T60	Unk-15 RPLP0 799 T60	Unk-20 RPLP0 811 T60	Unk-20 RPLP0 811 T60	Unk-26 RPLP0 805 T60	Unk-26 RPLP0 805 T60	Unk-32 RPLP0 816 T60	Unk-32 RPLP0 816 T60
D	Unk-4 RPLP0 001 T+N60	Unk-4 RPLP0 001 T+N60	Unk-10 RPLP0 002 T+N60	Unk-10 RPLP0 002 T+N60	Unk-16 RPLP0 799 T+N60	Unk-16 RPLP0 799 T+N60	Unk-21 RPLP0 811 T+N60	Unk-21 RPLP0 811 T+N60	Unk-27 RPLP0 805 T+N60	Unk-27 RPLP0 805 T+N60	Unk-33 RPLP0 816 T+N60	Unk-33 RPLP0 816 T+N60
E	Unk-5 RPLP0 001 V60	Unk-5 RPLP0 001 V60	Unk-11 RPLP0 002 V60	Unk-11 RPLP0 002 V60	Unk-17 RPLP0 799 Z60	Unk-17 RPLP0 799 Z60	Unk-22 RPLP0 811 V60	Unk-22 RPLP0 811 V60	Unk-28 RPLP0 805 V60	Unk-28 RPLP0 805 V60	Unk-34 RPLP0 816 V60	Unk-34 RPLP0 816 V60
F	Unk-6 RPLP0 001 Z60	Unk-6 RPLP0 001 Z60	Unk-12 RPLP0 002 Z60	Unk-12 RPLP0 002 Z60			Unk-23 RPLP0 811 Z60	Unk-23 RPLP0 811 Z60	Unk-29 RPLP0 805 Z60	Unk-29 RPLP0 805 Z60	Unk-35 RPLP0 816 Z60	Unk-35 RPLP0 816 Z60
G	Pos-36 RPLP0 804 PC	Pos-36 RPLP0 804 PC	NTC-37 RPLP0 H2O	NTC-37 RPLP0 H2O	NTC-38 RPLP0 H2O	NTC-38 RPLP0 H2O	Unk-39 RPLP0 Pooled MC 10ng	Unk-39 RPLP0 Pooled MC 10ng	Unk-40 RPLP0 Pooled MC 15ng	Unk-40 RPLP0 Pooled MC 15ng	Unk-41 RPLP0 Pooled MC 5ng	Unk-41 RPLP0 Pooled MC 5ng
H												

Quantification



Quantification Data

Well	Fluor	Target	Content	Sample	Cq	Cq Mean	Cq Std. Dev
A01	FAM	RPLP0	Unkn-01	001 S60	24.08	24.21	0.189
A02	FAM	RPLP0	Unkn-01	001 S60	24.35	24.21	0.189
A03	FAM	RPLP0	Unkn-07	002 S60	23.49	23.70	0.295
A04	FAM	RPLP0	Unkn-07	002 S60	23.91	23.70	0.295
A05	FAM	RPLP0	Unkn-13	799 S60	23.73	23.54	0.259
A06	FAM	RPLP0	Unkn-13	799 S60	23.36	23.54	0.259
A07	FAM	RPLP0	Unkn-18	811 S60	24.97	24.79	0.258
A08	FAM	RPLP0	Unkn-18	811 S60	24.61	24.79	0.258
A09	FAM	RPLP0	Unkn-24	805 S60	24.80	24.93	0.189
A10	FAM	RPLP0	Unkn-24	805 S60	25.07	24.93	0.189
A11	FAM	RPLP0	Unkn-30	816 S60	26.35	26.42	0.102
A12	FAM	RPLP0	Unkn-30	816 S60	26.49	26.42	0.102
B01	FAM	RPLP0	Unkn-02	001 N60	25.00	25.18	0.253
B02	FAM	RPLP0	Unkn-02	001 N60	25.36	25.18	0.253
B03	FAM	RPLP0	Unkn-08	002 N60	26.58	26.87	0.415
B04	FAM	RPLP0	Unkn-08	002 N60	27.17	26.87	0.415
B05	FAM	RPLP0	Unkn-14	799 N60	26.24	26.52	0.395
B06	FAM	RPLP0	Unkn-14	799 N60	26.80	26.52	0.395
B07	FAM	RPLP0	Unkn-19	811 N60	24.03	24.16	0.186
B08	FAM	RPLP0	Unkn-19	811 N60	24.29	24.16	0.186
B09	FAM	RPLP0	Unkn-25	805 N60	24.35	24.47	0.171
B10	FAM	RPLP0	Unkn-25	805 N60	24.59	24.47	0.171
B11	FAM	RPLP0	Unkn-31	816 N60	25.54	25.75	0.286
B12	FAM	RPLP0	Unkn-31	816 N60	25.95	25.75	0.286
C01	FAM	RPLP0	Unkn-03	001 T60	24.36	24.29	0.100
C02	FAM	RPLP0	Unkn-03	001 T60	24.22	24.29	0.100
C03	FAM	RPLP0	Unkn-09	002 T60	25.18	24.78	0.568
C04	FAM	RPLP0	Unkn-09	002 T60	24.38	24.78	0.568
C05	FAM	RPLP0	Unkn-15	799 T60	24.62	24.31	0.427
C06	FAM	RPLP0	Unkn-15	799 T60	24.01	24.31	0.427
C07	FAM	RPLP0	Unkn-20	811 T60	25.96	26.04	0.109
C08	FAM	RPLP0	Unkn-20	811 T60	26.12	26.04	0.109
C09	FAM	RPLP0	Unkn-26	805 T60	27.17	27.01	0.226
C10	FAM	RPLP0	Unkn-26	805 T60	26.85	27.01	0.226
C11	FAM	RPLP0	Unkn-32	816 T60	25.98	26.06	0.116
C12	FAM	RPLP0	Unkn-32	816 T60	26.14	26.06	0.116
D01	FAM	RPLP0	Unkn-04	001 T+N60	24.06	24.35	0.412
D02	FAM	RPLP0	Unkn-04	001 T+N60	24.64	24.35	0.412
D03	FAM	RPLP0	Unkn-10	002 T+N60	24.58	24.43	0.208
D04	FAM	RPLP0	Unkn-10	002 T+N60	24.28	24.43	0.208
D05	FAM	RPLP0	Unkn-16	799 T+N60	24.04	24.13	0.117
D06	FAM	RPLP0	Unkn-16	799 T+N60	24.21	24.13	0.117
D07	FAM	RPLP0	Unkn-21	811 T+N60	25.44	25.47	0.031
D08	FAM	RPLP0	Unkn-21	811 T+N60	25.49	25.47	0.031
D09	FAM	RPLP0	Unkn-27	805 T+N60	26.45	26.27	0.250
D10	FAM	RPLP0	Unkn-27	805 T+N60	26.10	26.27	0.250
D11	FAM	RPLP0	Unkn-33	816 T+N60	26.14	26.02	0.179

Well	Fluor	Target	Content	Sample	Cq	Cq Mean	Cq Std. Dev
D12	FAM	RPLP0	Unkn-33	816 T+N60	25.89	26.02	0.179
E01	FAM	RPLP0	Unkn-05	001 V60	24.19	24.19	0.003
E02	FAM	RPLP0	Unkn-05	001 V60	24.19	24.19	0.003
E03	FAM	RPLP0	Unkn-11	002 V60	23.76	23.94	0.253
E04	FAM	RPLP0	Unkn-11	002 V60	24.12	23.94	0.253
E05	FAM	RPLP0	Unkn-17	799 Z60	24.25	24.27	0.034
E06	FAM	RPLP0	Unkn-17	799 Z60	24.30	24.27	0.034
E07	FAM	RPLP0	Unkn-22	811 V60	24.51	24.70	0.268
E08	FAM	RPLP0	Unkn-22	811 V60	24.89	24.70	0.268
E09	FAM	RPLP0	Unkn-28	805 V60	23.73	23.93	0.293
E10	FAM	RPLP0	Unkn-28	805 V60	24.14	23.93	0.293
E11	FAM	RPLP0	Unkn-34	816 V60	25.38	25.35	0.046
E12	FAM	RPLP0	Unkn-34	816 V60	25.31	25.35	0.046
F01	FAM	RPLP0	Unkn-06	001 Z60	24.49	24.47	0.036
F02	FAM	RPLP0	Unkn-06	001 Z60	24.44	24.47	0.036
F03	FAM	RPLP0	Unkn-12	002 Z60	24.59	24.37	0.306
F04	FAM	RPLP0	Unkn-12	002 Z60	24.16	24.37	0.306
F07	FAM	RPLP0	Unkn-23	811 Z60	24.64	24.92	0.397
F08	FAM	RPLP0	Unkn-23	811 Z60	25.20	24.92	0.397
F09	FAM	RPLP0	Unkn-29	805 Z60	27.13	27.26	0.192
F10	FAM	RPLP0	Unkn-29	805 Z60	27.40	27.26	0.192
F11	FAM	RPLP0	Unkn-35	816 Z60	26.12	25.87	0.355
F12	FAM	RPLP0	Unkn-35	816 Z60	25.62	25.87	0.355
G01	FAM	RPLP0	Pos Ctrl-36	804 PC	25.08	24.88	0.284
G02	FAM	RPLP0	Pos Ctrl-36	804 PC	24.68	24.88	0.284
G03	FAM	RPLP0	NTC-37	H2O	N/A	0.00	0.000
G04	FAM	RPLP0	NTC-37	H2O	N/A	0.00	0.000
G05	FAM	RPLP0	NTC-38	H2O	N/A	0.00	0.000
G06	FAM	RPLP0	NTC-38	H2O	N/A	0.00	0.000
G07	FAM	RPLP0	Unkn-39	Pooled MC 10ng	27.18	27.09	0.127
G08	FAM	RPLP0	Unkn-39	Pooled MC 10ng	27.00	27.09	0.127
G09	FAM	RPLP0	Unkn-40	Pooled MC 15ng	27.19	27.18	0.019
G10	FAM	RPLP0	Unkn-40	Pooled MC 15ng	27.16	27.18	0.019
G11	FAM	RPLP0	Unkn-41	Pooled MC 5ng	28.66	28.58	0.113
G12	FAM	RPLP0	Unkn-41	Pooled MC 5ng	28.50	28.58	0.113

Gene Expression

Target Names

Name	Full Name	Reference	Auto Efficiency	Efficiency
RPLP0	RPLP0	False	Yes	100.0%

RPLP0 90d.pcrd

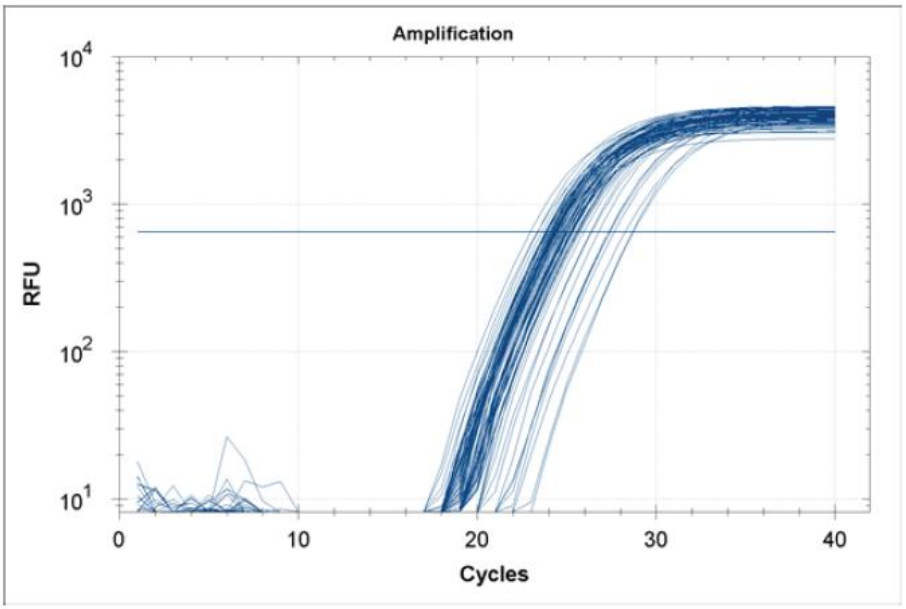
2013/08/21 12:44 PM

Run Setup

Plate Display

	1	2	3	4	5	6	7	8	9	10	11	12
A	Unk-1 RPLP0 001 S90	Unk-1 RPLP0 001 S90	Unk-8 RPLP0 002 S90	Unk-8 RPLP0 002 S90	Unk-15 RPLP0 799 S90	Unk-15 RPLP0 799 S90	Unk-21 RPLP0 811 S90	Unk-21 RPLP0 811 S90	Unk-28 RPLP0 805 S90	Unk-28 RPLP0 805 S90	Unk-35 RPLP0 816 S90	Unk-35 RPLP0 816 S90
B	Unk-2 RPLP0 001 N90	Unk-2 RPLP0 001 N90	Unk-9 RPLP0 002 N90	Unk-9 RPLP0 002 N90	Unk-16 RPLP0 799 N90	Unk-16 RPLP0 799 N90	Unk-22 RPLP0 811 N90	Unk-22 RPLP0 811 N90	Unk-29 RPLP0 805 N90	Unk-29 RPLP0 805 N90	Unk-36 RPLP0 816 N90	Unk-36 RPLP0 816 N90
C	Unk-3 RPLP0 001 T90	Unk-3 RPLP0 001 T90	Unk-10 RPLP0 002 T90	Unk-10 RPLP0 002 T90	Unk-17 RPLP0 799 T90	Unk-17 RPLP0 799 T90	Unk-23 RPLP0 811 T90	Unk-23 RPLP0 811 T90	Unk-30 RPLP0 805 T90	Unk-30 RPLP0 805 T90	Unk-37 RPLP0 816 T90	Unk-37 RPLP0 816 T90
D	Unk-4 RPLP0 001 T+N90	Unk-4 RPLP0 001 T+N90	Unk-11 RPLP0 002 T+N90	Unk-11 RPLP0 002 T+N90	Unk-18 RPLP0 799 T+N90	Unk-18 RPLP0 799 T+N90	Unk-24 RPLP0 811 T+N90	Unk-24 RPLP0 811 T+N90	Unk-31 RPLP0 805 T+N90	Unk-31 RPLP0 805 T+N90	Unk-38 RPLP0 816 T+N90	Unk-38 RPLP0 816 T+N90
E	Unk-5 RPLP0 001 V90	Unk-5 RPLP0 001 V90	Unk-12 RPLP0 002 V90	Unk-12 RPLP0 002 V90	Unk-19 RPLP0 799 Z90	Unk-19 RPLP0 799 Z90	Unk-25 RPLP0 811 V90	Unk-25 RPLP0 811 V90	Unk-32 RPLP0 805 V90	Unk-32 RPLP0 805 V90	Unk-39 RPLP0 816 V90	Unk-39 RPLP0 816 V90
F	Unk-6 RPLP0 001 Z90	Unk-6 RPLP0 001 Z90	Unk-13 RPLP0 002 Z90	Unk-13 RPLP0 002 Z90			Unk-26 RPLP0 811 Z90	Unk-26 RPLP0 811 Z90	Unk-33 RPLP0 805 Z90	Unk-33 RPLP0 805 Z90	Unk-40 RPLP0 816 Z90	Unk-40 RPLP0 816 Z90
G	Unk-7 RPLP0 001 MC	Unk-7 RPLP0 001 MC	Unk-14 RPLP0 002 MC	Unk-14 RPLP0 002 MC	Unk-20 RPLP0 799 MC	Unk-20 RPLP0 799 MC	Unk-27 RPLP0 811 MC	Unk-27 RPLP0 811 MC	Unk-34 RPLP0 805 MC	Unk-34 RPLP0 805 MC	Unk-41 RPLP0 816 MC	Unk-41 RPLP0 816 MC
H	Pos-42 RPLP0 804 PC	Pos-42 RPLP0 804 PC	NTC-43 RPLP0 H2O	NTC-43 RPLP0 H2O	NTC-44 RPLP0 H2O	NTC-44 RPLP0 H2O	Unk-45 RPLP0 Pooled MC 15ng	Unk-45 RPLP0 Pooled MC 15ng	Unk-46 RPLP0 Pooled MC 10ng	Unk-46 RPLP0 Pooled MC 10ng	Unk-47 RPLP0 Pooled MC 5ng	Unk-47 RPLP0 Pooled MC 5ng

Quantification



Quantification Data

Well	Fluor	Target	Content	Sample	Cq	Cq Mean	Cq Std. Dev
A01	FAM	RPLP0	Unkn-01	001 S90	24.28	24.42	0.205
A02	FAM	RPLP0	Unkn-01	001 S90	24.57	24.42	0.205
A03	FAM	RPLP0	Unkn-08	002 S90	23.82	23.88	0.089
A04	FAM	RPLP0	Unkn-08	002 S90	23.95	23.88	0.089
A05	FAM	RPLP0	Unkn-15	799 S90	24.68	24.27	0.567
A06	FAM	RPLP0	Unkn-15	799 S90	23.87	24.27	0.567
A07	FAM	RPLP0	Unkn-21	811 S90	23.31	23.13	0.256
A08	FAM	RPLP0	Unkn-21	811 S90	22.95	23.13	0.256
A09	FAM	RPLP0	Unkn-28	805 S90	25.47	25.32	0.212
A10	FAM	RPLP0	Unkn-28	805 S90	25.17	25.32	0.212
A11	FAM	RPLP0	Unkn-35	816 S90	25.70	25.66	0.061
A12	FAM	RPLP0	Unkn-35	816 S90	25.61	25.66	0.061
B01	FAM	RPLP0	Unkn-02	001 N90	24.37	24.37	0.012
B02	FAM	RPLP0	Unkn-02	001 N90	24.38	24.37	0.012
B03	FAM	RPLP0	Unkn-09	002 N90	24.11	24.07	0.063
B04	FAM	RPLP0	Unkn-09	002 N90	24.02	24.07	0.063
B05	FAM	RPLP0	Unkn-16	799 N90	25.12	24.67	0.643
B06	FAM	RPLP0	Unkn-16	799 N90	24.21	24.67	0.643
B07	FAM	RPLP0	Unkn-22	811 N90	25.26	25.39	0.183
B08	FAM	RPLP0	Unkn-22	811 N90	25.52	25.39	0.183
B09	FAM	RPLP0	Unkn-29	805 N90	24.40	24.36	0.058
B10	FAM	RPLP0	Unkn-29	805 N90	24.31	24.36	0.058
B11	FAM	RPLP0	Unkn-36	816 N90	24.74	24.46	0.401
B12	FAM	RPLP0	Unkn-36	816 N90	24.18	24.46	0.401
C01	FAM	RPLP0	Unkn-03	001 T90	24.50	24.86	0.505
C02	FAM	RPLP0	Unkn-03	001 T90	25.21	24.86	0.505
C03	FAM	RPLP0	Unkn-10	002 T90	24.97	24.93	0.045
C04	FAM	RPLP0	Unkn-10	002 T90	24.90	24.93	0.045
C05	FAM	RPLP0	Unkn-17	799 T90	25.01	25.02	0.009
C06	FAM	RPLP0	Unkn-17	799 T90	25.02	25.02	0.009
C07	FAM	RPLP0	Unkn-23	811 T90	24.03	24.13	0.139
C08	FAM	RPLP0	Unkn-23	811 T90	24.23	24.13	0.139
C09	FAM	RPLP0	Unkn-30	805 T90	26.35	26.31	0.047
C10	FAM	RPLP0	Unkn-30	805 T90	26.28	26.31	0.047
C11	FAM	RPLP0	Unkn-37	816 T90	25.20	25.12	0.119
C12	FAM	RPLP0	Unkn-37	816 T90	25.03	25.12	0.119
D01	FAM	RPLP0	Unkn-04	001 T+N90	24.60	24.68	0.112
D02	FAM	RPLP0	Unkn-04	001 T+N90	24.76	24.68	0.112
D03	FAM	RPLP0	Unkn-11	002 T+N90	24.32	24.10	0.314
D04	FAM	RPLP0	Unkn-11	002 T+N90	23.88	24.10	0.314
D05	FAM	RPLP0	Unkn-18	799 T+N90	24.12	23.95	0.233
D06	FAM	RPLP0	Unkn-18	799 T+N90	23.79	23.95	0.233
D07	FAM	RPLP0	Unkn-24	811 T+N90	23.83	23.94	0.146
D08	FAM	RPLP0	Unkn-24	811 T+N90	24.04	23.94	0.146
D09	FAM	RPLP0	Unkn-31	805 T+N90	25.58	25.54	0.057
D10	FAM	RPLP0	Unkn-31	805 T+N90	25.50	25.54	0.057
D11	FAM	RPLP0	Unkn-38	816 T+N90	27.29	27.01	0.397

Well	Fluor	Target	Content	Sample	Cq	Cq Mean	Cq Std. Dev
D12	FAM	RPLP0	Unkn-38	816 T+N90	26.73	27.01	0.397
E01	FAM	RPLP0	Unkn-05	001 V90	24.59	24.43	0.224
E02	FAM	RPLP0	Unkn-05	001 V90	24.27	24.43	0.224
E03	FAM	RPLP0	Unkn-12	002 V90	24.35	24.32	0.043
E04	FAM	RPLP0	Unkn-12	002 V90	24.29	24.32	0.043
E05	FAM	RPLP0	Unkn-19	799 Z90	24.38	24.32	0.084
E06	FAM	RPLP0	Unkn-19	799 Z90	24.26	24.32	0.084
E07	FAM	RPLP0	Unkn-25	811 V90	25.35	25.22	0.186
E08	FAM	RPLP0	Unkn-25	811 V90	25.09	25.22	0.186
E09	FAM	RPLP0	Unkn-32	805 V90	24.35	24.40	0.076
E10	FAM	RPLP0	Unkn-32	805 V90	24.45	24.40	0.076
E11	FAM	RPLP0	Unkn-39	816 V90	25.21	25.23	0.035
E12	FAM	RPLP0	Unkn-39	816 V90	25.26	25.23	0.035
F01	FAM	RPLP0	Unkn-06	001 Z90	24.13	24.57	0.614
F02	FAM	RPLP0	Unkn-06	001 Z90	25.00	24.57	0.614
F03	FAM	RPLP0	Unkn-13	002 Z90	24.10	23.92	0.252
F04	FAM	RPLP0	Unkn-13	002 Z90	23.74	23.92	0.252
F07	FAM	RPLP0	Unkn-26	811 Z90	24.88	25.05	0.251
F08	FAM	RPLP0	Unkn-26	811 Z90	25.23	25.05	0.251
F09	FAM	RPLP0	Unkn-33	805 Z90	24.09	24.13	0.055
F10	FAM	RPLP0	Unkn-33	805 Z90	24.16	24.13	0.055
F11	FAM	RPLP0	Unkn-40	816 Z90	25.27	25.60	0.466
F12	FAM	RPLP0	Unkn-40	816 Z90	25.93	25.60	0.466
G01	FAM	RPLP0	Unkn-07	001 MC	24.70	24.70	0.004
G02	FAM	RPLP0	Unkn-07	001 MC	24.70	24.70	0.004
G03	FAM	RPLP0	Unkn-14	002 MC	24.24	24.12	0.160
G04	FAM	RPLP0	Unkn-14	002 MC	24.01	24.12	0.160
G05	FAM	RPLP0	Unkn-20	799 MC	24.41	24.46	0.077
G06	FAM	RPLP0	Unkn-20	799 MC	24.52	24.46	0.077
G07	FAM	RPLP0	Unkn-27	811 MC	23.32	23.43	0.162
G08	FAM	RPLP0	Unkn-27	811 MC	23.55	23.43	0.162
G09	FAM	RPLP0	Unkn-34	805 MC	24.29	24.44	0.215
G10	FAM	RPLP0	Unkn-34	805 MC	24.59	24.44	0.215
G11	FAM	RPLP0	Unkn-41	816 MC	24.83	24.93	0.130
G12	FAM	RPLP0	Unkn-41	816 MC	25.02	24.93	0.130
H01	FAM	RPLP0	Pos Ctrl-42	804 PC	25.26	25.12	0.205
H02	FAM	RPLP0	Pos Ctrl-42	804 PC	24.97	25.12	0.205
H03	FAM	RPLP0	NTC-43	H2O	N/A	0.00	0.000
H04	FAM	RPLP0	NTC-43	H2O	N/A	0.00	0.000
H05	FAM	RPLP0	NTC-44	H2O	N/A	0.00	0.000
H06	FAM	RPLP0	NTC-44	H2O	N/A	0.00	0.000
H07	FAM	RPLP0	Unkn-45	Pooled MC 15ng	27.38	27.80	0.598
H08	FAM	RPLP0	Unkn-45	Pooled MC 15ng	28.22	27.80	0.598
H09	FAM	RPLP0	Unkn-46	Pooled MC 10ng	27.31	27.45	0.203
H10	FAM	RPLP0	Unkn-46	Pooled MC 10ng	27.59	27.45	0.203
H11	FAM	RPLP0	Unkn-47	Pooled MC 5ng	28.60	28.64	0.058
H12	FAM	RPLP0	Unkn-47	Pooled MC 5ng	28.68	28.64	0.058

Gene Expression

Target Names

Name	Full Name	Reference	Auto Efficiency	Efficiency
RPLP0	RPLP0	False	Yes	100.0%

SDHA 15d.pcrd

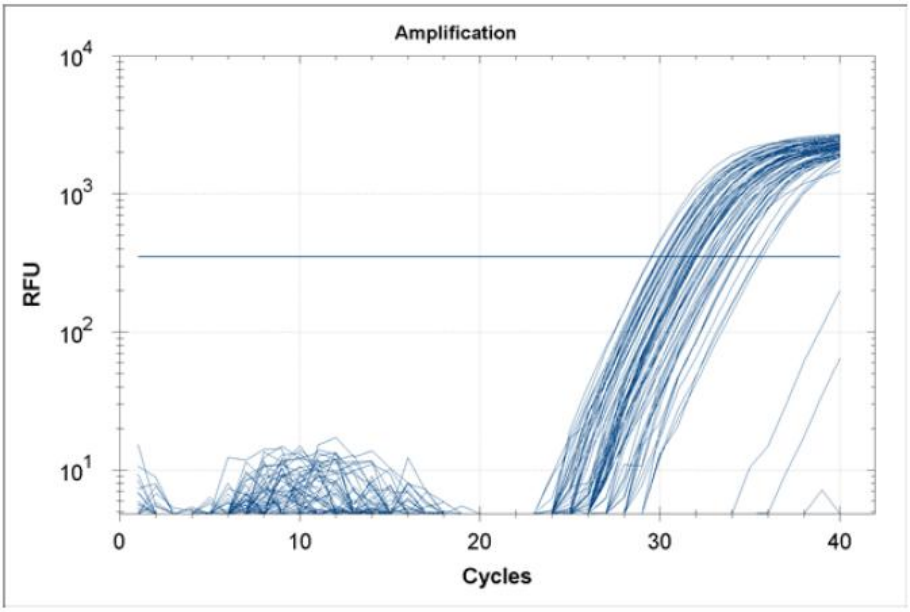
2013/08/21 12:51 PM

Run Setup

Plate Display

	1	2	3	4	5	6	7	8	9	10	11	12
A	Unk-1 SDHA 001 S15	Unk-1 SDHA 001 S15	Unk-7 SDHA 002 S15	Unk-7 SDHA 002 S15	Unk-13 SDHA 799 S15	Unk-13 SDHA 799 S15	Unk-18 SDHA 811 S15	Unk-18 SDHA 811 S15	Unk-24 SDHA 805 S15	Unk-24 SDHA 805 S15	Unk-30 SDHA 816 S15	Unk-30 SDHA 816 S15
B	Unk-2 SDHA 001 N15	Unk-2 SDHA 001 N15	Unk-8 SDHA 002 N15	Unk-8 SDHA 002 N15	Unk-14 SDHA 799 N15	Unk-14 SDHA 799 N15	Unk-19 SDHA 811 N15	Unk-19 SDHA 811 N15	Unk-25 SDHA 805 N15	Unk-25 SDHA 805 N15	Unk-31 SDHA 816 N15	Unk-31 SDHA 816 N15
C	Unk-3 SDHA 001 T15	Unk-3 SDHA 001 T15	Unk-9 SDHA 002 T15	Unk-9 SDHA 002 T15	Unk-15 SDHA 799 T15	Unk-15 SDHA 799 T15	Unk-20 SDHA 811 T15	Unk-20 SDHA 811 T15	Unk-26 SDHA 805 T15	Unk-26 SDHA 805 T15	Unk-32 SDHA 816 T15	Unk-32 SDHA 816 T15
D	Unk-4 SDHA 001 T+N15	Unk-4 SDHA 001 T+N15	Unk-10 SDHA 002 T+N15	Unk-10 SDHA 002 T+N15	Unk-16 SDHA 799 T+N15	Unk-16 SDHA 799 T+N15	Unk-21 SDHA 811 T+N15	Unk-21 SDHA 811 T+N15	Unk-27 SDHA 805 T+N15	Unk-27 SDHA 805 T+N15	Unk-33 SDHA 816 T+N15	Unk-33 SDHA 816 T+N15
E	Unk-5 SDHA 001 V15	Unk-5 SDHA 001 V15	Unk-11 SDHA 002 V15	Unk-11 SDHA 002 V15	Unk-17 SDHA 799 Z15	Unk-17 SDHA 799 Z15	Unk-22 SDHA 811 V15	Unk-22 SDHA 811 V15	Unk-28 SDHA 805 V15	Unk-28 SDHA 805 V15	Unk-34 SDHA 816 V15	Unk-34 SDHA 816 V15
F	Unk-6 SDHA 001 Z15	Unk-6 SDHA 001 Z15	Unk-12 SDHA 002 Z15	Unk-12 SDHA 002 Z15			Unk-23 SDHA 811 Z15	Unk-23 SDHA 811 Z15	Unk-29 SDHA 805 Z15	Unk-29 SDHA 805 Z15	Unk-35 SDHA 816 Z15	Unk-35 SDHA 816 Z15
G	Pos-36 SDHA 804 PC	Pos-36 SDHA 804 PC	NTC-37 SDHA H2O	NTC-37 SDHA H2O	NTC-38 SDHA H2O	NTC-38 SDHA H2O	Unk-39 SDHA Pooled MC 10ng	Unk-39 SDHA Pooled MC 10ng	Unk-40 SDHA Pooled MC 15ng	Unk-40 SDHA Pooled MC 15ng	Unk-41 SDHA Pooled MC 5ng	Unk-41 SDHA Pooled MC 5ng
H												

Quantification



Quantification Data

Well	Fluor	Target	Content	Sample	Cq	Cq Mean	Cq Std. Dev
A01	FAM	SDHA	Unkn-01	001 S15	30.33	30.47	0.197
A02	FAM	SDHA	Unkn-01	001 S15	30.61	30.47	0.197
A03	FAM	SDHA	Unkn-07	002 S15	33.64	32.84	1.140
A04	FAM	SDHA	Unkn-07	002 S15	32.03	32.84	1.140
A05	FAM	SDHA	Unkn-13	799 S15	32.58	32.29	0.404
A06	FAM	SDHA	Unkn-13	799 S15	32.01	32.29	0.404
A07	FAM	SDHA	Unkn-18	811 S15	32.80	32.57	0.320
A08	FAM	SDHA	Unkn-18	811 S15	32.34	32.57	0.320
A09	FAM	SDHA	Unkn-24	805 S15	N/A	0.00	0.000
A10	FAM	SDHA	Unkn-24	805 S15	N/A	0.00	0.000
A11	FAM	SDHA	Unkn-30	816 S15	32.73	32.84	0.157
A12	FAM	SDHA	Unkn-30	816 S15	32.95	32.84	0.157
B01	FAM	SDHA	Unkn-02	001 N15	29.51	29.75	0.351
B02	FAM	SDHA	Unkn-02	001 N15	30.00	29.75	0.351
B03	FAM	SDHA	Unkn-08	002 N15	31.56	31.72	0.226
B04	FAM	SDHA	Unkn-08	002 N15	31.88	31.72	0.226
B05	FAM	SDHA	Unkn-14	799 N15	31.29	31.24	0.062
B06	FAM	SDHA	Unkn-14	799 N15	31.20	31.24	0.062
B07	FAM	SDHA	Unkn-19	811 N15	32.58	32.79	0.288
B08	FAM	SDHA	Unkn-19	811 N15	32.99	32.79	0.288
B09	FAM	SDHA	Unkn-25	805 N15	35.41	35.17	0.335
B10	FAM	SDHA	Unkn-25	805 N15	34.94	35.17	0.335
B11	FAM	SDHA	Unkn-31	816 N15	33.53	33.54	0.014
B12	FAM	SDHA	Unkn-31	816 N15	33.55	33.54	0.014
C01	FAM	SDHA	Unkn-03	001 T15	30.62	30.51	0.148
C02	FAM	SDHA	Unkn-03	001 T15	30.41	30.51	0.148
C03	FAM	SDHA	Unkn-09	002 T15	30.54	30.58	0.053
C04	FAM	SDHA	Unkn-09	002 T15	30.62	30.58	0.053
C05	FAM	SDHA	Unkn-15	799 T15	31.83	31.33	0.699
C06	FAM	SDHA	Unkn-15	799 T15	30.84	31.33	0.699
C07	FAM	SDHA	Unkn-20	811 T15	32.05	31.74	0.436
C08	FAM	SDHA	Unkn-20	811 T15	31.43	31.74	0.436
C09	FAM	SDHA	Unkn-26	805 T15	33.84	33.84	0.001
C10	FAM	SDHA	Unkn-26	805 T15	33.84	33.84	0.001
C11	FAM	SDHA	Unkn-32	816 T15	33.82	33.87	0.083
C12	FAM	SDHA	Unkn-32	816 T15	33.93	33.87	0.083
D01	FAM	SDHA	Unkn-04	001 T+N15	32.05	31.71	0.482
D02	FAM	SDHA	Unkn-04	001 T+N15	31.37	31.71	0.482
D03	FAM	SDHA	Unkn-10	002 T+N15	31.05	30.56	0.687
D04	FAM	SDHA	Unkn-10	002 T+N15	30.08	30.56	0.687
D05	FAM	SDHA	Unkn-16	799 T+N15	34.35	34.33	0.019
D06	FAM	SDHA	Unkn-16	799 T+N15	34.32	34.33	0.019
D07	FAM	SDHA	Unkn-21	811 T+N15	35.63	35.53	0.142
D08	FAM	SDHA	Unkn-21	811 T+N15	35.43	35.53	0.142
D09	FAM	SDHA	Unkn-27	805 T+N15	33.37	33.49	0.172
D10	FAM	SDHA	Unkn-27	805 T+N15	33.61	33.49	0.172
D11	FAM	SDHA	Unkn-33	816 T+N15	31.71	31.69	0.022

Well	Fluor	Target	Content	Sample	Cq	Cq Mean	Cq Std. Dev
D12	FAM	SDHA	Unkn-33	816 T+N15	31.68	31.69	0.022
E01	FAM	SDHA	Unkn-05	001 V15	31.16	31.36	0.289
E02	FAM	SDHA	Unkn-05	001 V15	31.57	31.36	0.289
E03	FAM	SDHA	Unkn-11	002 V15	30.02	30.11	0.128
E04	FAM	SDHA	Unkn-11	002 V15	30.20	30.11	0.128
E05	FAM	SDHA	Unkn-17	799 Z15	31.95	31.43	0.733
E06	FAM	SDHA	Unkn-17	799 Z15	30.91	31.43	0.733
E07	FAM	SDHA	Unkn-22	811 V15	32.35	32.39	0.068
E08	FAM	SDHA	Unkn-22	811 V15	32.44	32.39	0.068
E09	FAM	SDHA	Unkn-28	805 V15	34.26	33.96	0.422
E10	FAM	SDHA	Unkn-28	805 V15	33.66	33.96	0.422
E11	FAM	SDHA	Unkn-34	816 V15	31.89	31.97	0.103
E12	FAM	SDHA	Unkn-34	816 V15	32.04	31.97	0.103
F01	FAM	SDHA	Unkn-06	001 Z15	29.44	29.86	0.605
F02	FAM	SDHA	Unkn-06	001 Z15	30.29	29.86	0.605
F03	FAM	SDHA	Unkn-12	002 Z15	30.30	30.50	0.273
F04	FAM	SDHA	Unkn-12	002 Z15	30.69	30.50	0.273
F07	FAM	SDHA	Unkn-23	811 Z15	30.29	30.32	0.048
F08	FAM	SDHA	Unkn-23	811 Z15	30.35	30.32	0.048
F09	FAM	SDHA	Unkn-29	805 Z15	32.06	31.84	0.306
F10	FAM	SDHA	Unkn-29	805 Z15	31.63	31.84	0.306
F11	FAM	SDHA	Unkn-35	816 Z15	31.30	31.33	0.045
F12	FAM	SDHA	Unkn-35	816 Z15	31.36	31.33	0.045
G01	FAM	SDHA	Pos Ctrl-36	804 PC	29.94	29.98	0.057
G02	FAM	SDHA	Pos Ctrl-36	804 PC	30.02	29.98	0.057
G03	FAM	SDHA	NTC-37	H2O	N/A	0.00	0.000
G04	FAM	SDHA	NTC-37	H2O	N/A	0.00	0.000
G05	FAM	SDHA	NTC-38	H2O	N/A	0.00	0.000
G06	FAM	SDHA	NTC-38	H2O	N/A	0.00	0.000
G07	FAM	SDHA	Unkn-39	Pooled MC 10ng	31.95	31.60	0.486
G08	FAM	SDHA	Unkn-39	Pooled MC 10ng	31.26	31.60	0.486
G09	FAM	SDHA	Unkn-40	Pooled MC 15ng	32.05	32.34	0.412
G10	FAM	SDHA	Unkn-40	Pooled MC 15ng	32.64	32.34	0.412
G11	FAM	SDHA	Unkn-41	Pooled MC 5ng	33.01	33.14	0.183
G12	FAM	SDHA	Unkn-41	Pooled MC 5ng	33.27	33.14	0.183

Gene Expression

Target Names

Name	Full Name	Reference	Auto Efficiency	Efficiency
SDHA	SDHA	False	Yes	100.0%

SDHA 60d.pcrd

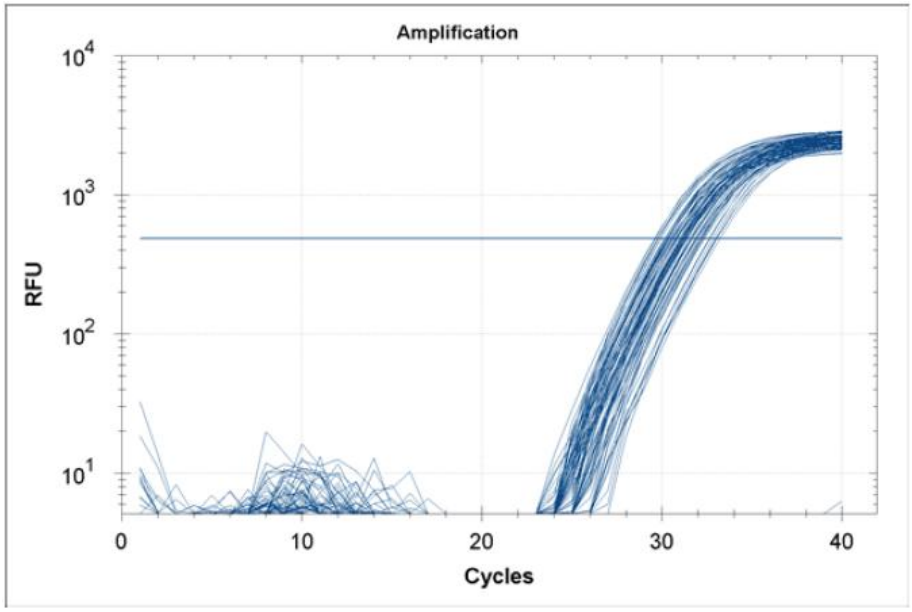
2013/08/21 12:52 PM

Run Setup

Plate Display

	1	2	3	4	5	6	7	8	9	10	11	12
A	Unk-1 SDHA 001 S60	Unk-1 SDHA 001 S60	Unk-7 SDHA 002 S60	Unk-7 SDHA 002 S60	Unk-13 SDHA 799 S60	Unk-13 SDHA 799 S60	Unk-18 SDHA 811 S60	Unk-18 SDHA 811 S60	Unk-24 SDHA 805 S60	Unk-24 SDHA 805 S60	Unk-30 SDHA 816 S60	Unk-30 SDHA 816 S60
B	Unk-2 SDHA 001 N60	Unk-2 SDHA 001 N60	Unk-8 SDHA 002 N60	Unk-8 SDHA 002 N60	Unk-14 SDHA 799 N60	Unk-14 SDHA 799 N60	Unk-19 SDHA 811 N60	Unk-19 SDHA 811 N60	Unk-25 SDHA 805 N60	Unk-25 SDHA 805 N60	Unk-31 SDHA 816 N60	Unk-31 SDHA 816 N60
C	Unk-3 SDHA 001 T60	Unk-3 SDHA 001 T60	Unk-9 SDHA 002 T60	Unk-9 SDHA 002 T60	Unk-15 SDHA 799 T60	Unk-15 SDHA 799 T60	Unk-20 SDHA 811 T60	Unk-20 SDHA 811 T60	Unk-26 SDHA 805 T60	Unk-26 SDHA 805 T60	Unk-32 SDHA 816 T60	Unk-32 SDHA 816 T60
D	Unk-4 SDHA 001 T+N60	Unk-4 SDHA 001 T+N60	Unk-10 SDHA 002 T+N60	Unk-10 SDHA 002 T+N60	Unk-16 SDHA 799 T+N60	Unk-16 SDHA 799 T+N60	Unk-21 SDHA 811 T+N60	Unk-21 SDHA 811 T+N60	Unk-27 SDHA 805 T+N60	Unk-27 SDHA 805 T+N60	Unk-33 SDHA 816 T+N60	Unk-33 SDHA 816 T+N60
E	Unk-5 SDHA 001 V60	Unk-5 SDHA 001 V60	Unk-11 SDHA 002 V60	Unk-11 SDHA 002 V60	Unk-17 SDHA 799 Z60	Unk-17 SDHA 799 Z60	Unk-22 SDHA 811 V60	Unk-22 SDHA 811 V60	Unk-28 SDHA 805 V60	Unk-28 SDHA 805 V60	Unk-34 SDHA 816 V60	Unk-34 SDHA 816 V60
F	Unk-6 SDHA 001 Z60	Unk-6 SDHA 001 Z60	Unk-12 SDHA 002 Z60	Unk-12 SDHA 002 Z60			Unk-23 SDHA 811 Z60	Unk-23 SDHA 811 Z60	Unk-29 SDHA 805 Z60	Unk-29 SDHA 805 Z60	Unk-35 SDHA 816 Z60	Unk-35 SDHA 816 Z60
G	Pos-36 SDHA 804 PC	Pos-36 SDHA 804 PC	NTC-37 SDHA H2O	NTC-37 SDHA H2O	NTC-38 SDHA H2O	NTC-38 SDHA H2O	Unk-39 SDHA Pooled MC 10ng	Unk-39 SDHA Pooled MC 10ng	Unk-40 SDHA Pooled MC 15ng	Unk-40 SDHA Pooled MC 15ng	Unk-41 SDHA Pooled MC 5ng	Unk-41 SDHA Pooled MC 5ng
H												

Quantification



Quantification Data

Well	Fluor	Target	Content	Sample	Cq	Cq Mean	Cq Std. Dev
A01	FAM	SDHA	Unkn-01	001 S60	31.11	30.96	0.218
A02	FAM	SDHA	Unkn-01	001 S60	30.80	30.96	0.218
A03	FAM	SDHA	Unkn-07	002 S60	30.43	30.44	0.020
A04	FAM	SDHA	Unkn-07	002 S60	30.46	30.44	0.020
A05	FAM	SDHA	Unkn-13	799 S60	31.27	31.31	0.059
A06	FAM	SDHA	Unkn-13	799 S60	31.35	31.31	0.059
A07	FAM	SDHA	Unkn-18	811 S60	31.17	31.20	0.051
A08	FAM	SDHA	Unkn-18	811 S60	31.24	31.20	0.051
A09	FAM	SDHA	Unkn-24	805 S60	30.57	30.66	0.123
A10	FAM	SDHA	Unkn-24	805 S60	30.75	30.66	0.123
A11	FAM	SDHA	Unkn-30	816 S60	31.93	31.90	0.044
A12	FAM	SDHA	Unkn-30	816 S60	31.87	31.90	0.044
B01	FAM	SDHA	Unkn-02	001 N60	30.61	30.93	0.449
B02	FAM	SDHA	Unkn-02	001 N60	31.25	30.93	0.449
B03	FAM	SDHA	Unkn-08	002 N60	31.87	31.99	0.175
B04	FAM	SDHA	Unkn-08	002 N60	32.12	31.99	0.175
B05	FAM	SDHA	Unkn-14	799 N60	30.78	30.97	0.269
B06	FAM	SDHA	Unkn-14	799 N60	31.16	30.97	0.269
B07	FAM	SDHA	Unkn-19	811 N60	30.95	31.03	0.106
B08	FAM	SDHA	Unkn-19	811 N60	31.10	31.03	0.106
B09	FAM	SDHA	Unkn-25	805 N60	30.32	30.31	0.004
B10	FAM	SDHA	Unkn-25	805 N60	30.31	30.31	0.004
B11	FAM	SDHA	Unkn-31	816 N60	31.11	31.12	0.014
B12	FAM	SDHA	Unkn-31	816 N60	31.13	31.12	0.014
C01	FAM	SDHA	Unkn-03	001 T60	30.62	30.57	0.076
C02	FAM	SDHA	Unkn-03	001 T60	30.51	30.57	0.076
C03	FAM	SDHA	Unkn-09	002 T60	30.29	30.40	0.155
C04	FAM	SDHA	Unkn-09	002 T60	30.51	30.40	0.155
C05	FAM	SDHA	Unkn-15	799 T60	31.25	31.72	0.653
C06	FAM	SDHA	Unkn-15	799 T60	32.18	31.72	0.653
C07	FAM	SDHA	Unkn-20	811 T60	32.09	32.21	0.164
C08	FAM	SDHA	Unkn-20	811 T60	32.32	32.21	0.164
C09	FAM	SDHA	Unkn-26	805 T60	33.03	33.03	0.012
C10	FAM	SDHA	Unkn-26	805 T60	33.04	33.03	0.012
C11	FAM	SDHA	Unkn-32	816 T60	31.19	31.52	0.468
C12	FAM	SDHA	Unkn-32	816 T60	31.86	31.52	0.468
D01	FAM	SDHA	Unkn-04	001 T+N60	30.13	30.18	0.070
D02	FAM	SDHA	Unkn-04	001 T+N60	30.23	30.18	0.070
D03	FAM	SDHA	Unkn-10	002 T+N60	30.12	30.16	0.052
D04	FAM	SDHA	Unkn-10	002 T+N60	30.19	30.16	0.052
D05	FAM	SDHA	Unkn-16	799 T+N60	31.60	31.60	0.000
D06	FAM	SDHA	Unkn-16	799 T+N60	31.60	31.60	0.000
D07	FAM	SDHA	Unkn-21	811 T+N60	31.99	31.82	0.247
D08	FAM	SDHA	Unkn-21	811 T+N60	31.64	31.82	0.247
D09	FAM	SDHA	Unkn-27	805 T+N60	32.25	32.17	0.121
D10	FAM	SDHA	Unkn-27	805 T+N60	32.08	32.17	0.121
D11	FAM	SDHA	Unkn-33	816 T+N60	31.25	31.27	0.030

Well	Fluor	Target	Content	Sample	Cq	Cq Mean	Cq Std. Dev
D12	FAM	SDHA	Unkn-33	816 T+N60	31.29	31.27	0.030
E01	FAM	SDHA	Unkn-05	001 V60	30.20	29.98	0.306
E02	FAM	SDHA	Unkn-05	001 V60	29.76	29.98	0.306
E03	FAM	SDHA	Unkn-11	002 V60	29.70	29.81	0.146
E04	FAM	SDHA	Unkn-11	002 V60	29.91	29.81	0.146
E05	FAM	SDHA	Unkn-17	799 Z60	31.38	31.49	0.158
E06	FAM	SDHA	Unkn-17	799 Z60	31.60	31.49	0.158
E07	FAM	SDHA	Unkn-22	811 V60	31.06	31.06	0.001
E08	FAM	SDHA	Unkn-22	811 V60	31.06	31.06	0.001
E09	FAM	SDHA	Unkn-28	805 V60	29.58	29.74	0.224
E10	FAM	SDHA	Unkn-28	805 V60	29.90	29.74	0.224
E11	FAM	SDHA	Unkn-34	816 V60	30.72	30.51	0.297
E12	FAM	SDHA	Unkn-34	816 V60	30.30	30.51	0.297
F01	FAM	SDHA	Unkn-06	001 Z60	29.76	29.65	0.154
F02	FAM	SDHA	Unkn-06	001 Z60	29.55	29.65	0.154
F03	FAM	SDHA	Unkn-12	002 Z60	30.82	30.58	0.344
F04	FAM	SDHA	Unkn-12	002 Z60	30.34	30.58	0.344
F07	FAM	SDHA	Unkn-23	811 Z60	31.79	31.44	0.494
F08	FAM	SDHA	Unkn-23	811 Z60	31.09	31.44	0.494
F09	FAM	SDHA	Unkn-29	805 Z60	32.79	32.68	0.153
F10	FAM	SDHA	Unkn-29	805 Z60	32.57	32.68	0.153
F11	FAM	SDHA	Unkn-35	816 Z60	31.59	31.44	0.218
F12	FAM	SDHA	Unkn-35	816 Z60	31.29	31.44	0.218
G01	FAM	SDHA	Pos Ctrl-36	804 PC	31.01	31.01	0.003
G02	FAM	SDHA	Pos Ctrl-36	804 PC	31.01	31.01	0.003
G03	FAM	SDHA	NTC-37	H2O	N/A	0.00	0.000
G04	FAM	SDHA	NTC-37	H2O	N/A	0.00	0.000
G05	FAM	SDHA	NTC-38	H2O	N/A	0.00	0.000
G06	FAM	SDHA	NTC-38	H2O	N/A	0.00	0.000
G07	FAM	SDHA	Unkn-39	Pooled MC 10ng	31.52	31.51	0.015
G08	FAM	SDHA	Unkn-39	Pooled MC 10ng	31.50	31.51	0.015
G09	FAM	SDHA	Unkn-40	Pooled MC 15ng	32.62	32.41	0.292
G10	FAM	SDHA	Unkn-40	Pooled MC 15ng	32.20	32.41	0.292
G11	FAM	SDHA	Unkn-41	Pooled MC 5ng	32.96	33.07	0.160
G12	FAM	SDHA	Unkn-41	Pooled MC 5ng	33.19	33.07	0.160

Gene Expression

Target Names

Name	Full Name	Reference	Auto Efficiency	Efficiency
SDHA	SDHA	False	Yes	100.0%

SDHA 90d.pcrd

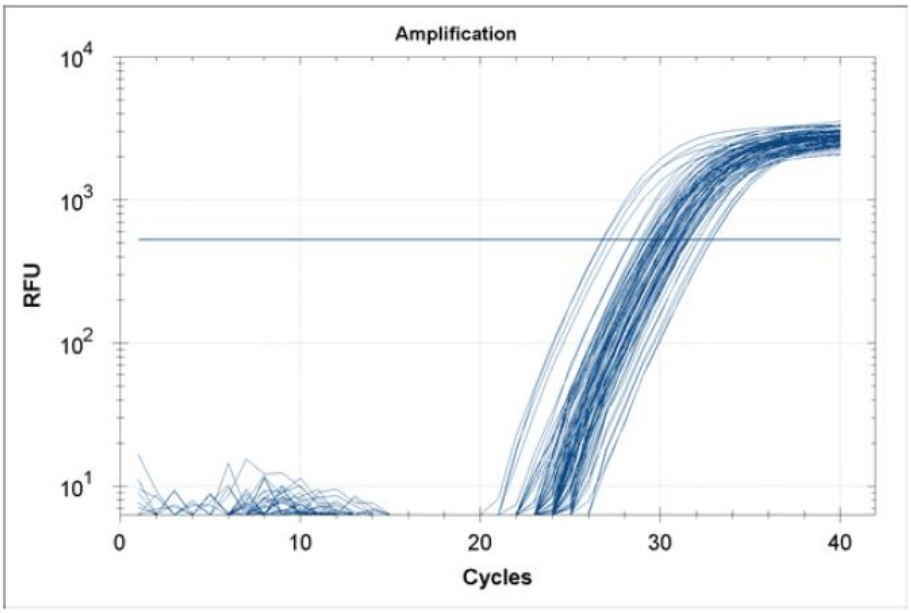
2013/08/21 12:52 PM

Run Setup

Plate Display

	1	2	3	4	5	6	7	8	9	10	11	12
A	Unk-1 SDHA 001 S90	Unk-1 SDHA 001 S90	Unk-8 SDHA 002 S90	Unk-8 SDHA 002 S90	Unk-15 SDHA 799 S90	Unk-15 SDHA 799 S90	Unk-21 SDHA 811 S90	Unk-21 SDHA 811 S90	Unk-28 SDHA 805 S90	Unk-28 SDHA 805 S90	Unk-35 SDHA 816 S90	Unk-35 SDHA 816 S90
B	Unk-2 SDHA 001 N90	Unk-2 SDHA 001 N90	Unk-9 SDHA 002 N90	Unk-9 SDHA 002 N90	Unk-16 SDHA 799 N90	Unk-16 SDHA 799 N90	Unk-22 SDHA 811 N90	Unk-22 SDHA 811 N90	Unk-29 SDHA 805 N90	Unk-29 SDHA 805 N90	Unk-36 SDHA 816 N90	Unk-36 SDHA 816 N90
C	Unk-3 SDHA 001 T90	Unk-3 SDHA 001 T90	Unk-10 SDHA 002 T90	Unk-10 SDHA 002 T90	Unk-17 SDHA 799 T90	Unk-17 SDHA 799 T90	Unk-23 SDHA 811 T90	Unk-23 SDHA 811 T90	Unk-30 SDHA 805 T90	Unk-30 SDHA 805 T90	Unk-37 SDHA 816 T90	Unk-37 SDHA 816 T90
D	Unk-4 SDHA 001 T+N90	Unk-4 SDHA 001 T+N90	Unk-11 SDHA 002 T+N90	Unk-11 SDHA 002 T+N90	Unk-18 SDHA 799 T+N90	Unk-18 SDHA 799 T+N90	Unk-24 SDHA 811 T+N90	Unk-24 SDHA 811 T+N90	Unk-31 SDHA 805 T+N90	Unk-31 SDHA 805 T+N90	Unk-38 SDHA 816 T+N90	Unk-38 SDHA 816 T+N90
E	Unk-5 SDHA 001 V90	Unk-5 SDHA 001 V90	Unk-12 SDHA 002 V90	Unk-12 SDHA 002 V90	Unk-19 SDHA 799 Z90	Unk-19 SDHA 799 Z90	Unk-25 SDHA 811 V90	Unk-25 SDHA 811 V90	Unk-32 SDHA 805 V90	Unk-32 SDHA 805 V90	Unk-39 SDHA 816 V90	Unk-39 SDHA 816 V90
F	Unk-6 SDHA 001 Z90	Unk-6 SDHA 001 Z90	Unk-13 SDHA 002 Z90	Unk-13 SDHA 002 Z90			Unk-26 SDHA 811 Z90	Unk-26 SDHA 811 Z90	Unk-33 SDHA 805 Z90	Unk-33 SDHA 805 Z90	Unk-40 SDHA 816 Z90	Unk-40 SDHA 816 Z90
G	Unk-7 SDHA 001 MC	Unk-7 SDHA 001 MC	Unk-14 SDHA 002 MC	Unk-14 SDHA 002 MC	Unk-20 SDHA 799 MC	Unk-20 SDHA 799 MC	Unk-27 SDHA 811 MC	Unk-27 SDHA 811 MC	Unk-34 SDHA 805 MC	Unk-34 SDHA 805 MC	Unk-41 SDHA 816 MC	Unk-41 SDHA 816 MC
H	Pos-42 SDHA 804 PC	Pos-42 SDHA 804 PC	NTC-43 SDHA H2O	NTC-43 SDHA H2O	NTC-44 SDHA H2O	NTC-44 SDHA H2O	Unk-45 SDHA Pooled MC 15ng	Unk-45 SDHA Pooled MC 15ng	Unk-46 SDHA Pooled MC 10ng	Unk-46 SDHA Pooled MC 10ng	Unk-47 SDHA Pooled MC 5ng	Unk-47 SDHA Pooled MC 5ng

Quantification



Quantification Data

Well	Fluor	Target	Content	Sample	Cq	Cq Mean	Cq Std. Dev
A01	FAM	SDHA	Unkn-01	001 S90	31.42	31.24	0.252
A02	FAM	SDHA	Unkn-01	001 S90	31.06	31.24	0.252
A03	FAM	SDHA	Unkn-08	002 S90	30.37	30.27	0.139
A04	FAM	SDHA	Unkn-08	002 S90	30.17	30.27	0.139
A05	FAM	SDHA	Unkn-15	799 S90	29.22	29.39	0.232
A06	FAM	SDHA	Unkn-15	799 S90	29.55	29.39	0.232
A07	FAM	SDHA	Unkn-21	811 S90	29.72	29.61	0.151
A08	FAM	SDHA	Unkn-21	811 S90	29.50	29.61	0.151
A09	FAM	SDHA	Unkn-28	805 S90	31.42	31.29	0.182
A10	FAM	SDHA	Unkn-28	805 S90	31.16	31.29	0.182
A11	FAM	SDHA	Unkn-35	816 S90	31.04	31.16	0.169
A12	FAM	SDHA	Unkn-35	816 S90	31.28	31.16	0.169
B01	FAM	SDHA	Unkn-02	001 N90	30.54	30.42	0.166
B02	FAM	SDHA	Unkn-02	001 N90	30.30	30.42	0.166
B03	FAM	SDHA	Unkn-09	002 N90	29.21	29.40	0.260
B04	FAM	SDHA	Unkn-09	002 N90	29.58	29.40	0.260
B05	FAM	SDHA	Unkn-16	799 N90	30.98	31.05	0.094
B06	FAM	SDHA	Unkn-16	799 N90	31.12	31.05	0.094
B07	FAM	SDHA	Unkn-22	811 N90	31.04	31.28	0.345
B08	FAM	SDHA	Unkn-22	811 N90	31.53	31.28	0.345
B09	FAM	SDHA	Unkn-29	805 N90	29.81	29.90	0.129
B10	FAM	SDHA	Unkn-29	805 N90	30.00	29.90	0.129
B11	FAM	SDHA	Unkn-36	816 N90	30.65	30.31	0.475
B12	FAM	SDHA	Unkn-36	816 N90	29.97	30.31	0.475
C01	FAM	SDHA	Unkn-03	001 T90	30.75	30.82	0.097
C02	FAM	SDHA	Unkn-03	001 T90	30.89	30.82	0.097
C03	FAM	SDHA	Unkn-10	002 T90	30.30	30.44	0.201
C04	FAM	SDHA	Unkn-10	002 T90	30.58	30.44	0.201
C05	FAM	SDHA	Unkn-17	799 T90	30.59	30.80	0.301
C06	FAM	SDHA	Unkn-17	799 T90	31.01	30.80	0.301
C07	FAM	SDHA	Unkn-23	811 T90	29.83	30.11	0.397
C08	FAM	SDHA	Unkn-23	811 T90	30.39	30.11	0.397
C09	FAM	SDHA	Unkn-30	805 T90	31.46	31.50	0.047
C10	FAM	SDHA	Unkn-30	805 T90	31.53	31.50	0.047
C11	FAM	SDHA	Unkn-37	816 T90	31.07	31.25	0.265
C12	FAM	SDHA	Unkn-37	816 T90	31.44	31.25	0.265
D01	FAM	SDHA	Unkn-04	001 T+N90	29.83	30.17	0.485
D02	FAM	SDHA	Unkn-04	001 T+N90	30.51	30.17	0.485
D03	FAM	SDHA	Unkn-11	002 T+N90	29.30	29.23	0.100
D04	FAM	SDHA	Unkn-11	002 T+N90	29.16	29.23	0.100
D05	FAM	SDHA	Unkn-18	799 T+N90	29.90	30.01	0.154
D06	FAM	SDHA	Unkn-18	799 T+N90	30.12	30.01	0.154
D07	FAM	SDHA	Unkn-24	811 T+N90	30.00	29.89	0.145
D08	FAM	SDHA	Unkn-24	811 T+N90	29.79	29.89	0.145
D09	FAM	SDHA	Unkn-31	805 T+N90	31.04	31.18	0.207
D10	FAM	SDHA	Unkn-31	805 T+N90	31.33	31.18	0.207
D11	FAM	SDHA	Unkn-38	816 T+N90	32.11	32.11	0.006

Well	Fluor	Target	Content	Sample	Cq	Cq Mean	Cq Std. Dev
D12	FAM	SDHA	Unkn-38	816 T+N90	32.11	32.11	0.006
E01	FAM	SDHA	Unkn-05	001 V90	29.75	29.69	0.088
E02	FAM	SDHA	Unkn-05	001 V90	29.63	29.69	0.088
E03	FAM	SDHA	Unkn-12	002 V90	30.49	30.53	0.059
E04	FAM	SDHA	Unkn-12	002 V90	30.58	30.53	0.059
E05	FAM	SDHA	Unkn-19	799 Z90	30.44	30.47	0.040
E06	FAM	SDHA	Unkn-19	799 Z90	30.50	30.47	0.040
E07	FAM	SDHA	Unkn-25	811 V90	31.07	30.89	0.259
E08	FAM	SDHA	Unkn-25	811 V90	30.70	30.89	0.259
E09	FAM	SDHA	Unkn-32	805 V90	30.09	29.87	0.319
E10	FAM	SDHA	Unkn-32	805 V90	29.64	29.87	0.319
E11	FAM	SDHA	Unkn-39	816 V90	30.30	30.32	0.017
E12	FAM	SDHA	Unkn-39	816 V90	30.33	30.32	0.017
F01	FAM	SDHA	Unkn-06	001 Z90	29.88	29.72	0.230
F02	FAM	SDHA	Unkn-06	001 Z90	29.56	29.72	0.230
F03	FAM	SDHA	Unkn-13	002 Z90	29.70	29.57	0.177
F04	FAM	SDHA	Unkn-13	002 Z90	29.45	29.57	0.177
F07	FAM	SDHA	Unkn-26	811 Z90	30.80	30.61	0.262
F08	FAM	SDHA	Unkn-26	811 Z90	30.43	30.61	0.262
F09	FAM	SDHA	Unkn-33	805 Z90	30.05	30.03	0.021
F10	FAM	SDHA	Unkn-33	805 Z90	30.02	30.03	0.021
F11	FAM	SDHA	Unkn-40	816 Z90	31.14	30.79	0.499
F12	FAM	SDHA	Unkn-40	816 Z90	30.43	30.79	0.499
G01	FAM	SDHA	Unkn-07	001 MC	27.48	27.31	0.244
G02	FAM	SDHA	Unkn-07	001 MC	27.13	27.31	0.244
G03	FAM	SDHA	Unkn-14	002 MC	26.72	26.75	0.044
G04	FAM	SDHA	Unkn-14	002 MC	26.78	26.75	0.044
G05	FAM	SDHA	Unkn-20	799 MC	28.98	29.10	0.169
G06	FAM	SDHA	Unkn-20	799 MC	29.22	29.10	0.169
G07	FAM	SDHA	Unkn-27	811 MC	28.85	28.95	0.141
G08	FAM	SDHA	Unkn-27	811 MC	29.05	28.95	0.141
G09	FAM	SDHA	Unkn-34	805 MC	29.18	29.30	0.172
G10	FAM	SDHA	Unkn-34	805 MC	29.43	29.30	0.172
G11	FAM	SDHA	Unkn-41	816 MC	28.34	28.37	0.046
G12	FAM	SDHA	Unkn-41	816 MC	28.40	28.37	0.046
H01	FAM	SDHA	Pos Ctrl-42	804 PC	31.18	31.37	0.273
H02	FAM	SDHA	Pos Ctrl-42	804 PC	31.57	31.37	0.273
H03	FAM	SDHA	NTC-43	H2O	N/A	0.00	0.000
H04	FAM	SDHA	NTC-43	H2O	N/A	0.00	0.000
H05	FAM	SDHA	NTC-44	H2O	N/A	0.00	0.000
H06	FAM	SDHA	NTC-44	H2O	N/A	0.00	0.000
H07	FAM	SDHA	Unkn-45	Pooled MC 15ng	31.87	31.41	0.655
H08	FAM	SDHA	Unkn-45	Pooled MC 15ng	30.94	31.41	0.655
H09	FAM	SDHA	Unkn-46	Pooled MC 10ng	32.82	32.83	0.013
H10	FAM	SDHA	Unkn-46	Pooled MC 10ng	32.84	32.83	0.013
H11	FAM	SDHA	Unkn-47	Pooled MC 5ng	32.62	32.56	0.086
H12	FAM	SDHA	Unkn-47	Pooled MC 5ng	32.50	32.56	0.086

Gene Expression

Target Names

Name	Full Name	Reference	Auto Efficiency	Efficiency
SDHA	SDHA	False	Yes	100.0%

BMP2 15d.pcrd

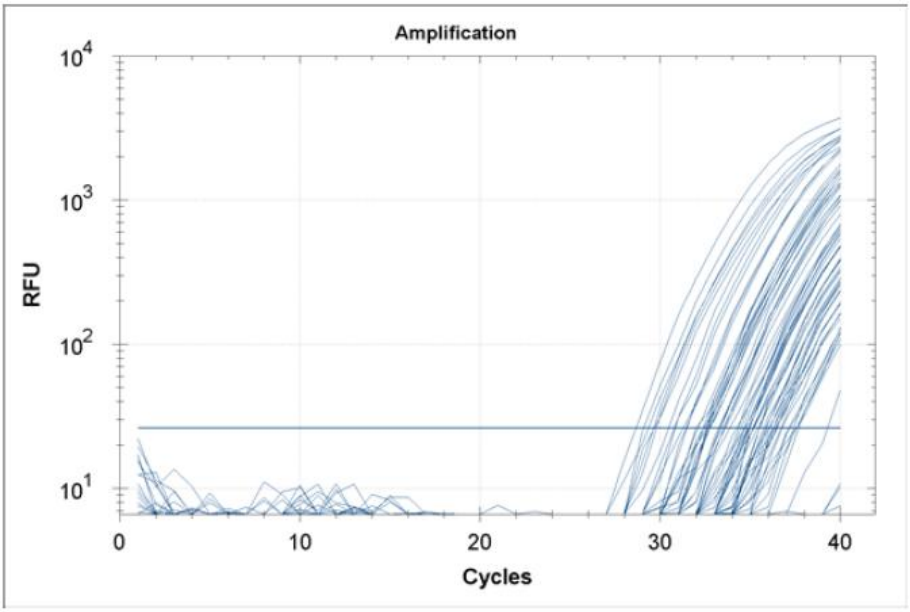
2013/08/21 12:58 PM

Run Setup

Plate Display

	1	2	3	4	5	6	7	8	9	10	11	12
A	Unk-1 BMP2 001 S15	Unk-1 BMP2 001 S15	Unk-7 BMP2 002 S15	Unk-7 BMP2 002 S15	Unk-13 BMP2 799 S15	Unk-13 BMP2 799 S15	Unk-18 BMP2 811 S15	Unk-18 BMP2 811 S15	Unk-24 BMP2 805 S15	Unk-24 BMP2 805 S15	Unk-30 BMP2 816 S15	Unk-30 BMP2 816 S15
B	Unk-2 BMP2 001 N15	Unk-2 BMP2 001 N15	Unk-8 BMP2 002 N15	Unk-8 BMP2 002 N15	Unk-14 BMP2 799 N15	Unk-14 BMP2 799 N15	Unk-19 BMP2 811 N15	Unk-19 BMP2 811 N15	Unk-25 BMP2 805 N15	Unk-25 BMP2 805 N15	Unk-31 BMP2 816 N15	Unk-31 BMP2 816 N15
C	Unk-3 BMP2 001 T15	Unk-3 BMP2 001 T15	Unk-9 BMP2 002 T15	Unk-9 BMP2 002 T15	Unk-15 BMP2 799 T15	Unk-15 BMP2 799 T15	Unk-20 BMP2 811 T15	Unk-20 BMP2 811 T15	Unk-26 BMP2 805 T15	Unk-26 BMP2 805 T15	Unk-32 BMP2 816 T15	Unk-32 BMP2 816 T15
D	Unk-4 BMP2 001 T+N15	Unk-4 BMP2 001 T+N15	Unk-10 BMP2 002 T+N15	Unk-10 BMP2 002 T+N15	Unk-16 BMP2 799 T+N15	Unk-16 BMP2 799 T+N15	Unk-21 BMP2 811 T+N15	Unk-21 BMP2 811 T+N15	Unk-27 BMP2 805 T+N15	Unk-27 BMP2 805 T+N15	Unk-33 BMP2 816 T+N15	Unk-33 BMP2 816 T+N15
E	Unk-5 BMP2 001 V15	Unk-5 BMP2 001 V15	Unk-11 BMP2 002 V15	Unk-11 BMP2 002 V15	Unk-17 BMP2 799 Z15	Unk-17 BMP2 799 Z15	Unk-22 BMP2 811 V15	Unk-22 BMP2 811 V15	Unk-28 BMP2 805 V15	Unk-28 BMP2 805 V15	Unk-34 BMP2 816 V15	Unk-34 BMP2 816 V15
F	Unk-6 BMP2 001 Z15	Unk-6 BMP2 001 Z15	Unk-12 BMP2 002 Z15	Unk-12 BMP2 002 Z15			Unk-23 BMP2 811 Z15	Unk-23 BMP2 811 Z15	Unk-29 BMP2 805 Z15	Unk-29 BMP2 805 Z15	Unk-35 BMP2 816 Z15	Unk-35 BMP2 816 Z15
G	Pos-36 BMP2 804 PC	Pos-36 BMP2 804 PC	NTC-37 BMP2 H2O	NTC-37 BMP2 H2O	NTC-38 BMP2 H2O	NTC-38 BMP2 H2O	*Unk-39 BMP2 Pooled MC 10ng	*Unk-39 BMP2 Pooled MC 10ng	*Unk-40 BMP2 Pooled MC 15ng	*Unk-40 BMP2 Pooled MC 15ng	*Unk-41 BMP2 Pooled MC 5ng	*Unk-41 BMP2 Pooled MC 5ng
H												

Quantification



Quantification Data

Well	Fluor	Target	Content	Sample	Cq	Cq Mean	Cq Std. Dev
A01	FAM	BMP2	Unkn-01	001 S15	33.40	33.05	0.494
A02	FAM	BMP2	Unkn-01	001 S15	32.70	33.05	0.494
A03	FAM	BMP2	Unkn-07	002 S15	30.37	30.55	0.245
A04	FAM	BMP2	Unkn-07	002 S15	30.72	30.55	0.245
A05	FAM	BMP2	Unkn-13	799 S15	29.06	28.81	0.342
A06	FAM	BMP2	Unkn-13	799 S15	28.57	28.81	0.342
A07	FAM	BMP2	Unkn-18	811 S15	32.44	32.37	0.099
A08	FAM	BMP2	Unkn-18	811 S15	32.30	32.37	0.099
A09	FAM	BMP2	Unkn-24	805 S15	36.31	36.91	0.847
A10	FAM	BMP2	Unkn-24	805 S15	37.50	36.91	0.847
A11	FAM	BMP2	Unkn-30	816 S15	36.03	35.45	0.827
A12	FAM	BMP2	Unkn-30	816 S15	34.86	35.45	0.827
B01	FAM	BMP2	Unkn-02	001 N15	33.27	33.23	0.054
B02	FAM	BMP2	Unkn-02	001 N15	33.19	33.23	0.054
B03	FAM	BMP2	Unkn-08	002 N15	32.07	31.73	0.485
B04	FAM	BMP2	Unkn-08	002 N15	31.39	31.73	0.485
B05	FAM	BMP2	Unkn-14	799 N15	30.76	31.00	0.329
B06	FAM	BMP2	Unkn-14	799 N15	31.23	31.00	0.329
B07	FAM	BMP2	Unkn-19	811 N15	35.37	35.78	0.591
B08	FAM	BMP2	Unkn-19	811 N15	36.20	35.78	0.591
B09	FAM	BMP2	Unkn-25	805 N15	N/A	0.00	0.000
B10	FAM	BMP2	Unkn-25	805 N15	N/A	0.00	0.000
B11	FAM	BMP2	Unkn-31	816 N15	N/A	0.00	0.000
B12	FAM	BMP2	Unkn-31	816 N15	36.41	36.41	0.000
C01	FAM	BMP2	Unkn-03	001 T15	36.41	36.41	0.000
C02	FAM	BMP2	Unkn-03	001 T15	N/A	0.00	0.000
C03	FAM	BMP2	Unkn-09	002 T15	34.87	34.90	0.048
C04	FAM	BMP2	Unkn-09	002 T15	34.94	34.90	0.048
C05	FAM	BMP2	Unkn-15	799 T15	31.98	32.32	0.470
C06	FAM	BMP2	Unkn-15	799 T15	32.65	32.32	0.470
C07	FAM	BMP2	Unkn-20	811 T15	29.62	29.44	0.250
C08	FAM	BMP2	Unkn-20	811 T15	29.27	29.44	0.250
C09	FAM	BMP2	Unkn-26	805 T15	34.86	35.27	0.587
C10	FAM	BMP2	Unkn-26	805 T15	35.69	35.27	0.587
C11	FAM	BMP2	Unkn-32	816 T15	36.73	35.64	1.550
C12	FAM	BMP2	Unkn-32	816 T15	34.54	35.64	1.550
D01	FAM	BMP2	Unkn-04	001 T+N15	35.12	34.48	0.904
D02	FAM	BMP2	Unkn-04	001 T+N15	33.84	34.48	0.904
D03	FAM	BMP2	Unkn-10	002 T+N15	37.50	37.55	0.069
D04	FAM	BMP2	Unkn-10	002 T+N15	37.60	37.55	0.069
D05	FAM	BMP2	Unkn-16	799 T+N15	34.64	35.23	0.834
D06	FAM	BMP2	Unkn-16	799 T+N15	35.82	35.23	0.834
D07	FAM	BMP2	Unkn-21	811 T+N15	N/A	0.00	0.000
D08	FAM	BMP2	Unkn-21	811 T+N15	39.21	39.21	0.000
D09	FAM	BMP2	Unkn-27	805 T+N15	37.17	36.90	0.381
D10	FAM	BMP2	Unkn-27	805 T+N15	36.64	36.90	0.381
D11	FAM	BMP2	Unkn-33	816 T+N15	33.47	33.36	0.159

Well	Fluor	Target	Content	Sample	Cq	Cq Mean	Cq Std. Dev
D12	FAM	BMP2	Unkn-33	816 T+N15	33.25	33.36	0.159
E01	FAM	BMP2	Unkn-05	001 V15	36.35	35.28	1.516
E02	FAM	BMP2	Unkn-05	001 V15	34.20	35.28	1.516
E03	FAM	BMP2	Unkn-11	002 V15	35.15	35.29	0.196
E04	FAM	BMP2	Unkn-11	002 V15	35.43	35.29	0.196
E05	FAM	BMP2	Unkn-17	799 Z15	34.94	34.59	0.485
E06	FAM	BMP2	Unkn-17	799 Z15	34.25	34.59	0.485
E07	FAM	BMP2	Unkn-22	811 V15	35.41	35.74	0.456
E08	FAM	BMP2	Unkn-22	811 V15	36.06	35.74	0.456
E09	FAM	BMP2	Unkn-28	805 V15	37.32	37.21	0.158
E10	FAM	BMP2	Unkn-28	805 V15	37.10	37.21	0.158
E11	FAM	BMP2	Unkn-34	816 V15	34.38	33.47	1.279
E12	FAM	BMP2	Unkn-34	816 V15	32.57	33.47	1.279
F01	FAM	BMP2	Unkn-06	001 Z15	32.67	32.51	0.224
F02	FAM	BMP2	Unkn-06	001 Z15	32.36	32.51	0.224
F03	FAM	BMP2	Unkn-12	002 Z15	33.53	32.99	0.770
F04	FAM	BMP2	Unkn-12	002 Z15	32.45	32.99	0.770
F07	FAM	BMP2	Unkn-23	811 Z15	29.54	29.62	0.121
F08	FAM	BMP2	Unkn-23	811 Z15	29.71	29.62	0.121
F09	FAM	BMP2	Unkn-29	805 Z15	35.86	35.50	0.516
F10	FAM	BMP2	Unkn-29	805 Z15	35.14	35.50	0.516
F11	FAM	BMP2	Unkn-35	816 Z15	36.21	35.45	1.077
F12	FAM	BMP2	Unkn-35	816 Z15	34.69	35.45	1.077
G01	FAM	BMP2	Pos Ctrl-36	804 PC	32.52	31.94	0.824
G02	FAM	BMP2	Pos Ctrl-36	804 PC	31.36	31.94	0.824
G03	FAM	BMP2	NTC-37	H2O	N/A	0.00	0.000
G04	FAM	BMP2	NTC-37	H2O	N/A	0.00	0.000
G05	FAM	BMP2	NTC-38	H2O	N/A	0.00	0.000
G06	FAM	BMP2	NTC-38	H2O	N/A	0.00	0.000

Gene Expression

Target Names

Name	Full Name	Reference	Auto Efficiency	Efficiency
BMP2	BMP2	False	Yes	100.0%

BMP2 60d.pcrd

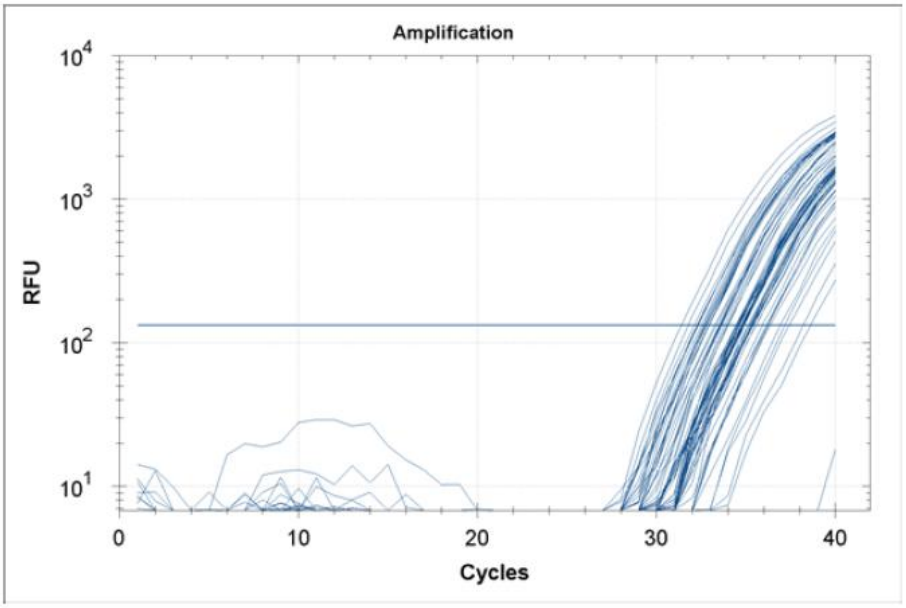
2013/08/21 12:59 PM

Run Setup

Plate Display

	1	2	3	4	5	6	7	8	9	10	11	12
A	Unk-1 BMP2 001 S60	Unk-1 BMP2 001 S60	Unk-7 BMP2 002 S60	Unk-7 BMP2 002 S60	Unk-13 BMP2 799 S60	Unk-13 BMP2 799 S60	Unk-18 BMP2 811 S60	Unk-18 BMP2 811 S60	Unk-24 BMP2 805 S60	Unk-24 BMP2 805 S60	Unk-30 BMP2 816 S60	Unk-30 BMP2 816 S60
B	Unk-2 BMP2 001 N60	Unk-2 BMP2 001 N60	Unk-8 BMP2 002 N60	Unk-8 BMP2 002 N60	Unk-14 BMP2 799 N60	Unk-14 BMP2 799 N60	Unk-19 BMP2 811 N60	Unk-19 BMP2 811 N60	Unk-25 BMP2 805 N60	Unk-25 BMP2 805 N60	Unk-31 BMP2 816 N60	Unk-31 BMP2 816 N60
C	Unk-3 BMP2 001 T60	Unk-3 BMP2 001 T60	Unk-9 BMP2 002 T60	Unk-9 BMP2 002 T60	Unk-15 BMP2 799 T60	Unk-15 BMP2 799 T60	Unk-20 BMP2 811 T60	Unk-20 BMP2 811 T60	Unk-26 BMP2 805 T60	Unk-26 BMP2 805 T60	Unk-32 BMP2 816 T60	Unk-32 BMP2 816 T60
D	Unk-4 BMP2 001 T+N60	Unk-4 BMP2 001 T+N60	Unk-10 BMP2 002 T+N60	Unk-10 BMP2 002 T+N60	Unk-16 BMP2 799 T+N60	Unk-16 BMP2 799 T+N60	Unk-21 BMP2 811 T+N60	Unk-21 BMP2 811 T+N60	Unk-27 BMP2 805 T+N60	Unk-27 BMP2 805 T+N60	Unk-33 BMP2 816 T+N60	Unk-33 BMP2 816 T+N60
E	Unk-5 BMP2 001 V60	Unk-5 BMP2 001 V60	Unk-11 BMP2 002 V60	Unk-11 BMP2 002 V60	Unk-17 BMP2 799 Z60	Unk-17 BMP2 799 Z60	Unk-22 BMP2 811 V60	Unk-22 BMP2 811 V60	Unk-28 BMP2 805 V60	Unk-28 BMP2 805 V60	Unk-34 BMP2 816 V60	Unk-34 BMP2 816 V60
F	Unk-6 BMP2 001 Z60	Unk-6 BMP2 001 Z60	Unk-12 BMP2 002 Z60	Unk-12 BMP2 002 Z60			Unk-23 BMP2 811 Z60	Unk-23 BMP2 811 Z60	Unk-29 BMP2 805 Z60	Unk-29 BMP2 805 Z60	Unk-35 BMP2 816 Z60	Unk-35 BMP2 816 Z60
G	Pos-36 BMP2 804 PC	Pos-36 BMP2 804 PC	NTC-37 BMP2 H2O	NTC-37 BMP2 H2O	NTC-38 BMP2 H2O	NTC-38 BMP2 H2O	*Unk-39 BMP2 Pooled MC 10ng	*Unk-39 BMP2 Pooled MC 10ng	*Unk-40 BMP2 Pooled MC 15ng	*Unk-40 BMP2 Pooled MC 15ng	*Unk-41 BMP2 Pooled MC 5ng	*Unk-41 BMP2 Pooled MC 5ng
H												

Quantification



Quantification Data

Well	Fluor	Target	Content	Sample	Cq	Cq Mean	Cq Std. Dev
A01	FAM	BMP2	Unkn-01	001 S60	34.74	35.01	0.389
A02	FAM	BMP2	Unkn-01	001 S60	35.29	35.01	0.389
A03	FAM	BMP2	Unkn-07	002 S60	33.29	32.87	0.607
A04	FAM	BMP2	Unkn-07	002 S60	32.44	32.87	0.607
A05	FAM	BMP2	Unkn-13	799 S60	32.73	32.63	0.134
A06	FAM	BMP2	Unkn-13	799 S60	32.54	32.63	0.134
A07	FAM	BMP2	Unkn-18	811 S60	34.84	34.62	0.302
A08	FAM	BMP2	Unkn-18	811 S60	34.41	34.62	0.302
A09	FAM	BMP2	Unkn-24	805 S60	34.45	34.91	0.641
A10	FAM	BMP2	Unkn-24	805 S60	35.36	34.91	0.641
A11	FAM	BMP2	Unkn-30	816 S60	38.55	37.96	0.842
A12	FAM	BMP2	Unkn-30	816 S60	37.36	37.96	0.842
B01	FAM	BMP2	Unkn-02	001 N60	34.88	34.80	0.119
B02	FAM	BMP2	Unkn-02	001 N60	34.71	34.80	0.119
B03	FAM	BMP2	Unkn-08	002 N60	36.90	36.53	0.516
B04	FAM	BMP2	Unkn-08	002 N60	36.17	36.53	0.516
B05	FAM	BMP2	Unkn-14	799 N60	32.91	33.19	0.392
B06	FAM	BMP2	Unkn-14	799 N60	33.47	33.19	0.392
B07	FAM	BMP2	Unkn-19	811 N60	32.25	32.43	0.249
B08	FAM	BMP2	Unkn-19	811 N60	32.60	32.43	0.249
B09	FAM	BMP2	Unkn-25	805 N60	34.69	34.63	0.091
B10	FAM	BMP2	Unkn-25	805 N60	34.56	34.63	0.091
B11	FAM	BMP2	Unkn-31	816 N60	35.50	35.04	0.656
B12	FAM	BMP2	Unkn-31	816 N60	34.57	35.04	0.656
C01	FAM	BMP2	Unkn-03	001 T60	33.42	33.48	0.089
C02	FAM	BMP2	Unkn-03	001 T60	33.54	33.48	0.089
C03	FAM	BMP2	Unkn-09	002 T60	32.09	31.71	0.536
C04	FAM	BMP2	Unkn-09	002 T60	31.33	31.71	0.536
C05	FAM	BMP2	Unkn-15	799 T60	32.27	33.14	1.230
C06	FAM	BMP2	Unkn-15	799 T60	34.01	33.14	1.230
C07	FAM	BMP2	Unkn-20	811 T60	34.51	34.01	0.707
C08	FAM	BMP2	Unkn-20	811 T60	33.51	34.01	0.707
C09	FAM	BMP2	Unkn-26	805 T60	35.15	35.68	0.754
C10	FAM	BMP2	Unkn-26	805 T60	36.21	35.68	0.754
C11	FAM	BMP2	Unkn-32	816 T60	35.08	35.60	0.732
C12	FAM	BMP2	Unkn-32	816 T60	36.12	35.60	0.732
D01	FAM	BMP2	Unkn-04	001 T+N60	34.37	34.45	0.113
D02	FAM	BMP2	Unkn-04	001 T+N60	34.53	34.45	0.113
D03	FAM	BMP2	Unkn-10	002 T+N60	32.22	31.97	0.353
D04	FAM	BMP2	Unkn-10	002 T+N60	31.72	31.97	0.353
D05	FAM	BMP2	Unkn-16	799 T+N60	35.49	35.90	0.577
D06	FAM	BMP2	Unkn-16	799 T+N60	36.30	35.90	0.577
D07	FAM	BMP2	Unkn-21	811 T+N60	33.22	33.59	0.533
D08	FAM	BMP2	Unkn-21	811 T+N60	33.97	33.59	0.533
D09	FAM	BMP2	Unkn-27	805 T+N60	35.25	36.71	2.066
D10	FAM	BMP2	Unkn-27	805 T+N60	38.17	36.71	2.066
D11	FAM	BMP2	Unkn-33	816 T+N60	35.32	36.23	1.284

Well	Fluor	Target	Content	Sample	Cq	Cq Mean	Cq Std. Dev
D12	FAM	BMP2	Unkn-33	816 T+N60	37.14	36.23	1.284
E01	FAM	BMP2	Unkn-05	001 V60	35.91	34.74	1.647
E02	FAM	BMP2	Unkn-05	001 V60	33.58	34.74	1.647
E03	FAM	BMP2	Unkn-11	002 V60	32.77	32.85	0.113
E04	FAM	BMP2	Unkn-11	002 V60	32.93	32.85	0.113
E05	FAM	BMP2	Unkn-17	799 Z60	32.91	32.92	0.020
E06	FAM	BMP2	Unkn-17	799 Z60	32.93	32.92	0.020
E07	FAM	BMP2	Unkn-22	811 V60	33.87	34.36	0.691
E08	FAM	BMP2	Unkn-22	811 V60	34.85	34.36	0.691
E09	FAM	BMP2	Unkn-28	805 V60	34.85	34.80	0.070
E10	FAM	BMP2	Unkn-28	805 V60	34.75	34.80	0.070
E11	FAM	BMP2	Unkn-34	816 V60	34.69	34.95	0.356
E12	FAM	BMP2	Unkn-34	816 V60	35.20	34.95	0.356
F01	FAM	BMP2	Unkn-06	001 Z60	34.58	34.68	0.146
F02	FAM	BMP2	Unkn-06	001 Z60	34.79	34.68	0.146
F03	FAM	BMP2	Unkn-12	002 Z60	32.67	33.19	0.745
F04	FAM	BMP2	Unkn-12	002 Z60	33.72	33.19	0.745
F07	FAM	BMP2	Unkn-23	811 Z60	35.20	34.85	0.505
F08	FAM	BMP2	Unkn-23	811 Z60	34.49	34.85	0.505
F09	FAM	BMP2	Unkn-29	805 Z60	N/A	0.00	0.000
F10	FAM	BMP2	Unkn-29	805 Z60	N/A	0.00	0.000
F11	FAM	BMP2	Unkn-35	816 Z60	34.77	35.03	0.357
F12	FAM	BMP2	Unkn-35	816 Z60	35.28	35.03	0.357
G01	FAM	BMP2	Pos Ctrl-36	804 PC	35.33	35.09	0.343
G02	FAM	BMP2	Pos Ctrl-36	804 PC	34.84	35.09	0.343
G03	FAM	BMP2	NTC-37	H2O	N/A	0.00	0.000
G04	FAM	BMP2	NTC-37	H2O	N/A	0.00	0.000
G05	FAM	BMP2	NTC-38	H2O	N/A	0.00	0.000
G06	FAM	BMP2	NTC-38	H2O	N/A	0.00	0.000

Gene Expression

Target Names

Name	Full Name	Reference	Auto Efficiency	Efficiency
BMP2	BMP2	False	Yes	100.0%

BMP2 90d.pcrd

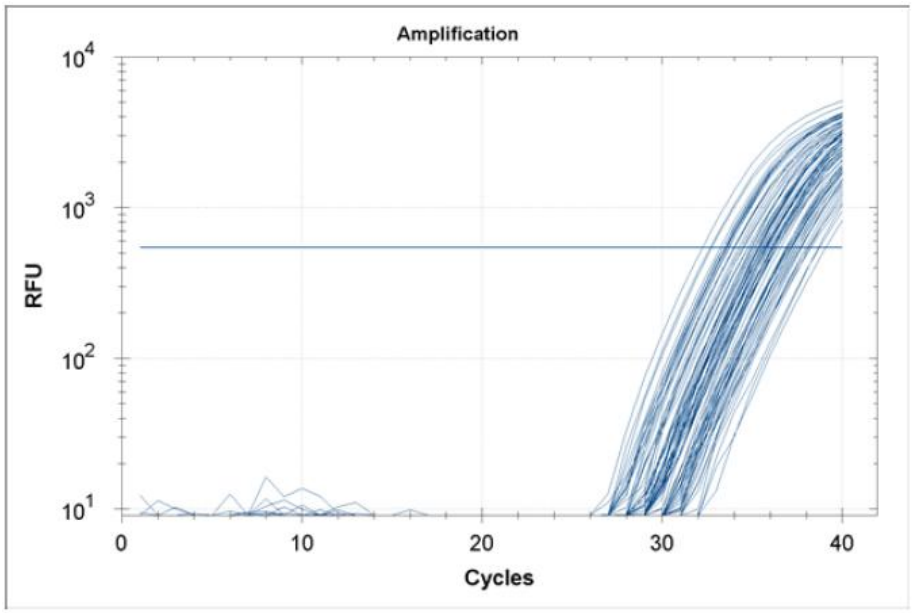
2013/08/21 01:00 PM

Run Setup

Plate Display

	1	2	3	4	5	6	7	8	9	10	11	12
A	Unk-1 BMP2 001 S90	Unk-1 BMP2 001 S90	Unk-8 BMP2 002 S90	Unk-8 BMP2 002 S90	Unk-15 BMP2 799 S90	Unk-15 BMP2 799 S90	Unk-21 BMP2 811 S90	Unk-21 BMP2 811 S90	Unk-28 BMP2 805 S90	Unk-28 BMP2 805 S90	Unk-35 BMP2 816 S90	Unk-35 BMP2 816 S90
B	Unk-2 BMP2 001 N90	Unk-2 BMP2 001 N90	Unk-9 BMP2 002 N90	Unk-9 BMP2 002 N90	Unk-16 BMP2 799 N90	Unk-16 BMP2 799 N90	Unk-22 BMP2 811 N90	Unk-22 BMP2 811 N90	Unk-29 BMP2 805 N90	Unk-29 BMP2 805 N90	Unk-36 BMP2 816 N90	Unk-36 BMP2 816 N90
C	Unk-3 BMP2 001 T90	Unk-3 BMP2 001 T90	Unk-10 BMP2 002 T90	Unk-10 BMP2 002 T90	Unk-17 BMP2 799 T90	Unk-17 BMP2 799 T90	Unk-23 BMP2 811 T90	Unk-23 BMP2 811 T90	Unk-30 BMP2 805 T90	Unk-30 BMP2 805 T90	Unk-37 BMP2 816 T90	Unk-37 BMP2 816 T90
D	Unk-4 BMP2 001 T+N90	Unk-4 BMP2 001 T+N90	Unk-11 BMP2 002 T+N90	Unk-11 BMP2 002 T+N90	Unk-18 BMP2 799 T+N90	Unk-18 BMP2 799 T+N90	Unk-24 BMP2 811 T+N90	Unk-24 BMP2 811 T+N90	Unk-31 BMP2 805 T+N90	Unk-31 BMP2 805 T+N90	Unk-38 BMP2 816 T+N90	Unk-38 BMP2 816 T+N90
E	Unk-5 BMP2 001 V90	Unk-5 BMP2 001 V90	Unk-12 BMP2 002 V90	Unk-12 BMP2 002 V90	Unk-19 BMP2 799 Z90	Unk-19 BMP2 799 Z90	Unk-25 BMP2 811 V90	Unk-25 BMP2 811 V90	Unk-32 BMP2 805 V90	Unk-32 BMP2 805 V90	Unk-39 BMP2 816 V90	Unk-39 BMP2 816 V90
F	Unk-6 BMP2 001 Z90	Unk-6 BMP2 001 Z90	Unk-13 BMP2 002 Z90	Unk-13 BMP2 002 Z90			Unk-26 BMP2 811 Z90	Unk-26 BMP2 811 Z90	Unk-33 BMP2 805 Z90	Unk-33 BMP2 805 Z90	Unk-40 BMP2 816 Z90	Unk-40 BMP2 816 Z90
G	Unk-7 BMP2 001 MC	Unk-7 BMP2 001 MC	Unk-14 BMP2 002 MC	Unk-14 BMP2 002 MC	Unk-20 BMP2 799 MC	Unk-20 BMP2 799 MC	Unk-27 BMP2 811 MC	Unk-27 BMP2 811 MC	Unk-34 BMP2 805 MC	Unk-34 BMP2 805 MC	Unk-41 BMP2 816 MC	Unk-41 BMP2 816 MC
H	Pos-42 BMP2 804 PC	Pos-42 BMP2 804 PC	NTC-43 BMP2 H2O	NTC-43 BMP2 H2O	NTC-44 BMP2 H2O	NTC-44 BMP2 H2O	*Unk-45 BMP2 Pooled MC 15ng	*Unk-45 BMP2 Pooled MC 15ng	*Unk-46 BMP2 Pooled MC 10ng	*Unk-46 BMP2 Pooled MC 10ng	*Unk-47 BMP2 Pooled MC 5ng	*Unk-47 BMP2 Pooled MC 5ng

Quantification



Quantification Data

Well	Fluor	Target	Content	Sample	Cq	Cq Mean	Cq Std. Dev
A01	FAM	BMP2	Unkn-01	001 S90	38.24	36.87	1.934
A02	FAM	BMP2	Unkn-01	001 S90	35.50	36.87	1.934
A03	FAM	BMP2	Unkn-08	002 S90	35.63	35.65	0.025
A04	FAM	BMP2	Unkn-08	002 S90	35.66	35.65	0.025
A05	FAM	BMP2	Unkn-15	799 S90	33.98	33.73	0.356
A06	FAM	BMP2	Unkn-15	799 S90	33.48	33.73	0.356
A07	FAM	BMP2	Unkn-21	811 S90	33.33	33.49	0.222
A08	FAM	BMP2	Unkn-21	811 S90	33.64	33.49	0.222
A09	FAM	BMP2	Unkn-28	805 S90	37.04	37.09	0.084
A10	FAM	BMP2	Unkn-28	805 S90	37.15	37.09	0.084
A11	FAM	BMP2	Unkn-35	816 S90	36.11	36.20	0.122
A12	FAM	BMP2	Unkn-35	816 S90	36.28	36.20	0.122
B01	FAM	BMP2	Unkn-02	001 N90	35.62	34.82	1.133
B02	FAM	BMP2	Unkn-02	001 N90	34.02	34.82	1.133
B03	FAM	BMP2	Unkn-09	002 N90	33.54	34.15	0.853
B04	FAM	BMP2	Unkn-09	002 N90	34.75	34.15	0.853
B05	FAM	BMP2	Unkn-16	799 N90	33.66	34.36	0.985
B06	FAM	BMP2	Unkn-16	799 N90	35.05	34.36	0.985
B07	FAM	BMP2	Unkn-22	811 N90	35.13	35.22	0.135
B08	FAM	BMP2	Unkn-22	811 N90	35.32	35.22	0.135
B09	FAM	BMP2	Unkn-29	805 N90	36.96	37.07	0.156
B10	FAM	BMP2	Unkn-29	805 N90	37.18	37.07	0.156
B11	FAM	BMP2	Unkn-36	816 N90	35.64	36.00	0.513
B12	FAM	BMP2	Unkn-36	816 N90	36.36	36.00	0.513
C01	FAM	BMP2	Unkn-03	001 T90	34.20	36.15	2.755
C02	FAM	BMP2	Unkn-03	001 T90	38.10	36.15	2.755
C03	FAM	BMP2	Unkn-10	002 T90	33.50	33.34	0.219
C04	FAM	BMP2	Unkn-10	002 T90	33.19	33.34	0.219
C05	FAM	BMP2	Unkn-17	799 T90	36.05	36.12	0.099
C06	FAM	BMP2	Unkn-17	799 T90	36.19	36.12	0.099
C07	FAM	BMP2	Unkn-23	811 T90	33.97	33.34	0.891
C08	FAM	BMP2	Unkn-23	811 T90	32.71	33.34	0.891
C09	FAM	BMP2	Unkn-30	805 T90	35.80	36.48	0.965
C10	FAM	BMP2	Unkn-30	805 T90	37.16	36.48	0.965
C11	FAM	BMP2	Unkn-37	816 T90	37.61	37.28	0.467
C12	FAM	BMP2	Unkn-37	816 T90	36.95	37.28	0.467
D01	FAM	BMP2	Unkn-04	001 T+N90	35.97	34.65	1.864
D02	FAM	BMP2	Unkn-04	001 T+N90	33.33	34.65	1.864
D03	FAM	BMP2	Unkn-11	002 T+N90	32.62	32.41	0.293
D04	FAM	BMP2	Unkn-11	002 T+N90	32.20	32.41	0.293
D05	FAM	BMP2	Unkn-18	799 T+N90	35.45	35.82	0.522
D06	FAM	BMP2	Unkn-18	799 T+N90	36.19	35.82	0.522
D07	FAM	BMP2	Unkn-24	811 T+N90	34.74	34.61	0.181
D08	FAM	BMP2	Unkn-24	811 T+N90	34.48	34.61	0.181
D09	FAM	BMP2	Unkn-31	805 T+N90	36.85	37.16	0.432
D10	FAM	BMP2	Unkn-31	805 T+N90	37.46	37.16	0.432
D11	FAM	BMP2	Unkn-38	816 T+N90	39.07	38.02	1.483

Well	Fluor	Target	Content	Sample	Cq	Cq Mean	Cq Std. Dev
D12	FAM	BMP2	Unkn-38	816 T+N90	36.97	38.02	1.483
E01	FAM	BMP2	Unkn-05	001 V90	34.33	35.31	1.375
E02	FAM	BMP2	Unkn-05	001 V90	36.28	35.31	1.375
E03	FAM	BMP2	Unkn-12	002 V90	35.52	35.41	0.161
E04	FAM	BMP2	Unkn-12	002 V90	35.29	35.41	0.161
E05	FAM	BMP2	Unkn-19	799 Z90	37.70	36.79	1.285
E06	FAM	BMP2	Unkn-19	799 Z90	35.88	36.79	1.285
E07	FAM	BMP2	Unkn-25	811 V90	37.08	36.22	1.221
E08	FAM	BMP2	Unkn-25	811 V90	35.36	36.22	1.221
E09	FAM	BMP2	Unkn-32	805 V90	35.22	34.84	0.538
E10	FAM	BMP2	Unkn-32	805 V90	34.46	34.84	0.538
E11	FAM	BMP2	Unkn-39	816 V90	37.31	36.54	1.088
E12	FAM	BMP2	Unkn-39	816 V90	35.77	36.54	1.088
F01	FAM	BMP2	Unkn-06	001 Z90	35.70	35.42	0.405
F02	FAM	BMP2	Unkn-06	001 Z90	35.13	35.42	0.405
F03	FAM	BMP2	Unkn-13	002 Z90	34.33	33.89	0.622
F04	FAM	BMP2	Unkn-13	002 Z90	33.45	33.89	0.622
F07	FAM	BMP2	Unkn-26	811 Z90	34.91	34.94	0.039
F08	FAM	BMP2	Unkn-26	811 Z90	34.97	34.94	0.039
F09	FAM	BMP2	Unkn-33	805 Z90	36.28	36.22	0.096
F10	FAM	BMP2	Unkn-33	805 Z90	36.15	36.22	0.096
F11	FAM	BMP2	Unkn-40	816 Z90	36.07	35.91	0.227
F12	FAM	BMP2	Unkn-40	816 Z90	35.75	35.91	0.227
G01	FAM	BMP2	Unkn-07	001 MC	38.07	38.12	0.067
G02	FAM	BMP2	Unkn-07	001 MC	38.17	38.12	0.067
G03	FAM	BMP2	Unkn-14	002 MC	38.62	37.88	1.047
G04	FAM	BMP2	Unkn-14	002 MC	37.14	37.88	1.047
G05	FAM	BMP2	Unkn-20	799 MC	36.88	37.17	0.416
G06	FAM	BMP2	Unkn-20	799 MC	37.47	37.17	0.416
G07	FAM	BMP2	Unkn-27	811 MC	35.33	35.93	0.851
G08	FAM	BMP2	Unkn-27	811 MC	36.53	35.93	0.851
G09	FAM	BMP2	Unkn-34	805 MC	36.12	35.71	0.582
G10	FAM	BMP2	Unkn-34	805 MC	35.29	35.71	0.582
G11	FAM	BMP2	Unkn-41	816 MC	37.32	38.01	0.975
G12	FAM	BMP2	Unkn-41	816 MC	38.70	38.01	0.975
H01	FAM	BMP2	Pos Ctrl-42	804 PC	37.64	37.80	0.215
H02	FAM	BMP2	Pos Ctrl-42	804 PC	37.95	37.80	0.215
H03	FAM	BMP2	NTC-43	H2O	N/A	0.00	0.000
H04	FAM	BMP2	NTC-43	H2O	N/A	0.00	0.000
H05	FAM	BMP2	NTC-44	H2O	N/A	0.00	0.000
H06	FAM	BMP2	NTC-44	H2O	N/A	0.00	0.000

Gene Expression

Target Names

Name	Full Name	Reference	Auto Efficiency	Efficiency
BMP2	BMP2	False	Yes	100.0%

TGF-b3 15d.pcrd

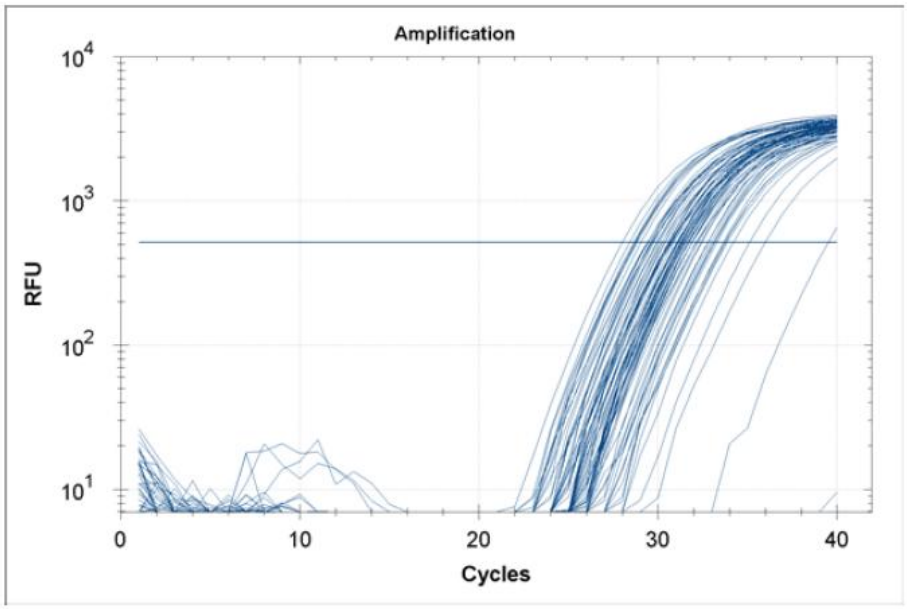
2013/08/21 01:03 PM

Run Setup

Plate Display

	1	2	3	4	5	6	7	8	9	10	11	12
A	Unk-1 TGF-b3 001 S15	Unk-1 TGF-b3 001 S15	Unk-7 TGF-b3 002 S15	Unk-7 TGF-b3 002 S15	Unk-13 TGF-b3 799 S15	Unk-13 TGF-b3 799 S15	Unk-18 TGF-b3 811 S15	Unk-18 TGF-b3 811 S15	Unk-24 TGF-b3 805 S15	Unk-24 TGF-b3 805 S15	Unk-30 TGF-b3 816 S15	Unk-30 TGF-b3 816 S15
B	Unk-2 TGF-b3 001 N15	Unk-2 TGF-b3 001 N15	Unk-8 TGF-b3 002 N15	Unk-8 TGF-b3 002 N15	Unk-14 TGF-b3 799 N15	Unk-14 TGF-b3 799 N15	Unk-19 TGF-b3 811 N15	Unk-19 TGF-b3 811 N15	*Unk-25 TGF-b3 805 N15	Unk-25 TGF-b3 805 N15	Unk-31 TGF-b3 816 N15	Unk-31 TGF-b3 816 N15
C	Unk-3 TGF-b3 001 T15	Unk-3 TGF-b3 001 T15	Unk-9 TGF-b3 002 T15	Unk-9 TGF-b3 002 T15	Unk-15 TGF-b3 799 T15	Unk-15 TGF-b3 799 T15	Unk-20 TGF-b3 811 T15	Unk-20 TGF-b3 811 T15	Unk-26 TGF-b3 805 T15	Unk-26 TGF-b3 805 T15	Unk-32 TGF-b3 816 T15	Unk-32 TGF-b3 816 T15
D	Unk-4 TGF-b3 001 T+N15	Unk-4 TGF-b3 001 T+N15	Unk-10 TGF-b3 002 T+N15	Unk-10 TGF-b3 002 T+N15	Unk-16 TGF-b3 799 T+N15	Unk-16 TGF-b3 799 T+N15	Unk-21 TGF-b3 811 T+N15	Unk-21 TGF-b3 811 T+N15	Unk-27 TGF-b3 805 T+N15	Unk-27 TGF-b3 805 T+N15	Unk-33 TGF-b3 816 T+N15	Unk-33 TGF-b3 816 T+N15
E	Unk-5 TGF-b3 001 V15	Unk-5 TGF-b3 001 V15	Unk-11 TGF-b3 002 V15	Unk-11 TGF-b3 002 V15	Unk-17 TGF-b3 799 Z15	Unk-17 TGF-b3 799 Z15	Unk-22 TGF-b3 811 V15	Unk-22 TGF-b3 811 V15	Unk-28 TGF-b3 805 V15	Unk-28 TGF-b3 805 V15	Unk-34 TGF-b3 816 V15	Unk-34 TGF-b3 816 V15
F	Unk-6 TGF-b3 001 Z15	Unk-6 TGF-b3 001 Z15	Unk-12 TGF-b3 002 Z15	Unk-12 TGF-b3 002 Z15			Unk-23 TGF-b3 811 Z15	Unk-23 TGF-b3 811 Z15	Unk-29 TGF-b3 805 Z15	Unk-29 TGF-b3 805 Z15	Unk-35 TGF-b3 816 Z15	Unk-35 TGF-b3 816 Z15
G	Pos-36 TGF-b3 804 PC	Pos-36 TGF-b3 804 PC	NTC-37 TGF-b3 H2O	NTC-37 TGF-b3 H2O	NTC-38 TGF-b3 H2O	NTC-38 TGF-b3 H2O	Unk-39 TGF-b3 Pooled MC 10ng	Unk-39 TGF-b3 Pooled MC 10ng	Unk-40 TGF-b3 Pooled MC 15ng	Unk-40 TGF-b3 Pooled MC 15ng	Unk-41 TGF-b3 Pooled MC 5ng	Unk-41 TGF-b3 Pooled MC 5ng
H												

Quantification



Quantification Data

Well	Fluor	Target	Content	Sample	Cq	Cq Mean	Cq Std. Dev
A01	FAM	TGF-b3	Unkn-01	001 S15	32.14	32.02	0.172
A02	FAM	TGF-b3	Unkn-01	001 S15	31.89	32.02	0.172
A03	FAM	TGF-b3	Unkn-07	002 S15	30.65	30.71	0.093
A04	FAM	TGF-b3	Unkn-07	002 S15	30.78	30.71	0.093
A05	FAM	TGF-b3	Unkn-13	799 S15	29.62	29.49	0.178
A06	FAM	TGF-b3	Unkn-13	799 S15	29.37	29.49	0.178
A07	FAM	TGF-b3	Unkn-18	811 S15	31.71	31.80	0.129
A08	FAM	TGF-b3	Unkn-18	811 S15	31.89	31.80	0.129
A09	FAM	TGF-b3	Unkn-24	805 S15	33.75	33.71	0.054
A10	FAM	TGF-b3	Unkn-24	805 S15	33.67	33.71	0.054
A11	FAM	TGF-b3	Unkn-30	816 S15	32.11	32.16	0.071
A12	FAM	TGF-b3	Unkn-30	816 S15	32.21	32.16	0.071
B01	FAM	TGF-b3	Unkn-02	001 N15	30.66	30.64	0.023
B02	FAM	TGF-b3	Unkn-02	001 N15	30.62	30.64	0.023
B03	FAM	TGF-b3	Unkn-08	002 N15	29.38	29.78	0.573
B04	FAM	TGF-b3	Unkn-08	002 N15	30.19	29.78	0.573
B05	FAM	TGF-b3	Unkn-14	799 N15	31.04	30.96	0.120
B06	FAM	TGF-b3	Unkn-14	799 N15	30.87	30.96	0.120
B07	FAM	TGF-b3	Unkn-19	811 N15	31.45	31.46	0.021
B08	FAM	TGF-b3	Unkn-19	811 N15	31.48	31.46	0.021
B10	FAM	TGF-b3	Unkn-25	805 N15	39.46	39.46	0.000
B11	FAM	TGF-b3	Unkn-31	816 N15	33.60	33.89	0.408
B12	FAM	TGF-b3	Unkn-31	816 N15	34.18	33.89	0.408
C01	FAM	TGF-b3	Unkn-03	001 T15	30.70	30.72	0.021
C02	FAM	TGF-b3	Unkn-03	001 T15	30.73	30.72	0.021
C03	FAM	TGF-b3	Unkn-09	002 T15	30.33	30.34	0.013
C04	FAM	TGF-b3	Unkn-09	002 T15	30.35	30.34	0.013
C05	FAM	TGF-b3	Unkn-15	799 T15	31.08	31.22	0.194
C06	FAM	TGF-b3	Unkn-15	799 T15	31.35	31.22	0.194
C07	FAM	TGF-b3	Unkn-20	811 T15	28.00	28.36	0.512
C08	FAM	TGF-b3	Unkn-20	811 T15	28.73	28.36	0.512
C09	FAM	TGF-b3	Unkn-26	805 T15	31.13	31.19	0.091
C10	FAM	TGF-b3	Unkn-26	805 T15	31.25	31.19	0.091
C11	FAM	TGF-b3	Unkn-32	816 T15	31.31	31.49	0.262
C12	FAM	TGF-b3	Unkn-32	816 T15	31.68	31.49	0.262
D01	FAM	TGF-b3	Unkn-04	001 T+N15	30.51	30.52	0.007
D02	FAM	TGF-b3	Unkn-04	001 T+N15	30.52	30.52	0.007
D03	FAM	TGF-b3	Unkn-10	002 T+N15	28.83	28.94	0.157
D04	FAM	TGF-b3	Unkn-10	002 T+N15	29.05	28.94	0.157
D05	FAM	TGF-b3	Unkn-16	799 T+N15	31.56	31.50	0.075
D06	FAM	TGF-b3	Unkn-16	799 T+N15	31.45	31.50	0.075
D07	FAM	TGF-b3	Unkn-21	811 T+N15	35.10	35.54	0.628
D08	FAM	TGF-b3	Unkn-21	811 T+N15	35.98	35.54	0.628
D09	FAM	TGF-b3	Unkn-27	805 T+N15	31.69	31.46	0.327
D10	FAM	TGF-b3	Unkn-27	805 T+N15	31.23	31.46	0.327
D11	FAM	TGF-b3	Unkn-33	816 T+N15	30.20	30.38	0.260
D12	FAM	TGF-b3	Unkn-33	816 T+N15	30.57	30.38	0.260

Well	Fluor	Target	Content	Sample	Cq	Cq Mean	Cq Std. Dev
E01	FAM	TGF-b3	Unkn-05	001 V15	31.10	31.08	0.020
E02	FAM	TGF-b3	Unkn-05	001 V15	31.07	31.08	0.020
E03	FAM	TGF-b3	Unkn-11	002 V15	30.06	29.99	0.096
E04	FAM	TGF-b3	Unkn-11	002 V15	29.93	29.99	0.096
E05	FAM	TGF-b3	Unkn-17	799 Z15	29.55	29.53	0.021
E06	FAM	TGF-b3	Unkn-17	799 Z15	29.52	29.53	0.021
E07	FAM	TGF-b3	Unkn-22	811 V15	31.87	31.63	0.350
E08	FAM	TGF-b3	Unkn-22	811 V15	31.38	31.63	0.350
E09	FAM	TGF-b3	Unkn-28	805 V15	33.84	33.09	1.061
E10	FAM	TGF-b3	Unkn-28	805 V15	32.34	33.09	1.061
E11	FAM	TGF-b3	Unkn-34	816 V15	31.63	31.75	0.166
E12	FAM	TGF-b3	Unkn-34	816 V15	31.87	31.75	0.166
F01	FAM	TGF-b3	Unkn-06	001 Z15	29.97	29.85	0.176
F02	FAM	TGF-b3	Unkn-06	001 Z15	29.72	29.85	0.176
F03	FAM	TGF-b3	Unkn-12	002 Z15	29.66	29.53	0.187
F04	FAM	TGF-b3	Unkn-12	002 Z15	29.39	29.53	0.187
F07	FAM	TGF-b3	Unkn-23	811 Z15	28.67	28.68	0.018
F08	FAM	TGF-b3	Unkn-23	811 Z15	28.70	28.68	0.018
F09	FAM	TGF-b3	Unkn-29	805 Z15	33.15	32.78	0.530
F10	FAM	TGF-b3	Unkn-29	805 Z15	32.40	32.78	0.530
F11	FAM	TGF-b3	Unkn-35	816 Z15	31.29	31.25	0.066
F12	FAM	TGF-b3	Unkn-35	816 Z15	31.20	31.25	0.066
G01	FAM	TGF-b3	Pos Ctrl-36	804 PC	28.37	28.48	0.157
G02	FAM	TGF-b3	Pos Ctrl-36	804 PC	28.59	28.48	0.157
G03	FAM	TGF-b3	NTC-37	H2O	N/A	0.00	0.000
G04	FAM	TGF-b3	NTC-37	H2O	N/A	0.00	0.000
G05	FAM	TGF-b3	NTC-38	H2O	N/A	0.00	0.000
G06	FAM	TGF-b3	NTC-38	H2O	N/A	0.00	0.000
G07	FAM	TGF-b3	Unkn-39	Pooled MC 10ng	32.76	32.75	0.011
G08	FAM	TGF-b3	Unkn-39	Pooled MC 10ng	32.75	32.75	0.011
G09	FAM	TGF-b3	Unkn-40	Pooled MC 15ng	33.06	33.16	0.140
G10	FAM	TGF-b3	Unkn-40	Pooled MC 15ng	33.26	33.16	0.140
G11	FAM	TGF-b3	Unkn-41	Pooled MC 5ng	32.94	33.04	0.134
G12	FAM	TGF-b3	Unkn-41	Pooled MC 5ng	33.13	33.04	0.134

Gene Expression

Target Names

Name	Full Name	Reference	Auto Efficiency	Efficiency
TGF-b3	TGF-b3	False	Yes	100.0%

TGF-b3 60d.pcrd

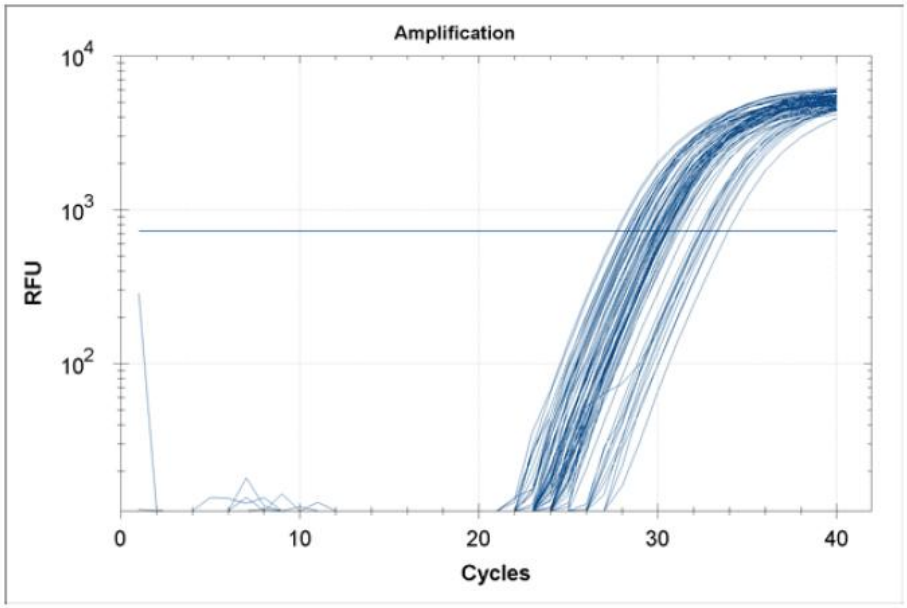
2013/08/21 01:04 PM

Run Setup

Plate Display

	1	2	3	4	5	6	7	8	9	10	11	12
A	Unk-1 TGF-b3 001 S60	Unk-1 TGF-b3 001 S60	Unk-7 TGF-b3 002 S60	Unk-7 TGF-b3 002 S60	Unk-13 TGF-b3 799 S60	Unk-13 TGF-b3 799 S60	Unk-18 TGF-b3 811 S60	Unk-18 TGF-b3 811 S60	Unk-24 TGF-b3 805 S60	Unk-24 TGF-b3 805 S60	Unk-30 TGF-b3 816 S60	Unk-30 TGF-b3 816 S60
B	Unk-2 TGF-b3 001 N60	Unk-2 TGF-b3 001 N60	Unk-8 TGF-b3 002 N60	Unk-8 TGF-b3 002 N60	Unk-14 TGF-b3 799 N60	Unk-14 TGF-b3 799 N60	Unk-19 TGF-b3 811 N60	Unk-19 TGF-b3 811 N60	Unk-25 TGF-b3 805 N60	Unk-25 TGF-b3 805 N60	Unk-31 TGF-b3 816 N60	Unk-31 TGF-b3 816 N60
C	Unk-3 TGF-b3 001 T60	Unk-3 TGF-b3 001 T60	Unk-9 TGF-b3 002 T60	Unk-9 TGF-b3 002 T60	Unk-15 TGF-b3 799 T60	Unk-15 TGF-b3 799 T60	Unk-20 TGF-b3 811 T60	Unk-20 TGF-b3 811 T60	Unk-26 TGF-b3 805 T60	Unk-26 TGF-b3 805 T60	Unk-32 TGF-b3 816 T60	Unk-32 TGF-b3 816 T60
D	Unk-4 TGF-b3 001 T+N60	Unk-4 TGF-b3 001 T+N60	Unk-10 TGF-b3 002 T+N60	Unk-10 TGF-b3 002 T+N60	Unk-16 TGF-b3 799 T+N60	Unk-16 TGF-b3 799 T+N60	Unk-21 TGF-b3 811 T+N60	Unk-21 TGF-b3 811 T+N60	Unk-27 TGF-b3 805 T+N60	Unk-27 TGF-b3 805 T+N60	Unk-33 TGF-b3 816 T+N60	Unk-33 TGF-b3 816 T+N60
E	Unk-5 TGF-b3 001 V60	Unk-5 TGF-b3 001 V60	Unk-11 TGF-b3 002 V60	Unk-11 TGF-b3 002 V60	Unk-17 TGF-b3 799 Z60	Unk-17 TGF-b3 799 Z60	Unk-22 TGF-b3 811 V60	Unk-22 TGF-b3 811 V60	Unk-28 TGF-b3 805 V60	Unk-28 TGF-b3 805 V60	Unk-34 TGF-b3 816 V60	Unk-34 TGF-b3 816 V60
F	Unk-6 TGF-b3 001 Z60	Unk-6 TGF-b3 001 Z60	Unk-12 TGF-b3 002 Z60	Unk-12 TGF-b3 002 Z60			Unk-23 TGF-b3 811 Z60	Unk-23 TGF-b3 811 Z60	Unk-29 TGF-b3 805 Z60	Unk-29 TGF-b3 805 Z60	Unk-35 TGF-b3 816 Z60	Unk-35 TGF-b3 816 Z60
G	Pos-36 TGF-b3 804 PC	Pos-36 TGF-b3 804 PC	NTC-37 TGF-b3 H2O	NTC-37 TGF-b3 H2O	NTC-38 TGF-b3 H2O	NTC-38 TGF-b3 H2O	Unk-39 TGF-b3 Pooled MC 10ng	Unk-39 TGF-b3 Pooled MC 10ng	Unk-40 TGF-b3 Pooled MC 15ng	Unk-40 TGF-b3 Pooled MC 15ng	Unk-41 TGF-b3 Pooled MC 5ng	Unk-41 TGF-b3 Pooled MC 5ng
H												

Quantification



Quantification Data

Well	Fluor	Target	Content	Sample	Cq	Cq Mean	Cq Std. Dev
A01	FAM	TGF-b3	Unkn-01	001 S60	29.87	29.64	0.321
A02	FAM	TGF-b3	Unkn-01	001 S60	29.41	29.64	0.321
A03	FAM	TGF-b3	Unkn-07	002 S60	29.41	29.30	0.156
A04	FAM	TGF-b3	Unkn-07	002 S60	29.19	29.30	0.156
A05	FAM	TGF-b3	Unkn-13	799 S60	28.95	28.61	0.485
A06	FAM	TGF-b3	Unkn-13	799 S60	28.26	28.61	0.485
A07	FAM	TGF-b3	Unkn-18	811 S60	30.73	30.95	0.309
A08	FAM	TGF-b3	Unkn-18	811 S60	31.17	30.95	0.309
A09	FAM	TGF-b3	Unkn-24	805 S60	30.45	30.11	0.477
A10	FAM	TGF-b3	Unkn-24	805 S60	29.77	30.11	0.477
A11	FAM	TGF-b3	Unkn-30	816 S60	30.16	30.34	0.255
A12	FAM	TGF-b3	Unkn-30	816 S60	30.52	30.34	0.255
B01	FAM	TGF-b3	Unkn-02	001 N60	30.89	30.94	0.067
B02	FAM	TGF-b3	Unkn-02	001 N60	30.98	30.94	0.067
B03	FAM	TGF-b3	Unkn-08	002 N60	32.33	32.25	0.109
B04	FAM	TGF-b3	Unkn-08	002 N60	32.17	32.25	0.109
B05	FAM	TGF-b3	Unkn-14	799 N60	28.29	28.38	0.126
B06	FAM	TGF-b3	Unkn-14	799 N60	28.47	28.38	0.126
B07	FAM	TGF-b3	Unkn-19	811 N60	30.37	30.42	0.068
B08	FAM	TGF-b3	Unkn-19	811 N60	30.47	30.42	0.068
B09	FAM	TGF-b3	Unkn-25	805 N60	29.76	29.61	0.205
B10	FAM	TGF-b3	Unkn-25	805 N60	29.47	29.61	0.205
B11	FAM	TGF-b3	Unkn-31	816 N60	30.18	30.12	0.092
B12	FAM	TGF-b3	Unkn-31	816 N60	30.05	30.12	0.092
C01	FAM	TGF-b3	Unkn-03	001 T60	30.21	30.15	0.082
C02	FAM	TGF-b3	Unkn-03	001 T60	30.09	30.15	0.082
C03	FAM	TGF-b3	Unkn-09	002 T60	29.50	29.48	0.022
C04	FAM	TGF-b3	Unkn-09	002 T60	29.47	29.48	0.022
C05	FAM	TGF-b3	Unkn-15	799 T60	27.74	27.69	0.072
C06	FAM	TGF-b3	Unkn-15	799 T60	27.64	27.69	0.072
C07	FAM	TGF-b3	Unkn-20	811 T60	30.49	30.68	0.269
C08	FAM	TGF-b3	Unkn-20	811 T60	30.87	30.68	0.269
C09	FAM	TGF-b3	Unkn-26	805 T60	31.54	31.30	0.344
C10	FAM	TGF-b3	Unkn-26	805 T60	31.05	31.30	0.344
C11	FAM	TGF-b3	Unkn-32	816 T60	30.44	30.36	0.115
C12	FAM	TGF-b3	Unkn-32	816 T60	30.28	30.36	0.115
D01	FAM	TGF-b3	Unkn-04	001 T+N60	28.16	28.14	0.018
D02	FAM	TGF-b3	Unkn-04	001 T+N60	28.13	28.14	0.018
D03	FAM	TGF-b3	Unkn-10	002 T+N60	29.54	29.76	0.311
D04	FAM	TGF-b3	Unkn-10	002 T+N60	29.98	29.76	0.311
D05	FAM	TGF-b3	Unkn-16	799 T+N60	32.41	32.37	0.050
D06	FAM	TGF-b3	Unkn-16	799 T+N60	32.34	32.37	0.050
D07	FAM	TGF-b3	Unkn-21	811 T+N60	30.47	30.46	0.014
D08	FAM	TGF-b3	Unkn-21	811 T+N60	30.45	30.46	0.014
D09	FAM	TGF-b3	Unkn-27	805 T+N60	30.38	30.38	0.008
D10	FAM	TGF-b3	Unkn-27	805 T+N60	30.39	30.38	0.008
D11	FAM	TGF-b3	Unkn-33	816 T+N60	30.35	30.15	0.282

Well	Fluor	Target	Content	Sample	Cq	Cq Mean	Cq Std. Dev
D12	FAM	TGF-b3	Unkn-33	816 T+N60	29.95	30.15	0.282
E01	FAM	TGF-b3	Unkn-05	001 V60	28.74	28.74	0.008
E02	FAM	TGF-b3	Unkn-05	001 V60	28.73	28.74	0.008
E03	FAM	TGF-b3	Unkn-11	002 V60	28.86	28.73	0.188
E04	FAM	TGF-b3	Unkn-11	002 V60	28.59	28.73	0.188
E05	FAM	TGF-b3	Unkn-17	799 Z60	28.63	28.59	0.058
E06	FAM	TGF-b3	Unkn-17	799 Z60	28.55	28.59	0.058
E07	FAM	TGF-b3	Unkn-22	811 V60	29.91	29.96	0.072
E08	FAM	TGF-b3	Unkn-22	811 V60	30.01	29.96	0.072
E09	FAM	TGF-b3	Unkn-28	805 V60	28.80	28.95	0.203
E10	FAM	TGF-b3	Unkn-28	805 V60	29.09	28.95	0.203
E11	FAM	TGF-b3	Unkn-34	816 V60	29.35	29.49	0.204
E12	FAM	TGF-b3	Unkn-34	816 V60	29.63	29.49	0.204
F01	FAM	TGF-b3	Unkn-06	001 Z60	29.49	29.65	0.228
F02	FAM	TGF-b3	Unkn-06	001 Z60	29.81	29.65	0.228
F03	FAM	TGF-b3	Unkn-12	002 Z60	29.13	29.16	0.035
F04	FAM	TGF-b3	Unkn-12	002 Z60	29.18	29.16	0.035
F07	FAM	TGF-b3	Unkn-23	811 Z60	30.64	30.46	0.258
F08	FAM	TGF-b3	Unkn-23	811 Z60	30.28	30.46	0.258
F09	FAM	TGF-b3	Unkn-29	805 Z60	32.62	32.81	0.266
F10	FAM	TGF-b3	Unkn-29	805 Z60	32.99	32.81	0.266
F11	FAM	TGF-b3	Unkn-35	816 Z60	30.09	30.04	0.076
F12	FAM	TGF-b3	Unkn-35	816 Z60	29.98	30.04	0.076
G01	FAM	TGF-b3	Pos Ctrl-36	804 PC	28.31	28.41	0.141
G02	FAM	TGF-b3	Pos Ctrl-36	804 PC	28.51	28.41	0.141
G03	FAM	TGF-b3	NTC-37	H2O	N/A	0.00	0.000
G04	FAM	TGF-b3	NTC-37	H2O	N/A	0.00	0.000
G05	FAM	TGF-b3	NTC-38	H2O	N/A	0.00	0.000
G06	FAM	TGF-b3	NTC-38	H2O	N/A	0.00	0.000
G07	FAM	TGF-b3	Unkn-39	Pooled MC 10ng	32.77	32.61	0.229
G08	FAM	TGF-b3	Unkn-39	Pooled MC 10ng	32.45	32.61	0.229
G09	FAM	TGF-b3	Unkn-40	Pooled MC 15ng	32.86	33.08	0.309
G10	FAM	TGF-b3	Unkn-40	Pooled MC 15ng	33.30	33.08	0.309
G11	FAM	TGF-b3	Unkn-41	Pooled MC 5ng	33.23	33.57	0.483
G12	FAM	TGF-b3	Unkn-41	Pooled MC 5ng	33.91	33.57	0.483

Gene Expression

Target Names

Name	Full Name	Reference	Auto Efficiency	Efficiency
TGF-b3	TGF-b3	False	Yes	100.0%

TGF-b3 90d.pcrd

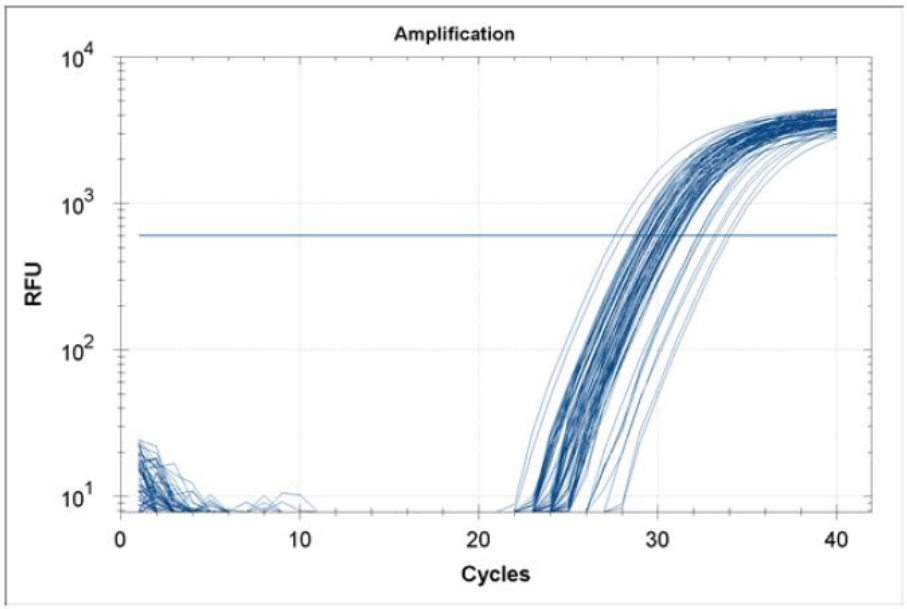
2013/08/21 01:04 PM

Run Setup

Plate Display

	1	2	3	4	5	6	7	8	9	10	11	12
A	Unk-1 TGF-b3 001 S90	Unk-1 TGF-b3 001 S90	Unk-8 TGF-b3 002 S90	Unk-8 TGF-b3 002 S90	Unk-15 TGF-b3 799 S90	Unk-15 TGF-b3 799 S90	Unk-21 TGF-b3 811 S90	Unk-21 TGF-b3 811 S90	Unk-28 TGF-b3 805 S90	Unk-28 TGF-b3 805 S90	Unk-35 TGF-b3 816 S90	Unk-35 TGF-b3 816 S90
B	Unk-2 TGF-b3 001 N90	Unk-2 TGF-b3 001 N90	Unk-9 TGF-b3 002 N90	Unk-9 TGF-b3 002 N90	Unk-16 TGF-b3 799 N90	Unk-16 TGF-b3 799 N90	Unk-22 TGF-b3 811 N90	Unk-22 TGF-b3 811 N90	Unk-29 TGF-b3 805 N90	Unk-29 TGF-b3 805 N90	Unk-36 TGF-b3 816 N90	Unk-36 TGF-b3 816 N90
C	Unk-3 TGF-b3 001 T90	Unk-3 TGF-b3 001 T90	Unk-10 TGF-b3 002 T90	Unk-10 TGF-b3 002 T90	Unk-17 TGF-b3 799 T90	Unk-17 TGF-b3 799 T90	Unk-23 TGF-b3 811 T90	Unk-23 TGF-b3 811 T90	Unk-30 TGF-b3 805 T90	Unk-30 TGF-b3 805 T90	Unk-37 TGF-b3 816 T90	Unk-37 TGF-b3 816 T90
D	Unk-4 TGF-b3 001 T+N90	Unk-4 TGF-b3 001 T+N90	Unk-11 TGF-b3 002 T+N90	Unk-11 TGF-b3 002 T+N90	Unk-18 TGF-b3 799 T+N90	Unk-18 TGF-b3 799 T+N90	Unk-24 TGF-b3 811 T+N90	Unk-24 TGF-b3 811 T+N90	Unk-31 TGF-b3 805 T+N90	Unk-31 TGF-b3 805 T+N90	Unk-38 TGF-b3 816 T+N90	Unk-38 TGF-b3 816 T+N90
E	Unk-5 TGF-b3 001 V90	Unk-5 TGF-b3 001 V90	Unk-12 TGF-b3 002 V90	Unk-12 TGF-b3 002 V90	Unk-19 TGF-b3 799 Z90	Unk-19 TGF-b3 799 Z90	Unk-25 TGF-b3 811 V90	Unk-25 TGF-b3 811 V90	Unk-32 TGF-b3 805 V90	Unk-32 TGF-b3 805 V90	Unk-39 TGF-b3 816 V90	Unk-39 TGF-b3 816 V90
F	Unk-6 TGF-b3 001 Z90	Unk-6 TGF-b3 001 Z90	Unk-13 TGF-b3 002 Z90	Unk-13 TGF-b3 002 Z90			Unk-26 TGF-b3 811 Z90	Unk-26 TGF-b3 811 Z90	Unk-33 TGF-b3 805 Z90	Unk-33 TGF-b3 805 Z90	Unk-40 TGF-b3 816 Z90	Unk-40 TGF-b3 816 Z90
G	Unk-7 TGF-b3 001 MC	Unk-7 TGF-b3 001 MC	Unk-14 TGF-b3 002 MC	Unk-14 TGF-b3 002 MC	Unk-20 TGF-b3 799 MC	Unk-20 TGF-b3 799 MC	Unk-27 TGF-b3 811 MC	Unk-27 TGF-b3 811 MC	Unk-34 TGF-b3 805 MC	Unk-34 TGF-b3 805 MC	Unk-41 TGF-b3 816 MC	Unk-41 TGF-b3 816 MC
H	Pos-42 TGF-b3 804 PC	Pos-42 TGF-b3 804 PC	NTC-43 TGF-b3 H2O	NTC-43 TGF-b3 H2O	NTC-44 TGF-b3 H2O	NTC-44 TGF-b3 H2O	Unk-45 TGF-b3 Pooled MC 15ng	Unk-45 TGF-b3 Pooled MC 15ng	Unk-46 TGF-b3 Pooled MC 10ng	Unk-46 TGF-b3 Pooled MC 10ng	Unk-47 TGF-b3 Pooled MC 5ng	Unk-47 TGF-b3 Pooled MC 5ng

Quantification



Quantification Data

Well	Fluor	Target	Content	Sample	Cq	Cq Mean	Cq Std. Dev
A01	FAM	TGF-b3	Unkn-01	001 S90	30.14	30.55	0.578
A02	FAM	TGF-b3	Unkn-01	001 S90	30.95	30.55	0.578
A03	FAM	TGF-b3	Unkn-08	002 S90	30.49	30.38	0.163
A04	FAM	TGF-b3	Unkn-08	002 S90	30.26	30.38	0.163
A05	FAM	TGF-b3	Unkn-15	799 S90	29.90	29.91	0.001
A06	FAM	TGF-b3	Unkn-15	799 S90	29.91	29.91	0.001
A07	FAM	TGF-b3	Unkn-21	811 S90	29.39	29.30	0.119
A08	FAM	TGF-b3	Unkn-21	811 S90	29.22	29.30	0.119
A09	FAM	TGF-b3	Unkn-28	805 S90	30.14	29.81	0.474
A10	FAM	TGF-b3	Unkn-28	805 S90	29.47	29.81	0.474
A11	FAM	TGF-b3	Unkn-35	816 S90	30.83	30.84	0.011
A12	FAM	TGF-b3	Unkn-35	816 S90	30.85	30.84	0.011
B01	FAM	TGF-b3	Unkn-02	001 N90	29.41	29.45	0.058
B02	FAM	TGF-b3	Unkn-02	001 N90	29.50	29.45	0.058
B03	FAM	TGF-b3	Unkn-09	002 N90	28.93	29.00	0.107
B04	FAM	TGF-b3	Unkn-09	002 N90	29.08	29.00	0.107
B05	FAM	TGF-b3	Unkn-16	799 N90	30.17	30.24	0.107
B06	FAM	TGF-b3	Unkn-16	799 N90	30.32	30.24	0.107
B07	FAM	TGF-b3	Unkn-22	811 N90	30.39	30.46	0.103
B08	FAM	TGF-b3	Unkn-22	811 N90	30.54	30.46	0.103
B09	FAM	TGF-b3	Unkn-29	805 N90	28.85	28.75	0.142
B10	FAM	TGF-b3	Unkn-29	805 N90	28.65	28.75	0.142
B11	FAM	TGF-b3	Unkn-36	816 N90	29.43	29.56	0.185
B12	FAM	TGF-b3	Unkn-36	816 N90	29.69	29.56	0.185
C01	FAM	TGF-b3	Unkn-03	001 T90	30.11	30.05	0.086
C02	FAM	TGF-b3	Unkn-03	001 T90	29.99	30.05	0.086
C03	FAM	TGF-b3	Unkn-10	002 T90	30.15	30.33	0.256
C04	FAM	TGF-b3	Unkn-10	002 T90	30.51	30.33	0.256
C05	FAM	TGF-b3	Unkn-17	799 T90	31.24	31.24	0.002
C06	FAM	TGF-b3	Unkn-17	799 T90	31.24	31.24	0.002
C07	FAM	TGF-b3	Unkn-23	811 T90	30.90	31.11	0.296
C08	FAM	TGF-b3	Unkn-23	811 T90	31.32	31.11	0.296
C09	FAM	TGF-b3	Unkn-30	805 T90	30.36	30.24	0.173
C10	FAM	TGF-b3	Unkn-30	805 T90	30.12	30.24	0.173
C11	FAM	TGF-b3	Unkn-37	816 T90	30.11	30.51	0.566
C12	FAM	TGF-b3	Unkn-37	816 T90	30.91	30.51	0.566
D01	FAM	TGF-b3	Unkn-04	001 T+N90	29.73	29.64	0.124
D02	FAM	TGF-b3	Unkn-04	001 T+N90	29.56	29.64	0.124
D03	FAM	TGF-b3	Unkn-11	002 T+N90	29.42	29.54	0.167
D04	FAM	TGF-b3	Unkn-11	002 T+N90	29.66	29.54	0.167
D05	FAM	TGF-b3	Unkn-18	799 T+N90	28.90	28.89	0.017
D06	FAM	TGF-b3	Unkn-18	799 T+N90	28.87	28.89	0.017
D07	FAM	TGF-b3	Unkn-24	811 T+N90	30.82	30.74	0.109
D08	FAM	TGF-b3	Unkn-24	811 T+N90	30.67	30.74	0.109
D09	FAM	TGF-b3	Unkn-31	805 T+N90	30.16	30.07	0.129
D10	FAM	TGF-b3	Unkn-31	805 T+N90	29.98	30.07	0.129
D11	FAM	TGF-b3	Unkn-38	816 T+N90	31.01	31.10	0.124

Well	Fluor	Target	Content	Sample	Cq	Cq Mean	Cq Std. Dev
D12	FAM	TGF-b3	Unkn-38	816 T+N90	31.19	31.10	0.124
E01	FAM	TGF-b3	Unkn-05	001 V90	29.00	28.90	0.144
E02	FAM	TGF-b3	Unkn-05	001 V90	28.80	28.90	0.144
E03	FAM	TGF-b3	Unkn-12	002 V90	29.44	29.48	0.061
E04	FAM	TGF-b3	Unkn-12	002 V90	29.53	29.48	0.061
E05	FAM	TGF-b3	Unkn-19	799 Z90	30.78	30.66	0.168
E06	FAM	TGF-b3	Unkn-19	799 Z90	30.54	30.66	0.168
E07	FAM	TGF-b3	Unkn-25	811 V90	30.80	30.76	0.054
E08	FAM	TGF-b3	Unkn-25	811 V90	30.72	30.76	0.054
E09	FAM	TGF-b3	Unkn-32	805 V90	29.18	29.23	0.059
E10	FAM	TGF-b3	Unkn-32	805 V90	29.27	29.23	0.059
E11	FAM	TGF-b3	Unkn-39	816 V90	29.63	29.63	0.005
E12	FAM	TGF-b3	Unkn-39	816 V90	29.64	29.63	0.005
F01	FAM	TGF-b3	Unkn-06	001 Z90	29.24	29.15	0.128
F02	FAM	TGF-b3	Unkn-06	001 Z90	29.06	29.15	0.128
F03	FAM	TGF-b3	Unkn-13	002 Z90	29.21	28.95	0.365
F04	FAM	TGF-b3	Unkn-13	002 Z90	28.69	28.95	0.365
F07	FAM	TGF-b3	Unkn-26	811 Z90	30.11	30.12	0.005
F08	FAM	TGF-b3	Unkn-26	811 Z90	30.12	30.12	0.005
F09	FAM	TGF-b3	Unkn-33	805 Z90	30.11	29.50	0.860
F10	FAM	TGF-b3	Unkn-33	805 Z90	28.90	29.50	0.860
F11	FAM	TGF-b3	Unkn-40	816 Z90	30.25	30.27	0.029
F12	FAM	TGF-b3	Unkn-40	816 Z90	30.29	30.27	0.029
G01	FAM	TGF-b3	Unkn-07	001 MC	31.27	31.06	0.289
G02	FAM	TGF-b3	Unkn-07	001 MC	30.86	31.06	0.289
G03	FAM	TGF-b3	Unkn-14	002 MC	30.57	30.91	0.476
G04	FAM	TGF-b3	Unkn-14	002 MC	31.24	30.91	0.476
G05	FAM	TGF-b3	Unkn-20	799 MC	32.37	32.27	0.138
G06	FAM	TGF-b3	Unkn-20	799 MC	32.18	32.27	0.138
G07	FAM	TGF-b3	Unkn-27	811 MC	30.27	29.86	0.578
G08	FAM	TGF-b3	Unkn-27	811 MC	29.45	29.86	0.578
G09	FAM	TGF-b3	Unkn-34	805 MC	30.37	30.38	0.018
G10	FAM	TGF-b3	Unkn-34	805 MC	30.40	30.38	0.018
G11	FAM	TGF-b3	Unkn-41	816 MC	30.60	30.71	0.147
G12	FAM	TGF-b3	Unkn-41	816 MC	30.81	30.71	0.147
H01	FAM	TGF-b3	Pos Ctrl-42	804 PC	28.01	27.78	0.330
H02	FAM	TGF-b3	Pos Ctrl-42	804 PC	27.54	27.78	0.330
H03	FAM	TGF-b3	NTC-43	H2O	N/A	0.00	0.000
H04	FAM	TGF-b3	NTC-43	H2O	N/A	0.00	0.000
H05	FAM	TGF-b3	NTC-44	H2O	N/A	0.00	0.000
H06	FAM	TGF-b3	NTC-44	H2O	N/A	0.00	0.000
H07	FAM	TGF-b3	Unkn-45	Pooled MC 15ng	33.25	33.18	0.097
H08	FAM	TGF-b3	Unkn-45	Pooled MC 15ng	33.11	33.18	0.097
H09	FAM	TGF-b3	Unkn-46	Pooled MC 10ng	32.22	32.34	0.162
H10	FAM	TGF-b3	Unkn-46	Pooled MC 10ng	32.45	32.34	0.162
H11	FAM	TGF-b3	Unkn-47	Pooled MC 5ng	34.02	33.89	0.183
H12	FAM	TGF-b3	Unkn-47	Pooled MC 5ng	33.77	33.89	0.183

Gene Expression

Target Names

Name	Full Name	Reference	Auto Efficiency	Efficiency
TGF-b3	TGF-b3	False	Yes	100.0%

Collagen IV 15d (2).pcrd

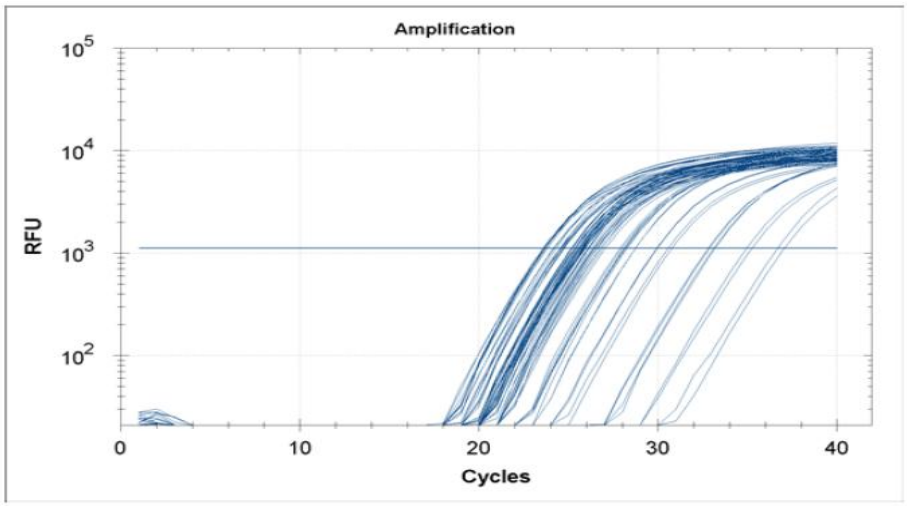
2013/08/21 01:09 PM

Run Setup

Plate Display

	1	2	3	4	5	6	7	8	9	10	11	12
A	Unk-1 Collagen IV 001 S15	Unk-1 Collagen IV 001 S15	Unk-7 Collagen IV 002 S15	Unk-7 Collagen IV 002 S15	Unk-13 Collagen IV 799 S15	Unk-13 Collagen IV 799 S15	Unk-18 Collagen IV 811 S15	Unk-18 Collagen IV 811 S15	Unk-24 Collagen IV 805 S15	Unk-24 Collagen IV 805 S15	Unk-30 Collagen IV 816 S15	Unk-30 Collagen IV 816 S15
B	Unk-2 Collagen IV 001 N15	Unk-2 Collagen IV 001 N15	Unk-8 Collagen IV 002 N15	Unk-8 Collagen IV 002 N15	Unk-14 Collagen IV 799 N15	Unk-14 Collagen IV 799 N15	Unk-19 Collagen IV 811 N15	Unk-19 Collagen IV 811 N15	Unk-25 Collagen IV 805 N15	Unk-25 Collagen IV 805 N15	Unk-31 Collagen IV 816 N15	Unk-31 Collagen IV 816 N15
C	Unk-3 Collagen IV 001 T15	Unk-3 Collagen IV 001 T15	Unk-9 Collagen IV 002 T15	Unk-9 Collagen IV 002 T15	Unk-15 Collagen IV 799 T15	Unk-15 Collagen IV 799 T15	Unk-20 Collagen IV 811 T15	Unk-20 Collagen IV 811 T15	Unk-26 Collagen IV 805 T15	Unk-26 Collagen IV 805 T15	Unk-32 Collagen IV 816 T15	Unk-32 Collagen IV 816 T15
D	Unk-4 Collagen IV 001 T+N15	Unk-4 Collagen IV 001 T+N15	Unk-10 Collagen IV 002 T+N15	Unk-10 Collagen IV 002 T+N15	Unk-16 Collagen IV 799 T+N15	Unk-16 Collagen IV 799 T+N15	Unk-21 Collagen IV 811 T+N15	Unk-21 Collagen IV 811 T+N15	Unk-27 Collagen IV 805 T+N15	Unk-27 Collagen IV 805 T+N15	Unk-33 Collagen IV 816 T+N15	Unk-33 Collagen IV 816 T+N15
E	Unk-5 Collagen IV 001 V15	Unk-5 Collagen IV 001 V15	Unk-11 Collagen IV 002 V15	Unk-11 Collagen IV 002 V15	Unk-17 Collagen IV 799 Z15	Unk-17 Collagen IV 799 Z15	Unk-22 Collagen IV 811 V15	Unk-22 Collagen IV 811 V15	Unk-28 Collagen IV 805 V15	Unk-28 Collagen IV 805 V15	Unk-34 Collagen IV 816 V15	Unk-34 Collagen IV 816 V15
F	Unk-6 Collagen IV 001 Z15	Unk-6 Collagen IV 001 Z15	Unk-12 Collagen IV 002 Z15	Unk-12 Collagen IV 002 Z15			Unk-23 Collagen IV 811 Z15	Unk-23 Collagen IV 811 Z15	Unk-29 Collagen IV 805 Z15	Unk-29 Collagen IV 805 Z15	Unk-35 Collagen IV 816 Z15	Unk-35 Collagen IV 816 Z15
G	Pos-36 Collagen IV 804 PC	Pos-36 Collagen IV 804 PC	NTC-37 Collagen IV H2O	NTC-37 Collagen IV H2O	NTC-38 Collagen IV H2O	NTC-38 Collagen IV H2O	Unk-39 Collagen IV Pooled MC 10ng	Unk-39 Collagen IV Pooled MC 10ng	Unk-40 Collagen IV Pooled MC 15ng	Unk-40 Collagen IV Pooled MC 15ng	Unk-41 Collagen IV Pooled MC 5ng	Unk-41 Collagen IV Pooled MC 5ng
H												

Quantification



Quantification Data

Well	Fluor	Target	Content	Sample	Cq	Cq Mean	Cq Std. Dev
A01	FAM	Collagen IV	Unkn-01	001 S15	25.36	25.43	0.093
A02	FAM	Collagen IV	Unkn-01	001 S15	25.50	25.43	0.093
A03	FAM	Collagen IV	Unkn-07	002 S15	24.53	24.49	0.055
A04	FAM	Collagen IV	Unkn-07	002 S15	24.45	24.49	0.055
A05	FAM	Collagen IV	Unkn-13	799 S15	23.62	23.57	0.070
A06	FAM	Collagen IV	Unkn-13	799 S15	23.52	23.57	0.070
A07	FAM	Collagen IV	Unkn-18	811 S15	30.51	30.62	0.155
A08	FAM	Collagen IV	Unkn-18	811 S15	30.73	30.62	0.155
A09	FAM	Collagen IV	Unkn-24	805 S15	34.94	35.08	0.193
A10	FAM	Collagen IV	Unkn-24	805 S15	35.21	35.08	0.193
A11	FAM	Collagen IV	Unkn-30	816 S15	25.63	25.77	0.191
A12	FAM	Collagen IV	Unkn-30	816 S15	25.90	25.77	0.191
B01	FAM	Collagen IV	Unkn-02	001 N15	25.85	25.78	0.092
B02	FAM	Collagen IV	Unkn-02	001 N15	25.72	25.78	0.092
B03	FAM	Collagen IV	Unkn-08	002 N15	25.32	25.40	0.106
B04	FAM	Collagen IV	Unkn-08	002 N15	25.47	25.40	0.106
B05	FAM	Collagen IV	Unkn-14	799 N15	24.14	24.15	0.013
B06	FAM	Collagen IV	Unkn-14	799 N15	24.16	24.15	0.013
B07	FAM	Collagen IV	Unkn-19	811 N15	24.63	24.66	0.037
B08	FAM	Collagen IV	Unkn-19	811 N15	24.69	24.66	0.037
B09	FAM	Collagen IV	Unkn-25	805 N15	29.94	29.93	0.016
B10	FAM	Collagen IV	Unkn-25	805 N15	29.92	29.93	0.016
B11	FAM	Collagen IV	Unkn-31	816 N15	27.86	27.92	0.090
B12	FAM	Collagen IV	Unkn-31	816 N15	27.98	27.92	0.090
C01	FAM	Collagen IV	Unkn-03	001 T15	25.71	25.74	0.039
C02	FAM	Collagen IV	Unkn-03	001 T15	25.77	25.74	0.039
C03	FAM	Collagen IV	Unkn-09	002 T15	25.27	25.21	0.089
C04	FAM	Collagen IV	Unkn-09	002 T15	25.14	25.21	0.089
C05	FAM	Collagen IV	Unkn-15	799 T15	25.59	25.57	0.021
C06	FAM	Collagen IV	Unkn-15	799 T15	25.56	25.57	0.021
C07	FAM	Collagen IV	Unkn-20	811 T15	23.62	23.71	0.123
C08	FAM	Collagen IV	Unkn-20	811 T15	23.79	23.71	0.123
C09	FAM	Collagen IV	Unkn-26	805 T15	28.12	28.14	0.040
C10	FAM	Collagen IV	Unkn-26	805 T15	28.17	28.14	0.040
C11	FAM	Collagen IV	Unkn-32	816 T15	26.55	26.65	0.129
C12	FAM	Collagen IV	Unkn-32	816 T15	26.74	26.65	0.129
D01	FAM	Collagen IV	Unkn-04	001 T+N15	26.34	26.35	0.025
D02	FAM	Collagen IV	Unkn-04	001 T+N15	26.37	26.35	0.025
D03	FAM	Collagen IV	Unkn-10	002 T+N15	25.14	25.16	0.025
D04	FAM	Collagen IV	Unkn-10	002 T+N15	25.17	25.16	0.025
D05	FAM	Collagen IV	Unkn-16	799 T+N15	26.10	26.08	0.022
D06	FAM	Collagen IV	Unkn-16	799 T+N15	26.07	26.08	0.022
D07	FAM	Collagen IV	Unkn-21	811 T+N15	28.69	28.69	0.003
D08	FAM	Collagen IV	Unkn-21	811 T+N15	28.69	28.69	0.003
D09	FAM	Collagen IV	Unkn-27	805 T+N15	28.09	28.17	0.107
D10	FAM	Collagen IV	Unkn-27	805 T+N15	28.24	28.17	0.107
D11	FAM	Collagen IV	Unkn-33	816 T+N15	26.11	26.17	0.085

Well	Fluor	Target	Content	Sample	Cq	Cq Mean	Cq Std. Dev
D12	FAM	Collagen IV	Unkn-33	816 T+N15	26.23	26.17	0.085
E01	FAM	Collagen IV	Unkn-05	001 V15	27.05	26.96	0.115
E02	FAM	Collagen IV	Unkn-05	001 V15	26.88	26.96	0.115
E03	FAM	Collagen IV	Unkn-11	002 V15	24.26	24.38	0.174
E04	FAM	Collagen IV	Unkn-11	002 V15	24.51	24.38	0.174
E05	FAM	Collagen IV	Unkn-17	799 Z15	23.56	23.58	0.036
E06	FAM	Collagen IV	Unkn-17	799 Z15	23.61	23.58	0.036
E07	FAM	Collagen IV	Unkn-22	811 V15	25.37	25.44	0.087
E08	FAM	Collagen IV	Unkn-22	811 V15	25.50	25.44	0.087
E09	FAM	Collagen IV	Unkn-28	805 V15	25.69	25.81	0.169
E10	FAM	Collagen IV	Unkn-28	805 V15	25.93	25.81	0.169
E11	FAM	Collagen IV	Unkn-34	816 V15	25.13	25.20	0.097
E12	FAM	Collagen IV	Unkn-34	816 V15	25.27	25.20	0.097
F01	FAM	Collagen IV	Unkn-06	001 Z15	24.58	24.65	0.095
F02	FAM	Collagen IV	Unkn-06	001 Z15	24.71	24.65	0.095
F03	FAM	Collagen IV	Unkn-12	002 Z15	25.75	25.72	0.046
F04	FAM	Collagen IV	Unkn-12	002 Z15	25.69	25.72	0.046
F07	FAM	Collagen IV	Unkn-23	811 Z15	23.62	23.66	0.053
F08	FAM	Collagen IV	Unkn-23	811 Z15	23.70	23.66	0.053
F09	FAM	Collagen IV	Unkn-29	805 Z15	25.81	25.84	0.041
F10	FAM	Collagen IV	Unkn-29	805 Z15	25.87	25.84	0.041
F11	FAM	Collagen IV	Unkn-35	816 Z15	26.39	26.56	0.238
F12	FAM	Collagen IV	Unkn-35	816 Z15	26.72	26.56	0.238
G01	FAM	Collagen IV	Pos Ctrl-36	804 PC	26.49	26.53	0.057
G02	FAM	Collagen IV	Pos Ctrl-36	804 PC	26.57	26.53	0.057
G03	FAM	Collagen IV	NTC-37	H2O	N/A	0.00	0.000
G04	FAM	Collagen IV	NTC-37	H2O	N/A	0.00	0.000
G05	FAM	Collagen IV	NTC-38	H2O	N/A	0.00	0.000
G06	FAM	Collagen IV	NTC-38	H2O	N/A	0.00	0.000
G07	FAM	Collagen IV	Unkn-39	Pooled MC 10ng	32.76	32.81	0.067
G08	FAM	Collagen IV	Unkn-39	Pooled MC 10ng	32.85	32.81	0.067
G09	FAM	Collagen IV	Unkn-40	Pooled MC 15ng	33.16	33.12	0.049
G10	FAM	Collagen IV	Unkn-40	Pooled MC 15ng	33.09	33.12	0.049
G11	FAM	Collagen IV	Unkn-41	Pooled MC 5ng	36.63	36.84	0.295
G12	FAM	Collagen IV	Unkn-41	Pooled MC 5ng	37.05	36.84	0.295

Gene Expression

Target Names

Name	Full Name	Reference	Auto Efficiency	Efficiency
Collagen IV	Collagen IV	False	Yes	100.0%

Collagen IV 60d.pcrd

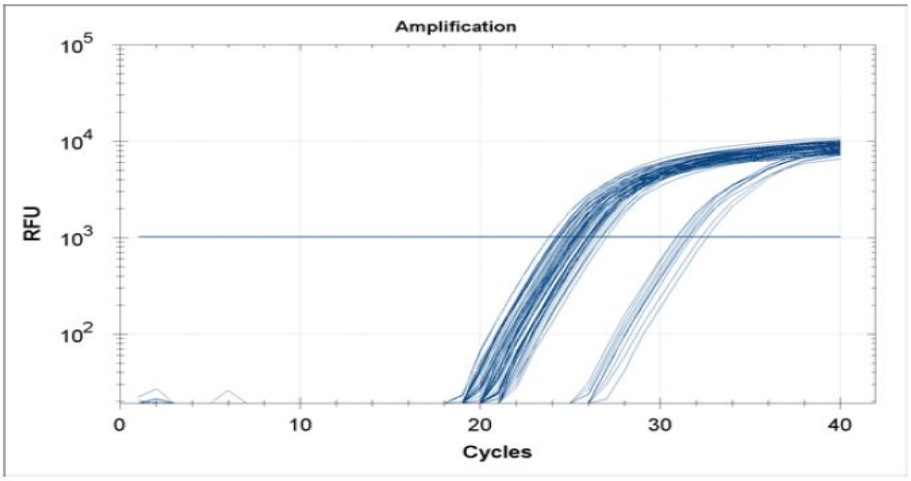
2013/08/21 01:11 PM

Run Setup

Plate Display

	1	2	3	4	5	6	7	8	9	10	11	12
A	Unk-1 Collagen IV 001 S60	Unk-1 Collagen IV 001 S60	Unk-7 Collagen IV 002 S60	Unk-7 Collagen IV 002 S60	Unk-13 Collagen IV 799 S60	Unk-13 Collagen IV 799 S60	Unk-18 Collagen IV 811 S60	Unk-18 Collagen IV 811 S60	Unk-24 Collagen IV 805 S60	Unk-24 Collagen IV 805 S60	Unk-30 Collagen IV 816 S60	Unk-30 Collagen IV 816 S60
B	Unk-2 Collagen IV 001 N60	Unk-2 Collagen IV 001 N60	Unk-8 Collagen IV 002 N60	Unk-8 Collagen IV 002 N60	Unk-14 Collagen IV 799 N60	Unk-14 Collagen IV 799 N60	Unk-19 Collagen IV 811 N60	Unk-19 Collagen IV 811 N60	Unk-25 Collagen IV 805 N60	Unk-25 Collagen IV 805 N60	Unk-31 Collagen IV 816 N60	Unk-31 Collagen IV 816 N60
C	Unk-3 Collagen IV 001 T60	Unk-3 Collagen IV 001 T60	Unk-9 Collagen IV 002 T60	Unk-9 Collagen IV 002 T60	Unk-15 Collagen IV 799 T60	Unk-15 Collagen IV 799 T60	Unk-20 Collagen IV 811 T60	Unk-20 Collagen IV 811 T60	Unk-26 Collagen IV 805 T60	Unk-26 Collagen IV 805 T60	Unk-32 Collagen IV 816 T60	Unk-32 Collagen IV 816 T60
D	Unk-4 Collagen IV 001 T+N60	Unk-4 Collagen IV 001 T+N60	Unk-10 Collagen IV 002 T+N60	Unk-10 Collagen IV 002 T+N60	Unk-16 Collagen IV 799 T+N60	Unk-16 Collagen IV 799 T+N60	Unk-21 Collagen IV 811 T+N60	Unk-21 Collagen IV 811 T+N60	Unk-27 Collagen IV 805 T+N60	Unk-27 Collagen IV 805 T+N60	Unk-33 Collagen IV 816 T+N60	Unk-33 Collagen IV 816 T+N60
E	Unk-5 Collagen IV 001 V60	Unk-5 Collagen IV 001 V60	Unk-11 Collagen IV 002 V60	Unk-11 Collagen IV 002 V60	Unk-17 Collagen IV 799 Z60	Unk-17 Collagen IV 799 Z60	Unk-22 Collagen IV 811 V60	Unk-22 Collagen IV 811 V60	Unk-28 Collagen IV 805 V60	Unk-28 Collagen IV 805 V60	Unk-34 Collagen IV 816 V60	Unk-34 Collagen IV 816 V60
F	Unk-6 Collagen IV 001 Z60	Unk-6 Collagen IV 001 Z60	Unk-12 Collagen IV 002 Z60	Unk-12 Collagen IV 002 Z60			Unk-23 Collagen IV 811 Z60	Unk-23 Collagen IV 811 Z60	Unk-29 Collagen IV 805 Z60	Unk-29 Collagen IV 805 Z60	Unk-35 Collagen IV 816 Z60	Unk-35 Collagen IV 816 Z60
G	Pos-36 Collagen IV 804 PC	Pos-36 Collagen IV 804 PC	NTC-37 Collagen IV H2O	NTC-37 Collagen IV H2O	NTC-38 Collagen IV H2O	NTC-38 Collagen IV H2O	Unk-39 Collagen IV Pooled MC 10ng	Unk-39 Collagen IV Pooled MC 10ng	Unk-40 Collagen IV Pooled MC 15ng	Unk-40 Collagen IV Pooled MC 15ng	Unk-41 Collagen IV Pooled MC 5ng	Unk-41 Collagen IV Pooled MC 5ng
H												

Quantification



Quantification Data

Well	Fluor	Target	Content	Sample	Cq	Cq Mean	Cq Std. Dev
A01	FAM	Collagen IV	Unkn-01	001 S60	25.17	25.20	0.040
A02	FAM	Collagen IV	Unkn-01	001 S60	25.23	25.20	0.040
A03	FAM	Collagen IV	Unkn-07	002 S60	24.49	24.40	0.129
A04	FAM	Collagen IV	Unkn-07	002 S60	24.31	24.40	0.129
A05	FAM	Collagen IV	Unkn-13	799 S60	24.76	24.69	0.097
A06	FAM	Collagen IV	Unkn-13	799 S60	24.63	24.69	0.097
A07	FAM	Collagen IV	Unkn-18	811 S60	25.96	26.00	0.049
A08	FAM	Collagen IV	Unkn-18	811 S60	26.03	26.00	0.049
A09	FAM	Collagen IV	Unkn-24	805 S60	25.27	25.28	0.014
A10	FAM	Collagen IV	Unkn-24	805 S60	25.29	25.28	0.014
A11	FAM	Collagen IV	Unkn-30	816 S60	26.58	26.65	0.100
A12	FAM	Collagen IV	Unkn-30	816 S60	26.72	26.65	0.100
B01	FAM	Collagen IV	Unkn-02	001 N60	24.57	24.47	0.145
B02	FAM	Collagen IV	Unkn-02	001 N60	24.37	24.47	0.145
B03	FAM	Collagen IV	Unkn-08	002 N60	25.46	25.43	0.035
B04	FAM	Collagen IV	Unkn-08	002 N60	25.41	25.43	0.035
B05	FAM	Collagen IV	Unkn-14	799 N60	26.22	26.06	0.221
B06	FAM	Collagen IV	Unkn-14	799 N60	25.90	26.06	0.221
B07	FAM	Collagen IV	Unkn-19	811 N60	25.24	25.27	0.042
B08	FAM	Collagen IV	Unkn-19	811 N60	25.30	25.27	0.042
B09	FAM	Collagen IV	Unkn-25	805 N60	25.01	24.95	0.078
B10	FAM	Collagen IV	Unkn-25	805 N60	24.90	24.95	0.078
B11	FAM	Collagen IV	Unkn-31	816 N60	26.10	26.10	0.005
B12	FAM	Collagen IV	Unkn-31	816 N60	26.11	26.10	0.005
C01	FAM	Collagen IV	Unkn-03	001 T60	25.50	25.56	0.093
C02	FAM	Collagen IV	Unkn-03	001 T60	25.63	25.56	0.093
C03	FAM	Collagen IV	Unkn-09	002 T60	25.32	25.26	0.094
C04	FAM	Collagen IV	Unkn-09	002 T60	25.19	25.26	0.094
C05	FAM	Collagen IV	Unkn-15	799 T60	23.79	23.79	0.007
C06	FAM	Collagen IV	Unkn-15	799 T60	23.80	23.79	0.007
C07	FAM	Collagen IV	Unkn-20	811 T60	25.63	25.59	0.057
C08	FAM	Collagen IV	Unkn-20	811 T60	25.55	25.59	0.057
C09	FAM	Collagen IV	Unkn-26	805 T60	27.01	26.85	0.220
C10	FAM	Collagen IV	Unkn-26	805 T60	26.70	26.85	0.220
C11	FAM	Collagen IV	Unkn-32	816 T60	25.97	26.09	0.175
C12	FAM	Collagen IV	Unkn-32	816 T60	26.22	26.09	0.175
D01	FAM	Collagen IV	Unkn-04	001 T+N60	24.35	24.33	0.022
D02	FAM	Collagen IV	Unkn-04	001 T+N60	24.32	24.33	0.022
D03	FAM	Collagen IV	Unkn-10	002 T+N60	25.16	25.08	0.117
D04	FAM	Collagen IV	Unkn-10	002 T+N60	24.99	25.08	0.117
D05	FAM	Collagen IV	Unkn-16	799 T+N60	31.72	31.48	0.340
D06	FAM	Collagen IV	Unkn-16	799 T+N60	31.24	31.48	0.340
D07	FAM	Collagen IV	Unkn-21	811 T+N60	26.22	26.24	0.022
D08	FAM	Collagen IV	Unkn-21	811 T+N60	26.25	26.24	0.022
D09	FAM	Collagen IV	Unkn-27	805 T+N60	26.15	26.15	0.004
D10	FAM	Collagen IV	Unkn-27	805 T+N60	26.14	26.15	0.004
D11	FAM	Collagen IV	Unkn-33	816 T+N60	25.95	25.99	0.054

Well	Fluor	Target	Content	Sample	Cq	Cq Mean	Cq Std. Dev
D12	FAM	Collagen IV	Unkn-33	816 T+N60	26.03	25.99	0.054
E01	FAM	Collagen IV	Unkn-05	001 V60	25.09	25.01	0.113
E02	FAM	Collagen IV	Unkn-05	001 V60	24.93	25.01	0.113
E03	FAM	Collagen IV	Unkn-11	002 V60	24.19	24.18	0.019
E04	FAM	Collagen IV	Unkn-11	002 V60	24.17	24.18	0.019
E05	FAM	Collagen IV	Unkn-17	799 Z60	24.68	25.54	1.217
E06	FAM	Collagen IV	Unkn-17	799 Z60	26.40	25.54	1.217
E07	FAM	Collagen IV	Unkn-22	811 V60	24.98	24.91	0.108
E08	FAM	Collagen IV	Unkn-22	811 V60	24.83	24.91	0.108
E09	FAM	Collagen IV	Unkn-28	805 V60	24.16	24.24	0.118
E10	FAM	Collagen IV	Unkn-28	805 V60	24.33	24.24	0.118
E11	FAM	Collagen IV	Unkn-34	816 V60	25.01	25.04	0.051
E12	FAM	Collagen IV	Unkn-34	816 V60	25.08	25.04	0.051
F01	FAM	Collagen IV	Unkn-06	001 Z60	25.71	25.71	0.009
F02	FAM	Collagen IV	Unkn-06	001 Z60	25.70	25.71	0.009
F03	FAM	Collagen IV	Unkn-12	002 Z60	25.37	25.28	0.120
F04	FAM	Collagen IV	Unkn-12	002 Z60	25.20	25.28	0.120
F07	FAM	Collagen IV	Unkn-23	811 Z60	25.90	25.92	0.029
F08	FAM	Collagen IV	Unkn-23	811 Z60	25.94	25.92	0.029
F09	FAM	Collagen IV	Unkn-29	805 Z60	32.54	32.39	0.219
F10	FAM	Collagen IV	Unkn-29	805 Z60	32.23	32.39	0.219
F11	FAM	Collagen IV	Unkn-35	816 Z60	26.01	26.06	0.068
F12	FAM	Collagen IV	Unkn-35	816 Z60	26.11	26.06	0.068
G01	FAM	Collagen IV	Pos Ctrl-36	804 PC	24.37	24.30	0.090
G02	FAM	Collagen IV	Pos Ctrl-36	804 PC	24.24	24.30	0.090
G03	FAM	Collagen IV	NTC-37	H2O	N/A	0.00	0.000
G04	FAM	Collagen IV	NTC-37	H2O	N/A	0.00	0.000
G05	FAM	Collagen IV	NTC-38	H2O	N/A	0.00	0.000
G06	FAM	Collagen IV	NTC-38	H2O	N/A	0.00	0.000
G07	FAM	Collagen IV	Unkn-39	Pooled MC 10ng	30.85	30.90	0.077
G08	FAM	Collagen IV	Unkn-39	Pooled MC 10ng	30.96	30.90	0.077
G09	FAM	Collagen IV	Unkn-40	Pooled MC 15ng	31.13	31.31	0.251
G10	FAM	Collagen IV	Unkn-40	Pooled MC 15ng	31.49	31.31	0.251
G11	FAM	Collagen IV	Unkn-41	Pooled MC 5ng	31.39	31.48	0.122
G12	FAM	Collagen IV	Unkn-41	Pooled MC 5ng	31.56	31.48	0.122

Gene Expression

Target Names

Name	Full Name	Reference	Auto Efficiency	Efficiency
Collagen IV	Collagen IV	False	Yes	100.0%

Collagen IV 90d.pcrd

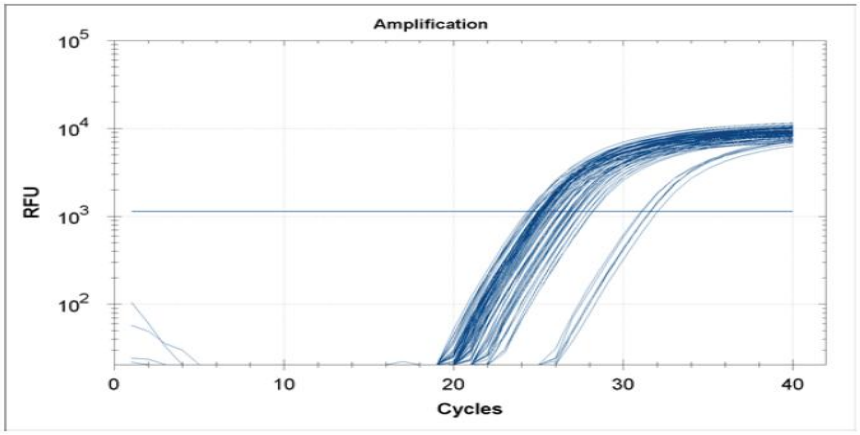
2013/08/21 01:12 PM

Run Setup

Plate Display

	1	2	3	4	5	6	7	8	9	10	11	12
A	Unk-1 Collagen IV 001 S90	Unk-1 Collagen IV 001 S90	Unk-8 Collagen IV 002 S90	Unk-8 Collagen IV 002 S90	Unk-15 Collagen IV 799 S90	Unk-15 Collagen IV 799 S90	Unk-21 Collagen IV 811 S90	Unk-21 Collagen IV 811 S90	Unk-28 Collagen IV 805 S90	Unk-28 Collagen IV 805 S90	Unk-35 Collagen IV 816 S90	Unk-35 Collagen IV 816 S90
B	Unk-2 Collagen IV 001 N90	Unk-2 Collagen IV 001 N90	Unk-9 Collagen IV 002 N90	Unk-9 Collagen IV 002 N90	Unk-16 Collagen IV 799 N90	Unk-16 Collagen IV 799 N90	Unk-22 Collagen IV 811 N90	Unk-22 Collagen IV 811 N90	Unk-29 Collagen IV 805 N90	Unk-29 Collagen IV 805 N90	Unk-36 Collagen IV 816 N90	Unk-36 Collagen IV 816 N90
C	Unk-3 Collagen IV 001 T90	Unk-3 Collagen IV 001 T90	Unk-10 Collagen IV 002 T90	Unk-10 Collagen IV 002 T90	Unk-17 Collagen IV 799 T90	Unk-17 Collagen IV 799 T90	Unk-23 Collagen IV 811 T90	Unk-23 Collagen IV 811 T90	Unk-30 Collagen IV 805 T90	Unk-30 Collagen IV 805 T90	Unk-37 Collagen IV 816 T90	Unk-37 Collagen IV 816 T90
D	Unk-4 Collagen IV 001 T+N90	Unk-4 Collagen IV 001 T+N90	Unk-11 Collagen IV 002 T+N90	Unk-11 Collagen IV 002 T+N90	Unk-18 Collagen IV 799 T+N90	Unk-18 Collagen IV 799 T+N90	Unk-24 Collagen IV 811 T+N90	Unk-24 Collagen IV 811 T+N90	Unk-31 Collagen IV 805 T+N90	Unk-31 Collagen IV 805 T+N90	Unk-38 Collagen IV 816 T+N90	Unk-38 Collagen IV 816 T+N90
E	Unk-5 Collagen IV 001 V90	Unk-5 Collagen IV 001 V90	Unk-12 Collagen IV 002 V90	Unk-12 Collagen IV 002 V90	Unk-19 Collagen IV 799 Z90	Unk-19 Collagen IV 799 Z90	Unk-25 Collagen IV 811 V90	Unk-25 Collagen IV 811 V90	Unk-32 Collagen IV 805 V90	Unk-32 Collagen IV 805 V90	Unk-39 Collagen IV 816 V90	Unk-39 Collagen IV 816 V90
F	Unk-6 Collagen IV 001 Z90	Unk-6 Collagen IV 001 Z90	Unk-13 Collagen IV 002 Z90	Unk-13 Collagen IV 002 Z90			Unk-26 Collagen IV 811 Z90	Unk-26 Collagen IV 811 Z90	Unk-33 Collagen IV 805 Z90	Unk-33 Collagen IV 805 Z90	Unk-40 Collagen IV 816 Z90	Unk-40 Collagen IV 816 Z90
G	Unk-7 Collagen IV 001 MC	Unk-7 Collagen IV 001 MC	Unk-14 Collagen IV 002 MC	Unk-14 Collagen IV 002 MC	Unk-20 Collagen IV 799 MC	Unk-20 Collagen IV 799 MC	Unk-27 Collagen IV 811 MC	Unk-27 Collagen IV 811 MC	Unk-34 Collagen IV 805 MC	Unk-34 Collagen IV 805 MC	Unk-41 Collagen IV 816 MC	Unk-41 Collagen IV 816 MC
H	Pos-42 Collagen IV 804 PC	Pos-42 Collagen IV 804 PC	NTC-43 Collagen IV H2O	NTC-43 Collagen IV H2O	NTC-44 Collagen IV H2O	NTC-44 Collagen IV H2O	Unk-45 Collagen IV Pooled MC 15ng	Unk-45 Collagen IV Pooled MC 15ng	Unk-46 Collagen IV Pooled MC 10ng	Unk-46 Collagen IV Pooled MC 10ng	Unk-47 Collagen IV Pooled MC 5ng	Unk-47 Collagen IV Pooled MC 5ng

Quantification



Quantification Data

Well	Fluor	Target	Content	Sample	Cq	Cq Mean	Cq Std. Dev
A01	FAM	Collagen IV	Unkn-01	001 S90	25.36	25.42	0.095
A02	FAM	Collagen IV	Unkn-01	001 S90	25.49	25.42	0.095
A03	FAM	Collagen IV	Unkn-08	002 S90	24.61	24.59	0.028
A04	FAM	Collagen IV	Unkn-08	002 S90	24.57	24.59	0.028
A05	FAM	Collagen IV	Unkn-15	799 S90	25.18	25.28	0.138
A06	FAM	Collagen IV	Unkn-15	799 S90	25.37	25.28	0.138
A07	FAM	Collagen IV	Unkn-21	811 S90	25.08	25.04	0.049
A08	FAM	Collagen IV	Unkn-21	811 S90	25.01	25.04	0.049
A09	FAM	Collagen IV	Unkn-28	805 S90	25.38	25.41	0.045
A10	FAM	Collagen IV	Unkn-28	805 S90	25.44	25.41	0.045
A11	FAM	Collagen IV	Unkn-35	816 S90	25.50	25.66	0.227
A12	FAM	Collagen IV	Unkn-35	816 S90	25.82	25.66	0.227
B01	FAM	Collagen IV	Unkn-02	001 N90	25.16	25.14	0.019
B02	FAM	Collagen IV	Unkn-02	001 N90	25.13	25.14	0.019
B03	FAM	Collagen IV	Unkn-09	002 N90	25.17	25.08	0.133
B04	FAM	Collagen IV	Unkn-09	002 N90	24.99	25.08	0.133
B05	FAM	Collagen IV	Unkn-16	799 N90	26.31	26.16	0.214
B06	FAM	Collagen IV	Unkn-16	799 N90	26.01	26.16	0.214
B07	FAM	Collagen IV	Unkn-22	811 N90	25.55	25.51	0.051
B08	FAM	Collagen IV	Unkn-22	811 N90	25.47	25.51	0.051
B09	FAM	Collagen IV	Unkn-29	805 N90	24.99	24.98	0.012
B10	FAM	Collagen IV	Unkn-29	805 N90	24.97	24.98	0.012
B11	FAM	Collagen IV	Unkn-36	816 N90	25.05	25.07	0.035
B12	FAM	Collagen IV	Unkn-36	816 N90	25.10	25.07	0.035
C01	FAM	Collagen IV	Unkn-03	001 T90	26.67	26.65	0.033
C02	FAM	Collagen IV	Unkn-03	001 T90	26.63	26.65	0.033
C03	FAM	Collagen IV	Unkn-10	002 T90	26.00	25.86	0.200
C04	FAM	Collagen IV	Unkn-10	002 T90	25.72	25.86	0.200
C05	FAM	Collagen IV	Unkn-17	799 T90	27.10	27.10	0.005
C06	FAM	Collagen IV	Unkn-17	799 T90	27.11	27.10	0.005
C07	FAM	Collagen IV	Unkn-23	811 T90	25.23	25.23	0.003
C08	FAM	Collagen IV	Unkn-23	811 T90	25.22	25.23	0.003
C09	FAM	Collagen IV	Unkn-30	805 T90	26.30	26.33	0.042
C10	FAM	Collagen IV	Unkn-30	805 T90	26.36	26.33	0.042
C11	FAM	Collagen IV	Unkn-37	816 T90	25.61	25.74	0.183
C12	FAM	Collagen IV	Unkn-37	816 T90	25.87	25.74	0.183
D01	FAM	Collagen IV	Unkn-04	001 T+N90	26.28	26.31	0.043
D02	FAM	Collagen IV	Unkn-04	001 T+N90	26.34	26.31	0.043
D03	FAM	Collagen IV	Unkn-11	002 T+N90	25.37	25.22	0.202
D04	FAM	Collagen IV	Unkn-11	002 T+N90	25.08	25.22	0.202
D05	FAM	Collagen IV	Unkn-18	799 T+N90	25.09	25.05	0.062
D06	FAM	Collagen IV	Unkn-18	799 T+N90	25.00	25.05	0.062
D07	FAM	Collagen IV	Unkn-24	811 T+N90	25.09	25.10	0.016
D08	FAM	Collagen IV	Unkn-24	811 T+N90	25.12	25.10	0.016
D09	FAM	Collagen IV	Unkn-31	805 T+N90	25.74	25.86	0.162
D10	FAM	Collagen IV	Unkn-31	805 T+N90	25.97	25.86	0.162
D11	FAM	Collagen IV	Unkn-38	816 T+N90	26.93	26.87	0.082

Well	Fluor	Target	Content	Sample	Cq	Cq Mean	Cq Std. Dev
D12	FAM	Collagen IV	Unkn-38	816 T+N90	26.82	26.87	0.082
E01	FAM	Collagen IV	Unkn-05	001 V90	25.34	25.29	0.075
E02	FAM	Collagen IV	Unkn-05	001 V90	25.24	25.29	0.075
E03	FAM	Collagen IV	Unkn-12	002 V90	25.28	25.28	0.000
E04	FAM	Collagen IV	Unkn-12	002 V90	25.28	25.28	0.000
E05	FAM	Collagen IV	Unkn-19	799 Z90	27.07	27.31	0.334
E06	FAM	Collagen IV	Unkn-19	799 Z90	27.55	27.31	0.334
E07	FAM	Collagen IV	Unkn-25	811 V90	25.17	25.13	0.058
E08	FAM	Collagen IV	Unkn-25	811 V90	25.09	25.13	0.058
E09	FAM	Collagen IV	Unkn-32	805 V90	24.51	24.59	0.119
E10	FAM	Collagen IV	Unkn-32	805 V90	24.67	24.59	0.119
E11	FAM	Collagen IV	Unkn-39	816 V90	25.85	25.93	0.123
E12	FAM	Collagen IV	Unkn-39	816 V90	26.02	25.93	0.123
F01	FAM	Collagen IV	Unkn-06	001 Z90	24.95	24.99	0.062
F02	FAM	Collagen IV	Unkn-06	001 Z90	25.04	24.99	0.062
F03	FAM	Collagen IV	Unkn-13	002 Z90	24.45	24.41	0.063
F04	FAM	Collagen IV	Unkn-13	002 Z90	24.36	24.41	0.063
F07	FAM	Collagen IV	Unkn-26	811 Z90	25.17	25.19	0.023
F08	FAM	Collagen IV	Unkn-26	811 Z90	25.21	25.19	0.023
F09	FAM	Collagen IV	Unkn-33	805 Z90	24.89	24.94	0.064
F10	FAM	Collagen IV	Unkn-33	805 Z90	24.98	24.94	0.064
F11	FAM	Collagen IV	Unkn-40	816 Z90	26.21	26.25	0.069
F12	FAM	Collagen IV	Unkn-40	816 Z90	26.30	26.25	0.069
G01	FAM	Collagen IV	Unkn-07	001 MC	28.12	28.14	0.034
G02	FAM	Collagen IV	Unkn-07	001 MC	28.17	28.14	0.034
G03	FAM	Collagen IV	Unkn-14	002 MC	27.55	27.51	0.057
G04	FAM	Collagen IV	Unkn-14	002 MC	27.47	27.51	0.057
G05	FAM	Collagen IV	Unkn-20	799 MC	27.86	27.87	0.009
G06	FAM	Collagen IV	Unkn-20	799 MC	27.87	27.87	0.009
G07	FAM	Collagen IV	Unkn-27	811 MC	27.18	27.02	0.225
G08	FAM	Collagen IV	Unkn-27	811 MC	26.86	27.02	0.225
G09	FAM	Collagen IV	Unkn-34	805 MC	26.72	26.74	0.037
G10	FAM	Collagen IV	Unkn-34	805 MC	26.77	26.74	0.037
G11	FAM	Collagen IV	Unkn-41	816 MC	27.13	27.19	0.082
G12	FAM	Collagen IV	Unkn-41	816 MC	27.25	27.19	0.082
H01	FAM	Collagen IV	Pos Ctrl-42	804 PC	24.68	24.48	0.277
H02	FAM	Collagen IV	Pos Ctrl-42	804 PC	24.29	24.48	0.277
H03	FAM	Collagen IV	NTC-43	H2O	N/A	0.00	0.000
H04	FAM	Collagen IV	NTC-43	H2O	N/A	0.00	0.000
H05	FAM	Collagen IV	NTC-44	H2O	N/A	0.00	0.000
H06	FAM	Collagen IV	NTC-44	H2O	N/A	0.00	0.000
H07	FAM	Collagen IV	Unkn-45	Pooled MC 15ng	31.10	31.06	0.050
H08	FAM	Collagen IV	Unkn-45	Pooled MC 15ng	31.02	31.06	0.050
H09	FAM	Collagen IV	Unkn-46	Pooled MC 10ng	31.48	31.51	0.049
H10	FAM	Collagen IV	Unkn-46	Pooled MC 10ng	31.55	31.51	0.049
H11	FAM	Collagen IV	Unkn-47	Pooled MC 5ng	31.54	31.77	0.330
H12	FAM	Collagen IV	Unkn-47	Pooled MC 5ng	32.01	31.77	0.330

Gene Expression

Target Names

Name	Full Name	Reference	Auto Efficiency	Efficiency
Collagen IV	Collagen IV	False	Yes	100.0%

Noggin 15d.pcrd

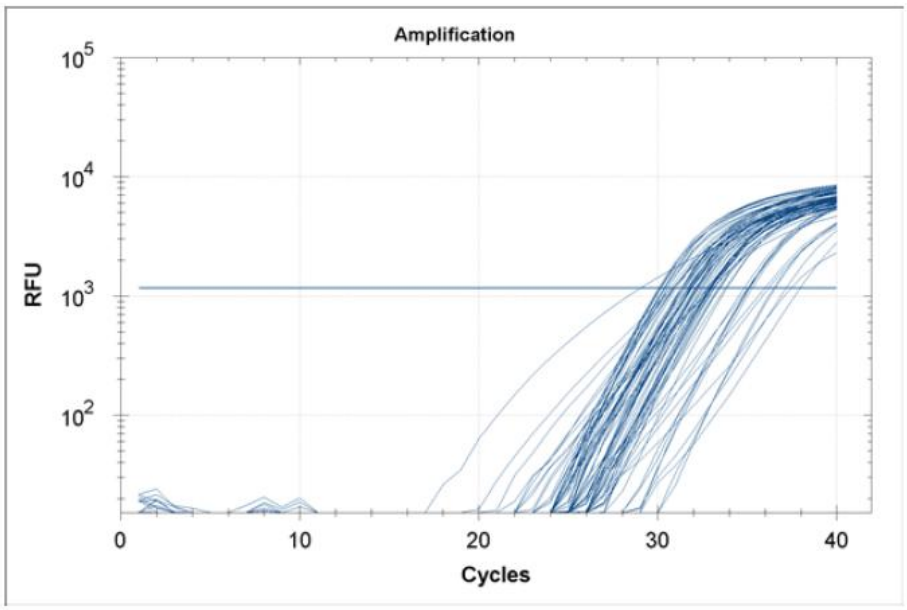
2013/08/21 01:16 PM

Run Setup

Plate Display

	1	2	3	4	5	6	7	8	9	10	11	12
A	Unk-1 Noggin 001 S15	Unk-1 Noggin 001 S15	Unk-7 Noggin 002 S15	Unk-7 Noggin 002 S15	Unk-13 Noggin 799 S15	Unk-13 Noggin 799 S15	Unk-18 Noggin 811 S15	Unk-18 Noggin 811 S15	Unk-24 Noggin 805 S15	Unk-24 Noggin 805 S15	Unk-30 Noggin 816 S15	Unk-30 Noggin 816 S15
B	Unk-2 Noggin 001 N15	Unk-2 Noggin 001 N15	Unk-8 Noggin 002 N15	Unk-8 Noggin 002 N15	Unk-14 Noggin 799 N15	Unk-14 Noggin 799 N15	Unk-19 Noggin 811 N15	Unk-19 Noggin 811 N15	Unk-25 Noggin 805 N15	Unk-25 Noggin 805 N15	Unk-31 Noggin 816 N15	Unk-31 Noggin 816 N15
C	Unk-3 Noggin 001 T15	Unk-3 Noggin 001 T15	Unk-9 Noggin 002 T15	Unk-9 Noggin 002 T15	Unk-15 Noggin 799 T15	Unk-15 Noggin 799 T15	Unk-20 Noggin 811 T15	Unk-20 Noggin 811 T15	Unk-26 Noggin 805 T15	Unk-26 Noggin 805 T15	Unk-32 Noggin 816 T15	Unk-32 Noggin 816 T15
D	Unk-4 Noggin 001 T+N15	Unk-4 Noggin 001 T+N15	Unk-10 Noggin 002 T+N15	Unk-10 Noggin 002 T+N15	Unk-16 Noggin 799 T+N15	Unk-16 Noggin 799 T+N15	Unk-21 Noggin 811 T+N15	Unk-21 Noggin 811 T+N15	Unk-27 Noggin 805 T+N15	Unk-27 Noggin 805 T+N15	Unk-33 Noggin 816 T+N15	Unk-33 Noggin 816 T+N15
E	Unk-5 Noggin 001 V15	Unk-5 Noggin 001 V15	Unk-11 Noggin 002 V15	Unk-11 Noggin 002 V15	Unk-17 Noggin 799 Z15	Unk-17 Noggin 799 Z15	Unk-22 Noggin 811 V15	Unk-22 Noggin 811 V15	Unk-28 Noggin 805 V15	Unk-28 Noggin 805 V15	Unk-34 Noggin 816 V15	Unk-34 Noggin 816 V15
F	Unk-6 Noggin 001 Z15	Unk-6 Noggin 001 Z15	Unk-12 Noggin 002 Z15	Unk-12 Noggin 002 Z15			Unk-23 Noggin 811 Z15	Unk-23 Noggin 811 Z15	Unk-29 Noggin 805 Z15	Unk-29 Noggin 805 Z15	Unk-35 Noggin 816 Z15	Unk-35 Noggin 816 Z15
G	Pos-36 Noggin 804 PC	Pos-36 Noggin 804 PC	NTC-37 Noggin H2O	NTC-37 Noggin H2O	NTC-38 Noggin H2O	NTC-38 Noggin H2O	Unk-39 Noggin Pooled MC 10ng	Unk-39 Noggin Pooled MC 10ng	Unk-40 Noggin Pooled MC 15ng	Unk-40 Noggin Pooled MC 15ng	Unk-41 Noggin Pooled MC 5ng	Unk-41 Noggin Pooled MC 5ng
H												

Quantification



Quantification Data

Well	Fluor	Target	Content	Sample	Cq	Cq Mean	Cq Std. Dev
A01	FAM	Noggin	Unkn-01	001 S15	32.33	32.41	0.115
A02	FAM	Noggin	Unkn-01	001 S15	32.50	32.41	0.115
A03	FAM	Noggin	Unkn-07	002 S15	32.24	32.01	0.329
A04	FAM	Noggin	Unkn-07	002 S15	31.77	32.01	0.329
A05	FAM	Noggin	Unkn-13	799 S15	30.90	30.70	0.282
A06	FAM	Noggin	Unkn-13	799 S15	30.50	30.70	0.282
A07	FAM	Noggin	Unkn-18	811 S15	36.16	36.08	0.125
A08	FAM	Noggin	Unkn-18	811 S15	35.99	36.08	0.125
A09	FAM	Noggin	Unkn-24	805 S15	37.94	37.54	0.561
A10	FAM	Noggin	Unkn-24	805 S15	37.14	37.54	0.561
A11	FAM	Noggin	Unkn-30	816 S15	32.66	32.73	0.101
A12	FAM	Noggin	Unkn-30	816 S15	32.80	32.73	0.101
B01	FAM	Noggin	Unkn-02	001 N15	30.88	30.95	0.109
B02	FAM	Noggin	Unkn-02	001 N15	31.03	30.95	0.109
B03	FAM	Noggin	Unkn-08	002 N15	32.16	32.02	0.191
B04	FAM	Noggin	Unkn-08	002 N15	31.89	32.02	0.191
B05	FAM	Noggin	Unkn-14	799 N15	32.87	32.94	0.097
B06	FAM	Noggin	Unkn-14	799 N15	33.01	32.94	0.097
B07	FAM	Noggin	Unkn-19	811 N15	33.13	33.48	0.488
B08	FAM	Noggin	Unkn-19	811 N15	33.82	33.48	0.488
B09	FAM	Noggin	Unkn-25	805 N15	31.82	31.75	0.103
B10	FAM	Noggin	Unkn-25	805 N15	31.68	31.75	0.103
B11	FAM	Noggin	Unkn-31	816 N15	36.51	36.46	0.070
B12	FAM	Noggin	Unkn-31	816 N15	36.41	36.46	0.070
C01	FAM	Noggin	Unkn-03	001 T15	33.30	33.34	0.051
C02	FAM	Noggin	Unkn-03	001 T15	33.38	33.34	0.051
C03	FAM	Noggin	Unkn-09	002 T15	31.65	31.48	0.233
C04	FAM	Noggin	Unkn-09	002 T15	31.32	31.48	0.233
C05	FAM	Noggin	Unkn-15	799 T15	30.68	30.78	0.135
C06	FAM	Noggin	Unkn-15	799 T15	30.87	30.78	0.135
C07	FAM	Noggin	Unkn-20	811 T15	30.38	30.44	0.091
C08	FAM	Noggin	Unkn-20	811 T15	30.51	30.44	0.091
C09	FAM	Noggin	Unkn-26	805 T15	32.98	32.96	0.029
C10	FAM	Noggin	Unkn-26	805 T15	32.94	32.96	0.029
C11	FAM	Noggin	Unkn-32	816 T15	35.23	35.13	0.137
C12	FAM	Noggin	Unkn-32	816 T15	35.04	35.13	0.137
D01	FAM	Noggin	Unkn-04	001 T+N15	32.78	32.88	0.135
D02	FAM	Noggin	Unkn-04	001 T+N15	32.97	32.88	0.135
D03	FAM	Noggin	Unkn-10	002 T+N15	30.08	30.10	0.031
D04	FAM	Noggin	Unkn-10	002 T+N15	30.12	30.10	0.031
D05	FAM	Noggin	Unkn-16	799 T+N15	31.46	31.53	0.096
D06	FAM	Noggin	Unkn-16	799 T+N15	31.59	31.53	0.096
D07	FAM	Noggin	Unkn-21	811 T+N15	34.79	34.91	0.171
D08	FAM	Noggin	Unkn-21	811 T+N15	35.03	34.91	0.171
D09	FAM	Noggin	Unkn-27	805 T+N15	33.12	33.43	0.437
D10	FAM	Noggin	Unkn-27	805 T+N15	33.74	33.43	0.437
D11	FAM	Noggin	Unkn-33	816 T+N15	31.31	31.27	0.052

Well	Fluor	Target	Content	Sample	Cq	Cq Mean	Cq Std. Dev
D12	FAM	Noggin	Unkn-33	816 T+N15	31.24	31.27	0.052
E01	FAM	Noggin	Unkn-05	001 V15	32.05	31.68	0.521
E02	FAM	Noggin	Unkn-05	001 V15	31.31	31.68	0.521
E03	FAM	Noggin	Unkn-11	002 V15	31.74	31.52	0.310
E04	FAM	Noggin	Unkn-11	002 V15	31.30	31.52	0.310
E05	FAM	Noggin	Unkn-17	799 Z15	30.32	30.30	0.026
E06	FAM	Noggin	Unkn-17	799 Z15	30.28	30.30	0.026
E07	FAM	Noggin	Unkn-22	811 V15	31.83	31.98	0.213
E08	FAM	Noggin	Unkn-22	811 V15	32.13	31.98	0.213
E09	FAM	Noggin	Unkn-28	805 V15	35.11	35.09	0.015
E10	FAM	Noggin	Unkn-28	805 V15	35.08	35.09	0.015
E11	FAM	Noggin	Unkn-34	816 V15	32.41	32.76	0.498
E12	FAM	Noggin	Unkn-34	816 V15	33.12	32.76	0.498
F01	FAM	Noggin	Unkn-06	001 Z15	31.45	31.42	0.040
F02	FAM	Noggin	Unkn-06	001 Z15	31.39	31.42	0.040
F03	FAM	Noggin	Unkn-12	002 Z15	31.90	31.90	0.004
F04	FAM	Noggin	Unkn-12	002 Z15	31.90	31.90	0.004
F07	FAM	Noggin	Unkn-23	811 Z15	30.15	30.09	0.087
F08	FAM	Noggin	Unkn-23	811 Z15	30.03	30.09	0.087
F09	FAM	Noggin	Unkn-29	805 Z15	32.09	32.14	0.073
F10	FAM	Noggin	Unkn-29	805 Z15	32.19	32.14	0.073
F11	FAM	Noggin	Unkn-35	816 Z15	32.92	33.17	0.356
F12	FAM	Noggin	Unkn-35	816 Z15	33.42	33.17	0.356
G01	FAM	Noggin	Pos Ctrl-36	804 PC	30.86	30.81	0.070
G02	FAM	Noggin	Pos Ctrl-36	804 PC	30.76	30.81	0.070
G03	FAM	Noggin	NTC-37	H2O	N/A	0.00	0.000
G04	FAM	Noggin	NTC-37	H2O	N/A	0.00	0.000
G05	FAM	Noggin	NTC-38	H2O	N/A	0.00	0.000
G06	FAM	Noggin	NTC-38	H2O	N/A	0.00	0.000
G07	FAM	Noggin	Unkn-39	Pooled MC 10ng	32.85	32.77	0.118
G08	FAM	Noggin	Unkn-39	Pooled MC 10ng	32.69	32.77	0.118
G09	FAM	Noggin	Unkn-40	Pooled MC 15ng	32.84	32.94	0.148
G10	FAM	Noggin	Unkn-40	Pooled MC 15ng	33.05	32.94	0.148
G11	FAM	Noggin	Unkn-41	Pooled MC 5ng	29.03	33.23	5.932
G12	FAM	Noggin	Unkn-41	Pooled MC 5ng	37.42	33.23	5.932

Gene Expression

Target Names

Name	Full Name	Reference	Auto Efficiency	Efficiency
Noggin	Noggin	False	Yes	100.0%

Noggin 60d.pcrd

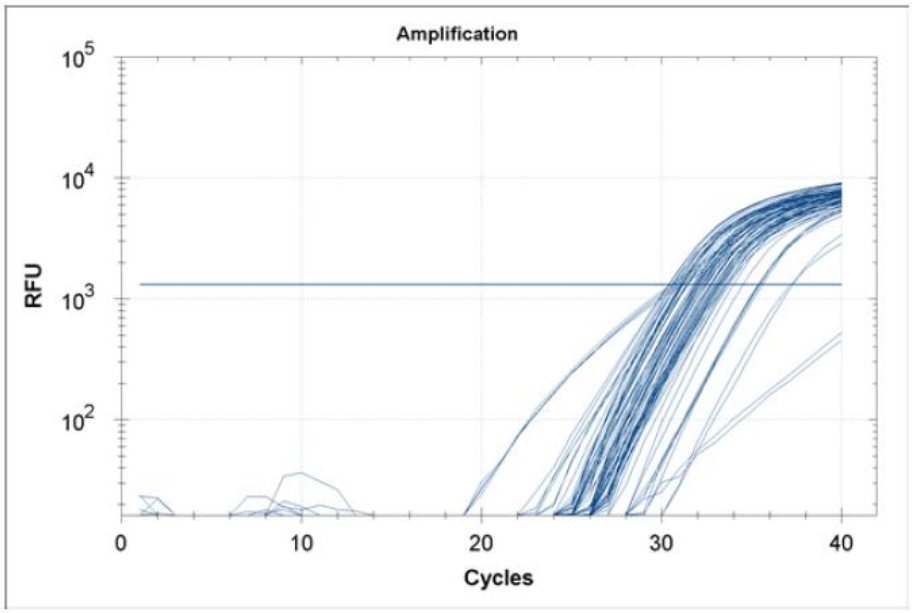
2013/08/21 01:17 PM

Run Setup

Plate Display

	1	2	3	4	5	6	7	8	9	10	11	12
A	Unk-1 Noggin 001 S60	Unk-1 Noggin 001 S60	Unk-7 Noggin 002 S60	Unk-7 Noggin 002 S60	Unk-13 Noggin 799 S60	Unk-13 Noggin 799 S60	Unk-18 Noggin 811 S60	Unk-18 Noggin 811 S60	Unk-24 Noggin 805 S60	Unk-24 Noggin 805 S60	Unk-30 Noggin 816 S60	Unk-30 Noggin 816 S60
B	Unk-2 Noggin 001 N60	Unk-2 Noggin 001 N60	Unk-8 Noggin 002 N60	Unk-8 Noggin 002 N60	Unk-14 Noggin 799 N60	Unk-14 Noggin 799 N60	Unk-19 Noggin 811 N60	Unk-19 Noggin 811 N60	Unk-25 Noggin 805 N60	Unk-25 Noggin 805 N60	Unk-31 Noggin 816 N60	Unk-31 Noggin 816 N60
C	Unk-3 Noggin 001 T60	Unk-3 Noggin 001 T60	Unk-9 Noggin 002 T60	Unk-9 Noggin 002 T60	Unk-15 Noggin 799 T60	Unk-15 Noggin 799 T60	Unk-20 Noggin 811 T60	Unk-20 Noggin 811 T60	Unk-26 Noggin 805 T60	Unk-26 Noggin 805 T60	Unk-32 Noggin 816 T60	Unk-32 Noggin 816 T60
D	Unk-4 Noggin 001 T+N60	Unk-4 Noggin 001 T+N60	Unk-10 Noggin 002 T+N60	Unk-10 Noggin 002 T+N60	Unk-16 Noggin 799 T+N60	Unk-16 Noggin 799 T+N60	Unk-21 Noggin 811 T+N60	Unk-21 Noggin 811 T+N60	Unk-27 Noggin 805 T+N60	Unk-27 Noggin 805 T+N60	Unk-33 Noggin 816 T+N60	Unk-33 Noggin 816 T+N60
E	Unk-5 Noggin 001 V60	Unk-5 Noggin 001 V60	Unk-11 Noggin 002 V60	Unk-11 Noggin 002 V60	Unk-17 Noggin 799 Z60	Unk-17 Noggin 799 Z60	Unk-22 Noggin 811 V60	Unk-22 Noggin 811 V60	Unk-28 Noggin 805 V60	Unk-28 Noggin 805 V60	Unk-34 Noggin 816 V60	Unk-34 Noggin 816 V60
F	Unk-6 Noggin 001 Z60	Unk-6 Noggin 001 Z60	Unk-12 Noggin 002 Z60	Unk-12 Noggin 002 Z60			Unk-23 Noggin 811 Z60	Unk-23 Noggin 811 Z60	Unk-29 Noggin 805 Z60	Unk-29 Noggin 805 Z60	Unk-35 Noggin 816 Z60	Unk-35 Noggin 816 Z60
G	Pos-36 Noggin 804 PC	Pos-36 Noggin 804 PC	NTC-37 Noggin H2O	NTC-37 Noggin H2O	NTC-38 Noggin H2O	NTC-38 Noggin H2O	Unk-39 Noggin Pooled MC 10ng	Unk-39 Noggin Pooled MC 10ng	Unk-40 Noggin Pooled MC 15ng	Unk-40 Noggin Pooled MC 15ng	Unk-41 Noggin Pooled MC 5ng	Unk-41 Noggin Pooled MC 5ng
H												

Quantification



Quantification Data

Well	Fluor	Target	Content	Sample	Cq	Cq Mean	Cq Std. Dev
A01	FAM	Noggin	Unkn-01	001 S60	33.27	33.43	0.228
A02	FAM	Noggin	Unkn-01	001 S60	33.59	33.43	0.228
A03	FAM	Noggin	Unkn-07	002 S60	32.41	32.52	0.151
A04	FAM	Noggin	Unkn-07	002 S60	32.62	32.52	0.151
A05	FAM	Noggin	Unkn-13	799 S60	31.42	31.27	0.208
A06	FAM	Noggin	Unkn-13	799 S60	31.12	31.27	0.208
A07	FAM	Noggin	Unkn-18	811 S60	31.32	31.57	0.343
A08	FAM	Noggin	Unkn-18	811 S60	31.81	31.57	0.343
A09	FAM	Noggin	Unkn-24	805 S60	32.36	32.20	0.226
A10	FAM	Noggin	Unkn-24	805 S60	32.04	32.20	0.226
A11	FAM	Noggin	Unkn-30	816 S60	32.63	32.82	0.259
A12	FAM	Noggin	Unkn-30	816 S60	33.00	32.82	0.259
B01	FAM	Noggin	Unkn-02	001 N60	31.91	31.80	0.156
B02	FAM	Noggin	Unkn-02	001 N60	31.69	31.80	0.156
B03	FAM	Noggin	Unkn-08	002 N60	35.32	36.28	1.357
B04	FAM	Noggin	Unkn-08	002 N60	37.24	36.28	1.357
B05	FAM	Noggin	Unkn-14	799 N60	30.92	31.17	0.359
B06	FAM	Noggin	Unkn-14	799 N60	31.42	31.17	0.359
B07	FAM	Noggin	Unkn-19	811 N60	31.02	31.35	0.466
B08	FAM	Noggin	Unkn-19	811 N60	31.68	31.35	0.466
B09	FAM	Noggin	Unkn-25	805 N60	30.73	30.66	0.105
B10	FAM	Noggin	Unkn-25	805 N60	30.58	30.66	0.105
B11	FAM	Noggin	Unkn-31	816 N60	31.35	31.52	0.240
B12	FAM	Noggin	Unkn-31	816 N60	31.69	31.52	0.240
C01	FAM	Noggin	Unkn-03	001 T60	32.88	33.18	0.425
C02	FAM	Noggin	Unkn-03	001 T60	33.48	33.18	0.425
C03	FAM	Noggin	Unkn-09	002 T60	33.09	32.78	0.436
C04	FAM	Noggin	Unkn-09	002 T60	32.47	32.78	0.436
C05	FAM	Noggin	Unkn-15	799 T60	31.09	31.12	0.039
C06	FAM	Noggin	Unkn-15	799 T60	31.14	31.12	0.039
C07	FAM	Noggin	Unkn-20	811 T60	33.01	32.89	0.180
C08	FAM	Noggin	Unkn-20	811 T60	32.76	32.89	0.180
C09	FAM	Noggin	Unkn-26	805 T60	35.54	35.45	0.132
C10	FAM	Noggin	Unkn-26	805 T60	35.36	35.45	0.132
C11	FAM	Noggin	Unkn-32	816 T60	35.34	34.90	0.617
C12	FAM	Noggin	Unkn-32	816 T60	34.47	34.90	0.617
D01	FAM	Noggin	Unkn-04	001 T+N60	33.14	33.24	0.143
D02	FAM	Noggin	Unkn-04	001 T+N60	33.34	33.24	0.143
D03	FAM	Noggin	Unkn-10	002 T+N60	33.72	33.47	0.346
D04	FAM	Noggin	Unkn-10	002 T+N60	33.23	33.47	0.346
D05	FAM	Noggin	Unkn-16	799 T+N60	30.66	30.57	0.122
D06	FAM	Noggin	Unkn-16	799 T+N60	30.49	30.57	0.122
D07	FAM	Noggin	Unkn-21	811 T+N60	32.28	32.18	0.141
D08	FAM	Noggin	Unkn-21	811 T+N60	32.08	32.18	0.141
D09	FAM	Noggin	Unkn-27	805 T+N60	32.26	34.71	3.465
D10	FAM	Noggin	Unkn-27	805 T+N60	37.16	34.71	3.465
D11	FAM	Noggin	Unkn-33	816 T+N60	33.58	33.35	0.326

Well	Fluor	Target	Content	Sample	Cq	Cq Mean	Cq Std. Dev
D12	FAM	Noggin	Unkn-33	816 T+N60	33.12	33.35	0.326
E01	FAM	Noggin	Unkn-05	001 V60	31.98	32.07	0.127
E02	FAM	Noggin	Unkn-05	001 V60	32.16	32.07	0.127
E03	FAM	Noggin	Unkn-11	002 V60	31.06	31.46	0.566
E04	FAM	Noggin	Unkn-11	002 V60	31.86	31.46	0.566
E05	FAM	Noggin	Unkn-17	799 Z60	30.33	30.35	0.028
E06	FAM	Noggin	Unkn-17	799 Z60	30.37	30.35	0.028
E07	FAM	Noggin	Unkn-22	811 V60	N/A	0.00	0.000
E08	FAM	Noggin	Unkn-22	811 V60	32.63	32.63	0.000
E09	FAM	Noggin	Unkn-28	805 V60	31.91	32.03	0.174
E10	FAM	Noggin	Unkn-28	805 V60	32.15	32.03	0.174
E11	FAM	Noggin	Unkn-34	816 V60	32.70	32.93	0.322
E12	FAM	Noggin	Unkn-34	816 V60	33.15	32.93	0.322
F01	FAM	Noggin	Unkn-06	001 Z60	31.69	31.95	0.361
F02	FAM	Noggin	Unkn-06	001 Z60	32.20	31.95	0.361
F03	FAM	Noggin	Unkn-12	002 Z60	31.13	31.16	0.051
F04	FAM	Noggin	Unkn-12	002 Z60	31.20	31.16	0.051
F07	FAM	Noggin	Unkn-23	811 Z60	30.84	30.84	0.000
F08	FAM	Noggin	Unkn-23	811 Z60	30.84	30.84	0.000
F09	FAM	Noggin	Unkn-29	805 Z60	33.98	34.71	1.031
F10	FAM	Noggin	Unkn-29	805 Z60	35.44	34.71	1.031
F11	FAM	Noggin	Unkn-35	816 Z60	32.06	32.22	0.222
F12	FAM	Noggin	Unkn-35	816 Z60	32.38	32.22	0.222
G01	FAM	Noggin	Pos Ctrl-36	804 PC	30.62	30.56	0.091
G02	FAM	Noggin	Pos Ctrl-36	804 PC	30.49	30.56	0.091
G03	FAM	Noggin	NTC-37	H2O	N/A	0.00	0.000
G04	FAM	Noggin	NTC-37	H2O	N/A	0.00	0.000
G05	FAM	Noggin	NTC-38	H2O	N/A	0.00	0.000
G06	FAM	Noggin	NTC-38	H2O	N/A	0.00	0.000
G07	FAM	Noggin	Unkn-39	Pooled MC 10ng	32.98	32.84	0.195
G08	FAM	Noggin	Unkn-39	Pooled MC 10ng	32.71	32.84	0.195
G09	FAM	Noggin	Unkn-40	Pooled MC 15ng	33.26	33.36	0.140
G10	FAM	Noggin	Unkn-40	Pooled MC 15ng	33.46	33.36	0.140
G11	FAM	Noggin	Unkn-41	Pooled MC 5ng	30.90	31.03	0.191
G12	FAM	Noggin	Unkn-41	Pooled MC 5ng	31.17	31.03	0.191

Gene Expression

Target Names

Name	Full Name	Reference	Auto Efficiency	Efficiency
Noggin	Noggin	False	Yes	100.0%

Noggin 90d.pcrd

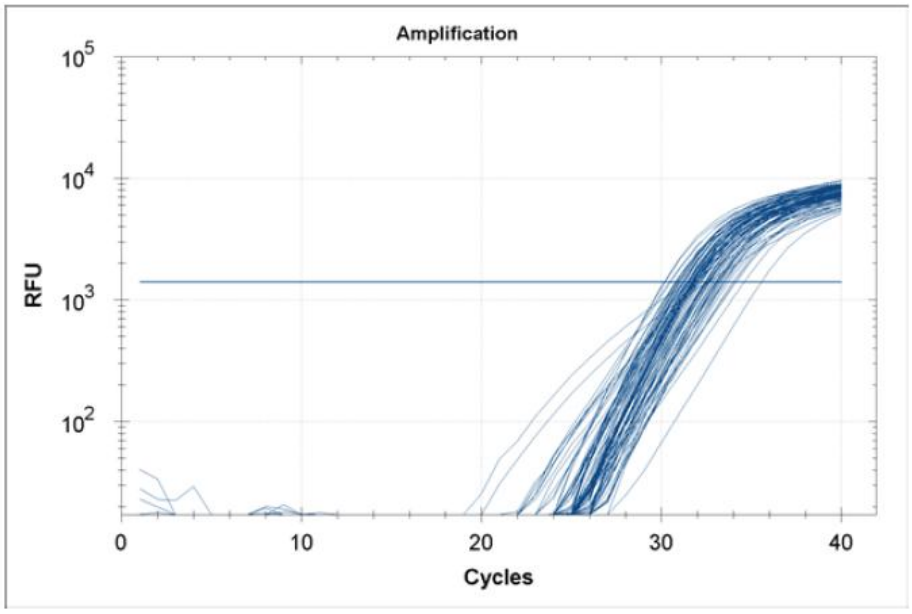
2013/08/21 01:17 PM

Run Setup

Plate Display

	1	2	3	4	5	6	7	8	9	10	11	12
A	Unk-1 Noggin 001 S90	Unk-1 Noggin 001 S90	Unk-8 Noggin 002 S90	Unk-8 Noggin 002 S90	Unk-15 Noggin 799 S90	Unk-15 Noggin 799 S90	Unk-21 Noggin 811 S90	Unk-21 Noggin 811 S90	Unk-28 Noggin 805 S90	Unk-28 Noggin 805 S90	Unk-35 Noggin 816 S90	Unk-35 Noggin 816 S90
B	Unk-2 Noggin 001 N90	Unk-2 Noggin 001 N90	Unk-9 Noggin 002 N90	Unk-9 Noggin 002 N90	Unk-16 Noggin 799 N90	Unk-16 Noggin 799 N90	Unk-22 Noggin 811 N90	Unk-22 Noggin 811 N90	Unk-29 Noggin 805 N90	Unk-29 Noggin 805 N90	Unk-36 Noggin 816 N90	Unk-36 Noggin 816 N90
C	Unk-3 Noggin 001 T90	Unk-3 Noggin 001 T90	Unk-10 Noggin 002 T90	Unk-10 Noggin 002 T90	Unk-17 Noggin 799 T90	Unk-17 Noggin 799 T90	Unk-23 Noggin 811 T90	Unk-23 Noggin 811 T90	Unk-30 Noggin 805 T90	Unk-30 Noggin 805 T90	Unk-37 Noggin 816 T90	Unk-37 Noggin 816 T90
D	Unk-4 Noggin 001 T+N90	Unk-4 Noggin 001 T+N90	Unk-11 Noggin 002 T+N90	Unk-11 Noggin 002 T+N90	Unk-18 Noggin 799 T+N90	Unk-18 Noggin 799 T+N90	Unk-24 Noggin 811 T+N90	Unk-24 Noggin 811 T+N90	Unk-31 Noggin 805 T+N90	Unk-31 Noggin 805 T+N90	Unk-38 Noggin 816 T+N90	Unk-38 Noggin 816 T+N90
E	Unk-5 Noggin 001 V90	Unk-5 Noggin 001 V90	Unk-12 Noggin 002 V90	Unk-12 Noggin 002 V90	Unk-19 Noggin 799 Z90	Unk-19 Noggin 799 Z90	Unk-25 Noggin 811 V90	Unk-25 Noggin 811 V90	Unk-32 Noggin 805 V90	Unk-32 Noggin 805 V90	Unk-39 Noggin 816 V90	Unk-39 Noggin 816 V90
F	Unk-6 Noggin 001 Z90	Unk-6 Noggin 001 Z90	Unk-13 Noggin 002 Z90	Unk-13 Noggin 002 Z90			Unk-26 Noggin 811 Z90	Unk-26 Noggin 811 Z90	Unk-33 Noggin 805 Z90	Unk-33 Noggin 805 Z90	Unk-40 Noggin 816 Z90	Unk-40 Noggin 816 Z90
G	Unk-7 Noggin 001 MC	Unk-7 Noggin 001 MC	Unk-14 Noggin 002 MC	Unk-14 Noggin 002 MC	Unk-20 Noggin 799 MC	Unk-20 Noggin 799 MC	Unk-27 Noggin 811 MC	Unk-27 Noggin 811 MC	Unk-34 Noggin 805 MC	Unk-34 Noggin 805 MC	Unk-41 Noggin 816 MC	Unk-41 Noggin 816 MC
H	Pos-42 Noggin 804 PC	Pos-42 Noggin 804 PC	NTC-43 Noggin H2O	NTC-43 Noggin H2O	NTC-44 Noggin H2O	NTC-44 Noggin H2O	Unk-45 Noggin Pooled MC 15ng	Unk-45 Noggin Pooled MC 15ng	Unk-46 Noggin Pooled MC 10ng	Unk-46 Noggin Pooled MC 10ng	Unk-47 Noggin Pooled MC 5ng	Unk-47 Noggin Pooled MC 5ng

Quantification



Quantification Data

Well	Fluor	Target	Content	Sample	Cq	Cq Mean	Cq Std. Dev
A01	FAM	Noggin	Unkn-01	001 S90	33.56	33.62	0.093
A02	FAM	Noggin	Unkn-01	001 S90	33.69	33.62	0.093
A03	FAM	Noggin	Unkn-08	002 S90	32.11	31.99	0.173
A04	FAM	Noggin	Unkn-08	002 S90	31.86	31.99	0.173
A05	FAM	Noggin	Unkn-15	799 S90	31.73	31.78	0.069
A06	FAM	Noggin	Unkn-15	799 S90	31.83	31.78	0.069
A07	FAM	Noggin	Unkn-21	811 S90	31.53	31.85	0.443
A08	FAM	Noggin	Unkn-21	811 S90	32.16	31.85	0.443
A09	FAM	Noggin	Unkn-28	805 S90	33.02	32.78	0.334
A10	FAM	Noggin	Unkn-28	805 S90	32.54	32.78	0.334
A11	FAM	Noggin	Unkn-35	816 S90	31.72	31.81	0.128
A12	FAM	Noggin	Unkn-35	816 S90	31.90	31.81	0.128
B01	FAM	Noggin	Unkn-02	001 N90	32.57	32.60	0.037
B02	FAM	Noggin	Unkn-02	001 N90	32.63	32.60	0.037
B03	FAM	Noggin	Unkn-09	002 N90	31.87	31.81	0.079
B04	FAM	Noggin	Unkn-09	002 N90	31.76	31.81	0.079
B05	FAM	Noggin	Unkn-16	799 N90	31.80	31.92	0.168
B06	FAM	Noggin	Unkn-16	799 N90	32.04	31.92	0.168
B07	FAM	Noggin	Unkn-22	811 N90	31.15	31.09	0.084
B08	FAM	Noggin	Unkn-22	811 N90	31.03	31.09	0.084
B09	FAM	Noggin	Unkn-29	805 N90	31.19	31.08	0.146
B10	FAM	Noggin	Unkn-29	805 N90	30.98	31.08	0.146
B11	FAM	Noggin	Unkn-36	816 N90	31.84	31.95	0.150
B12	FAM	Noggin	Unkn-36	816 N90	32.05	31.95	0.150
C01	FAM	Noggin	Unkn-03	001 T90	30.80	30.97	0.248
C02	FAM	Noggin	Unkn-03	001 T90	31.15	30.97	0.248
C03	FAM	Noggin	Unkn-10	002 T90	31.87	31.66	0.289
C04	FAM	Noggin	Unkn-10	002 T90	31.46	31.66	0.289
C05	FAM	Noggin	Unkn-17	799 T90	31.91	31.98	0.098
C06	FAM	Noggin	Unkn-17	799 T90	32.05	31.98	0.098
C07	FAM	Noggin	Unkn-23	811 T90	33.31	33.23	0.115
C08	FAM	Noggin	Unkn-23	811 T90	33.14	33.23	0.115
C09	FAM	Noggin	Unkn-30	805 T90	34.06	33.73	0.468
C10	FAM	Noggin	Unkn-30	805 T90	33.40	33.73	0.468
C11	FAM	Noggin	Unkn-37	816 T90	33.18	33.66	0.671
C12	FAM	Noggin	Unkn-37	816 T90	34.13	33.66	0.671
D01	FAM	Noggin	Unkn-04	001 T+N90	32.86	32.62	0.340
D02	FAM	Noggin	Unkn-04	001 T+N90	32.38	32.62	0.340
D03	FAM	Noggin	Unkn-11	002 T+N90	32.99	33.05	0.081
D04	FAM	Noggin	Unkn-11	002 T+N90	33.11	33.05	0.081
D05	FAM	Noggin	Unkn-18	799 T+N90	31.21	31.20	0.016
D06	FAM	Noggin	Unkn-18	799 T+N90	31.19	31.20	0.016
D07	FAM	Noggin	Unkn-24	811 T+N90	31.77	31.70	0.101
D08	FAM	Noggin	Unkn-24	811 T+N90	31.63	31.70	0.101
D09	FAM	Noggin	Unkn-31	805 T+N90	32.21	32.51	0.417
D10	FAM	Noggin	Unkn-31	805 T+N90	32.80	32.51	0.417
D11	FAM	Noggin	Unkn-38	816 T+N90	34.55	35.03	0.672

Well	Fluor	Target	Content	Sample	Cq	Cq Mean	Cq Std. Dev
D12	FAM	Noggin	Unkn-38	816 T+N90	35.50	35.03	0.672
E01	FAM	Noggin	Unkn-05	001 V90	32.51	32.28	0.326
E02	FAM	Noggin	Unkn-05	001 V90	32.05	32.28	0.326
E03	FAM	Noggin	Unkn-12	002 V90	32.36	32.43	0.096
E04	FAM	Noggin	Unkn-12	002 V90	32.49	32.43	0.096
E05	FAM	Noggin	Unkn-19	799 Z90	30.39	30.43	0.054
E06	FAM	Noggin	Unkn-19	799 Z90	30.47	30.43	0.054
E07	FAM	Noggin	Unkn-25	811 V90	31.39	31.38	0.009
E08	FAM	Noggin	Unkn-25	811 V90	31.38	31.38	0.009
E09	FAM	Noggin	Unkn-32	805 V90	31.66	31.67	0.024
E10	FAM	Noggin	Unkn-32	805 V90	31.69	31.67	0.024
E11	FAM	Noggin	Unkn-39	816 V90	33.24	33.16	0.109
E12	FAM	Noggin	Unkn-39	816 V90	33.09	33.16	0.109
F01	FAM	Noggin	Unkn-06	001 Z90	32.41	32.49	0.121
F02	FAM	Noggin	Unkn-06	001 Z90	32.58	32.49	0.121
F03	FAM	Noggin	Unkn-13	002 Z90	31.75	31.85	0.141
F04	FAM	Noggin	Unkn-13	002 Z90	31.95	31.85	0.141
F07	FAM	Noggin	Unkn-26	811 Z90	31.09	31.06	0.046
F08	FAM	Noggin	Unkn-26	811 Z90	31.03	31.06	0.046
F09	FAM	Noggin	Unkn-33	805 Z90	31.43	31.41	0.027
F10	FAM	Noggin	Unkn-33	805 Z90	31.39	31.41	0.027
F11	FAM	Noggin	Unkn-40	816 Z90	32.37	32.52	0.213
F12	FAM	Noggin	Unkn-40	816 Z90	32.67	32.52	0.213
G01	FAM	Noggin	Unkn-07	001 MC	30.94	31.11	0.243
G02	FAM	Noggin	Unkn-07	001 MC	31.28	31.11	0.243
G03	FAM	Noggin	Unkn-14	002 MC	31.57	31.22	0.494
G04	FAM	Noggin	Unkn-14	002 MC	30.87	31.22	0.494
G05	FAM	Noggin	Unkn-20	799 MC	31.52	31.59	0.111
G06	FAM	Noggin	Unkn-20	799 MC	31.67	31.59	0.111
G07	FAM	Noggin	Unkn-27	811 MC	30.16	30.15	0.023
G08	FAM	Noggin	Unkn-27	811 MC	30.13	30.15	0.023
G09	FAM	Noggin	Unkn-34	805 MC	31.40	31.39	0.020
G10	FAM	Noggin	Unkn-34	805 MC	31.38	31.39	0.020
G11	FAM	Noggin	Unkn-41	816 MC	32.02	32.22	0.290
G12	FAM	Noggin	Unkn-41	816 MC	32.43	32.22	0.290
H01	FAM	Noggin	Pos Ctrl-42	804 PC	30.78	30.76	0.023
H02	FAM	Noggin	Pos Ctrl-42	804 PC	30.74	30.76	0.023
H03	FAM	Noggin	NTC-43	H2O	N/A	0.00	0.000
H04	FAM	Noggin	NTC-43	H2O	N/A	0.00	0.000
H05	FAM	Noggin	NTC-44	H2O	N/A	0.00	0.000
H06	FAM	Noggin	NTC-44	H2O	N/A	0.00	0.000
H07	FAM	Noggin	Unkn-45	Pooled MC 15ng	33.44	33.24	0.287
H08	FAM	Noggin	Unkn-45	Pooled MC 15ng	33.04	33.24	0.287
H09	FAM	Noggin	Unkn-46	Pooled MC 10ng	33.96	33.70	0.363
H10	FAM	Noggin	Unkn-46	Pooled MC 10ng	33.44	33.70	0.363
H11	FAM	Noggin	Unkn-47	Pooled MC 5ng	31.52	32.04	0.738
H12	FAM	Noggin	Unkn-47	Pooled MC 5ng	32.56	32.04	0.738

Gene Expression

Target Names

Name	Full Name	Reference	Auto Efficiency	Efficiency
Noggin	Noggin	False	Yes	100.0%

Additional quantitative RT-PCR runs on new genes

Results Runx2 15days.pcrd

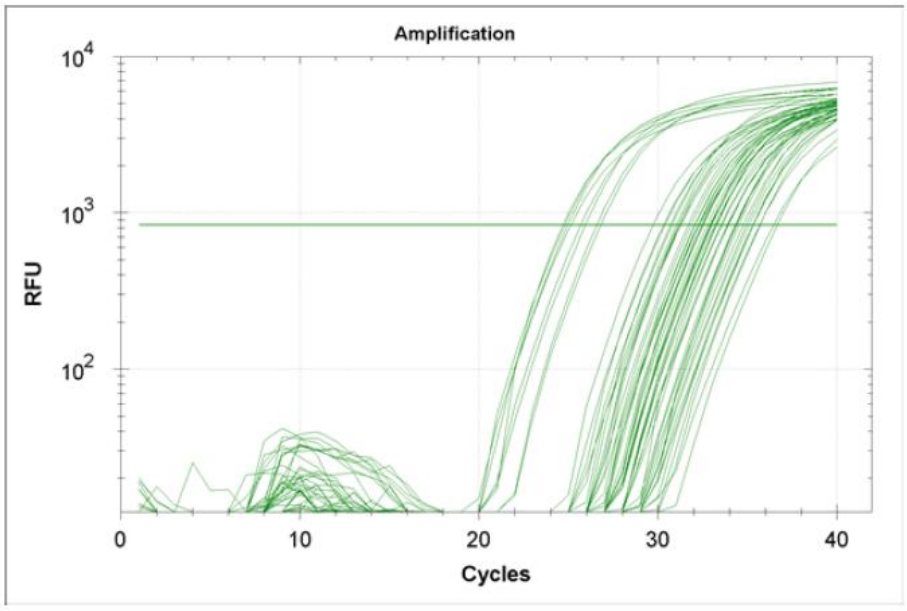
2013/08/21 01:20 PM

Run Setup

Plate Display

	1	2	3	4	5	6	7	8	9	10	11	12
A	Unk-1 Runx2 1 S 15	Unk-1 Runx2 1 S 15	Unk-2 Runx2 2 S 15	Unk-2 Runx2 2 S 15	Unk-3 Runx2 3 S 15	Unk-3 Runx2 3 S 15	Unk-4 Runx2 4 S 15	Unk-4 Runx2 4 S 15	Unk-5 Runx2 5 S 15	Unk-5 Runx2 5 S 15	Unk-6 Runx2 6 S 15	Unk-6 Runx2 6 S 15
B	Unk-7 Runx2 1 N 15	Unk-7 Runx2 1 N 15	Unk-8 Runx2 2 N 15	Unk-8 Runx2 2 N 15	Unk-9 Runx2 3 N 15	Unk-9 Runx2 3 N 15	Unk-10 Runx2 4 N 15	Unk-10 Runx2 4 N 15	Unk-11 Runx2 5 N 15	Unk-11 Runx2 5 N 15	Unk-12 Runx2 6 N 15	Unk-12 Runx2 6 N 15
C	Unk-13 Runx2 1 T 15	Unk-13 Runx2 1 T 15	Unk-14 Runx2 2 T 15	Unk-14 Runx2 2 T 15	Unk-15 Runx2 3 T 15	Unk-15 Runx2 3 T 15	Unk-16 Runx2 4 T 15	Unk-16 Runx2 4 T 15	Unk-17 Runx2 5 T 15	Unk-17 Runx2 5 T 15	Unk-18 Runx2 6 T 15	Unk-18 Runx2 6 T 15
D	Unk-19 Runx2 1 TN 15	Unk-19 Runx2 1 TN 15	Unk-20 Runx2 2 TN 15	Unk-20 Runx2 2 TN 15	Unk-21 Runx2 3 TN 15	Unk-21 Runx2 3 TN 15	Unk-22 Runx2 4 TN 15	Unk-22 Runx2 4 TN 15	Unk-23 Runx2 5 TN 15	Unk-23 Runx2 5 TN 15	Unk-24 Runx2 6 TN 15	Unk-24 Runx2 6 TN 15
E	Pos Runx2 PC 001 15	Pos Runx2 PC 001 15	Neg Runx2 H2O	Neg Runx2 H2O	Neg Runx2 H2O	Neg Runx2 H2O	Unk Runx2 PMC 15 15	Unk Runx2 PMC 15 15	Unk Runx2 PMC 10 15	Unk Runx2 PMC 10 15	Unk Runx2 PMC 5 15	Unk Runx2 PMC 5 15
F												
G												
H												

Quantification



Quantification Data

Well	Fluor	Target	Content	Sample	Cq	Cq Mean	Cq Std. Dev
A01	SYBR	Runx2	Unkn-01	1 S 15	32.27	32.70	0.611
A02	SYBR	Runx2	Unkn-01	1 S 15	33.14	32.70	0.611
A03	SYBR	Runx2	Unkn-02	2 S 15	29.69	30.01	0.461
A04	SYBR	Runx2	Unkn-02	2 S 15	30.34	30.01	0.461
A05	SYBR	Runx2	Unkn-03	3 S 15	30.27	30.72	0.642
A06	SYBR	Runx2	Unkn-03	3 S 15	31.18	30.72	0.642
A07	SYBR	Runx2	Unkn-04	4 S 15	33.84	33.88	0.061
A08	SYBR	Runx2	Unkn-04	4 S 15	33.92	33.88	0.061
A09	SYBR	Runx2	Unkn-05	5 S 15	36.42	36.52	0.142
A10	SYBR	Runx2	Unkn-05	5 S 15	36.62	36.52	0.142
A11	SYBR	Runx2	Unkn-06	6 S 15	32.20	32.54	0.476
A12	SYBR	Runx2	Unkn-06	6 S 15	32.88	32.54	0.476
B01	SYBR	Runx2	Unkn-07	1 N 15	33.01	33.24	0.323
B02	SYBR	Runx2	Unkn-07	1 N 15	33.47	33.24	0.323
B03	SYBR	Runx2	Unkn-08	2 N 15	31.25	31.67	0.581
B04	SYBR	Runx2	Unkn-08	2 N 15	32.08	31.67	0.581
B05	SYBR	Runx2	Unkn-09	3 N 15	30.64	31.45	1.138
B06	SYBR	Runx2	Unkn-09	3 N 15	32.25	31.45	1.138
B07	SYBR	Runx2	Unkn-10	4 N 15	33.51	33.91	0.560
B08	SYBR	Runx2	Unkn-10	4 N 15	34.30	33.91	0.560
B09	SYBR	Runx2	Unkn-11	5 N 15	35.23	35.26	0.049
B10	SYBR	Runx2	Unkn-11	5 N 15	35.29	35.26	0.049
B11	SYBR	Runx2	Unkn-12	6 N 15	35.63	35.64	0.009
B12	SYBR	Runx2	Unkn-12	6 N 15	35.65	35.64	0.009
C01	SYBR	Runx2	Unkn-13	1 T 15	32.39	32.55	0.223
C02	SYBR	Runx2	Unkn-13	1 T 15	32.70	32.55	0.223
C03	SYBR	Runx2	Unkn-14	2 T 15	31.19	31.50	0.441
C04	SYBR	Runx2	Unkn-14	2 T 15	31.81	31.50	0.441
C05	SYBR	Runx2	Unkn-15	3 T 15	31.11	31.38	0.376
C06	SYBR	Runx2	Unkn-15	3 T 15	31.64	31.38	0.376
C07	SYBR	Runx2	Unkn-16	4 T 15	24.64	24.88	0.334
C08	SYBR	Runx2	Unkn-16	4 T 15	25.11	24.88	0.334
C09	SYBR	Runx2	Unkn-17	5 T 15	24.77	24.86	0.130
C10	SYBR	Runx2	Unkn-17	5 T 15	24.95	24.86	0.130
C11	SYBR	Runx2	Unkn-18	6 T 15	32.48	33.60	1.578
C12	SYBR	Runx2	Unkn-18	6 T 15	34.71	33.60	1.578
D01	SYBR	Runx2	Unkn-19	1 TN 15	32.02	32.48	0.640
D02	SYBR	Runx2	Unkn-19	1 TN 15	32.93	32.48	0.640
D03	SYBR	Runx2	Unkn-20	2 TN 15	33.24	33.10	0.204
D04	SYBR	Runx2	Unkn-20	2 TN 15	32.96	33.10	0.204
D05	SYBR	Runx2	Unkn-21	3 TN 15	32.43	32.82	0.548
D06	SYBR	Runx2	Unkn-21	3 TN 15	33.21	32.82	0.548
D07	SYBR	Runx2	Unkn-22	4 TN 15	30.75	30.89	0.190
D08	SYBR	Runx2	Unkn-22	4 TN 15	31.02	30.89	0.190
D09	SYBR	Runx2	Unkn-23	5 TN 15	26.53	26.65	0.170
D10	SYBR	Runx2	Unkn-23	5 TN 15	26.77	26.65	0.170
D11	SYBR	Runx2	Unkn-24	6 TN 15	33.20	33.55	0.493

Well	Fluor	Target	Content	Sample	Cq	Cq Mean	Cq Std. Dev
D12	SYBR	Runx2	Unkn-24	6 TN 15	33.90	33.55	0.493
E01	SYBR	Runx2	Pos Ctrl	PC 001 15	25.64	25.64	0.000
E02	SYBR	Runx2	Pos Ctrl	PC 001 15	25.93	25.93	0.000
E03	SYBR	Runx2	Neg Ctrl	H2O	N/A	0.00	0.000
E04	SYBR	Runx2	Neg Ctrl	H2O	N/A	0.00	0.000
E05	SYBR	Runx2	Neg Ctrl	H2O	N/A	0.00	0.000
E06	SYBR	Runx2	Neg Ctrl	H2O	N/A	0.00	0.000
E07	SYBR	Runx2	Unkn	PMC 15 15	34.46	34.46	0.000
E08	SYBR	Runx2	Unkn	PMC 15 15	34.26	34.26	0.000
E09	SYBR	Runx2	Unkn	PMC 10 15	34.34	34.34	0.000
E10	SYBR	Runx2	Unkn	PMC 10 15	34.90	34.90	0.000
E11	SYBR	Runx2	Unkn	PMC 5 15	35.29	35.29	0.000
E12	SYBR	Runx2	Unkn	PMC 5 15	35.06	35.06	0.000

Gene Expression

Target Names

Name	Full Name	Reference	Auto Efficiency	Efficiency
Runx2	Runx2	False	Yes	100.0%

Results Runx2 60days.pcrd

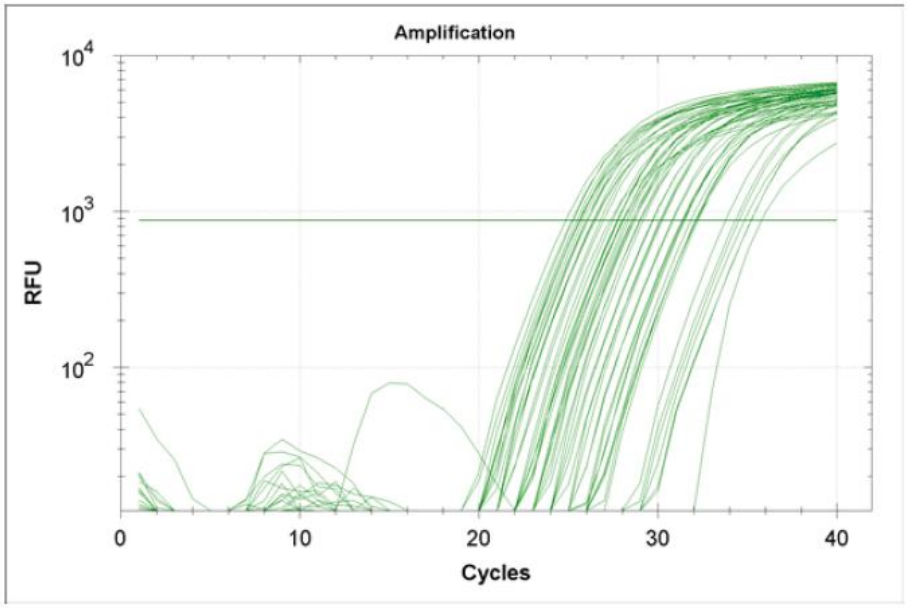
2013/08/21 01:21 PM

Run Setup

Plate Display

	1	2	3	4	5	6	7	8	9	10	11	12
A	Unk-1 Runx2 1 S 60	Unk-1 Runx2 1 S 60	Unk-2 Runx2 2 S 60	Unk-2 Runx2 2 S 60	Unk-3 Runx2 3 S 60	Unk-3 Runx2 3 S 60	Unk-4 Runx2 4 S 60	Unk-4 Runx2 4 S 60	Unk-5 Runx2 5 S 60	Unk-5 Runx2 5 S 60	Unk-6 Runx2 6 S 60	Unk-6 Runx2 6 S 60
B	Unk-7 Runx2 1 N 60	Unk-7 Runx2 1 N 60	Unk-8 Runx2 2 N 60	Unk-8 Runx2 2 N 60	Unk-9 Runx2 3 N 60	Unk-9 Runx2 3 N 60	Unk-10 Runx2 4 N 60	Unk-10 Runx2 4 N 60	Unk-11 Runx2 5 N 60	Unk-11 Runx2 5 N 60	Unk-12 Runx2 6 N 60	Unk-12 Runx2 6 N 60
C	Unk-13 Runx2 1 T 60	Unk-13 Runx2 1 T 60	Unk-14 Runx2 2 T 60	Unk-14 Runx2 2 T 60	Unk-15 Runx2 3 T 60	Unk-15 Runx2 3 T 60	Unk-16 Runx2 4 T 60	Unk-16 Runx2 4 T 60	Unk-17 Runx2 5 T 60	Unk-17 Runx2 5 T 60	Unk-18 Runx2 6 T 60	Unk-18 Runx2 6 T 60
D	Unk-19 Runx2 1 TN 60	Unk-19 Runx2 1 TN 60	Unk-20 Runx2 2 TN 60	Unk-20 Runx2 2 TN 60	Unk-21 Runx2 3 TN 60	Unk-21 Runx2 3 TN 60	Unk-22 Runx2 4 TN 60	Unk-22 Runx2 4 TN 60	Unk-23 Runx2 5 TN 60	Unk-23 Runx2 5 TN 60	Unk-24 Runx2 6 TN 60	Unk-24 Runx2 6 TN 60
E	Pos Runx2 PC 001 60	Pos Runx2 PC 001 60	Neg Runx2 H2O	Neg Runx2 H2O	Neg Runx2 H2O	Neg Runx2 H2O	Unk Runx2 PMC 15 60	Unk Runx2 PMC 15 60	Unk Runx2 PMC 10 60	Unk Runx2 PMC 10 60	Unk Runx2 PMC 5 60	Unk Runx2 PMC 5 60
F												
G												
H												

Quantification



Quantification Data

Well	Fluor	Target	Content	Sample	Cq	Cq Mean	Cq Std. Dev
A01	SYBR	Runx2	Unkn-01	1 S 60	28.05	28.27	0.301
A02	SYBR	Runx2	Unkn-01	1 S 60	28.48	28.27	0.301
A03	SYBR	Runx2	Unkn-02	2 S 60	26.37	26.40	0.040
A04	SYBR	Runx2	Unkn-02	2 S 60	26.43	26.40	0.040
A05	SYBR	Runx2	Unkn-03	3 S 60	25.98	26.15	0.239
A06	SYBR	Runx2	Unkn-03	3 S 60	26.32	26.15	0.239
A07	SYBR	Runx2	Unkn-04	4 S 60	31.33	31.31	0.039
A08	SYBR	Runx2	Unkn-04	4 S 60	31.28	31.31	0.039
A09	SYBR	Runx2	Unkn-05	5 S 60	27.40	27.53	0.178
A10	SYBR	Runx2	Unkn-05	5 S 60	27.66	27.53	0.178
A11	SYBR	Runx2	Unkn-06	6 S 60	31.78	31.96	0.246
A12	SYBR	Runx2	Unkn-06	6 S 60	32.13	31.96	0.246
B01	SYBR	Runx2	Unkn-07	1 N 60	27.29	27.95	0.932
B02	SYBR	Runx2	Unkn-07	1 N 60	28.60	27.95	0.932
B03	SYBR	Runx2	Unkn-08	2 N 60	29.63	29.88	0.354
B04	SYBR	Runx2	Unkn-08	2 N 60	30.13	29.88	0.354
B05	SYBR	Runx2	Unkn-09	3 N 60	29.01	29.33	0.456
B06	SYBR	Runx2	Unkn-09	3 N 60	29.65	29.33	0.456
B07	SYBR	Runx2	Unkn-10	4 N 60	28.49	28.81	0.456
B08	SYBR	Runx2	Unkn-10	4 N 60	29.13	28.81	0.456
B09	SYBR	Runx2	Unkn-11	5 N 60	30.80	30.76	0.048
B10	SYBR	Runx2	Unkn-11	5 N 60	30.73	30.76	0.048
B11	SYBR	Runx2	Unkn-12	6 N 60	32.08	32.13	0.083
B12	SYBR	Runx2	Unkn-12	6 N 60	32.19	32.13	0.083
C01	SYBR	Runx2	Unkn-13	1 T 60	26.07	26.03	0.059
C02	SYBR	Runx2	Unkn-13	1 T 60	25.99	26.03	0.059
C03	SYBR	Runx2	Unkn-14	2 T 60	25.40	25.49	0.136
C04	SYBR	Runx2	Unkn-14	2 T 60	25.59	25.49	0.136
C05	SYBR	Runx2	Unkn-15	3 T 60	25.57	25.67	0.131
C06	SYBR	Runx2	Unkn-15	3 T 60	25.76	25.67	0.131
C07	SYBR	Runx2	Unkn-16	4 T 60	28.97	28.79	0.248
C08	SYBR	Runx2	Unkn-16	4 T 60	28.62	28.79	0.248
C09	SYBR	Runx2	Unkn-17	5 T 60	28.18	28.24	0.079
C10	SYBR	Runx2	Unkn-17	5 T 60	28.29	28.24	0.079
C11	SYBR	Runx2	Unkn-18	6 T 60	35.74	33.55	3.089
C12	SYBR	Runx2	Unkn-18	6 T 60	31.37	33.55	3.089
D01	SYBR	Runx2	Unkn-19	1 TN 60	28.00	27.87	0.189
D02	SYBR	Runx2	Unkn-19	1 TN 60	27.73	27.87	0.189
D03	SYBR	Runx2	Unkn-20	2 TN 60	25.15	25.18	0.043
D04	SYBR	Runx2	Unkn-20	2 TN 60	25.21	25.18	0.043
D05	SYBR	Runx2	Unkn-21	3 TN 60	24.81	25.17	0.509
D06	SYBR	Runx2	Unkn-21	3 TN 60	25.53	25.17	0.509
D07	SYBR	Runx2	Unkn-22	4 TN 60	28.02	27.84	0.247
D08	SYBR	Runx2	Unkn-22	4 TN 60	27.67	27.84	0.247
D09	SYBR	Runx2	Unkn-23	5 TN 60	30.20	30.14	0.083
D10	SYBR	Runx2	Unkn-23	5 TN 60	30.08	30.14	0.083
D11	SYBR	Runx2	Unkn-24	6 TN 60	31.42	31.76	0.472

Well	Fluor	Target	Content	Sample	Cq	Cq Mean	Cq Std. Dev
D12	SYBR	Runx2	Unkn-24	6 TN 60	32.09	31.76	0.472
E01	SYBR	Runx2	Pos Ctrl	PC 001 60	26.92	26.92	0.000
E02	SYBR	Runx2	Pos Ctrl	PC 001 60	26.72	26.72	0.000
E03	SYBR	Runx2	Neg Ctrl	H2O	N/A	0.00	0.000
E04	SYBR	Runx2	Neg Ctrl	H2O	N/A	0.00	0.000
E05	SYBR	Runx2	Neg Ctrl	H2O	N/A	0.00	0.000
E06	SYBR	Runx2	Neg Ctrl	H2O	N/A	0.00	0.000
E07	SYBR	Runx2	Unkn	PMC 15 60	34.78	34.78	0.000
E08	SYBR	Runx2	Unkn	PMC 15 60	33.72	33.72	0.000
E09	SYBR	Runx2	Unkn	PMC 10 60	35.17	35.17	0.000
E10	SYBR	Runx2	Unkn	PMC 10 60	34.27	34.27	0.000
E11	SYBR	Runx2	Unkn	PMC 5 60	34.45	34.45	0.000
E12	SYBR	Runx2	Unkn	PMC 5 60	35.16	35.16	0.000

Gene Expression

Target Names

Name	Full Name	Reference	Auto Efficiency	Efficiency
Runx2	Runx2	False	Yes	100.0%

Results Runx2 90days.pcrd

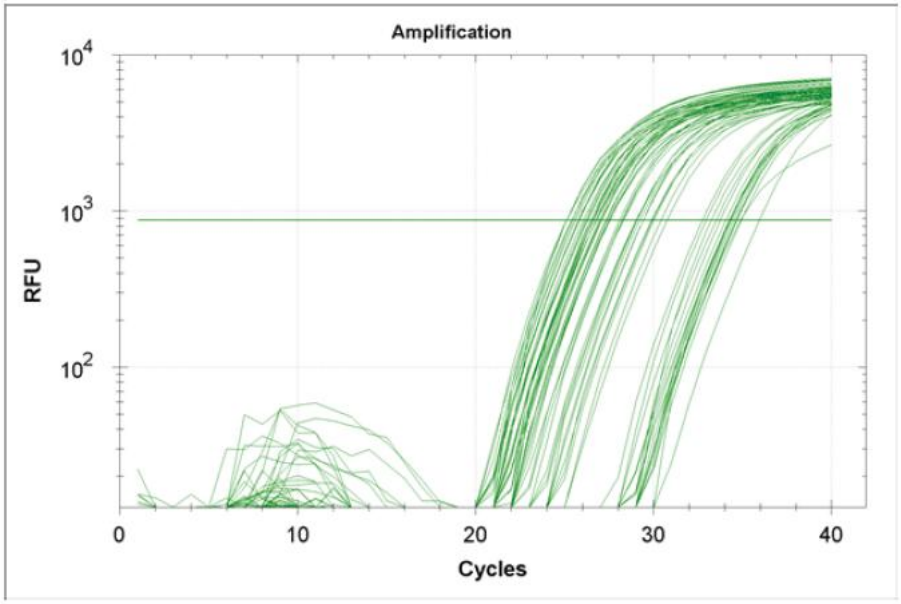
2013/08/21 01:24 PM

Run Setup

Plate Display

	1	2	3	4	5	6	7	8	9	10	11	12
A	Unk-1 Runx2 1 S 90	Unk-1 Runx2 1 S 90	Unk-2 Runx2 2 S 90	Unk-2 Runx2 2 S 90	Unk-3 Runx2 3 S 90	Unk-3 Runx2 3 S 90	Unk-4 Runx2 4 S 90	Unk-4 Runx2 4 S 90	Unk-5 Runx2 5 S 90	Unk-5 Runx2 5 S 90	Unk-6 Runx2 6 S 90	Unk-6 Runx2 6 S 90
B	Unk-7 Runx2 1 N 90	Unk-7 Runx2 1 N 90	Unk-8 Runx2 2 N 90	Unk-8 Runx2 2 N 90	Unk-9 Runx2 3 N 90	Unk-9 Runx2 3 N 90	Unk-10 Runx2 4 N 90	Unk-10 Runx2 4 N 90	Unk-11 Runx2 5 N 90	Unk-11 Runx2 5 N 90	Unk-12 Runx2 6 N 90	Unk-12 Runx2 6 N 90
C	Unk-13 Runx2 1 T 90	Unk-13 Runx2 1 T 90	Unk-14 Runx2 2 T 90	Unk-14 Runx2 2 T 90	Unk-15 Runx2 3 T 90	Unk-15 Runx2 3 T 90	Unk-16 Runx2 4 T 90	Unk-16 Runx2 4 T 90	Unk-17 Runx2 5 T 90	Unk-17 Runx2 5 T 90	Unk-18 Runx2 6 T 90	Unk-18 Runx2 6 T 90
D	Unk-19 Runx2 1 TN 90	Unk-19 Runx2 1 TN 90	Unk-20 Runx2 2 TN 90	Unk-20 Runx2 2 TN 90	Unk-21 Runx2 3 TN 90	Unk-21 Runx2 3 TN 90	Unk-22 Runx2 4 TN 90	Unk-22 Runx2 4 TN 90	Unk-23 Runx2 5 TN 90	Unk-23 Runx2 5 TN 90	Unk-24 Runx2 6 TN 90	Unk-24 Runx2 6 TN 90
E	Unk-25 Runx2 MC 1	Unk-25 Runx2 MC 1	Unk-26 Runx2 MC 2	Unk-26 Runx2 MC 2	Unk-27 Runx2 MC 3	Unk-27 Runx2 MC 3	Unk-28 Runx2 MC 4	Unk-28 Runx2 MC 4	Unk-29 Runx2 MC 5	Unk-29 Runx2 MC 5	Unk-30 Runx2 MC 6	Unk-30 Runx2 MC 6
F	Pos Runx2 PC 001 90	Pos Runx2 PC 001 90	Neg Runx2 H2O	Neg Runx2 H2O	Neg Runx2 H2O	Neg Runx2 H2O	Unk Runx2 PMC 15 90	Unk Runx2 PMC 15 90	Unk Runx2 PMC 10 90	Unk Runx2 PMC 10 90	Unk Runx2 PMC 5 90	Unk Runx2 PMC 5 90
G												
H												

Quantification



Quantification Data

Well	Fluor	Target	Content	Sample	Cq	Cq Mean	Cq Std. Dev
A01	SYBR	Runx2	Unkn-01	1 S 90	27.48	27.47	0.012
A02	SYBR	Runx2	Unkn-01	1 S 90	27.46	27.47	0.012
A03	SYBR	Runx2	Unkn-02	2 S 90	26.72	26.64	0.114
A04	SYBR	Runx2	Unkn-02	2 S 90	26.56	26.64	0.114
A05	SYBR	Runx2	Unkn-03	3 S 90	26.75	26.73	0.027
A06	SYBR	Runx2	Unkn-03	3 S 90	26.71	26.73	0.027
A07	SYBR	Runx2	Unkn-04	4 S 90	29.18	29.55	0.518
A08	SYBR	Runx2	Unkn-04	4 S 90	29.91	29.55	0.518
A09	SYBR	Runx2	Unkn-05	5 S 90	28.26	28.64	0.540
A10	SYBR	Runx2	Unkn-05	5 S 90	29.02	28.64	0.540
A11	SYBR	Runx2	Unkn-06	6 S 90	29.86	30.29	0.603
A12	SYBR	Runx2	Unkn-06	6 S 90	30.71	30.29	0.603
B01	SYBR	Runx2	Unkn-07	1 N 90	27.48	27.82	0.483
B02	SYBR	Runx2	Unkn-07	1 N 90	28.16	27.82	0.483
B03	SYBR	Runx2	Unkn-08	2 N 90	26.24	26.19	0.079
B04	SYBR	Runx2	Unkn-08	2 N 90	26.13	26.19	0.079
B05	SYBR	Runx2	Unkn-09	3 N 90	26.40	26.84	0.616
B06	SYBR	Runx2	Unkn-09	3 N 90	27.27	26.84	0.616
B07	SYBR	Runx2	Unkn-10	4 N 90	29.36	29.86	0.708
B08	SYBR	Runx2	Unkn-10	4 N 90	30.36	29.86	0.708
B09	SYBR	Runx2	Unkn-11	5 N 90	29.02	29.51	0.698
B10	SYBR	Runx2	Unkn-11	5 N 90	30.01	29.51	0.698
B11	SYBR	Runx2	Unkn-12	6 N 90	28.06	28.14	0.114
B12	SYBR	Runx2	Unkn-12	6 N 90	28.23	28.14	0.114
C01	SYBR	Runx2	Unkn-13	1 T 90	26.03	26.53	0.708
C02	SYBR	Runx2	Unkn-13	1 T 90	27.03	26.53	0.708
C03	SYBR	Runx2	Unkn-14	2 T 90	27.01	27.16	0.205
C04	SYBR	Runx2	Unkn-14	2 T 90	27.30	27.16	0.205
C05	SYBR	Runx2	Unkn-15	3 T 90	26.41	26.66	0.353
C06	SYBR	Runx2	Unkn-15	3 T 90	26.91	26.66	0.353
C07	SYBR	Runx2	Unkn-16	4 T 90	25.09	25.43	0.484
C08	SYBR	Runx2	Unkn-16	4 T 90	25.78	25.43	0.484
C09	SYBR	Runx2	Unkn-17	5 T 90	26.71	27.05	0.488
C10	SYBR	Runx2	Unkn-17	5 T 90	27.40	27.05	0.488
C11	SYBR	Runx2	Unkn-18	6 T 90	25.77	26.15	0.546
C12	SYBR	Runx2	Unkn-18	6 T 90	26.54	26.15	0.546
D01	SYBR	Runx2	Unkn-19	1 TN 90	25.09	25.22	0.186
D02	SYBR	Runx2	Unkn-19	1 TN 90	25.35	25.22	0.186
D03	SYBR	Runx2	Unkn-20	2 TN 90	25.77	25.95	0.255
D04	SYBR	Runx2	Unkn-20	2 TN 90	26.13	25.95	0.255
D05	SYBR	Runx2	Unkn-21	3 TN 90	25.09	25.27	0.259
D06	SYBR	Runx2	Unkn-21	3 TN 90	25.46	25.27	0.259
D07	SYBR	Runx2	Unkn-22	4 TN 90	25.34	25.45	0.154
D08	SYBR	Runx2	Unkn-22	4 TN 90	25.56	25.45	0.154
D09	SYBR	Runx2	Unkn-23	5 TN 90	25.74	26.11	0.536
D10	SYBR	Runx2	Unkn-23	5 TN 90	26.49	26.11	0.536
D11	SYBR	Runx2	Unkn-24	6 TN 90	29.05	29.20	0.212

Well	Fluor	Target	Content	Sample	Cq	Cq Mean	Cq Std. Dev
D12	SYBR	Runx2	Unkn-24	6 TN 90	29.35	29.20	0.212
E01	SYBR	Runx2	Unkn-25	MC 1	33.46	34.18	1.029
E02	SYBR	Runx2	Unkn-25	MC 1	34.91	34.18	1.029
E03	SYBR	Runx2	Unkn-26	MC 2	33.20	33.45	0.349
E04	SYBR	Runx2	Unkn-26	MC 2	33.69	33.45	0.349
E05	SYBR	Runx2	Unkn-27	MC 3	34.22	34.43	0.293
E06	SYBR	Runx2	Unkn-27	MC 3	34.63	34.43	0.293
E07	SYBR	Runx2	Unkn-28	MC 4	32.70	32.81	0.169
E08	SYBR	Runx2	Unkn-28	MC 4	32.93	32.81	0.169
E09	SYBR	Runx2	Unkn-29	MC 5	34.26	34.41	0.219
E10	SYBR	Runx2	Unkn-29	MC 5	34.57	34.41	0.219
E11	SYBR	Runx2	Unkn-30	MC 6	34.34	34.29	0.071
E12	SYBR	Runx2	Unkn-30	MC 6	34.24	34.29	0.071
F01	SYBR	Runx2	Pos Ctrl	PC 001 90	26.21	26.21	0.000
F02	SYBR	Runx2	Pos Ctrl	PC 001 90	27.07	27.07	0.000
F03	SYBR	Runx2	Neg Ctrl	H2O	N/A	0.00	0.000
F04	SYBR	Runx2	Neg Ctrl	H2O	N/A	0.00	0.000
F05	SYBR	Runx2	Neg Ctrl	H2O	N/A	0.00	0.000
F06	SYBR	Runx2	Neg Ctrl	H2O	N/A	0.00	0.000
F07	SYBR	Runx2	Unkn	PMC 15 90	34.25	34.25	0.000
F08	SYBR	Runx2	Unkn	PMC 15 90	34.62	34.62	0.000
F09	SYBR	Runx2	Unkn	PMC 10 90	35.92	35.92	0.000
F10	SYBR	Runx2	Unkn	PMC 10 90	34.05	34.05	0.000
F11	SYBR	Runx2	Unkn	PMC 5 90	34.44	34.44	0.000
F12	SYBR	Runx2	Unkn	PMC 5 90	34.87	34.87	0.000

Gene Expression

Target Names

Name	Full Name	Reference	Auto Efficiency	Efficiency
Runx2	Runx2	False	Yes	100.0%

Oc results 15days.pcrd

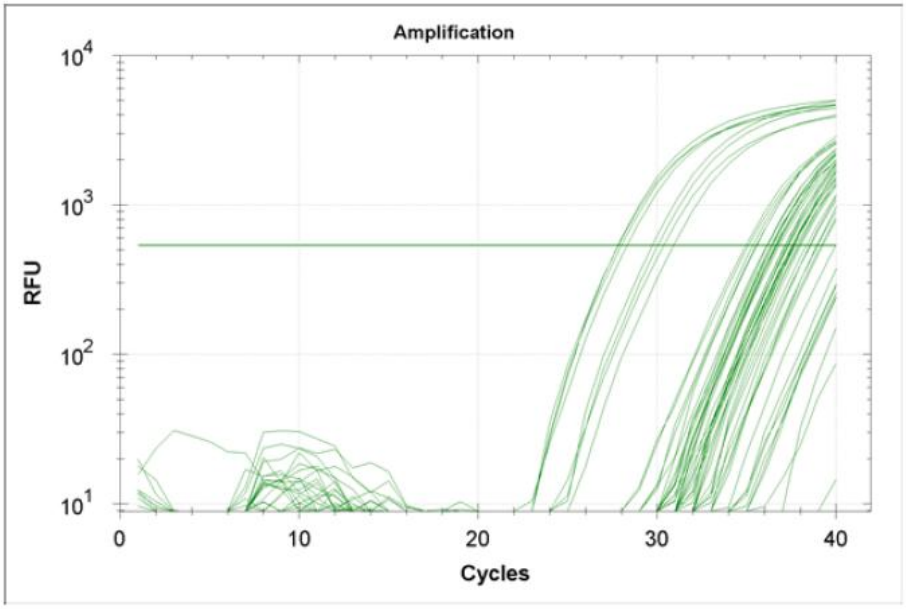
2013/08/21 01:27 PM

Run Setup

Plate Display

	1	2	3	4	5	6	7	8	9	10	11	12
A	Unk-1 OC 1 S 15	Unk-1 OC 1 S 15	Unk-2 OC 2 S 15	Unk-2 OC 2 S 15	Unk-3 OC 3 S 15	Unk-3 OC 3 S 15	Unk-4 OC 4 S 15	Unk-4 OC 4 S 15	Unk-5 OC 5 S 15	Unk-5 OC 5 S 15	Unk-6 OC 6 S 15	Unk-6 OC 6 S 15
B	Unk-7 OC 1 N 15	Unk-7 OC 1 N 15	Unk-8 OC 2 N 15	Unk-8 OC 2 N 15	Unk-9 OC 3 N 15	Unk-9 OC 3 N 15	Unk-10 OC 4 N 15	Unk-10 OC 4 N 15	Unk-11 OC 5 N 15	Unk-11 OC 5 N 15	Unk-12 OC 6 N 15	Unk-12 OC 6 N 15
C	Unk-13 OC 1 T 15	Unk-13 OC 1 T 15	Unk-14 OC 2 T 15	Unk-14 OC 2 T 15	Unk-15 OC 3 T 15	Unk-15 OC 3 T 15	Unk-16 OC 4 T 15	Unk-16 OC 4 T 15	Unk-17 OC 5 T 15	Unk-17 OC 5 T 15	Unk-18 OC 6 T 15	Unk-18 OC 6 T 15
D	Unk-19 OC 1 TN 15	Unk-19 OC 1 TN 15	Unk-20 OC 2 TN 15	Unk-20 OC 2 TN 15	Unk-21 OC 3 TN 15	Unk-21 OC 3 TN 15	Unk-22 OC 4 TN 15	Unk-22 OC 4 TN 15	Unk-23 OC 5 TN 15	Unk-23 OC 5 TN 15	Unk-24 OC 6 TN 15	Unk-24 OC 6 TN 15
E	Pos OC PC 001 15	Pos OC PC 001 15	Neg OC H2O	Neg OC H2O	Neg OC H2O	Neg OC H2O	Unk OC PMC 15 15	Unk OC PMC 15 15	Unk OC PMC 10 15	Unk OC PMC 10 15	Unk OC PMC 5 15	Unk OC PMC 5 15
F												
G												
H												

Quantification



Quantification Data

Well	Fluor	Target	Content	Sample	Cq	Cq Mean	Cq Std. Dev
A01	SYBR	OC	Unkn-01	1 S 15	37.72	37.04	0.959
A02	SYBR	OC	Unkn-01	1 S 15	36.36	37.04	0.959
A03	SYBR	OC	Unkn-02	2 S 15	37.55	37.12	0.614
A04	SYBR	OC	Unkn-02	2 S 15	36.68	37.12	0.614
A05	SYBR	OC	Unkn-03	3 S 15	36.64	36.50	0.195
A06	SYBR	OC	Unkn-03	3 S 15	36.36	36.50	0.195
A07	SYBR	OC	Unkn-04	4 S 15	N/A	0.00	0.000
A08	SYBR	OC	Unkn-04	4 S 15	N/A	0.00	0.000
A09	SYBR	OC	Unkn-05	5 S 15	N/A	0.00	0.000
A10	SYBR	OC	Unkn-05	5 S 15	N/A	0.00	0.000
A11	SYBR	OC	Unkn-06	6 S 15	35.09	35.03	0.088
A12	SYBR	OC	Unkn-06	6 S 15	34.96	35.03	0.088
B01	SYBR	OC	Unkn-07	1 N 15	35.30	35.70	0.570
B02	SYBR	OC	Unkn-07	1 N 15	36.11	35.70	0.570
B03	SYBR	OC	Unkn-08	2 N 15	36.81	36.68	0.183
B04	SYBR	OC	Unkn-08	2 N 15	36.55	36.68	0.183
B05	SYBR	OC	Unkn-09	3 N 15	37.57	37.52	0.065
B06	SYBR	OC	Unkn-09	3 N 15	37.48	37.52	0.065
B07	SYBR	OC	Unkn-10	4 N 15	36.41	37.35	1.332
B08	SYBR	OC	Unkn-10	4 N 15	38.29	37.35	1.332
B09	SYBR	OC	Unkn-11	5 N 15	37.57	37.75	0.253
B10	SYBR	OC	Unkn-11	5 N 15	37.93	37.75	0.253
B11	SYBR	OC	Unkn-12	6 N 15	38.95	38.28	0.954
B12	SYBR	OC	Unkn-12	6 N 15	37.60	38.28	0.954
C01	SYBR	OC	Unkn-13	1 T 15	38.47	38.47	0.000
C02	SYBR	OC	Unkn-13	1 T 15	N/A	0.00	0.000
C03	SYBR	OC	Unkn-14	2 T 15	37.49	37.40	0.128
C04	SYBR	OC	Unkn-14	2 T 15	37.31	37.40	0.128
C05	SYBR	OC	Unkn-15	3 T 15	36.58	36.85	0.384
C06	SYBR	OC	Unkn-15	3 T 15	37.12	36.85	0.384
C07	SYBR	OC	Unkn-16	4 T 15	27.99	28.13	0.200
C08	SYBR	OC	Unkn-16	4 T 15	28.27	28.13	0.200
C09	SYBR	OC	Unkn-17	5 T 15	27.80	27.79	0.022
C10	SYBR	OC	Unkn-17	5 T 15	27.77	27.79	0.022
C11	SYBR	OC	Unkn-18	6 T 15	39.96	39.96	0.000
C12	SYBR	OC	Unkn-18	6 T 15	N/A	0.00	0.000
D01	SYBR	OC	Unkn-19	1 TN 15	39.21	39.21	0.000
D02	SYBR	OC	Unkn-19	1 TN 15	N/A	0.00	0.000
D03	SYBR	OC	Unkn-20	2 TN 15	35.51	35.49	0.018
D04	SYBR	OC	Unkn-20	2 TN 15	35.48	35.49	0.018
D05	SYBR	OC	Unkn-21	3 TN 15	36.30	36.22	0.108
D06	SYBR	OC	Unkn-21	3 TN 15	36.15	36.22	0.108
D07	SYBR	OC	Unkn-22	4 TN 15	N/A	0.00	0.000
D08	SYBR	OC	Unkn-22	4 TN 15	N/A	0.00	0.000
D09	SYBR	OC	Unkn-23	5 TN 15	30.03	29.86	0.247
D10	SYBR	OC	Unkn-23	5 TN 15	29.68	29.86	0.247
D11	SYBR	OC	Unkn-24	6 TN 15	38.91	39.02	0.159

Well	Fluor	Target	Content	Sample	Cq	Cq Mean	Cq Std. Dev
D12	SYBR	OC	Unkn-24	6 TN 15	39.14	39.02	0.159
E01	SYBR	OC	Pos Ctrl	PC 001 15	30.91	30.91	0.000
E02	SYBR	OC	Pos Ctrl	PC 001 15	30.32	30.32	0.000
E03	SYBR	OC	Neg Ctrl	H2O	N/A	0.00	0.000
E04	SYBR	OC	Neg Ctrl	H2O	N/A	0.00	0.000
E05	SYBR	OC	Neg Ctrl	H2O	N/A	0.00	0.000
E06	SYBR	OC	Neg Ctrl	H2O	N/A	0.00	0.000
E07	SYBR	OC	Unkn	PMC 15 15	37.23	37.23	0.000
E08	SYBR	OC	Unkn	PMC 15 15	38.02	38.02	0.000
E09	SYBR	OC	Unkn	PMC 10 15	37.85	37.85	0.000
E10	SYBR	OC	Unkn	PMC 10 15	37.14	37.14	0.000
E11	SYBR	OC	Unkn	PMC 5 15	38.51	38.51	0.000
E12	SYBR	OC	Unkn	PMC 5 15	37.26	37.26	0.000

Gene Expression

Target Names

Name	Full Name	Reference	Auto Efficiency	Efficiency
OC	OC	False	Yes	100.0%

Oc results 60days.pcrd

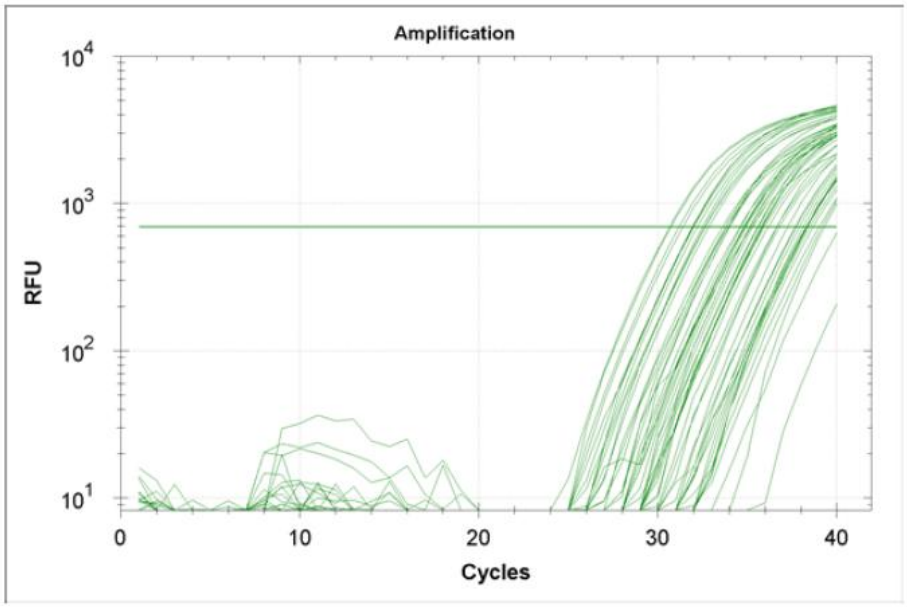
2013/08/21 01:27 PM

Run Setup

Plate Display

	1	2	3	4	5	6	7	8	9	10	11	12
A	Unk-1 OC 1 S 60	Unk-1 OC 1 S 60	Unk-2 OC 2 S 60	Unk-2 OC 2 S 60	Unk-3 OC 3 S 60	Unk-3 OC 3 S 60	Unk-4 OC 4 S 60	Unk-4 OC 4 S 60	Unk-5 OC 5 S 60	Unk-5 OC 5 S 60	Unk-6 OC 6 S 60	Unk-6 OC 6 S 60
B	Unk-7 OC 1 N 60	Unk-7 OC 1 N 60	Unk-8 OC 2 N 60	Unk-8 OC 2 N 60	Unk-9 OC 3 N 60	Unk-9 OC 3 N 60	Unk-10 OC 4 N 60	Unk-10 OC 4 N 60	Unk-11 OC 5 N 60	Unk-11 OC 5 N 60	Unk-12 OC 6 N 60	Unk-12 OC 6 N 60
C	Unk-13 OC 1 T 60	Unk-13 OC 1 T 60	Unk-14 OC 2 T 60	Unk-14 OC 2 T 60	Unk-15 OC 3 T 60	Unk-15 OC 3 T 60	Unk-16 OC 4 T 60	Unk-16 OC 4 T 60	Unk-17 OC 5 T 60	Unk-17 OC 5 T 60	Unk-18 OC 6 T 60	Unk-18 OC 6 T 60
D	Unk-19 OC 1 TN 60	Unk-19 OC 1 TN 60	Unk-20 OC 2 TN 60	Unk-20 OC 2 TN 60	Unk-21 OC 3 TN 60	Unk-21 OC 3 TN 60	Unk-22 OC 4 TN 60	Unk-22 OC 4 TN 60	Unk-23 OC 5 TN 60	Unk-23 OC 5 TN 60	Unk-24 OC 6 TN 60	Unk-24 OC 6 TN 60
E	Pos OC PC 001 60	Pos OC PC 001 60	Neg OC H2O	Neg OC H2O	Neg OC H2O	Neg OC H2O	Unk OC PMC 15 60	Unk OC PMC 15 60	Unk OC PMC 10 60	Unk OC PMC 10 60	Unk OC PMC 5 60	Unk OC PMC 5 60
F												
G												
H												

Quantification



Quantification Data

Well	Fluor	Target	Content	Sample	Cq	Cq Mean	Cq Std. Dev
A01	SYBR	OC	Unkn-01	1 S 60	35.22	35.03	0.264
A02	SYBR	OC	Unkn-01	1 S 60	34.85	35.03	0.264
A03	SYBR	OC	Unkn-02	2 S 60	33.57	34.05	0.679
A04	SYBR	OC	Unkn-02	2 S 60	34.53	34.05	0.679
A05	SYBR	OC	Unkn-03	3 S 60	33.84	33.92	0.115
A06	SYBR	OC	Unkn-03	3 S 60	34.00	33.92	0.115
A07	SYBR	OC	Unkn-04	4 S 60	36.60	35.93	0.943
A08	SYBR	OC	Unkn-04	4 S 60	35.26	35.93	0.943
A09	SYBR	OC	Unkn-05	5 S 60	33.84	33.78	0.084
A10	SYBR	OC	Unkn-05	5 S 60	33.72	33.78	0.084
A11	SYBR	OC	Unkn-06	6 S 60	36.15	36.04	0.148
A12	SYBR	OC	Unkn-06	6 S 60	35.94	36.04	0.148
B01	SYBR	OC	Unkn-07	1 N 60	38.24	38.26	0.017
B02	SYBR	OC	Unkn-07	1 N 60	38.27	38.26	0.017
B03	SYBR	OC	Unkn-08	2 N 60	N/A	0.00	0.000
B04	SYBR	OC	Unkn-08	2 N 60	N/A	0.00	0.000
B05	SYBR	OC	Unkn-09	3 N 60	38.32	38.29	0.036
B06	SYBR	OC	Unkn-09	3 N 60	38.27	38.29	0.036
B07	SYBR	OC	Unkn-10	4 N 60	34.59	34.85	0.370
B08	SYBR	OC	Unkn-10	4 N 60	35.11	34.85	0.370
B09	SYBR	OC	Unkn-11	5 N 60	36.61	37.15	0.768
B10	SYBR	OC	Unkn-11	5 N 60	37.69	37.15	0.768
B11	SYBR	OC	Unkn-12	6 N 60	36.76	35.95	1.146
B12	SYBR	OC	Unkn-12	6 N 60	35.14	35.95	1.146
C01	SYBR	OC	Unkn-13	1 T 60	31.35	31.25	0.139
C02	SYBR	OC	Unkn-13	1 T 60	31.16	31.25	0.139
C03	SYBR	OC	Unkn-14	2 T 60	32.62	32.72	0.140
C04	SYBR	OC	Unkn-14	2 T 60	32.82	32.72	0.140
C05	SYBR	OC	Unkn-15	3 T 60	32.55	32.49	0.081
C06	SYBR	OC	Unkn-15	3 T 60	32.44	32.49	0.081
C07	SYBR	OC	Unkn-16	4 T 60	34.81	34.88	0.103
C08	SYBR	OC	Unkn-16	4 T 60	34.95	34.88	0.103
C09	SYBR	OC	Unkn-17	5 T 60	35.70	35.77	0.096
C10	SYBR	OC	Unkn-17	5 T 60	35.84	35.77	0.096
C11	SYBR	OC	Unkn-18	6 T 60	37.89	38.26	0.526
C12	SYBR	OC	Unkn-18	6 T 60	38.63	38.26	0.526
D01	SYBR	OC	Unkn-19	1 TN 60	35.56	35.69	0.183
D02	SYBR	OC	Unkn-19	1 TN 60	35.82	35.69	0.183
D03	SYBR	OC	Unkn-20	2 TN 60	32.18	32.04	0.191
D04	SYBR	OC	Unkn-20	2 TN 60	31.91	32.04	0.191
D05	SYBR	OC	Unkn-21	3 TN 60	32.00	31.98	0.035
D06	SYBR	OC	Unkn-21	3 TN 60	31.95	31.98	0.035
D07	SYBR	OC	Unkn-22	4 TN 60	34.78	34.37	0.570
D08	SYBR	OC	Unkn-22	4 TN 60	33.97	34.37	0.570
D09	SYBR	OC	Unkn-23	5 TN 60	35.79	35.66	0.180
D10	SYBR	OC	Unkn-23	5 TN 60	35.53	35.66	0.180
D11	SYBR	OC	Unkn-24	6 TN 60	38.46	38.80	0.481

Well	Fluor	Target	Content	Sample	Cq	Cq Mean	Cq Std. Dev
D12	SYBR	OC	Unkn-24	6 TN 60	39.14	38.80	0.481
E01	SYBR	OC	Pos Ctrl	PC 001 60	30.61	30.61	0.000
E02	SYBR	OC	Pos Ctrl	PC 001 60	30.69	30.69	0.000
E03	SYBR	OC	Neg Ctrl	H2O	N/A	0.00	0.000
E04	SYBR	OC	Neg Ctrl	H2O	N/A	0.00	0.000
E05	SYBR	OC	Neg Ctrl	H2O	N/A	0.00	0.000
E06	SYBR	OC	Neg Ctrl	H2O	N/A	0.00	0.000
E07	SYBR	OC	Unkn	PMC 15 60	39.26	39.26	0.000
E08	SYBR	OC	Unkn	PMC 15 60	38.31	38.31	0.000
E09	SYBR	OC	Unkn	PMC 10 60	38.10	38.10	0.000
E10	SYBR	OC	Unkn	PMC 10 60	37.62	37.62	0.000
E11	SYBR	OC	Unkn	PMC 5 60	37.22	37.22	0.000
E12	SYBR	OC	Unkn	PMC 5 60	39.01	39.01	0.000

Gene Expression

Target Names

Name	Full Name	Reference	Auto Efficiency	Efficiency
OC	OC	False	Yes	100.0%

Oc results 90days.pcrd

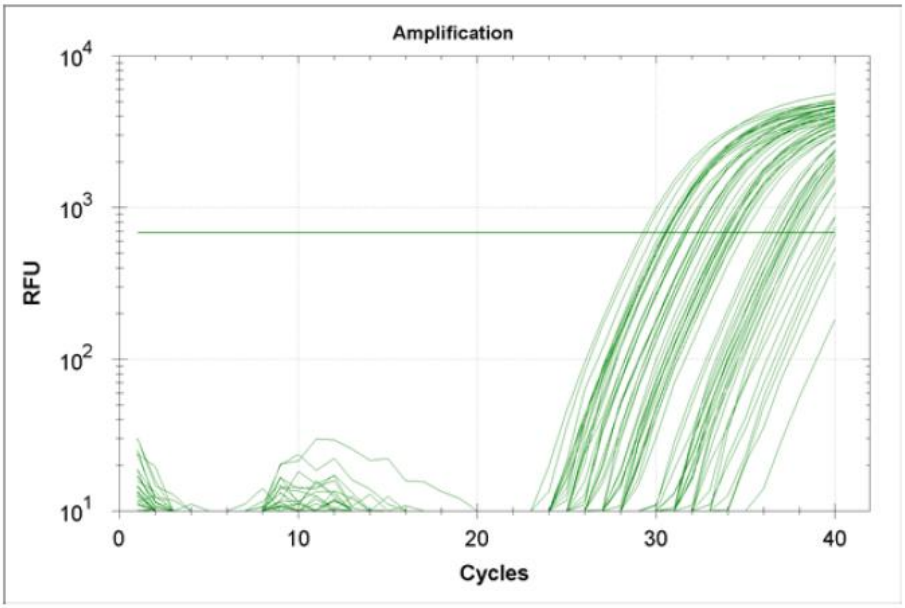
2013/08/21 01:34 PM

Run Setup

Plate Display

	1	2	3	4	5	6	7	8	9	10	11	12
A	Unk-1 OC 1 S 90	Unk-1 OC 1 S 90	Unk-2 OC 2 S 90	Unk-2 OC 2 S 90	Unk-3 OC 3 S 90	Unk-3 OC 3 S 90	Unk-4 OC 4 S 90	Unk-4 OC 4 S 90	Unk-5 OC 5 S 90	Unk-5 OC 5 S 90	Unk-6 OC 6 S 90	Unk-6 OC 6 S 90
B	Unk-7 OC 1 N 90	Unk-7 OC 1 N 90	Unk-8 OC 2 N 90	Unk-8 OC 2 N 90	Unk-9 OC 3 N 90	Unk-9 OC 3 N 90	Unk-10 OC 4 N 90	Unk-10 OC 4 N 90	Unk-11 OC 5 N 90	Unk-11 OC 5 N 90	Unk-12 OC 6 N 90	Unk-12 OC 6 N 90
C	Unk-13 OC 1 T 90	Unk-13 OC 1 T 90	Unk-14 OC 2 T 90	Unk-14 OC 2 T 90	Unk-15 OC 3 T 90	Unk-15 OC 3 T 90	Unk-16 OC 4 T 90	Unk-16 OC 4 T 90	Unk-17 OC 5 T 90	Unk-17 OC 5 T 90	Unk-18 OC 6 T 90	Unk-18 OC 6 T 90
D	Unk-19 OC 1 TN 90	Unk-19 OC 1 TN 90	Unk-20 OC 2 TN 90	Unk-20 OC 2 TN 90	Unk-21 OC 3 TN 90	Unk-21 OC 3 TN 90	Unk-22 OC 4 TN 90	Unk-22 OC 4 TN 90	Unk-23 OC 5 TN 90	Unk-23 OC 5 TN 90	Unk-24 OC 6 TN 90	Unk-24 OC 6 TN 90
E	Unk-25 OC MC 1	Unk-25 OC MC 1	Unk-26 OC MC 2	Unk-26 OC MC 2	Unk-27 OC MC 3	Unk-27 OC MC 3	Unk-28 OC MC 4	Unk-28 OC MC 4	Unk-29 OC MC 5	Unk-29 OC MC 5	Unk-30 OC MC 6	Unk-30 OC MC 6
F	Pos OC PC 001 90	Pos OC PC 001 90	Neg OC H2O	Neg OC H2O	Neg OC H2O	Neg OC H2O	Unk OC PMC 15 90	Unk OC PMC 15 90	Unk OC PMC 10 90	Unk OC PMC 10 90	Unk OC PMC 5 90	Unk OC PMC 5 90
G												
H												

Quantification



Quantification Data

Well	Fluor	Target	Content	Sample	Cq	Cq Mean	Cq Std. Dev
A01	SYBR	OC	Unkn-01	1 S 90	33.47	33.82	0.500
A02	SYBR	OC	Unkn-01	1 S 90	34.18	33.82	0.500
A03	SYBR	OC	Unkn-02	2 S 90	30.43	30.73	0.416
A04	SYBR	OC	Unkn-02	2 S 90	31.02	30.73	0.416
A05	SYBR	OC	Unkn-03	3 S 90	33.80	33.74	0.083
A06	SYBR	OC	Unkn-03	3 S 90	33.68	33.74	0.083
A07	SYBR	OC	Unkn-04	4 S 90	34.24	34.09	0.215
A08	SYBR	OC	Unkn-04	4 S 90	33.94	34.09	0.215
A09	SYBR	OC	Unkn-05	5 S 90	34.33	34.15	0.258
A10	SYBR	OC	Unkn-05	5 S 90	33.97	34.15	0.258
A11	SYBR	OC	Unkn-06	6 S 90	37.21	37.49	0.406
A12	SYBR	OC	Unkn-06	6 S 90	37.78	37.49	0.406
B01	SYBR	OC	Unkn-07	1 N 90	34.53	34.73	0.281
B02	SYBR	OC	Unkn-07	1 N 90	34.93	34.73	0.281
B03	SYBR	OC	Unkn-08	2 N 90	32.30	32.41	0.160
B04	SYBR	OC	Unkn-08	2 N 90	32.53	32.41	0.160
B05	SYBR	OC	Unkn-09	3 N 90	34.47	34.37	0.142
B06	SYBR	OC	Unkn-09	3 N 90	34.27	34.37	0.142
B07	SYBR	OC	Unkn-10	4 N 90	36.03	36.12	0.134
B08	SYBR	OC	Unkn-10	4 N 90	36.22	36.12	0.134
B09	SYBR	OC	Unkn-11	5 N 90	38.14	37.59	0.770
B10	SYBR	OC	Unkn-11	5 N 90	37.05	37.59	0.770
B11	SYBR	OC	Unkn-12	6 N 90	33.71	33.79	0.114
B12	SYBR	OC	Unkn-12	6 N 90	33.87	33.79	0.114
C01	SYBR	OC	Unkn-13	1 T 90	31.60	31.62	0.029
C02	SYBR	OC	Unkn-13	1 T 90	31.65	31.62	0.029
C03	SYBR	OC	Unkn-14	2 T 90	32.25	32.28	0.039
C04	SYBR	OC	Unkn-14	2 T 90	32.31	32.28	0.039
C05	SYBR	OC	Unkn-15	3 T 90	31.44	31.55	0.152
C06	SYBR	OC	Unkn-15	3 T 90	31.66	31.55	0.152
C07	SYBR	OC	Unkn-16	4 T 90	29.21	29.29	0.116
C08	SYBR	OC	Unkn-16	4 T 90	29.38	29.29	0.116
C09	SYBR	OC	Unkn-17	5 T 90	32.75	32.62	0.192
C10	SYBR	OC	Unkn-17	5 T 90	32.48	32.62	0.192
C11	SYBR	OC	Unkn-18	6 T 90	32.69	32.93	0.341
C12	SYBR	OC	Unkn-18	6 T 90	33.17	32.93	0.341
D01	SYBR	OC	Unkn-19	1 TN 90	30.24	30.05	0.269
D02	SYBR	OC	Unkn-19	1 TN 90	29.85	30.05	0.269
D03	SYBR	OC	Unkn-20	2 TN 90	30.38	30.43	0.067
D04	SYBR	OC	Unkn-20	2 TN 90	30.48	30.43	0.067
D05	SYBR	OC	Unkn-21	3 TN 90	30.50	31.00	0.707
D06	SYBR	OC	Unkn-21	3 TN 90	31.50	31.00	0.707
D07	SYBR	OC	Unkn-22	4 TN 90	30.53	30.53	0.001
D08	SYBR	OC	Unkn-22	4 TN 90	30.53	30.53	0.001
D09	SYBR	OC	Unkn-23	5 TN 90	30.82	30.79	0.051
D10	SYBR	OC	Unkn-23	5 TN 90	30.75	30.79	0.051
D11	SYBR	OC	Unkn-24	6 TN 90	37.01	37.16	0.200

Well	Fluor	Target	Content	Sample	Cq	Cq Mean	Cq Std. Dev
D12	SYBR	OC	Unkn-24	6 TN 90	37.30	37.16	0.200
E01	SYBR	OC	Unkn-25	MC 1	N/A	0.00	0.000
E02	SYBR	OC	Unkn-25	MC 1	39.79	39.79	0.000
E03	SYBR	OC	Unkn-26	MC 2	38.67	38.02	0.914
E04	SYBR	OC	Unkn-26	MC 2	37.38	38.02	0.914
E05	SYBR	OC	Unkn-27	MC 3	N/A	0.00	0.000
E06	SYBR	OC	Unkn-27	MC 3	N/A	0.00	0.000
E07	SYBR	OC	Unkn-28	MC 4	36.78	36.58	0.280
E08	SYBR	OC	Unkn-28	MC 4	36.38	36.58	0.280
E09	SYBR	OC	Unkn-29	MC 5	39.50	39.50	0.000
E10	SYBR	OC	Unkn-29	MC 5	N/A	0.00	0.000
E11	SYBR	OC	Unkn-30	MC 6	37.36	37.03	0.473
E12	SYBR	OC	Unkn-30	MC 6	36.69	37.03	0.473
F01	SYBR	OC	Pos Ctrl	PC 001 90	30.53	30.53	0.000
F02	SYBR	OC	Pos Ctrl	PC 001 90	30.50	30.50	0.000
F03	SYBR	OC	Neg Ctrl	H2O	N/A	0.00	0.000
F04	SYBR	OC	Neg Ctrl	H2O	N/A	0.00	0.000
F05	SYBR	OC	Neg Ctrl	H2O	N/A	0.00	0.000
F06	SYBR	OC	Neg Ctrl	H2O	N/A	0.00	0.000
F07	SYBR	OC	Unkn	PMC 15 90	38.20	38.20	0.000
F08	SYBR	OC	Unkn	PMC 15 90	37.60	37.60	0.000
F09	SYBR	OC	Unkn	PMC 10 90	37.47	37.47	0.000
F10	SYBR	OC	Unkn	PMC 10 90	37.00	37.00	0.000
F11	SYBR	OC	Unkn	PMC 5 90	38.05	38.05	0.000
F12	SYBR	OC	Unkn	PMC 5 90	39.36	39.36	0.000

Gene Expression

Target Names

Name	Full Name	Reference	Auto Efficiency	Efficiency
OC	OC	False	Yes	100.0%

Results ALP 15days.pcrd

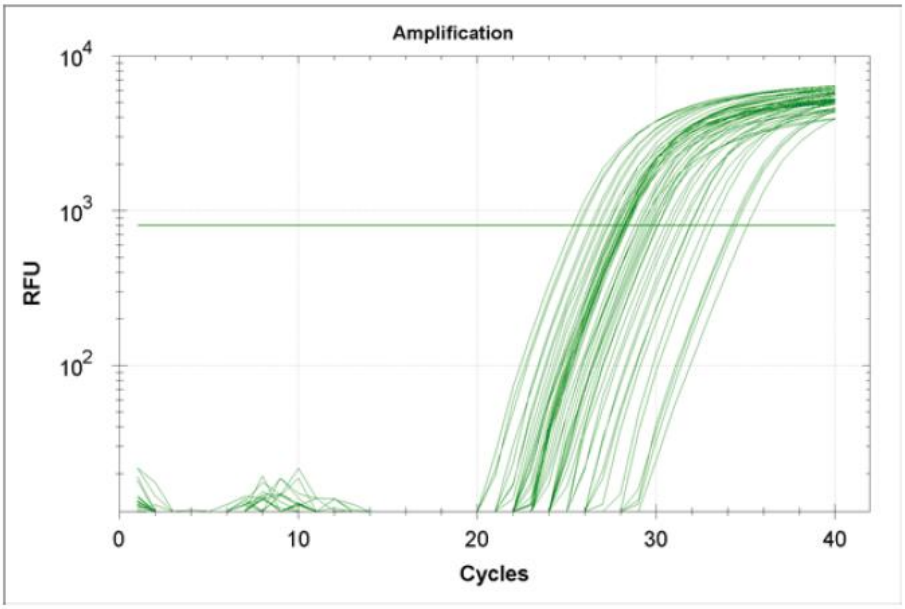
2013/08/21 01:36 PM

Run Setup

Plate Display

	1	2	3	4	5	6	7	8	9	10	11	12
A	Unk-1 ALPase 1 S 15	Unk-1 ALPase 1 S 15	Unk-2 ALPase 2 S 15	Unk-2 ALPase 2 S 15	Unk-3 ALPase 3 S 15	Unk-3 ALPase 3 S 15	Unk-4 ALPase 4 S 15	Unk-4 ALPase 4 S 15	Unk-5 ALPase 5 S 15	Unk-5 ALPase 5 S 15	Unk-6 ALPase 6 S 15	Unk-6 ALPase 6 S 15
B	Unk-7 ALPase 1 N 15	Unk-7 ALPase 1 N 15	Unk-8 ALPase 2 N 15	Unk-8 ALPase 2 N 15	Unk-9 ALPase 3 N 15	Unk-9 ALPase 3 N 15	Unk-10 ALPase 4 N 15	Unk-10 ALPase 4 N 15	Unk-11 ALPase 5 N 15	Unk-11 ALPase 5 N 15	Unk-12 ALPase 6 N 15	Unk-12 ALPase 6 N 15
C	Unk-13 ALPase 1 T 15	Unk-13 ALPase 1 T 15	Unk-14 ALPase 2 T 15	Unk-14 ALPase 2 T 15	Unk-15 ALPase 3 T 15	Unk-15 ALPase 3 T 15	Unk-16 ALPase 4 T 15	Unk-16 ALPase 4 T 15	Unk-17 ALPase 5 T 15	Unk-17 ALPase 5 T 15	Unk-18 ALPase 6 T 15	Unk-18 ALPase 6 T 15
D	Unk-19 ALPase 1 TN 15	Unk-19 ALPase 1 TN 15	Unk-20 ALPase 2 TN 15	Unk-20 ALPase 2 TN 15	Unk-21 ALPase 3 TN 15	Unk-21 ALPase 3 TN 15	Unk-22 ALPase 4 TN 15	Unk-22 ALPase 4 TN 15	Unk-23 ALPase 5 TN 15	Unk-23 ALPase 5 TN 15	Unk-24 ALPase 6 TN 15	Unk-24 ALPase 6 TN 15
E	Pos ALPase PC 001 15	Pos ALPase PC 001 15	Neg ALPase H2O	Neg ALPase H2O	Neg ALPase H2O	Neg ALPase H2O	Unk ALPase PMC 15 15	Unk ALPase PMC 15 15	Unk ALPase PMC 10 15	Unk ALPase PMC 10 15	Unk ALPase PMC 5 15	Unk ALPase PMC 5 15
F												
G												
H												

Quantification



Quantification Data

Well	Fluor	Target	Content	Sample	Cq	Cq Mean	Cq Std. Dev
A01	SYBR	ALPase	Unkn-01	1 S 15	29.65	30.04	0.555
A02	SYBR	ALPase	Unkn-01	1 S 15	30.43	30.04	0.555
A03	SYBR	ALPase	Unkn-02	2 S 15	28.23	28.91	0.949
A04	SYBR	ALPase	Unkn-02	2 S 15	29.58	28.91	0.949
A05	SYBR	ALPase	Unkn-03	3 S 15	27.23	27.62	0.558
A06	SYBR	ALPase	Unkn-03	3 S 15	28.02	27.62	0.558
A07	SYBR	ALPase	Unkn-04	4 S 15	30.91	31.17	0.362
A08	SYBR	ALPase	Unkn-04	4 S 15	31.43	31.17	0.362
A09	SYBR	ALPase	Unkn-05	5 S 15	31.27	31.73	0.641
A10	SYBR	ALPase	Unkn-05	5 S 15	32.18	31.73	0.641
A11	SYBR	ALPase	Unkn-06	6 S 15	28.77	28.89	0.165
A12	SYBR	ALPase	Unkn-06	6 S 15	29.00	28.89	0.165
B01	SYBR	ALPase	Unkn-07	1 N 15	28.20	28.66	0.649
B02	SYBR	ALPase	Unkn-07	1 N 15	29.11	28.66	0.649
B03	SYBR	ALPase	Unkn-08	2 N 15	27.60	27.89	0.409
B04	SYBR	ALPase	Unkn-08	2 N 15	28.18	27.89	0.409
B05	SYBR	ALPase	Unkn-09	3 N 15	27.11	27.44	0.474
B06	SYBR	ALPase	Unkn-09	3 N 15	27.78	27.44	0.474
B07	SYBR	ALPase	Unkn-10	4 N 15	28.99	29.38	0.546
B08	SYBR	ALPase	Unkn-10	4 N 15	29.76	29.38	0.546
B09	SYBR	ALPase	Unkn-11	5 N 15	29.43	29.63	0.281
B10	SYBR	ALPase	Unkn-11	5 N 15	29.83	29.63	0.281
B11	SYBR	ALPase	Unkn-12	6 N 15	30.08	30.37	0.418
B12	SYBR	ALPase	Unkn-12	6 N 15	30.67	30.37	0.418
C01	SYBR	ALPase	Unkn-13	1 T 15	27.88	28.13	0.353
C02	SYBR	ALPase	Unkn-13	1 T 15	28.38	28.13	0.353
C03	SYBR	ALPase	Unkn-14	2 T 15	27.75	27.71	0.048
C04	SYBR	ALPase	Unkn-14	2 T 15	27.68	27.71	0.048
C05	SYBR	ALPase	Unkn-15	3 T 15	26.82	27.05	0.325
C06	SYBR	ALPase	Unkn-15	3 T 15	27.28	27.05	0.325
C07	SYBR	ALPase	Unkn-16	4 T 15	25.69	26.04	0.492
C08	SYBR	ALPase	Unkn-16	4 T 15	26.39	26.04	0.492
C09	SYBR	ALPase	Unkn-17	5 T 15	25.30	25.43	0.190
C10	SYBR	ALPase	Unkn-17	5 T 15	25.57	25.43	0.190
C11	SYBR	ALPase	Unkn-18	6 T 15	29.32	29.68	0.515
C12	SYBR	ALPase	Unkn-18	6 T 15	30.05	29.68	0.515
D01	SYBR	ALPase	Unkn-19	1 TN 15	28.33	28.76	0.619
D02	SYBR	ALPase	Unkn-19	1 TN 15	29.20	28.76	0.619
D03	SYBR	ALPase	Unkn-20	2 TN 15	28.02	28.03	0.017
D04	SYBR	ALPase	Unkn-20	2 TN 15	28.04	28.03	0.017
D05	SYBR	ALPase	Unkn-21	3 TN 15	27.52	27.77	0.347
D06	SYBR	ALPase	Unkn-21	3 TN 15	28.01	27.77	0.347
D07	SYBR	ALPase	Unkn-22	4 TN 15	31.84	31.87	0.039
D08	SYBR	ALPase	Unkn-22	4 TN 15	31.90	31.87	0.039
D09	SYBR	ALPase	Unkn-23	5 TN 15	26.26	26.47	0.300
D10	SYBR	ALPase	Unkn-23	5 TN 15	26.68	26.47	0.300
D11	SYBR	ALPase	Unkn-24	6 TN 15	28.24	28.18	0.081

Well	Fluor	Target	Content	Sample	Cq	Cq Mean	Cq Std. Dev
D12	SYBR	ALPase	Unkn-24	6 TN 15	28.12	28.18	0.081
E01	SYBR	ALPase	Pos Ctrl	PC 001 15	28.16	28.16	0.000
E02	SYBR	ALPase	Pos Ctrl	PC 001 15	28.29	28.29	0.000
E03	SYBR	ALPase	Neg Ctrl	H2O	N/A	0.00	0.000
E04	SYBR	ALPase	Neg Ctrl	H2O	N/A	0.00	0.000
E05	SYBR	ALPase	Neg Ctrl	H2O	N/A	0.00	0.000
E06	SYBR	ALPase	Neg Ctrl	H2O	N/A	0.00	0.000
E07	SYBR	ALPase	Unkn	PMC 15 15	34.17	34.17	0.000
E08	SYBR	ALPase	Unkn	PMC 15 15	32.71	32.71	0.000
E09	SYBR	ALPase	Unkn	PMC 10 15	33.11	33.11	0.000
E10	SYBR	ALPase	Unkn	PMC 10 15	34.27	34.27	0.000
E11	SYBR	ALPase	Unkn	PMC 5 15	34.40	34.40	0.000
E12	SYBR	ALPase	Unkn	PMC 5 15	35.07	35.07	0.000

Gene Expression

Target Names

Name	Full Name	Reference	Auto Efficiency	Efficiency
ALPase	ALPase	False	Yes	100.0%

Results ALP 60days.pcrd

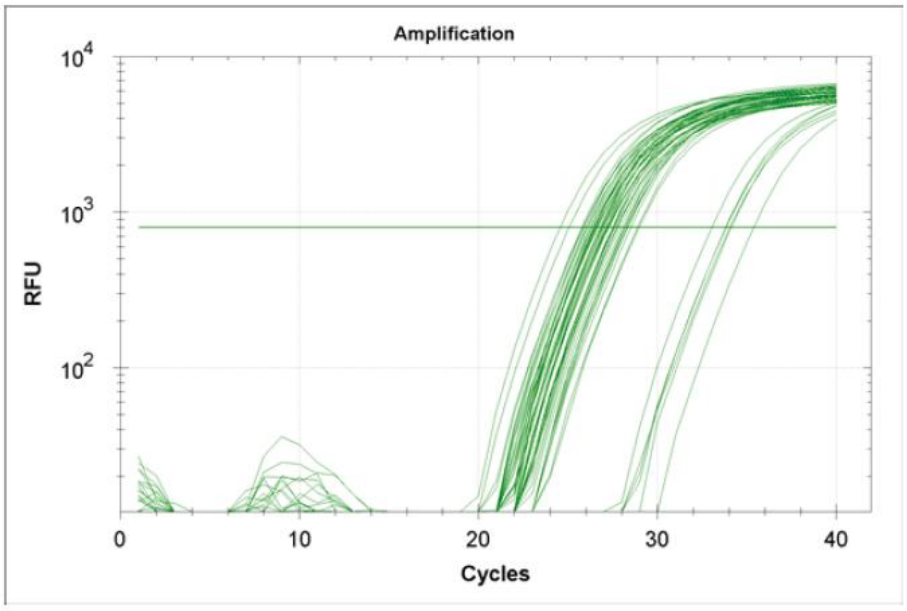
2013/08/21 01:37 PM

Run Setup

Plate Display

	1	2	3	4	5	6	7	8	9	10	11	12
A	Unk-1 ALPase 1 S 60	Unk-1 ALPase 1 S 60	Unk-2 ALPase 2 S 60	Unk-2 ALPase 2 S 60	Unk-3 ALPase 3 S 60	Unk-3 ALPase 3 S 60	Unk-4 ALPase 4 S 60	Unk-4 ALPase 4 S 60	Unk-5 ALPase 5 S 60	Unk-5 ALPase 5 S 60	Unk-6 ALPase 6 S 60	Unk-6 ALPase 6 S 60
B	Unk-7 ALPase 1 N 60	Unk-7 ALPase 1 N 60	Unk-8 ALPase 2 N 60	Unk-8 ALPase 2 N 60	Unk-9 ALPase 3 N 60	Unk-9 ALPase 3 N 60	Unk-10 ALPase 4 N 60	Unk-10 ALPase 4 N 60	Unk-11 ALPase 5 N 60	Unk-11 ALPase 5 N 60	Unk-12 ALPase 6 N 60	Unk-12 ALPase 6 N 60
C	Unk-13 ALPase 1 T 60	Unk-13 ALPase 1 T 60	Unk-14 ALPase 2 T 60	Unk-14 ALPase 2 T 60	Unk-15 ALPase 3 T 60	Unk-15 ALPase 3 T 60	Unk-16 ALPase 4 T 60	Unk-16 ALPase 4 T 60	Unk-17 ALPase 5 T 60	Unk-17 ALPase 5 T 60	Unk-18 ALPase 6 T 60	Unk-18 ALPase 6 T 60
D	Unk-19 ALPase 1 TN 60	Unk-19 ALPase 1 TN 60	Unk-20 ALPase 2 TN 60	Unk-20 ALPase 2 TN 60	Unk-21 ALPase 3 TN 60	Unk-21 ALPase 3 TN 60	Unk-22 ALPase 4 TN 60	Unk-22 ALPase 4 TN 60	Unk-23 ALPase 5 TN 60	Unk-23 ALPase 5 TN 60	Unk-24 ALPase 6 TN 60	Unk-24 ALPase 6 TN 60
E	Pos ALPase PC 001 60	Pos ALPase PC 001 60	Neg ALPase H2O	Neg ALPase H2O	Neg ALPase H2O	Neg ALPase H2O	Unk ALPase PMC 15 60	Unk ALPase PMC 15 60	Unk ALPase PMC 10 60	Unk ALPase PMC 10 60	Unk ALPase PMC 5 60	Unk ALPase PMC 5 60
F												
G												
H												

Quantification



Quantification Data

Well	Fluor	Target	Content	Sample	Cq	Cq Mean	Cq Std. Dev
A01	SYBR	ALPase	Unkn-01	1 S 60	27.18	27.43	0.350
A02	SYBR	ALPase	Unkn-01	1 S 60	27.68	27.43	0.350
A03	SYBR	ALPase	Unkn-02	2 S 60	26.39	26.66	0.372
A04	SYBR	ALPase	Unkn-02	2 S 60	26.92	26.66	0.372
A05	SYBR	ALPase	Unkn-03	3 S 60	26.32	26.44	0.180
A06	SYBR	ALPase	Unkn-03	3 S 60	26.57	26.44	0.180
A07	SYBR	ALPase	Unkn-04	4 S 60	28.03	27.94	0.127
A08	SYBR	ALPase	Unkn-04	4 S 60	27.85	27.94	0.127
A09	SYBR	ALPase	Unkn-05	5 S 60	26.05	26.56	0.722
A10	SYBR	ALPase	Unkn-05	5 S 60	27.07	26.56	0.722
A11	SYBR	ALPase	Unkn-06	6 S 60	27.48	28.23	1.051
A12	SYBR	ALPase	Unkn-06	6 S 60	28.97	28.23	1.051
B01	SYBR	ALPase	Unkn-07	1 N 60	27.21	27.10	0.151
B02	SYBR	ALPase	Unkn-07	1 N 60	26.99	27.10	0.151
B03	SYBR	ALPase	Unkn-08	2 N 60	28.22	28.25	0.040
B04	SYBR	ALPase	Unkn-08	2 N 60	28.28	28.25	0.040
B05	SYBR	ALPase	Unkn-09	3 N 60	27.24	27.70	0.641
B06	SYBR	ALPase	Unkn-09	3 N 60	28.15	27.70	0.641
B07	SYBR	ALPase	Unkn-10	4 N 60	28.12	27.63	0.699
B08	SYBR	ALPase	Unkn-10	4 N 60	27.13	27.63	0.699
B09	SYBR	ALPase	Unkn-11	5 N 60	27.14	27.02	0.175
B10	SYBR	ALPase	Unkn-11	5 N 60	26.90	27.02	0.175
B11	SYBR	ALPase	Unkn-12	6 N 60	27.50	28.18	0.959
B12	SYBR	ALPase	Unkn-12	6 N 60	28.85	28.18	0.959
C01	SYBR	ALPase	Unkn-13	1 T 60	26.75	26.64	0.157
C02	SYBR	ALPase	Unkn-13	1 T 60	26.53	26.64	0.157
C03	SYBR	ALPase	Unkn-14	2 T 60	27.67	26.36	1.850
C04	SYBR	ALPase	Unkn-14	2 T 60	25.05	26.36	1.850
C05	SYBR	ALPase	Unkn-15	3 T 60	26.61	26.36	0.349
C06	SYBR	ALPase	Unkn-15	3 T 60	26.11	26.36	0.349
C07	SYBR	ALPase	Unkn-16	4 T 60	26.41	26.92	0.719
C08	SYBR	ALPase	Unkn-16	4 T 60	27.43	26.92	0.719
C09	SYBR	ALPase	Unkn-17	5 T 60	26.43	26.76	0.458
C10	SYBR	ALPase	Unkn-17	5 T 60	27.08	26.76	0.458
C11	SYBR	ALPase	Unkn-18	6 T 60	26.20	26.49	0.411
C12	SYBR	ALPase	Unkn-18	6 T 60	26.78	26.49	0.411
D01	SYBR	ALPase	Unkn-19	1 TN 60	25.86	26.06	0.284
D02	SYBR	ALPase	Unkn-19	1 TN 60	26.26	26.06	0.284
D03	SYBR	ALPase	Unkn-20	2 TN 60	24.51	25.25	1.050
D04	SYBR	ALPase	Unkn-20	2 TN 60	25.99	25.25	1.050
D05	SYBR	ALPase	Unkn-21	3 TN 60	25.80	25.76	0.057
D06	SYBR	ALPase	Unkn-21	3 TN 60	25.72	25.76	0.057
D07	SYBR	ALPase	Unkn-22	4 TN 60	26.46	26.66	0.284
D08	SYBR	ALPase	Unkn-22	4 TN 60	26.86	26.66	0.284
D09	SYBR	ALPase	Unkn-23	5 TN 60	27.54	27.63	0.117
D10	SYBR	ALPase	Unkn-23	5 TN 60	27.71	27.63	0.117
D11	SYBR	ALPase	Unkn-24	6 TN 60	26.41	26.92	0.718

Well	Fluor	Target	Content	Sample	Cq	Cq Mean	Cq Std. Dev
D12	SYBR	ALPase	Unkn-24	6 TN 60	27.42	26.92	0.718
E01	SYBR	ALPase	Pos Ctrl	PC 001 60	28.29	28.29	0.000
E02	SYBR	ALPase	Pos Ctrl	PC 001 60	28.45	28.45	0.000
E03	SYBR	ALPase	Neg Ctrl	H2O	N/A	0.00	0.000
E04	SYBR	ALPase	Neg Ctrl	H2O	N/A	0.00	0.000
E05	SYBR	ALPase	Neg Ctrl	H2O	N/A	0.00	0.000
E06	SYBR	ALPase	Neg Ctrl	H2O	N/A	0.00	0.000
E07	SYBR	ALPase	Unkn	PMC 15 60	34.10	34.10	0.000
E08	SYBR	ALPase	Unkn	PMC 15 60	33.80	33.80	0.000
E09	SYBR	ALPase	Unkn	PMC 10 60	33.78	33.78	0.000
E10	SYBR	ALPase	Unkn	PMC 10 60	33.04	33.04	0.000
E11	SYBR	ALPase	Unkn	PMC 5 60	35.33	35.33	0.000
E12	SYBR	ALPase	Unkn	PMC 5 60	34.03	34.03	0.000

Gene Expression

Target Names

Name	Full Name	Reference	Auto Efficiency	Efficiency
ALPase	ALPase	False	Yes	100.0%

Results ALP 90days.pcrd

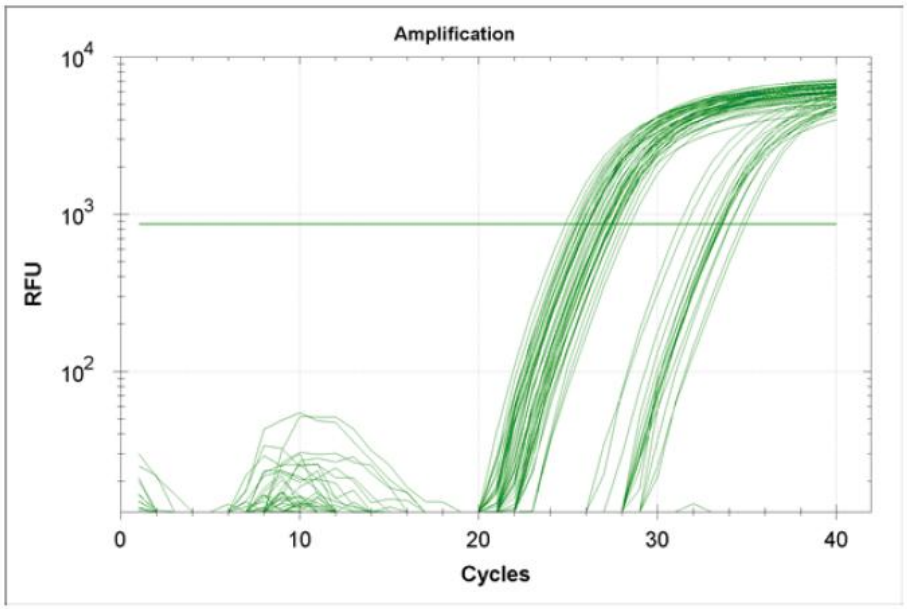
2013/08/21 01:38 PM

Run Setup

Plate Display

	1	2	3	4	5	6	7	8	9	10	11	12
A	Unk-1 ALPase 1 S 90	Unk-1 ALPase 1 S 90	Unk-2 ALPase 2 S 90	Unk-2 ALPase 2 S 90	Unk-3 ALPase 3 S 90	Unk-3 ALPase 3 S 90	Unk-4 ALPase 4 S 90	Unk-4 ALPase 4 S 90	Unk-5 ALPase 5 S 90	Unk-5 ALPase 5 S 90	Unk-6 ALPase 6 S 90	Unk-6 ALPase 6 S 90
B	Unk-7 ALPase 1 N 90	Unk-7 ALPase 1 N 90	Unk-8 ALPase 2 N 90	Unk-8 ALPase 2 N 90	Unk-9 ALPase 3 N 90	Unk-9 ALPase 3 N 90	Unk-10 ALPase 4 N 90	Unk-10 ALPase 4 N 90	Unk-11 ALPase 5 N 90	Unk-11 ALPase 5 N 90	Unk-12 ALPase 6 N 90	Unk-12 ALPase 6 N 90
C	Unk-13 ALPase 1 T 90	Unk-13 ALPase 1 T 90	Unk-14 ALPase 2 T 90	Unk-14 ALPase 2 T 90	Unk-15 ALPase 3 T 90	Unk-15 ALPase 3 T 90	Unk-16 ALPase 4 T 90	Unk-16 ALPase 4 T 90	Unk-17 ALPase 5 T 90	Unk-17 ALPase 5 T 90	Unk-18 ALPase 6 T 90	Unk-18 ALPase 6 T 90
D	Unk-19 ALPase 1 TN 90	Unk-19 ALPase 1 TN 90	Unk-20 ALPase 2 TN 90	Unk-20 ALPase 2 TN 90	Unk-21 ALPase 3 TN 90	Unk-21 ALPase 3 TN 90	Unk-22 ALPase 4 TN 90	Unk-22 ALPase 4 TN 90	Unk-23 ALPase 5 TN 90	Unk-23 ALPase 5 TN 90	Unk-24 ALPase 6 TN 90	Unk-24 ALPase 6 TN 90
E	Unk-25 ALPase MC 1	Unk-25 ALPase MC 1	Unk-26 ALPase MC 2	Unk-26 ALPase MC 2	Unk-27 ALPase MC 3	Unk-27 ALPase MC 3	Unk-28 ALPase MC 4	Unk-28 ALPase MC 4	Unk-29 ALPase MC 5	Unk-29 ALPase MC 5	Unk-30 ALPase MC 6	Unk-30 ALPase MC 6
F	Pos ALPase PC 001 90	Pos ALPase PC 001 90	Neg ALPase H2O	Neg ALPase H2O	Neg ALPase H2O	Neg ALPase H2O	Unk ALPase PMC 15 90	Unk ALPase PMC 15 90	Unk ALPase PMC 10 90	Unk ALPase PMC 10 90	Unk ALPase PMC 5 90	Unk ALPase PMC 5 90
G												
H												

Quantification



Quantification Data

Well	Fluor	Target	Content	Sample	Cq	Cq Mean	Cq Std. Dev
A01	SYBR	ALPase	Unkn-01	1 S 90	26.97	27.21	0.338
A02	SYBR	ALPase	Unkn-01	1 S 90	27.45	27.21	0.338
A03	SYBR	ALPase	Unkn-02	2 S 90	27.01	27.25	0.336
A04	SYBR	ALPase	Unkn-02	2 S 90	27.49	27.25	0.336
A05	SYBR	ALPase	Unkn-03	3 S 90	25.72	26.25	0.750
A06	SYBR	ALPase	Unkn-03	3 S 90	26.78	26.25	0.750
A07	SYBR	ALPase	Unkn-04	4 S 90	27.31	27.47	0.220
A08	SYBR	ALPase	Unkn-04	4 S 90	27.62	27.47	0.220
A09	SYBR	ALPase	Unkn-05	5 S 90	27.01	27.34	0.462
A10	SYBR	ALPase	Unkn-05	5 S 90	27.67	27.34	0.462
A11	SYBR	ALPase	Unkn-06	6 S 90	27.38	27.90	0.738
A12	SYBR	ALPase	Unkn-06	6 S 90	28.43	27.90	0.738
B01	SYBR	ALPase	Unkn-07	1 N 90	27.00	27.16	0.231
B02	SYBR	ALPase	Unkn-07	1 N 90	27.32	27.16	0.231
B03	SYBR	ALPase	Unkn-08	2 N 90	25.11	25.88	1.098
B04	SYBR	ALPase	Unkn-08	2 N 90	26.66	25.88	1.098
B05	SYBR	ALPase	Unkn-09	3 N 90	26.06	26.53	0.673
B06	SYBR	ALPase	Unkn-09	3 N 90	27.01	26.53	0.673
B07	SYBR	ALPase	Unkn-10	4 N 90	27.63	27.91	0.385
B08	SYBR	ALPase	Unkn-10	4 N 90	28.18	27.91	0.385
B09	SYBR	ALPase	Unkn-11	5 N 90	26.36	26.87	0.732
B10	SYBR	ALPase	Unkn-11	5 N 90	27.39	26.87	0.732
B11	SYBR	ALPase	Unkn-12	6 N 90	26.05	26.48	0.612
B12	SYBR	ALPase	Unkn-12	6 N 90	26.91	26.48	0.612
C01	SYBR	ALPase	Unkn-13	1 T 90	25.53	26.06	0.750
C02	SYBR	ALPase	Unkn-13	1 T 90	26.59	26.06	0.750
C03	SYBR	ALPase	Unkn-14	2 T 90	26.12	26.12	0.008
C04	SYBR	ALPase	Unkn-14	2 T 90	26.11	26.12	0.008
C05	SYBR	ALPase	Unkn-15	3 T 90	25.45	25.85	0.572
C06	SYBR	ALPase	Unkn-15	3 T 90	26.26	25.85	0.572
C07	SYBR	ALPase	Unkn-16	4 T 90	25.76	26.10	0.481
C08	SYBR	ALPase	Unkn-16	4 T 90	26.44	26.10	0.481
C09	SYBR	ALPase	Unkn-17	5 T 90	26.04	26.50	0.642
C10	SYBR	ALPase	Unkn-17	5 T 90	26.95	26.50	0.642
C11	SYBR	ALPase	Unkn-18	6 T 90	25.26	25.96	0.987
C12	SYBR	ALPase	Unkn-18	6 T 90	26.65	25.96	0.987
D01	SYBR	ALPase	Unkn-19	1 TN 90	24.81	25.37	0.789
D02	SYBR	ALPase	Unkn-19	1 TN 90	25.92	25.37	0.789
D03	SYBR	ALPase	Unkn-20	2 TN 90	25.43	25.73	0.432
D04	SYBR	ALPase	Unkn-20	2 TN 90	26.04	25.73	0.432
D05	SYBR	ALPase	Unkn-21	3 TN 90	25.72	25.83	0.155
D06	SYBR	ALPase	Unkn-21	3 TN 90	25.94	25.83	0.155
D07	SYBR	ALPase	Unkn-22	4 TN 90	25.36	25.52	0.225
D08	SYBR	ALPase	Unkn-22	4 TN 90	25.68	25.52	0.225
D09	SYBR	ALPase	Unkn-23	5 TN 90	26.09	26.58	0.693
D10	SYBR	ALPase	Unkn-23	5 TN 90	27.07	26.58	0.693
D11	SYBR	ALPase	Unkn-24	6 TN 90	27.12	27.55	0.609

Well	Fluor	Target	Content	Sample	Cq	Cq Mean	Cq Std. Dev
D12	SYBR	ALPase	Unkn-24	6 TN 90	27.98	27.55	0.609
E01	SYBR	ALPase	Unkn-25	MC 1	33.38	34.01	0.885
E02	SYBR	ALPase	Unkn-25	MC 1	34.63	34.01	0.885
E03	SYBR	ALPase	Unkn-26	MC 2	33.45	33.37	0.124
E04	SYBR	ALPase	Unkn-26	MC 2	33.28	33.37	0.124
E05	SYBR	ALPase	Unkn-27	MC 3	33.08	33.58	0.701
E06	SYBR	ALPase	Unkn-27	MC 3	34.07	33.58	0.701
E07	SYBR	ALPase	Unkn-28	MC 4	31.58	31.38	0.281
E08	SYBR	ALPase	Unkn-28	MC 4	31.18	31.38	0.281
E09	SYBR	ALPase	Unkn-29	MC 5	32.33	32.48	0.211
E10	SYBR	ALPase	Unkn-29	MC 5	32.63	32.48	0.211
E11	SYBR	ALPase	Unkn-30	MC 6	33.45	33.49	0.068
E12	SYBR	ALPase	Unkn-30	MC 6	33.54	33.49	0.068
F01	SYBR	ALPase	Pos Ctrl	PC 001 90	27.14	27.14	0.000
F02	SYBR	ALPase	Pos Ctrl	PC 001 90	27.35	27.35	0.000
F03	SYBR	ALPase	Neg Ctrl	H2O	N/A	0.00	0.000
F04	SYBR	ALPase	Neg Ctrl	H2O	N/A	0.00	0.000
F05	SYBR	ALPase	Neg Ctrl	H2O	N/A	0.00	0.000
F06	SYBR	ALPase	Neg Ctrl	H2O	N/A	0.00	0.000
F07	SYBR	ALPase	Unkn	PMC 15 90	33.50	33.50	0.000
F08	SYBR	ALPase	Unkn	PMC 15 90	33.05	33.05	0.000
F09	SYBR	ALPase	Unkn	PMC 10 90	33.57	33.57	0.000
F10	SYBR	ALPase	Unkn	PMC 10 90	33.30	33.30	0.000
F11	SYBR	ALPase	Unkn	PMC 5 90	34.90	34.90	0.000
F12	SYBR	ALPase	Unkn	PMC 5 90	34.03	34.03	0.000

Gene Expression

Target Names

Name	Full Name	Reference	Auto Efficiency	Efficiency
ALPase	ALPase	False	Yes	100.0%

GENERAL REFERENCES

Alliston, T.N & Derynck, R. (2000) Transforming growth factor-β in skeletal development and maintenance. *In Skeletal growth factors* (ed. Canalis, E.), p. 233-249. Lippincot Williams and Wilkins, Philadelphia.

Alliston, T., Piek, E. & Derynck, R. (2008) TGF-β family signalling in skeletal development, maintenance and disease. *In The TGF-β Family* (ed. Derynck, R., Miyazono, K.) p.667-723.CHSL Press, USA.

Chou, L., Firth, J.D., Uitto, V.J. & Brunette, D.M. (1995) Substratum surface topography allows cell shape and regulates fibronectin mRNA levels, mRNA stability, secretion and assembly in human fibroblasts. *J Cell Sci*, 4, 1563–1573.

Curran, J.M., Chen, R. & Hunt, J.A. (2006) The guidance of human mesenchymal stem cell differentiation in vitro by controlled modifications to cell substrate. *Biomaterials*, 27, 4783–93.

Bais, M.V., Wigner, N., Yong, M., Toholka, R., Graves, D.T., Morgan, E.F, *et al.* (2009) BMP2 is essential for post natal osteogenesis but not for recruitment of osteogenic stem cells. *Bone.* 45, 254-266.

Balooch, G., Balooch, M., Nalla, R.K., Schilling, S., Filvaroff, E.H., Marshall, G.W., *et al*. (2005). TGF-β regulates the mechanical properties and composition of bone matrix. *Proc Natl Acad Sci USA,* 102, 18813–18818.

Bandyopadhyay, A., Tsuji, K., Cox, K., Harfe, B.D., Rosen, V. & Tabin, C.J. (2006) Genetic analysis of the roles of BMP2, BMP4, and BMP7 in limb patterning and skeletogenesis. *PLoS Genet*,12, e216.

Barbado, M., Fablet, K., Ronjat, M. & de Waard, M. (2009) Gene regulation by voltage-dependent calcium channels. *Biochem et Biophys Acta,* 1793, 1096-1104.

Berk, M., Desai, S.V., Heyman, H.C. & Colmenares, C. (1997) Mice lacking the *ski* proto-oncogene have defects in neurulation, craniofacial, patterning and skeletal muscle development. *Genes Dev*, 11, 2029-2039.

Boyce, B.F., Rosenberg, E., de Papp, A.E. & Duong Le, T. (2012) The osteoclast, bone remodelling and treatment of metabolic bone disease. *Eur J Clin Invest,* 42, 1332-1341.

Boyle, W.J., Simonet, W.S. & Lacey, D.L. (2003) Osteoclast differentiation and activation. *Nature*, 423, 337-342.

Bruder, S.P. & Caplan, A.I. (1989) Cellular and molecular events during embryonic bone development. *Connect Tissue Res*, 20, 65-71.

Canalis, E., Economides, A.N. & Gazzerro, E. (2003) Bone morphogenetic proteins their antagonists and the skeleton. *Endocr Rev*, 24, 218-235.

Caudarella, R., Vescini, F., Buffa, A., Rizzoli, E., Cecoli, L. & Francucci, C.M. (2011) Role of calcium-sensing receptor in bone biology. *J Endocrinol Invest,* 34, 13-17.

Celeste, A.J., Iannazzi, J.A., Taylor, R.C., Hewick, R.M., Rosen, V., Wang, E.A., *et al.* (1990) Identification of transforming growth factor β family members present in bone inductive protein purified from bovine bone. *Proc Natl Acad Sci USA*, 87, 9843-9847.

Chang, S.C., Hoang, B., Thomas, J.T., Vukicevic, S., Luyten, F.P., Ryba, N.J. *et al.* (1994) Cartilage-derived morphogenetic proteins. New members of the transforming growth factor-β superfamily predominantly expressed in long bones during human embryonic development. *J Biol Chem*, 269, 28227-28234.

Chen, G., Deng, C. & Li, Y.P. (2012) TGF-β and BMP signaling in osteoblast differentiation and bone formation. *Int J Biol Sci*, 8, 272-288.

Cooper, G.M., Usas, A., Olshanski, A., Mooney, M.P., Losee, J.E. & Huard, J. (2009) Ex vivo Noggin gene therapy inhibits bone formation in a mouse model of postoperative resynostosis. *Plast Reconstr Surg*, 123, 94S-103S.

Cserjesi, P., Brown, D., Liqon, K.L., Lyons, G.E., Copeland, N.G., Gilbert, D.J., *et al.* (1995) Scleraxis: a basic helix-loop-helix protein that prefigures skeletal formation during mouse embryogenesis. *Development,* 121, 1099-1110.

Csiszar, A., Smith, K.E., Koller, A., Kaley, G., Edwards, J.G. & Ungavi, Z. (2005) Regulation of bone morphogenetic protein-2 expression in endothelial cells: Role of nuclear factor-K_b activation by tumor necrosis factor-2, H2O2, and high intravascular pressure. *Circulation* 111, 2364-2372.

Dallas, S.L., Rosser, J.L., Mundy, G.R. & Bonewald, L.F. (2002) Proteolysis of latent transforming growth factor-β (TGF-β) – binding protein-1 by osteoclasts. A cellular mechanism of release of TGF-β from bone matrix. *J Biol Chem,* 277, 21352-21360.

Domingos, P.M., Itasaki, N., Jones, C.M., Mercurio, S., Sargent, M.G., Smith, J.C., *et al*. (2001) The Wnt/beta-catenin pathway posteriorizes neural tissue in *Xenopus* by an indirect mechanism requiring FGF signalling. *Dev Biol*, 239, 148–160

Dougall, W.C., Glaccum, M., Charrier, K., Rohrbach, K., Brasel, K., de Smedt, T. *et al.* (1999) RANK is essential for osteoclasts and lymph node development. *Genes Dev*, 13, 2412-2424.

Ducy, P., Zhang, R., Geoffroy, V., Ridall, A.L. & Karsenty, G. (1997) Osf2/Cbfa1: a transcriptional activator of osteoblast differentiation. *Cell,* 89, 747-754.

Ehnert, S., Baur, J., Schmitt, A., Neumaier, M., Lucke, M., Dooley, S., *et al*. (2010) TGF-β_1 as possible link between loss of bone mineral density and chronic inflammation. *PLoS One*, 5: e14073.

Ehnert, S., Zhao, J., Pscherer, S., Freude, T., Dooley, S., Kolk, A., *et al*. (2012) Transforming growth factor β_1 inhibits bone morphogenic protein (BMP)-2 and BMP-7 signaling via upregulation of Ski-related novel protein N (SnoN): possible mechanism for the failure of BMP therapy? *BMC Med*, 10, 101.

Eriksen, E.F. (1986) Normal and pathological remodelling of human trabecular bone: three dimensional reconstruction of the remodelling sequence in normals and in metabolic bone disease. *Endocrinol Rev,* 7, 379-408.

Erlacher, L., Ny, C.K., Ullrich, R., Krieger, S. & Luyten, F.P. (1998) Presence of cartilage-derived morphogenetic proteins in articular cartilage and enhancement of matrix replacement *in vitro*. *Arthritis Rheum,* 41, 639-643.

Friedenstein, A.J. (1962). Humoral nature of osteogenic activity of transitional epithelium. *Nature,* 194, 698–699.Friedenstein, A.Y. (1968). Induction of bone tissue by transitional epithelium. *Clin Orthop Relat Res*, 59, 21–37.

Friedlaender, G.E., Perry, C.R., Cole, J.D., Cook, S.D., Cierny, G., Muschler, G.F., *et al*. (2001). Osteogenic protein-1 (bone morphogenetic protein-7) in the treatment of tibial non-unions. *J Bone Joint Surg Am,* 83A, S151–S158.

Frost, H.M. (1990) Skeletal structural adaptations to mechanical usage (SATMU): 2. Redefining Wolff's Law: the remodelling problem. *Anat Rec,* 226, 414-422.

Fu, J., Wang, Y.-K., Yang, M.T., Desai, R.A., Yu, X., Liu, Z., *et al*. (2010) Mechanical regulation of cell function with geometrically modulated elastomeric substrates. *Nat Methods,* 7, 733-736.

Garrison, K.R., Donell, S., Ryder, J., Shemilt, I., Mugford, M., Harvey, I., *et al*. (2007). Clinical effectiveness and cost-effectiveness of bone morphogenetic proteins in the non-healing of fractures and spinal fusion: a systematic review. *Health Technol. Assess,* 11, 1–150.

Gautschi, O.P., Frey, S.P. & Zellweger, R. (2007). Bone morphogenetic proteins in clinical applications. *ANZ J Surg,* 77, 626–631.

Gazzerro, E., Gangji, V. & Canalis, E. (1998) Bone morphogenetic proteins induce the expression of Noggin, which limits their activity in cultured rat osteoblasts. *J Clin Invest,* 102, 2106-2114.

Gilbert, S.F. (2000) Developmental Biology (6th ed.); Chapter 14: Osteogenesis: The development of bones. Sinhauer Associates, MA, USA.

Gittens R A, Mclachlan T, Olivares-Navarrete R, Cai Y, Berner S, Tannenbaum R, Schwartz Z, *et al.* (2011) The effects of combined micron-submicron-scale surface roughness and nanoscale features on cell proliferation and differentiation. *Biomaterials,* 32, 3395-3403.

Ghosh-Choudhury, N., Choudhury, G.G., Harris, M.A., Wozney, J., Mundy, G.R., Abboud, S.L. *et al.* (2001) Autoregulation of mouse BMP-2 gene transcription is directed by the proximal promoter element. *Biochem Biophys Res Commun,* 286, 101-108.

Govender, S., Csimma, C., Genant, H. K., Valentin-Opran, A., Amit, Y., Arbel, R., *et al*. (2002). Recombinant human bone morphogenetic protein-2 for treatment of open tibial fractures: A prospective, controlled, randomized study of four hundred and fifty patients. *J Bone Joint Surg Am,* 84-A, 2123–2134.

Groppe, J., Greenwald, J., Wiater, E., Rodriguez, L., Economides, A.N., Kwiatkowski. W., *et al*. (2003) Structural basis of BMP signaling inhibition by Noggin a novel twelve membered cysteine knot protein. *J Bone Joint Surg A*, 85-A Suppl 3, 52-58.

Habibovic, P., Sees, T.M., van den Doel, M.A., van Blitterswijk, C.A. & de Groot, K. (2006) Osteoinduction by biomaterials – Physicochemical and structural influences. *J Biomed Mater Res A*, 77, 747-762.

Hadjidakis, D.J. & Androulakis, J.I. (2006) Bone remodelling. *Ann NY Acad Sc,*; 1092, 385-396.

Hammonds, R.G.Jr., Schwall, R., Dudley, A., Berkemeier, L., Lai, C., Lee, J., *et al.* (1991) Bone inducing activity of mature BMP-2b produced from a hybrid BMP-2a/2b precursor. *Mol Endocrinal*, 5, 149-155.

Hatori, M., Klatle, K.J., Teixeira, C.C. & Shapiro, I.M. (1995) End labelling studies of fragmented DNA in avian growth plate: Evidence for apoptosis in terminally differentiated chondrocytes. *J Bone Miner Res*, 10, 1960-1968.

Hayashi, H., Abdollah, S., Qiu, Y., Cai, J., Xu, Y.Y., Grinnell, B.W., *et al.* (1997) The MAD-related protein Smad7 associates with the TGF-β receptor and functions as an antagonist of TGF-β signalling. *Cell*, 89, 1165-1173.

Helvering, L.M., Sharp, R.L., Ou, X. & Greiser, A.G. (2000) Regulation of the promoters for the human bone morphogenetic protein 2 and 4 genes. *Gene*, 256, 123-138.

Horner, A., Kemp, P., Summers, C., Bord, S., Bishop, N.J., Kelsall, A.W., *et al.* (1998) Expression and distribution of transforming growth factor-β isoforms and their signalling receptors in growing human bone. *Bone*, 23, 95-102.

Horton, W.A. (1990) The biology of bone growth. *Growth Genet Horm*, 6, 1-3.

Huang Z, Ren PG, Ma T, Smith RL & Goodman SB. (2010) Modulating osteogenesis of mesenchymal stem cells by modifying growth factor availability. *Cytokine*, 51, 305-310.

Huggins, G. (1931) The formation of bone under the influence of epithelium of the urinary tract. *Arch Surg*, 22, 377-408.

Hwang, S.Y. & Putney, J.W.Jr. (2011) Calcium signalling in osteoclasts. *Biochem Biophys Acta*, 1813, 979-983.

Imamura, T., Takase, M., Nishihara, A., Oeda, E., Hanai, J., Kawababata, M., *et al.* (1997) Smad6 inhibits signalling by the TGF-β superfamily. *Nature*, 389, 622-626.

Ishidou, Y., Kitajuma, I., Obama, H., Maruyama, I., Murata, F., Imamura, T., *et al.* (1995) Enhanced expression of type 1 receptors for bone morphogenetic proteins during bone formation. *J Bone Miner Res*, 10, 1651-1659.

Ishisaki, A., Yamato, K., Hashimoto, S., Nakao, A., Tamaki, K., Nonaka, K., *et al.* (1999) Differential inhibition of Smad6 and Smad7 on bone morphogenetic protein-and activin-mediated growth arrest and apoptosis in B cells. *J Biol Chem*, 274, 13637-13642.

Kaartinen, V., Voncken, J.W., Shuler, C., Warburton, D., Bu, D., Heisterkamp, N., *et al.* (1995) Abnormal lung development and cleft palate in mice lacking TGF-β_3 indicates defects of epithelial-mesenchymal interaction. *Nat Genet*, 11, 415-421.

Kanatani, M., Sugimoto, T., Fukase, M. & Fujita, T. (1991) Effect of elevated extracellular calcium on the proliferation of osteoblastic MC3T3-ES1 cells: its direct and indirect effects via human monocytes. *Biophys Res Commun*, 181, 1425-1430.

Kawabata, M., Chytil, A. & Moses, H.L. (1995) Cloning of a novel type II serine/threonine kinase receptor through interaction with the type I transforming growth factor β receptor. *J Biol Chem*, 270, 5625-5630.

Klar, R.M. (2011) Bone induction: regeneration through chaos. *Front Physiol*, 2, 1-2.

Khouri, R.K., Koudsi, B. & Reddi, H. (1991). Tissue transformation into bone in vivo. A potential practical application. *Am Med Assoc*, 266, 1953–1955.

Kulkarni, A.B., Huh, C.-G., Becker, D., Geiser, A., Lyght, M., Flanders, K.C., *et al*. (1993). Transforming growth factor-b1 null mutation in mice causes excessive inflammatory response and early death. *Proc Natl Acad Sci USA* 90, 770-774.

Kwok, S., Qin, I., Portridge, N.C. & Selvamunigan, N. (2005) Parathyroid hormone stimulation and PKA signalling of latent transforming growth factor β binding protein-1 (LTBP-1) mRNA expression in osteoblastic cells. *J Cell Biochem*, 95, 1002-1011.

Lacroix, P. (1945). Recent investigations on the growth of bone. *Nature*, 156, 576.

Levander, G. (1938) A study of bone regeneration. *Surg Gynec Obstet*, 67, 705-712.

Levander, G., & Willestaedt, H. (1946). Alcohol-soluble osteogenetic substance from bone marrow. *Nature*, 3992, 587.

Luyten, F.P., Cunningham, N.S., Ma, S., Muthukamaran, N., Hammonds, R.G., Nevins, W.B., *et al.* (1989) Purification and partial amino acid sequence of osteogenin, a protein initiating bone differentiation. *J Biol Chem*, 264, 13377-13380.

Magan, A. & Ripamonti, U. (1996) Geometry of porous hydroxyapatite implants influences osteogenesis in baboons (*Papio ursinus*). *J Craniofac Surg*, 7, 71-78.

Matsunobu, T., Torigoe, K., Ishikawa, M., de Vega, S., Kulkarni, A.B., Iwamoto, Y., *et al*. (2009) Critical roles of the TGF-β type I receptor ALK5 in perichondrial formation and function, cartilage integrity, and osteoblast differentiation during growth plate development. *Dev Biol*, 2, 325-338.

McNamara LE, McMurray RJ, Biggs MJ, Kantawong F, Oreffo RO, Dalby MJ. (2010) Nanotopographical control of stem cell differentiation. *J Tissue Eng*, 18, 1-13.

McNamara, L.E., Sjöström, T., Burgess, K.E., Kim, J.J., Liu, E., Gordonov, S., *et al*. (2011) Skeletal stem cell physiology on functionally distinct titania nanotopographies. *Biomaterials*, 32, 7403–7410.

Mendel, J.G. (1866). Versuche über PflanzenhybridenVerhandlungen des naturforschenden Vereines in Brünn. *Bd,* IV**,** 3–47

Mikic, B., Battaglia, T.C., Taylor, E.A. & Clark, R.T. (2002) The effect of growth/differentiation factor-5 deficiency on femoral composition and mechanical behaviour in mice. *Bone*, 30, 733-737.

Millian, F.A., Denhez, F., Kondaiah, P. & Akhurst, R.J. (1991) Embryonic gene expression patterns of TGF-β_1, β_2 and β_3 suggest different developmental functions *in vivo*. *Development*, 111, 131-143.

Mundy, G., Garrett, R., Harris, S., Chan, J., Chen, D., Rossini, G., *et al.* (1999) Stimulation of bone formation *in vitro* and in rodents by statins. *Science*, 286, 1946-1949.

Müller, P., Bulnheim, U., Diener, A., Luthen, F., Teller, M., Klinkenberg, E.D., *et al.* (2008) Calcium phosphate surfaces promote osteogenic differentiation of mesenchymal stem cells. *J Cell Mol Med*, 12, 281-291.

Mussano, F., Ciccone, G., Ceccarelli, M., Baldi, I. & Bassi, F. (2007) Bone morphogenetic proteins and bone defects: a systematic review. *Spine*, 32, 824–830.

Onishi, T., Ishidou, Y., Nagamine, T., Yone, K., Imamura, T., Kato, M., *et al.* (1998) Distinct and overlapping patterns of localization of bone morphogenetic protein (BMP) family members and a BMP type II receptor during fracture healing in rats. *Bone*, 22 605-612.

Oreffo, R.O., Mundy, G.R., Seyedin, S.M. & Bonewald, L.F. (1989) Activation of the bone-derived latent TGF-β complex by isolated osteoclasts. *Biochem Biophys Res Commun*, 158, 817-823.

Oursler, M.J. (1994) Osteoclast synthesis and secretion and activation of latent transforming growth factor β. *J Bone Miner Res*, 9, 443-452.

Özkaynak, E., Rueger, D.C., Drier, E.A., Corbett, C., Ridge, R. J., Sampath, T.K., *et al.* (1990) OP-1 cDNA encodes an osteogenic protein in the TGF-β family. *EMBO J*, 9, 2085-2093

Parfitt, A.M. (1994) Osteonal and hemi-osteonal remodelling: the spatial and temporal framework for signalling traffic in adult human bone. *J Cell Biochem*, 55, 273-286.

Pelton, R.W., Dickinson, M.E., Moses, H.L. & Hogan, B.L. (1990) *In situ* hybridization analysis of TGF-β_3 RNA expression during mouse development: Comparative studies with TGF-β_1 and β_2. *Development*, 110, 609-620.

Pelton, R.W., Saxena, B., Jones, M., Moses, H.L. & Gold, L.I. (1991) Immunohistochemical localization of TGF-β_1, TGF-β_2 and TGF-β_3 in mouse embryo: Expression patterns suggest multiple roles during embryonic development. *J Cell Biol*, 115, 1091-1105.

Pereira, R.C., Economides, A.N. & Canalis, E. (2000) Bone morphogenetic proteins induce gremlin, a protein that limits their activity in osteoblasts. *Endocrinology*, 141, 4558-4563.

Petryl. M., Hert, J. & Fiala, P. (1996) Spatial organization of the Haversian bone in man. *J Biomech*, 29, 161-169.

Pretheeban, T., Lemos, D.R., Paylor, B., Zhang, R. & Rossi, F.M. (2012) Role of stem/progenitor cells in reparative disorders. *Fibrogenesis of Tissue Repair*, 5, 1-12.

Proetzel, G., Pawlowski, S.A., Wiles, M.V. Yin, M., Boivin, G.P., Howles, P.N., *et al.* (1995) Transforming growth factor-β_3 is required for secondary palate fusion. *Nat Genet*, 11, 409-414.

Raisz, L.G. (1999) Physiology and pathophysiology of bone remodelling. *Clinical Chem*, 45, 1353-1358.

Rajpurokit, R., Mansfield, K., Ohyama, K., Ewert, D. & Shapiro, I.M. (1999) Chondrocyte death is linked to development of a mitochondrial membrane permeability transition in the growth plate. *J Cell Physiol*, 179, 287-296.

Rawadi, G., Vayssiere, B., Dunn, F., Baron, R. & Roman-Roman, S. (2003) BMP-2 controls alkaline phosphotase expression and osteoblast mineralization by a Wnt autocrine loop. *J Bone Miner Res*, 18s, 1842-1853.

Reddi, A.H. (1984) Extracellular Matrix Biochemistry; Chapter: Extracellular matrix and development. Elsevier, New York, p. 375–412.

Reddi, A.H. (1994) Symbiosis of biotechnology and biomaterials: Applications in tissue engineering of bone and cartilage. *J Cell Biochem*, 56, 192-195.

Reddi, A.H. (1997) Bone morphogenesis and modeling: soluble signals sculpt osteosomes in the solid state. *Cell*, 89, 159–161.

Reddi, A.H. (2000) Role of bone morphogenetic proteins in skeletal tissue engineering of bone and cartilage: inductive signals, stem cells, and biomimetic biomaterials. *Tissue Eng*, 6, 351–359.

Reddi, A.H. (2005) BMPs: from bone morphogenetic proteins to body morphogenetic proteins. *Cytokine Growth Factor Rev,*16, 249–50.

Reddi, A.H. & Huggins, C.B. (1972) Biochemical sequences in the transformation of normal fibroblasts in adolescent rats. *Proc Natl Acad Sci USA,* 69, 1601-1605.

Reddi, A.H & Huggins, C.B. (1973) Influence of geometry of transplanted tooth and bone on transformation of fibroblasts. *Proc Soc Exp Biol Med,* 143, 634-637.

Rickard, D.J., Hofbauer, L.C., Bonde, S.K., Gori, F., Spelsberg, T.C. & Riggs, B.L. (1998) Bone morphogenetic protein-6 production in human osteoblastic cell-lines. Selective regulation by estrogen. *J Clin Invest*, 101, 413-422.

Ripamonti, U. (1990) Handbook of Bioactive Ceramics (Volume II: Calcium Phosphate and Hydroxylapatite Ceramics); Inductive bone matrix and porous hydroxyapatite composites in rodents and nonhuman primates. CRC Press, Boca Raton, Florida, p 245-253.

Ripamonti, U. (1991) The morphogenesis of bone replicas of porous hydroxyapatite obtained from conversion of calcium carbonate exoskeletons of coral. *J Bone Joint Surg Am,* 73, 692-703.

Ripamonti, U. (1996) Osteoinduction in porous hydroxyapatite implanted in heterotopic sites of different animal models. *Biomaterials*, 17, 31-35.

Ripamonti, U. (2000) Bone Engineering; Chapter: Smart biomaterials with intrinsic osteoinductivity; Geometric control of bone differentiation. EM2 Corporation, Toronto, Canada, p. 215-222.

Ripamonti, U. (2004) Soluble, insoluble and geometric signals sculpt the architecture of mineralized tissues. *J Cell Mol Med,* 8, 169-180.

Ripamonti, U. (2005) Bone induction by recombinant human osteogenic protein-1 (hOP-1, BMP-7) in the primate *Papio ursinus* with expression of mRNA of gene products of the TGF-β superfamily. *J Cell Mol Med*, 9, 911–928.

Ripamonti, U. (2006) Soluble osteogenic molecular signals and the induction of bone formation. *Biomaterials,* 27, 807-822.

Ripamonti, U. (2009) Biomimetism, biomimetic matrices and the induction of bone formation. *J Cell Mol Med,* 13, 2953-2972.

Ripamonti, U. (2010) Soluble and insoluble signals sculpt osteogenesis in angiogenesis. *World J Biol Chem*, 1, 109–132.

Ripamonti, U. & Duneas, N. (1996) Tissue engineering of bone by osteoinductive biomaterials. *Material Research Society Bulletin*, 21, 36-39.

Ripamonti, U. & Duneas, N. (1998) Tissue morphogenesis and regeneration by bone morphogenetic proteins. *Plast Reconstr Surg,* 101, 227-239.

Ripamonti, U., Duneas, N., van den Heever, B., Bosch, C. & Crooks, J. (1997) Recombinant transforming growth factor-β_1 induces endochondral bone in the baboon and synergizes with recombinant osteogenic protein-1 (bone morphogenetic protein-7) to initiate rapid bone formation. *J Bone Miner Res,* 2, 1584-1595.

Ripamonti, U., Crooks, J. & Kirkbride, A.N. (1999) Sintered porous hydroxyapatites with intrinsic osteoinductive activity: Geometric induction of bone formation. *S Afr J Sci*, 95, 335-343.

Ripamonti, U., Crooks, J., Khoali, L. & Roden, L. (2009) The induction of bone formation by coral-derived calcium carbonate/hydroxyapatite constructs. *Biomaterials*, 30, 1428-1439.

Ripamonti, U., Crooks, J., Matsaba, T. & Taskar, J, (2000) Induction of endochondral bone formation by recombinant human transforming growth factor-β_2 in the baboon (*Papio ursinus*). *Growth Factors,* 17, 269-285.

Ripamonti, U., Ferretti, C. & Heliotis, M. (2006) Soluble and insoluble signals and the induction of bone formation: Molecular therapeutics recapitulating development. *J. Anat,* 209, 447–468.

Ripamonti, U., Ferretti, C., Teare, J. & Blann, L. (2009) Transforming growth factor-β isoforms and the induction of bone formation: Implications for reconstructive craniofacial surgery. *J Craniofac Surg,* 20, 1544-1555.

Ripamonti, U. & Ferretti, C. (2012) Keystone symposia on regenerative tissue engineering. Grand challenges for craniomandibularfacialreconstruction by human recombinant transforming growth factor-β_3. Breckenridge CO. http://www.keystonesymposia.org; 2012.

Ripamonti, U., Klar, R.M., Duarte, R. & Dix-Peek, T. (2014) Keystone Symposia on Molecular and Cellular Biology, Engineering Cell fate and Function. Engineering microenvironments super activated by hTGF-β_3 reprogramming recruited differentiated pericytes into highly active secreting osteoblasts in primate striated muscles. Squaw Creek, Olympic valley, CA, 2014.

Ripamonti, U., Heliotis, M. & Ferretti, C. (2007) Bone morphogenetic proteins and the induction of bone formation: From laboratory to patients. *Oral Maxillofac Surg Clin North Am*, 19, 575–589.

Ripamonti, U., Ma, S., Cunningham, N.S., Yeates, L. & Reddi, A.H. (1992) Initiation of bone regeneration in adult baboons by osteogenin, a bone morphogenetic protein. *Matrix*, 12, 369-380.

Ripamonti, U., Ramoshebi, L.N., Matsaba, T., Tasker, J., Crooks, J. & Teare J. (2001) Bone induction by BMPs/OPs and related family members in primates. *J Bone Joint Surg*,83-A Suppl 1(Pt 2)**,** S116-127.

Ripamonti, U., Ramoshebi, L.N., Patton, J., Matsaba, T., Teare, J. & Renton, L. (2004) The Skeleton; Chapter 15: Soluble signals and insoluble substrata: Novel molecular cues instructing the induction of bone. Humana Press, USA, p 217-227.

Ripamonti, U., Ramoshebi, L.N., Patton, J., Teare, J., Matsaba, T. & Renton, L. (2004a) Pharmaceutical Biotechnology; Chapter 16: Sculpturing the architecture of mineralized tissues: Tissue engineering of bone from soluble signals to smart biomimetic matrices. Wiley-VCH, USA, 281-297.

Ripamonti, U., Ramoshebi, L.N., Teare. J., Renton, L. & Ferretti, C. (2008) The induction of endochondral bone formation by transforming growth factor-β_3: experimental studies in the non-human primate *Papio ursinus*. *J Cell Mol Med*, 12, 1029-1048.

Ripamonti, U. & Roden, L.C. (2010) The induction of bone formation by transforming growth factor-β_2 in the non-human primate *Papio ursinus* and its modulation by skeletal muscle responding stem cells. *Cell Proliferation,* 43, 207-218.

Ripamonti, U., Roden, L.C., Ferretti, C. & Klar, R. (2011) Biomimetic matrices self-initiating the induction of bone formation. *J Craniofacial Surg*, 22, 1859-1870.

Ripamonti, U., Roden, L., Renton, L., Klar, R. & Jean-Claude, P. (2012) The influence of geometry on bone: formation by autoinduction. *Science in Africa*, 5, 1-51.

Ripamonti, U. & Reddi, A.H. (1995) Bone morphogenetic proteins: applications in plastic and reconstructive surgery. *Adv Plast Reconstr Surg*, 11, 47–73.

Ripamonti, U., Richter, P.W. & Thomas, M.E. (2007a) Self-inducing shape memory geometric cues embedded within *smart* hydroxyapatite-based biomimetic matrices. *Plast Reconstr Surg*, 120, 1796-1807.

Ripamonti, U., Teare, J. & Ferretti C. (2012a) A macroporous bioreactor super activated by the recombinant human transforming growth factor-β_3. *Front Physiol*, 3, 1-18.

Ripamonti, U., van den Heever, B., Crooks, J., Tucker, M.M., Sampath, T.K., *et al*. (2000a) Long-term evaluation of bone formation by osteogenic protein 1 in the baboon and relative efficacy of bone-derived bone morphogenetic proteins delivered by irradiated xenogeneic collagenous matrices. *J Bone Miner Res*, 15, 1798-1809.

Ripamonti, U., van den Heever, B. & van Wyk, J. (1993) Expression of the osteogenic phenotype in porous hydroxyapatite implanted extraskeletally in baboons. *Matrix*, 13, 491-502.

Roberts, A.B., Sporn, M.B., Assoian, R.K., Smith, J.M., Roche, N.S., Wakefield, L.M., *et al.* (1986) Transforming growth factor type β: Rapid induction of fibrosis and angiogenesis *in vivo* and stimulation of collagen formation *in vitro*. *Proc Natl Acad Sci USA*, 83, 4167-4171.

Saadeh, P.B., Mehrara, B.J., Steinbrech, D.S., Dudziak, M.E., Greenwald, J.A., Luchs, J.S., *et al*. (1999) Transforming growth factor-β1 modulates the expression of vascular endothelial growth factor by osteoblasts. *Am J Physiol,* 277(Pt 1), C628–C637.

Sacerdotti, C. & Frattin, G. (1901) Sulla produzione eteroplastica dell'osso. *R Accad MedTorino*, 825-836.

Sakou, T., Onishi, T., Yamamoto, T., Nagamine, T., Sampath, T. & ten Dijke, P. (1999) Localization of Smads, the TGF-β family intracellular signalling components during endochondral ossification. *J Bone Miner Res*, 14, 1145-1152.

Sampath, T.K., Maliakal, J.C., Hauschka, P.V., Jones, W.K., Sasak, H., Tucker, R.F, *et al.* (1992) Recombinant hOP-1 induces new bone formation in vivo with specific activity comparable to natural bovine OP-1, and stimulates osteoblast proliferation and differentiation in vitro. *J Biol Chem*, 267, 20352–20362.

Sampath, T.K., Muthukumaran, N. & Reddi, A.H. (1987) Isolation of osteogenin, an extracellular matrix-associated, bone-inductive protein, by heparin affinity chromatography. *Proc Natl Acad Sc. USA*, 84, 7109–7113.

Sampath, T.K., Rashka, K.E., Doctor, J.S., Tucker, R.F. & Hoffmann, F.M. (1993). Drosophila transforming growth factor superfamily proteins induce endochondral bone formation in mammals. *Proc Natl Acad Sci USA*, **13,** 6004-6008.

Sampath, T.K. & Reddi, A.H. (1981) Dissociative extraction and reconstitution of extracellular matrix components involved in local bone differentiation. *Proc Natl Acad Sci USA*, 78, 7599–7603.

Sampath, T.K. & Reddi, A.H. (1983) Homology of bone-inductive proteins from human, monkey, bovine, and rat extracellular matrix. *Proc Natl Acad Sci USA*, 80, 6591–6595.

Sampath, T.K. & Reddi, A.H. (1984) Distribution of bone inductive proteins in mineralized and demineralized extracellular matrix. *Biochem Biophys Res Commun*, 119, 949–954.

Sandberg, M., Vuorio, T., Hirvonen, H., Alitalo, K. & Vuorio, E. (1988) Enhanced expression of TGF-β and *c-fos* mRNA in the growth plates of developing human long bones. *Development*, 102, 461-470.

Sandford, L.P., Ormsby, I., Gittenberger-de Groot, A.C., Sariola, H., Friedman, R., Boivin, G.P., *et al.* (1997) TGFβ_2 knockout mice have multiple developmental defects that are non-overlapping with other TGFβ knockout phenotypes. *Development*, 124, 2659-2670.

Sasso, R.C., Williams, J.I., Dimasi, N. & Meyer, P.R. Jr. (1998) Postoperative drains at the donor site of iliac-crest bone grafts. A prospective, randomized study of morbidity at the donor site in patients who had a traumatic injury of the spine. *J Bone Joint Surg Am*, 80, 631-635.

Senn, N. (1889) On the healing of aseptic bone cavities by implantation of antiseptic decalcified bone. *Am J Med Sci*, 98, 219–243.

Seyedin, S.M., Segarini, P.R., Rosen, D.M., Thompson, A.Y., Bentz, H. & Gaycar, J. (1987) Cartilage-inducing factor-B is a unique protein structurally and functionally related to transforming growth factor-β. *J Biol Chem*, 262, 1946-1949.

Selye, H., Lemire, Y. & Bajusz, E. (1960) Induction of bone, cartilage and hemopoietic tissue by subcutaneously implanted tissue diaphragms. *Roux' Arch Entwicklungsmech,* 151, 572-585.

Shah, M., Foreman, D.M. & Ferguson, M.W. (1995) Neutralisation of TGF-β1 and TGF- β 2 or exogenous addition of TGF- β 3 to cutaneous rat wounds reduces scarring. *J Cell Sci*, 108, 985-1002.

Shi,Y. & Massagué, J. (2003) Mechanisms of TGF-β signaling from cell membrane to the nucleus. *Cell*,113, 685-700.

Shinozak, M., Kawara, S., Hayashi, N., Kakinuma, T., Igarashi, A. & Takehara, K. (1997) Induction of subcutaneous tissue fibrosis in newborn mice by transforming growth factor b-simultaneous application with basic fibroblast growth factor causes persistent fibrosis. *Biochem Biophys Res Commun,* 240, 292-297.

Shipley, J.M., Mecham, R.P., Maus, E., Bonadio, J., Rosenbloom, J., McCarthy, R.T., *et al.* (2000) Developmental expression of latent transforming growth factor β binding protein 2 and its requirement early in mouse development. *Mol Cell Biol*, 20, 4879-4887.

Shull, M.M., Ormsby, I., Kier, A.B., Pawlowski, S., Diebold, R.J., Yin, M., *et al*. (1992) Targeted disruption of the mouse transforming growth factor-β 1 gene results in multifocal inflammatory disease. *Nature,* 359, 693-699.

Solloway, M.J., Dudley, A.T., Bikoff, E.K., Lyons, K.M., Hogan, B.L. & Robertson, E.J. (1998) Mice lacking BMP-6 function. *Dev Genet*, 22, 321-339.

Sosic, D., Brand-Saberi, B., Schmidt, C., Christ, B. & Olson, E. (1997) Regulation of *paraxis* expression and somite formation by ectoderm-and neural tube-derived signals. *Dev Biol*, 185, 229-243.

Sowa, H., Kaji, H., Hendy, G.N., Canaff, L., Komori, T., Sugimoto, T., *et al.* (2004) Menin is required for bone morphogenetic protein 2 – and transforming growth factor β – regulated osteoblastic differentiation through interaction with Smads and Runx2. *J Biol Chem*, 279, 40267-40275.

Spagnoli, A., O'Rear, L., Chandler, R.L., Granero-Molto, F., Mortlock, D.P., Gorska, A., E., *et al*. (2007). TGF-β signaling is essential for joint morphogenesis. *J Cell Biol*, 177, 1105–1117.

Spemann, H. (1938). Embryonic Development and Induction. New Haven: Yale University Press.

Storm, E.E., Huynh, T.V., Copeland, N.G., Jenkins, N.A., Kingsley, D.M. & Lee, S.J. (1994) Limb alterations in brachypodism mice due to mutations in a new member of the TGF-β superfamily. *Nature*, 368, 639-643.

Storm, E.E. & Kingsley, D.M. (1996) Joint patterning defects caused by single and double mutations in members of the bone morphogenetic protein (BMP) family. *Development*, 122, 3969-3979.

Storm, E.E. & Kingsley, D.M. (1999) GDF co-ordinates bone and joint formation during digit development. *Dev Biol*, 209, 11-27.

Takase, M., Imamura, T., Sampath, T.K., Takeda, K., Ichijo, H., Miyazono, K., *et al.* (1998) Induction of Smad6 mRNA by bone morphogenetic proteins. *Biochem Biophys Res Commun*, 244, 26-29.

ten Dijke, P., Iwata, K.K., Goddard, C., Pieter, C., Canalis, E., McCarthy, T.L., *et al*. (1990) Recombinant transforming growth factor type β_3: biological activities and receptor-binding properties in isolated bone cells. *Mol Cell Biol*,10, 4473-4479.

Teitelbaum, S.L. (2000) Bone resorption by osteoclasts. *Science*, 289, 1504-1508.

Thorp, B.H., Anderson, I. & Jakowlew, S.B. (1992) Transforming growth factor-β_1, -β_2 and –β_3 in cartilage and bone cells during endochondral ossification in the chick. *Development*, 114, 907-911.

Trueta, J. (1963) The role of the vessels in osteogenesis. . *Bone Joint Surg*, 45B, 402–418.

Urist, M.R. (1965) Bone: formation by autoinduction. *Science*, 150, 1136-1138.

Urist, M.R., Silverman, B.F., Buring, K., Dubuc, F.L. & Rosenberg, J.M. (1967) The bone induction principle. *Clin Orthop*, 53, 243-283.

Urist, M.R. & Strates, B.S. (1971) Bone morphogenetic protein. *J Den Res*, 50, 1392-1406.

Vaananen, H.K., Zhao, H., Mulari, M. & Halleen, J.M. (2000) The cell biology of osteoclast function. *J Cell Sci*, 113, 377-381.

Vlacic-Zischke, J., Hamlet, S.M., Friis, T., Tonetti, M.S. & Ivanovski, S. (2011) The influence of surface microroughness and hydrophilicity of titanium on the up-regulation of TGF-β/BMP signalling in osteoblasts. *Biomaterials*, 32, 665–671.

Van Bezooijen, R.L., Papapoulos, S.E. & Lowik, C.W. (2005) Bone morphogenetic proteins and their antagonists: The sclerostin paradigm. *J Endocrinol Invest* & 28 & 15-17.

Van Eeden, S.P. & Ripamonti, U. (1994) Bone differentiation in porous hydroxyapatite in baboons is regulated by the geometry of the substratum: Implications for reconstructive craniofacial surgery. *Plast Reconstr Surg*, 93, 959-966.

Wang, E.A., Rosend, V., Cordes, P., Hewick, R.M., Kriz, M.J., Luxenberg, D.P., *et al*. (1988) Purification and characterization of other distinct bone-inducing factors. *Proc Natl Acad Sci USA*, 85, 9480-9488.

Wang, E.A., Rosen, V., D'Alessandro, J.S., Bauduy, M., Cordes, P., Harada, T., *et al.* (1990) Recombinant human bone morphogenetic protein induces bone formation. *Proc Natl Acad Sci USA*, 87, 2220-2224.

Wei, W. & Wan, Y. (2013) Translational Endocrinology; Chapter: Regulation of Bone Resorption by PPARγ. Academic Press, USA p.103-135.

Wilkinson, A., Hewitt, R.N., McNamara, L.E., Mccloy, D., Dominic Meek, R.M. & Dalby, M.J. (2011). Biomimetic microtopography to enhance osteogenesis in vitro. *Acta Biomater*, 7, 2919–2925.

Winter, G.D. & Simpson, B.J. (1996) Heterotopic bone formed in a synthetic sponge in the skin of young pigs. *Nature,*233, 88–90.

Wozney, J.M., Rosen, V., Celeste, A.J., Mitsocks, L.M., Whitters, M.J., Kriz, R.W., *et al.* (1988) Novel regulators of bone formation: molecular clones and activities. *Science,* 242, 1528-1534.

Wu, L.N., Genge, B.R., Dunkelberger, D.G., LeGeros, R.Z., Concannon, B. & Wuthier, R.E. (1997) Physiochemical characterization of the nucleational core of matrix vesicles. *J Biol Chem,* 272, 4404-4411.

Yeh, L.C., Tsai, A.D. & Lee, J.C. (2005) Cartilage-derived morphogenetic proteins induce osteogenic gene expression in the C2C12 mesenchymal cell line. *J Cell Biochem,* 95, 173-188.

Yoshida, Y., Tanaka, S., Umemori, H., Minowa, O., Usui, M., Ikematsu, N., *et al.* (2000) Negative regulation of BMP/Smad signalling by Tob in osteoblasts. *Cell,* 103, 1085-1097.

Zimmerman, L.B., De Jesus-Escobar, J.M. & Harland, R.M. (1996) The Spemann organizer signal Noggin binds and inactivates bone morphogenetic protein 4. *Cell,* 96, 599-606.

Zhang, R., Edwards, J.R., Ko, S., Dong, S., Liu, H., Oyajobi, B.O., *et al.* (2011) Transcriptional regulation of BMP2 expression by the PTH-CREB signalling pathway in osteoblasts. *PLOS ONE,* 6, 1-12.

Zhao, M., Edwards, J., Ko, S., Parlato, R., Harris, S. & Mundy, G. (2009) CREB induces BMP-2 transcription in osteoblasts and CREB knockout reduces bone mass in mice. *Bone*, 44(suppl1), S27.

Zhou, Z., Xie, J., Lee, D., Liu, Y., Jung, J., Zhou, L., *et al*. (2010) Neogenin regulation of BMP induced canonical Smad signaling and endochondral bone formation. *Dev Cell*, 19, 90-102.

Zyzafoon, M. (2009) Calcium/calmodulin signalling controls osteoblasts growth and differentiation. *J Cell Mol Med*, 13, 1-10.